

Towards Improved Practicality in Iron-Catalyzed Suzuki-Miyaura Cross-Coupling Reactions

Alexander Shun-Wai Wong

A dissertation
submitted to the Faculty of
the department of Chemistry
in partial fulfillment
of the requirements for the degree of
Doctor of Philosophy

Boston College
Morrissey College of Arts and Sciences
Graduate School

August 2021

Towards Improved Practicality in Iron-Catalyzed Suzuki-Miyaura Cross-Coupling Reactions

Alexander Shun-Wai Wong

Advisor: Professor Jeffery A. Byers, Ph.D.

Abstract: This dissertation will discuss the development of Suzuki-Miyaura cross-coupling reactions catalyzed by iron-based complexes with an emphasis on addressing limitations to their practical application in industrial contexts. *Chapter 1* will provide an overview of the development of the palladium-catalyzed Suzuki-Miyaura cross-coupling reaction and key factors which have enabled its prevalent use in various industries, with a comparison to how those factors have limited similar development of iron-catalyzed analogues. *Chapter 2* will discuss the initial discovery and subsequent development of a series of iron-based precatalysts for the cross-coupling reaction of unactivated aryl boronic esters and alkyl halides. *Chapter 3* will discuss the development and validation of a bench-stable iron(III)-based complex capable of catalyzing the Suzuki-Miyaura cross-coupling reaction between unactivated aryl boronic esters and alkyl halides. To conclude, *Chapter 4* will discuss the ability of iron-based complexes to participate in the Suzuki-Miyaura cross-coupling reaction with alkyl tosylate electrophiles and its implications for harnessing the ability of iron catalysis to operate under different mechanistic manifolds.

TABLE OF CONTENTS

Table of Contents	iv
List of tables.....	viii
List of figures.....	xii
List of schemes.....	xxiii
List of abbreviations	xxi
Acknowledgments	xxiv
Dedication	xxxiii
Chapter 1. The Development of Versatile Palladium-Catalyzed Suzuki-Miyaura Cross-Coupling Reactions and Comparisons to Iron-Catalyzed Analogues.....	1
1.1 Introduction.....	2
1.2 The palladium-catalyzed Suzuki-Miyaura cross-coupling reaction and its operative mechanism	4
1.2.1 Oxidative addition	5
1.2.2 Transmetalation.....	7
1.2.3 Reductive elimination.....	10
1.3 The dialkylbiaryl monophosphines: logically designed supporting ligand frameworks to promote palladium-catalyzed Suzuki-Miyaura reactions	11
1.4 The development of bench-stable palladacycle-based catalyst precursors for Suzuki-Miyaura cross-coupling reactions	15
1.5 Transition metal-catalyzed Suzuki-Miyaura cross-coupling reactions involving C—O electrophiles	19
1.5.1 Suzuki-Miyaura cross-coupling reactions of activated C—O bonds.....	20
1.5.2 Suzuki-Miyaura cross-coupling reactions of unactivated C—O bonds.....	22
1.6 Recent developments in first-row transition metal catalysis to address limitations of the palladium-catalyzed Suzuki-Miyaura cross-coupling reaction	25
1.7 An overview of the development of iron-catalyzed cross-coupling reactions	30

1.8	Conclusion	38
1.9	References.....	40
Chapter 2. Suzuki-Miyaura Cross-Coupling Reactions of Alkyl Halides and Unactivated Aryl Boronic Esters Catalyzed by Iron-Based Complexes Developed Through Rational Ligand Design..... 62		
2.1	Introduction.....	63
2.2	The impact of promoting transmetalation and regulating aggregation on cross-coupling reactions catalyzed by iron-based complexes	66
2.3	Evaluation of substrate scope of a Suzuki-Miyaura cross-coupling reaction catalyzed by iron-based complexes and extension to a pharmaceutical target	72
2.4	Working mechanistic hypothesis and the development of principles for future ligand design	75
2.5	Examining the viability of β -diketiminato ligand frameworks to promote Suzuki-Miyaura cross-coupling reactions catalyzed by iron-based complexes	79
2.6	Optimization of catalyst structure and reaction conditions.....	84
2.7	Evaluation of substrate scope.....	88
2.8	Revised mechanistic hypothesis featuring a bifunctional iron amide intermediate...	91
2.9	Examining the transmetalation step with low-temperature nuclear magnetic resonance spectroscopy.....	93
2.10	Conclusion and outlook	104
2.11	Experimental section.....	106
2.12	References.....	142
Chapter 3. Synthesis and Characterization of Air-Stable Iron-Based Catalyst Precursors for the Suzuki-Miyaura Cross-Coupling Reaction of Alkyl Halides and Unactivated Aryl Boronic Esters..... 156		
3.1	Introduction.....	157
3.2	Practical limitations to the general application of iron-based complexes for catalyzing Suzuki-Miyaura cross-coupling reactions.....	158
3.3	Synthesis and characterization of iron(III)-based catalyst precursors supported by β -diketiminato ligands.....	160
3.4	Evaluation of catalytic competence and bench stability of β -diketiminato iron(III)-based complexes for the Suzuki-Miyaura cross-coupling reaction.....	163

3.5	Examining the mechanism of activation for iron(III)-based complexes in the Suzuki-Miyaura cross-coupling reaction.....	168
3.6	Reaction optimization	169
3.7	Evaluation of substrate scope.....	172
3.8	Conclusion and outlook	175
3.9	Experimental section.....	177
3.10	References.....	190
Chapter 4. Progress Towards Suzuki-Miyaura Cross-Coupling Reactions of Alkyl Sulfonate Esters and Unactivated Aryl Boronic Esters Catalyzed by Iron-Based Complexes.....		197
4.1	Introduction.....	198
4.2	Initial discovery and catalyst optimization	203
4.3	Inconsistencies in the working mechanistic hypothesis when explaining the reactivity of alkyl sulfonate ester electrophiles.....	205
4.4	Optimization of reaction conditions.....	206
4.4.1	Screening of substrate equivalents	206
4.4.2	Screening of sulfonate ester identity and boronic ester identity.....	208
4.4.3	Screening of lithium amide bases.....	209
4.4.4	Screening of reaction conditions	210
4.4.5	Screening of additive effects	211
4.5	Examining the equilibrium of the salt metathesis step and the inhibitory effect of lithium tosylate	213
4.6	Examining the possibility of a catalytic cycle featuring two-electron processes.....	217
4.7	Evaluation of substrate scope.....	220
4.8	Conclusion and outlook	221
4.9	Experimental section.....	222
4.10	References.....	231
Appendix A. Nuclear magnetic resonance spectral data.....		238
A.1	Nuclear magnetic resonance spectral data from Chapter 2.....	239

A.2	Nuclear magnetic resonance spectral data from Chapter 3.....	261
A.3	Nuclear magnetic resonance spectral data from Chapter 4.....	262
Appendix B. X-ray crystallographic data.....		263
B.1	X-ray crystallographic data from Chapter 2	264
B.1.1	X-ray crystallographic data for compound 2.46	264
B.1.2	X-ray crystallographic data for compound 2.47	273
B.2	X-ray crystallographic data from Chapter 3	288
B.2.1	X-ray crystallographic data for compound 3.2	288
B.2.2	X-ray crystallographic data for compound 3.3	314
Appendix C. Assorted spectral data.....		331
C.1	Mössbauer and electron paramagnetic resonance spectral data from Chapter 3	332

LIST OF TABLES

Table 2.1. Screen of iron-based complexes supported by bis(oxazoline) ligands for promoting the Suzuki-Miyaura cross-coupling reaction between PhB(pin) and bromocycloheptane.....	71
Table 2.2. Substrate scope of a Suzuki-Miyaura cross-coupling reaction between aryl boronic acid pinacol esters and alkyl halides catalyzed by iron-based complex 2.10 . Isolated yields are reported with yields based on recovered starting material appearing in parentheses.....	73
Table 2.3. Screening of iron(II) complexes supported by β -diketiminato ligands for catalytic activity in the Suzuki-Miyaura cross-coupling reaction between PhB(pin) and bromocycloheptane.....	85
Table 2.4. Screening of reaction conditions for the Suzuki-Miyaura cross-coupling reaction between PhB(pin) and bromocycloheptane catalyzed by iron(II) complexes supported by β -diketiminato ligands.....	87
Table 2.5. Substrate scope of a Suzuki-Miyaura cross-coupling reaction between aryl boronic acid pinacol esters and alkyl halides catalyzed by iron-based complex 2.48 or 2.49 . Compounds synthesized using complex 2.48 are highlighted in gray. Isolated yields are reported with yields based on recovered starting material appearing in parentheses.....	89
Table 3.1. Optimization of reaction conditions.....	171
Table 3.2. Substrate scope for cross-coupling reactions performed without the aid of a glovebox using air-stable complex 3.3 as a catalyst precursor. Isolated yields are reported with yields based on recovered starting material in parentheses. Yields from reactions employing the iron(II) catalyst 3.1 in the glovebox are reported below in italics.....	173
Table 3.3. Cross-coupling reactions performed without the aid of a glovebox using uniformly sieved lithium amide and complex 3.3 as catalyst precursor.....	175
Table 4.1. Screening of iron-based catalysts for the cross-coupling of cycloheptyl tosylate and phenyl boronic acid pinacol ester.....	204
Table 4.2. Screening of substrate equivalents for the cross-coupling of cycloheptyl tosylate and phenyl boronic acid pinacol ester catalyzed by an iron-based complex....	207
Table 4.3. Screening of sulfonate esters and boronic esters for the cross-coupling of cycloheptyl sulfonate ester and phenyl boronic ester catalyzed by an iron-based complex.....	209

Table 4.4. Screening of lithium amides for the cross-coupling of cycloheptyl tosylate and phenyl boronic acid pinacol ester catalyzed by an iron-based complex	210
Table 4.5. Screening of reaction conditions including solvent, temperature, time, and catalyst loading for the cross-coupling of cycloheptyl tosylate and phenyl boronic acid pinacol ester catalyzed by an iron-based complex	211
Table 4.6. Screening of the effect of additives for the cross-coupling of cycloheptyl tosylate and phenyl boronic acid pinacol ester catalyzed by an iron-based complex....	213
Table 4.7. Screening of the effect of adding reagents halfway through the cross-coupling of cycloheptyl tosylate and phenyl boronic acid pinacol ester catalyzed by an iron-based complex	217
Table 4.8. Stoichiometric reactions of <i>in situ</i> reduced iron amide species 4.13 to test for reactivity with cycloheptyl tosylate 4.1 and formation of 4.3	219
Table 4.9. Substrate scope of the cross-coupling of alkyl tosylate and aryl boronic acid pinacol ester.....	220
Table B.1.1.1. Crystal data and structure refinement for dimeric 2,4-bis[(2,6-dimethylphenyl)imino]pentane iron <i>N,N</i> -diethylamide complex (2.46).....	264
Table B.1.1.2. Atomic coordinates ($\times 10^4$) and equivalent isotropic displacement parameters ($\text{\AA}^2 \times 10^3$) for dimeric 2,4-bis[(2,6-dimethylphenyl)imino]pentane iron <i>N,N</i> -diethylamide complex (2.46). $U(\text{eq})$ is defined as one third of the trace of the orthogonalized U^{ij} tensor.	266
Table B.1.1.3. Bond lengths [\AA] and angles [$^\circ$] for dimeric 2,4-bis[(2,6-dimethylphenyl)imino]pentane iron <i>N,N</i> -diethylamide complex (2.46).....	267
Table B.1.1.4. Anisotropic displacement parameters ($\text{\AA}^2 \times 10^3$) for dimeric 2,4-bis[(2,6-dimethylphenyl)imino]pentane iron <i>N,N</i> -diethylamide complex (2.46). The anisotropic displacement factor exponent takes the form: $-2\pi^2 [h^2 a^{*2} U^{11} + \dots + 2 h k a^* b^* U^{12}]$	272
Table B.1.2.1. Crystal data and structure refinement for dimeric 2,4-bis[(2,6-dimethylphenyl)imino]pentane iron phenyl complex (2.47)	273
Table B.1.2.2. Atomic coordinates ($\times 10^4$) and equivalent isotropic displacement parameters ($\text{\AA}^2 \times 10^3$) for dimeric 2,4-bis[(2,6-dimethylphenyl)imino]pentane iron phenyl complex (2.47). $U(\text{eq})$ is defined as one third of the trace of the orthogonalized U^{ij} tensor.	275
Table B.1.2.3. Bond lengths [\AA] and angles [$^\circ$] for dimeric 2,4-bis[(2,6-dimethylphenyl)imino]pentane iron phenyl complex (2.47)	277

Table B.1.2.4. Anisotropic displacement parameters ($\text{\AA}^2 \times 10^3$) for dimeric 2,4-bis[(2,6-dimethylphenyl)imino]pentane iron phenyl complex (2.47). The anisotropic displacement factor exponent takes the form: $-2\pi^2 [h^2 a^{*2} U^{11} + \dots + 2 h k a^* b^* U^{12}]$	286
Table B.2.1.1. Crystal data and structure refinement for 2,4-bis[(2,6-dimethylphenyl)imino]pentane iron(III) dichloride complex (3.2)	288
Table B.2.1.2. Atomic coordinates ($\times 10^4$) and equivalent isotropic displacement parameters ($\text{\AA}^2 \times 10^3$) for 2,4-bis[(2,6-dimethylphenyl)imino]pentane iron(III) dichloride complex (3.2). $U(\text{eq})$ is defined as one third of the trace of the orthogonalized U^{ij} tensor.	290
Table B.2.1.3. Bond lengths [\AA] and angles [$^\circ$] for 2,4-bis[(2,6-dimethylphenyl)imino]pentane iron(III) dichloride complex (3.2)	293
Table B.2.1.4. Anisotropic displacement parameters ($\text{\AA}^2 \times 10^3$) for 2,4-bis[(2,6-dimethylphenyl)imino]pentane iron(III) dichloride complex (3.2). The anisotropic displacement factor exponent takes the form: $-2\pi^2 [h^2 a^{*2} U^{11} + \dots + 2 h k a^* b^* U^{12}]$	304
Table B.2.1.5. Hydrogen coordinates ($\times 10^4$) and isotropic displacement parameters ($\text{\AA}^2 \times 10^3$) for 2,4-bis[(2,6-dimethylphenyl)imino]pentane iron(III) dichloride complex (3.2)	307
Table B.2.1.6. Torsion angles [$^\circ$] for 2,4-bis[(2,6-dimethylphenyl)imino]pentane iron(III) dichloride complex (3.2).....	310
Table B.2.2.1. Crystal data and structure refinement for 2,4-bis[(2,6-dimethylphenyl)imino]pentane iron(III) bis(acetylacetonate) complex (3.3)	314
Table B.2.2.2. Atomic coordinates ($\times 10^4$) and equivalent isotropic displacement parameters ($\text{\AA}^2 \times 10^3$) for 2,4-bis[(2,6-dimethylphenyl)imino]pentane iron(III) bis(acetylacetonate) complex (3.3). $U(\text{eq})$ is defined as one third of the trace of the orthogonalized U^{ij} tensor.	316
Table B.2.2.3. Bond lengths [\AA] and angles [$^\circ$] for 2,4-bis[(2,6-dimethylphenyl)imino]pentane iron(III) bis(acetylacetonate) complex (3.3)	318
Table B.2.2.4. Anisotropic displacement parameters ($\text{\AA}^2 \times 10^3$) for 2,4-bis[(2,6-dimethylphenyl)imino]pentane iron(III) bis(acetylacetonate) complex (3.3). The anisotropic displacement factor exponent takes the form: $-2\pi^2 [h^2 a^{*2} U^{11} + \dots + 2 h k a^* b^* U^{12}]$	325
Table B.2.2.5. Hydrogen coordinates ($\times 10^4$) and isotropic displacement parameters ($\text{\AA}^2 \times 10^3$) for 2,4-bis[(2,6-dimethylphenyl)imino]pentane iron(III) bis(acetylacetonate) complex (3.3)	327

Table B.2.2.6. Torsion angles [°] for 2,4-bis[(2,6-dimethylphenyl)imino]pentane iron(III) bis(acetylacetonate) complex (3.3).....	329
--	-----

LIST OF FIGURES

Figure 1.1. Palladium-catalyzed cross-coupling reactions.....	2
Figure 1.2. General mechanism of the palladium-catalyzed Suzuki-Miyaura cross-coupling reaction.....	5
Figure 1.3. <i>Cis-trans</i> isomerization following oxidative addition of palladium <i>via</i> 3-membered transition state	6
Figure 1.4. a) Suzuki-Miyaura cross-coupling reactions of diastereomers of sterically hindered primary alkylborane 1.1 which proceeded with retention of stereochemistry, b) pathways toward a four-centered hydroxo μ_2 -bridged transition state which facilitates stereoretentive alkyl group transfer	8
Figure 1.5. Stoichiometric studies by Hartwig and co-workers to evaluate the relative rates of a) the borate and b) the palladium hydroxide pathways commonly proposed for transmetalation in the Suzuki-Miyaura cross-coupling reaction.....	9
Figure 1.6. Pre-transmetalation intermediates containing Pd—O—B linkages observed by Denmark and co-workers through the use of rapid injection nuclear magnetic resonance spectroscopy that led to successful transfer of boron aryl groups to palladium and subsequent formation of cross-coupled product	10
Figure 1.7. Electronic influence on the reductive elimination of biaryls from platinum complexes	11
Figure 1.8. Structural features of dialkylbiaryl monophosphine ligands and the impacts of those features on palladium-catalyzed cross-coupling reactions	12
Figure 1.9. Examples of dialkylbiaryl monophosphine ligands developed by Buchwald and co-workers.....	14
Figure 1.10. a) Initial discovery of palladacycle complexes capable of catalyzing Mizoroki-Heck cross-coupling reactions by Beller and Herrmann, b) Examples of palladacycle precatalysts for cross-coupling reactions developed by Buchwald and co-workers through rational iterative ligand design, c) Proposed mechanism of activation for palladacycle precatalysts to generate the active monoligated palladium(0) species in cross-coupling reactions	17
Figure 1.11. C—O electrophiles for transition metal-catalyzed cross-coupling reactions	20
Figure 1.12. Catalytic cycle for the palladium-catalyzed Suzuki-Miyaura cross-coupling reaction of alkyl electrophiles with possible inhibitory pathways highlighted using dashed arrows.....	26

Figure 1.13. Catalytic cycle for the iron-catalyzed Suzuki-Miyaura cross-coupling reaction between C(sp ²)-hybridized organoboron reagents and C(sp ³)-hybridized electrophiles proposed by Nakamura and Neidig featuring iron(II)/iron(III) intermediates.	36
Figure 1.14. Catalytic cycle for the iron-catalyzed Suzuki-Miyaura cross-coupling reaction between C(sp ²)-hybridized organoboron reagents and C(sp ³)-hybridized electrophiles proposed by Bedford and Norrby featuring iron(I)/iron(II)/iron(III) intermediates.	37
Figure 2.1. a) Mechanistic comparison between palladium-catalyzed and iron-catalyzed Suzuki-Miyaura cross-coupling reactions of halide electrophiles and organoboron nucleophiles. The base-facilitated transmetalation step is highlighted in red. b) Proposed pathways for transmetalation in palladium-catalyzed Suzuki-Miyaura cross-coupling reactions and a spectroscopically identified intermediate likely involved in transmetalation.....	67
Figure 2.2. Density functional theory (B3LYP/6-31G*) computed energies for the transmetalation from boron to iron in reactions between PhB(pin) and (dppe)Fe ^{II} X ₂	68
Figure 2.3. Working mechanistic hypothesis for the Suzuki-Miyaura cross-coupling reaction of alkyl electrophiles and unactivated aryl boronic acid pinacol esters catalyzed by an iron-based complex supported by a cyanated phenylbis(oxazoline) ligand (2.10).	78
Figure 2.4. Survey of journal articles describing Suzuki-Miyaura reactions for: a) hybridization of nucleophiles/electrophiles and types of nucleophiles/electrophiles involved in C(sp ²)-C(sp ³) cross-coupling reactions (inset), and b) types of nucleophiles/electrophiles used in C(sp ²)-C(sp ³) cross-coupling reactions for primary, secondary, or tertiary sp ³ -hybridized substrates. The dataset was generated using SciFinder [®]	80
Figure 2.5. a) Ligand design principles for the development of new iron-based complexes b) First- and second-generation iron-based complexes for Suzuki-Miyaura cross-coupling reactions of aryl boronic esters and alkyl halides.....	81
Figure 2.6. Conversion vs. time plots over the first 8 hours of reaction for the cross-coupling of PhB(pin) and bromocycloheptane using representative β-diketimate iron complexes.....	86
Figure 2.7. Revised working mechanistic hypothesis for the Suzuki-Miyaura cross-coupling reaction of alkyl halides and unactivated aryl boronic esters catalyzed by iron complexes supported by β-diketimate ligands	93
Figure 2.8. Conversion vs. time data for the consumption of PhB(pin) (blue traces) and the production of Et ₂ NB(pin) 2.80 (red traces) from reaction of PhB(pin) with 2.46 at a) -30 °C, b) -15 °C, and c) 0 °C.....	95

Figure 2.9. a) Conversion vs. time data for the consumption of PhB(neo) (green trace) and the production of Et₂NB(neo) **2.81** (purple trace) from reaction of PhB(neo) with **2.46** at -30 °C. b) Overlaid comparison of conversion vs. time data for transmetalation reactions between PhB(pin) and **2.46** (blue and red traces) and between PhB(neo) and **2.46** (green and purple traces) 98

Figure 2.10. Conversion vs. time data for the reaction of (PhBO)₃ with **2.46** at ambient temperature. NMR resonances corresponding to (PhBO)₃ were not observed; the data points trace the production of Et₂NB(OH) **2.82** over the course of 24 hours 99

Figure 2.11. Hypothesis for the formation of pre-transmetalation intermediates from iron amide complex **2.46** with a) PhB(pin), b) PhB(neo), and c) (PhBO)₃, and density functional theory computations (B3LYP/6-31G*) of ground-state enthalpy values 100

Figure 2.12. a) Conversion vs. time data for the consumption of 2-thiophenyl-B(pin) (blue trace) with **2.46** and the production of Et₂NB(pin) **2.80** (red traces) from reaction of 2-thiophenyl-B(pin) with **2.46** at -30 °C. b) Hypothesis for pre-transmetalation intermediates which inhibit transmetalation of 2-thiophenyl-B(pin). c) Pre-transmetalation intermediates for transmetalation of 3-thiophenyl-B(pin) which avoid inhibitory interactions 103

Figure 3.1. Appearance of iron complex **3.1** while stored under N₂ (left image) and appearance of iron complex **3.1** following 3 minutes of exposure to air (right image). 159

Figure 3.2. X-ray crystal structures of complexes **3.2** and **3.3** with selected bond metrics. Thermal ellipsoids are drawn at the 50% probability level; co-crystallized solvent molecules and hydrogen atoms are omitted for clarity. Crystal refinement tables are located in Appendix B.2 162

Figure 3.3. a) Comparison of the 80 K ⁵⁷Fe Mössbauer spectra of a powder of **3.3**, i) prior to and ii) following exposure to air for four months. b) Comparison of the 80 K ⁵⁷Fe Mössbauer spectra of the previously synthesized iron(II)-based cross-coupling precatalyst **3.1** i) prior to and ii) following exposure to air for one hour. The latter spectrum features three iron species with the following parameters: red component, δ = 0.38 mm/s, |ΔE_Q| = 1.37 mm/s (46% of total iron); blue component, δ = 0.42 mm/s, |ΔE_Q| = 0.81 mm/s (48% of total iron) and green component, δ = 1.34 mm/s, |ΔE_Q| = 2.55 mm/s (6% of total iron) 166

Figure 3.4. Comparison of the ¹H NMR spectra (solvent-suppressed, THF) of iron complex **3.1** a) prior to and b) after exposure to air for 1 hour 167

Figure 3.5. Working mechanistic hypothesis for the cross-coupling reaction of alkyl halides and aryl boronic esters catalyzed by β-diketiminato iron(II) complexes. Possible pathways for activation of the iron(III) analogues are highlighted in red 168

Figure 4.1. Representative synthesis of sulfonate esters from alcohols 198

Figure 4.2. Working mechanistic hypothesis for the Suzuki-Miyaura cross-coupling reaction of alkyl halides and unactivated boronic esters catalyzed by β -diketiminato iron(II) complexes applied to alkyl tosylate electrophiles. Changes resulting from replacement of the electrophile with an alkyl tosylate are highlighted	206
Figure A.1.1. ^1H NMR spectrum of compound 2.10 using solvent suppression for THF peaks.....	239
Figure A.1.2. ^1H NMR spectrum of compound 2.27	239
Figure A.1.3. ^{13}C NMR spectrum of compound 2.27	240
Figure A.1.4. ^{19}F NMR spectrum of compound 2.27	240
Figure A.1.5. ^1H NMR spectrum of compound 2.31	241
Figure A.1.6. ^{13}C NMR spectrum of compound 2.31	241
Figure A.1.7. ^{19}F NMR spectrum of compound 2.31	242
Figure A.1.8. ^1H NMR spectrum of compound 2.44 using solvent suppression for THF peaks.....	242
Figure A.1.9. ^1H NMR spectrum of compound 2.46	243
Figure A.1.10. DOSY NMR spectrum of compound 2.46	243
Figure A.1.11. ^1H NMR spectrum of compound 2.47	244
Figure A.1.12. ^1H NMR spectrum of compound 2.48 using solvent suppression for THF peaks.....	245
Figure A.1.13. ^1H NMR spectrum of compound 2.49 using solvent suppression for THF peaks.....	245
Figure A.1.14. ^1H NMR spectrum of compound 2.50 using solvent suppression for THF peaks.....	245
Figure A.1.15. ^1H NMR spectrum of compound 2.51 using solvent suppression for THF peaks.....	246
Figure A.1.16. ^1H NMR spectrum of compound 2.52 using solvent suppression for THF peaks.....	246
Figure A.1.17. ^1H NMR spectrum of compound 2.53 using solvent suppression for THF peaks.....	247
Figure A.1.18. ^1H NMR spectrum of compound 2.54 using solvent suppression for THF peaks.....	247

Figure A.1.19. ^1H NMR spectrum of compound 2.55 using solvent suppression for THF peaks.....	248
Figure A.1.20. ^1H NMR spectrum of compound 2.56 using solvent suppression for THF peaks.....	248
Figure A.1.21. ^1H NMR spectrum of compound 2.59 using solvent suppression for THF peaks.....	249
Figure A.1.22. ^1H NMR spectrum of compound 2.60 using solvent suppression for THF peaks.....	249
Figure A.1.23. ^1H NMR spectrum of compound 2.61 using solvent suppression for THF peaks.....	250
Figure A.1.24. ^1H NMR spectrum of compound 2.62	250
Figure A.1.25. ^{13}C NMR spectrum of compound 2.62	251
Figure A.1.26. ^1H NMR spectrum of compound 2.29	251
Figure A.1.27. ^{13}C NMR spectrum of compound 2.29	252
Figure A.1.28. ^1H NMR spectrum of compound 2.64	252
Figure A.1.29. ^{13}C NMR spectrum of compound 2.64	253
Figure A.1.30. ^1H NMR spectrum of compound 2.65	253
Figure A.1.31. ^{13}C NMR spectrum of compound 2.65	254
Figure A.1.32. ^1H NMR spectrum of compound 2.66	254
Figure A.1.33. ^{13}C NMR spectrum of compound 2.66	255
Figure A.1.34. ^1H NMR spectrum of compound 2.28	255
Figure A.1.35. ^{13}C NMR spectrum of compound 2.28	256
Figure A.1.36. ^1H NMR spectrum of compound 2.67	256
Figure A.1.37. ^{13}C NMR spectrum of compound 2.67	257
Figure A.1.38. ^1H NMR spectrum of compound 2.68	257
Figure A.1.39. ^{13}C NMR spectrum of compound 2.68	258
Figure A.1.40. ^1H NMR spectrum of compound 2.69	258

Figure A.1.41. ^{13}C NMR spectrum of compound 2.69	259
Figure A.1.42. ^1H NMR spectrum of compound 2.73	259
Figure A.1.43. ^{13}C NMR spectrum of compound 2.73	260
Figure A.2.1. ^1H NMR spectrum of compound 3.2 using solvent suppression for THF peaks.	261
Figure A.2.2. ^1H NMR spectrum of compound 3.3	261
Figure A.3.1. ^1H NMR spectrum of compound 4.12	262
Figure B.1.1.1. ORTEP diagram of compound 2.46	264
Figure B.1.2.1. ORTEP diagram of compound 2.47	273
Figure B.2.1.1. ORTEP diagram of compound 3.2	288
Figure B.2.2.1. ORTEP diagram of compound 3.3	314
Figure C.1.1. Mössbauer spectra of 3.3 synthesized at various concentrations. The fourth spectrum is a sample of ^{57}Fe -enriched 3.3 , which displays reduced signal broadening (though signal broadening is common for Fe(III) complexes)	332
Figure C.1.2. Two possible fits for the Mössbauer spectra of a sample of 3.3 dissolved in C_6H_6 after 24 hours. The compound is converted into a mixture of iron species in solution. At this time, the iron speciation of the compound in solution is unclear.	333
Figure C.1.3. a) 80 K ^{57}Fe Mössbauer spectra of 3.3 in C_6H_6 , b) 80 K ^{57}Fe Mössbauer spectra of 3.3 5 minutes following the addition of 1 equivalent LiNMeEt in C_6H_6 , c) 80 K ^{57}Fe Mössbauer spectra of 3.3 5 minutes following the addition of 1 equivalent PhB(pin) in C_6H_6 , d) 80 K ^{57}Fe Mössbauer spectra of 3.3 5 minutes following the addition of 1 equivalent LiNMeEt and 1 equivalent PhB(pin) in C_6H_6 . All spectra feature two iron species in varying ratios, with the following parameters: green component, $\delta = 0.47$ mm/s, $ \Delta E_Q = 0.82$ mm/s; blue component, $\delta = 0.85$ mm/s, $ \Delta E_Q = 1.64$ mm/s.	333
Figure C.1.4. Electron paramagnetic spectrum of 3.3 in C_6H_6 at 10 K.....	334
Figure C.1.5. Electron paramagnetic spectrum of 3.3 following the addition of 1 equivalent of LiNMeEt in C_6H_6 at 10 K.....	334
Figure C.1.6. Electron paramagnetic spectrum of 3.3 following the addition of 2 equivalents of LiNMeEt in C_6H_6 at 10 K.....	335

LIST OF SCHEMES

Scheme 1.1. a) First example of palladium-catalyzed Suzuki-Miyaura reaction of aryl triflates. b) First example of palladium-catalyzed Suzuki-Miyaura reaction of unactivated aryl tosylates.....	21
Scheme 1.2. a) First example of palladium-catalyzed Suzuki-Miyaura cross-coupling reaction of benzyl acetates. b,c) Independently reported examples of nickel-catalyzed Suzuki-Miyaura cross-coupling reactions of aryl pivalate esters. d,e) First independently reported examples of nickel-catalyzed Suzuki-Miyaura cross-coupling reactions of aryl carbamates.....	22
Scheme 1.3. a) Initial example of Suzuki-Miyaura cross-coupling reaction between aryl boronic ester and aryl methyl ether catalyzed by ruthenium in the presence of a directing group, b) nickel-catalyzed Suzuki-Miyaura cross-coupling reaction between aryl boronic ester and aryl methyl ether in the absence of a directing group, c) initial example of a nickel-catalyzed Suzuki-Miyaura cross-coupling reaction between an unprotected naphthyl alcohol with aryl boroxine	24
Scheme 1.4. Examples by Fu and co-workers of Suzuki-Miyaura cross-coupling reactions of C(sp ²)-hybridized organoboron reagents with substituted C(sp ³)-hybridized electrophiles catalyzed by nickel-based complexes, and proposed mechanism for c).....	28
Scheme 1.5. First example of a stereoconvergent Suzuki-Miyaura cross-coupling reaction of C(sp ³)-hybridized organoboron reagents with substituted C(sp ³)-hybridized electrophiles catalyzed by nickel-based complexes.....	29
Scheme 1.6. Early examples of cross-coupling reactions between organometallic nucleophiles and organic halides catalyzed by iron salts.....	31
Scheme 1.7. Examples of Negishi-type cross-coupling reactions between C(sp ²)-hybridized organozinc reagents and substituted C(sp ³)-hybridized electrophiles catalyzed by iron-based complexes	33
Scheme 1.8. Examples of Suzuki-Miyaura-type cross-coupling reactions between C(sp ²)-hybridized organoboron reagents and C(sp ³)-hybridized electrophiles catalyzed by iron-based complexes	35
Scheme 2.1. Examples of Suzuki-Miyaura-type cross-coupling reactions of aryl organoboron reagents catalyzed by iron-based complexes which require magnesium bromide additives for high yields.	65
Scheme 2.2. Attempted synthesis of (dppe)Fe(OR) ₂ <i>via</i> a) salt metathesis, b) protonolysis; c) Synthesis of (dppe)Fe(NR ₂) ₂ and evaluation of activity towards cross-coupling reaction of PhB(pin) and bromocycloheptane with screening of various LiNR ₂ sources.	69

Scheme 2.3. a) Retrosynthetic analysis of previously reported synthetic routes to cinacalcet (Sensipar [®]), b) a two-step synthesis of cinacalcet (Sensipar [®]) using an iron-catalyzed Suzuki-Miyaura cross-coupling reaction between an aryl boronic ester and an alkyl halide	75
Scheme 2.4. Reactions of radical clock substrates to examine the intermediacy of organic radicals in the iron-catalyzed Suzuki-Miyaura cross-coupling reaction.....	76
Scheme 2.5. Reactions involving preactivated borate species in the Suzuki-Miyaura cross-coupling reaction catalyzed by iron-based complex 2.10	77
Scheme 2.6. Stoichiometric reactions relevant to Suzuki-Miyaura cross-coupling reactions involving iron complexes supported by β -diketiminato ligands.....	83
Scheme 2.7. Stoichiometric reaction between 2.46 , 2.47 , and bromocycloheptane, which leads to rapid and quantitative formation of cross-coupled product 2.4	92
Scheme 2.8. Scope of phenyl boronic esters for the Suzuki-Miyaura cross-coupling reaction with bromocycloheptane catalyzed by β -diketiminato iron complex 2.49 featuring 2- ^t BuPh imine substituents	97
Scheme 3.1. a) Attempted synthesis of an iron(III) complex supported by a β -diketiminato ligand through the addition of FeCl ₃ , b) synthesis of a neutral iron(III) dichloride complex supported by a β -diketiminato ligand via the oxidation of the analogous iron (II) complex, c) synthesis of an air-stable iron(III) complex supported by a β -diketiminato ligand and two acetylacetonate (acac) ligands.....	161
Scheme 3.2. Suzuki-Miyaura cross-coupling reaction of bromocycloheptane and phenyl boronic acid pinacol ester catalyzed by iron complexes 3.1 , 3.2 , and 3.3 prior to and after exposure to air for one hour.....	164
Scheme 4.1. a) First example of palladium-catalyzed Suzuki-Miyaura reaction of aryl triflates. b) First example of palladium-catalyzed Suzuki-Miyaura reaction of unactivated aryl tosylates.....	199
Scheme 4.2. a-c) Examples of palladium-catalyzed cross-coupling reactions of alkyl tosylates, d-e) examples of first-row transition metal-catalyzed cross-coupling reactions of alkyl tosylates.....	200
Scheme 4.3. Examples of nickel-catalyzed reductive cross-electrophile cross-coupling reactions involving alkyl sulfonate esters	202
Scheme 4.4. a) Synthesis of iron tosylate complex supported by β -diketiminato ligand. b) ¹ H NMR spectrum in C ₆ D ₆ of 4.12 , c) ¹ H NMR spectrum in C ₆ D ₆ of reaction between 4.12 and LiNMeEt	214
Scheme 4.5. a) Cross-coupling reaction of cycloheptyl bromide and phenyl boronic acid pinacol ester catalyzed by iron tosylate complex 4.12 , b) Cross-coupling reaction	

of cycloheptyl tosylate and phenyl boronic acid pinacol ester catalyzed by iron tosylate complex **4.12** 215

Scheme 4.6. a) Inhibition of the cross-coupling reaction of bromocycloheptane and phenyl boronic acid pinacol ester catalyzed by iron tosylate complex **4.12** with the addition of 1 equiv. lithium tosylate, b) Inhibition of the cross-coupling reaction of cycloheptyl tosylate and phenyl boronic acid pinacol ester catalyzed by iron tosylate complex **4.12** with the addition of 1 equiv. lithium tosylate 216

Scheme 4.7. a) Stoichiometric reaction to probe reactivity of cycloheptyl tosylate **4.1** with discretely synthesized iron amide intermediate **4.13**, b) Stoichiometric reaction to probe reactivity of cycloheptyl tosylate **4.1** with *in situ* generated iron intermediates **4.13** and **4.14** 218

LIST OF ABBREVIATIONS

$^{\circ}\text{C}$	degree(s) Celsius
ΔG	change in Gibbs free energy
$\Delta\text{G}^{\ddagger}$	free energy activation energy
ΔH	change in enthalpy
$\Delta\text{H}^{\ddagger}$	enthalpic activation energy
δ	chemical shift (NMR), isomer shift (Mössbauer)
$ \Delta\text{E}_\text{Q} $	quadrupole splitting (Mössbauer)
μ_B	Bohr magneton
μ_eff	effective magnetic moment
1,3,5-TMB	1,3,5-trimethoxybenzene
12-crown-4	1,4,7,10-tetraoxacyclododecane
18-crown-6	1,4,7,10,13,16-hexaoxacyclooctadecane
9-BBN	9-borabicyclo[3.3.1]nonane
\AA	ångström
acac	acetylacetonate
Ad	adamantyl
Ar	aryl
Bn	benzyl
Boc	<i>tert</i> -butyloxycarbonyl
Box	bis(oxazoline)
BrettPhos	2-(dicyclohexylphosphino)-3,6-dimethoxy-2',4',6'-triisopropyl-1,1'-biphenyl
brsm	based on recovered starting material
cal	calorie(s)
cat.	catalyst
CBz	benzyl chloroformate
CCDC	Cambridge Crystallographic Data Centre
cod	1,5-cyclooctadiene
Cp	cyclopentadienyl
Cp*	pentamethylcyclopentadienyl
CV	cyclic voltammetry or cyclic voltammogram
d	doublet
DART	direct analysis in real time
dba	dibenzylideneacetone
DCM	dichloromethane
DFT	density functional theory
DMA	dimethylacetamide
DMF	dimethylformamide
DOSY	diffusion-ordered spectroscopy

dppbz	1,2-bis(diphenylphosphino)benzene
dppe	1,2-bis(diphenylphosphino)ethane
dppf	1,1'-bis(diphenylphosphino)ferrocene
dppm	bis(diphenylphosphino)methane
dtbbpy	4,4'-di- <i>tert</i> -butyl-2,2'-bipyridine
EPR	electron paramagnetic resonance spectroscopy
equiv.	equivalent(s)
ESI	electrospray ionization
Et	ethyl
Fc	ferrocenyl
g	gram(s)
GC	gas chromatography
glyme	1,2-dimethoxyethane
h	hour(s)
HMDS	hexamethyldisilazide
HRMS	high resolution mass spectrometry
Hz	Hertz
IMes	1,3-bis(2,4,6-trimethylphenyl)-1,3-dihydro-2H-imidazol-2-ylidene
ⁱPr	isopropyl
FT-IR	Fourier transform infrared spectroscopy
<i>J</i>-value	coupling constant
K	Kelvin
<i>k</i>_{obs}	observed rate constant
<i>k</i>_{rel}	relative rate constant
L	liter(s)
m	multiplet (NMR), meter(s) (length)
M	molarity
Me	methyl
MIDA	<i>N</i> -methyliminodiacetic acid
min.	minute(s) (time)
mol	mole(s)
mol %	mole percent
MS	mass spectrometry
m/z	mass-to-charge ratio
<i>n</i>-Bu	<i>n</i> -butyl
<i>n</i>-Dodec	<i>n</i> -dodecyl
<i>n</i>-Hex	<i>n</i> -hexyl
<i>n</i>-Oct	<i>n</i> -octyl
neo	2,2-dimethylpropane-1,3-diol (neopentyl glycol)

NHC	<i>N</i> -heterocyclic carbene
NMP	<i>N</i> -methyl-2-pyrrolidone
NMR	nuclear magnetic resonance spectroscopy
OAc	acetate
OEt	ethoxide
OMs	methanesulfonate (mesylate)
OTf	trifluoromethanesulfonate (triflate)
OTs	<i>para</i> -toluenesulfonate (tosylate)
PCy₃	tricyclohexylphosphine
PCyp₃	tricyclopentylphosphine
Ph	phenyl
pin	2,3-dimethylbutane-2,3-diol (pinacol)
Piv	2,2-dimethylpropanoate (pivalate)
p<i>K</i>_a	logarithmic acid dissociation constant
PPh₃	triphenylphosphine
ppm	part(s) per million
P(<i>i</i>Pr)₃	triisopropylphosphine
P(<i>t</i>Bu)₃	tri- <i>tert</i> -butylphosphine
q	quartet
rt	room temperature
s	second(s) (time), singlet (NMR)
SciOPP	spin-control-intended <i>ortho</i> -phenylenebisphosphine
SPS	solvent purification system
T	temperature
t	triplet
TBS	<i>tert</i> -butyldimethylsilyl
tmeda	tetramethylethylenediamine
TMS	trimethylsilyl
<i>t</i>Bu	<i>tert</i> -butyl
THF	tetrahydrofuran
<i>w</i>_{1/2}	peak width at half-height
XPhos	2-dicyclohexylphosphino-2',4',6'-triisopropylbiphenyl

ACKNOWLEDGMENTS

Wer nichts als Chemie versteht, versteht auch die nicht recht.

Georg Christoph Lichtenberg

I began to write this section about a year before my graduation, because the next few pages are, by far, the most important pages contained within this dissertation and deserve that special consideration. Deep in the doldrums of failed experiments, a worldwide pandemic, and writing this dissertation, it was heartening to come back to this document and reflect upon the people who have brought me this far. Despite presenting the conclusions contained herein as my own original contribution to the scientific community and society at large, no PhD journey is truly a solitary endeavor, and my time in graduate school was certainly not an exception. While this work is fully mine, it also fully belongs to the countless mentors, family, friends, and communities who have supported me along the way. My every accomplishment is the direct result of your investment.

I am exceedingly grateful to my thesis advisor, **Prof. Jeffery Byers**, for his mentorship and guidance over the past few years. I am incredibly fortunate to have trained with a remarkably knowledgeable, attentive, and passionate chemist who has always had my best interests in mind. Jeff has been my toughest critic and most tireless advocate, continually challenging me to be more rigorous and more imaginative while always making himself available for encouragement and new ideas. I am a better scientist today because of him.

I would like to thank **Prof. Shih-Yuan Liu** and **Prof. Jim Morken** for having devoted the time and effort to review this document and serve on my dissertation committee. Their insights, questions, and attention to detail have significantly enhanced the quality of my research and of this document. Additionally, I would like to thank Prof. Liu and **Prof. Masayuki Wasa** for having served on my second-year candidacy committee and my original research proposal committee, and Prof. Morken for his guidance while serving together on the Chemistry Department Diversity and Inclusion Committee, an opportunity for which I am humbled to have participated in.

My interest in organic chemistry first took root in **Dr. Steven O'Malley's** classroom at Stuyvesant High School. I am thankful for his exceptional teaching, which first inspired me to pursue chemistry and continues to reverberate over a decade later—the notes and lessons I used for every discussion section I led as a teaching assistant were adapted from his class. At Northwestern University, **Prof. Karl Scheidt** provided me my first chance to conduct independent research in his lab, an opportunity for which I will eternally be grateful. I would not be here today without his unwaveringly high standards of excellence and continuous dedication to the development of my scientific career. **Dr. Chris Check** and **Dr. Michael Wang**, my mentors in the Scheidt lab, demonstrated an exorbitant amount of patience in dealing with this lackadaisical and inexperienced undergraduate during those few years, for which hindsight has made me especially thankful. I enjoyed every course I took with **Prof. Fred Northrup**, **Prof. Owen Priest**, and **Prof. Regan Thomson**; my experience in their classes created the foundation for deciding to pursue a research career.

When I began research in the Byers group as a first-year graduate student, **Dr. Kayla Delle Chiaie** was there to teach me everything I did not know how to do. She was also there to graciously correct everything I had *thought* I knew how to do. My two years with her as a deskmate were never boring (especially during March Madness). Her mentorship and friendship have made me a more careful chemist and a better crossword solver, and I hope that I have been able to repay that kindness in the smallest way by helping her to better differentiate when to use “affect” versus “effect.”

It has been the honor of a lifetime to have been part of the small molecule subgroup with two remarkably talented chemists in **Dr. Michael Crockett** and **Dr. Chet Tyrol** during my graduate studies. Discussions with them in the pod or over lunch were often insightful and always a good time. I never left a conversation with Michael without a better understanding of chemistry and at least ten new ideas to try. Working with him on developing the β -diketiminato iron complexes made for the smoothest and most productive two months I've ever had in graduate school. I am especially grateful for his generous spirit and calm demeanor as a foil to my dramatic antics. Chet has been my best friend since day one of graduate school, and I am fortunate to have had him around every step of the way—

from late nights at Deep Ellum as first years, to being emergency roommates during the home stretch. I know that I can always count on him for unending optimism in the face of my cynicism, and to drain a well-defended three-pointer from a ludicrous distance on the basketball court. Michael and Chet have been extraordinary co-workers, and still better friends.

I am privileged to have always been surrounded with supportive co-workers who made it easy for me to want to be in the lab during my time in the Byers group. **Dr. Miao Qi**'s friendship, humorous candor, and willingness to get hot pot in any season were deeply appreciated. Some of my most treasured memories of the past few years took place during summer evenings in **Dr. Stella Gonsales**'s backyard; I am thankful for her hospitality and kindness. **Dr. Matt Thompson** is the final part of the entering cohort that included me and Chet, and I appreciated how I could count on him to match my cynicism in kind whenever Chet would not (especially during our coinciding month of dissertation writing). We made a great trio, and my time in graduate school would have been diminished with any other classmates. Competing with **Adam Bensalah** during March Madness and in fantasy football provided a welcome reprieve from the toil of graduate school. Weekly lunches at El Pelón Taquería with **Marcin Kazmierczak** were a highlight of my last few months at Boston College. One of the few misfortunes of finishing graduate school now is how little overlap I will have had with **Bill Thompson**; I am thankful for our fast friendship and his willingness to take a chance on continuing our research, despite our perpetual funding issues. I am excited to see the directions in which he will take our research in the coming years, and wish him all the (likely necessary) luck in doing so. Lastly, I am confident that the lab remains in good hands with **Connor Gallin**, **Eric Liu**, **Kexing Xiao**, and **Stephanie Johnson**, and I wish them all the best. May all your experiments be informative, and may all your publications come out in a timely fashion.

The Byers group has always had remarkably impressive undergraduate students. Throughout my first few years, it was not uncommon to return to my desk and find **Alex Sudyn** lounging with his legs across my chair. I am thankful that our friendship has grown since his graduation and for the chance to grab a drink with him every time we are in the same town. **Enric Adillon**'s enthusiasm for chemistry is admirable and genuinely

contagious, and my hope is that he maintains that attitude at Caltech. I am excited to watch the continued growth of his scientific career, and to one day claim the steak dinner he owes me. **Nancy Yone** was the annoying little sister of the small molecule subgroup—the lab felt a little brighter when she was around, despite her incessant snooping around for pre-cut TLC plates and details about my love life. There is a special place in my heart for **Justin Wong**, my own undergraduate mentee, who tackled a daunting project with tireless dedication. I can only hope he learned half as much from me as I did from him.

Outside of the Byers group, **Dr. Lucas Parvin** dropped by often to talk sports and chemistry; I am thankful for the access he provided to borrowing Zhang lab chemicals and our few months of roommateship. I have always been especially appreciative of my entering cohort—with special acknowledgments to **Julia Falco, Katie Grasso, Paul Hicks, Sarah Jayawardene, Vincent Ovalle, and Chris Wilhelmsen**—and the many kind words and encouraging commiserations whenever I saw them in the hallways or at our many gatherings throughout the past few years. I wish I could have made it to more of them, and I will miss the camaraderie and support I felt amongst you all.

Teaching undergraduate students never felt like a burden for me. It will always be breathtakingly humbling to me to fathom how many lives will be saved by the doctors and medical professionals who will emerge from the 800+ students that have passed through my discussion sections over the past five years, and even more so when considering how those who have chosen other career paths will impact the world in myriad other ways. While I can not claim any credit for their future achievements, I count myself so very lucky to have been a part of their journey. I have had the distinct privilege of teaching with two exceptional educators in **Prof. T. Ross Kelly** and **Prof. Holly Deak**, who share an unparalleled commitment to their students' education and well-being. I am grateful for the example they have set for me and the kindness and support they have shown me throughout the years. In the future, I hope that I can approach mentorship with even just a fraction of Ross's enthusiasm and flair, Holly's dedication and compassion, and the effectiveness with which both communicated organic chemistry.

Special thanks are reserved for the staff of the Boston College Chemistry Department, who do so much to enable productive and safe research in Merkert. I am

especially grateful to **Dale Mahoney** and **Dr. Ian Parr** for all that they do to keep this department running as smoothly as possible. In particular, I always looked forward to saying hello to **Lynne Houlihan** whenever I stopped by the main office. **Dr. Thusitha Jayasundera** and **Dr. Jing Jin** provided immense amounts of assistance when it came to nuclear magnetic resonance and electron paramagnetic resonance experiments, for which I am especially thankful. Additionally, I am proud to have never been the unnamed subject of one of TJ's departmental emails (which really should be a low bar to clear, to be fair...). **Dr. Bo Li** is a crystallographic sorcerer; his ability to solve X-ray crystal structures from the gunk I handed him never ceased to amaze me. **Sally Wyman's** kind assistance with finding information in the chemical literature was deeply appreciated.

Many parts of the research presented here would not have been possible without the generosity of various collaborators. I am grateful to **Prof. Michael Neidig** and **Bufan Zhang** at the University of Rochester for their assistance with collecting Mössbauer spectra and their insights toward elucidating the mechanisms of iron-catalyzed cross-coupling reactions. **Dr. Brian Sparling** and **Dr. Jason Tedrow** provided advice and access to the heteroaromatic substrates for developing the iron-catalyzed cross-coupling reactions described in Chapters 2 and 3; their perspectives on the implementation of our methodologies in the pharmaceutical industry were particularly valuable. It cannot be overstated how much their early belief and investment in our ideas gave us the confidence to successfully accomplish the research presented herein. Funding for this research has been provided in part by the ACS Green Chemistry Institute Pharmaceutical Roundtable and the ACS Petroleum Research Fund.

Despite two Patriots Super Bowl victories and one Red Sox World Series championship, my time in the city of Boston has been surprisingly pleasant, in no small part due to the people who have filled this chapter of my life. Back in 2016, **Phil Toomey** was the first person I told about deciding to pursue my PhD in chemistry at Boston College—which was especially meaningful because he was one of my first friends in college, whom I met in the first month of taking Prof. Thomson's Chem 212 together. When I decided to move into enemy territory, I took solace in knowing that I would get to hang out with Phil all the time over the next five years; unfortunately, I greatly

overestimated the amount of free time that would be available to me during graduate school. Nevertheless, I always looked forward to watching various sporting events together (despite usually rooting for opposite sides, with the exception of Northwestern) and lunches with him. Phil has been one of my closest friends since we met; I will always be thankful for his steadfast friendship across the past decade and the way he welcomed me to Boston.

Despite what can only be characterized as a strange start to our friendship, **Michelle Duan** became one of my closest friends during my time in graduate school. From second-year orals, to my third-year research proposal, to writing this dissertation, she has tried to keep me accountable whenever I needed to do work almost every step of the way (whether it worked all the time... is debatable). Since meeting her, I have never once forgotten that Chick-fil-A is closed on Sundays. Her friendship is one of the most valuable things I have gained from these past few years, and I am so very grateful and fortunate to have her in my life. I am excited for her to join me in doctorhood (twice over!) in the near future.

My time in graduate school became immeasurably better the summer that **Amanda Cheng** and **Grace Lee** moved to Boston. Thanks for putting up with my perpetual lateness to our pre-pandemic monthly dinners, dragging me out to awkward Northwestern alumni events, and imparting upon me the secondhand anxiety of your annual roommate searches. Amanda could always be counted on for blunt assessments of how poorly I was taking care of myself, and for never actually being in town to hang out at any given moment. On the other hand, I could always count on Grace to drop everything to go to a Celtics game with me, and then have postgame drinks at the Tip Tap Room. Their friendship and support through college, and especially since college, have meant a lot to me.

I sought a certain set of characteristics in my roommates: enjoyable to spend time with, minimizes time in the shared bathroom, friendly and four-legged... their owners turned out okay, too. Though my time living with Pinto the pug and **Bethany Ao** was short, I am thankful for Bethany's friendship and reading recommendations throughout the years even after she left Boston. Instead, most of my time was spent living with Yoshi the Shiba Inu and **Brian Wan**, for whom I am especially thankful. Though it took the world shutting down for us to actually spend time together outside of Costco and Wegmans, Brian has become one of my closest friends and his friendship over the past few years has been

indispensable to the successful completion of my PhD. Thanks for leaving dinner out on Monday nights, supporting local businesses with me, enabling one another's worst cravings while grocery shopping, and teaching me how to apply topspin to a volleyball (successfully getting it over a net may be a different story). While our roommateship ended once **Sarah Kim** moved up to Boston, I am glad that the two of them decided to move in only a block away. I am grateful for Sarah's ready willingness to trade pantry goods and to go with me to get egg tarts and bubble tea (but not so much the low-quality chemistry memes she would send me in the middle of the night). I am also appreciative of Luna the husky and her owners, **Alina Chaiyasarikul** and **Nickolas Cruz**, who were fantastic neighbors and hot pot buddies to have these last two years. Thanks for always thinking of me every time you went to get bubble tea. I will always hold dear the memories of idyllic afternoons with Luna and Yoshi at the field behind the McMullen Museum of Art during the height of the pandemic, and perhaps less fondly, the ignominious (for me) afternoons with Nick and Brian on the basketball court.

I was fortunate enough to have many old friends from high school already here in Boston to welcome me with open arms when I first arrived in 2016. In addition to Brian, **Oscar Cheung**, **Xiao Gao**, and **Jason Huang** have been reliable companions these past few years. Thanks for helping me with moving all the time and always being understanding of my poor availability—sorry that I will never get to finish *Betrayal Legacy* with you all. I always looked forward to our annual apple (cider donut) picking trips and regular gatherings over dim sum and hot pot. In particular, our trip to Acadia National Park will forever be a treasured memory of mine. Special thanks to Oscar for not leaving me to die on the face of Mount Washington, and to Xiao for the company of her (now thriving) ZZ plant and the harsh doses of reality when it was needed. I had promised to include a special acknowledgment of Jason in my dissertation in an exchange while playing *Bohnanza* on New Year's Eve, 2019. I probably still lost the game despite that deal, but my debt is repaid here in full.

Various people at Cambridge Community Fellowship Church have been valuable pillars of support for me during my time in Boston. I am indebted to **Juan Santos** for his incredible cooking (but especially his coquito), and for making Thanksgivings in Boston a

little less lonely. Thanks to **Heidi Liu** for convincing me that going to law school after completing my PhD would be a bad idea, and for always keeping it real with me. Wednesday nights at White Horse Tavern (and at Phoenix Landing, despite the tougher competition) with **Sherwin Chen, Eunice Hong, Sarah Hong, Ash Vallier**, and a rotating cast of sixth trivia team members got me through many stressful weeks, though I apologize if my competitiveness imparted any of that stress upon you all (mostly Sarah). Despite not being married, I always felt welcomed amongst **Brian and Cerina Li, Annie and Caleb Kim**, and **Phoebe Tse** and **Aaron Zalewski**. Thanks for looking out for me since the very beginning, and for being great friends. Lastly, I will fondly remember the many adventures and laughs with the crew at Norfolk Terrace. I can't believe you all literally flew to Chicago with me to satisfy my cravings for deep-dish pizza and Jeni's ice cream as the pandemic loomed; you all have an open invitation to stay with me and relive that adventure in the immediate future. In particular, I am deeply appreciative of **Christie Lau** for her tremendous friendship, hospitality, and adventurous spirit; thanks for dragging me out for the various escapades over the years. Thanks also to Ash for her indispensable presence throughout those many exploits, and to **June Shin** for tolerating my existence and always being open to commiserate about our time in graduate school.

I must extend my gratitude to **Ming Nagasawa** for her patient guidance, listening ear, and clear-eyed perspective these past few years. There should be no stigma in seeking out counseling, and I strongly believe that it is a beneficial and necessary step for every person, perhaps even more critically so for those of us traversing through the highs and lows of graduate school.

A very special thanks are due to a number of people who have contributed to this dissertation not in the form of research support nor company throughout my time in Boston, but perhaps even more importantly, in the form of various friendships that have transcended and thrived across time and space. To **Wasi Ahmed, Janus Chan, Shannon Chatham, Jimmy Cheung, Jeanne Hou, Cathy Lee, Patrick Moy, Mohammad Radiyat, Katie Rim, Rick Rodriguez, Darwin Seeto**, and **Calvin Zhu**—thank you for all the visits, messages of encouragement, and nodding along politely whenever I described my research to you. The unfailing love and support you have shown me throughout the

years are inextricably woven into the words contained within these pages, and I could fill several more dissertations in trying to properly express the immense debt of gratitude I have for you all.

I have spent much of the past decade away from my home of New York City to pursue my education, which would not have been possible without my brother, **Nicholas Wong**, holding down the fort. I know that my absence has been inconvenient for our family, but I am grateful for all the ways he has grown to fill those shoes and more. Any worries I had from hundreds of miles away were always reassured by the trust I had in his capabilities. Despite the different paths we have taken, I am so very proud of him for finding his own path and all that he has accomplished in his own career.

媽媽，我可以喺世間上獲得每一個學位，但仍然不能完全理解母親對孩子的愛。受過最多教育嘅人對如何像你每年夏天一樣養一個花園，抑或像我這樣的困難孩子，有咩可知道嘅？儘管我哋有好多分歧，多謝你撫養我，愛我，畀我實現我嘅夢想。冇你，我不可能完成呢個學位。如果我能畀你成個世界，它仍然會低於你應得嘅。

The completion of my PhD is a bittersweet occasion because my father, **Peter Wong**, passed away during my first year of graduate school after a long illness and is not here to see it. Every single day of the past four and a half years has been tinged with his memory, because all that I have done, and all that I will do, would not have been possible without his provisions, guidance, and sacrifices. I hope that I have made him proud, and that I will continue to make the most of all the doors he has opened for me.

DEDICATION

To my ancestors, to 妈妈, to 爸爸

Whereas, in the opinion of the Government of the United States the coming of Chinese laborers to this country endangers the good order of certain localities within the territory thereof: Therefore, Be it enacted by the Senate and House of Representatives of the United States of America in Congress assembled, That from and after the expiration of ninety days next after the passage of this act, and until the expiration of ten years next after the passage of this act, the coming of Chinese laborers to the United States be, and the same is hereby, suspended; and during such suspension it shall not be lawful for any Chinese laborer to come, or having so come after the expiration of said ninety days to remain within the United States.

Approved, May 6, 1882.

—the 47th United States Congress, *Pub.L. 47-126, 22 Stat. 58, Chap. 126.*

*“Such progress [you’ve] made in one generation that to progress beyond [you],
I feel as if I must leave America and colonize the moon.”*

—Weike Wang, *Chemistry*, p. 22.

Chapter 1.

The Development of Versatile Palladium-Catalyzed
Suzuki-Miyaura Cross-Coupling Reactions and
Comparisons to Iron-Catalyzed Analogues

1.1 Introduction

In the last half-century, the advent of metal-catalyzed cross-coupling reactions has fundamentally changed the way we think about the formation of carbon-carbon bonds in synthetic organic chemistry.¹ Among many other transition metals capable of enabling the formation of carbon-carbon bonds, palladium-catalyzed cross-coupling reactions are especially notable for their ability to employ a wide variety of organometallic nucleophiles and organic electrophiles (Figure 1.1).^{2,3} Development of palladium-catalyzed cross-coupling reactions have led to its widespread applicability for the preparation of C(sp²)-C(sp²) bonds in pharmaceutically relevant compounds,⁴ polymeric materials,⁵ and complex natural products.⁶

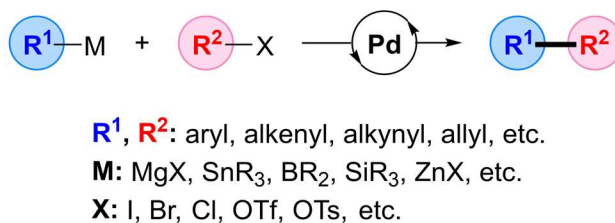


Figure 1.1. Palladium-catalyzed cross-coupling reactions.

Despite the applicability and reliability of these methods, the reliance on noble metals such as palladium has raised concerns over the toxicity⁷ and availability⁸ of the metal catalysts and their associated ligands. Biaryl products in which the C(sp²)-C(sp²) bond is forged through palladium-catalyzed cross-coupling compose a significant portion of cross-coupling products,⁹ and the extension of cross-coupling methodology to C(sp³)-hybridized substrates has been a central focus of the past three decades.¹⁰ However, undesired side reactivity in the form of β -hydride elimination often plagues palladium(II) alkyl complexes to deliver palladium-alkene complexes.¹⁰ In contrast, such a pathway is

not observed in palladium(II) aryl complexes that are common intermediates in the cross-coupling of C(sp²)-hybridized substrates, leading to a disproportionate representation of biaryl products. These concerns are especially magnified in the pharmaceutical industry, where costs associated with removal of toxic metal salts and associated ligands can impact the implementation of these methodologies on a large scale,⁷ and flat molecules have become overrepresented among medicinally relevant compounds.¹¹

A promising avenue of research to address these challenges is the use of first-row transition metal catalysis for cross-coupling reactions. First-row non-noble transition metals^{1,12} such as nickel, iron, and cobalt are more abundant than noble metals, and have demonstrated the ability to undergo one- or two-electron redox events which enable access to C(sp³)-hybridized substrates.¹³ Among the first-row transition metals, nickel-catalyzed systems have received extensive attention over the past two decades for the efficient cross-coupling of C(sp³)-hybridized substrates.¹⁰ Despite these successes, nickel-based complexes are also associated with toxicity concerns.⁷ More recently, our group and several others have directed efforts toward the development of iron-catalyzed systems for cross-coupling reactions.¹⁴ This growing interest in iron-catalyzed systems is motivated in part by iron's low levels of toxicity, high abundance in the Earth's crust, and demonstrated ability to access novel reactivity.

In this chapter, a brief discussion of the palladium-catalyzed Suzuki-Miyaura cross-coupling reaction and seminal studies from the historical development of our mechanistic understanding are presented. A thorough understanding of the operative mechanism has led to a number of key advances that have enabled the versatile application of cross-coupling technologies catalyzed by palladium-based complexes across various industries.

In parallel to the advances of palladium-catalyzed chemistry, the development of iron-catalyzed analogues will be highlighted, with a special emphasis on overcoming limitations that have discouraged the practical implementation of iron-catalyzed cross-coupling reactions for widespread use. Among other reasons, one such limitation is that our mechanistic understanding of cross-coupling reactions catalyzed by iron-based complexes severely lags that of palladium catalysis.

1.2 The palladium-catalyzed Suzuki-Miyaura cross-coupling reaction and its operative mechanism

Of the palladium-catalyzed cross-coupling reactions, the Suzuki-Miyaura reaction has emerged as the premier method for carbon-carbon bond formation due to its reliability, broad functional group compatibility, and ready access to a wide variety of commercially available boron-based transmetalating reagents that are stable to air and moisture.¹⁵ At a fundamental level, the palladium-catalyzed cross-coupling reactions proceed through an operative mechanism featuring three elementary steps: oxidative addition, transmetalation, and reductive elimination (Figure 1.2).¹⁶ These reactions are distinguished from one another by the identity of the organometallic donor which participates in transmetalation with the palladium(II) oxidative addition complex. In the case of the Suzuki-Miyaura reaction, the organometallic donor is an organoboron reagent (e.g. boranes, boronic acids, boronic esters, borates). Since Suzuki and Miyaura reported their now-eponymous reaction between an aryl boronic acid and an aryl halide in 1981,¹⁷ significant efforts have been directed at mechanistic investigations of these elementary steps in order to improve catalytic performance. The prevalence of the Suzuki-Miyaura cross-coupling reaction in

various industries is due in part to insights gained from these extensive mechanistic studies, which have informed its continued development over the past four decades.¹⁸

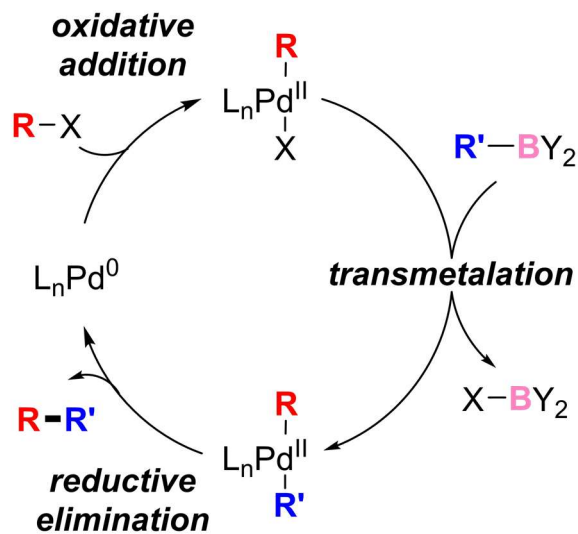


Figure 1.2. General mechanism of the palladium-catalyzed Suzuki-Miyaura cross-coupling reaction.

1.2.1 Oxidative addition

Many investigations have been directed at studying the oxidative addition of aryl and alkenyl halides with palladium, which is a common entry point for all palladium-catalyzed cross-coupling reactions.¹⁹ The oxidative addition occurs at a palladium(0) species,^{20–22} generating palladium(II) aryl intermediates through a two-electron process. Notably, it has been shown that the palladium(0) species must have at least two open coordination sites (of the form L_2Pd^0) formed through reversible ligand dissociation for the oxidative addition to occur.²³ The oxidative addition occurs *via* a three-membered transition state, initially forming a *cis*- $L_2Pd^{II}(aryl)(X)$ complex which rapidly isomerizes to the *trans*- $L_2Pd^{II}(aryl)(X)$ conformation (Figure 1.3).²⁴

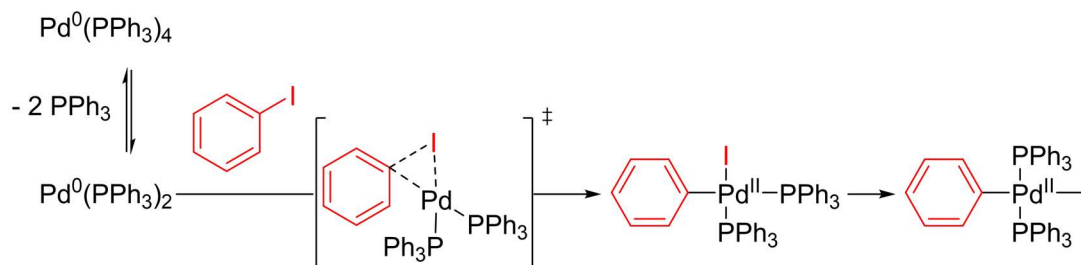


Figure 1.3. *Cis-trans* isomerization following oxidative addition of palladium *via* 3-membered transition state.

It has been established that the rate of reactivity decreases depending on the identity of the aryl halide, in the order of $\text{Ar-I} > \text{Ar-Br} \gg \text{Ar-Cl}$.^{25,26} Moreover, an examination of the oxidative addition rates of palladium(0) species to aryl iodides with electronically variable substituents at the *para* position demonstrated that electron-deficient groups more effectively facilitate oxidative addition.^{20,25} The activity of palladium complexes towards aryl chlorides could be enhanced by changing the identity of the supporting ligands from arylphosphines to sterically hindered alkylphosphine ligands.²⁷ Fu and co-workers determined that the use of large, aliphatic, electron-rich phosphines P^tBu_3 and PCy_3 in combination with palladium-based species could catalyze the coupling of aryl chlorides at room temperature,^{28,29} which was a significant advance for substrates that displayed poor reactivity with traditional palladium precatalysts such as $\text{Pd}(\text{PPh}_3)_4$, even at elevated temperatures. Mechanistic studies suggest that the enhanced rate of sterically-hindered phosphines toward oxidative addition originate from a prior ligand dissociation event to form a sterically unencumbered palladium monophosphine complex that is the active species,²² despite the preponderance of $\text{Pd}(\text{PR}_3)_2$ and phosphine-free palladium observed in these reactions.

1.2.2 Transmetalation

While the transmetalation step remains the least well-understood of the three elementary steps in the Suzuki-Miyaura cross-coupling reaction, significant strides have been made in recent years towards elucidating our understanding.³⁰ It should be noted that the following mechanistic studies are applicable only to the simple aryl boronic esters used herein, and that other mechanisms can be operative with more highly functionalized organoboron reagents (e.g. geminal diborons,^{31,32} β -hydroxy boronic esters,³³ and β -amido boronic esters^{34,35}). A unique hallmark of the Suzuki-Miyaura cross-coupling reaction that distinguishes it from palladium-catalyzed cross-coupling reactions involving other organometallic nucleophiles is that transmetalation does not occur in the absence of a base additive.³⁶ The base additive is hypothesized to create a hydroxo μ^2 -bridge between palladium and boron that facilitates transmetalation (Figure 1.4).³⁷ Soderquist and co-workers examined the diastereoselectivity of the transmetalation step by subjecting *syn* and *anti* deuterium-labeled isomers of a sterically hindered primary alkylborane (**1.1a** and **1.1b**) to standard Suzuki-Miyaura cross-coupling conditions (Figure 1.4a).³⁷ It was observed that the reaction proceeded with complete retention of stereoconfiguration, leading Soderquist and co-workers to propose that a Pd—O—B linkage is involved in the transmetalation event (Figure 1.4b). Independently, Woerpel and co-workers observed similar retention of stereochemistry.³⁸

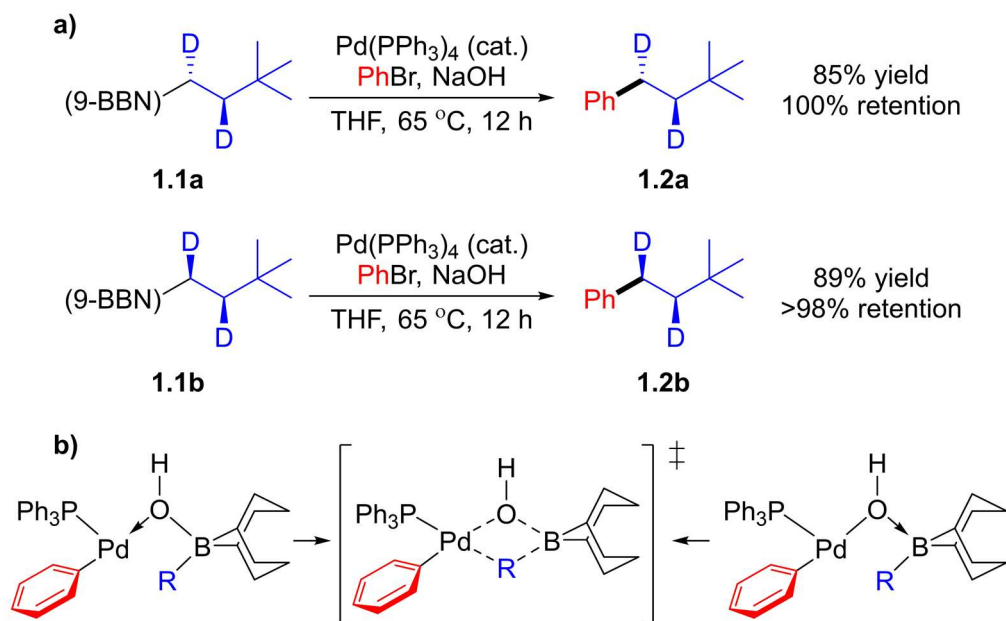
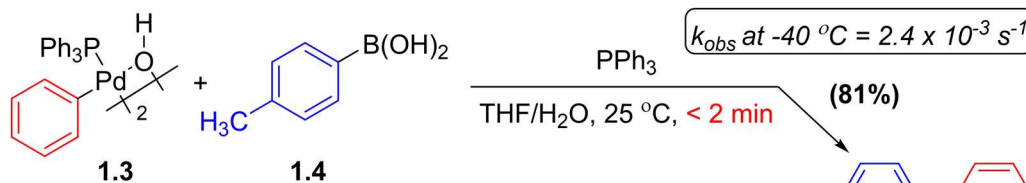


Figure 1.4. a) Suzuki-Miyaura cross-coupling reactions of diastereomers of sterically hindered primary alkylborane **1.1** which proceeded with retention of stereochemistry, b) pathways toward a four-centered hydroxo μ_2 -bridged transition state which facilitates stereoretentive alkyl group transfer.

Generally, there exist two possible pathways proposed for the putative Pd—O—B linkage to form: *via* a palladium hydroxide that reacts with the boronic acid (Figure 1.5a) or *via* a hydroxide-activated borate with increased nucleophilicity toward reaction with a palladium halide formed from oxidative addition (Figure 1.5b). In 2011, Hartwig and co-workers demonstrated that the pathway featuring palladium hydroxide species **1.3** is faster compared to that of the pathway featuring borate species **1.6** by over 4 orders of magnitude (Figure 1.5).³⁹ While both species led to the formation of the cross-coupled product, these findings suggested that the palladium hydroxide is more kinetically relevant, and the Hartwig group concluded that the role of the base is to activate the palladium catalyst.

Hartwig and co-workers (2011)

a) palladium hydroxide pathway



b) borate pathway

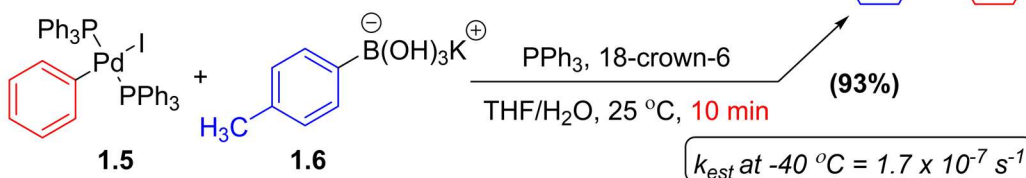


Figure 1.5. Stoichiometric studies by Hartwig and co-workers to evaluate the relative rates of a) the borate and b) the palladium hydroxide pathways commonly proposed for transmetalation in the Suzuki-Miyaura cross-coupling reaction.

Through the use of low-temperature, rapid injection nuclear magnetic resonance spectroscopy, Denmark and co-workers were able to characterize pre-transmetalation intermediates containing Pd—O—B linkages which underwent the Suzuki-Miyaura cross-coupling reaction (Figure 1.6).⁴⁰ The identification and characterization of the tetracoordinate and tricoordinate boron complexes provided strong evidence of the involvement of Pd—O—B linkages in the transmetalation event of the Suzuki-Miyaura cross-coupling reaction. It was determined that the formation of an empty coordination site on the palladium center was required for successful transmetalation, an assertion which has been supported by other groups.⁴¹ A subsequent study demonstrated that catechol and glycol boronic esters underwent transmetalation at enhanced rates, suggesting that the nucleophilic character of the *ipso* carbon bound to boron played a crucial role in successful transmetalation.⁴² While a variety of organoboron reagents have been reported as successful coupling partners in Suzuki-Miyaura reactions,¹⁵ investigations by Lloyd-Jones and co-workers have shown that hydrolysis of certain boronic esters to the boronic acid

(i.e. trifluoroborate salts,^{43,44} MIDA boronates⁴⁵) is required before the transmetalation event takes place.³⁰ At this time, the precise nature of the active transmetalating organoboron species remains unclear.

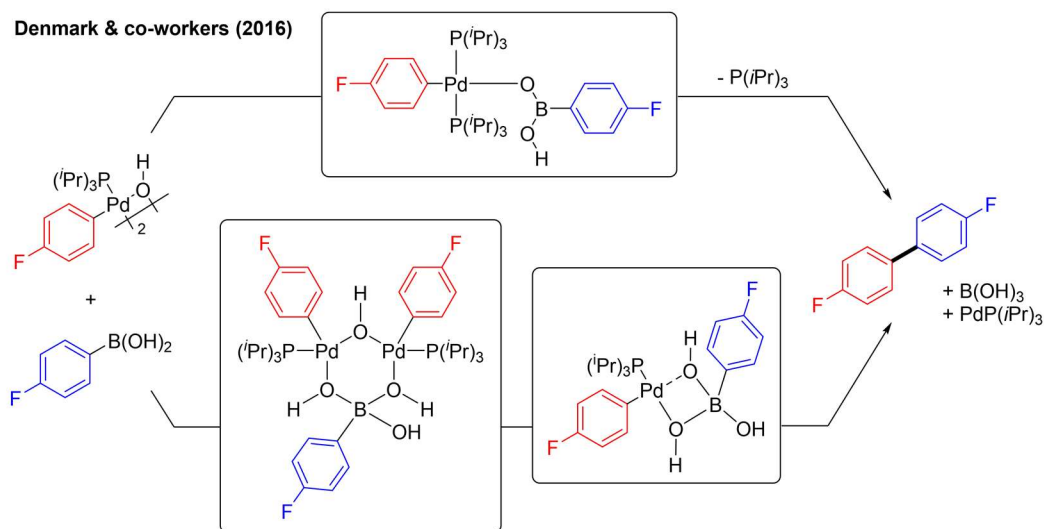


Figure 1.6. Pre-transmetalation intermediates containing Pd—O—B linkages observed by Denmark and co-workers through the use of rapid injection nuclear magnetic resonance spectroscopy that led to successful transfer of boron aryl groups to palladium and subsequent formation of cross-coupled product.

1.2.3 Reductive elimination

Reductive elimination of two covalent ligands from a metal complex is the final elementary step in the catalytic cycle of palladium-catalyzed cross-coupling reactions, and the one in which the carbon-carbon bond in the product is formed. Concurrent studies by the groups of Stille^{46–48} and Yamamoto^{49,50} demonstrated that reductive elimination from palladium complexes with two monophosphine ligands displayed an inverse dependence on the concentration of added phosphine, suggesting that the reversible loss of one phosphine ligand to form a tricoordinate palladium complex enhanced the rate of reductive elimination. Reductive elimination has been shown to proceed more slowly from

tetracoordinate palladium complexes^{51,52} and palladium complexes supported by bidentate phosphines,^{53,54} which do not readily dissociate to form tricoordinate palladium complexes.

Hartwig and co-workers demonstrated that the reductive elimination step can be significantly influenced by the electronic nature of the reactive ligands (Figure 1.7).⁵⁵ The reductive elimination of symmetrically electron-deficient aryl fragments from a dppf-supported platinum complex **1.7** proceeded slower than that of symmetrically electron-rich aryl fragments from the same complex. A further significant enhancement in the rate of reductive elimination was observed when there existed a greater discrepancy in the electronic nature of the two aryl fragments (i.e. an asymmetric complex with one electron-donating aryl and one electron-withdrawing aryl).

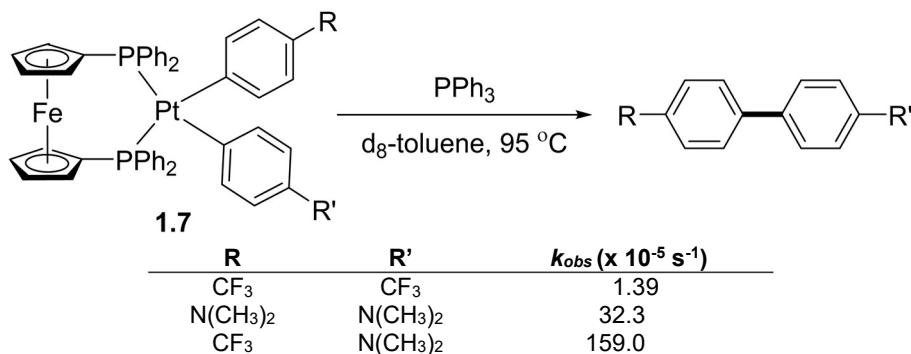


Figure 1.7. Electronic influence on the reductive elimination of biaryls from platinum complexes.

1.3 The dialkylbiaryl monophosphines: logically designed supporting ligand frameworks to promote palladium-catalyzed Suzuki-Miyaura reactions

The efficacy of transition metal catalysis to provide expedient access to complex molecular structures is often derived from the ability to modulate reactivity through changing the ancillary ligands. In particular, the discovery that certain characteristics of phosphine ligands (i.e. sterically hindered and electron-donating) could promote the

catalytic activity of palladium-based complexes^{56,57} are directly responsible for their emergence as dependable tools for cross-coupling reactions to assemble substituted aromatic compounds. While a variety of sterically hindered and electron-rich ligand frameworks that promote cross-coupling reactions have been developed as a result of contributions from various groups including Fu,^{28,29} Nolan,^{58–60} Hartwig,^{61–64} Beller,^{65,66} and Stradiotto,^{67–69} this overview will focus on the development of one pivotal class of ligands discovered by Buchwald and co-workers. In 1998, Buchwald and co-workers reported the room-temperature Suzuki-Miyaura cross-coupling of aryl chlorides catalyzed by palladium-based complexes supported by dialkylbiaryl monophosphine ligands.^{70–72} Since then, iterative development of this family of ligands has enabled broad applicability of palladium-based catalysts toward promoting a diverse array of cross-coupling reactions, including C—C,⁷³ C—F,⁷⁴ C—N,⁷⁵ and C—O⁷⁶ bond formation. The reactivity of palladium-based catalysts can be tailored in accordance to a variety of structural modifications to steric and electronic properties of these supporting ligands (Figure 1.8).⁷³

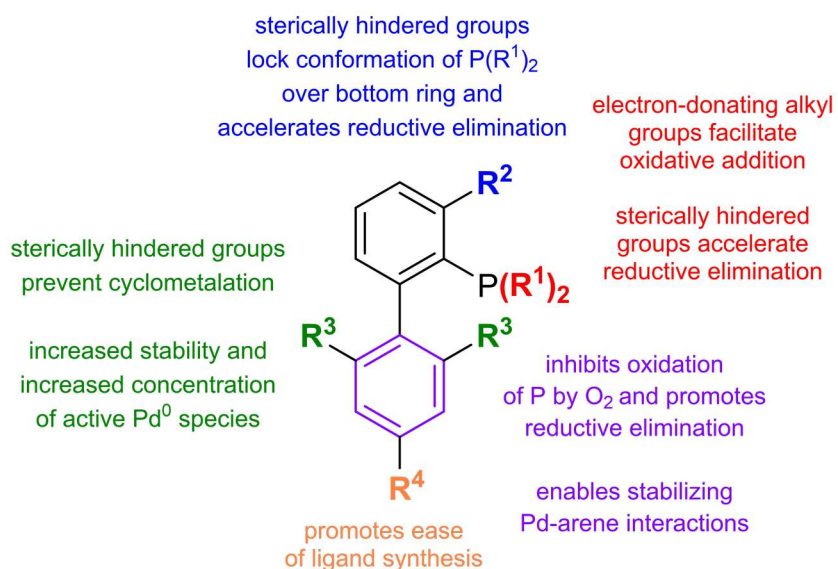


Figure 1.8. Structural features of dialkylbiaryl monophosphine ligands and the impacts of those features on palladium-catalyzed cross-coupling reactions.

The sterically hindered and electron-donating nature of the dialkylbiaryl monophosphine ligands are believed to impact the oxidative addition and reductive elimination steps by stabilizing an increased population of monoligated palladium(0) species. Palladium(0) species with lower coordination numbers have displayed faster rates of oxidative addition and reductive elimination than their polyligated counterparts (*vide supra*). The dialkylbiaryl monophosphine ligand DavePhos was initially used for Suzuki-Miyaura cross-coupling reactions,⁷⁰ but further studies revealed substantially higher reactivity at room temperature when catalysts supported by JohnPhos⁷¹ were used (Figure 1.9). These results demonstrated that the dimethylamino group on the non-phosphinated ring of DavePhos was not necessary for effective catalysis. Reactions employing CyJohnPhos, the cyclohexyl analogue to JohnPhos, were more active when using low catalyst loadings or more hindered substrate combinations.⁷² The higher level of reactivity observed for JohnPhos in comparison to CyJohnPhos at room temperature is attributed to a higher concentration of monoligated palladium(0) intermediates.

effective supporting ligands for the cross-coupling reactions of aminopyridines,⁸¹ aminopyrimidines,⁸¹ thiophenes,⁸² and pyridines.⁸² The isopropyl groups on the non-phosphinated ring help to discourage deactivating cyclometalative pathways.⁸³

Lastly, C—N cross-coupling reactions of less reactive aryl sulfonate esters were achieved through the use of the BrettPhos ligand (Figure 1.9), featuring two methoxy groups on the phosphinated ring.⁸⁴ The inclusion of these substituents serve to favor a conformation in which the palladium atom sits over the bottom ring, which improves the stability of catalytically important intermediates through palladium-arene interactions and accelerates reductive elimination. More recently, the combination of these guiding principles for ligand design contributed to the development of the dialkylbiaryl monophosphine AlPhos (Figure 1.9), which was applied toward the palladium-catalyzed fluorination of aryl electrophiles.⁸⁵ An electron-withdrawing arene on the non-phosphinated ring accelerates reductive elimination by destabilizing aromatic CH—F interactions in $L_nPd^{II}(Ar)(F)$ intermediates, leading to a highly active catalyst system capable of activating C—F bonds.

1.4 The development of bench-stable palladacycle-based catalyst precursors for Suzuki-Miyaura cross-coupling reactions

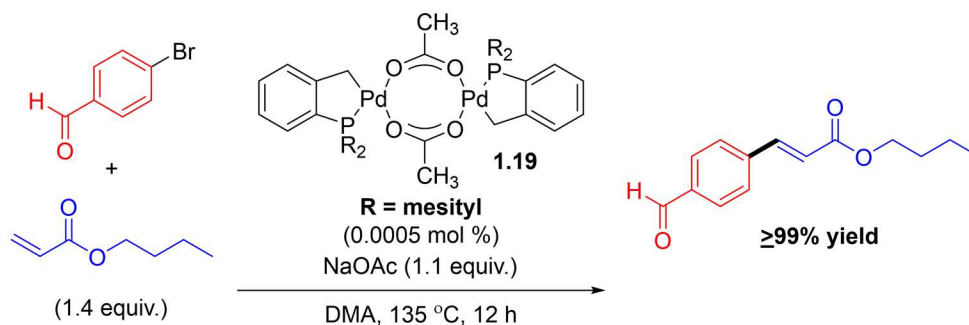
While the choice of ancillary ligands can have dramatic effects on the success or failure of a cross-coupling reaction, the source of palladium is of equally critical importance.^{86,87} However, traditionally used palladium sources (e.g. $Pd(OAc)_2$, $PdCl_2$, $PdCl_2(CH_3CN)_2$, $Pd_2(dba)_3$) often encounter problems in generating the catalytically active palladium(0) species. Due to their commercial availability and bench-stability, palladium(II) salts such as $Pd(OAc)_2$ and $PdCl_2$ are common choices as catalyst precursors.

However, their superior stability means that *in situ* reduction under the reaction conditions is required in order to enter the catalytic cycle as the active palladium(0) species, which can vary in efficiency.⁸⁸ Conversely, direct use of the active phosphine-ligated palladium(0) species is limited by their difficult preparation and sensitivity to air.⁸⁹ Pd₂(dba)₃ is a stable source of palladium(0) because of its strongly coordinating dba ligands, but can also lead to diminished reactivity and slower catalyst activation because catalyst formation often involves the *in situ* coordination of the appropriate ancillary ligand to palladium.⁹⁰ As a result, palladium-catalyzed cross-coupling reactions often required the practitioner to consider the tradeoff between practicality and reactivity.

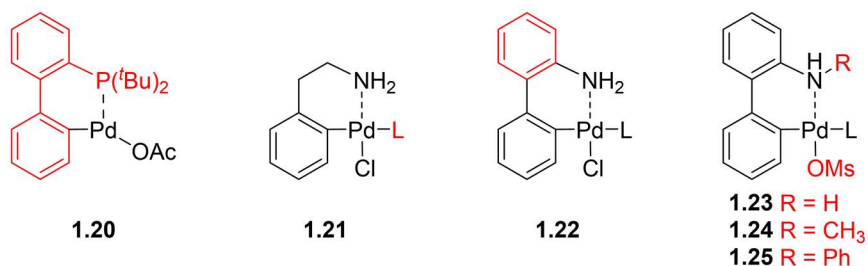
In response to these challenges, several innovations have been applied toward the synthesis of stable palladium complexes pre-ligated with monophosphines that could be activated under mild conditions to eliminate the need for *in situ* catalyst formation. One class of catalyst precursors that has demonstrated high activity for cross-coupling and benefited from extensive development are the palladacycle-based precatalysts. In 1995, Beller and Herrmann reported the synthesis of a pre-formed palladacycle dimer **1.19** which catalyzed the Mizoroki-Heck-type cross-coupling reaction between haloarenes and butyl acrylate (Figure 1.10a).⁹¹ Subsequently, the most significant developments of palladacycle precatalysts have been made by Buchwald and co-workers, who in 2003 demonstrated the ability of air-stable cyclopalladated complex **1.20** to catalyze amination reactions with superior efficiency compared to existing *in situ* systems (Figure 1.10b).⁹² The monophosphine ligand of **1.20** is incorporated into the palladacycle itself by carbopalladation of the ligand; future iterations of precatalysts instead form the palladacycle between palladium and a hemilabile ligand that dissociates in the course of

the reaction (Figure 1.10c). Importantly, these later iterations of palladacycles (**1.21-1.25**) can be modified with varying ancillary ligands, including different phosphines and NHCs.

a) Beller, Herrmann and co-workers (1995)



b) Palladacycle precatalysts developed by Buchwald and co-workers



c) Base-mediated activation of palladacycle precatalysts 1.21-1.25

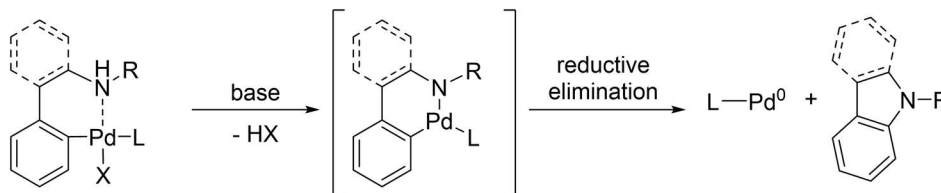


Figure 1.10. a) Initial discovery of palladacycle complexes capable of catalyzing Mizoroki-Heck cross-coupling reactions by Beller and Herrmann, b) Examples of palladacycle precatalysts for cross-coupling reactions developed by Buchwald and co-workers through rational iterative ligand design, c) Proposed mechanism of activation for palladacycle precatalysts to generate the active monoligated palladium(0) species in cross-coupling reactions.

In 2008, Buchwald and co-workers successfully incorporated an amine-bound oxidative addition palladium complex **1.21**^{93,94} capable of bearing a variety of phosphine ligands (Figure 1.10b). **1.21** could be converted into the catalytically active palladium(0) species through deprotonation of the coordinated amine to form an intermediate palladium amido species, which readily undergoes reductive elimination to generate LPd⁰ and an

indoline byproduct (Figure 1.10c). In comparison to traditional palladium sources, which generate the active species *in situ*, **1.21** enabled the amination of aryl chlorides in significantly higher yields when BrettPhos (*vide supra*, Figure 1.9) was the supporting ligand.⁸⁴ Despite these improvements, precatalysts based on **1.21** required high temperatures for activation and were unstable in solution.

One pathway to enabling the activation of the palladacycle precatalyst at lower temperatures was to increase the acidity of the coordinated amine by changing the structure of the palladacycle backbone. Palladacycles based on **1.22**, featuring 2-aminobiphenyl in place of phenylethylamine, could generate active palladium(0) species at ambient temperatures using a variety of bases and subsequently catalyze the Suzuki-Miyaura cross-coupling reaction between aryl chlorides and a variety of heteroaryl and aryl boronic acids.⁹⁵ However, **1.22** could not accommodate the use of larger dialkylbiaryl monophosphine ligands such as BrettPhos, and also generated carcinogenic⁹⁶ carbazole byproducts that were detrimental to certain cross-coupling reactions.⁹⁷ Replacement of the chloride anion with electron-withdrawing and poorly coordinating methanesulfonate in palladacycle **1.23** enabled the use of a wide variety of sterically hindered dialkylbiaryl phosphine ligands,⁹⁸ and palladacycles **1.24** and **1.25** produced *N*-substituted carbazoles that do not pose health risks.⁹⁹ Notably, palladacycles **1.23-1.25** demonstrated enhanced stability in solution compared to **1.21** and **1.22**.

The development of palladacycle-based precatalysts greatly expanded the utility and versatility of cross-coupling reactions by enabling the use of milder reaction conditions, bench-storable precursors, and a variety of ancillary ligand frameworks while maintaining reactivity and selectivity. This development was enabled by rational iterative

ligand design, which led to targeted modifications of ligand structure to address the limitations of previous generations of catalyst precursors.

1.5 Transition metal-catalyzed Suzuki-Miyaura cross-coupling reactions involving C—O electrophiles

The defining characteristic of the transition metal-catalyzed Suzuki-Miyaura cross-coupling reaction is the use of aryl boronic acids and esters as the nucleophilic coupling partner, which is highly advantageous due to the bench-stability and broad commercial availability of such reagents.¹⁵ Conversely, while aryl halides are most commonly used as the electrophilic coupling partner, they can be difficult to access in densely functionalized advanced synthetic intermediates and halogenated compounds pose severe toxicological risks to humans.¹⁰⁰ As a result, considerable attention has been directed toward exploring alternative electrophilic partners that engage in cross-coupling reactions in order to improve generality and applicability. Among these alternatives, C—O electrophiles are particularly appealing as naturally abundant and readily available reaction substrates.^{101,102} However, in comparison to organic halides, C—O bonds generally have higher bond dissociation energies and are relatively unreactive (Figure 1.11).^{101–104} Moreover, the two single bonds to oxygen in asymmetric ethers, esters, and alcohols have different levels of reactivity. It can be difficult to chemoselectively activate one of the two different bonds to the oxygen atom, which is a necessary consideration for any compound that is not a symmetric ether. Despite these challenges, the development of C—O electrophiles as cross-coupling partners offers tremendous economic and environmental benefits, and their divergent reactivity can be potentially leveraged for the design of orthogonal cross-coupling strategies in the presence of organic halides.

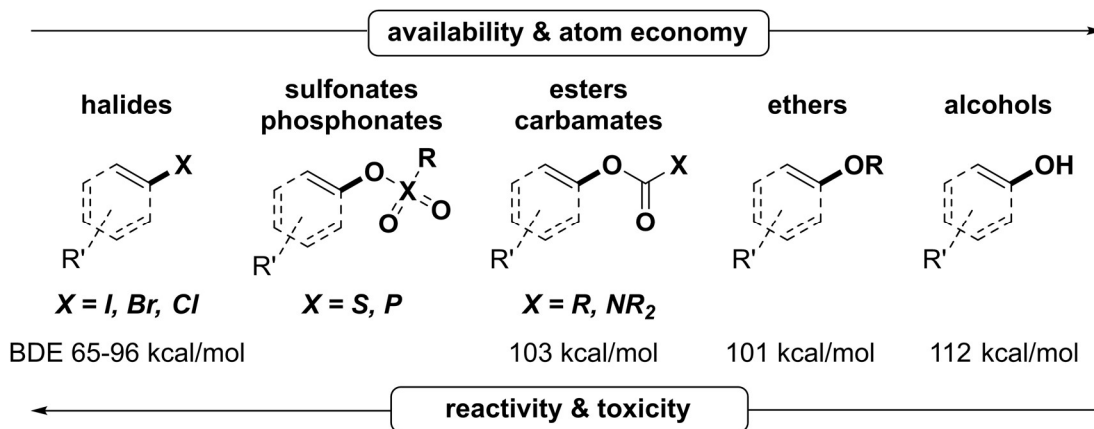
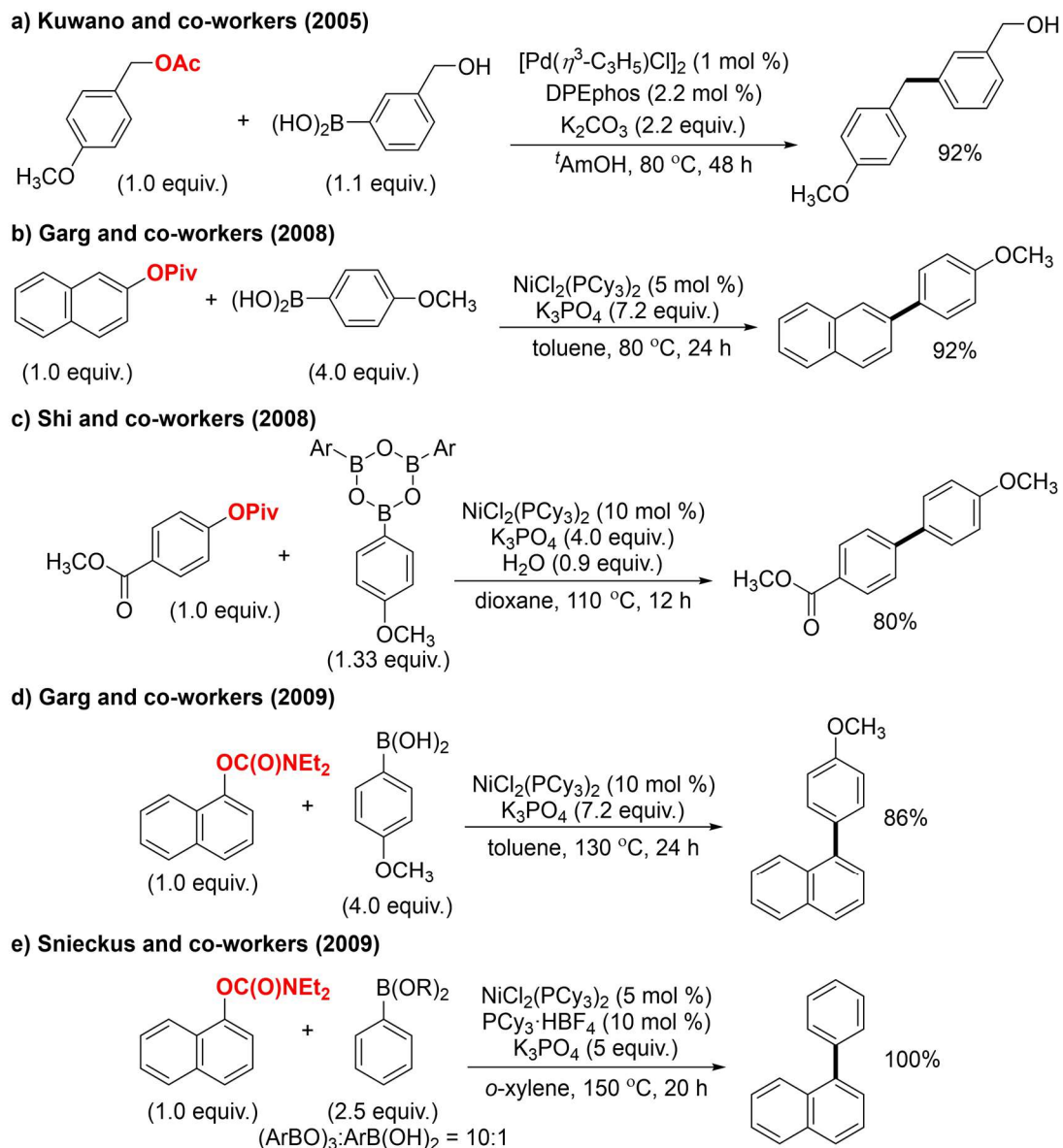


Figure 1.11. C—O electrophiles for transition metal-catalyzed cross-coupling reactions.

1.5.1 Suzuki-Miyaura cross-coupling reactions of activated C—O bonds

The majority of C—O electrophiles employed in palladium-catalyzed cross-coupling reactions are aryl sulfonate and phosphonate esters,^{105–109} which possess a relatively low activation barrier for C—O bond cleavage. Early examples employed alkenyl and aryl trifluoromethanesulfonate (triflate) electrophiles,¹¹⁰ including the first example of cross-coupling of these electrophiles with an organoboron reagent (Scheme 1.1a).¹¹¹ In 2003, Hartwig and co-workers reported the ability for palladium to engage in Kumada-Tamao-Corriu-type cross-coupling reactions with the less reactive but more readily available *para*-toluenesulfonate esters (tosylates),¹¹² which was followed shortly thereafter by a report from Buchwald and co-workers regarding successful palladium-catalyzed Suzuki-Miyaura-type reactions with the same electrophiles (Scheme 1.1b).¹¹³ Since then, triflates, tosylates, methanesulfonates (mesylates), and nonaflates have been gained wide acceptance as electrophiles in Suzuki-Miyaura cross-coupling reactions, even demonstrating reactivity in systems catalyzed by nickel-based complexes.^{114–116} However,



Scheme 1.2. a) First example of palladium-catalyzed Suzuki-Miyaura cross-coupling reaction of benzyl acetates. b,c) Independently reported examples of nickel-catalyzed Suzuki-Miyaura cross-coupling reactions of aryl pivalate esters. d,e) First independently reported examples of nickel-catalyzed Suzuki-Miyaura cross-coupling reactions of aryl carbamates.

1.5.2 Suzuki-Miyaura cross-coupling reactions of unactivated C—O bonds

Despite the success of nickel-based systems to catalyze the Suzuki-Miyaura cross-coupling reaction of aryl ester derivatives and carbamates, these substrates are not readily commercially available and their use generates a substantial amount of waste.¹⁰¹ An

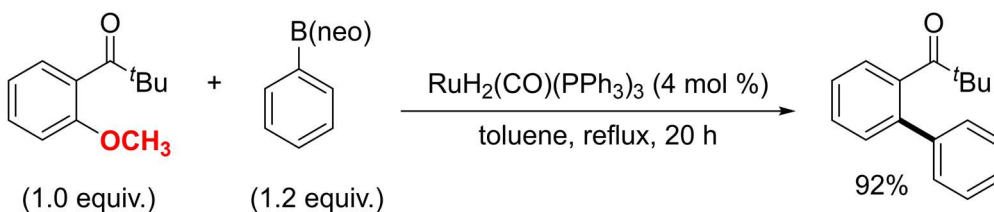
attractive advancement to address these drawbacks is the use of even simpler aryl alkyl ethers and phenols, but these C—O bonds have significantly higher bond dissociation energies and are more resistant to oxidative addition by transition metal complexes.¹⁰³ As a result, Suzuki-Miyaura cross-coupling reactions incorporating these substrates are typically catalyzed by transition metals other than palladium.

In 2004, Kakiuchi and co-workers reported the first example of a Suzuki-Miyaura cross-coupling reaction between aryl neopentyl boronic esters and aryl methyl ethers catalyzed by a ruthenium-based complex (Scheme 1.3a).¹²³ Notably, the scope of successfully coupled electrophiles was limited to those with ketones positioned *ortho* to the ether bond as a directing group for the ruthenium to activate the C—O bond. The requirement of a directing group was circumvented by Tobisu, Chatani, and co-workers in 2008, when they reported the successful nickel-catalyzed Suzuki-Miyaura cross-coupling reaction of aryl neopentyl boronic esters and aryl methyl ethers (Scheme 1.3b).¹²⁴ In both examples, π -extended aromatic electrophiles were significantly more reactive than their anisole-based counterparts, suggesting that the reaction proceeds through partial dearomatization of the aromatic ring.

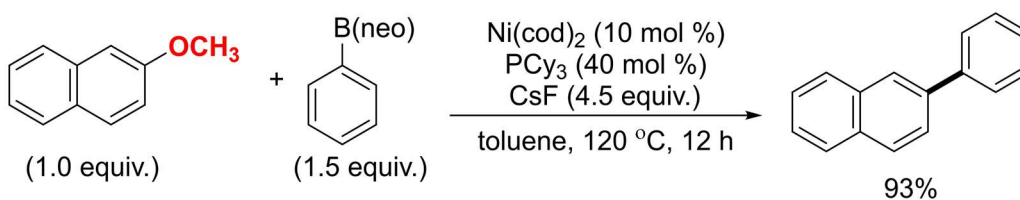
Suzuki-Miyaura cross-coupling reactions that employ alcohol electrophiles are rare and require the use of highly activated alcohol substrates, highly activating conditions, or both. In 2011, Shi and co-workers demonstrated the nickel-catalyzed cross-coupling reaction between naphthyl alcohol and aryl boroxine (Scheme 1.3c).¹²⁵ The authors propose that deprotonation of the alcohol followed by coordination to the triethylborane to form a borate are required to facilitate transmetalation. A similar “double activation” approach in which the organoboron both initiates the catalyst and activates the C—O bond

was invoked for their subsequent palladium-catalyzed Suzuki-Miyaura cross-coupling reaction of naphthyl benzylic alcohols, which demonstrated similar restrictions on the electrophile scope.¹²⁶ To date, the few examples of nickel-catalyzed systems for Suzuki-Miyaura cross-coupling reactions developed since then still require allylic¹²⁷ or π -extended benzylic alcohols¹²⁸ to deliver the desired products in high yields.

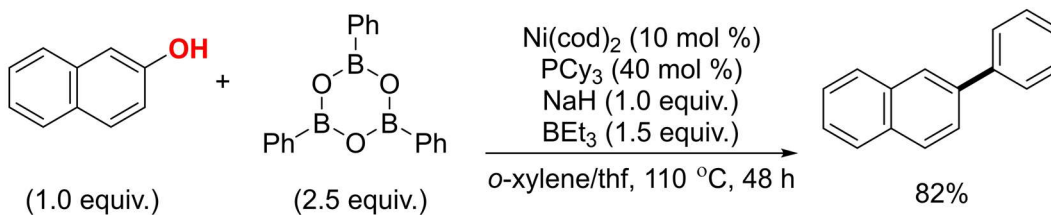
a) Kakiuchi and co-workers (2004)



b) Tobisu, Chatani, and co-workers (2008)



c) Shi and co-workers (2011)



Scheme 1.3. a) Initial example of Suzuki-Miyaura cross-coupling reaction between aryl boronic ester and aryl methyl ether catalyzed by ruthenium in the presence of a directing group, b) nickel-catalyzed Suzuki-Miyaura cross-coupling reaction between aryl boronic ester and aryl methyl ether in the absence of a directing group, c) initial example of a nickel-catalyzed Suzuki-Miyaura cross-coupling reaction between an unprotected naphthyl alcohol with aryl boroxine.

Recent developments directed toward the activation of C—O electrophiles for cross-coupling reactions have inspired a paradigm shift in the field. While palladium-based catalysts are tremendously effective for cross-coupling reactions of halide and activated

sulfonate esters, low-valent nickel-based catalysts have led to impressive results when it comes to the less reactive C—O functionalities, such as ethers and alcohols. While these methods have not yet achieved the same level of generality and applicability as the palladium-catalyzed analogues, they demonstrate the immense potential of new cross-coupling strategies based on first-row transition metal catalysis.

1.6 Recent developments in first-row transition metal catalysis to address limitations of the palladium-catalyzed Suzuki-Miyaura cross-coupling reaction

The synthetic utility and practical applicability of the palladium-catalyzed Suzuki-Miyaura cross-coupling reaction have been greatly enhanced as a result of four decades' worth of investigations by researchers around the world. Despite these advancements, a few limitations inherent to palladium-catalyzed systems have encouraged the exploration of reactions catalyzed by first-row transition metal complexes for the construction of carbon-carbon bonds. Palladium is toxic,⁷ and its most plentiful reserves are located in areas around the world often facing political upheaval (e.g. Russia, South Africa).^{8,129} Both of these concerns have economic consequences, in the form of increased costs associated with removal of toxic metal catalysts employed in the synthesis of small molecule drugs, and in the high costs and high cost volatility associated with its scarcity. As a result, the use of non-precious, first-row transition metals for important catalytic processes is motivated in part by their potential for improved environmental and economic sustainability.

However, another compelling motivation lies in the ability of first-row transition metals to participate in one- and two-electron processes and offer orthogonal reactivity to that of their second- and third-row counterparts. Unactivated alkyl electrophiles containing

β -hydrogen atoms are difficult substrates for methods catalyzed by palladium-based complexes.¹³⁰ Two hypotheses for the scarcity of palladium-catalyzed methods for these substrates concern the relatively slow oxidative addition of palladium into substituted $C(sp^3)$ -X bonds¹³¹ and the facile β -hydride elimination of the resultant palladium(II) alkyl complexes (Figure 1.12).¹⁰ As a result, successful examples of palladium-catalyzed Suzuki-Miyaura cross-coupling reactions are limited to those involving primary alkyl iodides¹³² and bromides¹³³ or alkyl- and aryl-(9-BBN) reagents.^{131,134} The ability to form bonds between $C(sp^3)$ -hybridized substrates is important because it could potentially enable access to stereogenic centers from cross-coupling methodologies. Methods for asymmetric catalysis remain highly valuable in chemical synthesis, and low-valent transition metals can participate in the single-electron processes that would circumvent some of the difficulties associated with palladium for these transformations.

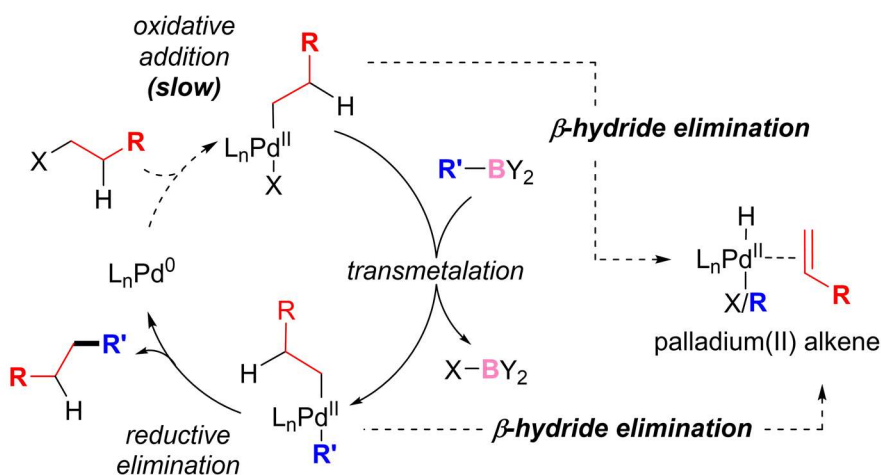
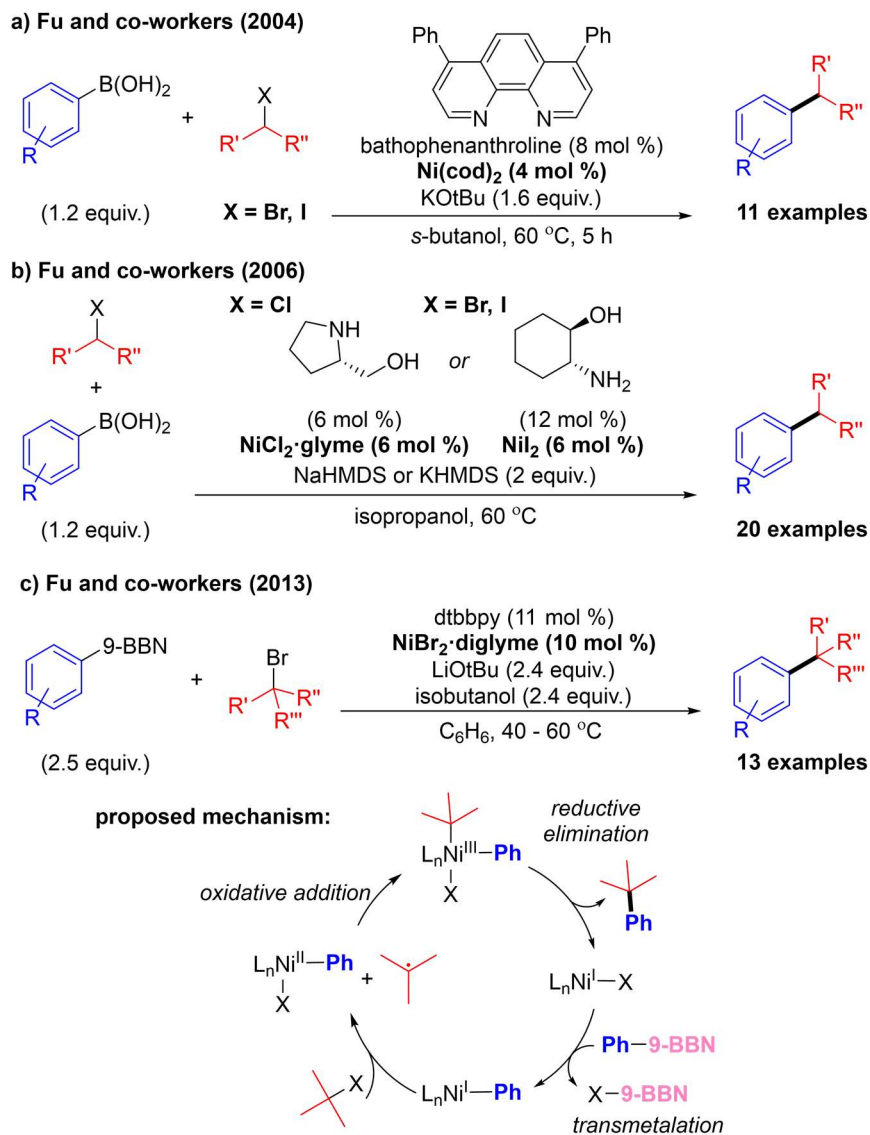


Figure 1.12. Catalytic cycle for the palladium-catalyzed Suzuki-Miyaura cross-coupling reaction of alkyl electrophiles with possible inhibitory pathways highlighted using dashed arrows.

Fu and co-workers have made significant progress toward expanding the capability of nickel-catalyzed systems to address these limitations. In 2004, they demonstrated the

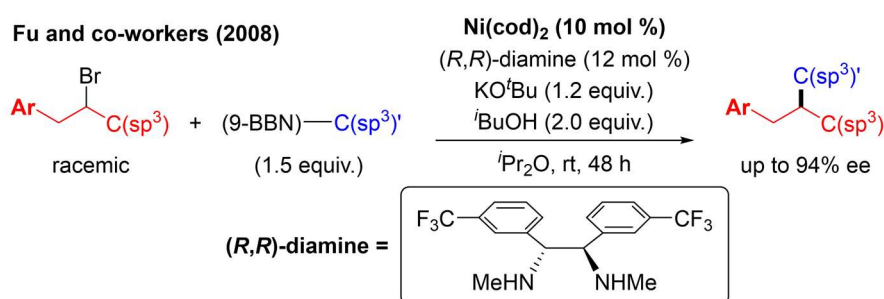
first Suzuki-Miyaura cross-coupling reaction of aryl boronic acids with unactivated secondary alkyl bromides and iodides, catalyzed by Ni(cod)₂ with bathophenanthroline ligand in the presence of KO^tBu (Scheme 1.4a).¹³⁵ Two years later, they expanded the scope of nickel-catalyzed Suzuki-Miyaura cross-coupling reactions to include unactivated secondary alkyl chlorides by changing the ligand in the catalyst system to readily available aminoalcohols (Scheme 1.4b).¹³⁶ Nickel(II) iodide with *trans*-2-aminocyclohexanol in the presence of NaHMDS displayed superior functional group compatibility compared to their previously reported system, and using prolinol as a ligand in combination with nickel(II) chloride glyme complex enabled the cross-coupling of secondary alkyl chlorides with a variety of electron-poor and electron-rich aryl boronic acids. Finally, the first example of a nickel-catalyzed Suzuki-Miyaura cross-coupling reaction of unactivated tertiary alkyl halides was achieved in 2012 by the Fu group (Scheme 1.4c).¹³⁷ A nickel complex supported by the dtbbpy ligand was an effective catalyst for this transformation involving a variety of tertiary alkyl halides, although the scope of the organoboron nucleophile was limited to *meta*-substituted or unsubstituted aryl-(9-BBN) reagents. Fu and co-workers propose a catalytic cycle in which a tertiary alkyl radical is generated from the electrophile and oxidatively adds to the nickel complex. At the onset of our investigations, this example was the most general method for the incorporation of highly sterically encumbered electrophiles in cross-coupling reactions to furnish products containing all-carbon quaternary centers.



Scheme 1.4. Examples by Fu and co-workers of Suzuki-Miyaura cross-coupling reactions of C(sp²)-hybridized organoboron reagents with substituted C(sp³)-hybridized electrophiles catalyzed by nickel-based complexes, and proposed mechanism for c).

Furthermore, Fu and co-workers have demonstrated successful nickel-catalyzed Suzuki-Miyaura cross-coupling reactions between alkyl nucleophiles and alkyl electrophiles,^{138,139} and extended them into stereoconvergent variants to furnish products containing stereogenic centers with high enantioselectivity. Using a chiral 1,2-diamine ligand, they were able to demonstrate the enantioselective Suzuki-Miyaura cross-coupling

reaction of homobenzylic halides in high yields (Scheme 1.5).¹⁴⁰ With similar catalytic systems featuring small alterations to the diamine ligand, the identity of the aryl group on the alkyl halide could be changed to a carbamate,^{141,142} sulfone,¹⁴² sulfonamide,¹⁴² or arylamine^{143,144} which acted as a directing group for the successful cross-coupling of unactivated alkyl halides. Notably, only one report describes the use of an aryl boronic ester nucleophile.¹⁴⁴



Scheme 1.5. First example of a stereoconvergent Suzuki-Miyaura cross-coupling reaction of C(sp³)-hybridized organoboron reagents with substituted C(sp³)-hybridized electrophiles catalyzed by nickel-based complexes.

While the scope of nickel-catalyzed Suzuki-Miyaura cross-coupling reactions of C(sp³)-hybridized substrates has expanded significantly over the past two decades, these methods share some limitations with the palladium-catalyzed analogues. Toxicity concerns likewise remain for nickel-based catalysts,⁷ and while nickel is significantly more abundant than palladium, sourcing nickel for chemical catalysis has tremendous competition in the longstanding stainless steel industry and in a growing demand for use in electric vehicle batteries.¹⁴⁵ Moreover, while nickel analogues overcome a limitation of the palladium-catalyzed Suzuki-Miyaura reaction in its ability to incorporate C(sp³)-hybridized substrates, these methods often require the use of 9-BBN boranes (*vide supra*), which are more reactive and difficult to handle than the bench-stable boronic esters from which the

Suzuki-Miyaura reaction derives much of its practical utility. Lastly, nickel-catalyzed methods involving tertiary alkyl halides often exhibit isomerization due to cascading elimination-reinsertion steps (i.e. chain-walking).¹⁴⁶⁻¹⁴⁸

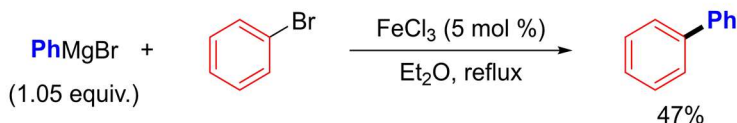
1.7 An overview of the development of iron-catalyzed cross-coupling reactions

Despite the predominance of palladium-catalyzed methods for cross-coupling reactions, first-row transition metals like iron actually predate palladium for catalyzing the formation of carbon-carbon bonds between organometallic nucleophiles and organic electrophiles.¹⁴⁹⁻¹⁵¹ Kharasch and co-workers initially discovered the synthesis of biaryls through the reaction of aryl Grignard reagents with aryl halides in the presence of simple metal salts (Scheme 1.6a).¹⁴⁹ Three decades passed before this reactivity was revisited by Kochi and co-workers, who demonstrated the vinylation of alkyl Grignard reagents in the presence of iron halide salts (Scheme 1.6b).^{150,151} However, these early approaches were low-yielding, due in part to significant homocoupling. Shortly after Kochi's reports, Kumada¹⁵² and Corriu¹⁵³ independently reported the ability of nickel-based catalysts to generate carbon-carbon bonds between Grignard reagents and organic halides, and Murahashi and co-workers soon introduced palladium-based catalysts¹⁵⁴ for the same transformation. As a result, rapid progress in the development of analogous palladium-catalyzed transformations rendered further investigations into iron-catalyzed cross-coupling reactions dormant for the next 30 years.

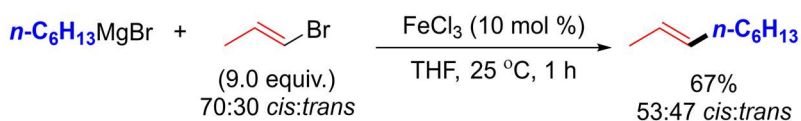
In 2002, Fürstner and co-workers revitalized the field of iron-catalyzed cross-coupling by demonstrating the ability of simple iron salts to efficiently catalyze what had since become known as the Kumada-Tamao-Corriu cross-coupling reaction of Grignard

reagents and organic electrophiles (Scheme 1.6c).^{14,155–157} Their efforts expanded the scope of iron-catalyzed cross-coupling reactions to include aryl and vinyl chlorides, tosylates, and triflates, and the potential of iron catalysts to employ these less reactive electrophiles and provide orthogonal reactivity to the well-established palladium-catalyzed processes¹³ sparked renewed interest in the field. In the present day, cross-coupling reactions catalyzed by iron-based complexes are still most commonly Kumada-Tamao-Corriu-type reactions employing organomagnesium nucleophiles. It is thought that the increased nucleophilic nature of the Grignard reagent aids transmetalation;¹⁵⁸ however, this same reagent displays poor functional group tolerance for reactions at ambient temperatures.¹⁵⁹ Paralleling the development of palladium-catalyzed cross-coupling reactions, the field shifted towards exploring the use of other transmetalating agents for the iron-catalyzed analogues.

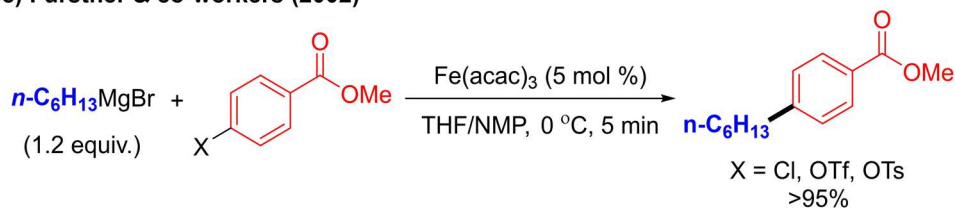
a) Kharasch & co-workers (1941)



b) Kochi & co-workers (1971)



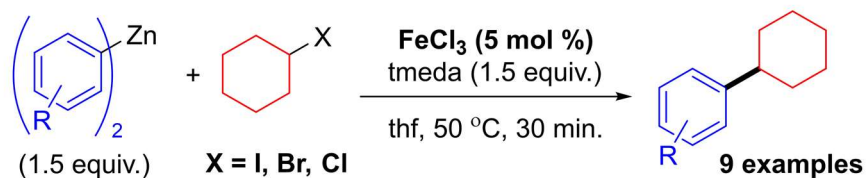
c) Fürstner & co-workers (2002)



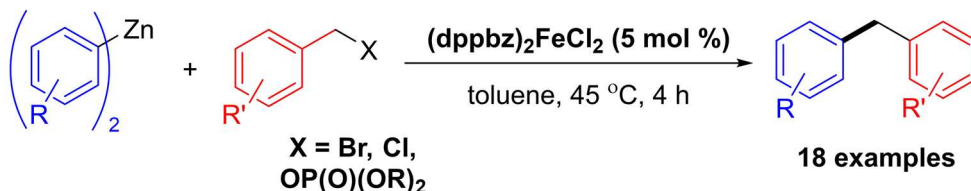
Scheme 1.6. Early examples of cross-coupling reactions between organometallic nucleophiles and organic halides catalyzed by iron salts.

Over the past 15 years, substantial progress has been made toward the development of iron-catalyzed systems for the Negishi-type cross-coupling reaction of aryl organozinc nucleophiles and alkyl electrophiles. In 2005, Nakamura and co-workers reported the first Negishi-type cross-coupling reaction catalyzed by iron salts (Scheme 1.7a).¹⁶⁰ A variety of diaryl and diheteroaryl organozinc nucleophiles were tolerated under these conditions, but the scope of the secondary alkyl halides was limited to those in 6-membered rings. Acyclic alkyl electrophiles were not reported. Bedford and co-workers expanded upon this discovery, demonstrating that iron-based catalysts supported by dppbz ligands enabled the coupling of benzylic halide and secondary alkyl phosphate electrophiles with diarylzinc nucleophiles (Scheme 1.7b).¹⁶¹ Almost concurrently, Nakamura and co-workers showed that the same system enabled the cross-coupling of fluoroaromatic zinc reagents (Scheme 1.7c)¹⁶² and that the addition of magnesium salts to the original system enabled the successful cross-coupling of secondary alkyl sulfonate ester electrophiles *via in situ* formation of the corresponding alkyl iodide (Scheme 1.7d).¹⁶³ These rapid enhancements in scope have motivated efforts to understand the effects of the phosphine ligands and the mechanistic features of this reaction, leading to further incremental improvements over time.¹⁶⁴⁻¹⁶⁶ A closer examination of the iron-phosphine precatalysts used shows that the diphosphine ligands preferentially coordinate to the zinc reagent over the iron species, raising questions about the nature of the catalytically active species in this transformation.¹⁶⁷

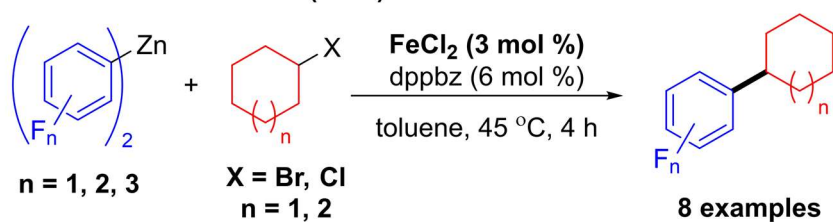
a) Nakamura and co-workers (2005)



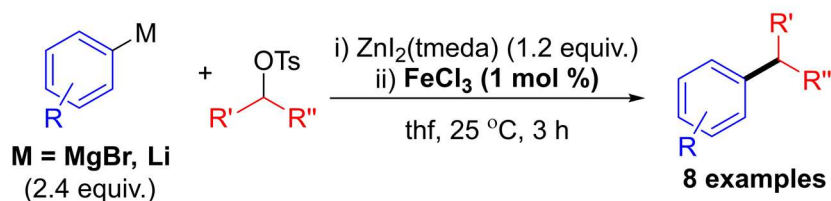
b) Bedford and co-workers (2008)



c) Nakamura and co-workers (2009)



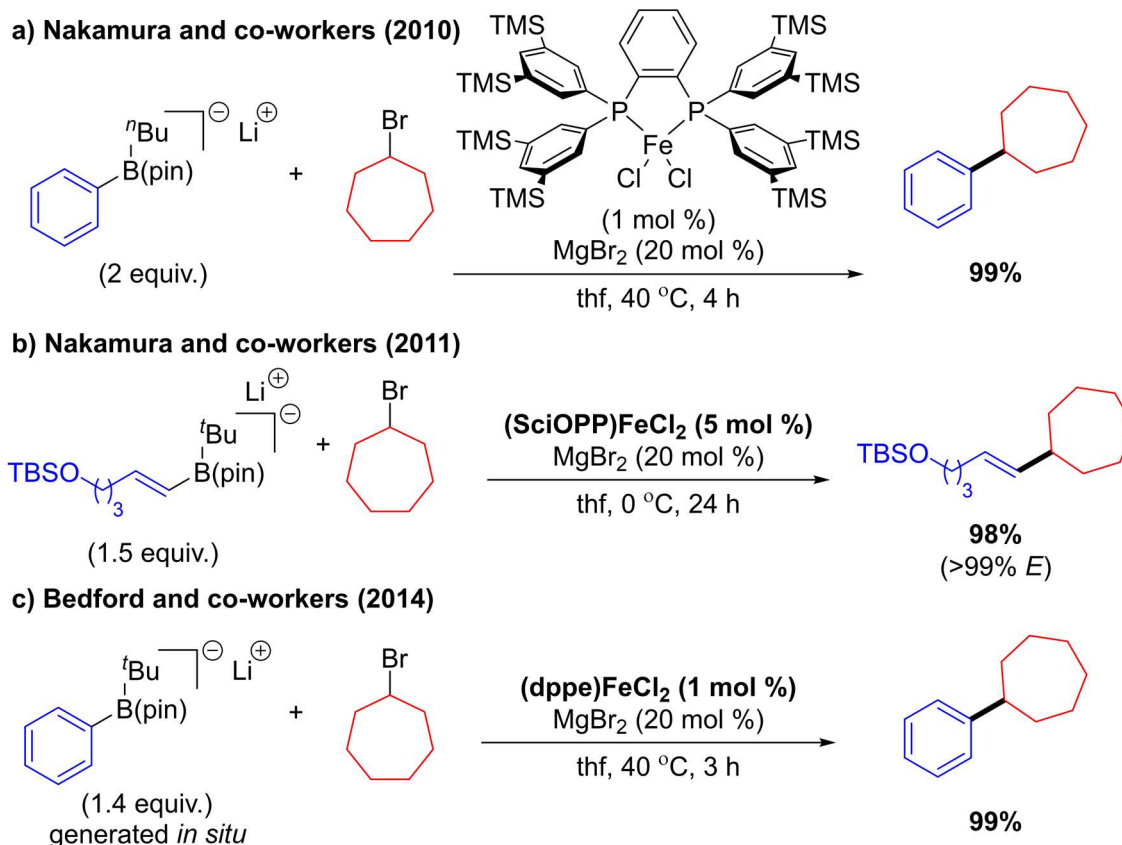
d) Nakamura and co-workers (2009)



Scheme 1.7. Examples of Negishi-type cross-coupling reactions between $\text{C}(\text{sp}^2)$ -hybridized organozinc reagents and substituted $\text{C}(\text{sp}^3)$ -hybridized electrophiles catalyzed by iron-based complexes.

Despite this progress, the Suzuki-Miyaura cross-coupling reaction remains the gold standard for cross-coupling reactions. Significant advancements towards the iron-catalyzed cross-coupling of aryl organoboron nucleophiles and highly substituted alkyl electrophiles have occurred within the past decade, signaling that this remains an attractive and thriving area of research. Nakamura and co-workers were the first to report such a transformation in 2010, when they successfully demonstrated the cross-coupling of preactivated aryl boronic acid pinacol esters (B(pin)) with a variety of primary and secondary alkyl halide electrophiles, catalyzed by an iron(II) chloride complex supported by the diphosphine

ligand 3,5-TMS-SciOPP (Scheme 1.8a).¹⁶⁸ The aryl boronic ester was preactivated by *in situ* borate formation upon reaction with an alkyllithium reagent, and the reaction was significantly lower-yielding in the absence of a MgBr₂ co-catalyst, which the authors propose accelerates the transmetalation between the borate and the iron catalyst. Two years later, Nakamura and co-workers expanded upon this work when they demonstrated that the same system could catalyze the stereospecific cross-coupling reaction of preactivated *E*- and *Z*-alkenyl boronic acid pinacol esters with alkyl halides (Scheme 1.8b).¹⁶⁹ In addition to high levels of stereospecificity, high yields and high functional group tolerance were observed, and mechanistic experiments suggested the intermediacy of alkyl radicals in the reaction. In 2014, Bedford and co-workers reported the cross-coupling reaction of preactivated aryl boronic acid pinacol esters with a variety of primary and secondary alkyl halide electrophiles, catalyzed by iron complexes supported by inexpensive and commercially available diphosphine ligands dppe or dppp (Scheme 1.8c).¹⁷⁰ Like the system reported by Nakamura and co-workers, the success of the reaction was dependent on preactivation of the boronic ester with alkyllithium and the inclusion of MgBr₂. As a result, neither group can rule out the possibility that the reaction may proceed *via* Kumada-type cross-coupling intermediates, in which a Grignard reagent is formed *in situ* upon reaction of the preactivated borate with the magnesium additive. Moreover, the reliance on pyrophoric alkyllithium reagents limits the practical application of these methods.



Scheme 1.8. Examples of Suzuki-Miyaura-type cross-coupling reactions between C(sp²)-hybridized organoboron reagents and C(sp³)-hybridized electrophiles catalyzed by iron-based complexes.

While Nakamura and Bedford reported similar catalytic systems for the cross-coupling of activated aryl boronic esters and alkyl halides, they offer divergent mechanistic hypotheses for the transformation. Nakamura and co-workers propose an iron(II)/iron(III) redox cycle, in which transmetalation between the iron(II) dihalide and aryl borate is facilitated by MgBr₂ (Figure 1.13).¹⁶⁸ Halogen abstraction of the alkyl halide forms an iron(III) aryl halide with concomitant generation of a carbon-centered radical, which recombines with the aryl group in a still-undetermined manner to forge the carbon-carbon bond. This mechanistic framework is supported by spectroscopic studies performed by Neidig and co-workers, who demonstrate that (SciOPP)—iron(II) species exhibit reactivity with the electrophile at catalytically relevant rates.¹⁷¹ Lower-valent iron(I) species are

formed in only very small amounts (< 0.5%) in solution, and do not react with the electrophile at catalytically relevant rates.

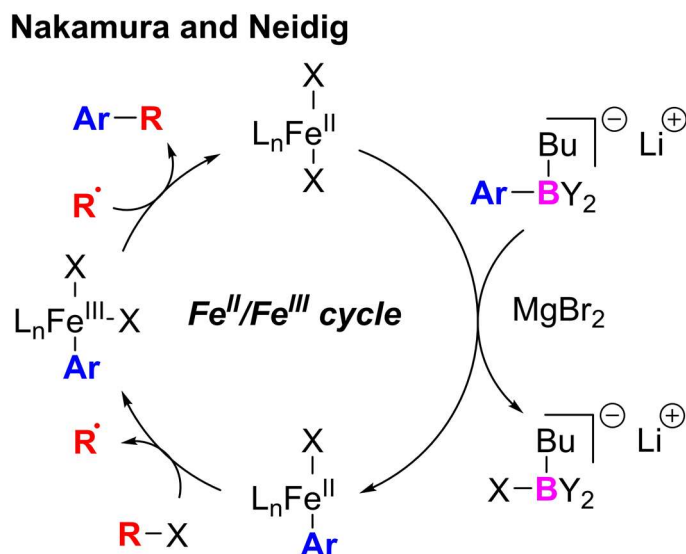


Figure 1.13. Catalytic cycle for the iron-catalyzed Suzuki-Miyaura cross-coupling reaction between C(sp²)-hybridized organoboron reagents and C(sp³)-hybridized electrophiles proposed by Nakamura and Neidig featuring iron(II)/iron(III) intermediates.

Conversely, Bedford and co-workers propose a catalytic cycle featuring iron(I)/iron(II)/iron(III) intermediates (Figure 1.14), in which the iron(II) precatalyst is reduced to an iron(I) species that undergoes transmetalation with the aryl borate, facilitated by MgBr₂.¹⁷⁰ The resultant iron(I) aryl species produces a carbon-centered radical upon halogen abstraction of the alkyl halide in the rate-determining step to generate an iron(II) aryl halide, which reacts with the carbon-centered radical to form an iron(III) intermediate poised for reductive elimination to forge the carbon-carbon bond and close the catalytic cycle. EPR analysis of the catalytic reaction identified an iron(I) species consistent with (dppe)₂FeX, which can undergo ligand dissociation to generate the catalytically active (dppe)FeX species. Norrby and co-workers support this framework, and employ a

combination of kinetics experiments and DFT calculations to justify the intermediacy of iron(I) species.¹⁷² The ongoing debate regarding the precise mechanism of these reactions underscores the difficulty of studying systems catalyzed by iron-based complexes, but also highlights the potential of harnessing its versatile reactivity.

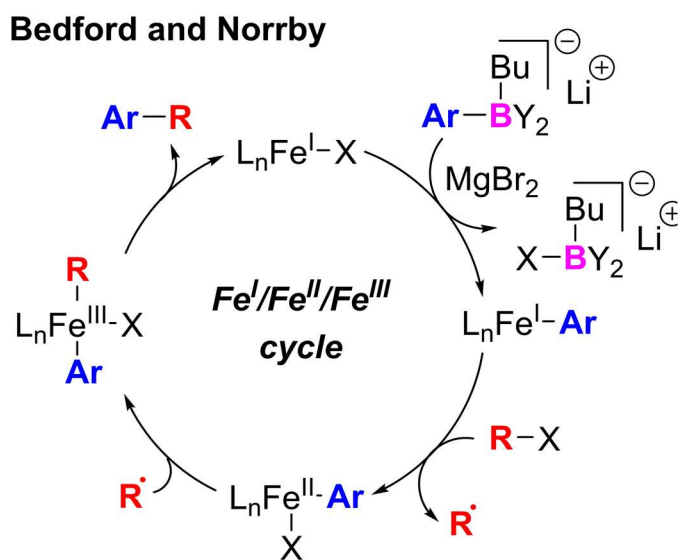


Figure 1.14. Catalytic cycle for the iron-catalyzed Suzuki-Miyaura cross-coupling reaction between C(sp²)-hybridized organoboron reagents and C(sp³)-hybridized electrophiles proposed by Bedford and Norrby featuring iron(I)/iron(II)/iron(III) intermediates.

While these few examples demonstrate tremendous promise for the future of iron-catalyzed Suzuki-Miyaura cross-coupling reactions, the dearth of examples is also a sign that development of these methods similar to that of their palladium analogues has been historically lacking. In comparison to the palladium-catalyzed analogues, iron-catalyzed cross-coupling reactions still demonstrate poor functional group tolerance due to the highly reactive transmetalating reagents. The iron sources used in iron-catalyzed cross-coupling reactions are typically simple iron salts, and the ancillary ligands used to promote the reactions are drawn from a pool of existing ligand frameworks that have been optimized

for other uses. Unlike the palladacycle precatalysts, the iron-based precatalysts used for cross-coupling reactions also remain significantly more susceptible to atmospheric conditions, demonstrating rapid deactivation in the presence of air or moisture and consequently require the use of inert gloveboxes for reaction assembly. Focused development of iron-catalyzed Suzuki-Miyaura cross-coupling reactions accompanied by rigorous mechanistic elucidation has the potential to elevate iron catalysis to provide complementary reactivity to existing methods while circumventing some of the remaining environmental and economic concerns of traditional cross-coupling reactions.

1.8 Conclusion

The development of cross-coupling technologies over the past half-century has predominantly focused on palladium-catalyzed methods.¹⁸ The reliable two-electron redox behavior of palladium has enabled thorough investigations of the operative mechanism by which palladium-catalyzed cross-coupling reactions proceed, which in turn have led to a plethora of advances aimed at improving their versatility and utility. Foremost among these advances is the application of air- and moisture-stable organoboron transmetalating reagents for what has become known as the Suzuki-Miyaura variant, and further improvements to the design of ligand frameworks,⁷³ the bench stability of the metal precatalysts,¹⁷³ and the breadth of incorporable substrates¹⁷⁴ have also contributed to the present-day prevalence of the palladium-catalyzed Suzuki-Miyaura cross-coupling reaction.

Despite these advancements, the remarkable success of the palladium-catalyzed Suzuki-Miyaura reaction has led to the overrepresentation of certain chemical motifs due to overreliance on the method across various industries,¹¹ high cost volatility due to

fluctuating demand of palladium for its various applications, and lagging innovation using other transition metals. In recent years, interest in the ability of other transition metals to catalyze cross-coupling reactions has grown in order to address these limitations.¹ While methods catalyzed by nickel have benefited from tremendous attention and developed rapidly in recent years, iron catalysis offers improved environmental and economic profiles⁷ that are important considerations for industrial relevance. Moreover, iron-based complexes are also able to access the one- and two-electron pathways which enable nickel catalysis to provide reactivity that palladium catalysis cannot. However, the development of iron-catalyzed methods has been held back by a poor understanding of its operative mechanism, which in turn has limited the rational development of ligand frameworks and reaction conditions that can effectively promote cross-coupling reactions demonstrating valuable reactivity inaccessible to palladium catalysis. Continued efforts toward investigating iron-catalyzed Suzuki-Miyaura cross-coupling reactions has the potential to initiate a rapid trajectory of development similar to that of palladium catalysis, with the goal of addressing remaining practical limitations in order to expand the toolbox of synthetic organic chemists.

1.9 References

- (1) Jana, R.; Pathak, T. P.; Sigman, M. S. Advances in Transition Metal (Pd,Ni,Fe)-Catalyzed Cross-Coupling Reactions Using Alkyl-Organometallics as Reaction Partners. *Chem. Rev.* **2011**, *111* (3), 1417–1492. <https://doi.org/10.1021/cr100327p>.
- (2) Negishi, E. A Genealogy of Pd-Catalyzed Cross-Coupling. *J. Organomet. Chem.* **2002**, *653* (1–2), 34–40. [https://doi.org/10.1016/S0022-328X\(02\)01273-1](https://doi.org/10.1016/S0022-328X(02)01273-1).
- (3) Farina, V. High-Turnover Palladium Catalysts in Cross-Coupling and Heck Chemistry: A Critical Overview. *Adv. Synth. Catal.* **2004**, *346* (13–15), 1553–1582. <https://doi.org/10.1002/adsc.200404178>.
- (4) Buskes, M. J.; Blanco, M. J. Impact of Cross-Coupling Reactions in Drug Discovery and Development. *Molecules* **2020**, *25* (15), 3493. <https://doi.org/10.3390/molecules25153493>.
- (5) Xu, S.; Kim, E. H.; Wei, A.; Negishi, E. I. Pd- and Ni-Catalyzed Cross-Coupling Reactions in the Synthesis of Organic Electronic Materials. *Sci. Technol. Adv. Mater.* **2014**, *15* (4), 1–23. <https://doi.org/10.1088/1468-6996/15/4/044201>.
- (6) Tabassum, S.; Zahoor, A. F.; Ahmad, S.; Noreen, R.; Khan, S. G.; Ahmad, H. Cross-Coupling Reactions towards the Synthesis of Natural Products. *Mol. Divers.* **2021**. <https://doi.org/10.1007/s11030-021-10195-6>.
- (7) Egorova, K. S.; Ananikov, V. P. Toxicity of Metal Compounds: Knowledge and Myths. *Organometallics* **2017**, *36* (21), 4071–4090. <https://doi.org/10.1021/acs.organomet.7b00605>.
- (8) Hunt, A. J.; Matharu, A. S.; King, A. H.; Clark, J. H. The Importance of Elemental Sustainability and Critical Element Recovery. *Green Chem.* **2015**, *17* (4), 1949–1950. <https://doi.org/10.1039/C5GC90019K>.
- (9) Hassan, J.; Sévignon, M.; Gozzi, C.; Schulz, E.; Lemaire, M. Aryl-Aryl Bond Formation One Century after the Discovery of the Ullmann Reaction. *Chem. Rev.* **2002**, *102* (5), 1359–1469. <https://doi.org/10.1021/cr000664r>.

- (10) Choi, J.; Fu, G. C. Transition Metal–Catalyzed Alkyl–Alkyl Bond Formation: Another Dimension in Cross-Coupling Chemistry. *Science* **2017**, *356* (6334), eaaf7230. <https://doi.org/10.1126/science.aaf7230>.
- (11) Brown, D. G.; Boström, J. Analysis of Past and Present Synthetic Methodologies on Medicinal Chemistry: Where Have All the New Reactions Gone? *J. Med. Chem.* **2016**, *59* (10), 4443–4458. <https://doi.org/10.1021/acs.jmedchem.5b01409>.
- (12) Kyne, S. H.; Lefèvre, G.; Ollivier, C.; Petit, M.; Ramis Cladera, V.-A.; Fensterbank, L. Iron and Cobalt Catalysis: New Perspectives in Synthetic Radical Chemistry. *Chem. Soc. Rev.* **2020**, *49* (23), 8501–8542. <https://doi.org/10.1039/D0CS00969E>.
- (13) Fürstner, A. Iron Catalysis in Organic Synthesis: A Critical Assessment of What It Takes to Make This Base Metal a Multitasking Champion. *ACS Cent. Sci.* **2016**, *2* (11), 778–789. <https://doi.org/10.1021/acscentsci.6b00272>.
- (14) Fürstner, A.; Leitner, A.; Méndez, M.; Krause, H. Iron-Catalyzed Cross-Coupling Reactions. *J. Am. Chem. Soc.* **2002**, *124* (46), 13856–13863. <https://doi.org/10.1021/ja027190t>.
- (15) Lennox, A. J. J.; Lloyd-Jones, G. C. Selection of Boron Reagents for Suzuki–Miyaura Coupling. *Chem. Soc. Rev.* **2014**, *43* (1), 412–443. <https://doi.org/10.1039/C3CS60197H>.
- (16) Suzuki, A. Organoboron Compounds in New Synthetic Reactions. *Pure Appl. Chem.* **1985**, *57* (12), 1749–1758. <https://doi.org/10.1351/pac198557121749>.
- (17) Miyaura, N.; Yanagi, T.; Suzuki, A. The Palladium-Catalyzed Cross-Coupling Reaction of Phenylboronic Acid with Haloarenes in the Presence of Bases. *Synth. Commun.* **1981**, *11* (7), 513–519. <https://doi.org/10.1080/00397918108063618>.
- (18) Miyaura, N.; Suzuki, A. Palladium-Catalyzed Cross-Coupling Reactions of Organoboron Compounds. *Chem. Rev.* **1995**, *95* (7), 2457–2483. <https://doi.org/10.1021/cr00039a007>.
- (19) Stille, J. K.; Lau, K. S. Y. Mechanisms of Oxidative Addition of Organic Halides

to Group 8 Transition-Metal Complexes. *Acc. Chem. Res.* **1977**, *10* (12), 434–442. <https://doi.org/10.1021/ar50120a002>.

(20) Amatore, C.; Pflüger, F. Mechanism of Oxidative Addition of Palladium(0) with Aromatic Iodides in Toluene, Monitored at Ultramicroelectrodes. *Organometallics* **1990**, *9* (8), 2276–2282. <https://doi.org/10.1021/om00158a026>.

(21) Portnoy, M.; Milstein, D. Mechanism of Aryl Chloride Oxidative Addition to Chelated Palladium(0) Complexes. *Organometallics* **1993**, *12* (5), 1665–1673. <https://doi.org/10.1021/om00029a026>.

(22) Hartwig, J. F.; Paul, F. Oxidative Addition of Aryl Bromide after Dissociation of Phosphine from a Two-Coordinate Palladium(0) Complex, Bis(Tri-*o*-Tolylphosphine)Palladium(0). *J. Am. Chem. Soc.* **1995**, *117* (19), 5373–5374. <https://doi.org/10.1021/ja00124a026>.

(23) Fauvarque, J. F.; Pflüger, F.; Troupel, M. Kinetics of Oxidative Addition of Zerovalent Palladium to Aromatic Iodides. *J. Organomet. Chem.* **1981**, *208* (3), 419–427. [https://doi.org/10.1016/S0022-328X\(00\)86726-1](https://doi.org/10.1016/S0022-328X(00)86726-1).

(24) Vicente, J.; Arcas, A.; Bautista, D.; Jones, P. G. The Difficulty of Coordinating Mutually Trans Phosphine and Aryl Ligands in Palladium Complexes and Its Relation to Important Coupling Processes. Syntheses and Crystal Structures of a Family of Palladium Phosphino, Triflato, Perchlorato, and Aquo-2-(Aryl). *Organometallics* **1997**, *16* (10), 2127–2138. <https://doi.org/10.1021/om961094h>.

(25) Fitton, P.; Rick, E. A. The Addition of Aryl Halides to Tetrakis(Triphenylphosphine)Palladium(0). *J. Organomet. Chem.* **1971**, *28* (2), 287–291. [https://doi.org/10.1016/S0022-328X\(00\)84578-7](https://doi.org/10.1016/S0022-328X(00)84578-7).

(26) Barrios-Landeros, F.; Hartwig, J. F. Distinct Mechanisms for the Oxidative Addition of Chloro-, Bromo-, and Iodoarenes to a Bisphosphine Palladium(0) Complex with Hindered Ligands. *J. Am. Chem. Soc.* **2005**, *127* (19), 6944–6945. <https://doi.org/10.1021/ja042959i>.

- (27) Fu, G. C. The Development of Versatile Methods for Palladium-Catalyzed Coupling Reactions of Aryl Electrophiles through the Use of P(*t*-Bu)₃ and PCy₃ as Ligands. *Acc. Chem. Res.* **2008**, *41* (11), 1555–1564. <https://doi.org/10.1021/ar800148f>.
- (28) Littke, A. F.; Fu, G. C. A Convenient and General Method for Pd-Catalyzed Suzuki Cross-Couplings of Aryl Chlorides and Arylboronic Acids. *Angew. Chemie Int. Ed.* **1998**, *37* (24), 3387–3388. [https://doi.org/10.1002/\(SICI\)1521-3773\(19981231\)37:24<3387::AID-ANIE3387>3.0.CO;2-P](https://doi.org/10.1002/(SICI)1521-3773(19981231)37:24<3387::AID-ANIE3387>3.0.CO;2-P).
- (29) Littke, A. F.; Dai, C.; Fu, G. C. Versatile Catalysts for the Suzuki Cross-Coupling of Arylboronic Acids with Aryl and Vinyl Halides and Triflates under Mild Conditions. *J. Am. Chem. Soc.* **2000**, *122* (17), 4020–4028. <https://doi.org/10.1021/ja0002058>.
- (30) Lennox, A. J. J.; Lloyd-Jones, G. C. Transmetalation in the Suzuki-Miyaura Coupling: The Fork in the Trail. *Angew. Chemie Int. Ed.* **2013**, *52* (29), 7362–7370. <https://doi.org/10.1002/anie.201301737>.
- (31) Endo, K.; Ohkubo, T.; Hirokami, M.; Shibata, T. Chemoselective and Regiospecific Suzuki Coupling on a Multisubstituted Sp³-Carbon in 1,1-Diborylalkanes at Room Temperature. *J. Am. Chem. Soc.* **2010**, *132* (32), 11033–11035. <https://doi.org/10.1021/ja105176v>.
- (32) Lee, J. C. H.; McDonald, R.; Hall, D. G. Enantioselective Preparation and Chemoselective Cross-Coupling of 1,1-Diboron Compounds. *Nat. Chem.* **2011**, *3* (11), 894–899. <https://doi.org/10.1038/nchem.1150>.
- (33) Blaisdell, T. P.; Caya, T. C.; Zhang, L.; Sanz-Marco, A.; Morken, J. P. Hydroxyl-Directed Stereoselective Diboration of Alkenes. *J. Am. Chem. Soc.* **2014**, *136* (26), 9264–9267. <https://doi.org/10.1021/ja504228p>.
- (34) Ohmura, T.; Awano, T.; Suginome, M. Stereospecific Suzuki-Miyaura Coupling of Chiral α -(Acylamino) Benzylboronic Esters with Inversion of Configuration. *J. Am. Chem. Soc.* **2010**, *132* (38), 13191–13193. <https://doi.org/10.1021/ja106632j>.
- (35) Sandrock, D. L.; Jean-Gérard, L.; Chen, C. Y.; Dreher, S. D.; Molander, G. A.

Stereospecific Cross-Coupling of Secondary Alkyl β - Trifluoroboratoamides. *J. Am. Chem. Soc.* **2010**, *132* (48), 17108–17110. <https://doi.org/10.1021/ja108949w>.

(36) Miyaura, N.; Yamada, K.; Suginome, H.; Suzuki, A. Novel and Convenient Method for the Stereo- and Regiospecific Synthesis of Conjugated Alkadienes and Alkynes via the Palladium-Catalyzed Cross-Coupling Reaction of 1-Alkenylboranes with Bromoalkenes and Bromoalkynes. *J. Am. Chem. Soc.* **1985**, *107* (4), 972–980. <https://doi.org/10.1021/ja00290a037>.

(37) Matos, K.; Soderquist, J. A. Alkylboranes in the Suzuki–Miyaura Coupling: Stereochemical and Mechanistic Studies. *J. Org. Chem.* **1998**, *63* (3), 461–470. <https://doi.org/10.1021/jo971681s>.

(38) Ridgway, B. H.; Woerpel, K. A. Transmetalation of Alkylboranes to Palladium in the Suzuki Coupling Reaction Proceeds with Retention of Stereochemistry. *J. Org. Chem.* **1998**, *63* (3), 458–460. <https://doi.org/10.1021/jo970803d>.

(39) Carrow, B. P.; Hartwig, J. F. Distinguishing Between Pathways for Transmetalation in Suzuki–Miyaura Reactions. *J. Am. Chem. Soc.* **2011**, *133* (7), 2116–2119. <https://doi.org/10.1021/ja1108326>.

(40) Thomas, A. A.; Denmark, S. E. Pre-Transmetalation Intermediates in the Suzuki–Miyaura Reaction Revealed: The Missing Link. *Science* **2016**, *352* (6283), 329–332. <https://doi.org/10.1126/science.aad6981>.

(41) Payard, P. A.; Bohn, A.; Tocqueville, D.; Jaouadi, K.; Escoude, E.; Ajig, S.; Dethoor, A.; Gontard, G.; Perego, L. A.; Vitale, M.; et al. Role of Dppf Monoxide in the Transmetalation Step of the Suzuki–Miyaura Coupling Reaction. *Organometallics* **2021**, *40* (8), 1120–1128. <https://doi.org/10.1021/acs.organomet.1c00090>.

(42) Thomas, A. A.; Zahrt, A. F.; Delaney, C. P.; Denmark, S. E. Elucidating the Role of the Boronic Esters in the Suzuki–Miyaura Reaction: Structural, Kinetic, and Computational Investigations. *J. Am. Chem. Soc.* **2018**, *140* (12), 4401–4416. <https://doi.org/10.1021/jacs.8b00400>.

- (43) Butters, M.; Harvey, J. N.; Jover, J.; Lennox, A. J. J.; Lloyd-Jones, G. C.; Murray, P. M. Aryl Trifluoroborates in Suzuki-Miyaura Coupling: The Roles of Endogenous Aryl Boronic Acid and Fluoride. *Angew. Chemie Int. Ed.* **2010**, *49* (30), 5156–5160. <https://doi.org/10.1002/anie.201001522>.
- (44) Lennox, A. J. J.; Lloyd-Jones, G. C. Organotrifluoroborate Hydrolysis: Boronic Acid Release Mechanism and an Acid–Base Paradox in Cross-Coupling. *J. Am. Chem. Soc.* **2012**, *134* (17), 7431–7441. <https://doi.org/10.1021/ja300236k>.
- (45) Gonzalez, J. A.; Ogba, O. M.; Morehouse, G. F.; Rosson, N.; Houk, K. N.; Leach, A. G.; Cheong, P. H.-Y.; Burke, M. D.; Lloyd-Jones, G. C. MIDA Boronates Are Hydrolysed Fast and Slow by Two Different Mechanisms. *Nat. Chem.* **2016**, *8* (11), 1067–1075. <https://doi.org/10.1038/nchem.2571>.
- (46) Gillie, A.; Stille, J. K. Mechanisms of 1,1-Reductive Elimination from Palladium. *J. Am. Chem. Soc.* **1980**, *102* (15), 4933–4941. <https://doi.org/10.1021/ja00535a018>.
- (47) Loar, M. K.; Stille, J. K. Mechanisms of 1,1-Reductive Elimination from Palladium: Coupling of Styrylmethylpalladium Complexes. *J. Am. Chem. Soc.* **1981**, *103* (14), 4174–4181. <https://doi.org/10.1021/ja00404a033>.
- (48) Moravskiy, A.; Stille, J. K. Mechanisms of 1,1-Reductive Elimination from Palladium: Elimination of Ethane from Dimethylpalladium(II) and Trimethylpalladium(IV). *J. Am. Chem. Soc.* **1981**, *103* (14), 4182–4186. <https://doi.org/10.1021/ja00404a034>.
- (49) Tatsumi, K.; Hoffmann, R.; Yamamoto, A.; Stille, J. K. Reductive Elimination of D⁸-Organotransition Metal Complexes. *Bull. Chem. Soc. Jpn.* **1981**, *54* (6), 1857–1867. <https://doi.org/10.1246/bcsj.54.1857>.
- (50) Ozawa, F.; Ito, T.; Nakamura, Y.; Yamamoto, A. Mechanisms of Thermal Decomposition of Trans - and Cis -Dialkylbis(Tertiary Phosphine)Palladium(II). Reductive Elimination and Trans to Cis Isomerization. *Bull. Chem. Soc. Jpn.* **1981**, *54* (6), 1868–1880. <https://doi.org/10.1246/bcsj.54.1868>.

- (51) Widenhoefer, R. A.; Buchwald, S. L. Electronic Dependence of C-O Reductive Elimination from Palladium (Aryl)Neopentoxide Complexes. *J. Am. Chem. Soc.* **1998**, *120* (26), 6504–6511. <https://doi.org/10.1021/ja9806581>.
- (52) Culkin, D. A.; Hartwig, J. F. Carbon-Carbon Bond-Forming Reductive Elimination from Arylpalladium Complexes Containing Functionalized Alkyl Groups. Influence of Ligand Steric and Electronic Properties on Structure, Stability, and Reactivity. *Organometallics* **2004**, *23* (14), 3398–3416. <https://doi.org/10.1021/om049726k>.
- (53) Paul, F.; Patt, J.; Hartwig, J. F. Palladium-Catalyzed Formation of Carbon-Nitrogen Bonds. Reaction Intermediates and Catalyst Improvements in the Hetero Cross-Coupling of Aryl Halides and Tin Amides. *J. Am. Chem. Soc.* **1994**, *116* (13), 5969–5970. <https://doi.org/10.1021/ja00092a058>.
- (54) Driver, M. S.; Hartwig, J. F. Carbon-Nitrogen-Bond-Forming Reductive Elimination of Arylamines from Palladium(II) Phosphine Complexes. *J. Am. Chem. Soc.* **1997**, *119* (35), 8232–8245. <https://doi.org/10.1021/ja971057x>.
- (55) Shekhar, S.; Hartwig, J. F. Distinct Electronic Effects on Reductive Eliminations of Symmetrical and Unsymmetrical Bis-Aryl Platinum Complexes. *J. Am. Chem. Soc.* **2004**, *126* (40), 13016–13027. <https://doi.org/10.1021/ja0480365>.
- (56) Huser, M.; Youinou, M. T.; Osborn, J. A. Chlorocarbon Activation: Catalytic Carbonylation of Dichloromethane and Chlorobenzene. *Angew. Chemie Int. Ed. English* **1989**, *28* (10), 1386–1388. <https://doi.org/10.1002/anie.198913861>.
- (57) Ben-David, Y.; Portnoy, M.; Milstein, D. Chelate-Assisted, Pd-Catalyzed Efficient Carbonylation of Aryl Chlorides. *J. Am. Chem. Soc.* **1989**, *111* (23), 8742–8744. <https://doi.org/10.1021/ja00205a039>.
- (58) Zhang, C.; Huang, J.; Trudell, M. L.; Nolan, S. P. Palladium-Imidazol-2-Ylidene Complexes as Catalysts for Facile and Efficient Suzuki Cross-Coupling Reactions of Aryl Chlorides with Arylboronic Acids. *J. Org. Chem.* **1999**, *64* (11), 3804–3805. <https://doi.org/10.1021/jo990554o>.

- (59) Marion, N.; Nolan, S. P. Well-Defined N-Heterocyclic Carbenes-Palladium(II) Precatalysts for Cross-Coupling Reactions. *Acc. Chem. Res.* **2008**, *41* (11), 1440–1449. <https://doi.org/10.1021/ar800020y>.
- (60) Díez-González, S.; Marion, N.; Nolan, S. P. N-Heterocyclic Carbenes in Late Transition Metal Catalysis. *Chem. Rev.* **2009**, *109* (8), 3612–3676. <https://doi.org/10.1021/cr900074m>.
- (61) Hama, T.; Liu, X.; Culkin, D. A.; Hartwig, J. F. Palladium-Catalyzed α -Arylation of Esters and Amides under More Neutral Conditions. *J. Am. Chem. Soc.* **2003**, *125* (37), 11176–11177. <https://doi.org/10.1021/ja036792p>.
- (62) Shelby, Q.; Kataoka, N.; Mann, G.; Hartwig, J. Unusual in Situ Ligand Modification to Generate a Catalyst for Room Temperature Aromatic C-O Bond Formation [8]. *J. Am. Chem. Soc.* **2000**, *122* (43), 10718–10719. <https://doi.org/10.1021/ja002543e>.
- (63) Kataoka, N.; Shelby, Q.; Stambuli, J. P.; Hartwig, J. F. Air Stable, Sterically Hindered Ferrocenyl Dialkylphosphines for Palladium-Catalyzed C-C, C-N, and C-O Bond-Forming Cross-Couplings. *J. Org. Chem.* **2002**, *67* (16), 5553–5566. <https://doi.org/10.1021/jo025732j>.
- (64) Vo, G. D.; Hartwig, J. F. Palladium-Catalyzed α -Arylation of Aldehydes with Bromo- and Chloroarenes Catalyzed by [$\text{Pd}(\text{Allyl})\text{Cl}$] $_2$ and Dppf or Q-Phos. *Angew. Chemie - Int. Ed.* **2008**, *47* (11), 2127–2130. <https://doi.org/10.1002/anie.200705357>.
- (65) Zapf, A.; Ehrentraut, A.; Beller, M. A New Highly Efficient Catalyst System for the Coupling of Nonactivated and Deactivated Aryl Chlorides with Arylboronic Acids. *Angew. Chemie - Int. Ed.* **2000**, *39* (22), 4153–4155. [https://doi.org/10.1002/1521-3773\(20001117\)39:22<4153::AID-ANIE4153>3.0.CO;2-T](https://doi.org/10.1002/1521-3773(20001117)39:22<4153::AID-ANIE4153>3.0.CO;2-T).
- (66) Klaus, S.; Neumann, H.; Zapf, A.; Strübing, D.; Hübner, S.; Almena, J.; Riermeier, T.; Groß, P.; Sarich, M.; Krahnert, W. R.; et al. A General and Efficient Method for the Formylation of Aryl and Heteroaryl Bromides. *Angew. Chemie - Int. Ed.* **2005**, *45* (1), 154–158. <https://doi.org/10.1002/anie.200502697>.

- (67) Lundgren, R. J.; Sapping-Kumankumah, A.; Stradiotto, M. A Highly Versatile Catalyst System for the Cross-Coupling of Aryl Chlorides and Amines. *Chem. - A Eur. J.* **2010**, *16* (6), 1983–1991. <https://doi.org/10.1002/chem.200902316>.
- (68) Lundgren, R. J.; Peters, B. D.; Alsabeh, P. G.; Stradiotto, M. A P,N-Ligand for Palladium-Catalyzed Ammonia Arylation: Coupling of Deactivated Aryl Chlorides, Chemoselective Arylations, and Room Temperature Reactions. *Angew. Chemie - Int. Ed.* **2010**, *49* (24), 4071–4074. <https://doi.org/10.1002/anie.201000526>.
- (69) Hesp, K. D.; Lundgren, R. J.; Stradiotto, M. Palladium-Catalyzed Mono- α -Arylation of Acetone with Aryl Halides and Tosylates. *J. Am. Chem. Soc.* **2011**, *133* (14), 5194–5197. <https://doi.org/10.1021/ja200009c>.
- (70) Old, D. W.; Wolfe, J. P.; Buchwald, S. L. A Highly Active Catalyst for Palladium-Catalyzed Cross-Coupling Reactions: Room-Temperature Suzuki Couplings and Amination of Unactivated Aryl Chlorides. *J. Am. Chem. Soc.* **1998**, *120* (37), 9722–9723. <https://doi.org/10.1021/ja982250+>.
- (71) Wolfe, J. P.; Buchwald, S. L. A Highly Active Catalyst for the Room-Temperature Amination and Suzuki Coupling of Aryl Chlorides. *Angew. Chemie - Int. Ed.* **1999**, *38* (16), 2413–2416. [https://doi.org/10.1002/\(SICI\)1521-3773\(19990816\)38:16<2413::AID-ANIE2413>3.0.CO;2-H](https://doi.org/10.1002/(SICI)1521-3773(19990816)38:16<2413::AID-ANIE2413>3.0.CO;2-H).
- (72) Wolfe, J. P.; Singer, R. A.; Yang, B. H.; Buchwald, S. L. Highly Active Palladium Catalysts for Suzuki Coupling Reactions. *J. Am. Chem. Soc.* **1999**, *121* (41), 9550–9561. <https://doi.org/10.1021/ja992130h>.
- (73) Martin, R.; Buchwald, S. L. Palladium-Catalyzed Suzuki–Miyaura Cross-Coupling Reactions Employing Dialkylbiaryl Phosphine Ligands. *Acc. Chem. Res.* **2008**, *41* (11), 1461–1473. <https://doi.org/10.1021/ar800036s>.
- (74) Sather, A. C.; Buchwald, S. L. The Evolution of Pd(0)/Pd(II)-Catalyzed Aromatic Fluorination. *Acc. Chem. Res.* **2016**, *49* (10), 2146–2157. <https://doi.org/10.1021/acs.accounts.6b00247>.

- (75) Ruiz-Castillo, P.; Buchwald, S. L. Applications of Palladium-Catalyzed C-N Cross-Coupling Reactions. *Chem. Rev.* **2016**, *116* (19), 12564–12649. <https://doi.org/10.1021/acs.chemrev.6b00512>.
- (76) Zhang, H.; Ruiz-Castillo, P.; Buchwald, S. L. Palladium-Catalyzed C-O Cross-Coupling of Primary Alcohols. *Org. Lett.* **2018**, *20* (6), 1580–1583. <https://doi.org/10.1021/acs.orglett.8b00325>.
- (77) Walker, S. D.; Barder, T. E.; Martinelli, J. R.; Buchwald, S. L. A Rationally Designed Universal Catalyst for Suzuki-Miyaura Coupling Processes. *Angew. Chemie - Int. Ed.* **2004**, *43* (14), 1871–1876. <https://doi.org/10.1002/anie.200353615>.
- (78) Barder, T. E.; Walker, S. D.; Martinelli, J. R.; Buchwald, S. L. Catalysts for Suzuki-Miyaura Coupling Processes: Scope and Studies of the Effect of Ligand Structure. *J. Am. Chem. Soc.* **2005**, *127* (13), 4685–4696. <https://doi.org/10.1021/ja042491j>.
- (79) Barder, T. E.; Biscoe, M. R.; Buchwald, S. L. Structural Insights into Active Catalyst Structures and Oxidative Addition to (Biaryl)Phosphine - Palladium Complexes via Density Functional Theory and Experimental Studies. *Organometallics* **2007**, *26* (9), 2183–2192. <https://doi.org/10.1021/om0701017>.
- (80) Itoh, T.; Mase, T. Direct Synthesis of Hetero-Biaryl Compounds Containing an Unprotected NH₂ Group via Suzuki-Miyaura Reaction. *Tetrahedron Lett.* **2005**, *46* (20), 3573–3577. <https://doi.org/10.1016/j.tetlet.2005.03.053>.
- (81) Billingsley, K. L.; Anderson, K. W.; Buchwald, S. L. A Highly Active Catalyst for Suzuki-Miyaura Cross-Coupling Reactions of Heteroaryl Compounds. *Angew. Chemie - Int. Ed.* **2006**, *45* (21), 3484–3488. <https://doi.org/10.1002/anie.200600493>.
- (82) Billingsley, K.; Buchwald, S. L. Highly Efficient Monophosphine-Based Catalyst for the Palladium-Catalyzed Suzuki-Miyaura Reaction of Heteroaryl Halides and Heteroaryl Boronic Acids and Esters. *J. Am. Chem. Soc.* **2007**, *129* (11), 3358–3366. <https://doi.org/10.1021/ja068577p>.
- (83) Allgeier, A. M.; Shaw, B. J.; Hwang, T. L.; Milne, J. E.; Tedrow, J. S.; Wilde, C.

N. Characterization of Two Stable Degradants of Palladium Tbxphos Catalyst and a Unique Dearomatization Reaction. *Organometallics* **2012**, *31* (2), 519–522. <https://doi.org/10.1021/om200988f>.

(84) Fors, B. P.; Watson, D. A.; Biscoe, M. R.; Buchwald, S. L. A Highly Active Catalyst for Pd-Catalyzed Amination Reactions: Cross-Coupling Reactions Using Aryl Mesylates and the Highly Selective Monoarylation of Primary Amines Using Aryl Chlorides. *J. Am. Chem. Soc.* **2008**, *130* (41), 13552–13554. <https://doi.org/10.1021/ja8055358>.

(85) Sather, A. C.; Lee, H. G.; De La Rosa, V. Y.; Yang, Y.; Müller, P.; Buchwald, S. L. A Fluorinated Ligand Enables Room-Temperature and Regioselective Pd-Catalyzed Fluorination of Aryl Triflates and Bromides. *J. Am. Chem. Soc.* **2015**, *137* (41), 13433–13438. <https://doi.org/10.1021/jacs.5b09308>.

(86) Svennebring, A.; Sjöberg, P. J. R.; Larhed, M.; Nilsson, P. A Mechanistic Study on Modern Palladium Catalyst Precursors as New Gateways to Pd(0) in Cationic Heck Reactions. *Tetrahedron* **2008**, *64* (8), 1808–1812. <https://doi.org/10.1016/j.tet.2007.11.111>.

(87) Carole, W. A.; Colacot, T. J. Understanding Palladium Acetate from a User Perspective. *Chem. - A Eur. J.* **2016**, *22* (23), 7686–7695. <https://doi.org/10.1002/chem.201601450>.

(88) Wei, C. S.; Davies, G. H. M.; Soltani, O.; Albrecht, J.; Gao, Q.; Pathirana, C.; Hsiao, Y.; Tummala, S.; Eastgate, M. D. The Impact of Palladium(II) Reduction Pathways on the Structure and Activity of Palladium(0) Catalysts. *Angew. Chemie Int. Ed.* **2013**, *52* (22), 5822–5826. <https://doi.org/10.1002/anie.201210252>.

(89) Fantasia, S.; Nolan, S. P. A General Synthetic Route to Mixed NHC-Phosphane Palladium(0) Complexes (NHC = N-Heterocyclic Carbene). *Chem. - A Eur. J.* **2008**, *14* (23), 6987–6993. <https://doi.org/10.1002/chem.200800815>.

(90) Amatore, C.; Broeker, G.; Jutand, A.; Khalil, F. Identification of the Effective Palladium(0) Catalytic Species Generated in Situ from Mixtures of Pd(dba)₂ and Bidentate

Phosphine Ligands. Determination of Their Rates and Mechanism in Oxidative Addition. *J. Am. Chem. Soc.* **1997**, *119* (22), 5176–5185. <https://doi.org/10.1021/ja9637098>.

(91) Herrmann, W. A.; Brossmer, C.; Öfele, K.; Reisinger, C.-P.; Priermeier, T.; Beller, M.; Fischer, H. Palladacycles as Structurally Defined Catalysts for the Heck Olefination of Chloro- and Bromoarenes. *Angew. Chemie Int. Ed. English* **1995**, *34* (17), 1844–1848. <https://doi.org/10.1002/anie.199518441>.

(92) Zim, D.; Buchwald, S. L. An Air and Thermally Stable One-Component Catalyst for the Amination of Aryl Chlorides. *Org. Lett.* **2003**, *5* (14), 2413–2415. <https://doi.org/10.1021/ol034561h>.

(93) Biscoe, M. R.; Barder, T. E.; Buchwald, S. L. Electronic Effects on the Selectivity of Pd-Catalyzed C–N Bond-Forming Reactions Using Biarylphosphine Ligands: The Competitive Roles of Amine Binding and Acidity. *Angew. Chemie Int. Ed.* **2007**, *46* (38), 7232–7235. <https://doi.org/10.1002/anie.200702122>.

(94) Biscoe, M. R.; Fors, B. P.; Buchwald, S. L. A New Class of Easily Activated Palladium Precatalysts for Facile C–N Cross-Coupling Reactions and the Low Temperature Oxidative Addition of Aryl Chlorides. *J. Am. Chem. Soc.* **2008**, *130* (21), 6686–6687. <https://doi.org/10.1021/ja801137k>.

(95) Kinzel, T.; Zhang, Y.; Buchwald, S. L. A New Palladium Precatalyst Allows for the Fast Suzuki–Miyaura Coupling Reactions of Unstable Polyfluorophenyl and 2-Heteroaryl Boronic Acids. *J. Am. Chem. Soc.* **2010**, *132* (40), 14073–14075. <https://doi.org/10.1021/ja1073799>.

(96) Feng, Z.; Hu, W.; Rom, W. N.; Beland, F. A.; Tang, M. S. 4-Aminobiphenyl Is a Major Etiological Agent of Human Bladder Cancer: Evidence from Its DNA Binding Spectrum in Human P53 Gene. *Carcinogenesis* **2002**, *23* (10), 1721–1727. <https://doi.org/10.1093/carcin/23.10.1721>.

(97) Lee, H. G.; Milner, P. J.; Buchwald, S. L. An Improved Catalyst System for the Pd-Catalyzed Fluorination of (Hetero)Aryl Triflates. *Org. Lett.* **2013**, *15* (21), 5602–5605. <https://doi.org/10.1021/ol402859k>.

- (98) Bruno, N. C.; Tudge, M. T.; Buchwald, S. L. Design and Preparation of New Palladium Precatalysts for C–C and C–N Cross-Coupling Reactions. *Chem. Sci.* **2013**, *4* (3), 916–920. <https://doi.org/10.1039/C2SC20903A>.
- (99) Bruno, N. C.; Niljianskul, N.; Buchwald, S. L. N-Substituted 2-Aminobiphenylpalladium Methanesulfonate Precatalysts and Their Use in C–C and C–N Cross-Couplings. *J. Org. Chem.* **2014**, *79* (9), 4161–4166. <https://doi.org/10.1021/jo500355k>.
- (100) Poland, A.; Knutson, J. C. 2,3,7,8-Tetrachlorodibenzo-p-Dioxin and Related Halogenated Aromatic Hydrocarbons: Examination of the Mechanism of Toxicity. *Annu. Rev. Pharmacol. Toxicol.* **1982**, *22* (1), 517–554. <https://doi.org/10.1146/annurev.pa.22.040182.002505>.
- (101) Cornella, J.; Zarate, C.; Martin, R. Metal-Catalyzed Activation of Ethers via C–O Bond Cleavage: A New Strategy for Molecular Diversity. *Chem. Soc. Rev.* **2014**, *43* (23), 8081–8097. <https://doi.org/10.1039/C4CS00206G>.
- (102) Zarate, C.; van Gemmeren, M.; Somerville, R. J.; Martin, R. Phenol Derivatives: Modern Electrophiles in Cross-Coupling Reactions. In *Advances in Organometallic Chemistry*; Elsevier, 2016; pp 143–222. <https://doi.org/10.1016/bs.adomc.2016.07.001>.
- (103) Pedley, J. B.; Naylor, R. D.; Kirby, S. P. *Thermochemical Data of Organic Compounds*; Springer Netherlands: Dordrecht, 1986. <https://doi.org/10.1007/978-94-009-4099-4>.
- (104) Luo, Y. R. *Handbook of Bond Dissociation Energies in Organic Compounds*; CRC Press LLC: Boca Raton: St. Petersburg, Florida, 2002. <https://doi.org/10.1201/9781420039863>.
- (105) Hansen, A. L.; Ebran, J. P.; Ahlquist, M.; Norrby, P. O.; Skrydstrup, T. Heck Coupling with Nonactivated Alkenyl Tosylates and Phosphates: Examples of Effective 1,2-Migrations of the Alkenyl Palladium(II) Intermediates. *Angew. Chemie - Int. Ed.* **2006**, *45* (20), 3349–3353. <https://doi.org/10.1002/anie.200600442>.

- (106) Munday, R. H.; Martinelli, J. R.; Buchwald, S. L. Palladium-Catalyzed Carbonylation of Aryl Tosylates and Mesylates. *J. Am. Chem. Soc.* **2008**, *130* (9), 2754–2755. <https://doi.org/10.1021/ja711449e>.
- (107) So, C. M.; Zhou, Z.; Lau, C. P.; Kwong, F. Y. Palladium-Catalyzed Amination of Aryl Mesylates. *Angew. Chemie - Int. Ed.* **2008**, *47* (34), 6402–6406. <https://doi.org/10.1002/anie.200802157>.
- (108) Zhang, L.; Wu, J. Palladium-Catalyzed Hiyama Cross-Couplings of Aryl Arenesulfonates with Arylsilanes. *J. Am. Chem. Soc.* **2008**, *130* (37), 12250–12251. <https://doi.org/10.1021/ja804672m>.
- (109) Albaneze-Walker, J.; Raju, R.; Vance, J. A.; Goodman, A. J.; Reeder, M. R.; Liao, J.; Maust, M. T.; Irish, P. A.; Espino, P.; Andrews, D. R. Imidazolylsulfonates: Electrophilic Partners in Cross-Coupling Reactions. *Org. Lett.* **2009**, *11* (7), 1463–1466. <https://doi.org/10.1021/ol802381k>.
- (110) Scott, W. J.; Crisp, G. T.; Stille, J. K. Palladium-Catalyzed Coupling of Vinyl Triflates with Organostannanes. A Short Synthesis of Pleraplysillin-1. *J. Am. Chem. Soc.* **1984**, *106* (16), 4630–4632. <https://doi.org/10.1021/ja00328a063>.
- (111) Oh-e, T.; Miyaura, N.; Suzuki, A. Palladium-Catalyzed Cross-Coupling Reaction of Organoboron Compounds with Organic Triflates. *J. Org. Chem.* **1993**, *58* (8), 2201–2208. <https://doi.org/10.1021/jo00060a041>.
- (112) Roy, A. H.; Hartwig, J. F. Oxidative Addition of Aryl Tosylates to Palladium(0) and Coupling of Unactivated Aryl Tosylates at Room Temperature. *J. Am. Chem. Soc.* **2003**, *125* (29), 8704–8705. <https://doi.org/10.1021/ja035835z>.
- (113) Nguyen, H. N.; Huang, X.; Buchwald, S. L. The First General Palladium Catalyst for the Suzuki-Miyaura and Carbonyl Enolate Coupling of Aryl Arenesulfonates. *J. Am. Chem. Soc.* **2003**, *125* (39), 11818–11819. <https://doi.org/10.1021/ja036947t>.
- (114) Percec, V.; Bae, J. Y.; Hill, D. H. Aryl Mesylates in Metal Catalyzed Homocoupling and Cross-Coupling Reactions. 2. Suzuki-Type Nickel-Catalyzed Cross-

Coupling of Aryl Arenesulfonates and Aryl Mesylates with Arylboronic Acids. *J. Org. Chem.* **1995**, *60* (4), 1060–1065. <https://doi.org/10.1021/jo00109a044>.

(115) Zim, D.; Lando, V. R.; Dupont, J.; Monteiro, A. L. NiCl₂(PCy₃)₂: A Simple and Efficient Catalyst Precursor for the Suzuki Cross-Coupling of Aryl Tosylates and Arylboronic Acids. *Org. Lett.* **2001**, *3* (19), 3049–3051. <https://doi.org/10.1021/ol016526l>.

(116) Percec, V.; Golding, G. M.; Smidrkal, J.; Weichold, O. NiCl₂(Dppe)-Catalyzed Cross-Coupling of Aryl Mesylates, Arenesulfonates, and Halides with Arylboronic Acids. *J. Org. Chem.* **2004**, *69* (10), 3447–3452. <https://doi.org/10.1021/jo049940i>.

(117) Cooper, A. K.; Burton, P. M.; Nelson, D. J. Nickel versus Palladium in Cross-Coupling Catalysis: On the Role of Substrate Coordination to Zerovalent Metal Complexes. *Synthesis (Stuttg.)* **2020**, *52* (4), 565–573. <https://doi.org/10.1055/s-0039-1690045>.

(118) Kuwano, R.; Yokogi, M. Cross-Coupling of Benzylic Acetates with Arylboronic Acids: One-Pot Transformation of Benzylic Alcohols to Diarylmethanes. *Chem. Commun.* **2005**, No. 47, 5899. <https://doi.org/10.1039/b513372f>.

(119) Quasdorf, K. W.; Tian, X.; Garg, N. K. Cross-Coupling Reactions of Aryl Pivalates with Boronic Acids. *J. Am. Chem. Soc.* **2008**, *130* (44), 14422–14423. <https://doi.org/10.1021/ja806244b>.

(120) Guan, B. T.; Wang, Y.; Li, B. J.; Yu, D. G.; Shi, Z. J. Biaryl Construction via Ni-Catalyzed C-O Activation of Phenolic Carboxylates. *J. Am. Chem. Soc.* **2008**, *130* (44), 14468–14470. <https://doi.org/10.1021/ja8056503>.

(121) Quasdorf, K. W.; Riener, M.; Petrova, K. V.; Garg, N. K. Suzuki-Miyaura Coupling of Aryl Carbamates, Carbonates, and Sulfamates. *J. Am. Chem. Soc.* **2009**, *131* (49), 17748–17749. <https://doi.org/10.1021/ja906477r>.

(122) Antoft-Finch, A.; Blackburn, T.; Snieckus, V. N,N-Diethyl O-Carbamate: Directed Metalation Group and Orthogonal Suzuki-Miyaura Cross-Coupling Partner. *J. Am. Chem. Soc.* **2009**, *131* (49), 17750–17752. <https://doi.org/10.1021/ja907700e>.

- (123) Kakiuchi, F.; Usui, M.; Ueno, S.; Chatani, N.; Murai, S. Ruthenium-Catalyzed Functionalization of Aryl Carbon–Oxygen Bonds in Aromatic Ethers with Organoboron Compounds. *J. Am. Chem. Soc.* **2004**, *126* (9), 2706–2707. <https://doi.org/10.1021/ja0393170>.
- (124) Tobisu, M.; Shimasaki, T.; Chatani, N. Nickel-Catalyzed Cross-Coupling of Aryl Methyl Ethers with Aryl Boronic Esters. *Angew. Chemie - Int. Ed.* **2008**, *47* (26), 4866–4869. <https://doi.org/10.1002/anie.200801447>.
- (125) Yu, D. G.; Shi, Z. J. Mutual Activation: Suzuki-Miyaura Coupling through Direct Cleavage of the Sp² C–O Bond of Naphtholate. *Angew. Chemie - Int. Ed.* **2011**, *50* (31), 7097–7100. <https://doi.org/10.1002/anie.201101461>.
- (126) Cao, Z. C.; Yu, D. G.; Zhu, R. Y.; Wei, J. B.; Shi, Z. J. Direct Cross-Coupling of Benzyl Alcohols to Construct Diarylmethanes via Palladium Catalysis. *Chem. Commun.* **2015**, *51* (13), 2683–2686. <https://doi.org/10.1039/c4cc10084k>.
- (127) Nazari, S. H.; Bourdeau, J. E.; Talley, M. R.; Valdivia-Berroeta, G. A.; Smith, S. J.; Michaelis, D. J. Nickel-Catalyzed Suzuki Cross Couplings with Unprotected Allylic Alcohols Enabled by Bidentate N-Heterocyclic Carbene (NHC)/Phosphine Ligands. *ACS Catal.* **2018**, *8* (1), 86–89. <https://doi.org/10.1021/acscatal.7b03079>.
- (128) Akkarasamiyo, S.; Margalef, J.; Samec, J. S. M. Nickel-Catalyzed Suzuki-Miyaura Cross-Coupling Reaction of Naphthyl and Quinolyl Alcohols with Boronic Acids. *Org. Lett.* **2019**, *21* (12), 4782–4787. <https://doi.org/10.1021/acs.orglett.9b01669>.
- (129) *Mineral Commodity Summaries*; 2021. <https://doi.org/10.3133/mcs2021>.
- (130) Cárdenas, D. J. Advances in Functional-Group-Tolerant Metal-Catalyzed Alkyl–Alkyl Cross-Coupling Reactions. *Angew. Chemie Int. Ed.* **2003**, *42* (4), 384–387. <https://doi.org/10.1002/anie.200390123>.
- (131) Netherton, M. R.; Dai, C.; Neuschütz, K.; Fu, G. C. Room-Temperature Alkyl–Alkyl Suzuki Cross-Coupling of Alkyl Bromides That Possess β Hydrogens [1]. *J. Am. Chem. Soc.* **2001**, *123* (41), 10099–10100. <https://doi.org/10.1021/ja011306o>.

- (132) Ishiyama, T.; Abe, S.; Miyaura, N.; Suzuki, A. Palladium-Catalyzed Alkyl-Alkyl Cross-Coupling Reaction of 9-Alkyl-9-BBN Derivatives with Iodoalkanes Possessing β -Hydrogens. *Chem. Lett.* **1992**, *21* (4), 691–694. <https://doi.org/10.1246/cl.1992.691>.
- (133) Kirchhoff, J. H.; Netherton, M. R.; Hills, I. D.; Fu, G. C. Boronic Acids: New Coupling Partners in Room-Temperature Suzuki Reactions of Alkyl Bromides. Crystallographic Characterization of an Oxidative-Addition Adduct Generated under Remarkably Mild Conditions. *J. Am. Chem. Soc.* **2002**, *124* (46), 13662–13663. <https://doi.org/10.1021/ja0283899>.
- (134) Kirchhoff, J. H.; Dai, C.; Fu, G. C. A Method for Palladium-Catalyzed Cross-Couplings of Simple Alkyl Chlorides: Suzuki Reactions Catalyzed by $[\text{Pd}_2(\text{dba})_3]/\text{PCy}_3$. *Angew. Chemie Int. Ed.* **2002**, *41* (11), 1945. [https://doi.org/10.1002/1521-3773\(20020603\)41:11<1945::aid-anie1945>3.0.co;2-7](https://doi.org/10.1002/1521-3773(20020603)41:11<1945::aid-anie1945>3.0.co;2-7).
- (135) Zhou, J.; Fu, G. C. Suzuki Cross-Couplings of Unactivated Secondary Alkyl Bromides and Iodides. *J. Am. Chem. Soc.* **2004**, *126* (5), 1340–1341. <https://doi.org/10.1021/ja039889k>.
- (136) González-Bobes, F.; Fu, G. C. Amino Alcohols as Ligands for Nickel-Catalyzed Suzuki Reactions of Unactivated Alkyl Halides, Including Secondary Alkyl Chlorides, with Arylboronic Acids. *J. Am. Chem. Soc.* **2006**, *128* (16), 5360–5361. <https://doi.org/10.1021/ja0613761>.
- (137) Zultanski, S. L.; Fu, G. C. Nickel-Catalyzed Carbon-Carbon Bond-Forming Reactions of Unactivated Tertiary Alkyl Halides: Suzuki Arylations. *J. Am. Chem. Soc.* **2013**, *135* (2), 624–627. <https://doi.org/10.1021/ja311669p>.
- (138) Saito, B.; Fu, G. C. Alkyl-Alkyl Suzuki Cross-Couplings of Unactivated Secondary Alkyl Halides at Room Temperature. *J. Am. Chem. Soc.* **2007**, *129* (31), 9602–9603. <https://doi.org/10.1021/ja074008l>.
- (139) Lu, Z.; Fu, G. C. Alkyl-Alkyl Suzuki Cross-Coupling of Unactivated Secondary Alkyl Chlorides. *Angew. Chemie Int. Ed.* **2010**, *49* (37), 6676–6678. <https://doi.org/10.1002/anie.201003272>.

- (140) Saito, B.; Fu, G. C. Enantioselective Alkyl-Alkyl Suzuki Cross-Couplings of Unactivated Homobenzylic Halides. *J. Am. Chem. Soc.* **2008**, *130* (21), 6694–6695. <https://doi.org/10.1021/ja8013677>.
- (141) Owston, N. A.; Fu, G. C. Asymmetric Alkyl-Alkyl Cross-Couplings of Unactivated Secondary Alkyl Electrophiles: Stereoconvergent Suzuki Reactions of Racemic Acylated Halohydrins. *J. Am. Chem. Soc.* **2010**, *132* (34), 11908–11909. <https://doi.org/10.1021/ja105924f>.
- (142) Wilsily, A.; Tramutola, F.; Owston, N. A.; Fu, G. C. New Directing Groups for Metal-Catalyzed Asymmetric Carbon-Carbon Bond-Forming Processes: Stereoconvergent Alkyl-Alkyl Suzuki Cross-Couplings of Unactivated Electrophiles. *J. Am. Chem. Soc.* **2012**, *134* (13), 5794–5797. <https://doi.org/10.1021/ja301612y>.
- (143) Lu, Z.; Wilsily, A.; Fu, G. C. Stereoconvergent Amine-Directed Alkyl-Alkyl Suzuki Reactions of Unactivated Secondary Alkyl Chlorides. *J. Am. Chem. Soc.* **2011**, *133* (21), 8154–8157. <https://doi.org/10.1021/ja203560q>.
- (144) Zultanski, S. L.; Fu, G. C. Catalytic Asymmetric γ -Alkylation of Carbonyl Compounds via Stereoconvergent Suzuki Cross-Couplings. *J. Am. Chem. Soc.* **2011**, *133* (39), 15362–15364. <https://doi.org/10.1021/ja2079515>.
- (145) Fraser, J.; Anderson, J.; Lazuen, J.; Lu, Y.; Heathman, O.; Brewster, N.; Bedder, J.; Masson, O. *Study on Future Demand and Supply Security of Nickel for Electric Vehicle Batteries*; Luxembourg, 2021. <https://doi.org/10.2760/212807>.
- (146) Wang, X.; Wang, S.; Xue, W.; Gong, H. Nickel-Catalyzed Reductive Coupling of Aryl Bromides with Tertiary Alkyl Halides. *J. Am. Chem. Soc.* **2015**, *137* (36), 11562–11565. <https://doi.org/10.1021/jacs.5b06255>.
- (147) Wang, X.; Ma, G.; Peng, Y.; Pitsch, C. E.; Moll, B. J.; Ly, T. D.; Wang, X.; Gong, H. Ni-Catalyzed Reductive Coupling of Electron-Rich Aryl Iodides with Tertiary Alkyl Halides. *J. Am. Chem. Soc.* **2018**, *140* (43), 14490–14497. <https://doi.org/10.1021/jacs.8b09473>.

- (148) Cherney, A. H.; Hedley, S. J.; Mennen, S. M.; Tedrow, J. S. Xantphos as a Branch-Selective Ligand for the Acyclic Sec-Alkyl Negishi Cross-Coupling of Heteroaryl Halides. *Organometallics* **2019**, *38* (1), 97–102. <https://doi.org/10.1021/acs.organomet.8b00590>.
- (149) Kharasch, M. S.; Fields, E. K. Factors Determining the Course and Mechanisms of Grignard Reactions. IV. The Effect of Metallic Halides on the Reaction of Aryl Grignard Reagents and Organic Halides. *J. Am. Chem. Soc.* **1941**, *63* (9), 2316–2320. <https://doi.org/10.1021/ja01854a006>.
- (150) Tamura, M.; Kochi, J. K. Vinylation of Grignard Reagents. Catalysis by Iron. *J. Am. Chem. Soc.* **1971**, *93* (6), 1487–1489. <https://doi.org/10.1021/ja00735a030>.
- (151) Tamura, M.; Kochi, J. Coupling of Grignard Reagents with Organic Halides. *Synth.* **1971**, (6), 303–305. <https://doi.org/10.1055/s-1971-35043>.
- (152) Tamao, K.; Sumitani, K.; Kumada, M. Selective Carbon-Carbon Bond Formation by Cross-Coupling of Grignard Reagents with Organic Halides. Catalysis by Nickel-Phosphine Complexes. *J. Am. Chem. Soc.* **1972**, *94* (12), 4374–4376. <https://doi.org/10.1021/ja00767a075>.
- (153) Corriu, R. J. P.; Masse, J. P. Activation of Grignard Reagents by Transition-Metal Complexes. A New and Simple Synthesis of Trans-Stilbenes and Polyphenyls. *J. Chem. Soc. Chem. Commun.* **1972**, 0 (3), 7062. <https://doi.org/10.1039/C3972000144a>.
- (154) Yamamura, M.; Moritani, I.; Murahashi, S. I. The Reaction of σ -Vinylpalladium Complexes with Alkylolithiums. Stereospecific Syntheses of Olefins from Vinyl Halides and Alkylolithiums. *J. Organomet. Chem.* **1975**, *91* (2). [https://doi.org/10.1016/S0022-328X\(00\)89636-9](https://doi.org/10.1016/S0022-328X(00)89636-9).
- (155) Fürstner, A.; Leitner, A. Iron-Catalyzed Cross-Coupling Reactions of Alkyl-Grignard Reagents with Aryl Chlorides, Tosylates, and Triflates. *Angew. Chemie - Int. Ed.* **2002**, *41* (4), 609–612. [https://doi.org/10.1002/1521-3773\(20020215\)41:4<609::AID-ANIE609>3.0.CO;2-M](https://doi.org/10.1002/1521-3773(20020215)41:4<609::AID-ANIE609>3.0.CO;2-M).
- (156) Scheiper, B.; Bonnekessel, M.; Krause, H.; Fürstner, A. Selective Iron-Catalyzed

Cross-Coupling Reactions of Grignard Reagents with Enol Triflates, Acid Chlorides, and Dichloroarenes. *J. Org. Chem.* **2004**, *69* (11), 3943–3949. <https://doi.org/10.1021/jo0498866>.

(157) Fürstner, A.; Martin, R.; Krause, H.; Seidel, G.; Goddard, R.; Lehmann, C. W. Preparation, Structure, and Reactivity of Nonstabilized Organoiron Compounds. Implications for Iron-Catalyzed Cross Coupling Reactions. *J. Am. Chem. Soc.* **2008**, *130* (27), 8773–8787. <https://doi.org/10.1021/ja801466t>.

(158) Hedström, A.; Bollmann, U.; Bravidor, J.; Norrby, P.-O. Iron-Catalyzed Coupling of Aryl Grignard Reagents with Alkyl Halides: A Competitive Hammett Study. *Chem. - A Eur. J.* **2011**, *17* (43), 11991–11993. <https://doi.org/10.1002/chem.201100467>.

(159) Adrio, J.; Carretero, J. C. Functionalized Grignard Reagents in Kumada Cross-Coupling Reactions. *ChemCatChem* **2010**, *2* (11), 1384–1386. <https://doi.org/10.1002/cctc.201000237>.

(160) Nakamura, M.; Ito, S.; Matsuo, K.; Nakamura, E. Iron-Catalyzed Chemoselective Cross-Coupling of Primary and Secondary Alkyl Halides with Arylzinc Reagents. *Synlett* **2005**, No. 11, 1794–1798. <https://doi.org/10.1055/s-2005-871541>.

(161) Bedford, R. B.; Huwe, M.; Wilkinson, M. C. Iron-Catalysed Negishi Coupling of Benzyl Halides and Phosphates. *Chem. Commun.* **2009**, No. 5, 600–602. <https://doi.org/10.1039/b818961g>.

(162) Hatakeyama, T.; Kondo, Y.; Fujiwara, Y. I.; Takaya, H.; Ito, S.; Nakamura, E.; Nakamura, M. Iron-Catalysed Fluoroaromatic Coupling Reactions under Catalytic Modulation with 1,2-Bis(Diphenylphosphino)Benzene. *Chem. Commun.* **2009**, No. 10, 1216–1218. <https://doi.org/10.1039/b820879d>.

(163) Ito, S.; Fujiwara, Y. I.; Nakamura, E.; Nakamura, M. Iron-Catalyzed Cross-Coupling of Alkyl Sulfonates with Arylzinc Reagents. *Org. Lett.* **2009**, *11* (19), 4306–4309. <https://doi.org/10.1021/ol901610a>.

(164) Adams, C. J.; Bedford, R. B.; Carter, E.; Gower, N. J.; Haddow, M. F.; Harvey, J.

N.; Huwe, M.; Cartes, M. Á.; Mansell, S. M.; Mendoza, C.; et al. Iron(I) in Negishi Cross-Coupling Reactions. *J. Am. Chem. Soc.* **2012**, *134* (25), 10333–10336. <https://doi.org/10.1021/ja303250t>.

(165) Bedford, R. B.; Carter, E.; Cogswell, P. M.; Gower, N. J.; Haddow, M. F.; Harvey, J. N.; Murphy, D. M.; Neeve, E. C.; Nunn, J. Simplifying Iron-Phosphine Catalysts for Cross-Coupling Reactions. *Angew. Chemie - Int. Ed.* **2013**, *52* (4), 1285–1288. <https://doi.org/10.1002/anie.201207868>.

(166) Brown, C. A.; Nile, T. A.; Mahon, M. F.; Webster, R. L. Iron Catalysed Negishi Cross-Coupling Using Simple Ethyl-Monophosphines. *Dalt. Trans.* **2015**, *44* (27), 12189–12195. <https://doi.org/10.1039/c5dt00112a>.

(167) Messinis, A. M.; Luckham, S. L. J.; Wells, P. P.; Gianolio, D.; Gibson, E. K.; O'Brien, H. M.; Sparkes, H. A.; Davis, S. A.; Callison, J.; Elorriaga, D.; et al. The Highly Surprising Behaviour of Diphosphine Ligands in Iron-Catalysed Negishi Cross-Coupling. *Nat. Catal.* **2019**, *2* (2), 123–133. <https://doi.org/10.1038/s41929-018-0197-z>.

(168) Hatakeyama, T.; Hashimoto, T.; Kondo, Y.; Fujiwara, Y.; Seike, H.; Takaya, H.; Tamada, Y.; Ono, T.; Nakamura, M. Iron-Catalyzed Suzuki-Miyaura Coupling of Alkyl Halides. *J. Am. Chem. Soc.* **2010**, *132* (31), 10674–10676. <https://doi.org/10.1021/ja103973a>.

(169) Hashimoto, T.; Hatakeyama, T.; Nakamura, M. Stereospecific Cross-Coupling between Alkenylboronates and Alkyl Halides Catalyzed by Iron-Bisphosphine Complexes. *J. Org. Chem.* **2012**, *77* (2), 1168–1173. <https://doi.org/10.1021/jo202151f>.

(170) Bedford, R. B.; Brenner, P. B.; Carter, E.; Carvell, T. W.; Cogswell, P. M.; Gallagher, T.; Harvey, J. N.; Murphy, D. M.; Neeve, E. C.; Nunn, J.; et al. Expedient Iron-Catalyzed Coupling of Alkyl, Benzyl and Allyl Halides with Arylboronic Esters. *Chem. - A Eur. J.* **2014**, *20* (26), 7935–7938. <https://doi.org/10.1002/chem.201402174>.

(171) Daifuku, S. L.; Kneebone, J. L.; Snyder, B. E. R.; Neidig, M. L. Iron(II) Active Species in Iron-Bisphosphine Catalyzed Kumada and Suzuki-Miyaura Cross-Couplings of Phenyl Nucleophiles and Secondary Alkyl Halides. *J. Am. Chem. Soc.* **2015**, *137* (35),

11432–11444. <https://doi.org/10.1021/jacs.5b06648>.

(172) Hedström, A.; Izakian, Z.; Vreto, I.; Wallentin, C. J.; Norrby, P. O. On the Radical Nature of Iron-Catalyzed Cross-Coupling Reactions. *Chem. - A Eur. J.* **2015**, *21* (15), 5946–5953. <https://doi.org/10.1002/chem.201406096>.

(173) Hazari, N.; Melvin, P. R.; Beromi, M. M. Well-Defined Nickel and Palladium Precatalysts for Cross-Coupling. *Nat. Rev. Chem.* **2017**, *1* (3), 0025. <https://doi.org/10.1038/s41570-017-0025>.

(174) Yu, D.-G.; Li, B.-J.; Shi, Z.-J. Exploration of New C–O Electrophiles in Cross-Coupling Reactions. *Acc. Chem. Res.* **2010**, *43* (12), 1486–1495. <https://doi.org/10.1021/ar100082d>.

Chapter 2.

Suzuki-Miyaura Cross-Coupling Reactions of Alkyl Halides and
Unactivated Aryl Boronic Esters Catalyzed by Iron-Based
Complexes Developed Through Rational Ligand Design

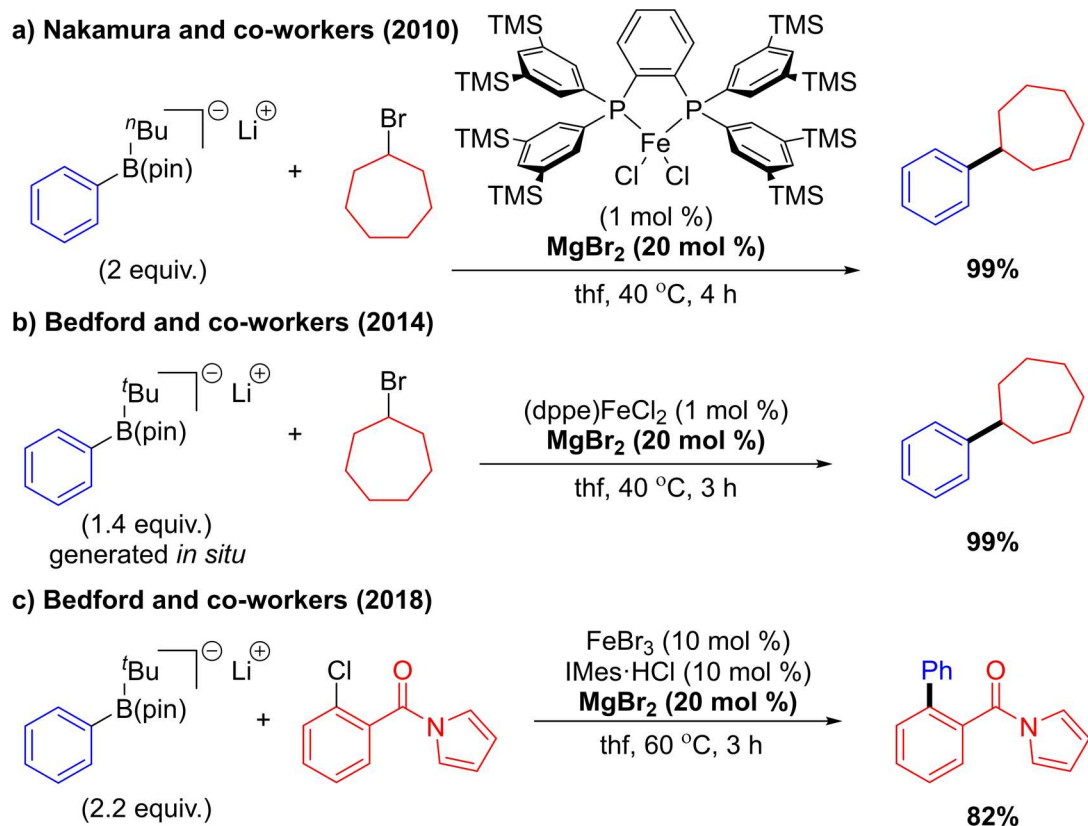
2.1 Introduction

Transition metal-catalyzed cross-coupling reactions are an important set of tools for the modern synthetic organic chemist to construct carbon-carbon and carbon-heteroatom bonds of increasing diversity and complexity.¹ Perhaps the most notable of the carbon-carbon bond-forming cross-coupling reactions is the Suzuki-Miyaura variant, which employs organoboron nucleophiles.^{2,3} The tremendous utility of the Suzuki-Miyaura cross-coupling reaction is largely due to the organoboron reagents, which are relatively nontoxic, easily synthesized, and generally stable to air and moisture⁴ compared to alternative organometallic nucleophiles.

Despite its widespread application across various industries, the Suzuki-Miyaura cross-coupling reaction is typically carried out using palladium-based catalysts. These catalysts have enabled the efficient incorporation of a wide variety of substrates under mild reaction conditions with low catalyst loadings, but palladium is toxic,⁵ costly, and suffers from high cost volatility. Moreover, palladium-based catalysts encounter an important substrate scope limitation in C(sp³)-hybridized electrophiles, due to facile β -hydride elimination side reactions which lead to catalyst deactivation.⁶ These concerns are especially magnified in the pharmaceutical industry, where extensive purification of toxic metal catalysts from the active pharmaceutical ingredient and sourcing of palladium can lead to higher costs for consumers, and substrate limitations lead to unexplored chemical motifs for therapeutic activity.⁷

In order to address these limitations, many groups have turned their attention to the exploration of more environmentally and economically sustainable first-row transition metal-based catalysts for cross-coupling reactions. Of the first-row transition metals, Cu

and co-workers have found that catalytic systems employing nickel-based complexes demonstrate considerable success for the cross-coupling reaction between alkyl halide substrates and organoborane nucleophiles.^{6,8,9} In recent years, less toxic iron-based catalytic systems have been developed for cross-coupling reactions of various organometallic nucleophiles by the groups of Fürstner,^{10,11} Nakamura,^{12–15} Bedford,^{16–18} and others.^{19–23} The majority of organometallic nucleophiles employed in cross-coupling reactions catalyzed by iron-based complexes are Grignard-type transmetalating reagents (i.e. Kumada-Tamao-Corriu-type cross-coupling reactions). At the onset of our investigations, iron-catalyzed Suzuki-Miyaura cross-coupling reactions using the potentially more easily handled aryl organoboron reagents were limited to only three examples (Scheme 2.1).^{14,17,18} However, the organoboron reagents employed in all three examples were borate species preactivated with pyrophoric alkyllithium reagents, and all required the addition of magnesium bromide for high yields. The requirement of difficult-to-handle preactivated borate species in these reactions nullifies one of the key advantages of the Suzuki-Miyaura cross-coupling reaction and limits the application of this methodology in industrial contexts. Moreover, it is possible that the magnesium additive in these examples is required to overcome a Schlenk equilibrium which disfavors iron-to-boron transmetalation,²⁴ and the reaction proceeds instead *via* iron-to-magnesium transmetalation.



Scheme 2.1. Examples of Suzuki-Miyaura-type cross-coupling reactions of aryl organoboron reagents catalyzed by iron-based complexes which require magnesium bromide additives for high yields.

In this chapter, we discuss the development of an iron-based catalyst system for the cross-coupling of alkyl halides and unactivated arylboronic esters in the absence of magnesium additives.²⁵ Mechanistic implications from these studies were applied toward the rationally guided development of a family of second-generation iron-based catalysts which demonstrated a broadened substrate scope including heteroaromatic boronic esters and tertiary alkyl halides.²⁶ An emphasis is placed on examining the transmetalation step in these reactions, which we believe is of particular importance due to the divergent levels of efficiency observed between iron-catalyzed Kumada-Tamao-Corriu-type reactions of Grignard reagents¹² and the corresponding Suzuki-Miyaura reactions of organoboron reagents.

2.2 The impact of promoting transmetalation and regulating aggregation on cross-coupling reactions catalyzed by iron-based complexes

The efficiency observed in iron-catalyzed cross-coupling reactions when the transmetalating reagent is a Grignard reagent led us to believe that transmetalation of the organoboron reagents was a limiting factor in iron-catalyzed Suzuki-Miyaura reactions. For comparison's sake, we turned to the significant body of work that had been established for the analogous palladium-catalyzed systems in order to better understand the transmetalation step in iron-catalyzed Suzuki-Miyaura cross-coupling reactions (Figure 2.1a). It should be noted that our understanding of these reactions follow the iron(II)/iron(III) mechanistic framework proposed by Nakamura¹⁴ and supported by Neidig,^{27,28} but we cannot definitively rule out other proposed mechanisms such as the iron(I)/iron(II)/iron(III) cycle favored by Bedford¹⁷ and Norrby.²⁹ As discussed in Chapter 1.2.2, extensive studies have been carried out to elucidate the role of base additives in palladium-catalyzed Suzuki-Miyaura reactions.³⁰⁻³⁵ Two viable pathways have been proposed: the base can form a nucleophilic organoborate species *in situ* or it converts the palladium(II) halide formed after oxidative addition into a palladium(II) hydroxide that is better suited for transmetalation with boronic acids³⁶ (Figure 2.1b). While neither pathway has been definitively ruled out, recent studies by the groups of Hartwig³³ and Denmark³⁴ have implicated the formation of palladium hydroxides in catalytic Suzuki-Miyaura cross-coupling reactions. While palladium hydroxide species can exist as mononuclear complexes in solution,³⁷ the analogous formation of iron hydroxides or alkoxides lead to irreversible aggregation of higher-ordered iron species,³⁸⁻⁴⁰ which we believe are deactivated for cross-coupling reactions.

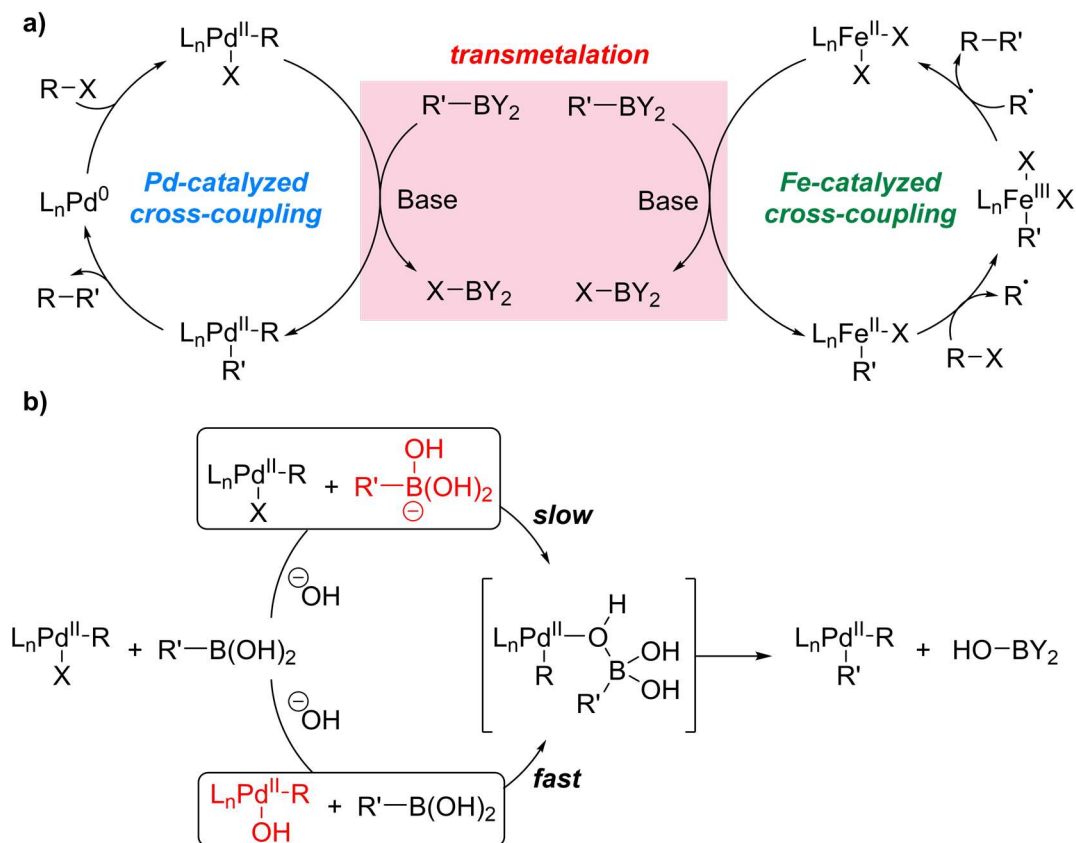


Figure 2.1. a) Mechanistic comparison between palladium-catalyzed and iron-catalyzed Suzuki-Miyaura cross-coupling reactions of halide electrophiles and organoboron nucleophiles. The base-facilitated transmetalation step is highlighted in red. b) Proposed pathways for transmetalation in palladium-catalyzed Suzuki-Miyaura cross-coupling reactions and a spectroscopically identified intermediate likely involved in transmetalation.

Transmetalation from boron to iron in iron-catalyzed Suzuki-Miyaura reactions could be inherently disfavored because iron is less electronegative than boron. To explore this hypothesis, Dr. Michael Crockett developed a computational model to evaluate the transmetalation from phenyl boronic acid pinacol ester (PhB(pin)) and (dppe)Fe^{II}X₂ complexes bearing various anionic ligands (Figure 2.2).^{25,41} The computations demonstrated that transmetalation reactions from PhB(pin) to iron chloride complexes feature prohibitively high thermodynamic barriers, which has also been observed in similar computations using palladium-based complexes (Figure 2.2, black trace).⁴² On the other hand, transmetalation reactions from PhB(pin) to iron methoxide complexes were

significantly less uphill than those from the iron chloride complexes, with thermodynamic barriers that are energetically surmountable at room temperature (Figure 2.2, red trace). Nonetheless, these values were still nearly 10 kcal/mol higher than those of analogous palladium-catalyzed systems,⁴² underscoring the reactivity differences between palladium- and iron-based complexes.

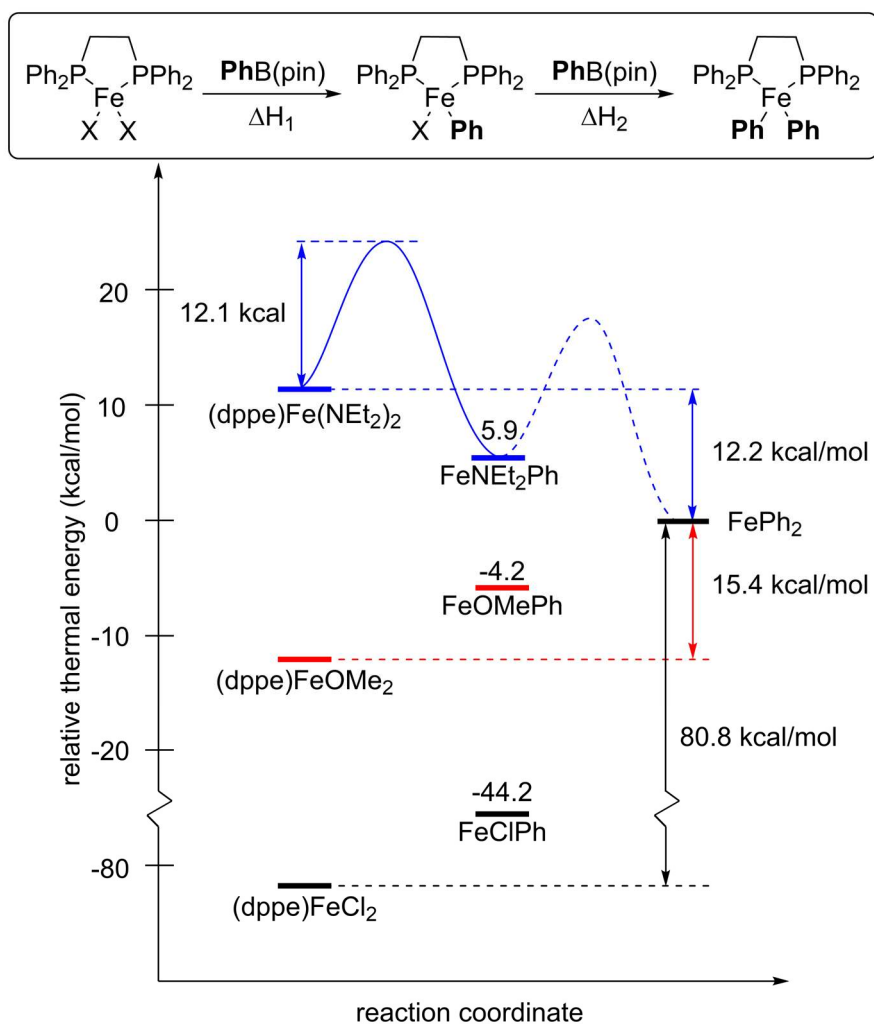
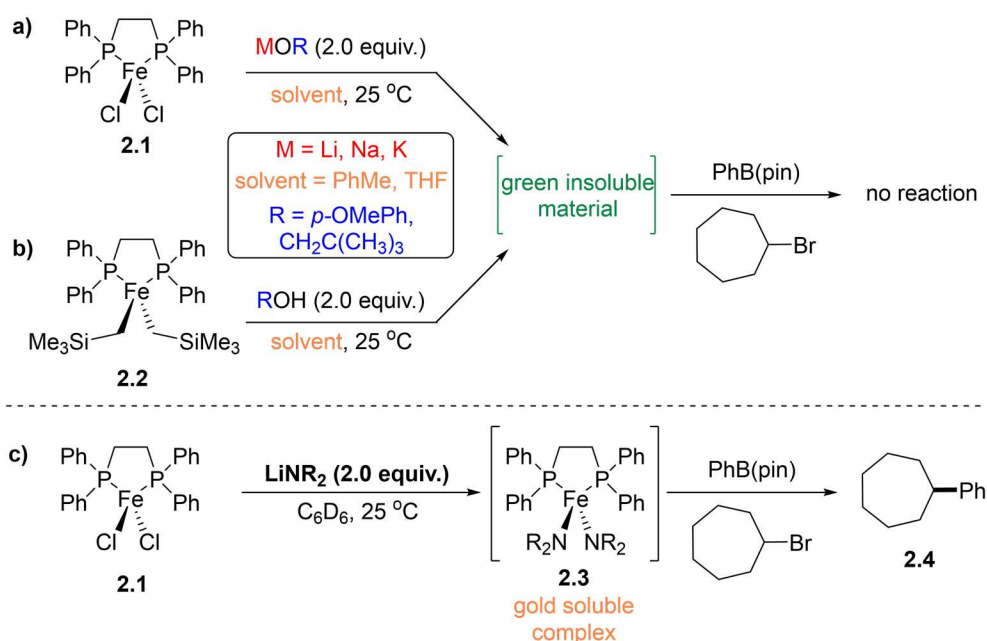


Figure 2.2. Density functional theory (B3LYP/6-31G*) computed energies for the transmetalation from boron to iron in reactions between PhB(pin) and (dppe)Fe^{II}X₂.

The implication that transmetalation from iron alkoxides could be thermodynamically accessible at room temperature compelled Dr. Crockett to attempt the

synthesis of mononuclear iron alkoxide complexes for use in cross-coupling reactions (Scheme 2.2). Unfortunately, neither a salt metathesis reaction of a metal alkoxide with (dppe)FeCl₂ (**2.1**) (Scheme 2.2a) nor a protonolysis reaction of (dppe)Fe(CH₂SiMe₃)₂ (**2.2**) (Scheme 2.2b)⁴⁰ cleanly produced the desired iron alkoxide. Instead, both reactions resulted in the formation of green insoluble material that proved inactive for cross-coupling reactions, which were presumed to be higher-ordered iron aggregates.



entry	R ¹	R ²	yield (%)
1	CH ₃	CH ₃	0%
2 ^a	CH ₃	Et	87%
3	Et	Et	38%
4	H	ⁿ Bu	7%
5	CH ₃	Ph	0%
6	ⁱ Pr	ⁱ Pr	7%
7	Si(CH ₃) ₃	Si(CH ₃) ₃	0%

Scheme 2.2. Attempted synthesis of (dppe)Fe(OR)₂ via a) salt metathesis, b) protonolysis; c) Synthesis of (dppe)Fe(NR₂)₂ and evaluation of activity towards cross-coupling reaction of PhB(pin) and bromocycloheptane with screening of various LiNR₂ sources. ^athe catalytic reaction employing 10 mol % (dppe)Fe(NMeEt)₂ produced the cross-coupled product in 31% yield.

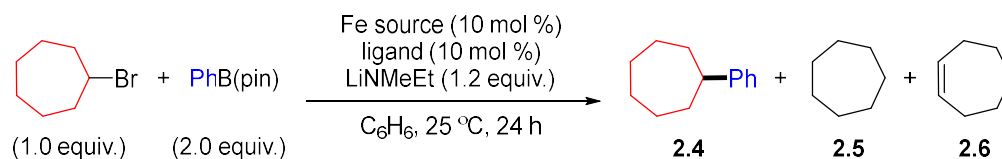
However, Dr. Crockett's computational studies of the transmetalation reaction also predicted that transmetalation from PhB(pin) to iron amide complexes would be

thermodynamically favorable and kinetically accessible at room temperature (Figure 2.2, blue trace).^{25,41} An attempt to synthesize the corresponding iron amide intermediate **2.3** through a salt metathesis reaction of lithium diethylamide and **2.1** resulted in a gold-colored homogeneous mixture that manifested as a single new paramagnetic species by ¹H NMR spectroscopy. Addition of a stoichiometric amount of coupling partners PhB(pin) and bromocycloheptane to the reaction mixture produced the cross-coupled product **2.4** in 38% yield (Scheme 2.2, entry 3). The ability to modify the amide substituents enabled a screen of various lithium amides for optimization, of which it was determined that lithium ethylmethylamide performed best (Scheme 2.2, entry 2). Successful cross-coupling was found to be particularly sensitive to the steric properties of the amide substituents, as amides that were significantly smaller or larger than ethylmethylamide resulted in much lower yields (Scheme 2.2, entries 1, 4-7). Most encouragingly, a catalytic amount of the iron amide resulting from salt metathesis with lithium ethylmethylamide (10 mol %) produced the cross-coupled product in 31% yield.

At this point, Dr. Crockett and Dr. Chet Tyrol evaluated a wide variety of monodentate and bidentate phosphorus-based and nitrogen-based ligands for their ability to promote catalytic cross-coupling between PhB(pin) and bromocycloheptane.^{41,43} Of the ligands screened, it was found that bis(oxazoline) ligands were exceptionally effective for the catalytic transformation (Table 2.1). Reactions carried out with iron dichloride in the absence of any ligand produced the cross-coupled product **2.4** in 25% yield, with significant byproduct formation resulting from elimination of the electrophile (**2.6**) (Table 2.1, entry 1). Byproduct formation was reduced and yields were significantly higher when the commercially available cyanated bis(oxazoline) ligand **2.9** was used (Table 2.1, entries

4-5) rather than the corresponding unsubstituted ligand **2.7** (Table 2.1, entry 2) or a bis(oxazoline) bearing geminal dimethyl substituents (**2.8**) (Table 2.1, entry 3).

Table 2.1. Screen of iron-based complexes supported by bis(oxazoline) ligands for promoting the Suzuki-Miyaura cross-coupling reaction between PhB(pin) and bromocycloheptane.



entry	Fe source	ligand	2.4 (%)	2.5 (%)	2.6 (%)
1	FeCl ₂	none	25	15	48
2	FeCl ₂	 2.7	36	14	16
3	FeCl ₂	 2.8	25	16	26
4	FeCl ₂	 2.9	58	14	10
5 ^a	FeCl ₂	2.9	72	6	6
6	 2.10	none	74	0	10
7 ^b	2.10	2.9	82	1	7
8 ^c	2.10	2.9	89	2	6
9 ^{bd}	2.10	2.9	75	2	13
10 ^{be}	2.10	2.9	69	1	19

^a 20% of **2.9**. ^b 48 h. ^c 48 h; 10% **2.10** and 60% LiNMeEt added after 24 h. ^d 5% **2.10** and **2.9**. ^e 1% **2.10** and **2.9**.

Moreover, it was determined that discretely synthesized iron complex **2.10** featuring a monoanionic cyanobis(oxazoline) ligand was more effective at carrying out the

cross-coupling reaction (Table 2.1, entry 6) than if the catalyst were formed *in situ* from **2.9** and iron dichloride. (*cf.* Table 2.1, entry 4.) The addition of 10 mol % exogenous ligand further improved yields when the reaction was allowed to run longer (Table 2.1, entry 7), which we believe is a critical component to discouraging aggregation (*vide infra*). Full consumption of the starting material could be achieved with the addition of catalyst and base at 24 hours (Table 2.1, entry 8). Catalyst loading could be reduced to as low as 1%, but formation of the cycloheptene byproduct **2.6** became more prevalent.

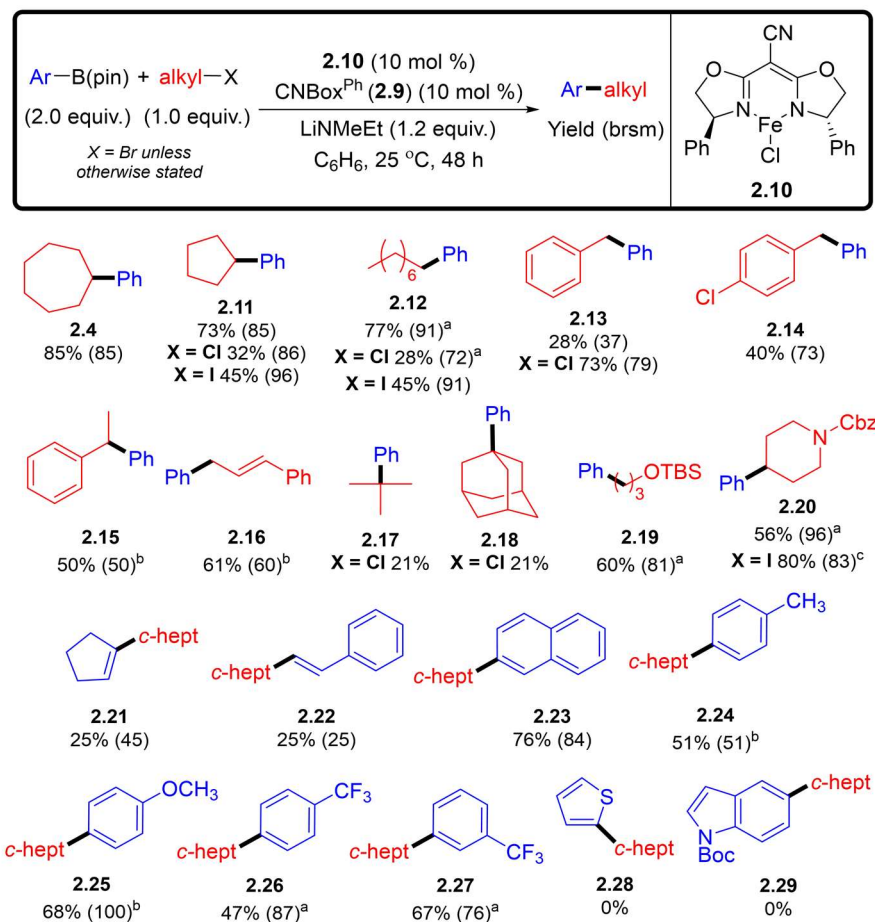
In summary, work by Dr. Crockett and Dr. Tyrol established that the key limitation that had previously limited iron-catalyzed Suzuki-Miyaura cross-coupling reactions was the irreversible formation of iron oxide aggregates. Computational studies demonstrated that lithium amides could serve as effective bases to promote transmetalation between boron and iron in order to enable the cross-coupling transformation. A wide-ranging survey of ligand frameworks highlighted the unique effectiveness of monoanionic cyanated phenylbis(oxazoline) ligands for high yields of cross-coupled product.

2.3 Evaluation of substrate scope of a Suzuki-Miyaura cross-coupling reaction catalyzed by iron-based complexes and extension to a pharmaceutical target

With optimal conditions in hand, the generality of the cross-coupling reaction towards a variety of substrates was explored (Table 2.2). Substrates **2.11-2.20** employing different alkyl halide coupling partners were synthesized by Dr. Tyrol. Primary and secondary alkyl halides were well tolerated (**2.4**, **2.11-2.12**), though the primary alkyl halides required heating to reach yields comparable to the secondary alkyl halides. Typically, the alkyl bromides were superior to the alkyl iodides, which were in turn

superior to the alkyl chlorides. This trend was reversed for **2.13-2.16** derived from activated alkyl halides, in which the chloride delivered the product in higher yield. It is believed that competitive homocoupling of the stabilized benzyl or allyl radical impedes formation of the cross-coupled product.⁴⁴ Tertiary alkyl chlorides could be used to deliver quaternary products **2.17-2.18**, albeit in low yields. Lastly, substrates containing a protected alcohol (**2.19**) and a protected amine (**2.20**) were tolerated, though the highly basic reaction conditions precluded toleration of functional groups containing labile protons (i.e. ketones, esters, amides, unprotected alcohols).

Table 2.2. Substrate scope of a Suzuki-Miyaura cross-coupling reaction between aryl boronic acid pinacol esters and alkyl halides catalyzed by iron-based complex **2.10**. Isolated yields are reported with yields based on recovered starting material appearing in parentheses.

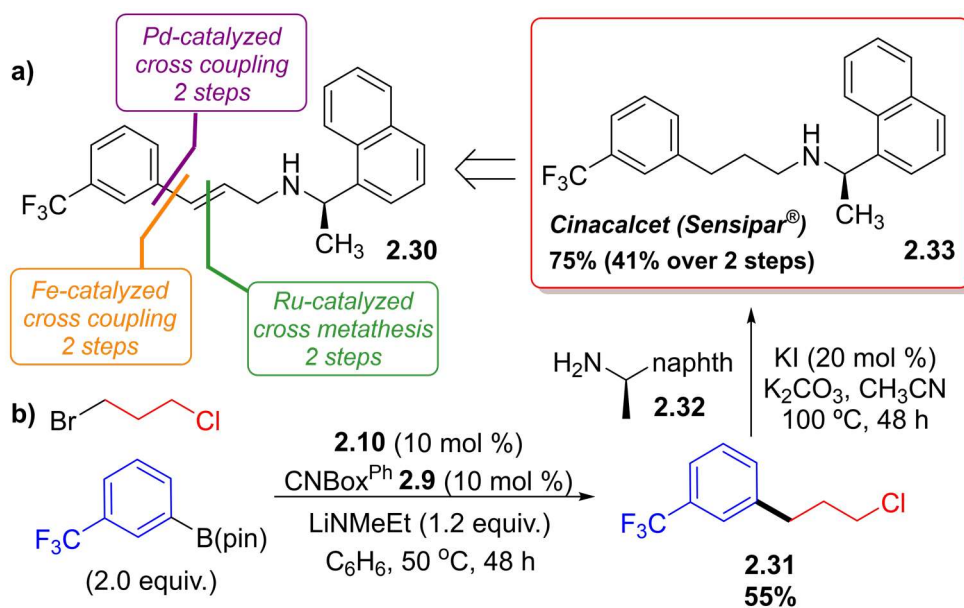


^a 50 °C. ^b 10 mol % **2.10** and 0.6 equiv. LiNMeEt added after 24 h. ^c toluene was used as solvent.

The identity of the boronic acid pinacol ester was screened in the cross-coupling reaction with bromocycloheptane to deliver substrates **2.21-2.29**. Alkenyl boronic esters could be incorporated to deliver **2.21-2.22** in low yields. Cross-coupling of naphthyl boronic ester to deliver **2.23** proceeded similarly to phenyl boronic ester to deliver **2.4**. Electron-donating substituents on the aryl boronic esters were tolerated (**2.24-2.25**), though these reactions were sluggish as a result of slower transmetalation. The lowered efficiency could be overcome with the addition of **2.10** and base midway through the reaction. Electron-withdrawing substituents on the aryl boronic esters resulted in lowered reactivity, likely due to the formation of less reactive borate species with the amide, and required heating to liberate the amide base and achieve appreciable yields (**2.26-2.27**). Unfortunately, this catalytic system was unreactive toward heteroaromatic boronic esters (**2.28-2.29**). In most cases, the cross-coupling reaction proceeded without formation of side products and gave high yields based on recovered starting material.

To demonstrate the utility of the iron-catalyzed Suzuki-Miyaura cross-coupling reaction, we envisioned its application toward the synthesis of the active pharmaceutical ingredient Cinacalcet (trade name, Sensipar®).⁴⁵ Cinacalcet is a calcimimetic which is used for the treatment of secondary hyperparathyroidism, and in 2018 it was the 39th top selling small molecule drug on the market, grossing \$1.774 billion.⁴⁶ At the time of these investigations, the most efficient established methods for the synthesis of Cinacalcet employed two-step synthetic routes using noble metal catalysts to form the precursor **2.30**,⁴⁷⁻⁵⁰ which could then be elaborated to Cinacalcet following alkene hydrogenation (Scheme 2.3a). We envisioned that this step could be circumvented if the aliphatic skeleton of Cinacalcet could be incorporated by an iron-catalyzed Suzuki-Miyaura cross-coupling

reaction with the *meta*-trifluoromethylphenyl ring. Taking advantage of the chemoselectivity of our method for unactivated alkyl bromides over the corresponding chlorides (*vide supra*), intermediate **2.31** could be synthesized from 1-bromo-3-chloropropane and *meta*-trifluoromethylphenyl boronic acid pinacol ester in 55% yield (Scheme 2.3b). Subsequent alkylation of commercially available chiral amine **2.32** by Dr. Tyrol delivered Cinacalcet in 75% yield (41% overall). At the time of this writing, this route is the shortest reported synthesis of Cinacalcet (**2.33**) from commercially available starting materials and avoids the use of noble metal catalysts.

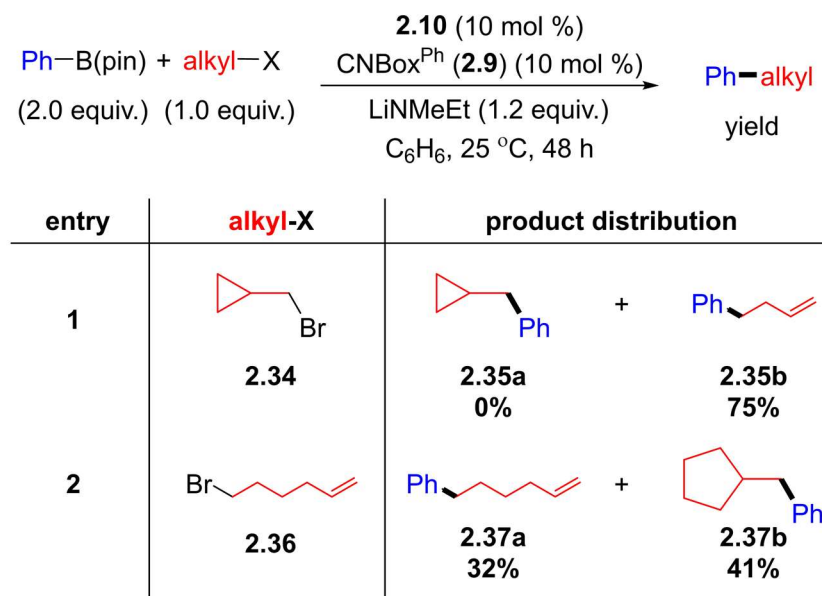


Scheme 2.3. a) Retrosynthetic analysis of previously reported synthetic routes to cinacalcet (Sensipar[®]), b) a two-step synthesis of cinacalcet (Sensipar[®]) using an iron-catalyzed Suzuki-Miyaura cross-coupling reaction between an aryl boronic ester and an alkyl halide.

2.4 Working mechanistic hypothesis and the development of principles for future ligand design

Our mechanistic understanding of the iron-catalyzed Suzuki-Miyaura cross-coupling reaction is chiefly guided by the iron(II)/iron(III) catalytic cycle proposed by Nakamura¹⁴ and supported by Neidig and co-workers^{27,28} for the coupling of alkyl

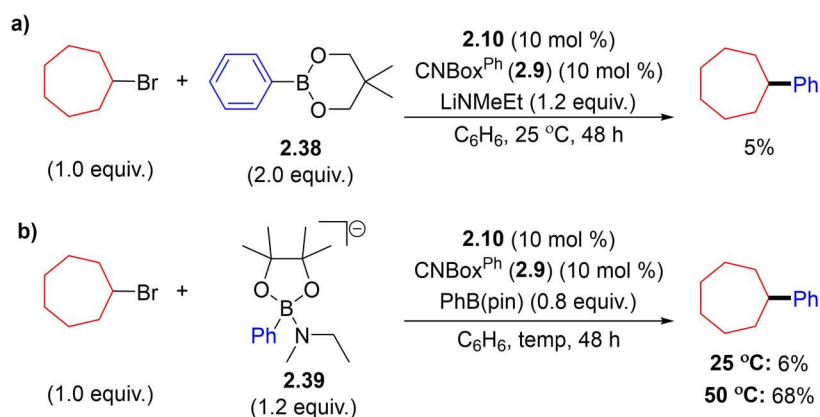
electrophiles with preactivated aryl borates. Regardless of the precise details of the mechanism, carbon-based radical intermediates are likely formed in our method because ring-opened product **2.35b** is exclusively formed in the cross-coupling reaction of PhB(pin) with radical clock substrate **2.34** (Scheme 2.4, entry 1). A mixture of the direct-cross-coupling product **2.37a** and ring-closure product **2.37b** is formed in the cross-coupling reaction between PhB(pin) and radical clock substrate **2.36** (Scheme 2.4, entry 2), which suggests that the radical intermediates have rearrangement rate constants on the order of 10^5 s^{-1} .⁵¹ Nakamura and co-workers observed similar results,¹⁴ which lead us to believe that the operative mechanism of our iron-catalyzed cross-coupling reaction follows a similar cycle.



Scheme 2.4. Reactions of radical clock substrates to examine the intermediacy of organic radicals in the iron-catalyzed Suzuki-Miyaura cross-coupling reaction.

A key distinction of our system compared to those reported by Nakamura and Bedford is our use of unactivated aryl boronic esters. While our reaction conditions also make use of a strong base capable of forming borate species upon reaction with the boronic

ester (pK_a of $\text{LiNR}_2 \approx 35$, *cf.* pK_a of $^n\text{BuLi} \approx 50$), several observations during optimization of reaction conditions lead us to believe that the role of the lithium amide is to activate the iron catalyst for transmetalation, rather than the boronic ester. While the conversion of $\text{PhB}(\text{pin})$ to a new boron species is observed by ^{11}B NMR spectroscopy ($\text{PhB}(\text{pin})$: 31.0 ppm, new species: 7.5 ppm, referenced to $\text{BF}_3 \cdot \text{O}(\text{C}_2\text{H}_5)_2$: 0.0 ppm) when lithium ethylmethanamide is added,⁴¹ aryl boronic ester substrates that are expected to more readily form borate species result in low yields at room temperature (e.g. electron-deficient boronic esters **2.26-2.27**, and less sterically encumbered boronic acid neopentyl glycol ester **2.38**) (Table 2.2; Scheme 2.5a). Moreover, the borate species **2.39** synthesized discretely from $\text{PhB}(\text{pin})$ and lithium ethylmethanamide likewise leads to low yields of cross-coupled product **2.4** at room temperature (Scheme 2.5b). However, heating the reaction employing the preformed borate as a coupling partner resulted in higher yields, though these yields are still lower than that of the reaction using the unactivated boronic ester (Scheme 2.5b). Presumably, heating reactions of substrates that are prone to form borate intermediates can liberate the amide base (*vide supra*, Table 2.2, entries **2.26-2.27**).



Scheme 2.5. Reactions involving preactivated borate species in the Suzuki-Miyaura cross-coupling reaction catalyzed by iron-based complex **2.10**.

These observations lead us to propose the mechanistic framework outlined in Figure 2.3. Iron halide **2.10** undergoes salt metathesis with the lithium ethylmethanamide to form iron amide complex **2.40**, which is thermodynamically favorable for the transmetalation reaction with PhB(pin). The iron phenyl species **2.41** formed from the transmetalation reaction abstracts the halogen from the alkyl halide to generate a carbon-centered radical, which subsequently recombines with the aryl fragment to deliver the cross-coupled product. Mechanistic understanding of the carbon-carbon bond-forming step remains limited, and it is possible that the carbon-carbon bond is formed by an inner-sphere (*via* **2.42**) or outer-sphere mechanism (*via* radical rebound).

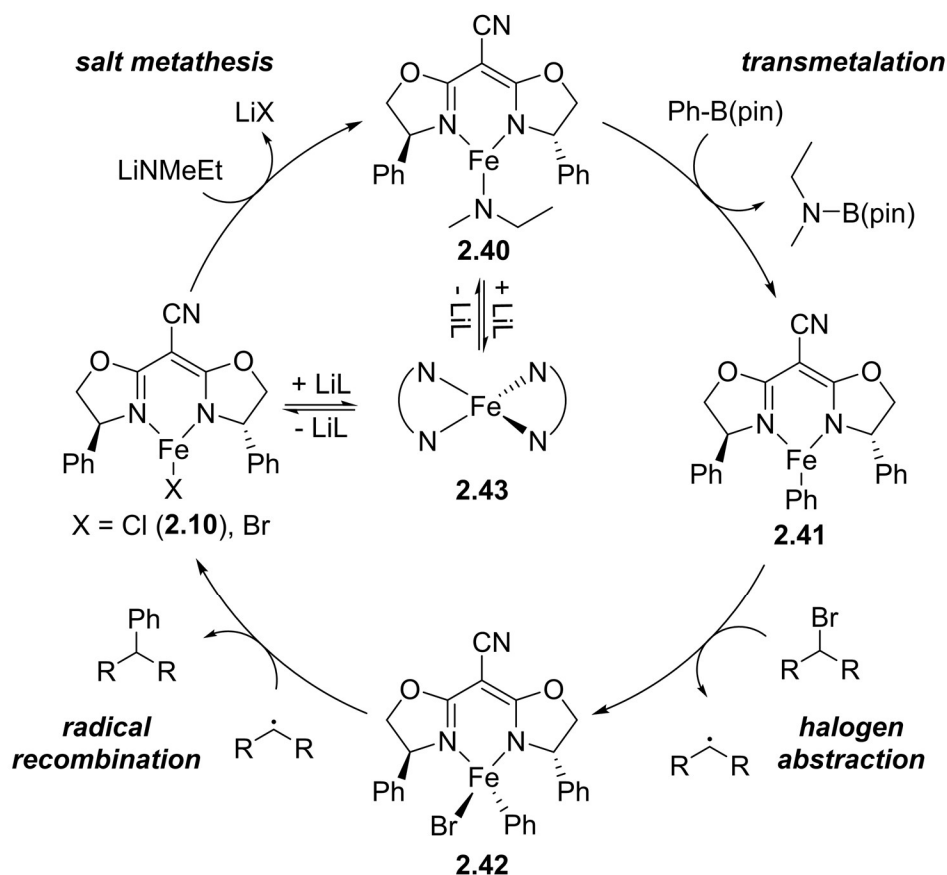


Figure 2.3. Working mechanistic hypothesis for the Suzuki-Miyaura cross-coupling reaction of alkyl electrophiles and unactivated aryl boronic acid pinacol esters catalyzed by an iron-based complex supported by a cyanated phenylbis(oxazoline) ligand (**2.10**).

Another key component of the reaction conditions which enabled higher yields of cross-coupled product and suppression of byproduct formation was the addition of a second equivalent of ligand **2.9** to the reaction mixture (*vide supra*, Table 2.1, entry 7). We hypothesize that the role of the second equivalent of ligand is to sequester the iron center and discourage aggregation by forming homoleptic complexes similar to **2.43** (Figure 2.3). Time course studies conducted by Dr. Crockett indicated that excess ligand provided greater selectivity at the cost of longer reaction times.⁴¹ The slower reaction rates lead us to believe that **2.43** is a catalyst resting state that exists off the catalytic cycle. Moreover, the increased acidity of ligand **2.9** in comparison to non-cyanated analogues **2.7-2.8** enable more facile deprotonation under the basic reaction conditions, which can then engage in reversible coordination with iron complexes **2.10** and **2.40** to access the homoleptic resting state and lead to superior performance.

In summary, our mechanistic understanding of the iron-catalyzed Suzuki-Miyaura reaction implicated two principles for promoting successful cross-coupling: 1) avoiding the formation of iron aggregates and 2) facilitating transmetalation from boron to iron.

2.5 Examining the viability of β -diketiminato ligand frameworks to promote Suzuki-Miyaura cross-coupling reactions catalyzed by iron-based complexes

Despite the success of our initial system for Suzuki-Miyaura cross-coupling reactions catalyzed by iron-based complexes, a significant substrate scope limitation remained in the inability to incorporate heteroaromatic boronic esters. It has been estimated that heterocycles are found in over 85% of biologically active compounds⁵² and over 70% of pharmaceutically relevant compounds.⁵³ A survey of Suzuki-Miyaura cross-coupling reactions in the literature confirms the well-known scarcity of such reactions involving at

least one sp^3 -hybridized substrate,⁷ and among those that do, fewer still are examples which react an sp^3 -hybridized substrate with a heteroaromatic coupling partner (Figure 2.4a). Moreover, the majority of aryl-alkyl Suzuki-Miyaura cross-coupling reactions involve primary alkyl fragments (Figure 2.4b). Successful reactions with more substituted aliphatic fragments remain uncommon, particularly when the alkyl fragment is the electrophilic coupling partner.⁶ Only four reports describe the successful incorporation of tertiary alkyl halide substrates,^{54–57} and only one tolerates heteroaromatic nucleophiles.⁵⁵

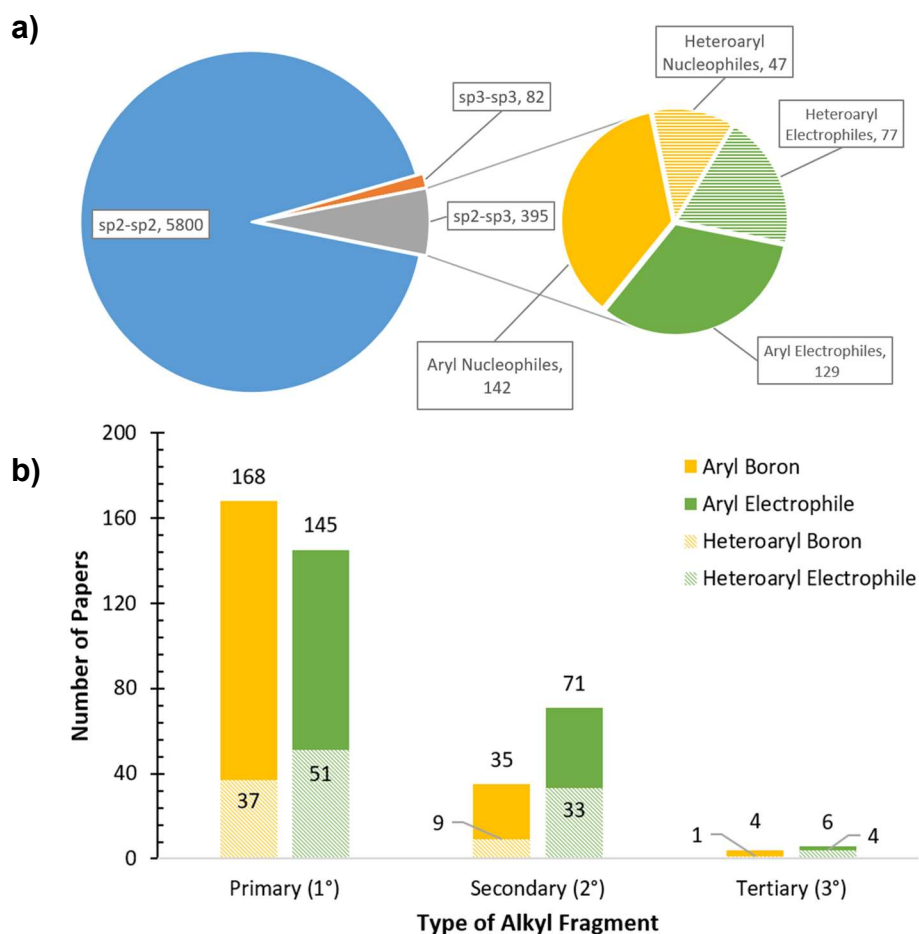


Figure 2.4. Survey of journal articles describing Suzuki-Miyaura reactions for: a) hybridization of nucleophiles/electrophiles and types of nucleophiles/electrophiles involved in $C(sp^2)$ - $C(sp^3)$ cross-coupling reactions (inset), and b) types of nucleophiles/electrophiles used in $C(sp^2)$ - $C(sp^3)$ cross-coupling reactions for primary, secondary, or tertiary sp^3 -hybridized substrates. The dataset was generated using SciFinder®.

Historically, significant attention has been dedicated toward the development of cross-coupling reactions of alkyl halide electrophiles using catalysts based on group 10 metals.^{58–61} However, existing toxicity⁵ and long-term viability concerns⁶² of group 10 metals compelled us to address these substrate limitations by further developing our Suzuki-Miyaura reaction catalyzed by an iron-based complex.²⁵ To expand the scope of our previous system, the development of new catalysts is required. Based on the working mechanistic hypothesis presented in Figure 2.3, we targeted ligand frameworks that 1) were sterically encumbered in order to discourage aggregation and 2) were sufficiently electron-donating in order to promote transmetalation (Figure 2.5a).

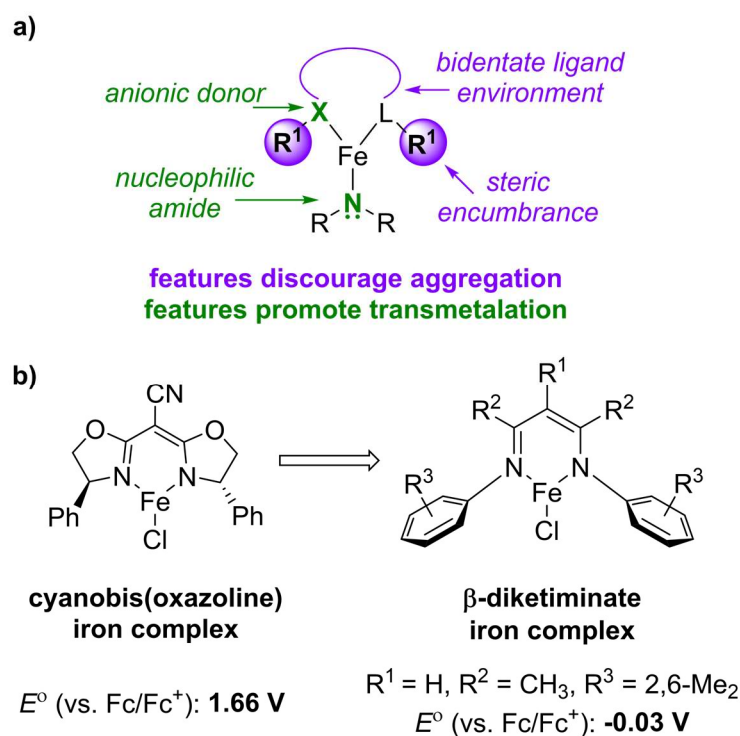
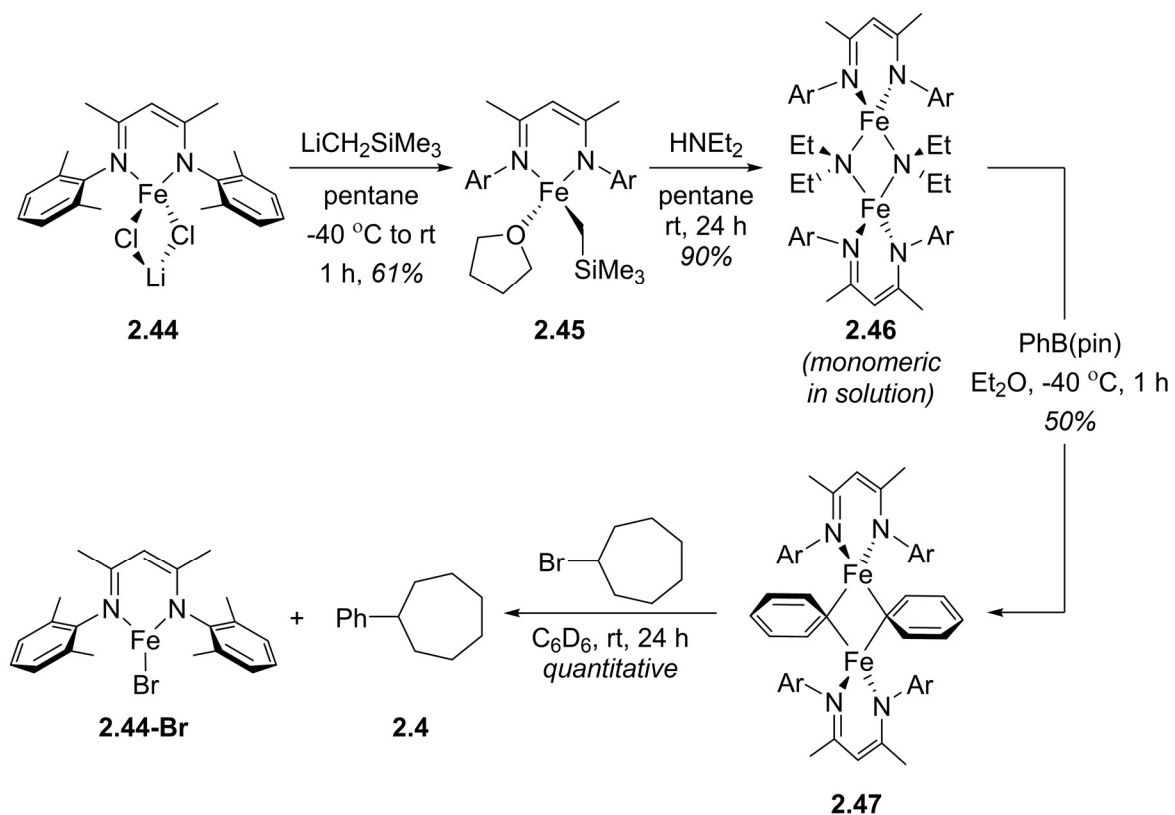


Figure 2.5. a) Ligand design principles for the development of new iron-based complexes b) First- and second-generation iron-based complexes for Suzuki-Miyaura cross-coupling reactions of aryl boronic esters and alkyl halides.

A class of ligands adhering to both design principles is the β -diketiminate ligands (Figure 2.5b). These ligands are better σ -donors than the less basic cyanobis(oxazoline) ligands previously used (E° of 2,6-dimethylphenyl imine iron complex (vs. Fc/Fc^+) = -0.03 V, *cf.* 1.66 V for the cyanobis(oxazoline) iron complex).²⁵ Among others,^{63–65} Holland and co-workers^{66–69} have demonstrated that these ligands are exceptional for stabilizing low-coordinate iron species, including 3-coordinate iron alkoxide and amide complexes.⁶⁷ Moreover, steric encumbrance in the β -diketiminate ligands located closer to the metal center more effectively hinders aggregation, and the ligand framework features many handles for modification of catalyst structure in order to tune steric and electronic properties. Following the working mechanistic hypothesis presented in Figure 2.3, Dr. Michael Crockett synthesized putative iron intermediates supported by β -diketiminate ligands (Scheme 2.6, **2.46–2.47**) in order to test for their ability to engage in cross-coupling reactions. Iron amide **2.46** could be accessed through the protonolysis⁴⁰ of iron alkyl complex **2.45** with diethylamine. X-ray crystallographic characterization of **2.46** confirmed the formation of an iron amide species that was dimeric by virtue of two μ^2 -diethylamide ligands (Appendix B.1.1). However, diffusion-ordered nuclear magnetic resonance spectroscopy (DOSY) suggested that the structure of **2.46** is mononuclear in solution.⁷⁰ This assessment is further supported by magnetic moments measured in the solid- and solution-states, which suggest that **2.46** is diamagnetic in the solid-state and paramagnetic in solution ($\mu_{\text{eff}} = 3.5$). Combining **2.46** with an equivalent of PhB(pin) in benzene resulted in an immediate color change that coincided with changes in the ^1H and ^{11}B NMR spectra consistent with the formation of iron phenyl complex **2.47**. Discrete synthesis of **2.47** in diethyl ether enabled the confirmation of its the structure by X-ray crystallography, which

determined that it exists as a dimer in the solid-state (Appendix B.1.2). Finally, treatment of **2.47** with bromocycloheptane delivered the cross-coupled product in nearly quantitative yields, with the concomitant formation of the iron bromide analogue of **2.44** (Scheme 2.6).



Scheme 2.6. Stoichiometric reactions relevant to Suzuki-Miyaura cross-coupling reactions involving iron complexes supported by β -diketiminato ligands.

Taken together, the monomer-dimer equilibrium of **2.46** suggested by DOSY and solution-state magnetic moment measurements are consistent with the hypothesis that the β -diketiminato ligands enable more reversible aggregation events than the cyanobis(oxazoline) ligand **2.9**. Moreover, the rapid conversion of the iron amide **2.46** to the iron phenyl **2.47** at ambient temperatures highlights the efficient transmetalation reaction afforded by the electron-releasing and sterically accommodating β -diketiminato ligands. The transmetalation reaction occurs in the absence of a preformed aryl borate

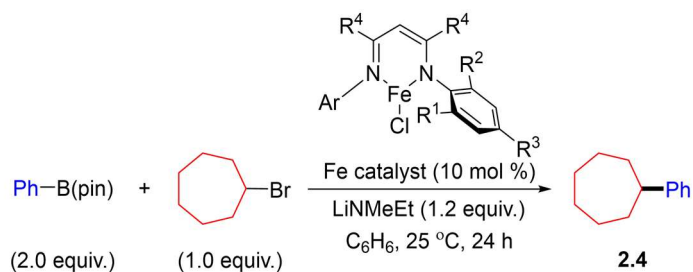
intermediate. Conversely, transmetalation between **2.44** and a preformed aryl borate required 24 hours to proceed to completion. Stoichiometric experiments between **2.44**, a preformed amino borate, and the alkyl halide produced the cross-coupled product in lower yields than the reaction between **2.47** and bromocycloheptane. These observations are consistent with a mechanistic proposal in which transmetalation proceeds predominantly through an iron amide intermediate, which is similar to results reported for metal hydroxide complexes proposed as intermediates in Suzuki-Miyaura cross-coupling reactions catalyzed by palladium-based complexes.³³

2.6 Optimization of catalyst structure and reaction conditions

Encouraged by the stoichiometric experiments, we sought to evaluate β -diketiminato iron complexes for their ability to catalyze the cross-coupling reaction between PhB(pin) and bromocycloheptane. In collaboration with Dr. Crockett, we synthesized a library of β -diketiminato ligands featuring a wide variety of substituents on the aryl rings (R^1 , R^2 , and R^3) and pentane backbone (R^4) (Table 2.3). Using 10% of complex **2.44**, the catalytic reaction proceeded efficiently to deliver >90% of the desired product. Importantly, the discrete iron complex must be made prior to cross-coupling; lower yields were observed if the catalyst were generated by combining the ligand with iron dichloride (entry 2). The rate of the reaction was sensitive to the identity of the aryl imines installed on the β -diketiminato ligands. In general, the reaction rate increased with decreasing steric bulk: complexes containing 2-aryl imine ligands (**2.49-2.52**) demonstrated superior catalytic performance compared to complexes containing 2,6-dimethyl aryl imine ligands (**2.44**, **2.48**, **2.53-2.56**). Further increased steric bulk (e.g. **2.57**) demonstrated efficient consumption of the starting material but failed to produce an

appreciable amount of the desired cross-coupled product. We hypothesize that this trend is due to the accessibility of a less crowded transmetalation pathway. Despite this trend, it appears that there is an optimal size for the ligands because 2-methylphenyl imine complex **2.52** was less efficient than 2-ethylphenyl imine complex **2.51**, and unsubstituted phenylimine complex **2.58** even less so. We hypothesize that the optimal size is due to the propensity for less hindered aryl imine complexes to engage in less reversible dimerization reactions, which hinder productive cross-coupling.

Table 2.3. Screening of iron(II) complexes supported by β -diketiminate ligands for catalytic activity in the Suzuki-Miyaura cross-coupling reaction between PhB(pin) and bromocycloheptane.



Fe complex	R ¹	R ²	R ³	R ⁴	$k_{app} (\times 10^{-5} \text{ s}^{-1})^a$	k_{rel}	$t_{1/2} \text{ (h)}$	yield (%)
2.44	CH ₃	CH ₃	H	CH ₃	2.43	1.0	7.96	91
2.44^b	CH ₃	CH ₃	H	CH ₃	n/a	n/a	n/a	57
2.48	CH ₃	CH ₃	H	CF ₃	2.34	1.0	8.25	99
2.49	^t Bu	H	H	CH ₃	7.95	3.3	2.43	96
2.50	ⁱ Pr	H	H	CH ₃	44.0	18.1	0.44	95
2.51	Et	H	H	CH ₃	45.4	18.7	0.43	99
2.52	CH ₃	H	H	CH ₃	29.9	12.3	0.65	85
2.53	CH ₃	CH ₃	CH ₃	CH ₃	3.38	1.4	5.72	99
2.54	CH ₃	CH ₃	Br	CH ₃	0.63	0.3	30.5	53
2.55	CH ₃	CH ₃	OCH ₃	CH ₃	3.47	1.4	5.56	99
2.56	CH ₃	CH ₃	N(CH ₃) ₂	CH ₃	2.67	1.1	7.44	99
2.57	ⁱ Pr	ⁱ Pr	H	CH ₃	2.31	1.0	8.35	1
2.58	H	H	H	CH ₃	n/a	n/a	2.83	28
2.59	CH ₃	CH ₃	H	Ph	5.64	2.9	8.25	28
2.60	CH ₃	CH ₃	H	^t Bu	n/a	n/a	n/a	1
2.61	CH ₃	CH ₃	H	N(CH ₃) ₂	2.55	1.3	44.9	50

^a k_{app} is based on the conversion of bromocycloheptane and only uses values up to 50% conversion.

^b **2.44** was generated *in situ* by reaction of the free ligand and FeCl₂.

In comparison to the steric influence of the ligand, electronic effects were minimally impactful. Iron complexes **2.54-2.56** with electron-donating and electron-withdrawing substituents on the aryl imines generally led to similar reaction rates and yields to the 2,6-dimethylphenyl imine complex **2.44**. Iron complexes **2.59-2.61** with various substituents on the pentane backbone generally resulted in lowered yields, likely due to an altered ligand bite angle which can restrict access to the iron center.⁷¹ Generally, all iron complexes were highly selective for generating the desired cross-coupled product. Unlike the previously reported system using cyanobis(oxazoline) iron complex **2.10**,²⁵ early catalyst decomposition was not observed (Figure 2.6). As a result, high conversions to the cross-coupled product were observed at early time points. With some β -diketiminato iron complexes, the reactions reached near completion within the first 8 hours.

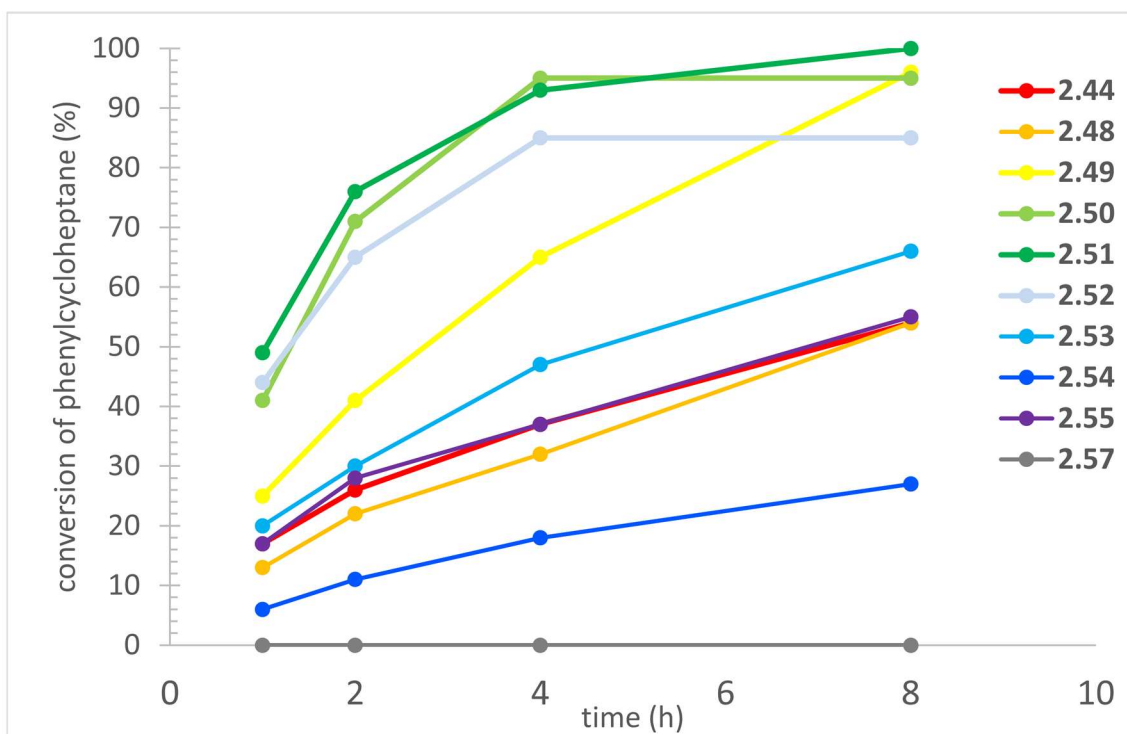


Figure 2.6. Conversion vs. time plots over the first 8 hours of reaction for the cross-coupling of PhB(pin) and bromocycloheptane using representative β -diketiminato iron complexes.

Table 2.4. Screening of reaction conditions for the Suzuki-Miyaura cross-coupling reaction between PhB(pin) and bromocycloheptane catalyzed by iron(II) complexes supported by β -diketiminato ligands.

entry	Fe complex (y equiv.)	x (cat loading) (1.0 equiv.)	y (equiv. B(pin))	solvent	yield (%)
1 ^a	2.49	10	2.0	benzene	67
2	2.49	5	2.0	benzene	45
3	2.49	1	2.0	benzene	5
4	2.49	10	1.3	benzene	80
5	2.49	10	1.5	benzene	90
6	2.49	10	2.0	benzene	95
7	2.49	10	2.2	benzene	96
8	2.49	10	2.5	benzene	97
9	2.44	10	2.0	benzene	91
10	2.44	10	2.0	toluene	73
11	2.44	10	2.0	anisole	40
12	2.44	10	2.0	methyl ^t Bu ether	43
13	2.44	10	2.0	THF	13
14	2.44	10	2.0	2-MeTHF	79

^a Reaction was carried out with 10 mol % of exogenous ligand.

Reaction conditions were screened using iron complexes **2.44** and **2.49** because a cursory exploration of boronic ester substrates demonstrated that these complexes were most general, despite not necessarily being the fastest catalyst precursors. These cross-coupling reactions demonstrated notable advantages compared to the previously reported system employing cyanobis(oxazoline) iron complexes.²⁵ Reactions proceeded to completion significantly faster due to prolonged catalyst lifetimes (Figure 2.6), obviating the need for additional equivalents of ligand, which now has a deleterious impact on reaction yield (Table 2.4, entry 1). The catalyst loading could not be lowered without significant loss in activity (Table 2.4, entries 2-3). The reaction also no longer required an excess of the boronic ester to be used; however, reactions with a superstoichiometric amount of the organoboron nucleophile were faster, slightly more selective, and void of

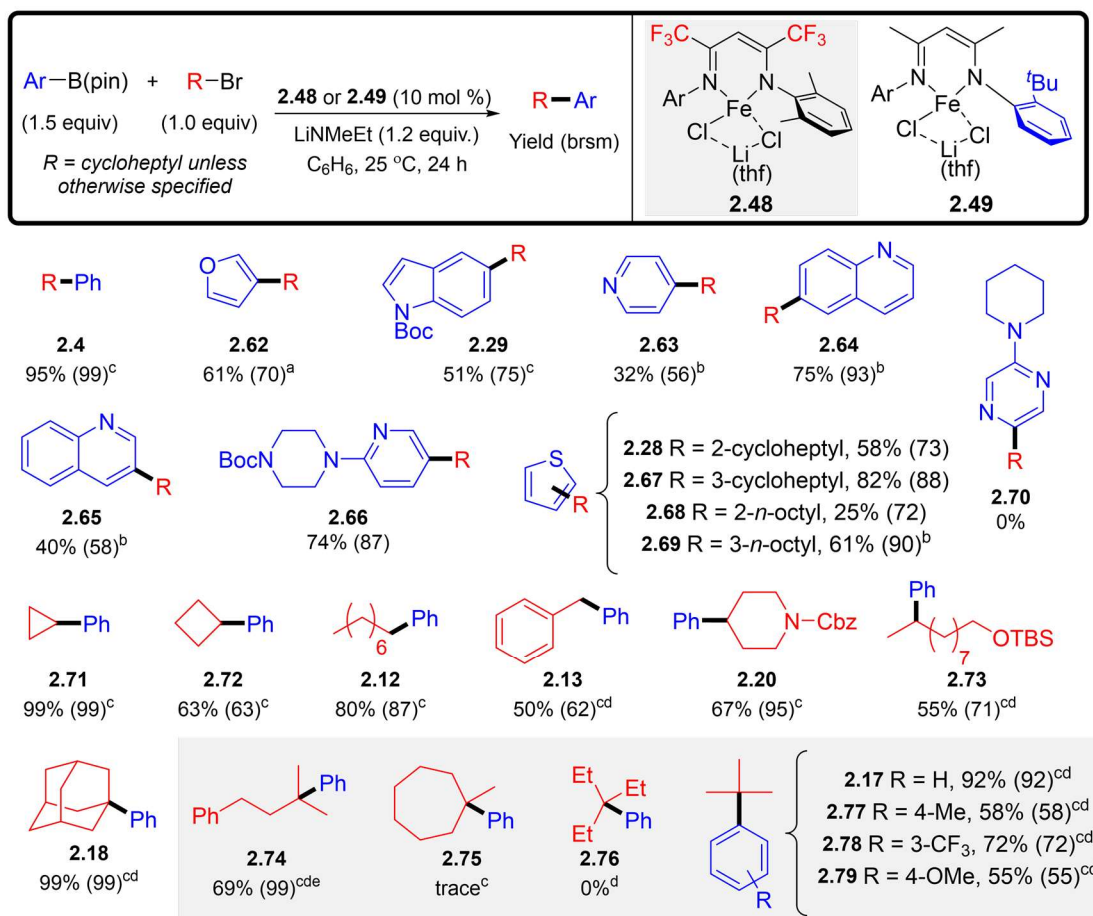
side reactions (Table 2.4, entries 4-8). Several different solvents enabled successful cross-coupling reactions (Table 2.4, entries 10-13); however, benzene remained the optimal solvent choice (*cf.* entry 9). Moreover, the cross-coupling reaction is readily scalable, as demonstrated by a reaction between PhB(pin) and bromocycloheptane to deliver **2.4** in 85% yield on a gram scale.

2.7 Evaluation of substrate scope

The generality of the cross-coupling reaction for a variety of heteroaromatic boronic ester substrates was evaluated next (Table 2.5). Catalyst precursor **2.49** was selected for this purpose because a cursory exploration of boronic ester substrates demonstrated that this complex led to higher yields. The sterically more encumbered ligand in **2.49** likely provides the optimal steric environment to overcome irreversible substrate binding of the heteroatom to the iron center while maintaining the accessibility required for transmetalation. With this precatalyst, several heteroaromatic boronic ester substrates produced the desired products in moderate to excellent yields (Table 2.5). Furans were compatible (**2.62**), as well as several nitrogen-containing heteroaromatic boronic esters (**2.29**, **2.63-2.66**). The latter substrates often required the reaction to be carried out at 50 °C or using an excess of boronic ester. Boc-protected indoles (**2.29**), quinolines (**2.64-2.65**), and sterically encumbered pyridines (**2.66**) were all tolerated. Such substrates were completely inactive when iron complexes supported by cyanobis(oxazoline) ligands (*i.e.* **2.9**) were used as precatalysts. Substrates more likely to bind to iron, such as unencumbered pyridine **2.63** and heterocycles containing multiple nitrogen atoms (**2.70**) did not undergo efficient cross-coupling. 2-thiophenyl-B(pin) and 3-thiophenyl-B(pin) produced the desired cross-coupling products **2.28** and **2.67-2.69** with primary and secondary alkyl

halides. These results demonstrated complementary reactivity with electrophilic aromatic substitution of thiophene rings, which selectively functionalize at the 2-position, and are prone to rearrangement when primary alkyl halides are used.^{72,73}

Table 2.5. Substrate scope of a Suzuki-Miyaura cross-coupling reaction between aryl boronic acid pinacol esters and alkyl halides catalyzed by iron-based complex **2.48** or **2.49**. Compounds synthesized using complex **2.48** are highlighted in gray. Isolated yields are reported with yields based on recovered starting material appearing in parentheses.



^a 0.1 mmol of electrophile. ^b at 50 °C. ^c 2.0 equiv. of B(pin). ^d corresponding chloride used. ^e isomer not observed.

In addition to the expanded boronic ester substrate scope, Dr. Michael Crockett demonstrated that the previously reported alkyl halide substrate scope was maintained to a high degree. Generally faster and cleaner reactions were observed using **2.49** as the catalyst precursor compared to cyanobis(oxazoline) iron complexes (Table 2.5, **2.12-2.13**, **2.20**,

2.71-2.73). Secondary alkyl halides (**2.71-2.72**) and primary alkyl halides (**2.12-2.13**) were well tolerated, with the alkyl bromide demonstrating superior performance compared to alkyl chlorides and iodides. Benzylic halide substrates (**2.13**) were a notable exception; a moderate yield of product could be achieved but the cyanobis(oxazoline) complexes performed better (*vide supra*, cf. Table 2.2). In these reactions, the product resulting from halide dimerization was observed in higher quantities, leading us to hypothesize that the higher reducing ability of the β -diketiminato iron complexes enabled more effective halogen abstraction to generate the carbon-centered radical in higher concentration, leading to irreversible dimerization. In addition to tolerating heterocycles, the cross-coupling reaction produced useful yields of products containing suitably protected amines (**2.20**) and alcohols (**2.73**).

Finally, tertiary alkyl halides proved to be excellent substrates for the cross-coupling reaction (Table 2.5, **2.17-2.18**, **2.74-2.79**). Previously, the cyanobis(oxazoline) iron complexes led to low yields of cross-coupled product **2.18** from 1-chloroadamantane,²⁵ but this result was not general across a variety of tertiary alkyl halides. In contrast, cross-coupling reactions using **2.49** resulted in near quantitative yield of **2.18** from 1-chloroadamantane. Despite this, fluorinated catalyst precursor **2.48** demonstrated more generality for a variety of tertiary alkyl chlorides. We believe that the more electron-deficient iron complex better facilitates reductive elimination, which can be difficult for the more hindered substrates. Using this catalyst, cross-coupling reactions between *tert*-butyl chloride and a variety of electron-rich and electron-deficient aryl boronic esters proceed in good to excellent yields (**2.77-2.79**). More sterically hindered tertiary alkyl halides of the general formula $R(\text{CH}_3)_2\text{CCl}$ also produced the desired cross-coupled

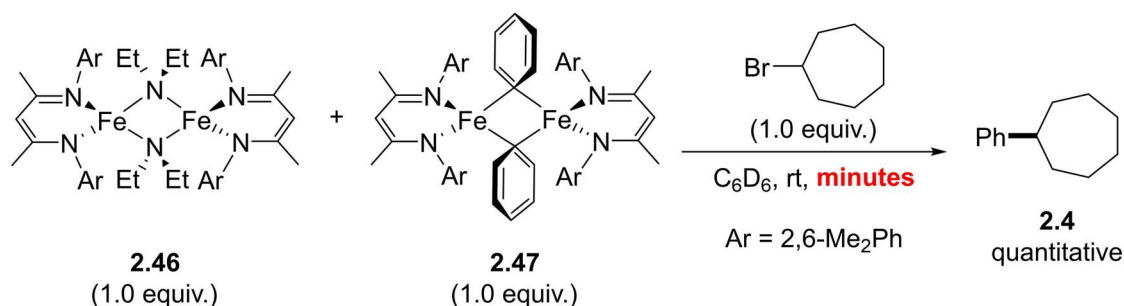
product in good yield (**2.74**), though it appeared that an upper limit existed for alkyl halides of the general formula $R_2(CH_3)CCl$ and larger (**2.75-2.76**). Notably, cross-coupled product **2.74** was produced in the absence of byproducts that can result from isomerization due to cascading insertion/elimination steps (i.e. “chain-walking”). This type of isomerization has been observed for nickel-catalyzed cross-electrophile cross-coupling reactions of similar substrates,⁷⁴⁻⁷⁶ and the byproducts can be difficult to remove from the desired product.

2.8 Revised mechanistic hypothesis featuring a bifunctional iron amide intermediate

Notably, the stoichiometric reaction between iron phenyl complex **2.47** and bromocycloheptane took nearly 24 hours to proceed to completion (*vide supra*, Scheme 2.6), which is significantly slower than one would expect based upon the catalytic reactions described in Chapters 2.6-2.7, which demonstrate high conversions to cross-coupled product within the first 8 hours (Figure 2.6). This inconsistency suggested that **2.47** was not sufficiently reducing enough to perform the halogen abstraction and generate the carbon-centered radical. We surmised that the iron amide species **2.46** could serve as a reducing agent in addition to engaging in transmetalation. To evaluate this possibility, a cyclic voltammogram of iron amide **2.46** was collected by Dr. Michael Crockett, which indicated that this complex possessed a reducing potential of -1.7 V vs. Fc/Fc^+ (*cf.* -0.03 V vs. Fc/Fc^+ for the analogous iron chloride complex **2.44**, Figure 2.5).⁴¹ Unfortunately, the instability of **2.47** at ambient temperatures precluded the collection of a cyclic voltammogram.

Furthermore, a 1:1 mixture of **2.46** and **2.47** rapidly produced the cross-coupled product following the addition of bromocycloheptane in stoichiometric quantity (Scheme

2.7). Taken together, these results imply that the iron phenyl species **2.47** is catalytically competent but not kinetically relevant. Instead, the iron amide is required for electrophile activation on the catalytic timescale.



Scheme 2.7. Stoichiometric reaction between **2.46**, **2.47**, and bromocycloheptane, which leads to rapid and quantitative formation of cross-coupled product **2.4**.

Because these results implicate the iron amide **2.46** in both the transmetalation step and the halogen abstraction step, we revised our mechanistic hypothesis to account for these observations (Figure 2.7).⁷⁷ In this revised catalytic cycle, iron halide precursor **I** is activated by salt metathesis with the lithium amide base. Iron amide **II** is bifunctional—it activates the alkyl halide electrophile *via* halogen abstraction to yield iron amide halide intermediate **IIIa**,^{11,17,23,27–29,78–81} and the organoboron nucleophile *via* transmetalation to yield iron aryl species **IIIb**.^{27,28,80} The carbon-centered radical generated from halogen abstraction recombines with **IIIb**, and reductive elimination from intermediate **IV** delivers the cross-coupled product.⁸⁰ It should be noted that the mechanism of the carbon-carbon bond forming step remains unclear, and could proceed *via* an outer-sphere mechanism in which **IIIb** is converted directly to **V**.⁸¹ Catalyst turnover is achieved by comproportionation between oxidized intermediate **IIIa** and low-valent intermediate **V** to regenerate an equivalent of **I** and an equivalent of **II**.

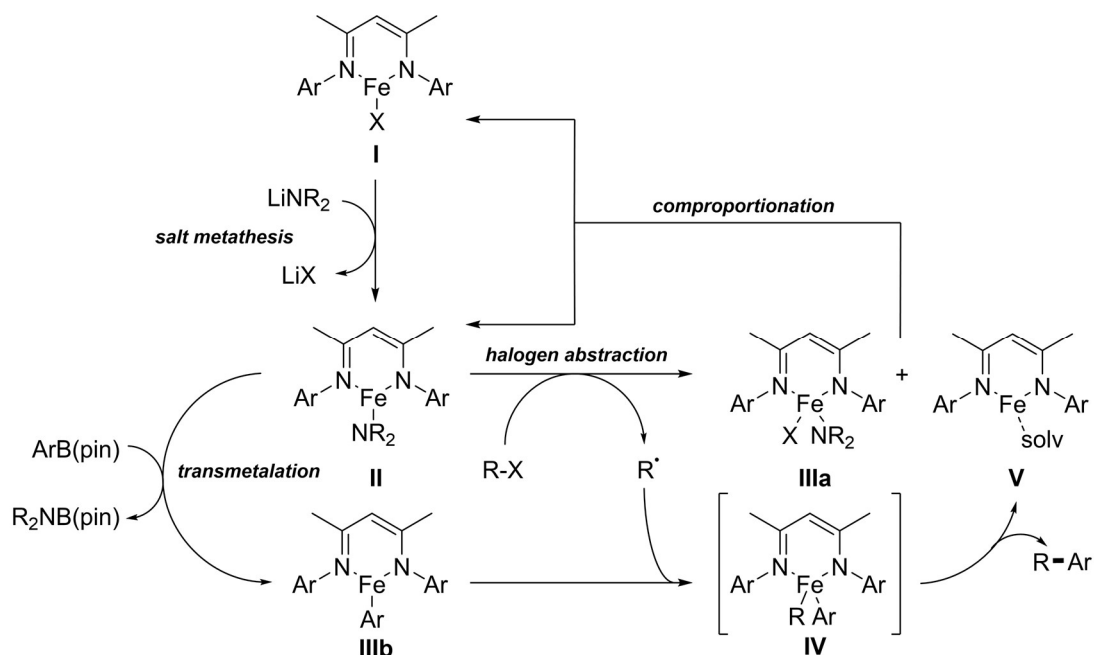


Figure 2.7. Revised working mechanistic hypothesis for the Suzuki-Miyaura cross-coupling reaction of alkyl halides and unactivated aryl boronic esters catalyzed by iron complexes supported by β -diketiminato ligands.

2.9 Examining the transmetalation step with low-temperature nuclear magnetic resonance spectroscopy

The working mechanistic hypothesis proposed in Figure 2.7 implies that the transmetalation reaction and the halogen abstraction reaction proceed at competitive rates from a common intermediate, and suggests that successful cross-coupling reactions hinge on mediating the delicate balance of the two reaction rates. It was determined that iron amide **2.46** reacted very rapidly with bromocycloheptane at ambient temperatures to produce a complex mixture of products as observed by ^1H NMR. As a result, we turned our attention towards gaining insight into the mechanism of the transmetalation reaction. While the rapid conversion of iron amide **2.46** to the iron phenyl complex **2.47** at ambient temperatures made the collection of reaction progress data not trivial, this issue could be ameliorated by tracking the transmetalation reaction at low temperatures using NMR spectroscopy.⁸² To do so, a stock solution of **2.46** was made in deuterated toluene and

dispensed into a J. Young tube, where it was frozen in the glovebox cold well. A stock solution of PhB(pin) in deuterated toluene was layered on top of the frozen iron complex solution, and allowed to freeze. The frozen multilayered sample was then transferred into a dewar of liquid nitrogen, which allowed the reaction mixture to be transported to the NMR instrument without transmetalation occurring prematurely. Once collection parameters were set up, the reaction mixture could be thawed in order to trigger the reaction and quickly inserted into the instrument to collect reaction progress data.

After screening various temperatures for the transmetalation of **2.46** with PhB(pin), it was determined that the reaction could be suitably slowed down at temperatures ranging from -30 °C to 0 °C (Figure 2.8). Unfortunately, the paramagnetic peaks were not well-resolved, and conversion of the iron complexes could only be determined indirectly from the diamagnetic resonances corresponding to the *ortho*-protons of PhB(pin) and the methylene protons of the aminoborane byproduct **2.80** resulting from transmetalation. From these plots of conversion vs. time, we observed that the consumption of PhB(pin) occurs rapidly early on and levels off in all cases, independent of temperature. The amount of **2.80** continues to grow steadily and reaches higher conversions in shorter times at higher temperatures. We hypothesized that a pre-equilibrium event preceding the transmetalation reaction could be responsible for the depletion of PhB(pin) early on. Pre-transmetalation intermediates have previously been identified for palladium-catalyzed systems,³⁴ the discovery of which substantially elucidated the mechanism of the transmetalation event. Attempts to determine the order of the reaction with respect to these intermediates by performing the reaction under pseudo first-order conditions were inconclusive because the obtained conversion vs. time plots did not fit first- or second-order trends.

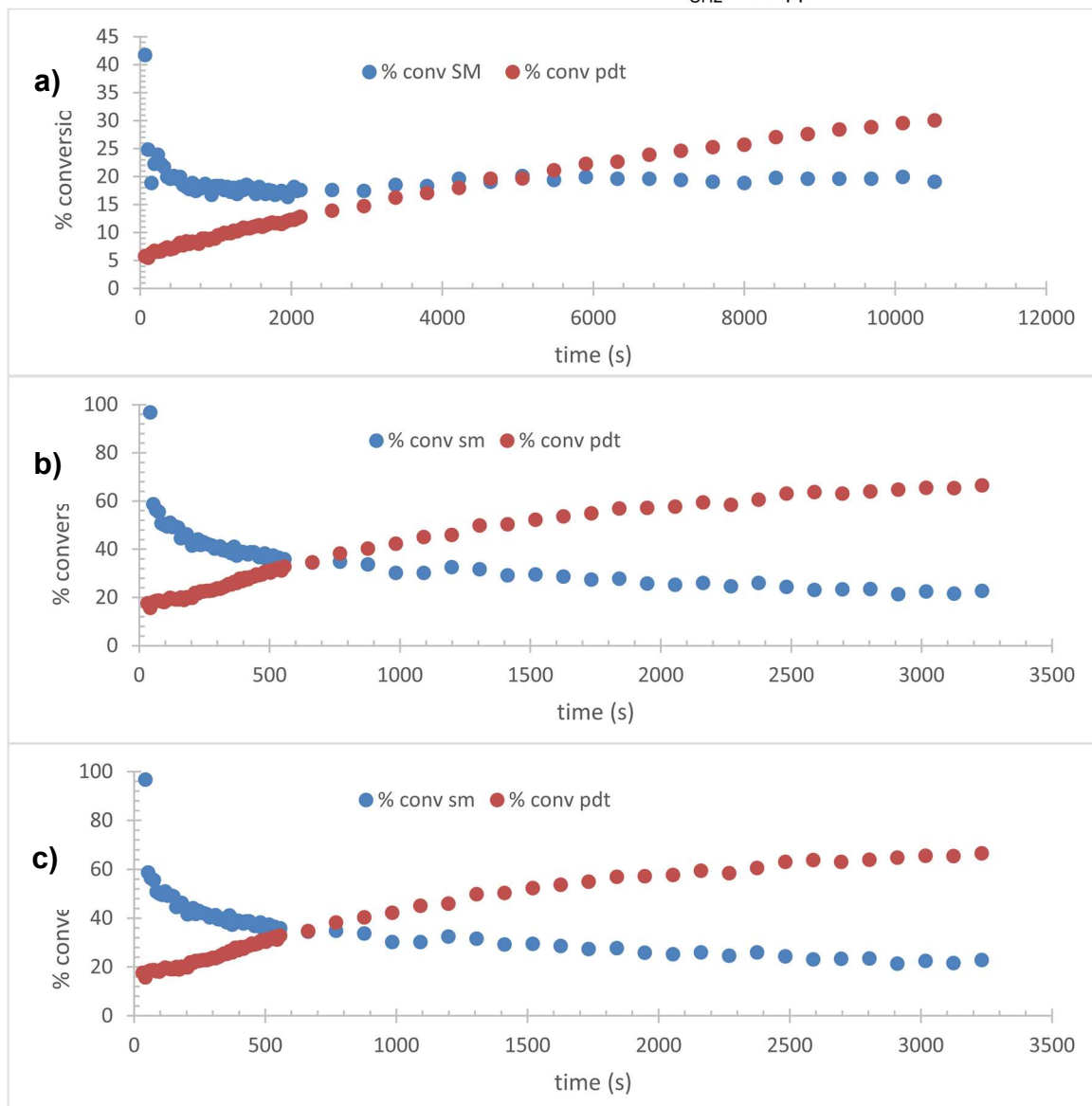
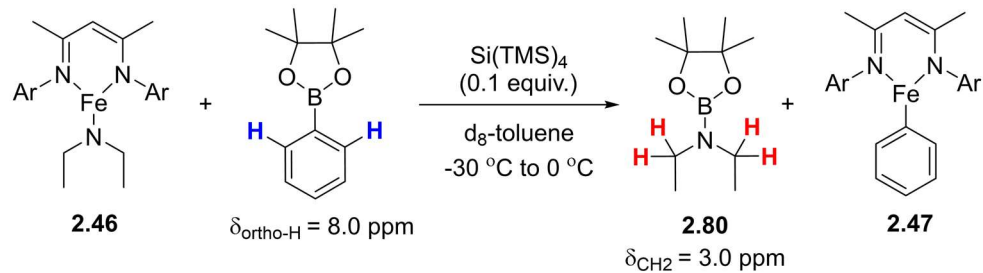
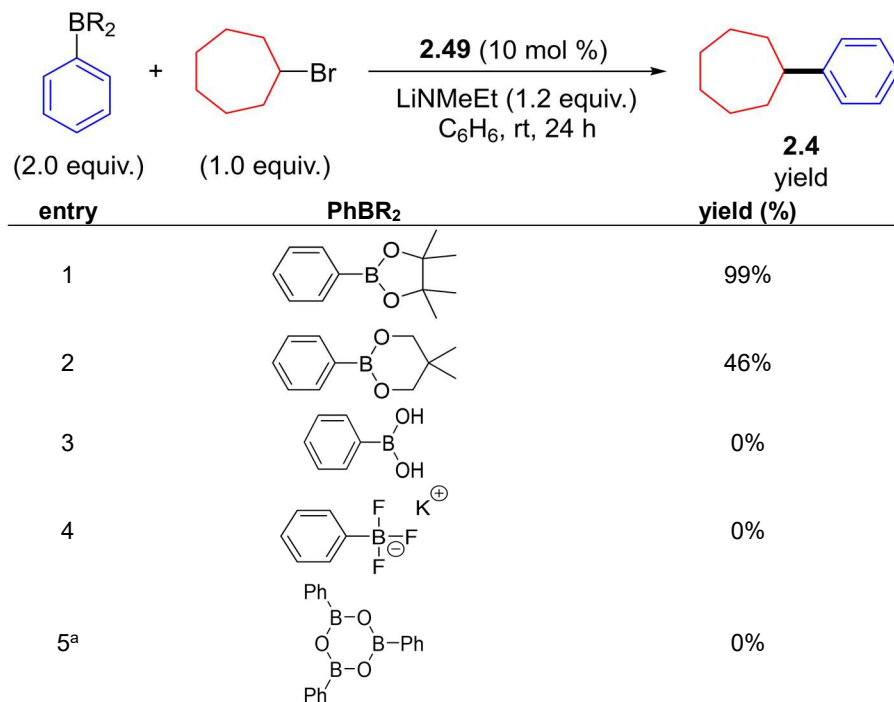


Figure 2.8. Conversion vs. time data for the consumption of PhB(pin) (blue traces) and the production of Et₂NB(pin) **2.80** (red traces) from reaction of PhB(pin) with **2.46** at a) -30 °C, b) -15 °C, and c) 0 °C.

We had previously demonstrated that the β -diketiminato complexes could perform the desired cross-coupling reaction with phenyl boronic acid neopentyl glycol ester (PhB(neo)), albeit with reduced yields (Scheme 2.8, entry 2). In attempting to screen the stoichiometric transmetalation reaction of iron amide **2.46** with different boronic esters, we expected that the lower yields of cross-coupled product resulting from the PhB(neo) substrate indicated that transmetalation would be less efficient, but to our surprise, the reaction between **2.46** and PhB(neo) resulted in an immediate color change at room temperature. Moreover, successful transmetalation was also observed between **2.46** and phenyl boroxine over 24 hours at room temperature, a substrate which was inactive for catalytic cross-coupling (Scheme 2.8, entry 5). Subsequent addition of bromocycloheptane to the putative iron phenyl complex resulted in slow formation of cross-coupled product in all cases. The successful transmetalation between these less active organoboron reagents and the iron amide complex **2.46** in stoichiometric reactions leads us to hypothesize that the success of the catalytic cross-coupling reaction is mediated by competing rates of transmetalation and halide abstraction by the *in situ*-formed iron amide. Halide abstraction with the iron amide complex **2.46** is extremely rapid at room temperature, demonstrating an immediate color change and a complex mixture of products in the ^1H NMR spectrum of the reaction mixture. However, when the transmetalation proceeds orders of magnitude too slowly compared to the fast halide abstraction, the reaction does not occur (i.e. phenyl boroxine). When transmetalation is competitive with the fast halide abstraction at room temperature (i.e. PhB(pin), PhB(neo)), the cross-coupling product is observed.



^a 0.33 equiv. PhBR₂ used in reaction.

Scheme 2.8. Scope of phenyl boronic esters for the Suzuki-Miyaura cross-coupling reaction with bromocycloheptane catalyzed by β -diketiminato iron complex **2.49** featuring 2'-BuPh imine substituents.

These findings compelled us to collect reaction progress data for transmetalation of **2.46** with other boronic esters at low temperature, in the hopes of elucidating the generally observed lower efficiency of catalytic reactions with boronic esters not containing pinacol. Specifically, it was unclear to us why PhB(neo) was less efficient under catalytic conditions, despite proceeding to completion in the transmetalation reaction almost instantaneously at ambient temperature. The stoichiometric transmetalation reaction was performed with PhB(neo) in place of PhB(pin) at -30 °C (Figure 2.9a). Similar to the stoichiometric transmetalation of PhB(pin) with iron amide complex, consumption of the boronic ester proceeded rapidly even at low temperatures; in fact, consumption of the PhB(neo) was faster than that of the PhB(pin) (Figure 2.9b). However, the production of

the analogous aminoborane was much slower than when PhB(pin) was used (Figure 2.9b).

Fitting to first- and second-order plots was likewise inconclusive.

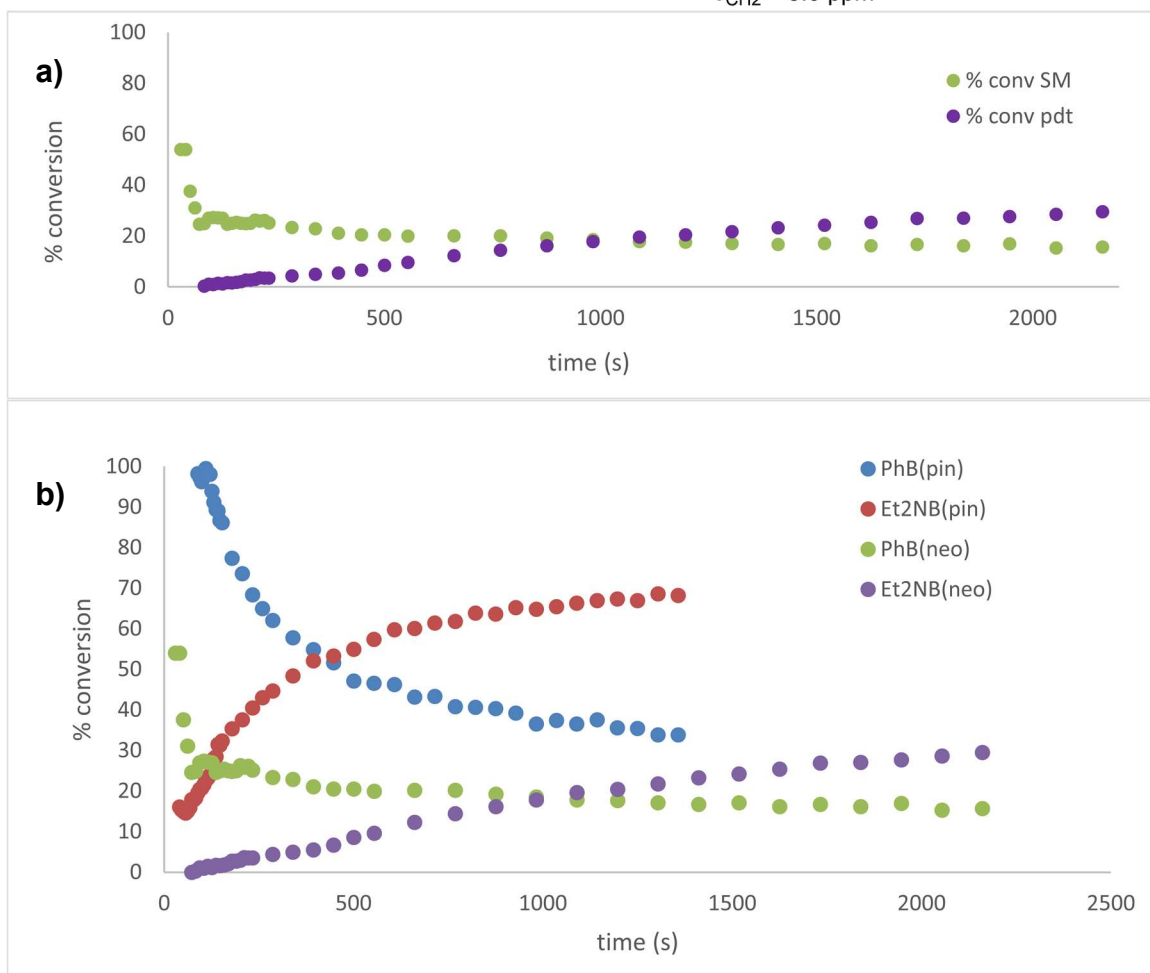
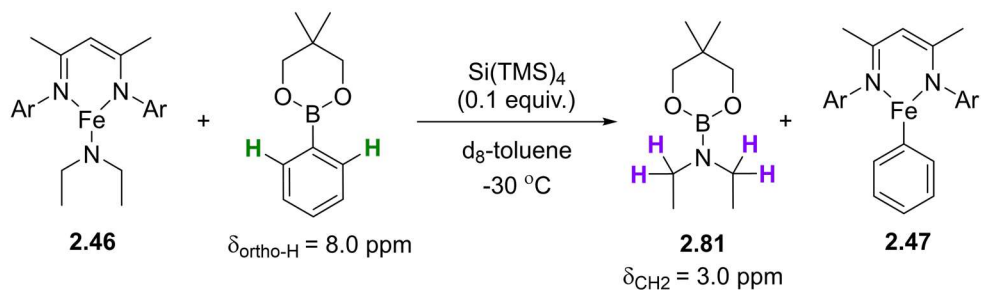


Figure 2.9. a) Conversion vs. time data for the consumption of PhB(neo) (green trace) and the production of Et₂NB(neo) **2.81** (purple trace) from reaction of PhB(neo) with **2.46** at -30°C . b) Overlaid comparison of conversion vs. time data for transmetalation reactions between PhB(pin) and **2.46** (blue and red traces) and between PhB(neo) and **2.46** (green and purple traces).

While the use of phenyl boroxine in the catalytic cross-coupling reaction produced no product (Scheme 2.8, entry 5), the stoichiometric transmetalation reaction displayed a change in the NMR spectrum consistent with completed transmetalation over the course of 24 hours. Thus, reaction progress data for the stoichiometric transmetalation between phenyl boroxine and **2.46** at room temperature was collected overnight (Figure 2.10). The transmetalation reaction resulted in the production of 16% of the analogous aminoborane product, which is consistent with destruction of the boroxine into its constituent monomer boronic acid products. Moreover, subsequent addition of bromocycloheptane to the completed transmetalation reaction mixture produced 16% of cross-coupled product, consistent with full conversion from the transmetalated reaction. Interestingly, NMR resonances corresponding to phenyl boroxine were not observed, suggesting that consumption of the starting material occurred prior to the collection of the first data point.

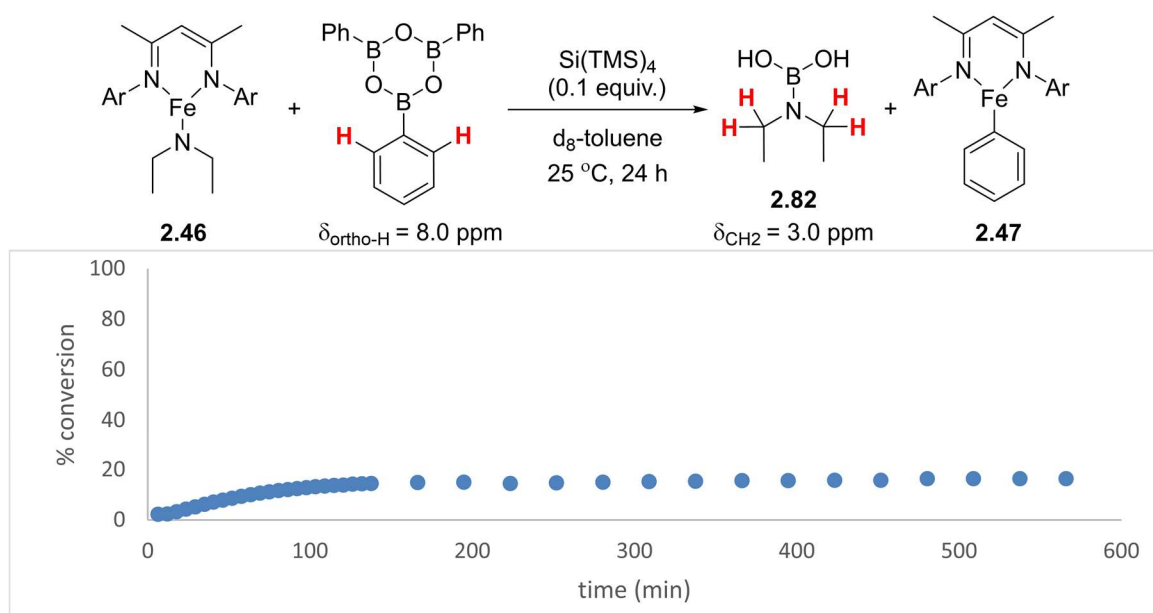


Figure 2.10. Conversion vs. time data for the reaction of $(\text{PhBO})_3$ with **2.46** at ambient temperature. NMR resonances corresponding to $(\text{PhBO})_3$ were not observed; the data points trace the production of $\text{Et}_2\text{NB}(\text{OH})$ **2.82** over the course of 24 hours.

The behavior of the transmetalation reaction of **2.46** with various boronic esters at different temperatures suggested the existence of pre-transmetalation intermediates. The productive transmetalation and cross-coupling reaction from phenyl boroxine further provided more evidence for how the pre-transmetalation intermediate could be formed. Taken together, a proposal to explain the different transmetalation rates of the different boronic esters is presented in Figure 2.11.

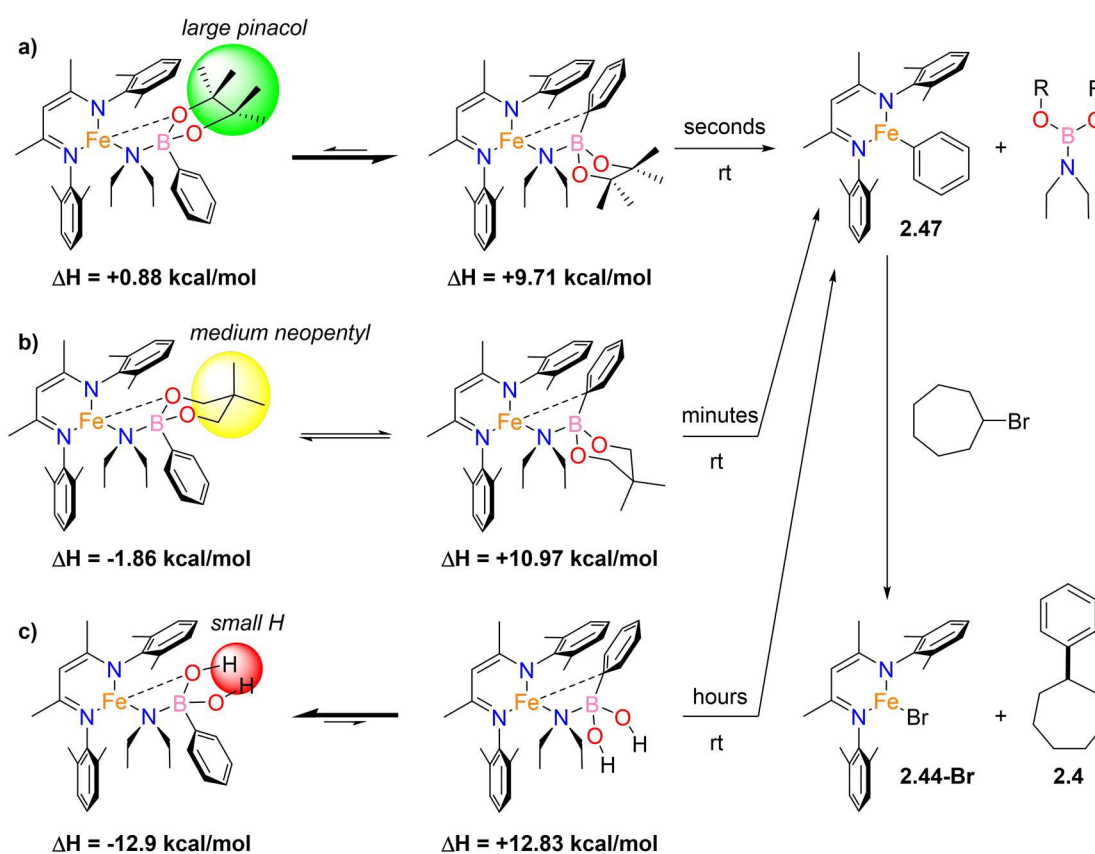


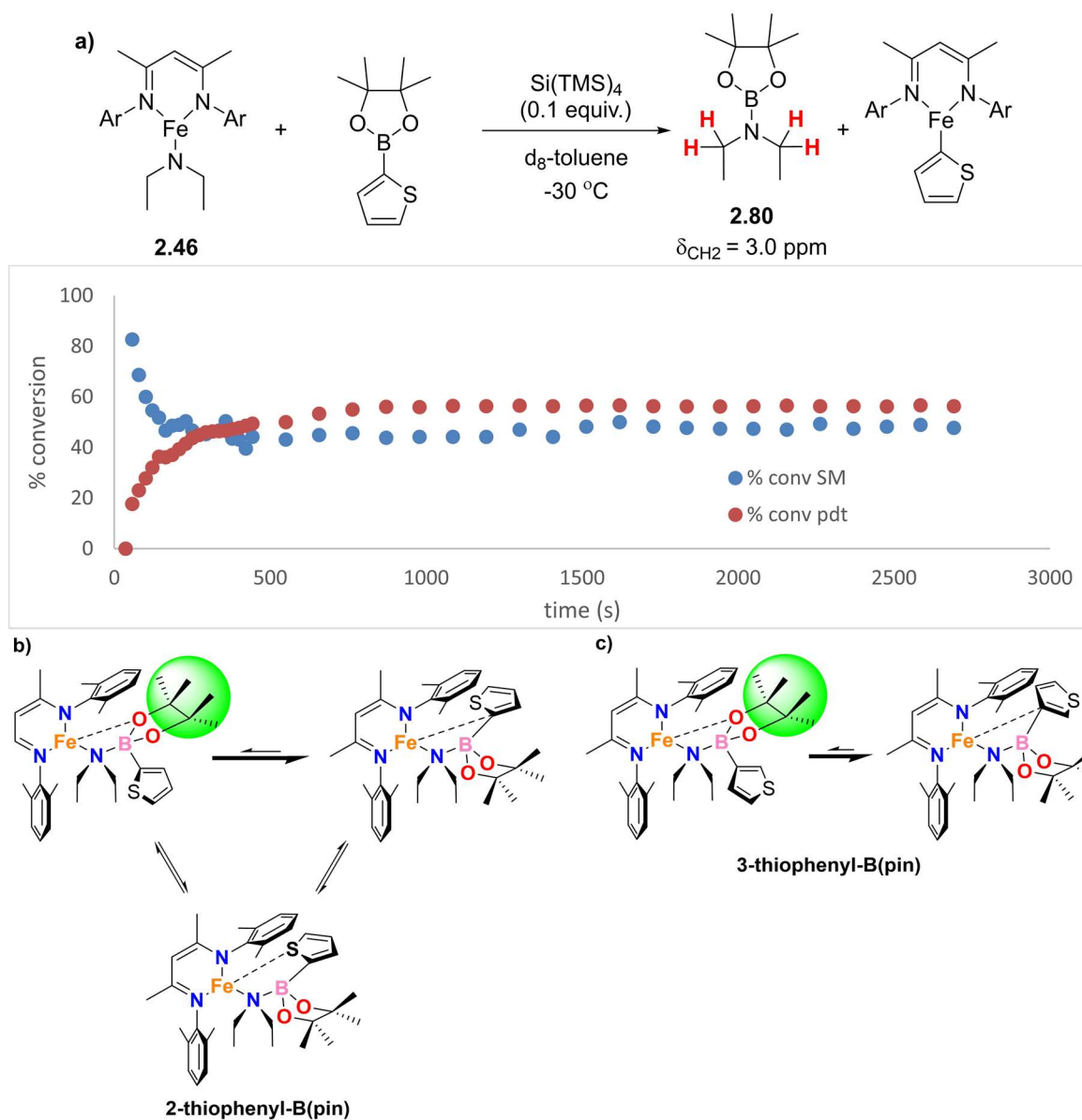
Figure 2.11. Hypothesis for the formation of pre-transmetalation intermediates from iron amide complex **2.46** with a) PhB(pin), b) PhB(neo), and c) (PhBO)₃, and density functional theory computations (B3LYP/6-31G*) of ground-state enthalpy values.

Formation of the putative pre-transmetalation intermediate is dependent on the equilibrium between an intermediate featuring inhibitory iron-oxygen interactions and an intermediate poised for iron-phenyl bond formation following the rapid formation of a

boron-nitrogen bond. In the case of boronic acid pinacol esters, the steric bulk provided by the pinacol group disfavors iron-oxygen bond formation and leads to complete transmetalation within seconds at room temperature (Figure 2.11a). The comparatively smaller neopentyl glycol group disfavors iron-oxygen interactions to a lesser extent, thereby slowing down the transmetalation reaction; however, the transmetalation still proceeds to completion within minutes (Figure 2.11b). The boronic acid resulting from cleavage of the phenyl boroxine has no steric bulk to disfavor iron-oxygen bond formation; thus, formation of the iron-phenyl bond necessary for transmetalation is inhibited by this competing pathway, though it proceeds to completion over the course of hours (Figure 2.11c). While transmetalation is gated by the rate with which boron-nitrogen bond formation is completed and a pre-transmetalation intermediate poised for iron-phenyl bond formation is accessed, the addition of bromocycloheptane following complete transmetalation leads to cross-coupled product formation in all cases. This hypothesis is supported by density functional theory computations, which indicate that the equilibrium between the pre-transmetalation intermediate formed from the pinacol and neopentyl glycol boronic esters and the putative four-membered transition state featuring an iron-phenyl interaction are thermodynamically feasible at ambient temperatures (8.83 kcal/mol and 12.83 kcal/mol, respectively) (Figure 2.11). However, the analogous pre-transmetalation intermediate formed from phenyl boronic acid is thermodynamically stable, and turnover to the transmetalation products is unfavorable from this pre-transmetalation intermediate, with an enthalpy difference of 25.73 kcal/mol.

This hypothesis is also consistent with results obtained for cross-coupling reactions of bromocycloheptane with thiophenyl boronic esters (Table 2.5, **2.28**, **2.67-2.69**). In those

reactions, regardless of the substitution of the alkyl halide, the 2-substituted thiophenyl boronic esters delivered the cross-coupled product in lower yield. This was surprising to us, because the data to this point suggested that the controlling factor for successful cross-coupling reactions was the use of an appropriately sterically hindered boronic ester such as pinacol to promote transmetalation. However, this divergence in yields could not be explained by the identity of the boronic ester. To gain further insight, the stoichiometric transmetalation reaction between 2-thiophenyl-B(pin) and iron amide complex **2.46** was studied at -30 °C. Interestingly, the consumption of 2-thiophenyl-B(pin) appeared to proceed faster than either of the transmetalations with phenyl boronic ester, though the production of the aminoborane **2.80** plateaued comparatively early (Figure 2.12a). The formation of hypothesized pre-transmetalation intermediates offers a possible explanation for these phenomena and the divergent yields (Figure 2.12b). The faster consumption of 2-thiophenyl-B(pin) and the early plateauing of the production of completed transmetalation byproduct **2.80** could be attributed to the appropriate positioning of the sulfur atom in 2-thiophenyl-B(pin) to form a five-membered ring chelate (Fe—N—B—C—S), which could assist the formation of the boron-nitrogen bond (manifesting as rapid consumption of starting material) but also inhibit the formation of the iron aryl complex necessary for product formation (inhibiting production of **2.80**, and leading to lower reaction yields). Conversely, the inherent geometry of the 3-thiophenyl-B(pin) substrate would position the sulfur atom in such a way that an inhibitory chelation interaction is not possible (Figure 2.12c), which is consistent with our observation that reactions employing that substrate proceed with greater efficiency.



Unfortunately, the future of the mechanistic studies by low-temperature nuclear magnetic resonance spectroscopy is limited by the ability of the NMR instrument to sufficiently resolve the structure of the observed pre-transmetalation species in solution. While diamagnetic species can be observed and quantified, paramagnetic species cannot

be effectively monitored at low temperatures. At this stage, it is unlikely that low temperature NMR spectroscopy is the appropriate tool to further elucidate the mechanism and kinetics of the transmetalation step. The speed of the reaction at ambient temperatures, and the poor resolution of the paramagnetic peaks at low temperatures, preclude the ability to study this reaction further using this method. Stopped-flow instrumentation may provide greater insight for elucidating this reaction.

2.10 Conclusion and outlook

The development of Suzuki-Miyaura cross-coupling reactions between alkyl halides and unactivated aryl boronic esters catalyzed by cyanobis(oxazoline) iron-based complexes is described. Overcoming the irreversible formation of iron oxide aggregates that are formed under conditions suitable for analogous palladium-catalyzed systems was key to the initial development of this method. A combination of computational studies and stoichiometric experiments indicated that lithium amide bases could promote effective transmetalation and discourage aggregation, enabling successful cross-coupling reactions to proceed catalytically with good yields.

A second-generation iron-based catalyst was developed to address substrate scope limitations of the initial method. Our mechanistic understanding of the iron-catalyzed cross-coupling reaction and stoichiometric experiments informed the rational choice of β -diketiminato ligand frameworks that favored reactive intermediates with low coordination numbers and promoted transmetalation. Iron complexes supported by these ligands are also less prone to ligand dissociation and irreversible aggregation. As a result, these complexes demonstrated high catalyst activity toward a broad substrate scope which included a variety

of heteroaromatic boronic ester nucleophiles and tertiary alkyl halide electrophiles. Both classes of substrates are particularly valuable motifs in chemical synthesis.

A deeper look at stoichiometric transmetalation reactions between discrete reactive iron-based intermediates and organoboron nucleophiles produced evidence of pre-transmetalation intermediates formed in the iron-catalyzed Suzuki-Miyaura reaction with alkyl halides. While these mechanistic studies were precluded by inherent limitations, valuable insights were gained toward a clearer mechanistic understanding, which we hope will allow us to develop ligand frameworks and reaction conditions that perform the cross-coupling reaction with greater efficiency, selectivity, and substrate tolerance.

2.11 Experimental section

General Considerations. Unless stated otherwise, all reactions were carried out in oven-dried glassware in a nitrogen-filled glovebox or using standard Schlenk-line techniques.⁸³ Solvents including dichloromethane, pentane, toluene, diethyl ether, and tetrahydrofuran were purified by passage through two activated alumina columns under a blanket of argon⁸⁴ and then degassed by brief exposure to vacuum. Deuterated solvents were dried over a sodium/benzophenone pot prior to distillation. All prepared boronic acid pinacol esters were used after passage through alumina under a nitrogen atmosphere. Methylethyl amine was purchased from TCI America; diisopropylamine and lithium dimethylamide were purchased from Alfa Aesar; butylamine and diethylamine were purchased from Sigma-Aldrich; phenylboronic acid, 2-naphthaleneboronic acid, 4-methoxyphenylboronic acid, *p*-tolylboronic acid, 4-trifluoromethylphenylboronic acid, and 3-trifluoromethylphenylboronic acid pinacol ester were purchased from Oakwood Chemicals. All amines that were liquids at room temperature were dried over calcium hydride for at least 24 hours before being vacuum-distilled. 2,3-dimethyl-2,3-butanediol and 2,2-dimethylpropane-1,3-diol were purchased from Alfa and used without further purification. Anhydrous iron (II) chloride was purchased from Sigma-Aldrich and used without further purification. (4*S*)-(+)-Phenyl- α -[(4*S*)-phenyloxazolidin-2-ylidene]-2-oxazoline-2-acetonitrile was purchased from Sigma-Aldrich and dried over P₂O₅ before use in the glovebox. Purchased alkyl halides were dried over calcium hydride for at least 24 hours before being vacuum-distilled, while all solids were dried over P₂O₅ before use in the glovebox. All alkyl halides were purchased from Sigma-Aldrich, Oakwood Chemicals and Fisher Scientific. Many of the heteroaromatic boronic esters were graciously provided

by Amgen. These compounds were then dried over P₂O₅, brought into a nitrogen glovebox, and passed through basic alumina before use.

¹H, ¹¹B, {¹H}¹³C, and ¹⁹F nuclear magnetic resonance (NMR) spectra were recorded at ambient temperature on Varian VNMRs operating at 400 MHz, 500 MHz, or 600 MHz for ¹H NMR at 160 MHz for ¹¹B NMR, 125 MHz for {¹H}¹³C or 470 MHz for ¹⁹F NMR. All {¹H}¹³C NMR spectra were collected while broad-band decoupling was applied to the ¹H region. The residual protio solvent impurity was used as an internal reference for ¹H NMR spectra and {¹H}¹³C NMR spectra. Boron trifluoride diethyl etherate was used as an external standard for ¹¹B NMR (BF₃·O(C₂H₅)₂: 0.0 ppm) and for ¹⁹F NMR (BF₃·O(C₂H₅)₂: -153.0 ppm). The line listing for NMR spectra of diamagnetic compounds are reported as follows: chemical shift (multiplicity, coupling constant, integration) while paramagnetic compounds are reported as: chemical shift (peak width at half height, number of protons). All paramagnetic spectra were collected at 25 °C. Solvent suppressed spectra were collected for paramagnetic precatalysts in THF using the PRESAT macro on the VNMR software. DOSY NMR are not usually collected for paramagnetic compounds due to complications with fast relaxation times. The DOSY spectra collected here were collected on a 600 MHz Agilent NMR spectrometer using the Doneshot macro. The diffusion delay was set to 8 ms and the gradients were arrayed between 1000 and 25000. Samples were typically collected with 4 scans per gradient. Infrared (IR) spectra were recorded on a Bruker Alpha attenuated total reflectance infrared spectrometer. High-resolution mass spectra were obtained at the Boston College Mass Spectrometry Facility on a JEOL AccuTOF DART instrument. Single crystal X-ray Intensity data were measured on a Bruker Kappa Apex Duo diffractometer using a high brightness I_μS copper source with

multi-layer mirrors. The low temperature device used is an Oxford 700 series Cryostream system with temperature range of 80-400 K. An Olympus SZ1145 stereo zoom microscope was used to view and mount crystals. The crystal structure was solved using ShellX. SQUID magnetometry measurements were performed on a Quantum Design MPMS3 Instrument as provided by National Science Foundation grant DMR-1337567. Samples were prepared by immobilization in eicosane. Solution magnetic moments were obtained by dissolving a known quantity of sample in a known volume of deuterated benzene and adding a capillary that contained benzene. Upon collection of the NMR spectrum, the peak separation for the two benzene species was measured and used to calculate an effective magnetic moment.⁸⁵

General procedure for literature survey featured in Figure 2.4. The data set was generated using the Substances: Chemical Structure search function on Scifinder®. In the reaction editor, a boron fragment and an electrophile fragment were drawn to match the desired functionality. The initial search set was first refined by the number of steps. We chose a step count of one to maximize the methodology papers included in the data set while eliminating some of the papers that simply use already known reactions in a broader synthesis. From the data set of single-step reactions, the Get References tool was used to consolidate reactions by document. The set of manuscripts was then refined by document type to only include journal articles. Finally, the data set was refined by research topic using the keyword “cross coupling” to generate the final data set used for the graphs. This procedure was repeated for every disconnection.

Computational procedures. All computations were carried out using Density Functional Theory (DFT) methodology employing the hybrid B3LYP functional (composed of

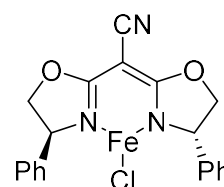
Becke's 1988 exchange functional⁸⁶ and Lee, Yang, and Parr's correlation functional⁸⁷) in conjunction with the 6-31G* basis set.⁸⁸ All calculations with phosphine ligands were carried out in a tetrahydrofuran (THF) solvent simulated by Tomasi's Polarizable Continuum Model (PCM).⁸⁹ Stationary-point characterization of all optimized geometries were carried out by means of frequency calculations utilizing the same level of theory as was used in the geometry optimizations. Gibbs free energies and enthalpies (computed at 298 K and 1 atm) and zero-point corrected energies were calculated using the computed normal mode frequencies (not scaled). All calculations were carried out using Gaussian 09 program. All iron complexes were calculated in the quintet state. In all cases for minima, the intermediate (triplet) and low (singlet) spin states were higher in energy between 15 and 40 kcal/mol.

General procedure for cross-coupling reaction of alkyl halides and aryl boronic esters. In a nitrogen-filled glovebox, iron complex (0.05 mmol) and lithium ethylmethanamide (0.60 mmol) were added to a 7 mL vial containing a stir bar. In reactions using cyanobis(oxazoline) iron complex **2.10**, ligand (0.05 mmol) was also weighed into the vial. A 1 mL benzene solution of boronic acid pinacol ester (1.0 mmol) and alkyl halide (0.50 mmol) was added to the stirring vial followed immediately by benzene (5 mL). The reaction was allowed to stir vigorously. Reactions employing **2.10** typically formed a precipitate after 15 minutes; reactions employing the β -diketiminato iron complexes turned homogeneous. Typically, the reaction turns a dark red-black, though in the case of certain heteroaromatic boronic esters other colors have been observed. If heating is required, the reaction vessels are sealed with Teflon cap and electrical tape, then removed and placed in an oil bath to stir. After 24 hours of stirring (48 hours for reactions using **2.10**), the typically

golden-colored reaction mixture was brought out of the glovebox and quenched with a saturated aqueous solution of ammonium chloride (10 mL). The aqueous phase was washed with dichloromethane (3 x 40 mL) and the combined organic phases were dried over sodium sulfate and filtered. Trimethoxybenzene (42 mg, 0.25 mmol) was added as an internal standard before evaporating the solvent *in vacuo*. An estimated yield was determined by analyzing the ¹H NMR spectrum of the crude reaction mixture, and yields based on recovered starting material were calculated from this spectrum. The product was then purified by silica gel flash column chromatography.

Synthesis of (2,2-bis((S)-4-phenyl-4,5-dihydrooxazol-2-

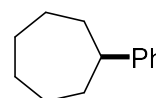
yl)acetonitrile)FeCl (2.10). In the glovebox, to a 7 mL scintillation vial equipped with stir bar was added 2,2-bis((S)-4-phenyl-4,5-dihydrooxazol-2-yl)acetonitrile (0.81 g, 2.5 mmol). This was then



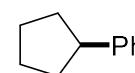
dissolved in THF (3 mL) and sodium hydride (0.065 g, 2.7 mmol) was added as a suspension in THF (2 mL). This mixture was stirred for 12 hours before being filtered through celite. The celite and vial were rinsed with THF (5 mL). To a 20 mL scintillation vial equipped with a stir-bar was added iron dichloride (0.310 g, 2.5 mmol) and THF (5 mL). After stirring for one hour, the Na{2,2-bis((S)-4-phenyl-4,5-dihydrooxazol-2-yl)acetonitrile} solution was added. The solution went from pale yellow-brown to a white suspension almost immediately. After stirring for 12 hours the solvent was removed *in vacuo* and the solid washed with THF and redried. This yielded an off-white solid (0.95 g, 81%). To generate X-ray quality crystals, a Soxhlet extraction in refluxing CH₃CN was carried out for two days to remove residual sodium chloride. Concentration of the filtrate

gave a white solid, and crystals suitable for X-ray diffraction were grown from a cold CH₃CN/toluene solution. The crystal structure contained two molecules of **2.10** in the asymmetric unit. Each iron was tetrahedral by virtue of coordinating to the nitrile moiety of the nearest neighbor iron complex. This interaction is presumed to be replaced by solvent during the cross-coupling reaction. ¹H NMR (500 MHz, THF) δ -30 (*w*_{1/2} = 307 Hz, 4H), -4.2 (*w*_{1/2} = 59 Hz, 2H), -3.8 (*w*_{1/2} = 33 Hz, 4H), -1.1 (*w*_{1/2} = 21 Hz, 2H), 10.8 (*w*_{1/2} = 76 Hz, 2H), 56.8 (*w*_{1/2} = 512 Hz, 1H) ppm. IR: 2203, 1606, 1533, 1440, 1067, 694 cm⁻¹.

Synthesis of phenylcycloheptane (2.4). Phenylcycloheptane was synthesized from bromocycloheptane and PhB(pin) using the general procedure with catalyst **2.10** and purified by silica gel flash column chromatography, eluting with 100% hexanes to afford product as a colorless oil (68 mg, 85% spectroscopic yield / 85% brsm, 80% isolated yield). ¹H NMR matched previously reported values.^{14,17} R_f = 0.60 (100% hexanes) ¹H NMR (500 MHz, CDCl₃): δ 1.46 – 1.78 (m, 8H), 1.80 (ddd, *J* = 13.4, 6.6, 3.4 Hz, 2H), 1.92 (ddt, *J* = 13.5, 6.6, 3.3 Hz, 2H), 2.66 (tt, *J* = 10.7, 3.7 Hz, 1H), 7.08 – 7.23 (m, 2H), 7.23 – 7.33 (m, 2H) ppm.



Synthesis of phenylcyclopentane (2.11). Phenylcyclopentane was synthesized from bromocyclopentane and PhB(pin) by the general procedure with catalyst **2.10** and purified by silica gel flash column chromatography, eluting with 100% hexanes to afford product as a colorless oil (53 mg, 80% spectroscopic yield / 85% brsm, 73% isolated yield). ¹H NMR matched previously reported values.¹⁷ R_f = 0.60 (100% hexane) ¹H NMR (500 MHz, CDCl₃) δ 1.53 – 1.74 (m, 4H), 1.75 – 1.87 (m, 2H), 1.99 – 2.14 (m, 2H), 2.99 (tt, *J* = 9.5, 7.4 Hz, 1H), 7.09 – 7.39 (m, 5H) ppm. Phenylcyclopentane was also synthesized from chlorocyclopentane and PhB(pin) by the

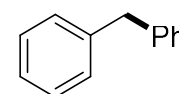


general procedure (32% spectroscopic yield / 86% brsm, 32% isolated yield) and iodocyclopentane and PhB(pin) by the general procedure (45% spectroscopic yield, / 96% brsm, 45% isolated yield).

Synthesis of phenyloctane (2.12). Phenyloctane was synthesized from octylbromide and PhB(pin) by the general procedure with heating to 50 °C



with catalyst **2.10** and purified by silica gel flash column chromatography, eluting with 100% hexanes to afford product as a colorless oil (73 mg, 85% spectroscopic yield / 91% brsm, 77% isolated

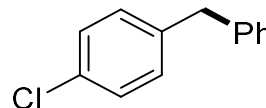


yield). 80% isolated yield / 82% spectroscopic yield / 87% brsm was obtained when using catalyst **2.49** at room temperature. ¹H NMR matched previously reported values.¹⁷ R_f = 0.60 (100% hexane) ¹H NMR (500 MHz, CDCl₃) δ 0.86 – 0.91 (m, 3H), 1.25 – 1.33 (m, 10H), 1.59 – 1.64 (m, 2H), 2.60 (t, *J* = 7.8 Hz, 2H), 7.18 (d, *J* = 7.6 Hz, 3H), 7.27 (t, *J* = 7.4 Hz, 2H) ppm. Phenyloctane was also synthesized from octyl chloride and PhB(pin) by the general procedure with heating to 50 °C (28% spectroscopic yield / 72% brsm, 28% isolated yield) and octyl iodide and PhB(pin) by the general procedure without heating (47% spectroscopic yield, / 91% brsm, 45% isolated yield).

Synthesis of diphenylmethane (2.13). Diphenylmethane was synthesized from benzyl chloride and PhB(pin) by the general procedure with catalyst **2.10** and purified by silica gel flash column chromatography, eluting with 100% hexanes to afford product as a colorless oil (61 mg, 79% spectroscopic yield / 79% brsm, 73% isolated yield). 50% isolated yield / 54% spectroscopic yield / 62% brsm was obtained when using catalyst **2.49**. ¹H NMR matched previously reported values.¹⁷ R_f = 0.50 (100% hexane) ¹H NMR (500 MHz, CDCl₃) δ 4.01 (s, 2H), 7.20 (s, 2H), 7.19 – 7.28 (m, 6H), 7.27 – 7.36 (m, 4H) ppm.

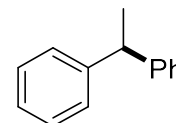
Diphenylmethane was also synthesized from benzyl bromide and PhB(pin) by the general procedure (28% spectroscopic yield / 37% brsm).

Synthesis of 1-benzyl-4-chlorobenzene (2.14). 1-benzyl-4-chlorobenzene was synthesized from 4-chlorobenzyl chloride and PhB(pin) by the general procedure with catalyst **2.10** and purified



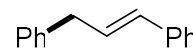
by silica gel flash column chromatography, eluting with 100% hexanes to afford product as a colorless oil (40 mg, 54% spectroscopic yield / 73% brsm, 40% isolated yield). ¹H NMR matched previously reported values.¹⁷ R_f = 0.50 (100% hexane) ¹H NMR (500 MHz, CDCl₃) δ 3.95 (s, 2H), 7.17 – 7.39 (m, 9H) ppm.

Synthesis of 1,1-diphenylethane (2.15). 1,1-diphenylethane was synthesized from 1-chloroethylbenzene and PhB(pin) by the general procedure with the addition of an extra equivalent of **2.10** and base at 24



h, then purified by silica gel flash column chromatography, eluting with 100% hexanes to afford product as a colorless oil (50% spectroscopic yield / 50% brsm, product isolated as a mixture with biphenyl—the dimer of the alkyl halide). ¹H NMR matched previously reported values.¹⁷ R_f = 0.50 (100% hexane) ¹H NMR (500 MHz, CDCl₃) δ 1.66 (d, *J* = 7.2 Hz, 3H), 4.17 (q, *J* = 7.3 Hz, 1H), 7.19 (t, *J* = 7.2 Hz, 2H), 7.22 – 7.25 (m, 4H), 7.29 (t, *J* = 7.6 Hz, 4H) ppm.

Synthesis of 1,3-diphenylpropene (2.16). 1,3-diphenylpropene was synthesized from 3-chloropropenylbenzene and PhB(pin) by the general



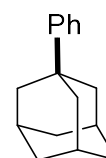
procedure with the addition of an extra equivalent of **2.10** and base at 24 h, then purified by silica gel flash column chromatography, eluting with 100% hexanes to afford product

as a colorless oil (58 mg, 61% spectroscopic yield / 61% brsm, 60% isolated yield). ^1H NMR matched previously reported values.¹⁷ $R_f = 0.20$ (100% hexane) ^1H NMR (500 MHz, CDCl_3) δ 3.56 (d, $J = 6.7$ Hz, 2H), 6.36 (dt, $J = 15.8, 6.9$ Hz, 1H), 6.46 (d, $J = 15.8$ Hz, 1H), 7.15 – 7.39 (m, 10H) ppm.

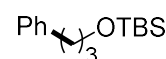
Synthesis of *tert*-butylbenzene (2.17). *Tert*-butylbenzene was synthesized from 2-chloro-2-methylpropane and PhB(pin) by the general procedure with catalyst **2.10**. Product was purified by silica gel flash column chromatography, eluting with 100% hexanes to afford purified product as a colorless oil (14 mg, 23% spectroscopic yield / 21% isolated yield). 85% isolated yield / 92% spectroscopic yield / 92% brsm was obtained when the fluorinated catalyst **2.48** was used. ^1H NMR matched previously reported values.⁹⁰ $R_f = 0.20$ (100% hexane) ^1H NMR (500 MHz, CDCl_3) δ 7.84 – 7.79 (m, 2H), 7.49 – 7.44 (m, 1H), 7.40 – 7.34 (m, 2H), 1.35 (s, 9H).



Synthesis of adamantylbenzene (2.18). Adamantylbenzene was synthesized from chloroadamantane and PhB(pin) by the general procedure with catalyst **2.10**. The yield of this compound was determined by GC because it is formed as a mixture with biadamantyl chloroadamantane which co-elutes with from silica gel (23% GC yield/spectroscopic yield). 99% GC yield / 99% brsm was obtained when using catalyst **2.49**. The identity of the peak was confirmed through an authentic sample as well as GCMS.



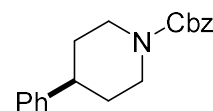
Synthesis of 3-phenylpropoxy-*tert*-butyldimethylsilane (2.19). 3-phenylpropoxy-*tert*-butyldimethylsilane was synthesized from 3-bromopropoxy-*tert*-butyldimethylsilane and PhB(pin) by the general procedure with



heating to 50 °C with catalyst **2.10**, then purified by silica gel flash column chromatography, eluting with 100% hexanes to afford product as a colorless oil (75 mg, 65% spectroscopic yield / 81% brsm, 60% isolated yield). ¹H NMR matched previously reported values.⁹¹ R_f = 0.15 (100% pentane) ¹H NMR (500 MHz, CDCl₃) δ 0.5 (s, 6H), 0.91 (s, 9H), 1.79 – 1.89 (m, 2H), 2.64 – 2.71 (m, 2H), 3.64 (t, *J* = 6.3 Hz, 2H), 3.64 (t, *J* = 5.7 Hz, 2H), 7.14 – 7.22 (m, 3H), 7.27 (m, 2H) ppm.

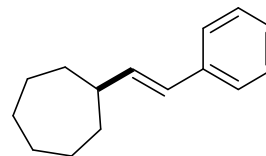
Synthesis of 4-phenylpiperidine-1-carboxylic acid benzyl ester

(2.20). 4-phenylpiperidine-1-carboxylic acid benzyl ester was synthesized from 4-bromopiperidine-1-carboxylic acid benzyl ester



and PhB(pin) by the general procedure with heating to 50 °C with catalyst **2.10** and purified by silica gel flash column chromatography, eluting with 1:5

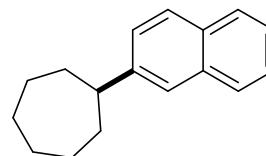
EtOAc/hexanes to afford product as a colorless oil (83 mg, 70% spectroscopic yield / 96% brsm, 56% isolated yield). 67%



isolated yield / 70% spectroscopic yield / 95% brsm was obtained when using catalyst **2.49**.

¹H NMR matched previously reported values.⁹² R_f = 0.2 (16% EtOAc/hexane) ¹H NMR (500 MHz, CDCl₃) δ 1.56 – 1.72 (m, 2H), 1.85 (d, *J* = 12.7 Hz, 2H), 2.67 (tt, *J* = 12.2, 3.6 Hz, 1H), 2.89 (t, *J* = 12.9 Hz, 2H), 4.32 (s, 2H), 5.16 (s, 2H), 7.17 – 7.25 (m, 3H), 7.26 – 7.42 (m, 7H) ppm.

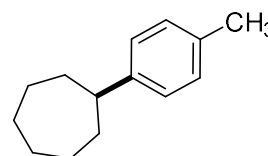
Synthesis of (*E*)-styrenylcycloheptane (2.22). (*E*)-styrenylcycloheptane was synthesized from bromocycloheptane and (*E*)-styrenyl boronic acid pinacol ester by the general procedure with catalyst **2.10**. Product was purified by silica gel flash column chromatography, eluting with pure hexane to afford purified product as a colorless oil (25 mg, 27% spectroscopic



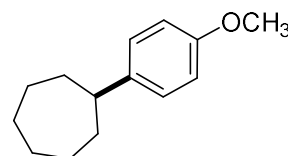
yield / 25% brsm, 25% isolated yield). ^1H NMR matched previously reported values.⁹³ $R_f = 0.8$ (100% hexane) ^1H NMR (500 MHz, CDCl_3) δ 1.39-1.75 (m, 10H), 1.79-1.86 (m, 2H), 2.33 (m, 1H), 6.22 (dd, $J = 15.9, 7.6$ Hz, 1H), 6.32 (d, $J = 15.9$ Hz, 1H), 7.18 (t, $J = 7.2$ Hz, 1H), 7.28 (t, $J = 7.6$ Hz, 2H), 7.34 (d, $J = 7.6$ Hz, 2H).

Synthesis of 2-cycloheptylnaphthalene (2.23). 2-cycloheptylnaphthalene was synthesized from bromocycloheptane and naphthalene-2-boronic acid pinacol ester by the general procedure with catalyst **2.10**. Product was purified by silica gel flash column chromatography, eluting with 100% hexanes to afford purified product as a white crystalline solid (85 mg, 84% spectroscopic yield / 84% brsm, 76% isolated yield). ^1H NMR matched previously reported values.⁹⁴ $R_f = 0.45$ (100% hexane) ^1H NMR (500 MHz, CDCl_3) $\delta = 1.85$ -1.58 (m, 10H), 2.01-1.98, (m, 2H), 2.86-2.81 (m, 1H), 7.44-7.45 (m, 3H), 7.61 (s, 1H), 7.79-7.75 (m, 3H) ppm.

Synthesis of *p*-tolylcycloheptane (2.24). *p*-tolylcycloheptane was synthesized from bromocycloheptane and *p*-tolylboronic acid pinacol ester by the general procedure with catalyst **2.10** and



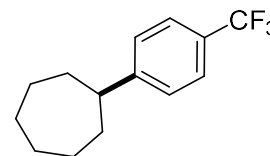
the addition of an extra equivalent of **2.10** and base at 24 hours. Product was purified by silica gel flash column chromatography, eluting with 30% EtOAc in hexane to afford purified product as a colorless oil (48 mg, 51% spectroscopic yield / 56% brsm, 51% isolated yield). ^1H NMR matched previously reported values.⁹⁵ $R_f = 0.70$ (100% hexane) ^1H NMR (400 MHz, CDCl_3) $\delta = 1.67$ -1.55 (m, 8H), 1.82-1.73 (2H), 1.93-1.84 (m, 2H), 2.31 (s, 3H), 2.66-2.58 (m, 1H), 7.08 (s, 4H) ppm.



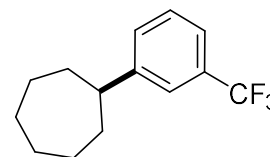
Synthesis of (4-methoxyphenyl)cycloheptane (2.25). (4-methoxyphenyl)cycloheptane was synthesized from bromocycloheptane and (4-methoxyphenyl) boronic acid pinacol ester by the general procedure with catalyst **2.10** and the addition of an extra equivalent of **2.10** and base at 24 hours. Product was purified by silica gel flash column chromatography, eluting with 30% EtOAc in hexane to afford purified product as a colorless oil (69 mg, 68% spectroscopic yield / 100% brsm, 68% isolated yield). ¹H NMR matched previously reported values.¹⁷ R_f = 0.60 (10% EtOAc in hexane) ¹H NMR (500 MHz, CDCl₃) δ = 1.65-1.49 (m, 6H), 1.72-1.65 (m, 2H), 1.82-1.73 (m, 2H), 1.93-1.83 (m, 2H), 2.66-2.57 (m, 1H), 3.78 (s, 3H), 6.83-6.81 (m, 2H), 7.12-7.10 (m, 2H) ppm.

Synthesis of (4-trifluoromethyl)phenyl)cycloheptane (2.26).

(4-trifluoromethyl) phenyl)cycloheptane was synthesized from bromocycloheptane and (4-trifluoromethyl)phenyl) boronic acid



pinacol ester by the general procedure with heating to 50 °C with catalyst **2.10**. Product was purified by silica gel flash column chromatography, eluting with 100% hexanes to afford purified product as a white crystalline solid (57 mg, 47% spectroscopic yield / 87% brsm, 47% isolated yield). ¹H NMR matched previously reported values.¹⁷ R_f = 0.50 (100% hexane)



¹H NMR (500 MHz, CDCl₃) δ 1.64 (m, 8H), 1.82 (s, 2H), 1.94 – 1.86 (m, 2H), 2.72 (tt, 1H), 7.52 (d, *J* = 8.0 Hz, 2H) ppm.

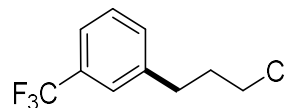
Synthesis of (3-trifluoromethyl)phenyl)cycloheptane (2.27).

(3-trifluoromethyl)phenyl)cycloheptane was synthesized from bromocycloheptane and (3-trifluoromethyl)phenyl) boronic acid pinacol ester by the general procedure with heating to 50 °C with catalyst **2.10**. Product was purified by silica gel flash column

chromatography, eluting with 100% hexanes to afford purified product as a white crystalline solid (81 mg, 67% spectroscopic yield / 76% brsm, 67% isolated yield). $R_f = 0.80$ (100% hexane), $^1\text{H NMR}$ (500 MHz, CDCl_3) δ 1.75 – 1.62, 1.82 (s, 2H), 1.90 (d, $J = 15.6$ Hz, 2H), 2.74 (m, 1H), 7.48 (t, $J = 7.7$ Hz, 2H), 7.70 (d, $J = 7.9$ Hz, 1H), 7.97 (d, $J = 7.5$ Hz, 1H) ppm. $\{^1\text{H}\}^{13}\text{C NMR}$ (125 MHz, CDCl_3) δ 27.1 (s), 27.8 (s), 36.7 (s), 46.9 (s), 122.4 (q, $J = 3.9$ Hz), 123.4 (q, $J = 3.8$ Hz), 124.3 (q, $J = 270.6$ Hz), 128.6 (s), 130.1 (q, $J = 1.4$ Hz), 130.5 (q, $J = 31.4$ Hz), 150.7 (s) ppm. $^{19}\text{F NMR}$ (470 MHz, CDCl_3) δ -62.1 (s) ppm. IR: 2922, 1446, 1327, 1158, 1121, 1073, 796, 702, 664 cm^{-1} . HRMS (ESI) m/z $[\text{M}]^+$ calcd. For $\text{C}_{14}\text{H}_{17}\text{F}_3$ 242.12769; found 242.12858.

Synthesis of 1-(3-chloropropyl)-3-

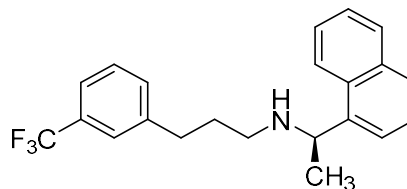
(trifluoromethyl)benzene (2.31). In a nitrogen filled glovebox, complex **2.10** (84 mg, 0.20 mmol),



cyanobis(oxazoline) ligand **2.9** (66 mg, 0.20 mmol) and lithium ethylmethylamide (156 mg, 2.40 mmol) were added to a 20 mL vial containing a stir bar. Benzene (15 mL) was added to the stirring vial followed immediately by a 5 mL benzene solution of *m*-trifluoromethylboronic acid pinacol ester (1.09 g, 4.00 mmol) and 1-bromo-3-chloropropane (197 μL , 314 mg, 2.00 mmol). The vial was sealed using electrical tape before being brought outside the glovebox. The reaction was stirred vigorously at 50 $^\circ\text{C}$. A precipitate formed on the vial wall after 10 minutes of stirring. After 48 hours, the reaction was quenched with a saturated aqueous solution of ammonium chloride (10 mL) and the aqueous phase was washed with dichloromethane (3 x 40 mL). The combined organic phases were dried over sodium sulfate and filtered. Trimethoxybenzene (42 mg, 0.25 mmol) was added as an internal standard before evaporating the solvent. A

spectroscopic yield of 60% was determined by ^1H NMR spectroscopy before the crude product was purified by silica gel flash column chromatography, eluting with hexanes to afford the product ($R_f = 0.50$), which was then further isolated from the bisarylated product (although it does not affect the subsequent reaction) through distillation ($R_f = 0.50$). The product was obtained as a colorless oil (244.9 mg, 55%). IR (neat): 2958, 2866, 2360, 1449, 1325, 1161, 1095, 1072, 900, 799, 701, 658 cm^{-1} ; ^1H NMR (400 MHz, CDCl_3): δ 2.04 – 2.14 (m, 2H), 2.85 (t, $J = 7.5$ Hz, 2H), 3.53 (t, $J = 6.3$ Hz, 2H), 7.37 – 7.49 (m, 4H); $\{^1\text{H}\}^{13}\text{C}$ NMR (125 MHz, CDCl_3): δ 32.55, 33.71, 43.88, 123.08 (q, $^3J = 3.9$ Hz), 124.10 (q, $^1J = 272.43$ Hz), 125.17 (q, $^3J = 3.9$ Hz), 128.9, 130.81 (q, $^2J = 32.41$ Hz), 131.93, 141.59. ^{19}F NMR (470 MHz, CDCl_3): δ -62.56 ppm. HRMS (ESI) m/z $[\text{M}]^+$ calcd. For $\text{C}_{10}\text{H}_{10}\text{F}_3\text{Cl}$ 222.64; found 222.04.

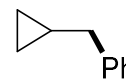
Synthesis of Cinacalcet (2.33). To a 20 mL Schlenk tube was added alkyl chloride **2.31** (240 mg, 1.08 mmol) (present as a mixture of **2.31** and bisarylated



product), potassium iodide (40 mg, 0.24 mmol) and potassium carbonate (331 mg, 2.40 mmol). On a Schlenk line, the Schlenk tube was evacuated and backfilled with nitrogen and then (*R*)-(+)-1-(1-naphthyl)ethylamine (**2.32**, 231 μL , 246 mg, 1.44 mmol) was added by syringe after addition of anhydrous acetonitrile (4 mL). The flask was sealed and then heated to 100 $^{\circ}\text{C}$ for 48 hours. At this time, the reaction was cooled, the insoluble material was filtered, and the solvent evaporated to yield a brown oil. The crude product was dissolved in dichloromethane (20 mL), washed with 5% aqueous hydrochloric acid (25 mL), saturated sodium bicarbonate solution (25 mL), and deionized water (25 mL). The combined organic phases were dried over sodium sulfate, filtered, and the solvent was

removed under reduced pressure. The product was isolated as a pure colorless oil (270 mg, 70%). ^1H NMR matched previously reported values.⁹⁵ $R_f = 0.30$ (1:1 EtOAc/hexane), ^1H NMR (400 MHz, CDCl_3): δ 1.36 (bs, 1H), 1.49 (d, $J = 6.6$ Hz, 3H), 1.84 (tt, $J = 7.4$ Hz, 2H), 2.55 – 2.79 (m, 4H), 4.62 (q, $J = 6.6$ Hz, 1H), 7.28 – 7.38 (m, 2H), 7.39 – 7.55 (m, 5H), 7.61 – 7.67 (m, 1H), 7.75 (d, $J = 8.1$ Hz, 1H), 7.88 (dd, $J = 7.6, 1.7$ Hz, 1H), 8.17 – 8.22 (m, 1H). ^{13}C NMR (500 MHz, CDCl_3) δ 23.56, 31.83, 33.37, 47.23, 53.73, 122.58 (q, $^3J = 4.3$ Hz), 122.62, 122.88, 124.24 (q, $^1J = 274.33$ Hz), 124.99 (q, $^3J = 3.7$ Hz), 125.27, 125.64, 125.72, 127.15, 128.6, 128.94, 130.52 (q, $^2J = 31.9$ Hz), 131.3, 131.72, 133.95, 141.17, 143.04. HRMS (ESI) m/z $[\text{M}]^+$ calcd. For $\text{C}_{22}\text{H}_{22}\text{F}_3\text{N}$ 357.41; found 357.18. $\alpha\text{-}^{24}_{589}$ (c = 1.0, CHCl_3) = +21.8°.

Cross-coupling reaction between PhB(pin) and cyclopropylmethylbromide (2.34). In a nitrogen-filled glovebox complex

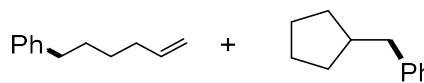


2.10 (21 mg, 0.05 mmol), 2,2-bis((*S*)-4-phenyl-4,5-dihydrooxazol-2-yl)acetonitrile ligand **2.9** (16.5 mg, 0.05 mmol) and lithium ethylmethylamide (38.5 mg, 0.6 mmol) were added to a 7 mL vial containing a stir bar. Benzene (5 mL) was added to the stirring vial followed immediately by a 1 mL benzene solution of phenylboronic acid pinacol ester (204 mg, 1.0 mmol) and cyclopropylmethylbromide (67 mg, 48 μL , 0.5 mmol). The reaction was stirred vigorously and after 15 minutes, a precipitate formed. After 48 hours of stirring, the reaction was brought out of the glovebox and quenched with a saturated aqueous solution of ammonium chloride (10 mL). The aqueous phase was washed with dichloromethane (3 x 40 mL) and the combined organic phases were dried over sodium sulfate and filtered. Trimethoxybenzene (42 mg, 0.25 mmol) was added as an internal standard before evaporating the solvent. A spectroscopic yield was determined by ^1H NMR spectroscopy

using trimethoxy benzene as an internal standard. before the crude product was further purified. This product was purified by silica gel flash column chromatography, eluting with 100% hexanes to afford single purified product **2.35a** as a colorless oil (76% spectroscopic yield / 76% brsm, 55% isolated yield)¹⁷ The product was volatile which complicated isolation. $R_f = 0.80$ (100% hexane), $^1\text{H NMR}$ (500 MHz, CDCl_3) δ 2.36 (q, $J = 7.3$ Hz, 2H), 2.69 (t, $J = 8.2$ Hz, 2H), 4.99 (dd, $J = 13.7, 26$ Hz, 2H), 5.84 (m, 1H), 7.17 (m, 2H), 7.25 (m, 2H), 7.44 (m, 1H) ppm.

Cross-coupling reaction between PhB(pin) and

6-bromohex-1-ene (2.36). In a nitrogen-filled



glovebox complex **2.10** (21 mg, 0.05 mmol), 2,2-bis((*S*)-4-phenyl-4,5-dihydrooxazol-2-yl)acetonitrile ligand **2.9** (16.5 mg, 0.05 mmol) and lithium ethylmethylamide (38.5 mg, 0.6 mmol) were added to a 7 mL vial containing a stir bar. Benzene (5 mL) was added to the stirring vial followed immediately by a 1 mL benzene solution of phenylboronic acid pinacol ester (204 mg, 1.0 mmol) and 6-bromohex-1-ene (81 mg, 67 μL , 0.5 mmol). The reaction was stirred vigorously and after 15 minutes, a precipitate formed. After 48 hours of stirring, the reaction was brought out of the glovebox and quenched with a saturated aqueous solution of ammonium chloride (10 mL). The aqueous phase was washed with dichloromethane (3 x 40 mL) and the combined organic phases were dried over sodium sulfate and filtered. Trimethoxybenzene (42 mg, 0.25 mmol) was added as an internal standard before evaporating the solvent. This reaction produced a mixture of the cyclized and uncyclized products. To verify the ratio, the mixture was also analyzed by gas chromatography as well as the relative integration of the alkene peaks to the overlapping benzylic peaks by NMR. The ratio is between 1.25:1 (GC) and 1.56:1 (NMR) for cyclized

to uncyclized products. Hex-5-enylbenzene (**2.37a**)⁹⁶: $R_f = 0.60$ (100% hexane). $^1\text{H NMR}$ (500 MHz, CDCl_3) δ 1.45 (m, 2H), 1.65 (m, 2H), 2.10 (m, 2H), 2.62 (t, $J = 7.5$ Hz, 2H), 5.00 (dd, $J = 13.7, 26$ Hz, 2H), 5.81 (ddt, $J = 16.9, 10.1, 6.7$ Hz, 1H), 7.18 (m, 3H), 7.26 (m, 2H) ppm. Cyclopentylmethylbenzene (**2.37b**)⁹⁷: $R_f = 0.60$ (100% hexane). $^1\text{H NMR}$ (500 MHz, CDCl_3) δ 1.21 (m, 2H), 1.53 (m, 2H), 1.65 (m, 2H) 1.71 (m, 2H) 2.10 (m, 1H) 2.6 (d, $J = 7.5$ Hz, 2H), 7.18 (m, 3H), 7.26 (m, 2H) ppm.

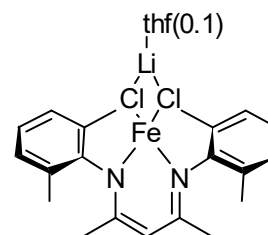
General procedure for synthesis of β -diketiminato ligands. To one-necked 250 mL round-bottom flask equipped with stir bar was added aniline (2.2 equiv.), 2,4-pentanedione (1.0 equiv.), and ethanol (50 mL). 12 M hydrochloric acid (1.2 equiv.) was added dropwise to the stirring reaction mixture. A reflux condenser was attached to the reaction vessel, and the reaction mixture heated to reflux under nitrogen on the Schlenk line for 3 days. The reaction mixture was removed from heat and allowed to cool to room temperature before evaporation *in vacuo*. The resulting tan solid was suspended in hexane, then further washed with hexane through a Büchner funnel. The collected hydrochloride salts were dissolved in dichloromethane and washed with saturated NaHCO_3 (aq) (5 x 20 mL). The collected aqueous layers were extracted with dichloromethane, and the combined organic layers were dried over sodium sulfate, filtered, and concentrated *in vacuo*. In some cases, the collected residue was distilled to remove excess aniline before it was dissolved in hot isopropanol or methanol and subsequently cooled to -40 °C overnight for crystallization. The crystals were collected by filtration and the mother liquor was concentrated and resubjected to recrystallization. Yields reported are the combined yields obtained from the initial crop of crystals and the second crop of crystals obtained from the mother liquor.

General procedure for synthesis of β -diketiminato iron chloride complexes. To an oven-dried round-bottom flask equipped with stirbar was added β -diketiminato ligand (9.8 mmol, 1.0 equiv) and pentane (40 mL, 0.244 M). On the Schlenk line, the mixture was cooled to $-78\text{ }^{\circ}\text{C}$ and degassed by placing the solution under vacuum for at least 5 minutes. A solution of butyl lithium in hexanes (4.21 mL, 2.3 M, 9.75 mmol) was added dropwise while stirring. In most cases, a white precipitate formed rapidly. The reaction mixture was warmed to room temperature while stirring before the solvent was removed under vacuum. The sealed reaction vessel was transferred into a glovebox, where the solid was collected on a frit and washed with cold pentane (5 mL at $-40\text{ }^{\circ}\text{C}$). The solid was dried and weighed to determine stoichiometry for the next step. No characterization of the lithium salts of the ligand were carried out. The collected deprotonated ligand (9.8 mmol) was then dissolved in THF (10 mL) in a 20 mL scintillation vial. This solution was added dropwise to a slurry of iron dichloride (9.8 mmol) in THF (10 mL) prepared in a separate scintillation vial equipped with stir bar. This mixture was allowed to stir overnight. The resulting solution was cooled and passed through celite which was washed with additional THF ($\sim 20\text{ mL}$), then concentrated under vacuum. The resulting semi-solid was then washed with pentane, dried, and collected. Spectra of the 2,4-bis(2,6-diethylphenylimido)pentane⁹⁸ and 2,4-bis(2,6-diisopropylphenylimido)pentane⁹⁹ complexes matched literature line listings.

Elemental analysis of the following iron complexes revealed samples with C, H, and N ratios that match what would be expected for the desired complexes containing variable amounts of THF (typically 2 or 3 equivalents). We have also independently identified that there appears to be exactly 1 equivalent of lithium chloride in the 2,4-bis(2,6-dimethylphenylimido)pentane iron chloride complex by ICP-OES, which is likely true for

all examined complexes. Discrepancies in the elemental analysis are an unidentified inorganic impurity that is not lithium chloride, which accounts for ~5-15 % of the mass. This difficulty has been observed previously in the purification of similar complexes.⁶⁷

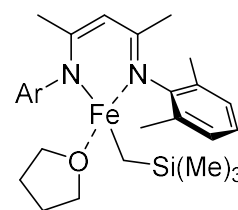
Synthesis of 2,4-bis[(2,6-dimethylphenyl)imino]pentane iron chloride complex (2.44). Synthesized according to general procedure using 2,4-bis[(2,6-dimethylphenyl)imino]pentane (3.0 g, 9.8 mmol) as the ligand which resulted in the formation



of a yellow crystalline solid (3.3 g, 58% yield). ¹H NMR (400 MHz, THF) δ -68.7 (*w*_{1/2} = 180 Hz, 6H), -52.0 (*w*_{1/2} = 100 Hz, 2H), -39.7 (*w*_{1/2} = 264 Hz, 1H), 6.2 (*w*_{1/2} = 254 Hz, 12H), 16.1 (*w*_{1/2} = 82 Hz, 4H) ppm. IR: 2916, 1519, 1373, 1038, 760 cm⁻¹. Elemental analysis for C₂₁H₂₅Cl₂FeLiN₂(C₄H₈O)_{0.1} calc'd C 66.09% H 6.69% N 7.20% Found C 55.71% H 5.69% N 6.06%.

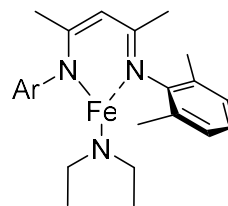
Synthesis of 2,4-bis[(2,6-dimethylphenyl)imino]pentane iron

CH₂TMS tetrahydrofuran adduct (2.45). In the glovebox, to a 7 mL scintillation vial equipped with magnetic stir bar was added 2,4-bis[(2-methylphenyl)imino]pentane iron chloride complex (2.44) (800 mg, 1.37 mmol) and pentane (2 mL). This mixture was allowed to cool to -40 °C in the freezer. A solution of LiCH₂TMS (129 mg, 1.0 equiv) in pentane (1 mL) was added to the stirring reaction mixture. The reaction vessel was sealed and a dark yellow precipitate formed immediately. The reaction was allowed to stir for 1 hour, at which point the precipitate was filtered off through celite and the filtrate concentrated *in vacuo*. The residue was dissolved in pentane and transferred to a vial to recrystallize in the freezer overnight. The mother liquor was decanted to afford the product as a yellow solid (434 mg, 61% yield). ¹H NMR (400 MHz,



C₆D₆) δ 81.30 ($w_{1/2}$ = 294 Hz, 6H), 34.65 ($w_{1/2}$ = 303 Hz, 9H), 3.31 ($w_{1/2}$ = 37 Hz, 4H), 1.58 ($w_{1/2}$ = 12 Hz, 4H), -4.97 ($w_{1/2}$ = 42 Hz, 4H), -61.48 ($w_{1/2}$ = 406 Hz, 12H), -69.12 ($w_{1/2}$ = 68 Hz, 2H). NMR spectrum is in agreement with literature precedence.¹⁰⁰

Synthesis of 2,4-bis[(2,6-dimethylphenyl)imino]pentane iron *N,N*-diethylamide (2.46). In the glovebox, to a 20 mL scintillation vial

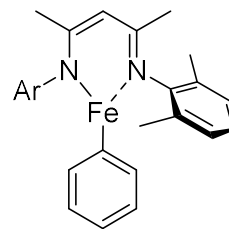


equipped with magnetic stir bar was added 2,4-bis[(2,6-dimethylphenyl)imino]pentane iron CH₂TMS tetrahydrofuran adduct (**2.45**) (200 mg, 390 μ mol) and pentane (5 mL). To this mixture was added diethylamine (40 μ L, 1.0 equiv). The resulting mixture was allowed to stir overnight, turning from yellow to red-orange. The reaction vessel was transferred to the freezer to recrystallize overnight. The pentane was decanted and the resultant red-orange solid washed with fresh cold pentane, and residual pentane removed *in vacuo* to afford the product as a red-orange solid (150 mg, 90% yield).

δ 121.30 ($w_{1/2}$ = 780 Hz, 1H), 50.20 ($w_{1/2}$ = 961 Hz, 6H), 37.77 ($w_{1/2}$ = 355 Hz, 6H), -14.89 ($w_{1/2}$ = 97 Hz, 4H), -73.44 ($w_{1/2}$ = 110 Hz, 2H), -78.58 ($w_{1/2}$ = 530 Hz, 12H). IR: 1506, 1378, 1173, 1096, 765 cm⁻¹. μ_{eff} (C₆D₆, 25 °C): 3.5(1) μ_{B} . When solid state magnetic moments were collected via SQUID spectrometry, there appeared to be little to no magnetic moment for this material, suggesting that it is diamagnetic in the solid state with some paramagnetic impurities. Elemental analysis for C₂₅H₃₅FeN₃ calc'd C 69.28% H 8.14% N 9.70% Found C 68.6% H 7.65% N 9.45%.

Synthesis of 2,4-bis[(2,6-dimethylphenyl)imino]pentane iron

phenyl (**2.47**). In the glovebox, to a 7 mL scintillation vial was added 2,4-bis[(2,6-dimethylphenyl)imino]pentane iron *N,N*-diethylamide (**2.46**) (100 mg, 190 μmol) and diethyl ether (1 mL). To this mixture



was added phenylboronic acid pinacol ester (42 mg, 200 μmol). The resulting mixture was cooled in a glovebox freezer to $-40\text{ }^\circ\text{C}$, turning from red-orange to yellow-black. After approximately one hour, the product precipitated as black metallic crystals that were of X-ray quality. The diethyl ether was decanted and the resultant solid was washed with fresh cold pentane (3 x 1 mL) to remove residual boron-containing compounds. Residual pentane was removed *in vacuo* to afford the product as a pure black solid (42 mg, 50% yield). ^1H NMR (600 MHz, C_6D_6) δ 158.37 ($w_{1/2}$ = 585 Hz, 1H), 116.81 ($w_{1/2}$ = 832 Hz, 1H), 71.76 ($w_{1/2}$ = 635 Hz, 6H), 23.39 ($w_{1/2}$ = 410 Hz, 2H), -6.76 ($w_{1/2}$ = 383 Hz, 4H), -72.87 ($w_{1/2}$ = 709 Hz, 12H), -78.37 ($w_{1/2}$ = 365 Hz, 2H). μ_{eff} (C_6D_6 , 25 $^\circ\text{C}$): 3.7(1) μ_{B} . When solid state magnetic moments were collected via SQUID spectrometry, there appeared to be little to no magnetic moment for this material, suggesting that it is diamagnetic in the solid state with some paramagnetic impurities. IR: 1518, 1377, 1180, 757, 709 cm^{-1} . Elemental analysis for $\text{C}_{27}\text{H}_{30}\text{FeN}_2$ calc'd C 73.97% H 6.90% N 6.39%.

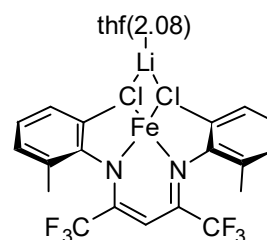
Procedure for the stoichiometric reaction of complex **2.47** with bromocycloheptane.

In a nitrogen-filled glovebox, complex **2.46** (12 mg, 0.03 mmol) was dissolved in C_6D_6 (0.5 mL) and transferred into a J. Young tube. A solution of phenylboronic acid pinacol ester (5.6 mg, 0.03 mmol) in C_6D_6 (0.1 mL) was then added. The reaction was checked by ^1H NMR to verify that complex **2.46** had fully converted to **2.47**. Bromocycloheptane (4.9 mg, 3.8 μL , 0.03 mmol) was added to the tube, it was sealed and then shaken to fully mix.

Over the course of the next 24 hours, the reaction was checked periodically by ^1H NMR until complex **2.47** was fully consumed to generate **2.4**.

Synthesis of 1,1,1,5,5,5-hexafluoro-2,4-bis[(2,6-dimethylphenyl)imino]pentane iron chloride complex (2.48).

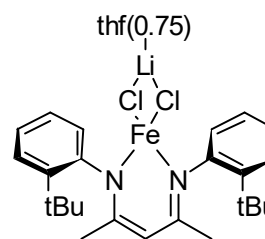
Synthesized according to general procedure using 1,1,1,5,5,5-hexafluoro-2,4-bis[(2,6-dimethylphenyl)imino]pentane (0.95 g,



2.3 mmol) as the ligand which resulted in the formation of a dark red-purple crystalline solid (1.44 g, 90% yield). ^1H NMR (400 MHz, THF) δ -53.9 ($w_{1/2}$ = 89 Hz, 1H), 15.5 ($w_{1/2}$ = 356 Hz, 12H), 18.7 ($w_{1/2}$ = 760 Hz, 4H) ppm. IR: 1564, 1173, 1136, 769 cm^{-1} . Elemental analysis for $\text{C}_{21}\text{H}_{19}\text{Cl}_2\text{F}_6\text{FeLiN}_2(\text{C}_4\text{H}_8\text{O})_{2.08}$ calc'd C 57.92% H 5.91% N 4.61% Found C 49.27% H 5.03% N 3.88%.

Synthesis of 2,4-bis[(2-tert-butylphenyl)imino]pentane iron chloride complex (2.49).

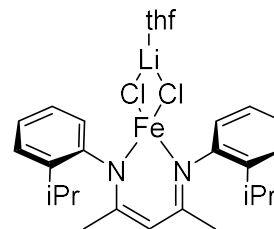
Synthesized according to general procedure using 2,4-bis[(2-tert-butylphenyl)imino]pentane (860 mg, 2.4 mmol) as the ligand which resulted in the



formation of a yellow crystalline solid (1.25 g, 82% yield). ^1H NMR (of the major rotameric species) (400 MHz, THF) δ -62.3 ($w_{1/2}$ = 137 Hz, 6H), -48.1 ($w_{1/2}$ = 69 Hz, 2H), -46.5 ($w_{1/2}$ = 206 Hz, 1H), -5.1 ($w_{1/2}$ = 210 Hz, 18H), 14.3 ($w_{1/2}$ = 60 Hz, 2H) 16.7 (three overlapping peaks, 4H) ppm. IR: 2914, 1377, 1187, 1037, 754 cm^{-1} . Elemental analysis for $\text{C}_{25}\text{H}_{33}\text{Cl}_2\text{FeLiN}_2(\text{C}_4\text{H}_8\text{O})_{0.75}$ calc'd C 62.46% H 8.07% N 3.94% Found C 54.29% H 6.44% N 4.61%.

Synthesis of 2,4-bis[(2-isopropylphenyl)imino]pentane iron

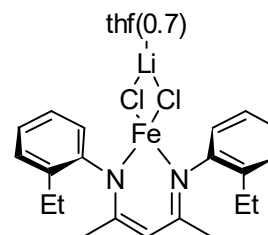
chloride complex (2.50). Synthesized according to the general procedure using 2,4-bis[(2-isopropylphenyl)imino]pentane (1.35 g, 4.0 mmol) as the ligand which resulted in the formation of a



yellow-orange crystalline solid (1.0 g, 40% yield). ^1H NMR (400 MHz, THF) δ -67.2 ($w_{1/2}$ = 161 Hz, 6H), -50.2 ($w_{1/2}$ = 68 Hz, 1H), -49.5 ($w_{1/2}$ = 61 Hz, 1H), -22.7 ($w_{1/2}$ = 116 Hz, 3H), -21.0 ($w_{1/2}$ = 186 Hz, 3H), -1.6 ($w_{1/2}$ = 59 Hz, 3H), 15.2 ($w_{1/2}$ = 42 Hz, 1H), 15.7 ($w_{1/2}$ = 32 Hz, 1H), 16.2 ($w_{1/2}$ = 50 Hz, 1H) ppm. IR: 3100, 1594, 1378, 1030, 751, 697 cm^{-1} . Elemental analysis for $\text{C}_{23}\text{H}_{29}\text{Cl}_2\text{FeLiN}_2(\text{C}_4\text{H}_8\text{O})_1$ calc'd C 69.37% H 7.98% N 5.99% Found C 52.29% H 6.14% N 4.66%.

Synthesis of 2,4-bis[(2-ethylphenyl)imino]pentane iron

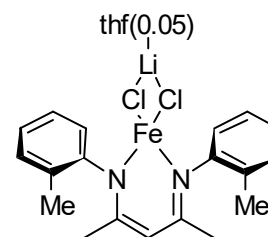
chloride complex (2.51). Synthesized according to the general procedure using 2,4-bis[(2-ethylphenyl)imino]pentane (1.45 g, 4.7 mmol) as the ligand which resulted in the formation of a



yellow-orange crystalline solid (0.90 g, 33% yield). ^1H NMR (400 MHz, THF) δ -67.2 ($w_{1/2}$ = 162 Hz, 6H), -52.1 ($w_{1/2}$ = 187 Hz, 2H), -14.2 ($w_{1/2}$ = 103 Hz, 3H), -11.3 ($w_{1/2}$ = 132 Hz, 3H), 15.9 ($w_{1/2}$ = 289 Hz, 4H) ppm. IR: 2963, 1518, 1373, 1021, 740 cm^{-1} . Elemental analysis for $\text{C}_{21}\text{H}_{25}\text{Cl}_2\text{FeLiN}_2(\text{C}_4\text{H}_8\text{O})_{0.7}$ calc'd C 67.64% H 7.30% N 6.63% Found C 53.35% H 5.87% N 5.35%.

Synthesis of 2,4-bis[(2-methylphenyl)imino]pentane iron chloride complex (2.52).

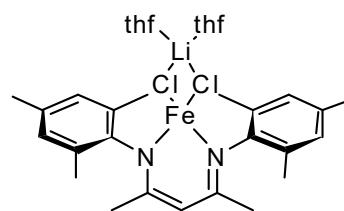
Synthesized according to the general procedure using 2,4-bis[(2-methylphenyl)imino]pentane (2.8 g, 9.9 mmol) as the ligand which resulted in a yellow-orange crystalline solid (1.1 g, 20% yield). A bisligated iron species is very difficult to



remove from this compound and was done by sequential recrystallization from pentane at $-40\text{ }^{\circ}\text{C}$. ^1H NMR (400 MHz, THF) δ -20.6 ($w_{1/2}$ = 427 Hz, 4H), -15.1 ($w_{1/2}$ = 169 Hz, 2H), -10.4 ($w_{1/2}$ = 180 Hz, 1H), 12.4 ($w_{1/2}$ = 180 Hz, 6H), 98.2 ($w_{1/2}$ = 437 Hz, 4H) ppm. IR: 3301, 1665, 1539, 1320, 752, 691 cm^{-1} . Elemental analysis for $\text{C}_{19}\text{H}_{21}\text{Cl}_2\text{FeLiN}_2(\text{C}_4\text{H}_8\text{O})_{0.05}$ calc'd C 64.40% H 6.02% N 7.82% Found C 68.77% H 6.49% N 8.28%.

Synthesis of 2,4-bis[(2,4,6-trimethylphenyl)imino]pentane iron chloride complex (2.53).

Synthesized according to general procedure using 2,4-bis[(2,4,6-trimethylphenyl)imino]pentane (2.0 g, 6

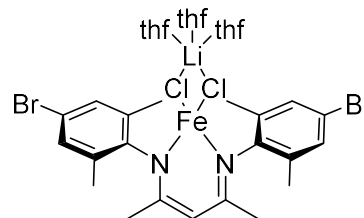


mmol) as the ligand which resulted in the formation of a bright yellow crystalline solid (1.9 g, 52% yield). ^1H NMR (400 MHz, THF) δ -71.6 ($w_{1/2}$ = 145 Hz, 6H), -41.3 ($w_{1/2}$ = 227 Hz, 1H), 6.7 ($w_{1/2}$ = 238 Hz, 12H), 16.6 ($w_{1/2}$ = 71 Hz, 4H), 45.1 ($w_{1/2}$ = 41 Hz, 6H) ppm. IR: 2883, 1524, 1375, 1198, 1038, 759 cm^{-1} . Elemental analysis for $\text{C}_{23}\text{H}_{29}\text{Cl}_2\text{FeLiN}_2(\text{C}_4\text{H}_8\text{O})_2$ calc'd C 71.11% H 8.66% N 5.35% Found C 58.63% H 7.15% N 4.35%.

Synthesis of 2,4-bis[(4-bromo-2,6-dimethylphenyl)imino]pentane iron chloride complex (2.54).

Synthesized according to general procedure using 2,4-bis[(4-bromo-2,6-dimethylphenyl)imino]pentane as

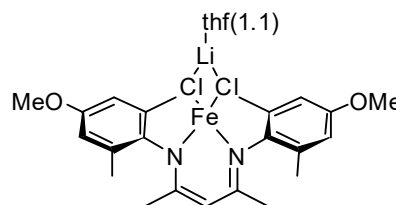
the ligand. ^1H NMR (500 MHz, THF) δ -64.5 ($w_{1/2}$ = 133 Hz, 6H), -35.5 ($w_{1/2}$ = 196 Hz, 1H), 6.1 ($w_{1/2}$ = 231 Hz, 12H), 16.1 ($w_{1/2}$ = 56 Hz, 4H) ppm. IR: 2974, 1573, 1375, 1180, 1039, 851 cm^{-1} .



Synthesis of 2,4-bis[(4-methoxy-2,6-dimethylphenyl)imino]pentane iron chloride complex (2.55).

Synthesized according to general procedure using 2,4-bis[(4-methoxy-2,6-

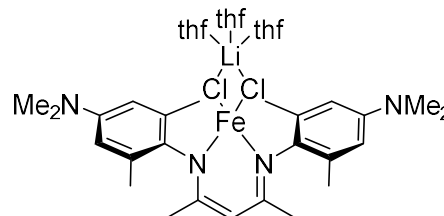
dimethylphenyl)imino]pentane (400 mg, 1.1 mmol) as the ligand which resulted in the formation of a yellow crystalline solid (400 mg, 56% yield). ^1H NMR (400 MHz, THF) δ -74.3 ($w_{1/2}$ = 197 Hz, 6H), -42.3 ($w_{1/2}$ = 310 Hz, 1H), 2.7 ($w_{1/2}$ = 82 Hz, 6H), 6.2 ($w_{1/2}$ = 244 Hz, 12H), 15.4 ($w_{1/2}$ = 74 Hz, 4H) ppm. IR: 2914, 1600, 1376, 1187, 1037, 892 cm^{-1} . Elemental analysis for $\text{C}_{23}\text{H}_{29}\text{Cl}_2\text{FeLiN}_2\text{O}_2(\text{C}_4\text{H}_8\text{O})_{1.1}$ calc'd C 65.16% H 7.54% N 5.55% Found C 50.80% H 5.90% N 4.32%.



Synthesis of 2,4-bis[(4-dimethylamino-2,6-dimethylphenyl)imino]pentane iron chloride complex (2.56).

Synthesized according to general procedure using 2,4-bis[(4-dimethylamino-2,6-

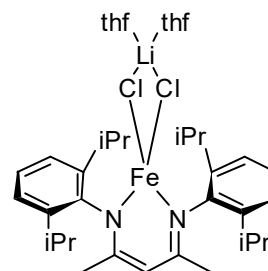
dimethylphenyl)imino]pentane as the ligand. ^1H NMR (400 MHz, THF) δ -77.6 ($w_{1/2}$ = 161



Hz, 6H), -44.8 ($w_{1/2} = 230$ Hz, 1H), 5.7 ($w_{1/2} = 249$ Hz, 12H), 7.9 ($w_{1/2} = 54$ Hz, 12H), 15.3 ($w_{1/2} = 62$ Hz, 4H) ppm. IR: 2912, 1602, 1377, 1353, 1029, 822 cm^{-1} .

Synthesis of 2,4-bis[(2,6-diisopropylphenyl)imino]pentane iron chloride complex (2.57).

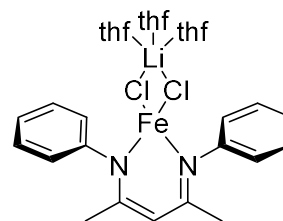
Synthesized according to general procedure using 2,4-bis[(2,6-diisopropylphenyl)imino]pentane (5.0 g, 11.9 mmol) as the ligand which resulted in the formation of a yellow crystalline solid (4.0 g, 48% yield). ^1H NMR (400



MHz, THF) δ 15.28 ($w_{1/2} = 40$ Hz, 4H), 2.23 ($w_{1/2} = 51$ Hz, 12H), -16.55 ($w_{1/2} = 115$ Hz, 12H), -42.97 ($w_{1/2} = 56$ Hz, 2H), -63.88 ($w_{1/2} = 116$ Hz, 6H). NMR spectrum is in agreement with literature precedence.⁹⁹

Synthesis of 2,4-bis(phenylimino)pentane iron chloride complex (2.58).

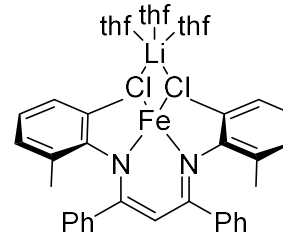
Synthesized according to general procedure using 2,4-bis(phenylimino)pentane as the ligand. ^1H NMR (400



MHz, THF) δ -20.6 ($w_{1/2} = 427$ Hz, 4H), -15.1 ($w_{1/2} = 169$ Hz, 2H), -10.4 ($w_{1/2} = 180$ Hz, 1H), 12.4 ($w_{1/2} = 180$ Hz, 6H), 98.2 ($w_{1/2} = 437$ Hz, 4H) ppm. IR: 3301, 1665, 1539, 1320, 752, 691 cm^{-1} .

Synthesis of 1,3-diphenyl-1,3-bis[(2,6-dimethylphenyl)imino]propane iron chloride complex (2.59).

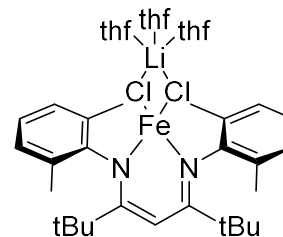
This complex was synthesized using 1,3-diphenyl-1,3-bis[(2,6-dimethylphenyl)imino]propane as the ligand.



Insufficient data for collection due to a spill of the compound.

Synthesis of 2,2,6,6-tetramethyl-3,5-bis[(2,6-dimethylphenyl)imino]heptane iron chloride complex (2.60).

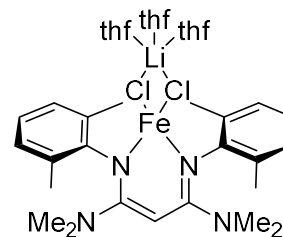
Synthesized according to general procedure using 2,2,6,6-tetramethyl-3,5-bis[(2,6-dimethylphenyl)imino]heptane as the



ligand. ^1H NMR (400 MHz, THF) δ -75.0 ($w_{1/2}$ = 105 Hz, 2H), -51.4 ($w_{1/2}$ = 348 Hz, 1H), 12.8 ($w_{1/2}$ = 152 Hz, 36H), 21.7 ($w_{1/2}$ = 383 Hz, 12H), 22.9 ($w_{1/2}$ = 82 Hz, 4H) ppm. IR: 3301, 1665, 1539, 1320, 752, 691 cm^{-1} .

Synthesis of *N,N,N,N*-tetramethyl-1,3-diamino-1,3-bis[(2,6-dimethylphenyl)imino]propane iron chloride complex (2.61).

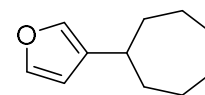
Synthesized according to general procedure using *N,N,N,N*-tetramethyl-1,3-diamino-1,3-bis[(2,6-dimethylphenyl)imino]



propane as the ligand. ^1H NMR (400 MHz, THF) δ -46.6 ($w_{1/2}$ = 837 Hz, 2H), -6.8 ($w_{1/2}$ = 295 Hz, 1H), 9.4 ($w_{1/2}$ = 666 Hz, 12H), 10.7 ($w_{1/2}$ = 147 Hz, 4H), 14.1 ($w_{1/2}$ = 386 Hz, 12H) ppm. IR: 3301, 1665, 1539, 1320, 752, 691 cm^{-1} .

Synthesis of 3-cycloheptyl furan (2.62). 3-cycloheptyl furan was

synthesized from bromocycloheptane and 3-furyl boronic acid



pinacol ester according to the general procedure using the 2-*tert*-

butylphenyl catalyst **2.49** and purified by silica gel flash column chromatography, eluting

with 100% hexanes (R_f = 0.95) to afford the product as a colorless oil (10 mg, 70%

spectroscopic yield, 70% based on recovered starting material, 61% isolated yield). ^1H

NMR (500 MHz, CDCl_3) δ 7.33 (s, 1H), 7.19 (s, 1H), 6.28 (s, 1H), 2.63 (septet, 1H), 1.94

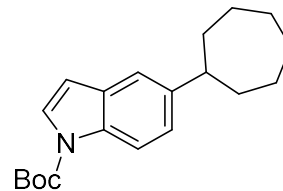
(m, 2H), 1.71 (m, 2H), 1.68 – 1.62 (m, 2H), 1.57 – 1.48 (m, 6H). ^{13}C NMR (126 MHz,

CDCl_3) δ 142.64, 137.53, 132.61, 110.10, 36.88, 35.77, 28.34, 26.50. IR: 2925, 2855, 1752,

1448, 1346, 1073, 1014 cm^{-1} . HRMS-DART (m/z): $[\text{M}+\text{H}]^+$ calculated for $\text{C}_{11}\text{H}_{16}\text{O}$, 164.25; found, 165.13.

Synthesis of 5-cycloheptyl-1-*N*-Boc-indole (2.29).

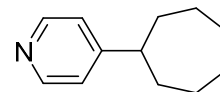
5-cycloheptyl-1-*N*-Boc-indole was synthesized from bromocycloheptane and 1-Boc-indole-5-boronic acid pinacol ester according to the general procedure using the 2-*tert*-



butylphenyl catalyst **2.49** and heated to 50 °C, then purified by silica gel flash column chromatography, eluting with 10% ethyl acetate in hexanes ($R_f = 0.30$) to afford the product as a colorless oil (40 mg, 61% spectroscopic yield, 51% based on recovered starting material, 75% isolated yield). ^1H NMR (500 MHz, CDCl_3) δ 8.06 – 7.98 (m, 1H), 7.62 – 7.54 (m, 1H), 7.37 (d, $J = 1.8$ Hz, 1H), 7.16 (dd, $J = 8.6, 1.8$ Hz, 1H), 6.51 (dd, $J = 3.7, 0.8$ Hz, 1H), 2.76 (tt, $J = 10.6, 3.6$ Hz, 1H), 2.00 – 1.91 (m, 2H), 1.91 – 1.78 (m, 1H), 1.80 – 1.65 (m, 12H), 1.67 (s, 9H), 1.65 – 1.58 (m, 1H), 1.61 – 1.50 (m, 1H). ^{13}C NMR (126 MHz, CDCl_3) δ 144.63, 130.68, 125.87, 123.44, 118.35, 114.87, 107.26, 83.36, 46.98, 37.28, 31.58, 28.20, 27.98, 27.26, 22.64, 14.10. IR: 2925, 2854, 1733, 1469, 1369, 1253, 1161 cm^{-1} . HRMS-DART (m/z): $[\text{M}+\text{H}]^+$ calculated for $\text{C}_{20}\text{H}_{27}\text{NO}_2$, 313.44; found, 314.21.

Synthesis of 4-cycloheptyl pyridine (2.63).

4-cycloheptyl pyridine was synthesized from bromocycloheptane and 4-pyridyl boronic acid pinacol ester according to the general procedure using the 2-

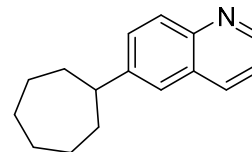


tert-butylphenyl catalyst **2.49** and heated to 50 °C, then purified by silica gel flash column chromatography, eluting with 100% hexanes ($R_f = 0.50$) to afford the product as a colorless oil (14 mg, 37% spectroscopic yield, 56% based on recovered starting material, 32% isolated yield). ^1H NMR (500 MHz, CDCl_3) δ 8.49 – 8.44 (m, 2H), 7.08 (m, 2H), 2.64,

(m, 1H), 1.90-1.83 (m, 2H), 1.82-1.74 (m, 2H), 1.71-1.49 (m, 8H). NMR spectrum is in agreement with literature precedence.¹⁰¹

Synthesis of 6-cycloheptyl quinoline (2.64). 6-cycloheptyl

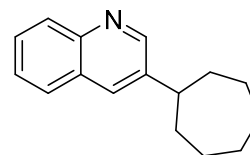
quinoline was synthesized from bromocycloheptane and 6-quinolyl boronic acid pinacol ester according to the general



procedure using the 2-*tert*-butylphenyl catalyst **2.49** and heated to 50 °C, then purified by silica gel flash column chromatography, eluting with 30% ethyl acetate in hexanes ($R_f = 0.45$) to afford the product as a colorless oil (42 mg, 80% spectroscopic yield, 93% based on recovered starting material, 75% isolated yield). ^1H NMR (500 MHz, CDCl_3) δ 8.85 (d, $J = 4.2$ Hz, 1H), 8.10 (d, $J = 8.4$ Hz, 1H), 8.03 (d, $J = 8.6$ Hz, 1H), 7.63 – 7.55 (m, 2H), 7.36 (dd, $J = 8.3, 4.2$ Hz, 1H), 2.87 (septet, 1H), 2.05 – 1.96 (m, 2H), 1.89 – 1.81 (m, 2H), 1.81 – 1.68 (m, 4H), 1.68 – 1.57 (m, 4H). ^{13}C NMR (101 MHz, CDCl_3) δ 149.59, 148.41, 147.16, 135.90, 129.98, 129.39, 128.52, 124.16, 121.11, 47.04, 36.84, 28.10, 27.41. IR: 2921, 2853, 1593, 1498, 1459, 827 cm^{-1} . HRMS-DART (m/z): $[\text{M}+\text{H}]^+$ calculated for $\text{C}_{16}\text{H}_{19}\text{N}$, 225.34; found, 226.16.

Synthesis of 3-cycloheptyl quinoline (2.65). 3-cycloheptyl

quinoline was synthesized from bromocycloheptane and 3-quinolyl boronic acid pinacol ester according to the general

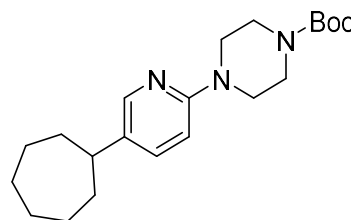


procedure using the 2-*tert*-butylphenyl catalyst **2.49** and heated to 50 °C, then purified by silica gel flash column chromatography, eluting with 30% ethyl acetate in hexanes ($R_f = 0.65$) to afford the product as a colorless oil (23 mg, 45% spectroscopic yield, 58% based on recovered starting material, 40% isolated yield). ^1H NMR (500 MHz, CDCl_3) δ 8.81 (s, 1H), 8.08 (s, 1H), 7.92 (s, 1H), 7.78 (d, $J = 8.2$ Hz, 1H), 7.65 (s, 1H), 7.52 (s, 1H), 2.90

(septet, 1H), 2.03 – 2.00 (m, 2H), 1.90 – 1.83 (m, 2H), 1.82 – 1.70 (m, 4H), 1.70 – 1.57 (m, 4H). ^{13}C NMR (151 MHz, CDCl_3) δ 151.50, 146.88, 142.35, 132.20, 129.19, 128.57, 128.45, 127.59, 126.60, 44.61, 36.69, 28.03, 27.29. IR: 2922, 2853, 1493, 1460, 787, 750 cm^{-1} . HRMS-DART (m/z): $[\text{M}+\text{H}]^+$ calculated for $\text{C}_{16}\text{H}_{19}\text{N}$, 225.34; found, 226.16.

Synthesis of 6-(4-Boc-piperazin-1-yl)-3-cycloheptyl

pyridine (2.66). 6-(4-Boc-piperazin-1-yl)-3-cycloheptylpyridine was synthesized from bromocycloheptane and 6-(4-Boc-piperazin-1-yl)pyridine-

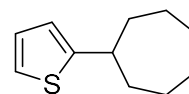


3-boronic acid pinacol ester according to the general procedure using the 2-*tert*-butylphenyl catalyst **2.49** and purified by silica gel flash column chromatography, eluting with 30% ethyl acetate in hexanes ($R_f = 0.75$) to afford the product as a white solid (66 mg, 81% spectroscopic yield, 87% based on recovered starting material, 74% isolated yield).

^1H NMR (500 MHz, CDCl_3) δ 8.04 (s, 1H), 7.35 (d, $J = 8.7$ Hz, 1H), 6.60 (d, $J = 8.7$ Hz, 1H), 3.54 (m, 4H), 3.46 (m, 4H), 2.58 (septet, 1H), 1.85 (m, 2H), 1.77 (m, 2H), 1.68 (m, 2H), 1.64 – 1.50 (m, 6H), 1.48 (s, 9H). ^{13}C NMR (151 MHz, CDCl_3) δ 154.96, 146.04, 136.40, 135.11, 107.59, 80.12, 45.87, 43.57, 36.82, 29.85, 28.58, 28.02, 27.12. IR: 2923, 2855, 1697, 1604, 1408, 1365, 1238, 1168 cm^{-1} . HRMS-DART (m/z): $[\text{M}+\text{H}]^+$ calculated for $\text{C}_{21}\text{H}_{33}\text{N}_3\text{O}_2$, 359.51; found, 360.30.

Synthesis of 2-cycloheptyl thiophene (2.28). 2-cycloheptyl

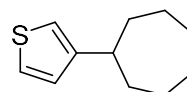
thiophene was synthesized from bromocycloheptane and 2-thiophene boronic acid pinacol ester according to the general procedure using the 2-*tert*-butylphenyl catalyst **2.49** and purified by



silica gel flash column chromatography, eluting with 100% hexanes ($R_f = 0.75$) to afford

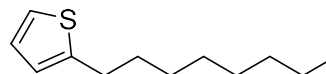
the product as a colorless oil (26 mg, 67% spectroscopic yield, 73% based on recovered starting material, 58% isolated yield). ^1H NMR (500 MHz, CDCl_3) δ 7.09 (dd, $J = 5.1, 1.2$ Hz, 1H), 6.90 (dd, $J = 5.1, 3.4$ Hz, 1H), 6.78 (d, 1H), 3.03 (septet, $J = 4.6$ Hz, 1H), 2.12 – 2.03 (m, 1H), 1.81 – 1.64 (m, 4H), 1.57 – 1.48 (m, 5H). ^{13}C NMR (126 MHz, CDCl_3) δ 153.65, 126.32, 122.00, 121.69, 41.61, 37.53, 28.13, 26.32. IR: 2923, 2853, 1459, 1442, 1234, 850, 815, 689 cm^{-1} . HRMS-DART (m/z): $[\text{M}+\text{H}]^+$ calculated for $\text{C}_{11}\text{H}_{16}\text{S}$, 180.31; found, 181.10.

Synthesis of 3-cycloheptyl thiophene (2.67). 3-cycloheptyl



thiophene was synthesized from bromocycloheptane and 3-thiophene boronic acid pinacol ester according to the general procedure using the 2-*tert*-butylphenyl catalyst **2.49** and purified by silica gel flash column chromatography, eluting with 100% hexanes ($R_f = 0.75$) to afford the product as a yellow oil (37 mg, 88% spectroscopic yield, 88% based on recovered starting material, 82% isolated yield). ^1H NMR (500 MHz, CDCl_3) δ 7.22 (t, $J = 3.9$ Hz, 1H), 6.97 (d, $J = 5.0$ Hz, 1H), 6.91 (s, 1H), 2.83 (septet, $J = 9.9, 4.0$ Hz, 1H), 1.98 (m, 2H), 1.80 – 1.72 (m, 2H), 1.71 – 1.47 (m, 8H). ^{13}C NMR (126 MHz, CDCl_3) δ 150.46, 127.34, 125.09, 118.10, 41.93, 36.39, 28.26, 26.80. IR: 2921, 2853, 1459, 771, 645 cm^{-1} . HRMS-DART (m/z): $[\text{M}+\text{H}]^+$ calculated for $\text{C}_{11}\text{H}_{16}\text{S}$, 180.31; found, 181.10.

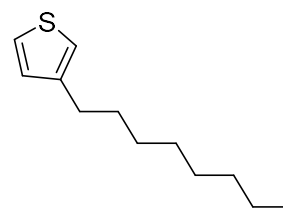
Synthesis of 2-octylthiophene (2.68). 2-octylthiophene



was synthesized from 1-bromooctane and 2-thiophene boronic acid pinacol ester according to the general procedure using the 2-*tert*-butylphenyl catalyst **2.49** and purified by silica gel flash column chromatography, eluting with 100% hexanes ($R_f = 0.65$) to afford the product as a colorless

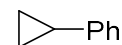
oil (12 mg, 28% spectroscopic yield, 72% based on recovered starting material, 25% isolated yield). ^1H NMR (400 MHz, CDCl_3) δ 7.10 (d, $J = 5.1$ Hz, 1H), 6.91 (dd, $J = 5.1$, 3.4 Hz, 1H), 6.77 (d, $J = 3.4$ Hz, 1H), 2.82 (t, $J = 7.7$ Hz, 2H), 1.67 (p, $J = 7.5$ Hz, 2H), 1.40 – 1.23 (m, 10H), 0.88 (t, $J = 6.7$ Hz, 3H). ^{13}C NMR (101 MHz, CDCl_3) δ 146.05, 126.77, 124.02, 122.84, 32.01, 31.96, 30.07, 29.48, 29.37, 29.29, 22.81, 14.25. IR: 2925, 2854, 1464, 907, 733, 690 cm^{-1} . HRMS-DART (m/z): $[\text{M}+\text{H}]^+$ calculated for $\text{C}_{12}\text{H}_{20}\text{S}$, 196.35; found, 197.14.

Synthesis of 3-octylthiophene (2.69). 3-octylthiophene was synthesized from 1-bromooctane and 3-thiophene boronic acid pinacol ester according to the general procedure using the 2-*tert*-butylphenyl catalyst **2.49** and heated to 50 $^\circ\text{C}$, then purified



by silica gel flash column chromatography, eluting with 100% hexanes ($R_f = 0.65$) to afford the product as a colorless oil (30 mg, 64% spectroscopic yield, 90% based on recovered starting material, 61% isolated yield). ^1H NMR (400 MHz, CDCl_3) δ 7.23 (m, 1H), 6.96 – 6.89 (m, 2H), 2.62 (t, $J = 7.7$ Hz, 2H), 1.62 (p, $J = 7.3$ Hz, 2H), 1.37 – 1.25 (m, 10H), 0.88 (t, $J = 6.5$ Hz, 3H). ^{13}C NMR (101 MHz, CDCl_3) δ 143.44, 128.45, 125.16, 119.89, 32.04, 30.72, 30.44, 29.59, 29.50, 29.41, 22.82, 14.26. IR: 2925, 2854, 1465, 907, 773, 733 cm^{-1} . HRMS-DART (m/z): $[\text{M}+\text{H}]^+$ calculated for $\text{C}_{12}\text{H}_{20}\text{S}$, 196.35; found, 197.14.

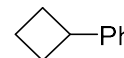
Synthesis of phenylcyclopropane (2.71). Phenylcyclopropane was synthesized from bromocyclobutane and phenyl boronic acid pinacol ester



according to the general procedure using the 2-*tert*-butylphenyl catalyst **2.49** and purified by silica gel flash column chromatography, eluting with 100% hexanes to afford product as a colorless oil (28 mg, 99% spectroscopic yield, 99% based on recovered starting

material, 95% isolated yield). ^1H NMR (500 MHz, CDCl_3) δ 7.47 (d, $J = 7.4$ Hz, 2H), 7.15 (t, $J = 7.5$ Hz, 1H), 7.09 (d, $J = 7.8$ Hz, 2H), 1.91 (tt, $J = 8.7, 5.1$ Hz, 1H), 0.97 (q, $J = 8.4$ Hz, 2H), 0.71 (q, $J = 4.6$ Hz, 2H) ppm. NMR spectrum is in agreement with literature precedence.¹⁰²

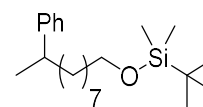
Synthesis of phenylcyclobutane (2.72). Phenylcyclobutane was synthesized from bromocyclobutane and phenyl boronic acid pinacol ester



according to general procedure using the 2-*tert*-butylphenyl catalyst **2.49** and purified by silica gel flash column chromatography, eluting with 100% hexanes to afford product as a colorless oil (20 mg, 63% spectroscopic yield, 63% based on recovered starting material, 61% isolated yield). $R_f = 0.70$ (100% hexanes) ^1H NMR (400 MHz, CDCl_3): δ 7.15 – 7.33 (m, 5H), 3.56 (p, $J = 8.8, 8.1$ Hz, 1H), 1.81 – 2.40 (m, 6H) ppm. NMR spectrum is in agreement with literature precedence.¹⁰³

Synthesis of *tert*-butyldimethyl((9-phenyldecyl)oxy)silane

(2.73). *tert*-butyldimethyl((9-phenyldecyl)oxy)silane was

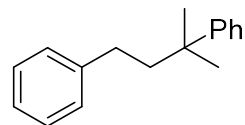


synthesized from *tert*-butyldimethyl((9-bromodecyl)oxy)silane

and phenyl boronic acid pinacol ester according to the general procedure using the 2-*tert*-butylphenyl catalyst **2.49** and purified by silica gel flash column chromatography, eluting with 100% hexanes to afford product as a colorless oil (48 mg, 71% spectroscopic yield, 71% based on recovered starting material, 55% isolated yield). Slight decomposition was observed on silica. $R_f = 0.45$ (100% hexanes) ^1H NMR (600 MHz, CDCl_3) δ 7.31 – 7.26 (m, 2H), 7.21 – 7.12 (m, 3H), 3.59 (t, $J = 6.7$ Hz, 2H), 2.67 (q, $J = 7.1$ Hz, 1H), 1.56 – 1.51 (m, 2H), 1.51 – 1.44 (m, 2H), 1.35 – 1.19 (m, 13H), 1.18 – 1.12 (m, 2H), 0.90 (s, 9H), 0.05 (s, 6H). ^{13}C NMR (151 MHz, CDCl_3) δ 150.61, 130.88, 129.62, 128.36, 65.98, 42.59,

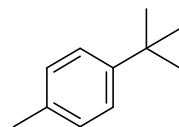
41.09, 35.52, 32.32, 32.19, 32.07, 30.35, 28.65, 28.43, 24.97, 21.03, -2.59. HRMS-DART (m/z): $[M+H]^+$ calculated for $C_{22}H_{41}OSi$, 349.29054; found, 349.29212.

Synthesis of 1,1-dimethyl-1,3-diphenylpropane (2.74). 1,1-dimethyl-1,3-diphenylpropane was synthesized from 3-chloro-1,1-dimethyl-1-phenylpropane and phenyl boronic acid pinacol ester



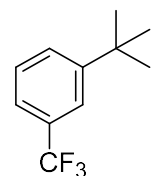
according to the general procedure using the fluorinated catalyst **2.48** and purified by silica gel flash column chromatography, eluting with 100% hexanes to afford product as a colorless oil (38 mg, 69% spectroscopic yield, 99% based on recovered starting material, 65% isolated yield). 1H NMR (500 MHz, $CDCl_3$) δ 7.47 – 7.08 (m, 10H), 2.36 (t, $J = 7.3$ Hz, 2H), 1.94 (t, $J = 8.6$ Hz, 2H), 1.39 (s, 6H). NMR spectrum is in agreement with literature precedence.¹⁰⁴

Synthesis of 1-tert-butyl-4-methylbenzene (2.77). 1-tert-butyl-4-methylbenzene was synthesized from 2-chloro-2-methylpropane and 4-tolyl boronic acid pinacol ester according to the general procedure using



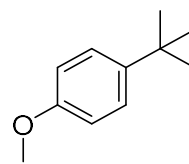
the fluorinated catalyst **2.48** and purified by silica gel flash column chromatography, eluting with 100% hexanes to afford purified product as a colorless oil (21 mg, 58% spectroscopic yield, 56% isolated yield). 1H NMR (500 MHz, $CDCl_3$) δ 7.31 (d, $J = 7.9$ Hz, 2H), 7.14 (d, $J = 7.9$ Hz, 2H), 2.34 (s, 3H), 1.33 (s, 9H). NMR spectrum is in agreement with literature precedence.¹⁰⁵

Synthesis of 1-tert-butyl-3-trifluoromethylbenzene (2.78). 1-tert-butyl-3-trifluoromethylbenzene was synthesized from 2-chloro-2-methylpropane and (*meta*-trifluoromethyl)phenyl boronic acid pinacol



ester according to the general procedure using the fluorinated catalyst **2.48** and purified by silica gel flash column chromatography, eluting with 100% hexanes to afford purified product as a colorless oil (35 mg, 72% spectroscopic yield, 69% isolated yield). ^1H NMR (500 MHz, CDCl_3) δ 7.05 (m, 5H), 1.27 (s, 9H). NMR spectrum is in agreement with literature precedence.¹⁰⁶

Synthesis of 1-tert-butyl-4-methoxybenzene (2.79). 1-tert-butyl-4-methoxybenzene was synthesized from 2-chloro-2-methylpropane and 4-anisoyl boronic acid pinacol ester according to the general procedure



using the fluorinated catalyst **2.48** and purified by silica gel flash column chromatography, eluting with 100% hexanes to afford purified product as a colorless oil (21 mg, 55% spectroscopic yield, 51% isolated yield). ^1H NMR (500 MHz, CDCl_3) δ 7.33 (d, $J = 8.3$ Hz, 2H), 6.87 (d, $J = 8.3$ Hz, 2H), 3.81 (s, 3H), 1.32 (s, 9H). NMR spectrum is in agreement with literature precedence.¹⁰⁷

General procedure for the monitoring of transmetallation kinetics at low temperature. At room temperature in the glovebox, a solution of iron amide **2.46** in deuterated toluene (500 μL , 0.0115 M) was added to a J. Young tube. To this solution was added $\text{Si}(\text{TMS})_4$ (50 μL , 0.0115 M) as internal standard. The J. Young tube was placed in the cold well, where the solution froze under liquid nitrogen. A cold solution of $\text{PhB}(\text{pin})$ in deuterated toluene (50 μL , 0.115 M) was added to the tube and allowed to freeze as a separate layer on top of the frozen solution of iron complex and standard. The layered tube was sealed, quickly removed from the glovebox, and immediately submerged in liquid nitrogen. The frozen tube was transported to a pre-cooled NMR machine. Once array parameters were set up on the NMR software, the frozen tube was thawed in a dry

ice/acetone bath to allow for homogenous mixing of the frozen layers. The tube was quickly inserted into the temperature-regulated NMR machine and the array started. Integrations were calculated using vNMRJ software.

2.12 References

- (1) Jana, R.; Pathak, T. P.; Sigman, M. S. Advances in Transition Metal (Pd,Ni,Fe)-Catalyzed Cross-Coupling Reactions Using Alkyl-Organometallics as Reaction Partners. *Chem. Rev.* **2011**, *111* (3), 1417–1492. <https://doi.org/10.1021/cr100327p>.
- (2) Miyaura, N.; Yamada, K.; Suzuki, A. A New Stereospecific Cross-Coupling by the Palladium-Catalyzed Reaction of 1-Alkenylboranes with 1-Alkenyl or 1-Alkynyl Halides. *Tetrahedron Lett.* **1979**, *20* (36), 3437–3440. [https://doi.org/10.1016/S0040-4039\(01\)95429-2](https://doi.org/10.1016/S0040-4039(01)95429-2).
- (3) Miyaura, N.; Yanagi, T.; Suzuki, A. The Palladium-Catalyzed Cross-Coupling Reaction of Phenylboronic Acid with Haloarenes in the Presence of Bases. *Synth. Commun.* **1981**, *11* (7), 513–519. <https://doi.org/10.1080/00397918108063618>.
- (4) Lennox, A. J. J.; Lloyd-Jones, G. C. Selection of Boron Reagents for Suzuki–Miyaura Coupling. *Chem. Soc. Rev.* **2014**, *43* (1), 412–443. <https://doi.org/10.1039/C3CS60197H>.
- (5) Egorova, K. S.; Ananikov, V. P. Toxicity of Metal Compounds: Knowledge and Myths. *Organometallics* **2017**, *36* (21), 4071–4090. <https://doi.org/10.1021/acs.organomet.7b00605>.
- (6) Choi, J.; Fu, G. C. Transition Metal–Catalyzed Alkyl–Alkyl Bond Formation: Another Dimension in Cross-Coupling Chemistry. *Science* **2017**, *356* (6334), eaaf7230. <https://doi.org/10.1126/science.aaf7230>.
- (7) Brown, D. G.; Boström, J. Analysis of Past and Present Synthetic Methodologies on Medicinal Chemistry: Where Have All the New Reactions Gone? *J. Med. Chem.* **2016**, *59* (10), 4443–4458. <https://doi.org/10.1021/acs.jmedchem.5b01409>.
- (8) Lundin, P. M.; Fu, G. C. Asymmetric Suzuki Cross-Couplings of Activated Secondary Alkyl Electrophiles: Arylations of Racemic α -Chloroamides. *J. Am. Chem. Soc.* **2010**, *132* (32), 11027–11029. <https://doi.org/10.1021/ja105148g>.
- (9) Owston, N. A.; Fu, G. C. Asymmetric Alkyl–Alkyl Cross-Couplings of Unactivated

Secondary Alkyl Electrophiles: Stereoconvergent Suzuki Reactions of Racemic Acylated Halohydrins. *J. Am. Chem. Soc.* **2010**, *132* (34), 11908–11909. <https://doi.org/10.1021/ja105924f>.

(10) Fürstner, A.; Leitner, A. Iron-Catalyzed Cross-Coupling Reactions of Alkyl-Grignard Reagents with Aryl Chlorides, Tosylates, and Triflates. *Angew. Chemie - Int. Ed.* **2002**, *41* (4), 609–612. [https://doi.org/10.1002/1521-3773\(20020215\)41:4<609::AID-ANIE609>3.0.CO;2-M](https://doi.org/10.1002/1521-3773(20020215)41:4<609::AID-ANIE609>3.0.CO;2-M).

(11) Martin, R.; Fürstner, A. Cross-Coupling of Alkyl Halides with Aryl Grignard Reagents Catalyzed by a Low-Valent Iron Complex. *Angew. Chemie - Int. Ed.* **2004**, *43* (30), 3955–3957. <https://doi.org/10.1002/anie.200460504>.

(12) Nakamura, M.; Matsuo, K.; Ito, S.; Nakamura, E. Iron-Catalyzed Cross-Coupling of Primary and Secondary Alkyl Halides with Aryl Grignard Reagents. *J. Am. Chem. Soc.* **2004**, *126* (12), 3686–3687. <https://doi.org/10.1021/ja049744t>.

(13) Ito, S.; Fujiwara, Y.; Nakamura, E.; Nakamura, M. Iron-Catalyzed Cross-Coupling of Alkyl Sulfonates with Arylzinc Reagents. *Org. Lett.* **2009**, *11* (19), 4306–4309. <https://doi.org/10.1021/ol901610a>.

(14) Hatakeyama, T.; Hashimoto, T.; Kondo, Y.; Fujiwara, Y.; Seike, H.; Takaya, H.; Tamada, Y.; Ono, T.; Nakamura, M. Iron-Catalyzed Suzuki-Miyaura Coupling of Alkyl Halides. *J. Am. Chem. Soc.* **2010**, *132* (31), 10674–10676. <https://doi.org/10.1021/ja103973a>.

(15) Iwamoto, T.; Okuzono, C.; Adak, L.; Jin, M.; Nakamura, M. Iron-Catalysed Enantioselective Suzuki–Miyaura Coupling of Racemic Alkyl Bromides. *Chem. Commun.* **2019**, *55* (8), 1128–1131. <https://doi.org/10.1039/C8CC09523J>.

(16) Bedford, R. B.; Bruce, D. W.; Frost, R. M.; Hird, M. Simple Iron-Amine Catalysts for the Cross-Coupling of Aryl Grignards with Alkyl Halides Bearing β -Hydrogens. *Chem. Commun.* **2005**, No. 33, 4161–4163. <https://doi.org/10.1039/b507133j>.

(17) Bedford, R. B.; Brenner, P. B.; Carter, E.; Carvell, T. W.; Cogswell, P. M.;

Gallagher, T.; Harvey, J. N.; Murphy, D. M.; Neeve, E. C.; Nunn, J.; et al. Expedient Iron-Catalyzed Coupling of Alkyl, Benzyl and Allyl Halides with Arylboronic Esters. *Chem. - A Eur. J.* **2014**, *20* (26), 7935–7938. <https://doi.org/10.1002/chem.201402174>.

(18) O'Brien, H. M.; Manzotti, M.; Abrams, R. D.; Elorriaga, D.; Sparkes, H. A.; Davis, S. A.; Bedford, R. B. Iron-Catalysed Substrate-Directed Suzuki Biaryl Cross-Coupling. *Nat. Catal.* **2018**, *1* (6), 429–437. <https://doi.org/10.1038/s41929-018-0081-x>.

(19) Nagano, T.; Hayashi, T. Iron-Catalyzed Grignard Cross-Coupling with Alkyl Halides Possessing β -Hydrogens. *Org. Lett.* **2004**, *6* (8), 1297–1299. <https://doi.org/10.1021/ol049779y>.

(20) Gao, H. H.; Yan, C. H.; Tao, X. P.; Xia, Y.; Sun, H. M.; Shen, Q.; Zhang, Y. Synthesis of Anionic Iron(II) Complex Bearing an n-Heterocyclic Carbene Ligand and Its Catalysis for Aryl Grignard Cross-Coupling of Alkyl Halides. *Organometallics* **2010**, *29* (18), 4189–4192. <https://doi.org/10.1021/om100482w>.

(21) Xue, F.; Zhao, J.; Hor, T. S. A. Iron(I) Complexes with Functionalized Amine-Pyrazolyl Tripodal Ligands in the Cross-Coupling of Aryl Grignard with Alkyl Halides. *Dalt. Trans.* **2011**, *40* (35), 8935. <https://doi.org/10.1039/c1dt10258c>.

(22) Yamaguchi, Y.; Ando, H.; Nagaya, M.; Hinago, H.; Ito, T.; Asami, M. Synthesis of Iron(III) Complex Bearing Tridentate β -Aminoketonato Ligand: Application to Iron-Catalyzed Cross-Coupling Reaction of Arylmagnesium Bromides with Alkyl Halides. *Chem. Lett.* **2011**, *40* (9), 983–985. <https://doi.org/10.1246/cl.2011.983>.

(23) Bauer, G.; Wodrich, M. D.; Scopelliti, R.; Hu, X. Iron Pincer Complexes as Catalysts and Intermediates in Alkyl-Aryl Kumada Coupling Reactions. *Organometallics* **2015**, *34* (1), 289–298. <https://doi.org/10.1021/om501122p>.

(24) Smith, M. B.; Becker, W. E. The Constitution of the Grignard Reagent—II. *Tetrahedron* **1966**, *22* (9), 3027–3036. [https://doi.org/10.1016/S0040-4020\(01\)82282-1](https://doi.org/10.1016/S0040-4020(01)82282-1).

(25) Crockett, M. P.; Tyrol, C. C.; Wong, A. S.; Li, B.; Byers, J. A. Iron-Catalyzed Suzuki–Miyaura Cross-Coupling Reactions between Alkyl Halides and Unactivated

Arylboronic Esters. *Org. Lett.* **2018**, *20* (17), 5233–5237.
<https://doi.org/10.1021/acs.orglett.8b02184>.

(26) Crockett, M. P.; Wong, A. S.; Li, B.; Byers, J. A. Rational Design of an Iron-Based Catalyst for Suzuki–Miyaura Cross-Couplings Involving Heteroaromatic Boronic Esters and Tertiary Alkyl Electrophiles. *Angew. Chemie Int. Ed.* **2020**, *59* (13), 5392–5397.
<https://doi.org/10.1002/anie.201914315>.

(27) Daifuku, S. L.; Al-Afyouni, M. H.; Snyder, B. E. R.; Kneebone, J. L.; Neidig, M. L. A Combined Mössbauer, Magnetic Circular Dichroism, and Density Functional Theory Approach for Iron Cross-Coupling Catalysis: Electronic Structure, in Situ Formation, and Reactivity of Iron-Mesityl-Bisphosphines. *J. Am. Chem. Soc.* **2014**, *136* (25), 9132–9143.
<https://doi.org/10.1021/ja503596m>.

(28) Daifuku, S. L.; Kneebone, J. L.; Snyder, B. E. R.; Neidig, M. L. Iron(II) Active Species in Iron–Bisphosphine Catalyzed Kumada and Suzuki–Miyaura Cross-Couplings of Phenyl Nucleophiles and Secondary Alkyl Halides. *J. Am. Chem. Soc.* **2015**, *137* (35), 11432–11444. <https://doi.org/10.1021/jacs.5b06648>.

(29) Hedström, A.; Izakian, Z.; Vreto, I.; Wallentin, C. J.; Norrby, P. O. On the Radical Nature of Iron-Catalyzed Cross-Coupling Reactions. *Chem. - A Eur. J.* **2015**, *21* (15), 5946–5953. <https://doi.org/10.1002/chem.201406096>.

(30) Butters, M.; Harvey, J. N.; Jover, J.; Lennox, A. J. J.; Lloyd-Jones, G. C.; Murray, P. M. Aryl Trifluoroborates in Suzuki–Miyaura Coupling: The Roles of Endogenous Aryl Boronic Acid and Fluoride. *Angew. Chemie Int. Ed.* **2010**, *49* (30), 5156–5160.
<https://doi.org/10.1002/anie.201001522>.

(31) Lennox, A. J. J.; Lloyd-Jones, G. C. Transmetalation in the Suzuki–Miyaura Coupling: The Fork in the Trail. *Angew. Chemie Int. Ed.* **2013**, *52* (29), 7362–7370.
<https://doi.org/10.1002/anie.201301737>.

(32) Matos, K.; Soderquist, J. A. Alkylboranes in the Suzuki–Miyaura Coupling: Stereochemical and Mechanistic Studies. *J. Org. Chem.* **1998**, *63* (3), 461–470.
<https://doi.org/10.1021/jo971681s>.

- (33) Carrow, B. P.; Hartwig, J. F. Distinguishing Between Pathways for Transmetalation in Suzuki–Miyaura Reactions. *J. Am. Chem. Soc.* **2011**, *133* (7), 2116–2119. <https://doi.org/10.1021/ja1108326>.
- (34) Thomas, A. A.; Denmark, S. E. Pre-Transmetalation Intermediates in the Suzuki–Miyaura Reaction Revealed: The Missing Link. *Science* **2016**, *352* (6283), 329–332. <https://doi.org/10.1126/science.aad6981>.
- (35) Thomas, A. A.; Zahrt, A. F.; Delaney, C. P.; Denmark, S. E. Elucidating the Role of the Boronic Esters in the Suzuki–Miyaura Reaction: Structural, Kinetic, and Computational Investigations. *J. Am. Chem. Soc.* **2018**, *140* (12), 4401–4416. <https://doi.org/10.1021/jacs.8b00400>.
- (36) Miyaura, N. Cross-Coupling Reaction of Organoboron Compounds via Base-Assisted Transmetalation to Palladium(II) Complexes. *J. Organomet. Chem.* **2002**, *653* (1–2), 54–57. [https://doi.org/10.1016/S0022-328X\(02\)01264-0](https://doi.org/10.1016/S0022-328X(02)01264-0).
- (37) Driver, M. S.; Hartwig, J. F. Energetics and Mechanism of Alkylamine N–H Bond Cleavage by Palladium Hydroxides: N–H Activation by Unusual Acid–Base Chemistry. *Organometallics* **1997**, *16* (26), 5706–5715. <https://doi.org/10.1021/om970856l>.
- (38) Schmidbaur, H.; Schmidt, M. Ferrosiloxanes and Ferrosilicate Anions. *J. Am. Chem. Soc.* **1962**, *84* (18), 3600–3601. <https://doi.org/10.1021/ja00877a050>.
- (39) Bochmann, M.; Wilkinson, G.; Young, G. B.; Hursthouse, M. B.; Malik, K. M. A. Preparation and Properties of 1-Adamantoxides, 2-Adamantoxides, and 1-Adamantylmethoxides of Ti (IV), V (IV), Nb (IV), Nb (V), Cr (III), Cr (IV), Mo (IV), Mn (II), Fe (III), and Co (II). The Crystal and Molecular Structure of Tetrakis(1-Adamantoxo)Dimet. *J. Chem. Soc. Dalt. Trans.* **1980**, No. 6, 901. <https://doi.org/10.1039/dt9800000901>.
- (40) Biernesser, A. B.; Li, B.; Byers, J. A. Redox-Controlled Polymerization of Lactide Catalyzed by Bis(Imino)Pyridine Iron Bis(Alkoxide) Complexes. *J. Am. Chem. Soc.* **2013**, *135* (44), 16553–16560. <https://doi.org/10.1021/ja407920d>.

- (41) Crockett, M. P. The Development of Iron Catalysts for Suzuki-Miyaura Cross-Coupling and the Reactivity Discovered Along the Way, PhD thesis, Boston College, 2020.
- (42) Audran, G.; Brémond, P.; Marque, S. R. A.; Siri, D.; Santelli, M. Calculated Linear Free Energy Relationships in the Course of the Suzuki-Miyaura Coupling Reaction. *Tetrahedron* **2014**, *70* (13), 2272–2279. <https://doi.org/10.1016/j.tet.2014.02.011>.
- (43) Tyrol, C. C. *Expanding the Scope of Available Iron-Based Catalysts for Suzuki-Miyaura Cross-Coupling Reactions Through Ligand Design and Mechanistic Investigation*; 2021.
- (44) Ackerman, L. K. G.; Anka-Lufford, L. L.; Naodovic, M.; Weix, D. J. Cobalt Co-Catalysis for Cross-Electrophile Coupling: Diarylmethanes from Benzyl Mesylates and Aryl Halides. *Chem. Sci.* **2015**, *6* (2), 1115–1119. <https://doi.org/10.1039/C4SC03106G>.
- (45) Torres, P. U. Cinacalcet HCl: A Novel Treatment for Secondary Hyperparathyroidism Caused by Chronic Kidney Disease. *J. Ren. Nutr.* **2006**, *16* (3), 253–258. <https://doi.org/10.1053/j.jrn.2006.04.010>.
- (46) McGrath, N. A.; Brichacek, M.; Njardarson, J. T. A Graphical Journey of Innovative Organic Architectures That Have Improved Our Lives. *J. Chem. Educ.* **2010**, *87* (12), 1348–1349. <https://doi.org/10.1021/ed1003806>.
- (47) Thiel, O.; Bernard, C.; Larsen, R.; Martinelli, M. J.; Raza, M. T. Methods of Synthesizing Cinacalcet and Salts Thereof. WO 2009/002427 A2, 2008.
- (48) Tewari, N.; Maheshwari, N.; Medhane, R.; Nizar, H.; Prasad, M. A Novel Method for the Large Scale Synthesis of Cinacalcet Hydrochloride Using Iron Catalyzed C–C Coupling. *Org. Process Res. Dev.* **2012**, *16* (9), 1566–1568. <https://doi.org/10.1021/op300164y>.
- (49) Barniol-Xicotá, M.; Leiva, R.; Escolano, C.; Vázquez, S. Syntheses of Cinacalcet: An Enantiopure Active Pharmaceutical Ingredient (API). *Synthesis (Stuttg.)* **2016**, *48* (06), 783–803. <https://doi.org/10.1055/s-0035-1561506>.
- (50) Lei, F.; Qu, B.; Li, X.; Guo, L.; Guan, M.; Hai, L.; Jin, H.; Wu, Y. Efficient

Synthesis of Substances Related to Cinacalcet Hydrochloride via Heck Coupling. *Synth. Commun.* **2014**, *44* (19), 2879–2885. <https://doi.org/10.1080/00397911.2014.895383>.

(51) Griller, D.; Ingold, K. U. Free-Radical Clocks. *Acc. Chem. Res.* **1980**, *13* (9), 317–323. <https://doi.org/10.1021/ar50153a004>.

(52) Heravi, M. M.; Zadsirjan, V. Prescribed Drugs Containing Nitrogen Heterocycles: An Overview. *RSC Adv.* **2020**, *10* (72), 44247–44311. <https://doi.org/10.1039/D0RA09198G>.

(53) Dinges, J.; Lamberth, C. *Bioactive Heterocyclic Compound Classes: Pharmaceuticals*; Lamberth, C., Dinges, J., Eds.; Wiley-VCH Verlag & Co.: Weinheim, Germany, 2013. <https://doi.org/10.1002/9783527664450>.

(54) Zultanski, S. L.; Fu, G. C. Nickel-Catalyzed Carbon–Carbon Bond-Forming Reactions of Unactivated Tertiary Alkyl Halides: Suzuki Arylations. *J. Am. Chem. Soc.* **2013**, *135* (2), 624–627. <https://doi.org/10.1021/ja311669p>.

(55) Yotsuji, K.; Hoshiya, N.; Kobayashi, T.; Fukuda, H.; Abe, H.; Arisawa, M.; Shuto, S. Nickel-Catalyzed Suzuki–Miyaura Coupling of a Tertiary Iodocyclopropane with Wide Boronic Acid Substrate Scope: Coupling Reaction Outcome Depends on Radical Species Stability. *Adv. Synth. Catal.* **2015**, *357* (5), 1022–1028. <https://doi.org/10.1002/adsc.201401000>.

(56) Zhou, Q.; Cobb, K. M.; Tan, T.; Watson, M. P. Stereospecific Cross Couplings To Set Benzylic, All-Carbon Quaternary Stereocenters in High Enantiopurity. *J. Am. Chem. Soc.* **2016**, *138* (37), 12057–12060. <https://doi.org/10.1021/jacs.6b08075>.

(57) Ariki, Z. T.; Maekawa, Y.; Nambo, M.; Crudden, C. M. Preparation of Quaternary Centers via Nickel-Catalyzed Suzuki–Miyaura Cross-Coupling of Tertiary Sulfones. *J. Am. Chem. Soc.* **2018**, *140* (1), 78–81. <https://doi.org/10.1021/jacs.7b10855>.

(58) Hills, I. D.; Netherton, M. R.; Fu, G. C. Toward an Improved Understanding of the Unusual Reactivity of Pd⁰/Trialkylphosphane Catalysts in Cross-Couplings of Alkyl Electrophiles: Quantifying the Factors That Determine the Rate of Oxidative Addition.

Angew. Chemie Int. Ed. **2003**, *42* (46), 5749–5752.
<https://doi.org/10.1002/anie.200352858>.

(59) Everson, D. A.; Weix, D. J. Cross-Electrophile Coupling: Principles of Reactivity and Selectivity. *J. Org. Chem.* **2014**, *79* (11), 4793–4798.
<https://doi.org/10.1021/jo500507s>.

(60) Rygus, J. P. G.; Crudden, C. M. Enantiospecific and Iterative Suzuki-Miyaura Cross-Couplings. *J. Am. Chem. Soc.* **2017**, *139* (50), 18124–18137.
<https://doi.org/10.1021/jacs.7b08326>.

(61) Zhao, S.; Gensch, T.; Murray, B.; Niemeyer, Z. L.; Sigman, M. S.; Biscoe, M. R. Enantiodivergent Pd-Catalyzed C–C Bond Formation Enabled through Ligand Parameterization. *Science* **2018**, *362* (6415), 670–674.
<https://doi.org/10.1126/science.aat2299>.

(62) Hunt, A. J.; Farmer, T. J.; Clark, J. H. CHAPTER 1. Elemental Sustainability and the Importance of Scarce Element Recovery; 2013; pp 1–28.
<https://doi.org/10.1039/9781849737340-00001>.

(63) Bart, S. C.; Hawrelak, E. J.; Lobkovsky, E.; Chirik, P. J. Low-Valent α -Diimine Iron Complexes for Catalytic Olefin Hydrogenation. *Organometallics* **2005**, *24* (23), 5518–5527. <https://doi.org/10.1021/om050625b>.

(64) Hennessy, E. T.; Betley, T. A. Complex N-Heterocycle Synthesis via Iron-Catalyzed, Direct C–H Bond Amination. *Science* **2013**, *340* (6132), 591–595.
<https://doi.org/10.1126/science.1233701>.

(65) Lee, W.-T.; Jeon, I.-R.; Xu, S.; Dickie, D. A.; Smith, J. M. Low-Coordinate Iron(II) Complexes of a Bulky Bis(Carbene)Borate Ligand. *Organometallics* **2014**, *33* (20), 5654–5659. <https://doi.org/10.1021/om500417y>.

(66) Smith, J. M.; Lachicotte, R. J.; Holland, P. L. Tuning Metal Coordination Number by Ancillary Ligand Steric Effects: Synthesis of a Three-Coordinate Iron(II) Complex. *Chem. Commun.* **2001**, No. 17, 1542–1543. <https://doi.org/10.1039/b103635c>.

- (67) Eckert, N. A.; Smith, J. M.; Lachicotte, R. J.; Holland, P. L. Low-Coordinate Iron(II) Amido Complexes of β -Diketiminates: Synthesis, Structure, and Reactivity. *Inorg. Chem.* **2004**, *43* (10), 3306–3321. <https://doi.org/10.1021/ic035483x>.
- (68) Vela, J.; Smith, J. M.; Yu, Y.; Ketterer, N. A.; Flaschenriem, C. J.; Lachicotte, R. J.; Holland, P. L. Synthesis and Reactivity of Low-Coordinate Iron(II) Fluoride Complexes and Their Use in the Catalytic Hydrodefluorination of Fluorocarbons. *J. Am. Chem. Soc.* **2005**, *127* (21), 7857–7870. <https://doi.org/10.1021/ja042672l>.
- (69) Holland, P. L. Electronic Structure and Reactivity of Three-Coordinate Iron Complexes. *Acc. Chem. Res.* **2008**, *41* (8), 905–914. <https://doi.org/10.1021/ar700267b>.
- (70) Crockett, M. P.; Zhang, H.; Thomas, C. M.; Byers, J. A. Adding Diffusion Ordered NMR Spectroscopy (DOSY) to the Arsenal for Characterizing Paramagnetic Complexes. *Chem. Commun.* **2019**, *55* (96), 14426–14429. <https://doi.org/10.1039/C9CC08229H>.
- (71) Tyrol, C. C.; Byers, J. A. A Broadly Applicable Alkyl-Alkyl Suzuki-Miyaura Cross-Coupling Reaction Catalyzed by an Iron-Based Complex. *ChemRxiv* **2021**. <https://doi.org/10.33774/chemrxiv-2021-wx9kh>.
- (72) Kamitori, Y.; Hojo, M.; Masuda, R.; Izumi, T.; Tsukamoto, S. Silica Gel as an Effective Catalyst for the Alkylation of Phenols and Some Heterocyclic Aromatic Compounds. *J. Org. Chem.* **1984**, *49* (22), 4161–4165. <https://doi.org/10.1021/jo00196a012>.
- (73) Huang, Z.; Zhang, J.; Zhou, Y.; Wang, N. X. Enantioselective Friedel-Crafts Alkylation of Thiophenes with Ethyl Glyoxylate: Easy Access to Chiral Secondary Alcohols. *European J. Org. Chem.* **2011**, No. 5, 843–847. <https://doi.org/10.1002/ejoc.201001455>.
- (74) Wang, X.; Wang, S.; Xue, W.; Gong, H. Nickel-Catalyzed Reductive Coupling of Aryl Bromides with Tertiary Alkyl Halides. *J. Am. Chem. Soc.* **2015**, *137* (36), 11562–11565. <https://doi.org/10.1021/jacs.5b06255>.
- (75) Wang, X.; Ma, G.; Peng, Y.; Pitsch, C. E.; Moll, B. J.; Ly, T. D.; Wang, X.; Gong,

H. Ni-Catalyzed Reductive Coupling of Electron-Rich Aryl Iodides with Tertiary Alkyl Halides. *J. Am. Chem. Soc.* **2018**. <https://doi.org/10.1021/jacs.8b09473>.

(76) Cherney, A. H.; Hedley, S. J.; Mennen, S. M.; Tedrow, J. S. Xantphos as a Branch-Selective Ligand for the Acyclic Sec-Alkyl Negishi Cross-Coupling of Heteroaryl Halides. *Organometallics* **2019**, *38* (1), 97–102. <https://doi.org/10.1021/acs.organomet.8b00590>.

(77) Tyrol, C. C.; Yone, N. S.; Gallin, C. F.; Byers, J. A. Iron-Catalysed Enantioconvergent Suzuki–Miyaura Cross-Coupling to Afford Enantioenriched 1,1-Diarylalkanes. *Chem. Commun.* **2020**, *56* (93), 14661–14664. <https://doi.org/10.1039/D0CC05003B>.

(78) Przyojski, J. A.; Veggeberg, K. P.; Arman, H. D.; Tonzetich, Z. J. Mechanistic Studies of Catalytic Carbon-Carbon Cross-Coupling by Well-Defined Iron NHC Complexes. *ACS Catal.* **2015**, *5* (10), 5938–5946. <https://doi.org/10.1021/acscatal.5b01445>.

(79) Noda, D.; Sunada, Y.; Hatakeyama, T.; Nakamura, M.; Nagashima, H. Effect of TMEDA on Iron-Catalyzed Coupling Reactions of ArMgX with Alkyl Halides. *J. Am. Chem. Soc.* **2009**, *131* (17), 6078–6079. <https://doi.org/10.1021/ja901262g>.

(80) Takaya, H.; Nakajima, S.; Nakagawa, N.; Isozaki, K.; Iwamoto, T.; Imayoshi, R.; Gower, N. J.; Adak, L.; Hatakeyama, T.; Honma, T.; et al. Investigation of Organoiron Catalysis in Kumada–Tamao–Corriu-Type Cross-Coupling Reaction Assisted by Solution-Phase X-Ray Absorption Spectroscopy. *Bull. Chem. Soc. Jpn.* **2015**, *88* (3), 410–418. <https://doi.org/10.1246/bcsj.20140376>.

(81) Adams, C. J.; Bedford, R. B.; Carter, E.; Gower, N. J.; Haddow, M. F.; Harvey, J. N.; Huwe, M.; Cartes, M. Á.; Mansell, S. M.; Mendoza, C.; et al. Iron(I) in Negishi Cross-Coupling Reactions. *J. Am. Chem. Soc.* **2012**, *134* (25), 10333–10336. <https://doi.org/10.1021/ja303250t>.

(82) Delle Chiaie, K. R. Exploration of Bis(Imino)Pyridine Iron Alkoxides for the Synthesis of Novel Degradable Polymers, PhD thesis, Boston College, 2018.

- (83) Burger, B. J.; Bercaw, J. E. Vacuum Line Techniques for Handling Air-Sensitive Organometallic Compounds. In *Experimental Organometallic Chemistry*; American Chemical Society, 1987; pp 79–115. <https://doi.org/10.1021/bk-1987-0357.ch004>.
- (84) Pangborn, A. B.; Giardello, M. A.; Grubbs, R. H.; Rosen, R. K.; Timmers, F. J. Safe and Convenient Procedure for Solvent Purification. *Organometallics* **1996**, *15* (5), 1518–1520. <https://doi.org/10.1021/om9503712>.
- (85) Evans, D. F. The Determination of the Paramagnetic Susceptibility of Substances in Solution by Nuclear Magnetic Resonance. *J. Chem. Soc.* **1959**, 2003–2005. <https://doi.org/10.1039/jr9590002003>.
- (86) Becke, A. D. Density-Functional Exchange-Energy Approximation with Correct Asymptotic Behavior. *Phys. Rev. A* **1988**, *38* (6), 3098–3100. <https://doi.org/10.1103/PhysRevA.38.3098>.
- (87) Lee, C.; Yang, W.; Parr, R. G. Development of the Colle-Salvetti Correlation-Energy Formula into a Functional of the Electron Density. *Phys. Rev. B* **1988**, *37* (2), 785–789. <https://doi.org/10.1103/PhysRevB.37.785>.
- (88) Rassolov, V. A.; Pople, J. A.; Ratner, M. A.; Windus, T. L. 6-31G* Basis Set for Atoms K through Zn. *J. Chem. Phys.* **1998**, *109* (4), 1223–1229. <https://doi.org/10.1063/1.476673>.
- (89) Miertuš, S.; Scrocco, E.; Tomasi, J. Electrostatic Interaction of a Solute with a Continuum. A Direct Utilizaion of AB Initio Molecular Potentials for the Prevision of Solvent Effects. *Chem. Phys.* **1981**, *55* (1), 117–129. [https://doi.org/10.1016/0301-0104\(81\)85090-2](https://doi.org/10.1016/0301-0104(81)85090-2).
- (90) Terao, J.; Nakamura, M.; Kambe, N. Non-Catalytic Conversion of C–F Bonds of Benzotrifluorides to C–C Bonds Using Organoaluminium Reagents. *Chem. Commun.* **2009**, No. 40, 6011. <https://doi.org/10.1039/b915620h>.
- (91) Ichikawa, T.; Netsu, M.; Mizuno, M.; Mizusaki, T.; Takagi, Y.; Sawama, Y.; Monguchi, Y.; Sajiki, H. Development of a Unique Heterogeneous Palladium Catalyst for

the Suzuki-Miyaura Reaction Using (Hetero)Aryl Chlorides and Chemoselective Hydrogenation. *Adv. Synth. Catal.* **2017**, *359* (13), 2269–2279. <https://doi.org/10.1002/adsc.201700156>.

(92) Huihui, K. M. M.; Caputo, J. A.; Melchor, Z.; Olivares, A. M.; Spiewak, A. M.; Johnson, K. A.; Dibenedetto, T. A.; Kim, S.; Ackerman, L. K. G.; Weix, D. J. Decarboxylative Cross-Electrophile Coupling of N-Hydroxyphthalimide Esters with Aryl Iodides. *J. Am. Chem. Soc.* **2016**, *138* (15), 5016–5019. <https://doi.org/10.1021/jacs.6b01533>.

(93) Yang, F.; Fu, S. Y.; Chu, W.; Li, C.; Tong, D. G. Monodisperse Amorphous CuB₂₃ Alloy Short Nanotubes: Novel Efficient Catalysts for Heck Coupling of Inactivated Alkyl Halides and Alkenes. *RSC Adv.* **2014**, *4* (86), 45838–45843. <https://doi.org/10.1039/C4RA08517E>.

(94) Tobisu, M.; Takahira, T.; Chatani, N. Nickel-Catalyzed Cross-Coupling of Anisoles with Alkyl Grignard Reagents via C–O Bond Cleavage. *Org. Lett.* **2015**, *17* (17), 4352–4355. <https://doi.org/10.1021/acs.orglett.5b02200>.

(95) Xia, C.-L.; Xie, C.-F.; Wu, Y.-F.; Sun, H.-M.; Shen, Q.; Zhang, Y. Efficient Cross-Coupling of Aryl Grignard Reagents with Alkyl Halides by Recyclable Ionic Iron(III) Complexes Bearing a Bis(Phenol)-Functionalized Benzimidazolium Cation. *Org. Biomol. Chem.* **2013**, *11* (46), 8135. <https://doi.org/10.1039/c3ob41376d>.

(96) Graham, T. J. A.; Poole, T. H.; Reese, C. N.; Goess, B. C. Regioselective Semihydrogenation of Dienes. *J. Org. Chem.* **2011**, *76* (10), 4132–4138. <https://doi.org/10.1021/jo200262r>.

(97) Yus, M.; Ortiz, R. Tandem Intramolecular Carbolithiation-Lithium/Zinc Transmetalation and Applications to Carbon-Carbon Bond-Forming Reactions. *European J. Org. Chem.* **2004**, No. 18, 3833–3841. <https://doi.org/10.1002/ejoc.200400349>.

(98) Bellows, S. M.; Arnet, N. A.; Gurubasavaraj, P. M.; Brennessel, W. W.; Bill, E.; Cundari, T. R.; Holland, P. L. The Mechanism of N–N Double Bond Cleavage by an Iron(II) Hydride Complex. *J. Am. Chem. Soc.* **2016**, *138* (37), 12112–12123.

<https://doi.org/10.1021/jacs.6b04654>.

(99) Smith, J. M.; Lachicotte, R. J.; Holland, P. L. Tuning Metal Coordination Number by Ancillary Ligand Steric Effects: Synthesis of a Three-Coordinate Iron(II) Complex. *Chem. Commun.* **2001**, 1 (17), 1542–1543. <https://doi.org/10.1039/b103635c>.

(100) King, A. K.; Buchard, A.; Mahon, M. F.; Webster, R. L. Facile, Catalytic Dehydrocoupling of Phosphines Using β -Diketiminato Iron(II) Complexes. *Chem. - A Eur. J.* **2015**, 21 (45), 15960–15963. <https://doi.org/10.1002/chem.201503399>.

(101) Molander, G. A.; Argintaru, O. A.; Aron, I.; Dreher, S. D. Nickel-Catalyzed Cross-Coupling of Potassium Aryl- and Heteroaryltrifluoroborates with Unactivated Alkyl Halides. *Org. Lett.* **2010**, 12 (24), 5783–5785. <https://doi.org/10.1021/ol102717x>.

(102) Finlay, J. D.; Smith, D. J. H. The Photolysis of 2-Phenylthietan-1,1-Dioxides: Preparation of Substituted Cyclopropanes. *Synthesis (Stuttg.)* **1978**, (8), 579–580.

(103) Maercker, A.; Oeffner, K. S.; Girreser, U. Polylithiumorganic Compounds. Part 29: C-C Bond Cleavage of Phenyl Substituted and Strained Carbocycles Using Lithium Metal. *Tetrahedron* **2004**, 60 (37), 8245–8256. <https://doi.org/10.1016/j.tet.2004.06.105>.

(104) Zultanski, S. L.; Fu, G. C. Nickel-Catalyzed Carbon-Carbon Bond-Forming Reactions of Unactivated Tertiary Alkyl Halides: Suzuki Arylations. *J. Am. Chem. Soc.* **2013**, 135 (2), 624–627. <https://doi.org/10.1021/ja311669p>.

(105) Tamura, Y.; Tsugoshi, T.; Annoura, H.; Ishibashi, H. Ethoxycarbonylmethylthiomethylation of Aromatic Compounds by Friedel-Crafts Reaction with Ethyl α -(Chloromethylthio)-Acetate. *Synthesis (Stuttg.)* **1984**, 1984 (04), 326–327. <https://doi.org/10.1055/s-1984-30830>.

(106) Sato, A.; Han, J.; Ono, T.; Wzorek, A.; Aceña, J. L.; Soloshonok, V. A. Introducing a New Radical Trifluoromethylation Reagent. *Chem. Commun.* **2015**, 51 (27), 5967–5970. <https://doi.org/10.1039/c5cc00905g>.

(107) Bauer, T.; Gajewiak, J. Diastereoselective Synthesis of 2-Alkoxy-5-Tert-Butylmandelic Acid. *Synthesis (Stuttg.)* **2003**, (01), 20–22. <https://doi.org/10.1055/s-2003->

42484.

Chapter 3.

Synthesis and Characterization of Air-Stable Iron-Based Catalyst
Precursors for the Suzuki-Miyaura Cross-Coupling Reaction of
Alkyl Halides and Unactivated Aryl Boronic Esters

3.1 Introduction

Over the past four decades, the palladium-catalyzed Suzuki-Miyaura cross-coupling reaction has become a prominent and powerful tool for the assembly of C(sp²)-C(sp²) bonds.¹ The impact of the Suzuki-Miyaura reaction is especially apparent in the pharmaceutical industry, where it is employed in nearly 25% of reported syntheses of medicinally active small molecule drugs.² The prevalence of the Suzuki-Miyaura reaction is due in large part to its success in incorporating a wide variety of substrates, but another contributing factor is the ability to use boronic esters and palladium catalyst precursors that are air- and moisture-stable. While most reactions are still run under inert gas conditions, its user-friendly assembly under atmospheric conditions and robust performance have made the Suzuki-Miyaura reaction a preferred tool for synthetic organic chemists.

Despite this impressive utility, cross-coupling reactions catalyzed by palladium-based complexes commonly undergo β -hydride elimination side reactions that often limit the reaction to sp²-hybridized substrates,³ which in turn is likely an underlying reason for the disproportionate representation of mostly flat molecules in medicinally relevant small molecule drugs.² In order to explore the efficacy of pharmaceutical targets possessing three-dimensional features, first-row transition metal catalysis has emerged as a promising alternative. Of the first-row transition metals, nickel-based complexes have been most commonly investigated for cross-coupling catalysis.⁴⁻⁹ In comparison, reactions catalyzed by iron-based complexes have historically received less attention,¹⁰⁻¹² despite the reduced cost and toxicity of iron when compared to that of palladium and nickel, respectively.¹³ Despite these advantages, the development and application of iron catalysis for cross-coupling reactions is often limited by inconvenient practical considerations compared to

cross-coupling reactions catalyzed by palladium-based complexes (see Chapter 2).¹⁴ In this chapter,¹⁵ we report our progress towards alleviating some of the practical limitations relevant to the application of iron-based complexes for cross-coupling reactions, so that they can be leveraged to provide reactivity complementary to that of the palladium-based analogues. We disclose the synthesis and characterization of a new iron(III)-based precatalyst that is air-stable, stable on the benchtop for at least nine months, and active for the Suzuki-Miyaura cross-coupling of alkyl halides with arylboronic esters.

3.2 Practical limitations to the general application of iron-based complexes for catalyzing Suzuki-Miyaura cross-coupling reactions

One challenge facing the broad implementation of iron-based catalysts in cross-coupling reactions is the propensity for catalyst precursors to undergo rapid deactivation upon exposure to air or water due to facile oxidation and hydrolysis reactions that form iron oxides (Figure 3.1). Bench-stable iron salts (e.g. FeCl_3 , $\text{Fe}(\text{acac})_3$) have been employed as catalyst precursors in cross-coupling reactions involving Grignard reagents^{16–19} and alkenes,^{20–23} but their efficient activity towards boron-containing coupling partners remains elusive. Moreover, examples of Suzuki-Miyaura reactions between alkyl halides and aryl boronic esters catalyzed by iron-based complexes often require the use of reactive lithium amide bases²⁴ or substrates preactivated by highly pyrophoric alkyllithium bases (see Chapter 2).^{25–27} Proposed catalytic cycles for these reactions often invoke the intermediacy of highly reactive and low-valent iron intermediates.^{28–31} As a result, cross-coupling reactions catalyzed by iron-based catalysts usually demand the use of stringently air- and water-free conditions, which limit their practical implementation on scale.

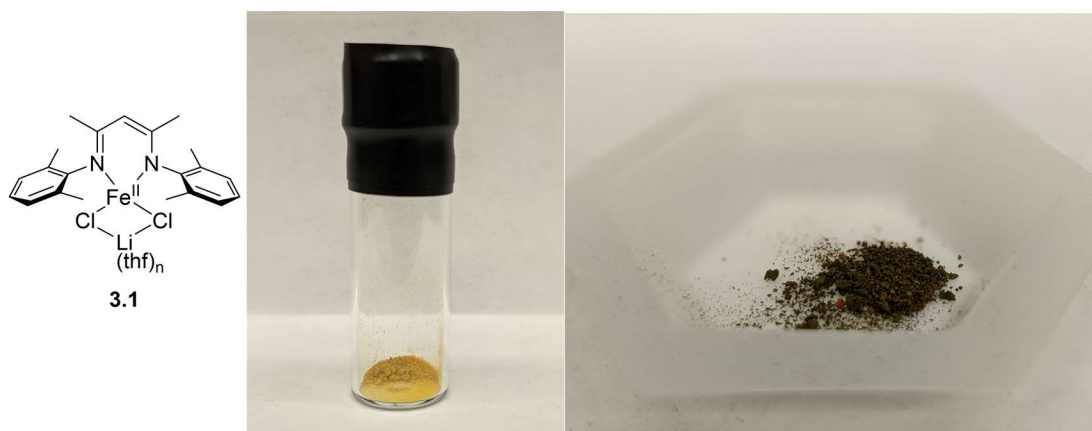


Figure 3.1. Appearance of iron complex **3.1** while stored under N₂ (left image) and appearance of iron complex **3.1** following 3 minutes of exposure to air (right image).

In Chapter 2, we reported the design of iron-based complexes (e.g. **3.1**) supported by β-diketiminato ligands that proved highly effective for catalyzing Suzuki-Miyaura cross-coupling reactions.³² The reaction was capable of assembling molecules with functionality common in many pharmaceuticals, such as functionalized heteroaromatic rings. It was also capable of carrying out difficult cross-coupling reactions, such as those involving tertiary alkyl halides. Utilizing these electrophiles in cross-coupling reactions result in the synthesis of all-carbon quaternary centers, a challenging motif to obtain for most synthetic methodologies. Despite their synthetic utility, the reactions required that discrete iron(II) complexes containing the β-diketiminato ligand be synthesized as opposed to reactions where ligands were added to iron-based catalyst precursors. These discrete complexes were not stable to oxygen or water, and they rapidly (i.e. within minutes) underwent decomposition when exposed to ambient air (Figure 3.1). We hypothesized that iron(III) catalyst precursors would be less prone to oxidation compared to iron(II) catalyst precursors we have used previously. Additionally, we believe that the highly reducing conditions of the cross-coupling reaction would generate *in situ* the iron(II)-based

intermediates that are often proposed to be catalytically relevant for successful cross-coupling.

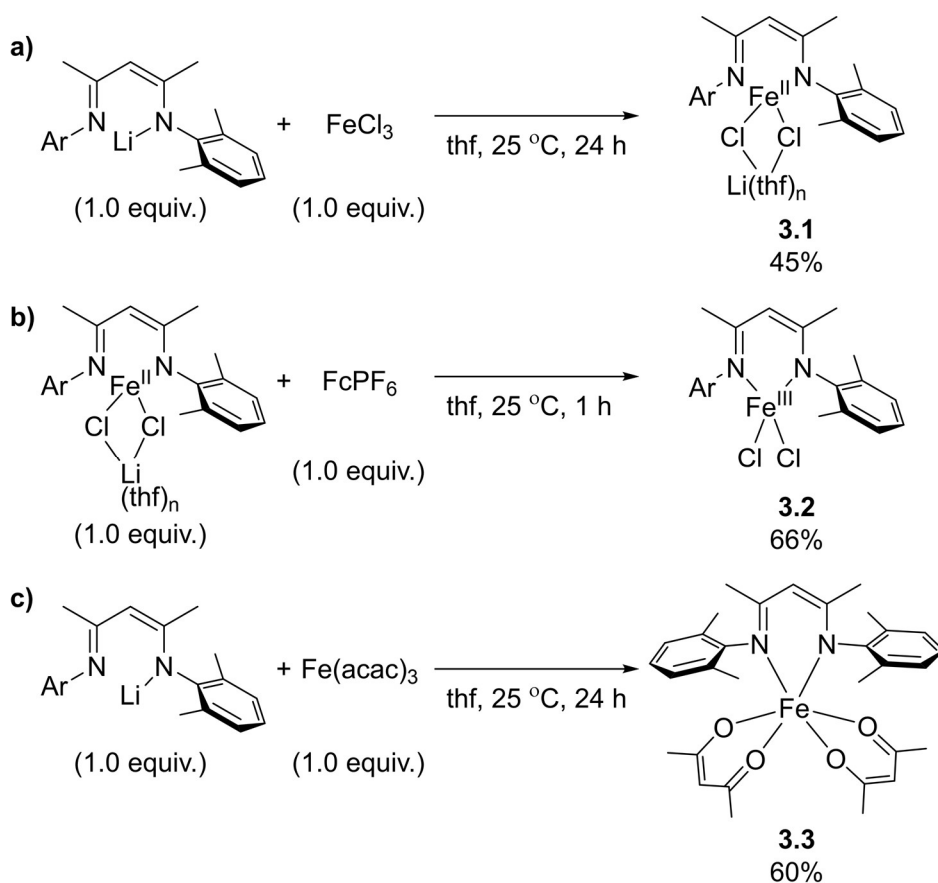
3.3 Synthesis and characterization of iron(III)-based catalyst precursors supported by β -diketiminato ligands

In order to obtain an air-stable catalyst precursor, we targeted discrete iron(III) catalyst precursors containing the β -diketiminato ligand. Initially, we attempted to synthesize an iron(III) halide complex by using the iron(III) salt FeCl_3 in place of FeCl_2 , but ^1H NMR spectroscopy of the resulting product was identical to that of the previously used iron(II) complex **3.1** (Scheme 3.1a). An effective magnetic moment ($\mu_{\text{eff}} = 5.20 \mu_{\text{B}}$) measured in the solution-state for the product suggested that the iron(III) catalyst precursor was reduced *in situ* by the deprotonated ligand. The spin-only magnetic moment can be approximated from the observed magnetic moment and correlated to the number of unpaired electrons in a coordination complex by the equation:

$$\mu_{\text{eff}} \approx \mu_{\text{spin-only}} = \sqrt{n(n+2)} \mu_{\text{B}} \quad (\text{eqn. 1})^{33}$$

where n is the number of unpaired electrons. As a result, a calculation of 4 unpaired electrons for iron complex **3.1** is consistent with a high-spin d^6 ion, for which the oxidation state of iron is iron(II). We next attempted to oxidize the iron(II) complex with the addition of an external oxidant, ferrocenium hexafluorophosphate (Scheme 3.1b).³⁴ An effective magnetic moment measured in the solution-state for the resultant purple crystals supported the successful oxidation to a high-spin iron(III) complex ($\mu_{\text{eff}} = 6.54 \mu_{\text{B}}$). This observed magnetic moment is significantly higher than what is normally observed for high-spin iron(III) complexes ($\mu_{\text{eff}} \approx 5.7\text{-}6.0 \mu_{\text{B}}$), which we attribute to contributions from orbital angular momentum or spin-orbit coupling.³⁵ Nevertheless, the calculation of

approximately 5 unpaired electrons for this compound is consistent with a high-spin d^5 ion. The structure was confirmed by X-ray crystallographic characterization as the monomeric, neutral iron(III) dichloride complex **3.2** (Figure 3.2a, CCDC 2088833). Iron(III) halide complexes that contain the β -diketiminato ligand have not been previously reported. However, Holland and co-workers have previously synthesized four-coordinate β -diketiminato iron(III) amido complexes³⁶ with similar Fe–N bond lengths compared to complex **3.2**. These Fe–N bond lengths are shorter than those reported for analogous four-coordinate iron(II) halide complexes,^{32,36} consistent with an increase in oxidation state.



Scheme 3.1. a) Attempted synthesis of an iron(III) complex supported by a β -diketiminato ligand through the addition of FeCl_3 , b) synthesis of a neutral iron(III) dichloride complex supported by a β -diketiminato ligand via the oxidation of the analogous iron (II) complex, c) synthesis of an air-stable iron(III) complex supported by a β -diketiminato ligand and two acetylacetonate (acac) ligands.

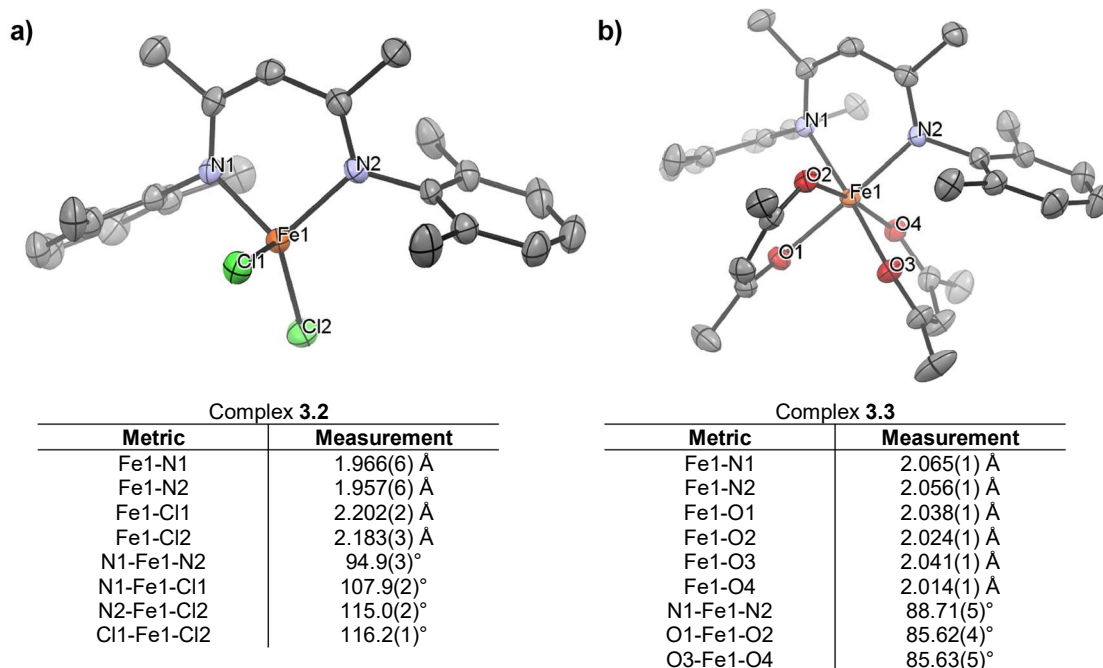


Figure 3.2. X-ray crystal structures of complexes **3.2** and **3.3** with selected bond metrics. Thermal ellipsoids are drawn at the 50% probability level; co-crystallized solvent molecules and hydrogen atoms are omitted for clarity. Crystal refinement tables are located in Appendix B.2.

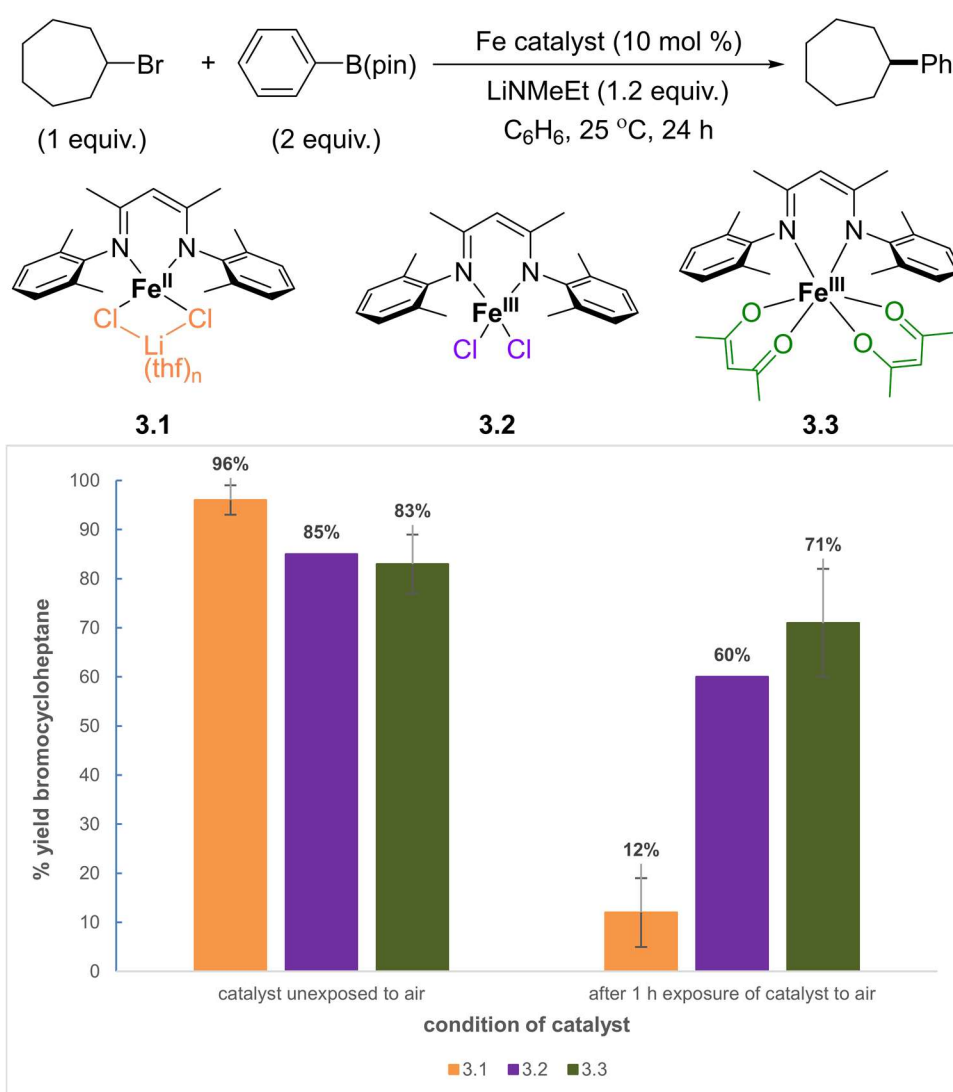
In addition to the iron(III) halide complex **3.2**, we also pursued the synthesis of the iron(III) complex **3.3**. Since the iron(III) salt $\text{Fe}(\text{acac})_3$ is often used as a bench-stable catalyst precursor^{21,37–39} and β -diketiminato ligands are isoelectronic and isolobal to acetylacetonate ligands,⁴⁰ we reasoned that replacing an acetylacetonate ligand in $\text{Fe}(\text{acac})_3$ with a β -diketiminato ligand could lead to an iron(III) complex containing the β -diketiminato ligand that was active for cross-coupling catalysis and was air-stable. We thought such a complex could be synthesized through ligand substitution reactions between $\text{Fe}(\text{acac})_3$ and the deprotonated β -diketiminato ligands. As expected, addition of the deprotonated β -diketiminato ligand to $\text{Fe}(\text{acac})_3$ resulted in the formation of a dark green compound **3.3** (Scheme 3.1c). An effective magnetic moment measured in the solution-state for complex **3.3** remains consistent with a high-spin iron(III) center ($\mu_{\text{eff}} = 7.04 \mu_{\text{B}}$).

Like complex **3.2**, the higher magnetic moment can be attributed to contributions from orbital angular momentum or spin-orbit coupling, but nonetheless suggests that there exist 5 unpaired electrons (a high-spin d^5 iron(III) ion). X-ray crystallographic characterization of this complex confirmed the formation of an octahedral iron complex supported by one β -diketiminato ligand and two acetylacetonate ligands (Figure 3.2b, CCDC 2088834). The Fe–N bond lengths of compound **3.3** are comparable to those found in previously reported β -diketiminato iron(II) complexes,⁴¹ but longer than those found in previously reported β -diketiminato iron(III) complexes,^{36,41–43} though the reported β -diketiminato iron(III) examples are limited to three- and four-coordinate iron(III) amido complexes. Hexacoordinate octahedral iron(III) complexes such as **3.3** would be expected to have longer Fe–N bonds due to steric hindrance.⁴⁴ The Fe–O bond lengths of compound **3.3** are likewise longer than those found in $\text{Fe}(\text{acac})_3$ (average bond length = 1.991(8)Å).⁴⁵ The octahedral geometry of complex **3.3** also gives rise to a smaller N–Fe–N bond angle than that observed in other β -diketiminato iron(III) complexes, though the O–Fe–O bond angles are also smaller than those observed in $\text{Fe}(\text{acac})_3$ (average O–Fe–O bond angle = 87.47(3)°).⁴⁵ In comparison to **3.2**, the Fe–N bond distances in **3.3** are significantly longer and the N–Fe–N bond angle is more acute. The differences in bond metrics between **3.2** and **3.3** may be due to the different geometry of the two complexes, or the *trans*-influence of the acac ligands in octahedral **3.3** that is absent in the distorted tetrahedral complex **3.2**.

3.4 Evaluation of catalytic competence and bench stability of β -diketiminato iron(III)-based complexes for the Suzuki-Miyaura cross-coupling reaction

When complex **3.1** was subjected to our previously established standard cross-coupling conditions³² (Scheme 3.2) following its exposure to in air for one hour, the Suzuki-Miyaura reaction between bromocycloheptane and phenyl boronic acid pinacol

ester produced phenylcycloheptane in significantly reduced yield ($12 \pm 7\%$), compared to reactions where **3.1** was not exposed to air ($96 \pm 3\%$). Conversely, an initial attempt to subject complex **3.2** to our standard cross-coupling conditions following exposure to air for one hour delivered the product in 60% yield (compared to 85% without air exposure) (Scheme 3.2), and complex **3.3** delivered the product in $71 \pm 11\%$ yield (compared to $83 \pm 6\%$ without air exposure) under the same conditions (Scheme 3.2).



Scheme 3.2. Suzuki-Miyaura cross-coupling reaction of bromocycloheptane and phenylboronic acid pinacol ester catalyzed by iron complexes **3.1**, **3.2**, and **3.3** prior to and after exposure to air for one hour.

With the competency of an iron(III) precatalyst for Suzuki-Miyaura cross-coupling established, we next sought to assess the benchtop stability of the iron complexes. The ^1H NMR spectrum of iron chloride complex **3.2** displayed no change immediately following exposure to air, which is consistent with our working hypothesis that these compounds would be less sensitive to oxidation. However, further exploration revealed that **3.2** was not indefinitely stable to air because a color change of the sample accompanied by loss of all paramagnetic resonances in the ^1H NMR were observed within 24 hours after initial exposure to air. This finding suggested that catalyst deactivation occurred. Conversely, complex **3.3** remained stable in the solid-state for up to nine months following its storage in a benchtop desiccator exposed to air, as determined by ^1H NMR spectroscopy. To gain further insight, the speciation of the iron center in complex **3.3** was also examined using ^{57}Fe Mössbauer spectroscopy. All ^{57}Fe Mössbauer spectra were obtained with the assistance of Bufan Zhang and Professor Michael Neidig at the University of Rochester. The 80 K ^{57}Fe Mössbauer spectrum of a powder of iron(III) complex **3.3** features a broad doublet with Mössbauer parameters of $\delta = 0.47$ mm/s and $|\Delta E_Q| = 0.82$ mm/s, consistent with a high-spin iron(III) species (Figure 3.3a). Similar broadening has been previously observed in other high-spin iron(III) complexes,^{46,47} though contributions to broadening from the presence of residual $\text{Fe}(\text{acac})_3$ cannot be excluded.⁴⁸ The degree of broadening can be reduced following extensive recrystallization of the compound. Most importantly, the spectrum of a sample of **3.3** taken after four months of continued exposure to air displayed no substantial changes from that of a freshly synthesized sample of the same complex. A similar analysis of the iron(II) complex **3.1** before and after only one hour of exposure to air (Figure 3.3b) displayed marked differences in the Mössbauer spectra that

suggest near-complete conversion of the iron(II) complex ($\delta = 0.90$ mm/s and $|\Delta E_Q| = 2.41$ mm/s) to a mixture of iron complexes, the two major components of which have Mössbauer parameters ($\delta = 0.42$ mm/s and $|\Delta E_Q| = 0.81$ mm/s, 48 % of total iron, blue component; $\delta = 0.38$ mm/s and $|\Delta E_Q| = 1.37$ mm/s, 46 % of total iron, red component) consistent with iron(III) complexes formed from rapid oxidation.^{49,50} This rapid oxidation is further supported from changes in the ^1H NMR spectrum of the complex as well as its physical appearance (Figure 3.4). These changes are also consistent with the decreased yield observed for reactions where **3.1** was exposed to air for one hour compared to reactions carried out entirely in the glovebox (*vide supra*).

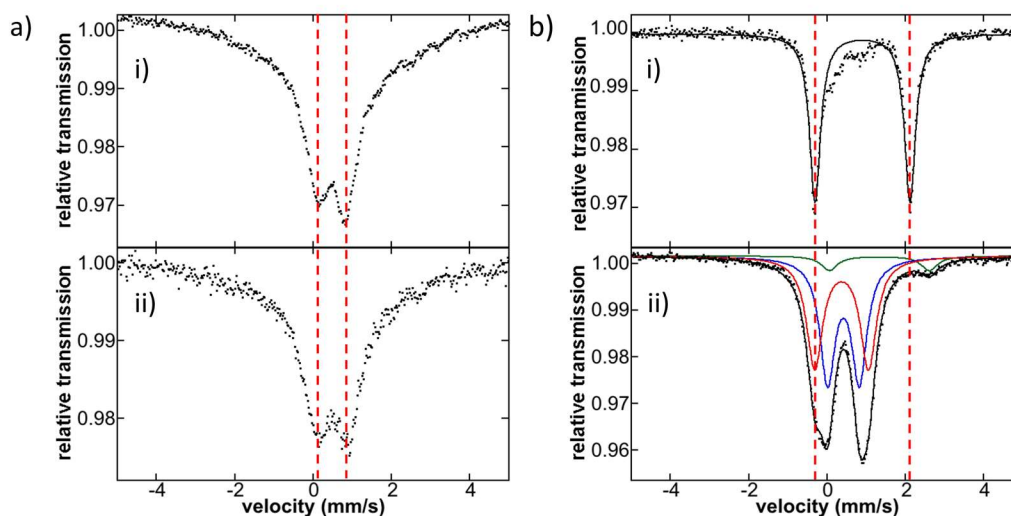


Figure 3.3. a) Comparison of the 80 K ^{57}Fe Mössbauer spectra of a powder of **3.3**, i) prior to and ii) following exposure to air for four months. b) Comparison of the 80 K ^{57}Fe Mössbauer spectra of the previously synthesized iron(II)-based cross-coupling precatalyst **3.1** i) prior to and ii) following exposure to air for one hour. The latter spectrum features three iron species with the following parameters: red component, $\delta = 0.38$ mm/s, $|\Delta E_Q| = 1.37$ mm/s (46% of total iron); blue component, $\delta = 0.42$ mm/s, $|\Delta E_Q| = 0.81$ mm/s (48% of total iron) and green component, $\delta = 1.34$ mm/s, $|\Delta E_Q| = 2.55$ mm/s (6% of total iron).

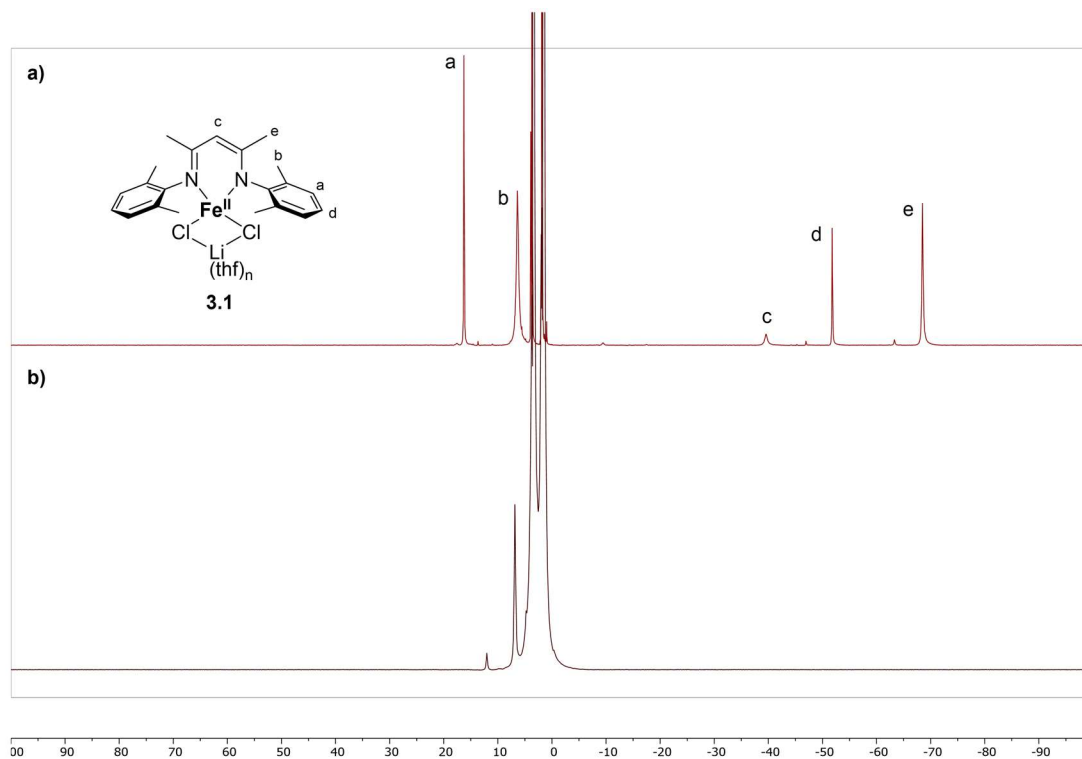


Figure 3.4. Comparison of the ¹H NMR spectra (solvent-suppressed, THF) of iron complex **3.1** a) prior to and b) after exposure to air for 1 hour.

These sets of experiments demonstrate that the iron(III) complex **3.3** is less prone to degradation in air, supporting our hypothesis that higher oxidation state iron species are less prone to decomposition on the benchtop than iron(II) catalyst precursors. In addition to oxidation state, we speculate that the iron(II) halide complex **3.1** is less stable to air than iron(III) complex **3.3** due to more rapid hydrolysis of iron halides⁵¹ compared to iron acetylacetonate complexes. This hypothesis is also consistent with the observed behavior of iron(III) halide complex **3.2**, which rapidly undergoes deactivation towards cross-coupling at room temperature, presumably because of hydrolysis rather than oxidation.⁵¹ Thus, with the proper choice of oxidation state and supporting ligands, air- and moisture-stable catalyst precursors for the Suzuki-Miyaura cross-coupling reaction can be obtained.

3.5 Examining the mechanism of activation for iron(III)-based complexes in the Suzuki-Miyaura cross-coupling reaction

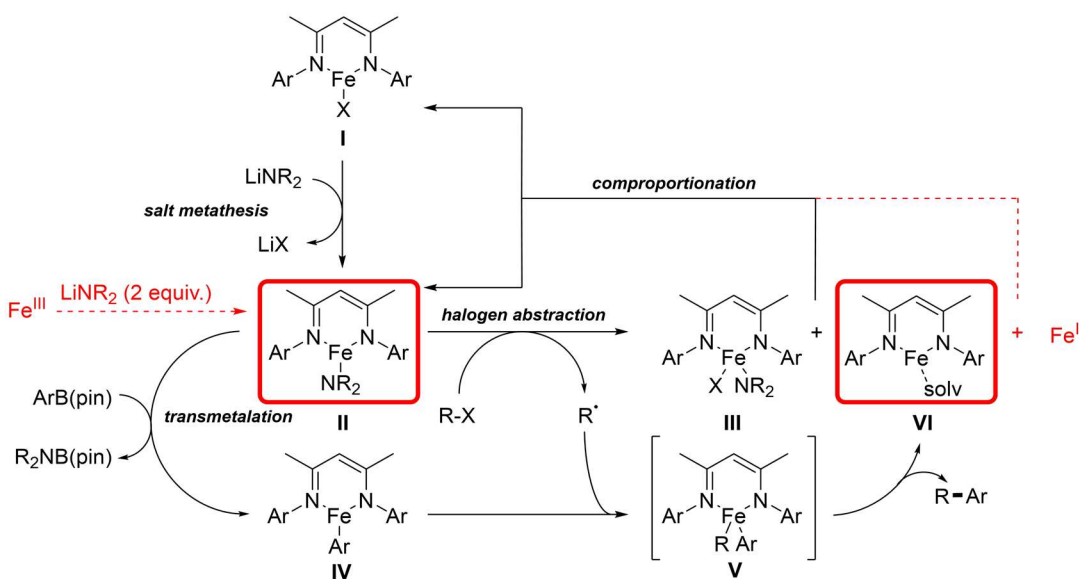


Figure 3.5. Working mechanistic hypothesis for the cross-coupling reaction of alkyl halides and aryl boronic esters catalyzed by β -diketiminato iron(II) complexes. Possible pathways for activation of the iron(III) analogues are highlighted in red.

We have previously proposed a catalytic cycle for the iron(II)-catalyzed Suzuki-Miyaura cross-coupling reaction, which is our current working mechanistic hypothesis for the cross-coupling reaction³¹ (Figure 3.5). In this proposed mechanism, iron(II) halide precatalyst **I** is activated by salt metathesis with the lithium amide base. Iron(II) amide species **II** activates the electrophile and the nucleophile via halogen abstraction to yield intermediate **III** and transmetalation to yield intermediate **IV**, respectively. The carbon-centered radical formed by halogen abstraction recombines with **IV**, followed by reductive elimination from **V** to deliver the cross-coupled product. Finally, catalyst turnover is achieved by comproportionation between **III** and **VI** to regenerate an equivalent of **I** and an equivalent of **II**. We hypothesized that the presence of a strong reductant like lithium amide⁵² could enable the iron(III) precursors to enter the catalytic cycle as presumably iron(II) amide species **II**. Alternatively, the iron(III) precursors could participate in

comproportionation with the low-coordinate iron(I) species **VI** generated from reductive elimination to enter the catalytic cycle.

To assess the possibility that the iron(III) catalyst precursors were being converted into iron(II) species *in situ*, we sought to examine the speciation of the iron centers in the presence of possible reductants using ^{57}Fe Mössbauer spectroscopy. A ^{57}Fe -enriched sample of iron complex **3.3** was discretely synthesized by Bufan Zhang at the University of Rochester for these studies; however, we cannot definitively conclude that the iron(III) species can be obtained cleanly (Appendix C). Reactions of iron(III) species **3.3** with possible reductants deliver a complex mixture of iron species observed by ^{57}Fe Mössbauer spectroscopy, the formation of which is not well understood. An attempt to examine the speciation of the iron centers under the same conditions with EPR spectroscopy was similarly inconclusive (Appendix C). We expected that clean reduction of the EPR-active iron(III) species to the EPR-inactive iron(II) species would result in the destruction of EPR signals. Instead, signals remained following the addition of lithium amide reductant. Investigations into the precise mechanism of activation of the iron(III) precatalysts are ongoing and will be reported in due course.

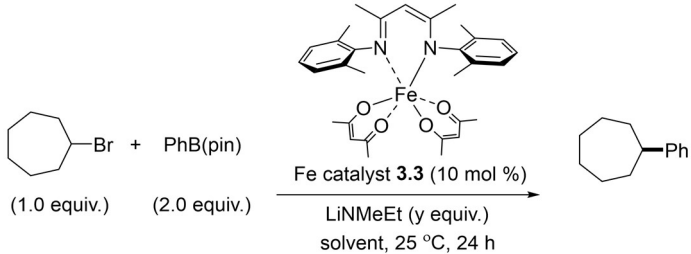
3.6 Reaction optimization

Having demonstrated the benchtop stability of the iron-based complex, we sought to evaluate conditions for the catalytic cross-coupling reaction in hopes of eliminating the need to use a glovebox for the reaction (Table 3.1). Low yields were obtained when the reaction was carried out with commercially available $\text{Fe}(\text{acac})_3$ and β -diketiminato ligand in place of iron complex **3.3** synthesized prior to the cross-coupling reaction (Table 3.1, entry 1). All other reactions reported in Table 3.1 were carried out with iron complex **3.3**

that was exposed to air for at least 4 weeks (see Experimental section for detailed procedure). The yield obtained after 4 weeks of exposure to air ($56 \pm 1\%$) was lower than the yield of the reaction carried out after one hour of exposure to air ($71 \pm 11\%$). However, we do not attribute these lower yields to catalyst decomposition in the air but rather due to incomplete activation of the iron(III) complex when using 1.2 equivalents of base because yields obtained with 1.2 equivalents of base varied from 50% to 80%. Increasing the equivalents of base to 2 resulted in increased average yield ($80 \pm 6\%$) compared to when 1.2 equivalents of base was used (Table 3.1, entries 2-6). These reaction conditions also led to more reproducible results with yield varying by only a few percent for multiple reactions carried out under these conditions, regardless of how long complex **3.3** was exposed to air: a reaction carried out with 2.0 equivalents of base with iron complex **3.3** that was not exposed to air gave nearly identical yield ($83 \pm 6\%$) as the reaction carried out after **3.3** was exposed to air for nine months (80%). Reactions carried out with 2 equivalents of base represent the optimal conditions to obtain high yields reproducibly, because further increasing the equivalents of base led to lower isolated yields (Table 3.1, entries 5-6). Cognizant of the toxicity of benzene as an ICH class 1 solvent,⁵³ more environmentally friendly solvents such as 2-methyl tetrahydrofuran and anisole (both ICH class 3 solvents) were also evaluated for the reaction (Table 3.1, entries 7-8). While reactions carried out in 2-methyl tetrahydrofuran led to a slight drop in yield compared to reactions carried out in benzene, reactions in anisole gave almost the same yield as reactions in benzene. While benzene was used as the primary solvent for the remainder of this study due to its relative ease of removal from the reaction mixture, we anticipate that anisole can be used as a

replacement for benzene in industrial settings where solvent toxicity is a significant concern.

Table 3.1. Optimization of reaction conditions.



entry	LiNMeEt (equiv.)	solvent	yield (brsm)	
			glovebox ^a	Schlenk line ^a
1 ^b	1.2	benzene	24 (40) ^c	n/a
2	1.2	benzene	56 (80) ^c	40 (61) ^d
3	1.5	benzene	66 (77) ^c	43 (52) ^d
4	2.0	benzene	81 (84) ^{df}	66 (75) ^d
5	2.5	benzene	45 (61) ^c	52 (59) ^d
6	3.0	benzene	22 (31) ^c	0 (0) ^d
7	2.0	2-MeTHF	69 (69) ^c	49 (49) ^d
8 ^c	2.0	anisole	78 (78) ^c	22 (25) ^d
9 ^c	2.0	1:6 anisole:benzene	99 (99) ^c	69 (73) ^d
10 ^e	2.0	1:6 anisole:benzene	n/a	74 (74) ^{df}

^a See Experimental Section for details regarding reaction assembly. ^b Fe(acac)₃ combined with β-diketiminato ligand in place of discrete catalyst. ^c LiNMeEt added as a uniformly sieved solid. ^d LiNMeEt added as a dispersion in anisole. ^e LiNMeEt synthesized in anisole in reaction vessel immediately prior to addition of catalyst and substrates. ^f average of five trials.

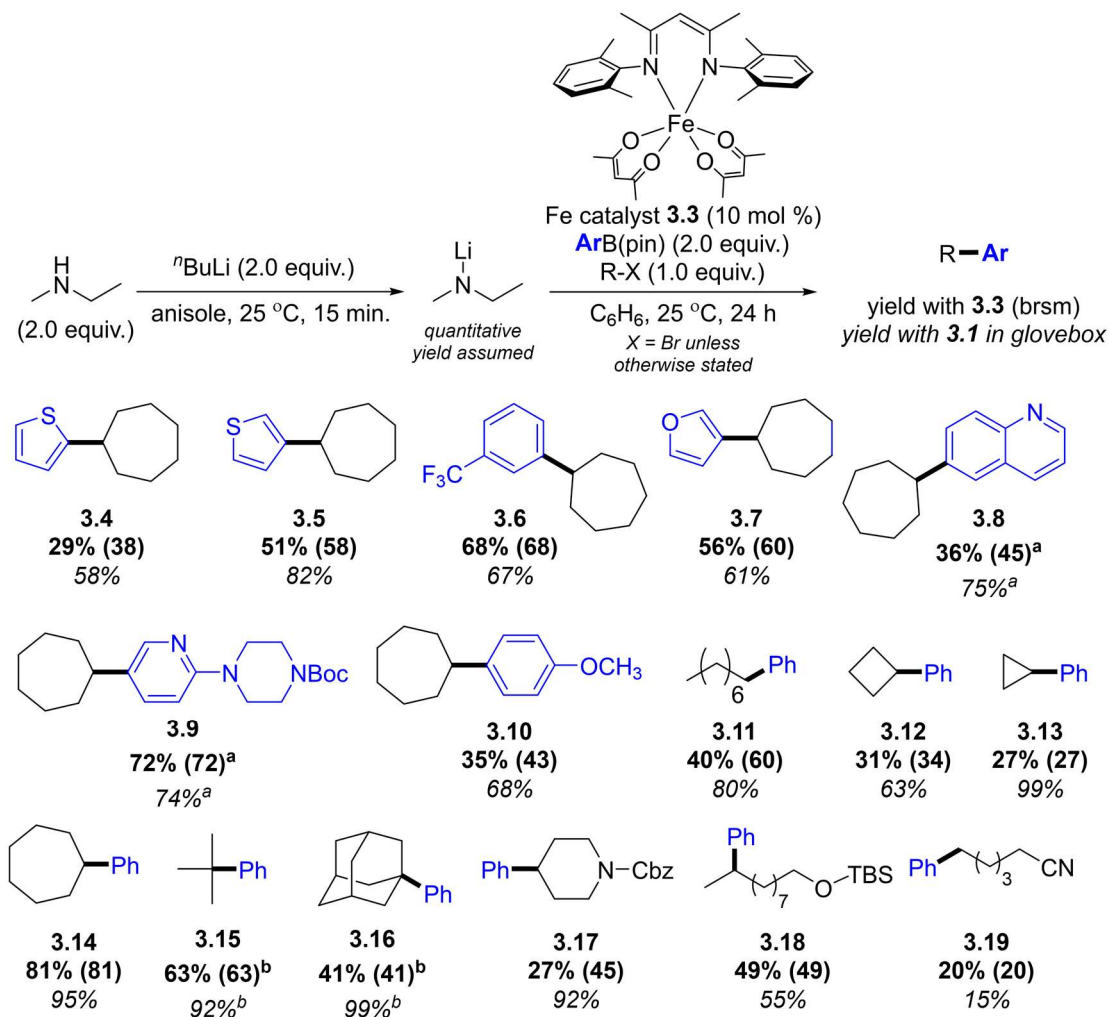
Our previous results suggest that using a lithium amide base is necessary for iron-catalyzed cross-coupling reactions in order to avoid the irreversible formation of inactive iron aggregates.²⁴ Unfortunately, using alkyl amide bases precludes facile reaction setup on the benchtop.⁵⁴ Because the lithium amide is moderately soluble in anisole and employing anisole as a solvent did not adversely affect the outcome of the reaction in the glovebox, a procedure was developed which involved dispensing a dispersion of the lithium amide in anisole into the reaction vessel for application on the Schlenk line. Reactions set up using this procedure produced the desired product, although lower yield was generally observed compared to reactions set up and carried out inside of a glovebox

with the same solvent ratio (Table 3.1, entry 9). Higher yields could be obtained by deprotonating the amine with *n*-butyllithium in anisole in the reaction vessel on the Schlenk line immediately prior to the addition of the catalyst and substrates under a positive flow of inert gas (Table 3.1, entry 10). Employing this procedure, yields were comparable to reactions assembled in the glovebox and employing benzene as the solvent (*cf.* Table 3.1, entry 4). This procedure also enabled the reaction to be carried out on a gram scale, enabling isolation of the desired cross-coupled product in 82% yield.

3.7 Evaluation of substrate scope

Having established an optimal procedure that does not require a glovebox, the substrate scope of the reaction was explored next (Table 3.2). Heteroaromatic-containing substrates **3.4-3.10**, which were amenable to our previously reported method,³² were also viable for cross-coupling with the air-stable catalyst. As discussed in Chapter 2, these substrates are highly represented in pharmaceutically relevant compounds and demonstrate how the new protocol may have value to medicinal and process chemists. Primary, secondary, and tertiary alkyl halides **3.11-3.16** were well-tolerated, as well as protected amine **3.17** and a protected alcohol **3.18**. While the need for the lithium amide base somewhat limited the functional group tolerance of the method (e.g., esters, ketones, and free amines were not tolerated), an alkyl halide containing a nitrile resulted in some cross-coupled product (**3.19**). All reactions delivered the desired cross-coupled product regardless of whether they were assembled in the glovebox or on the Schlenk line, although lower product yield is generally observed when compared to analogous reactions using the previously reported β -diketiminato iron(II) catalyst precursors in the glovebox.

Table 3.2. a) Substrate scope for cross-coupling reactions performed without the aid of a glovebox using air-stable complex **3.3** as a catalyst precursor. Isolated yields are reported with yields based on recovered starting material in parentheses. Yields from reactions employing the iron(II) catalyst **3.1** in the glovebox are reported below in italics.

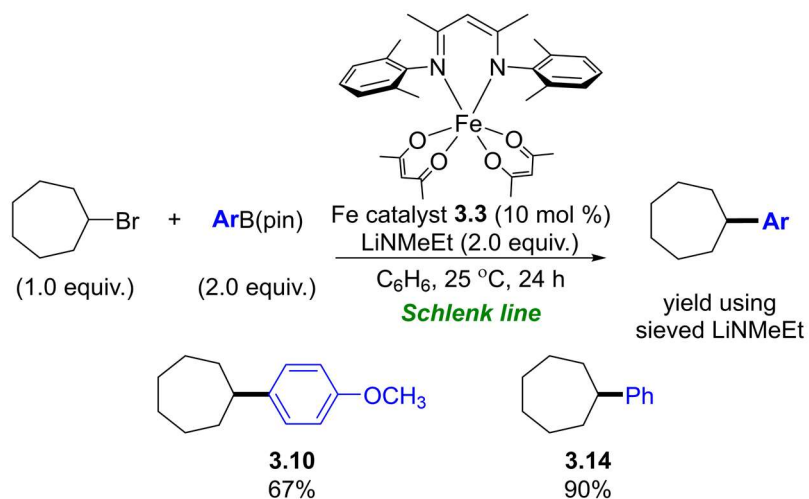


^a heated to 50 °C. ^b X = Cl.

It is important to mention that the discrepant yields between procedures are chiefly due to the manner in which the lithium amide is added to the reaction mixture, rather than the air sensitivity of the catalyst precursor or the fidelity of the air-free procedure. To illustrate this, reactions for compounds **3.10** and **3.14** were carried out using solid lithium amide that had been sieved to a particle size of 250 μm or smaller (Table 3.3). Lithium amide prepared in this way was weighed into a sealed reaction vessel inside a glovebox,

which was evacuated on a Schlenk line prior to addition of complex **3.3**, the reaction substrates, and the reaction solvent (dispensed on the bench) under positive pressure of inert gas. In both cases, the product yields were comparable to those from reactions using complex **3.1** inside of a glovebox, which also employed sieved lithium amide rather than an *in situ* suspension in anisole (*cf.* Table 3.2, entries **3.10** and **3.14**). We hypothesize that the particle size of the lithium amide helps regulate its dissolution, which is only partially soluble in the aromatic solvents used. Consequently, the partial solubility of the base in benzene and anisole is beneficial because the aromatic solvents provide a convenient way to gradually introduce the lithium amide to the reaction as it proceeds. Because anisole more readily solubilizes the base, it is detrimental for reactions when a slurry of lithium amide is made prior to initiating the reaction. Considering the environmental advantages of using anisole rather than benzene as the solvent, we have attempted to add the base as a slurry to reactions carried out in anisole *via* syringe pump, but such procedures have always led to lower yields compared to reactions in which all of the base is present at the onset. Nevertheless, we concluded that the procedure used for the substrates in Table 3.2 and Table 3.3 benefited from the convenience for assembling the reaction on the bench, avoiding the use of sieved solid lithium amide which would require access to a glovebox. While future optimization will still be needed for carrying out the reaction in more environmentally friendly solvents, access to the bench-stable iron(III) precursor **3.3** and a procedure that does not require a glovebox should make such optimizations easier for practitioners who require the use of such solvents.

Table 3.3. Cross-coupling reactions performed without the aid of a glovebox using uniformly sieved lithium amide and complex **3.3** as catalyst precursor.



3.8 Conclusion and outlook

In conclusion, an air-stable iron(III)-based catalyst precursor for the Suzuki-Miyaura cross-coupling between alkyl halides and aryl boronic esters was developed, and a protocol for carrying out the cross-coupling reactions without the aid of a glovebox was established. Bearing one β -diketiminato ligand and two acetylacetonate ligands, the new iron complex displayed long-term stability in the solid state, as assessed by a combination of ¹H NMR spectroscopy, Mössbauer spectroscopy, and its sustained catalytic activity after being exposed to air for months. We anticipate that this advance will enable the practical implementation of iron-based catalysts for the Suzuki-Miyaura cross-coupling reaction in industrial settings. Considering that the reaction is particularly effective at incorporating alkyl halide substrates and it is compatible with heterocycles commonly observed in pharmaceuticals, we expect that the iron-based complexes will provide complementary reactivity to the well-established palladium-based catalysts used for the Suzuki-Miyaura cross-coupling of two sp²-hybridized substrates. The low toxicity of iron compared to nickel may also make these catalysts advantageous compared to air-stable nickel-based

complexes that have previously been developed for similar reactions.⁷⁻⁹ Ultimately, we hope that this improved protocol for iron-catalyzed Suzuki-Miyaura cross-coupling reactions paves the way for facile access to previously inaccessible structures that may be useful for structure-activity relationship studies in the pharmaceutical industry.

3.9 Experimental section

General Considerations. Unless stated otherwise, all reactions were carried out in oven-dried glassware in a nitrogen-filled glovebox or using standard Schlenk line techniques.⁵⁵ Solvents including tetrahydrofuran, pentane, and benzene were used after passage through two activated alumina columns under a blanket of argon⁵⁶ and then degassed by brief exposure to vacuum. Deuterated solvents were dried over a sodium/benzophenone pot and distilled prior to their use. Boronic acid pinacol esters were used after passage through alumina under a nitrogen atmosphere. Methylethylamine was purchased from TCI America; diethylamine was purchased from Sigma-Aldrich. Amines that were liquids at room temperature were dried over calcium hydride for at least 24 hours and then distilled under vacuum. Lithium amides were passed through a 250 micron sieve to ensure homogenous particle size prior to use. The lithium amide salts are pyrophoric when exposed to air, but their flammability is mitigated when they are dissolved in solution. The β -diketiminato ligand used for the synthesis of iron complexes **3.1** and **3.3** was synthesized as described previously.³² Aryl boronic ester precursors for compounds **3.5**, **3.8**, and **3.9** were graciously provided by Amgen. Iron(III) chloride was purchased from Sigma-Aldrich and used without further purification. Iron(III) tris(acetoacetone) was purchased from Acros Organics and used without further purification. Alkyl halides were dried over calcium hydride for at least 24 hours and then distilled under vacuum. Nuclear magnetic resonance (NMR) spectra were recorded at ambient temperature on Varian vNMRs operating at 400 MHz, 500 MHz, or 600 MHz for ^1H NMR, at 160 MHz for ^{11}B NMR, and at 125 MHz for $\{^1\text{H}\}^{13}\text{C}$ NMR. Spectra were referenced using shifts corresponding to solvent residual protic impurities. Boron trifluoride diethyl etherate

(BF₃·Et₂O) was used as an external standard for ¹¹B NMR (0.0 ppm). The line listing for NMR spectra of diamagnetic compounds are reported as follows: chemical shift (multiplicity, coupling constant, integration); paramagnetic compounds are reported as follows: chemical shift (peak width at half height, number of protons). All paramagnetic spectra were collected at 25 °C. Solvent suppressed spectra were collected for paramagnetic complexes in THF using the PRESAT macro on the vNMR software. Infrared spectra were recorded on a Bruker Alpha attenuated total reflectance infrared spectrometer. High resolution mass spectra were obtained at the Boston College Mass Spectrometry Facility on a JEOL AccuTOF DART instrument. Single crystal X-ray Intensity data were measured on a Bruker Kappa Apex Duo diffractometer using a high brightness I μ S copper source with multi-layer mirrors. The low temperature device used is an Oxford 700 series Cryostream system with temperature range of 80-400 K. An Olympus SZ1145 stereo zoom microscope was used to view and mount crystals. The crystal structure was solved using ShellX. Solution state magnetic moments were obtained following the method described by Evans.⁵⁷ For Mössbauer spectroscopy, solid samples were prepared under an inert atmosphere within a glovebox with a liquid nitrogen fill port to freeze-trap solid samples at 77 K. Samples were loaded into Delrin sample cups and then frozen in liquid nitrogen. Low temperature ⁵⁷Fe Mössbauer measurements were performed using a Janis SVT-400T N₂ cryostat for analysis at 80 K. Isomer shift values were measured relative to an α -Fe standard at 298 K. All of the Mössbauer spectra were fit using WMoss (See Co.) software. The associated parameter errors in the fit analyses include the following: $\delta \pm 0.02$ mm/s, $\Delta E_Q \pm 3\%$. The multicomponent fit analyses have an associated

quantitation error of $\pm 3\%$. Since only zero-field Mössbauer measurements were performed, all quadrupole splitting parameters reported herein are absolute values.

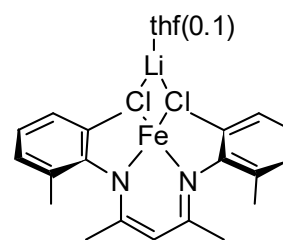
General procedure for the iron-catalyzed cross-coupling reaction of aryl boronic esters and alkyl halides performed in a glovebox. In a nitrogen-filled glovebox, iron complex **3.3** (0.025 mmol, 10 mol %, 14 mg) and lithium ethylmethyl amide (0.5 mmol, 2.0 equiv., 32 mg) were added to a 7 mL scintillation vial containing a magnetic stir bar. A 1 mL benzene solution of boronic acid pinacol ester (0.5 mmol, 2.0 equiv.) and alkyl halide (0.25 mmol, 1.0 equiv.) was added to the stirring vial, followed immediately by benzene (5 mL) and sealing of the reaction vessel. The reaction mixture was allowed to stir vigorously and quickly became homogenous. After 24 hours of stirring, the reaction was quenched with a saturated aqueous solution of ammonium chloride (10 mL). The aqueous phase was washed with dichloromethane (3 x 40 mL) and the combined organic phases were dried over sodium sulfate and filtered through celite. Trimethoxybenzene (42 mg, 0.25 mmol) was added as an internal standard before evaporating the solvent in vacuo. A spectroscopic yield was determined by ^1H NMR spectroscopy before the crude product was purified by silica flash column chromatography to give isolated yields.

General procedure for the iron-catalyzed cross-coupling reaction of aryl boronic esters and alkyl halides under nitrogen on a Schlenk line. On the Schlenk line, to an oven-dried 10 mL Schlenk tube equipped with stir bar and purged with N_2 was added ethylmethyl amine (0.55 mmol, 2.1 equiv., 31 mg, 45 μL) and anisole (0.5 mL). A solution of *n*-butyllithium in hexanes (2.5 M, 0.5 mmol, 2.0 equiv.) was added to the reaction vessel, whereupon the reaction mixture turned cloudy. The reaction mixture was allowed to stir at ambient temperature for 15 minutes. Iron complex **3.3** (0.025 mmol, 10 mol %) was

weighed into a round-bottom flask open to air, which was evacuated on the Schlenk line and backfilled with nitrogen. The iron complex was dissolved in benzene (1 mL) and then added simultaneously to the Schlenk tube by syringe with a 1 mL benzene solution of boronic acid pinacol ester (0.5 mmol, 2.0 equiv.) and alkyl halide (0.25 mmol, 1.0 equiv.) prepared in a separate syringe. The reaction mixture was diluted to a volume of 7 mL with benzene, then allowed to stir at room temperature under a nitrogen atmosphere. After 24 hours, the reaction was quenched with a saturated aqueous solution of ammonium chloride (10 mL). The aqueous phase was washed with dichloromethane (3 x 40 mL) and the combined organic phases were dried over sodium sulfate and filtered through celite. Trimethoxybenzene (42 mg, 0.25 mmol) was added as an internal standard before evaporating the solvent in vacuo. A spectroscopic yield was determined by ^1H NMR spectroscopy before the crude product was purified by silica flash column chromatography to give isolated yields.

Synthesis of 2,4-bis[(2,6-dimethylphenyl)imino]pentane iron chloride complex (3.1)

To an oven-dried 50 mL round-bottom flask equipped with stirbar was added 2,4-bis[(2,6-dimethylphenyl)imino]pentane (500 mg, 1.63 mmol, 1.0 equiv.) and pentane (25 mL). On the Schlenk line, the mixture was cooled to $-78\text{ }^\circ\text{C}$ and degassed by

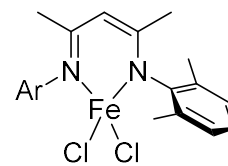


placing the solution under vacuum for at least 5 minutes. A solution of butyl lithium in hexanes (0.9 mL, 1.8 M, 1.63 mmol) was added dropwise while stirring. A pale yellow precipitate forms upon warming to ambient temperature. The reaction mixture was warmed to room temperature while stirring before the solvent was removed under vacuum. The sealed reaction vessel was transferred into a glovebox, where the solid was collected on a

frit and washed with cold pentane (5 mL at $-40\text{ }^{\circ}\text{C}$). The solid was dried and weighed to determine stoichiometry for the next step. No characterization of the lithium salts of the ligand were carried out. The collected deprotonated ligand (500 mg, 1.6 mmol, 1.0 equiv.) was then dissolved in THF (10 mL) in a 20 mL scintillation vial. This solution was added dropwise to a slurry of iron trichloride (260 mg, 1.6 mmol, 1.0 equiv.) in THF (10 mL) prepared in a separate scintillation vial equipped with stir bar. This mixture was allowed to stir for 1 hour before being placed in a $-40\text{ }^{\circ}\text{C}$ refrigerator overnight to precipitate. The reaction mixture was filtered through celite and washed with THF, then the filtrate concentrated *in vacuo*. The residue was washed with cold pentane (10 mL), dried, and collected as a dark yellow solid (450 mg, 45%). Spectral data matched that of the analogous iron (II) dihalide complex. ^1H NMR (400 MHz, THF) δ -68.7 ($w_{1/2}$ = 180 Hz, 6H), -52.0 ($w_{1/2}$ = 100 Hz, 2H), -39.7 ($w_{1/2}$ = 264 Hz, 1H), 6.2 ($w_{1/2}$ = 254 Hz, 12H), 16.1 ($w_{1/2}$ = 82 Hz, 4H) ppm.³² μ_{eff} (THF, $25\text{ }^{\circ}\text{C}$): $5.20\ \mu_{\text{B}}$.

Synthesis of 2,4-bis[(2,6-dimethylphenyl)imino]pentane iron (III) dichloride (3.2)

In a nitrogen-filled glovebox, to a 7 mL scintillation vial equipped with stir bar was added 2,4-bis[(2,6-dimethylphenyl)imino]pentane iron (II) chloride complex (100 mg, 0.17 mmol, 1.0 equiv.) and

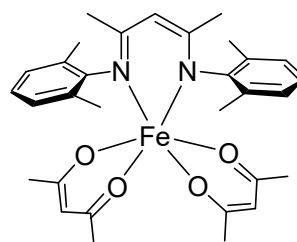


ferrocenium hexafluorophosphate (57 mg, 0.17 mmol, 1.0 equiv.). The solids were dissolved in THF (2 mL), at which point the reaction mixture turned a dark purple immediately. The reaction mixture was allowed to stir for 1 hour at ambient temperature, then the solvent evaporated *in vacuo*. The crude material was subjected to recrystallization from pentane at $-40\text{ }^{\circ}\text{C}$ overnight to afford the title compound as a dark purple solid of X-ray quality (25 mg, 66% yield). ^1H NMR (400 MHz, THF, solvent suppressed) δ 68.64

($w_{1/2} = 1007$ Hz, 12H), 16.12 ($w_{1/2} = 224$ Hz, 2H), -36.25 ($w_{1/2} = 800$ Hz, 4H), -52.01 ($w_{1/2} = 248$ Hz, 1H), -68.68 ($w_{1/2} = 335$ Hz, 6H). IR: 3357, 1560, 1523, 1473, 1446, 1276, 1193, 843, 773, 555 cm^{-1} . μ_{eff} (THF, 25 °C): 6.54 μ_{B} . HRMS-DART (m/z): $[\text{M}+\text{H}]^+$ calculated for $\text{C}_{21}\text{H}_{26}\text{N}_2\text{Cl}_2\text{Fe}$, 432.19; found, 432.08.

Synthesis of 2,4-bis[(2,6-dimethylphenyl)imino]pentane iron (III) bis(acetylacetonate) (3.3)

To an oven-dried 100 mL pear-shaped round-bottom flask equipped with stir bar was added 2,4-bis[(2,6-dimethylphenyl)imino]pentane ligand (4.59 g, 14.97 mmol, 1.05 equiv.) and pentane (25 mL). A 180° joint with stopcock was



attached and the apparatus was sealed with a rubberband and copper wire. On the Schlenk line, the mixture was cooled to -78 °C and degassed by placing the solution under vacuum for 5 minutes. A solution of butyllithium in hexanes (4.75 mL, 3 M, 1 equiv.) was added dropwise via sidearm while stirring at -78 °C. A pale yellow precipitate forms upon warming to ambient temperature. The reaction mixture was allowed to stir 30 minutes at ambient temperature before the solvent was removed under vacuum. The sealed reaction apparatus was transferred to a glovebox, and the solid was collected on a frit and washed with cold pentane (10 mL). The collected solid was dried and weighed to determine stoichiometry for the next step. The deprotonated ligand (4.56 g, 14.6 mmol, 1 equiv.) was dissolved in THF (5 mL) in a 20 mL scintillation vial. This solution was added dropwise to a suspension of $\text{Fe}(\text{acac})_3$ (5.16 g, 14.6 mmol, 1 equiv.) in THF (5 mL) prepared in a separate scintillation vial equipped with stir bar. This mixture was allowed to stir overnight, during which time it turned from red-orange to dark green. The reaction mixture was cooled

before being passed through celite, then washed with additional THF (~ 20 mL) before it was concentrated under vacuum. The resulting solid residue was washed with pentane, dried, and collected to afford the product as a dark green solid (4.9 g, 60% yield). ^1H NMR (500 MHz, C_6D_6) δ 42.94 ($w_{1/2}$ = 1550 Hz, 4H), 33.09 ($w_{1/2}$ = 4136 Hz, 6H), 20.19 ($w_{1/2}$ = 1827 Hz, 12H), 15.83 ($w_{1/2}$ = 1568 Hz, 8H), -31.79 ($w_{1/2}$ = 425 Hz, 3H), -47.02 ($w_{1/2}$ = 1410 Hz, 6H). IR: 2919, 1577, 1520, 1371, 1272, 1020, 764 cm^{-1} . μ_{eff} (THF, 25 °C): 7.04 μ_{B} . HRMS-DART (m/z): $[\text{M}+\text{H}]^+$ calculated for $\text{C}_{31}\text{H}_{39}\text{N}_2\text{O}_4\text{Fe}$, 559.51; found, 560.23. Elemental analysis for $\text{C}_{31}\text{H}_{39}\text{N}_2\text{O}_4\text{Fe}$: calculated C 66.55% H 7.03% N 5.01%; found C 63.17% H 6.65% N 4.52%. Discrepancies in the elemental analysis are believed to be due to the presence of residual $\text{Fe}(\text{acac})_3$.

Synthesis of 2-cycloheptyl thiophene (3.4)

3.4 was synthesized from bromocycloheptane and 2-thiophenyl boronic acid pinacol ester according to the general procedure on the Schlenk line, using catalyst **3.3** and purified by silica gel flash column chromatography, eluting with 100% hexanes to afford the product as a colorless oil (13 mg, 32% spectroscopic yield, 38% based on recovered starting material, 29% isolated). R_f = 0.75 (100% hexanes). ^1H NMR (400 MHz, CDCl_3): δ 7.07 (d, J = 5.1, 1H), 6.90 (t, J = 5.1, 3.4 Hz, 1H), 6.78 (d, 1H), 3.04 (septet, J = 4.6 Hz, 1H), 2.12 – 2.03 (m, 1H), 1.81 – 1.64 (m, 4H), 1.57 – 1.48 (m, 5H) ppm. NMR spectrum is in agreement with literature precedence.³²

Synthesis of 3-cycloheptyl thiophene (3.5)

3.5 was synthesized from bromocycloheptane and 3-thiophenyl boronic acid pinacol ester according to the general procedures in the glovebox and on the Schlenk line, using catalyst

3.3 and purified by silica gel flash column chromatography, eluting with 100% hexanes to afford the product as a colorless oil (23 mg, 53% spectroscopic yield, 58% based on recovered starting material, 51% isolated). $R_f = 0.75$ (100% hexanes). $^1\text{H NMR}$ (400 MHz, CDCl_3): δ 7.22 (dd, $J = 5.0, 3.0$ Hz, 1H), 6.97 (d, $J = 5.0$ Hz, 1H), 6.91 (s, 1H), 2.82 (septet, $J = 9.9, 4.7$ Hz, 1H), 1.98 (m, 2H), 1.80 – 1.72 (m, 2H), 1.71 – 1.47 (m, 8H) ppm. NMR spectrum is in agreement with literature precedence.³²

Synthesis of (3-(trifluoromethyl)phenyl) cycloheptane (3.6)

3.6 was synthesized from bromocycloheptane and (3-(trifluoromethyl)phenyl) boronic acid pinacol ester according to the general procedure on the Schlenk line, using catalyst **3.3** and purified by silica gel flash column chromatography, eluting with 100% hexanes to afford the product as a colorless oil (41 mg, 66% spectroscopic yield, 66% based on recovered starting material, 68% isolated). $R_f = 0.80$ (100% hexanes). $^1\text{H NMR}$ (400 MHz, CDCl_3): δ 7.43 – 7.36 (m, 4H), 2.73 (septet, 1H), 1.95 – 1.86 (m, 2H), 1.86 – 1.77 (m, 2H), 1.74 – 1.51 (m, 8H) ppm. NMR spectrum is in agreement with literature precedence.²⁴

Synthesis of 3-cycloheptyl furan (3.7)

3.7 was synthesized from bromocycloheptane and 3-furyl boronic acid pinacol ester according to the general procedure on the Schlenk line, using catalyst **3.3** and purified by silica gel flash column chromatography, eluting with 100% hexanes to afford the product as a colorless oil (23 mg, 55% spectroscopic yield, 60% based on recovered starting material, 56% isolated). $R_f = 0.95$ (100% hexanes). $^1\text{H NMR}$ (400 MHz, CDCl_3): δ 7.33 (s, 1H), 7.19 (s, 1H), 6.28 (s, 1H), 2.63 (septet, 1H), 1.94 (m, 2H), 1.76 – 1.62 (m, 4H), 1.57 – 1.48 (m, 6H) ppm. NMR spectrum is in agreement with literature precedence.³²

Synthesis of 6-cycloheptyl quinoline (3.8)

3.8 was synthesized from bromocycloheptane and 6-quinolyl boronic acid pinacol ester according to the general procedure on the Schlenk line heated to 50 °C, using catalyst **3.3** and purified by silica gel flash column chromatography, eluting with 100% hexanes to afford the product as a colorless oil (20 mg, 34% spectroscopic yield, 45% based on recovered starting material, 36% isolated). $R_f = 0.45$ (30% ethyl acetate in hexanes). ^1H NMR (400 MHz, CDCl_3): δ 8.85 (d, $J = 4.1$ Hz, 1H), 8.13 (d, $J = 8.3$ Hz, 1H), 8.03 (d, $J = 8.6$ Hz, 1H), 7.63 – 7.55 (m, 2H), 7.45 – 7.36 (m, 1H), 2.88i (septet, 1H), 2.04 – 1.95 (m, 2H), 1.89 – 1.79 (m, 2H), 1.79 – 1.71 (m, 4H), 1.71 – 1.57 (m, 4H) ppm. NMR spectrum is in agreement with literature precedence.³²

Synthesis of 6-(4-Boc-piperazin-1-yl)-3-cycloheptyl pyridine (3.9)

3.9 was synthesized from bromocycloheptane and 6-(4-Boc-piperazin-1-yl)pyridine-3-boronic acid pinacol ester according to the general procedure on the Schlenk line heated to 50 °C, using catalyst **3.3** and purified by silica gel flash column chromatography, eluting with 100% hexanes to afford the product as a colorless oil (65 mg, 72% spectroscopic yield, 72% based on recovered starting material, 72% isolated). $R_f = 0.45$ (30% ethyl acetate in hexanes). ^1H NMR (400 MHz, CDCl_3): δ 8.04 (s, 1H), 7.37 (m, 1H), 6.59 (m, 1H), 3.53 (m, 4H), 3.46 (m, 4H), 2.59 (septet, 1H), 1.89 – 1.81 (m, 2H), 1.81 – 1.73 (m, 2H), 1.72 – 1.65 (m, 2H), 1.65 – 1.51 (m, 6H), 1.48 (s, 9H) ppm. NMR spectrum is in agreement with literature precedence.³²

Synthesis of (4-methoxyphenyl) cycloheptane (3.10)

3.10 was synthesized from bromocycloheptane and (4-methoxyphenyl) boronic acid pinacol ester according to the general procedure on the Schlenk line, using catalyst **3.3** and purified by silica gel flash column chromatography, eluting with 100% hexanes to afford the product as a white solid (18 mg, 34% spectroscopic yield, 43% based on recovered starting material, 35% isolated). $R_f = 0.60$ (10% ethyl acetate in hexanes). $^1\text{H NMR}$ (500 MHz, CDCl_3): δ 7.11 (d, $J = 8.4$ Hz, 2H), 6.82 (d, $J = 8.4$ Hz, 2H), 2.61 (septet, $J = 10.3$, 5.1 Hz, 1H), 1.94 – 1.82 (m, 2H), 1.82 – 1.72 (m, 2H), 1.72 – 1.64 (m, 2H), 1.64 – 1.49 (m, 6H) ppm. NMR spectrum is in agreement with literature precedence.²⁴

Synthesis of phenyloctane (3.11)

3.11 was synthesized from bromooctane and phenyl boronic acid pinacol ester according to the general procedure on the Schlenk line, using catalyst **3.3** and purified by silica gel flash column chromatography, eluting with 100% hexanes to afford the product as a colorless oil (19 mg, 39% spectroscopic yield, 60% based on recovered starting material, 40% isolated). $R_f = 0.60$ (100% hexanes). $^1\text{H NMR}$ (400 MHz, CDCl_3): δ 7.27 (m, 2H), 7.18 (d, $J = 7.2$ Hz, 3H), 2.60 (t, $J = 7.5$ Hz, 2H), 1.65 – 1.57 (m, 2H), 1.32 – 1.26 (m, 10H), 0.90 – 0.86 (m, 3H) ppm. NMR spectrum is in agreement with literature precedence.³²

Synthesis of phenylcyclobutane (3.12)

3.12 was synthesized from bromocyclobutane and phenyl boronic acid pinacol ester according to the general procedure on the Schlenk line, using catalyst **3.3** and purified by silica gel flash column chromatography, eluting with 100% hexanes to afford the product as a colorless oil (10 mg, 34% spectroscopic yield, 34% based on recovered starting

material, 31% isolated). $R_f = 0.70$ (100% hexanes). $^1\text{H NMR}$ (400 MHz, CDCl_3): δ 7.33 – 7.14 (m, 5H), 3.56 (p, $J = 8.8$ Hz, 1H), 2.40 – 1.81 (m, 6H) ppm. NMR spectrum is in agreement with literature precedence.³²

Synthesis of phenylcyclopropane (3.13)

3.13 was synthesized from bromocyclopropane and phenyl boronic acid pinacol ester according to the general procedure on the Schlenk line, using catalyst **3.3** and purified by silica gel flash column chromatography, eluting with 100% hexanes to afford the product as a colorless oil (8 mg, 27% spectroscopic yield, 27% based on recovered starting material, 27% isolated). $R_f = 0.75$ (100% hexanes). $^1\text{H NMR}$ (400 MHz, CDCl_3) δ 7.47 (d, $J = 7.4$ Hz, 2H), 7.14 (t, $J = 7.5$ Hz, 1H), 7.09 (d, $J = 7.8$ Hz, 2H), 1.91 (m, 1H), 0.97 (q, $J = 8.4$ Hz, 2H), 0.71 (q, $J = 4.6$ Hz, 2H) ppm. NMR spectrum is in agreement with literature precedence.³²

Synthesis of phenylcycloheptane (3.14)

3.14 was synthesized from bromocycloheptane and phenyl boronic acid pinacol ester according to the general procedures in the glovebox and on the Schlenk line, using catalyst **3.3** and purified by silica gel flash column chromatography, eluting with 100% hexanes to afford the product as a colorless oil (13 mg, 32% spectroscopic yield, 38% based on recovered starting material, 29% isolated). $R_f = 0.60$ (100% hexanes). $^1\text{H NMR}$ (500 MHz, CDCl_3): δ 7.23 – 7.33 (m, 2H), 7.08 – 7.23 (m, 2H), 2.66 (tt, $J = 10.7, 3.7$ Hz, 1H), 1.92 (ddt, $J = 13.5, 6.6, 3.3$ Hz, 2H), 1.80 (ddd, $J = 13.4, 6.6, 3.4$ Hz, 2H), 1.46 – 1.78 (m, 8H) ppm. NMR spectrum is in agreement with literature precedence.²⁴

Synthesis of *tert*-butyl benzene (3.15)

3.15 was synthesized from *tert*-butyl chloride and phenyl boronic acid pinacol ester according to the general procedure on the Schlenk line, using catalyst **3.3** and purified by silica gel flash column chromatography, eluting with 100% hexanes to afford the product as a colorless oil (21 mg, 63% isolated). $R_f = 0.60$ (100% hexanes). ^1H NMR (400 MHz, CDCl_3) δ 7.84 – 7.78 (m, 2H), 7.48 – 7.42 (m, 1H), 7.37 (t, $J = 7.4$ Hz, 2H), 1.35 (s, 9H) ppm. NMR spectrum is in agreement with literature precedence.³²

Synthesis of adamantylbenzene (3.16)

3.16 was synthesized from chloroadamantane and phenyl boronic acid pinacol ester according to the general procedure on the Schlenk line, using catalyst **3.3** and purified by silica gel flash column chromatography, eluting with 100% hexanes to afford the product as a white solid (22 mg, 41% isolated). $R_f = 0.60$ (100% hexanes). ^1H NMR (500 MHz, CDCl_3): δ 7.2 – 7.4 (m, 5H), 2.10 (m, 3H), 1.92 (m, 6H), 1.77 (m, 6H) ppm. NMR spectrum is in agreement with literature precedence.³²

Synthesis of 4-phenylpiperidine-1-carboxylic acid benzyl ester (3.17)

3.17 was synthesized from 4-bromopiperidine-1-carboxylic acid benzyl ester and phenyl boronic acid pinacol ester according to the general procedure on the Schlenk line, using catalyst **3.3** and purified by silica gel flash column chromatography, eluting with 100% hexanes to afford the product as a colorless oil (20 mg, 31% spectroscopic yield, 45% based on recovered starting material, 27% isolated). $R_f = 0.20$ (15% ethyl acetate in hexanes). ^1H NMR (500 MHz, CDCl_3): δ 7.40 – 7.26 (m, 7H), 7.23 – 7.17 (m, 3H), 5.16 (s, 2H), 4.34 (br s, 2H), 2.89 (m, 2H), 2.67 (tt, $J = 12.0, 3.2$ Hz, 1H), 1.85 (d, $J = 13.2$ Hz, 2H), 1.70 – 1.61 (m, 2H) ppm. NMR spectrum is in agreement with literature precedence.³²

Synthesis of *tert*-butyldimethyl((9-phenyldecyl)oxy)silane (3.18)

3.18 was synthesized from *tert*-butyldimethyl((9-bromodecyl)oxy)silane and phenyl boronic acid pinacol ester according to the general procedure on the Schlenk line, using catalyst **3.3** and purified by silica gel flash column chromatography, eluting with 100% hexanes to afford the product as a colorless oil (43 mg, 48% spectroscopic yield, 48% based on recovered starting material, 49% isolated). $R_f = 0.15$ (100% pentane). $^1\text{H NMR}$ (500 MHz, CDCl_3): δ 7.32 – 7.26 (m, 2H), 7.20 – 7.10 (m, 3H), 3.58 (m, 2H), 2.67 (q, $J = 7.1$ Hz, 1H), 1.58 – 1.54 (m, 2H), 1.51 – 1.45 (m, 2H), 1.34 – 1.19 (m, 13H), 1.18 – 1.11 (m, 2H), 0.90 (s, 9H), 0.04 (s, 6H) ppm. NMR spectrum is in agreement with literature precedence.³²

Synthesis of 5-phenylpentyl cyanide (3.19)

3.19 was synthesized from 5-bromopentyl cyanide and phenyl boronic acid pinacol ester according to the general procedure on the Schlenk line, using catalyst **3.3** and purified by silica gel flash column chromatography, eluting with 100% hexanes to afford the product as a colorless oil (9 mg, 18% spectroscopic yield, 18% based on recovered starting material, 20% isolated). $R_f = 0.15$ (5% ethyl acetate in hexanes). $^1\text{H NMR}$ (400 MHz, CDCl_3): δ 7.28 (t, $J = 7.4$ Hz, 2H), 7.20 – 7.14 (m, 3H), 2.62 (t, $J = 7.5$ Hz, 2H), 2.33 (t, $J = 7.0$ Hz, 2H), 1.74 – 1.51 (m, 4H), 1.56 – 1.43 (m, 2H) ppm. NMR spectrum is in agreement with literature precedence.⁵⁸

3.10 References

- (1) Miyaura, N.; Yamada, K.; Suzuki, A. A New Stereospecific Cross-Coupling by the Palladium-Catalyzed Reaction of 1-Alkenylboranes with 1-Alkenyl or 1-Alkynyl Halides. *Tetrahedron Lett.* **1979**, *20* (36), 3437–3440. [https://doi.org/10.1016/S0040-4039\(01\)95429-2](https://doi.org/10.1016/S0040-4039(01)95429-2).
- (2) Brown, D. G.; Boström, J. Analysis of Past and Present Synthetic Methodologies on Medicinal Chemistry: Where Have All the New Reactions Gone? *J. Med. Chem.* **2016**, *59* (10), 4443–4458. <https://doi.org/10.1021/acs.jmedchem.5b01409>.
- (3) Choi, J.; Fu, G. C. Transition Metal–Catalyzed Alkyl–Alkyl Bond Formation: Another Dimension in Cross-Coupling Chemistry. *Science*, **2017**, *356* (6334), eaaf7230. <https://doi.org/10.1126/science.aaf7230>.
- (4) Han, F.-S. Transition-Metal-Catalyzed Suzuki–Miyaura Cross-Coupling Reactions: A Remarkable Advance from Palladium to Nickel Catalysts. *Chem. Soc. Rev.* **2013**, *42* (12), 5270–5298. <https://doi.org/10.1039/c3cs35521g>.
- (5) Balcells, D.; Nova, A. Designing Pd and Ni Catalysts for Cross-Coupling Reactions by Minimizing Off-Cycle Species. *ACS Catal.* **2018**, *8* (4), 3499–3515. <https://doi.org/10.1021/acscatal.8b00230>.
- (6) Ananikov, V. P. Nickel: The “Spirited Horse” of Transition Metal Catalysis. *ACS Catal.* **2015**, *5* (3), 1964–1971. <https://doi.org/10.1021/acscatal.5b00072>.
- (7) Zhou, J.; Fu, G. C. Suzuki Cross-Couplings of Unactivated Secondary Alkyl Bromides and Iodides. *J. Am. Chem. Soc.* **2004**, *126* (5), 1340–1341. <https://doi.org/10.1021/ja039889k>.
- (8) Zultanski, S. L.; Fu, G. C. Nickel-Catalyzed Carbon–Carbon Bond-Forming Reactions of Unactivated Tertiary Alkyl Halides: Suzuki Arylations. *J. Am. Chem. Soc.* **2013**, *135* (2), 624–627. <https://doi.org/10.1021/ja311669p>.
- (9) González-Bobes, F.; Fu, G. C. Amino Alcohols as Ligands for Nickel-Catalyzed Suzuki Reactions of Unactivated Alkyl Halides, Including Secondary Alkyl Chlorides,

with Arylboronic Acids. *J. Am. Chem. Soc.* **2006**, *128* (16), 5360–5361. <https://doi.org/10.1021/ja0613761>.

(10) Kharasch, M. S.; Fields, E. K. Factors Determining the Course and Mechanisms of Grignard Reactions. IV. The Effect of Metallic Halides on the Reaction of Aryl Grignard Reagents and Organic Halides. *J. Am. Chem. Soc.* **1941**, *63* (9), 2316–2320. <https://doi.org/10.1021/ja01854a006>.

(11) Tamura, M.; Kochi, J. K. Vinylation of Grignard Reagents. Catalysis by Iron. *J. Am. Chem. Soc.* **1971**, *93* (6), 1487–1489. <https://doi.org/10.1021/ja00735a030>.

(12) Fürstner, A.; Leitner, A.; Méndez, M.; Krause, H. Iron-Catalyzed Cross-Coupling Reactions. *J. Am. Chem. Soc.* **2002**, *124* (46), 13856–13863. <https://doi.org/10.1021/ja027190t>.

(13) Egorova, K. S.; Ananikov, V. P. Toxicity of Metal Compounds: Knowledge and Myths. *Organometallics* **2017**, *36* (21), 4071–4090. <https://doi.org/10.1021/acs.organomet.7b00605>.

(14) Fürstner, A. Iron Catalysis in Organic Synthesis: A Critical Assessment of What It Takes to Make This Base Metal a Multitasking Champion. *ACS Cent. Sci.* **2016**, *2* (11), 778–789. <https://doi.org/10.1021/acscentsci.6b00272>.

(15) Wong, A. S.; Zhang, B.; Li, B.; Neidig, M. L.; Byers, J. A. Air-Stable Iron-Based Precatalysts for Suzuki–Miyaura Cross-Coupling Reactions between Alkyl Halides and Aryl Boronic Esters. *Org. Process Res. Dev.* **2021**, *ASAP*. <https://doi.org/10.1021/acs.oprd.1c00235>.

(16) Cahiez, G.; Avedissian, H. Highly Stereo and Chemoselective Iron-Catalyzed Alkenylation of Organomagnesium Compounds. *Synthesis (Stuttg.)* **1998**, No. 8, 1199–1205. <https://doi.org/10.1055/s-1998-2135>.

(17) Fürstner, A.; Leitner, A. Iron-Catalyzed Cross-Coupling Reactions of Alkyl-Grignard Reagents with Aryl Chlorides, Tosylates, and Triflates. *Angew. Chemie - Int. Ed.* **2002**, *41* (4), 609–612. [https://doi.org/10.1002/1521-3773\(20020215\)41:4<609::AID-](https://doi.org/10.1002/1521-3773(20020215)41:4<609::AID-)

ANIE609>3.0.CO;2-M.

- (18) Nakamura, M.; Matsuo, K.; Ito, S.; Nakamura, E. Iron-Catalyzed Cross-Coupling of Primary and Secondary Alkyl Halides with Aryl Grignard Reagents. *J. Am. Chem. Soc.* **2004**, *126* (12), 3686–3687. <https://doi.org/10.1021/ja049744t>.
- (19) Bisz, E.; Szostak, M. Iron-Catalyzed C(Sp²)-C(Sp³) Cross-Coupling of Chlorobenzenesulfonamides with Alkyl Grignard Reagents: Entry to Alkylated Aromatics. *J. Org. Chem.* **2019**, *84* (3), 1640–1646. <https://doi.org/10.1021/acs.joc.8b02886>.
- (20) Lo, J. C.; Yabe, Y.; Baran, P. S. A Practical and Catalytic Reductive Olefin Coupling. *J. Am. Chem. Soc.* **2014**, *136* (4), 1304–1307. <https://doi.org/10.1021/ja4117632>.
- (21) Lo, J. C.; Gui, J.; Yabe, Y.; Pan, C.-M.; Baran, P. S. Functionalized Olefin Cross-Coupling to Construct Carbon–Carbon Bonds. *Nature* **2014**, *516* (7531), 343–348. <https://doi.org/10.1038/nature14006>.
- (22) Lo, J. C.; Kim, D.; Pan, C.-M.; Edwards, J. T.; Yabe, Y.; Gui, J.; Qin, T.; Gutiérrez, S.; Giacoboni, J.; Smith, M. W.; et al. Fe-Catalyzed C–C Bond Construction from Olefins via Radicals. *J. Am. Chem. Soc.* **2017**, *139* (6), 2484–2503. <https://doi.org/10.1021/jacs.6b13155>.
- (23) Kim, D.; Rahaman, S. M. W.; Mercado, B. Q.; Poli, R.; Holland, P. L. Roles of Iron Complexes in Catalytic Radical Alkene Cross-Coupling: A Computational and Mechanistic Study. *J. Am. Chem. Soc.* **2019**, *141* (18), 7473–7485. <https://doi.org/10.1021/jacs.9b02117>.
- (24) Crockett, M. P.; Tyrol, C. C.; Wong, A. S.; Li, B.; Byers, J. A. Iron-Catalyzed Suzuki–Miyaura Cross-Coupling Reactions between Alkyl Halides and Unactivated Arylboronic Esters. *Org. Lett.* **2018**, *20* (17), 5233–5237. <https://doi.org/10.1021/acs.orglett.8b02184>.
- (25) Hatakeyama, T.; Hashimoto, T.; Kondo, Y.; Fujiwara, Y.; Seike, H.; Takaya, H.; Tamada, Y.; Ono, T.; Nakamura, M. Iron-Catalyzed Suzuki–Miyaura Coupling of Alkyl

Halides. *J. Am. Chem. Soc.* **2010**, *132* (31), 10674–10676. <https://doi.org/10.1021/ja103973a>.

(26) Bedford, R. B.; Brenner, P. B.; Carter, E.; Carvell, T. W.; Cogswell, P. M.; Gallagher, T.; Harvey, J. N.; Murphy, D. M.; Neeve, E. C.; Nunn, J.; et al. Expedient Iron-Catalyzed Coupling of Alkyl, Benzyl and Allyl Halides with Arylboronic Esters. *Chem. - A Eur. J.* **2014**, *20* (26), 7935–7938. <https://doi.org/10.1002/chem.201402174>.

(27) O'Brien, H. M.; Manzotti, M.; Abrams, R. D.; Elorriaga, D.; Sparkes, H. A.; Davis, S. A.; Bedford, R. B. Iron-Catalysed Substrate-Directed Suzuki Biaryl Cross-Coupling. *Nat. Catal.* **2018**, *1* (6), 429–437. <https://doi.org/10.1038/s41929-018-0081-x>.

(28) Hedström, A.; Izakian, Z.; Vreto, I.; Wallentin, C. J.; Norrby, P. O. On the Radical Nature of Iron-Catalyzed Cross-Coupling Reactions. *Chem. - A Eur. J.* **2015**, *21* (15), 5946–5953. <https://doi.org/10.1002/chem.201406096>.

(29) Daifuku, S. L.; Al-Afyouni, M. H.; Snyder, B. E. R.; Kneebone, J. L.; Neidig, M. L. A Combined Mössbauer, Magnetic Circular Dichroism, and Density Functional Theory Approach for Iron Cross-Coupling Catalysis: Electronic Structure, in Situ Formation, and Reactivity of Iron-Mesityl-Bisphosphines. *J. Am. Chem. Soc.* **2014**, *136* (25), 9132–9143. <https://doi.org/10.1021/ja503596m>.

(30) Daifuku, S. L.; Kneebone, J. L.; Snyder, B. E. R.; Neidig, M. L. Iron(II) Active Species in Iron-Bisphosphine Catalyzed Kumada and Suzuki-Miyaura Cross-Couplings of Phenyl Nucleophiles and Secondary Alkyl Halides. *J. Am. Chem. Soc.* **2015**, *137* (35), 11432–11444. <https://doi.org/10.1021/jacs.5b06648>.

(31) Tyrol, C. C.; Yone, N. S.; Gallin, C. F.; Byers, J. A. Iron-Catalysed Enantioconvergent Suzuki–Miyaura Cross-Coupling to Afford Enantioenriched 1,1-Diarylalkanes. *Chem. Commun.* **2020**, *56* (93), 14661–14664. <https://doi.org/10.1039/D0CC05003B>.

(32) Crockett, M. P.; Wong, A. S.; Li, B.; Byers, J. A. Rational Design of an Iron-Based Catalyst for Suzuki–Miyaura Cross-Couplings Involving Heteroaromatic Boronic Esters and Tertiary Alkyl Electrophiles. *Angew. Chemie Int. Ed.* **2020**, *59* (13), 5392–5397.

<https://doi.org/10.1002/anie.201914315>.

(33) De Buysser, K.; Herman, G. G.; Bruneel, E.; Hoste, S.; Van Driessche, I. Determination of the Number of Unpaired Electrons in Metal-Complexes. A Comparison between the Evans' Method and Susceptometer Results. *Chem. Phys.* **2005**, *315* (3), 286–292. <https://doi.org/10.1016/j.chemphys.2005.04.022>.

(34) Connelly, N. G.; Geiger, W. E. Chemical Redox Agents for Organometallic Chemistry. *Chem. Rev.* **1996**, *96* (2), 877–910. <https://doi.org/10.1021/cr940053x>.

(35) Dai, D.; Xiang, H.; Whangbo, M.-H. Effects of Spin-Orbit Coupling on Magnetic Properties of Discrete and Extended Magnetic Systems. *J. Comput. Chem.* **2008**, *29* (13), 2187–2209. <https://doi.org/10.1002/jcc.21011>.

(36) Eckert, N. A.; Smith, J. M.; Lachicotte, R. J.; Holland, P. L. Low-Coordinate Iron(II) Amido Complexes of β -Diketiminates: Synthesis, Structure, and Reactivity. *Inorg. Chem.* **2004**, *43* (10), 3306–3321. <https://doi.org/10.1021/ic035483x>.

(37) Takacs, J. M.; Anderson, L. G.; Bindu Madhavan, G. V.; Creswell, M. W.; Seely, F. L.; Devroy, W. F. Transition-Metal-Catalyzed Carbon-Carbon Bond Forming Reactions: Regio- and Chemoselective Iron(0)-Catalyzed Diene to Olefin Cross-Coupling Reactions. *Organometallics* **1986**, *5* (11), 2395–2398. <https://doi.org/10.1021/om00142a044>.

(38) Williamson, K. S.; Yoon, T. P. Iron-Catalyzed Aminohydroxylation of Olefins. *J. Am. Chem. Soc.* **2010**, *132* (13), 4570–4571. <https://doi.org/10.1021/ja1013536>.

(39) Sudo, A.; Hirayama, S.; Endo, T. Highly Efficient Catalysts-Acetylacetonato Complexes of Transition Metals in the 4th Period for Ring-Opening Polymerization of 1,3-Benzoxazine. *J. Polym. Sci. Part A Polym. Chem.* **2010**, *48* (2), 479–484. <https://doi.org/10.1002/pola.23810>.

(40) McGeachin, S. G. Synthesis and Properties of Some β -Diketiminates Derived from Acetylacetonate, and Their Metal Complexes. *Can. J. Chem.* **1968**, *46* (11), 1903–1912. <https://doi.org/10.1139/v68-315>.

- (41) Cowley, R. E.; Deyonker, N. J.; Eckert, N. A.; Cundari, T. R.; Debeer, S.; Bill, E.; Ottenwaelder, X.; Flaschenriem, C.; Holland, P. L. Three-Coordinate Terminal Imidoiron(III) Complexes: Structure, Spectroscopy, and Mechanism of Formation. *Inorg. Chem.* **2010**, *49* (13), 6172–6187. <https://doi.org/10.1021/ic100846b>.
- (42) Cowley, R. E.; Eckert, N. A.; Vaddadi, S.; Figg, T. M.; Cundari, T. R.; Holland, P. L. Selectivity and Mechanism of Hydrogen Atom Transfer by an Isolable Imidoiron(III) Complex. *J. Am. Chem. Soc.* **2011**, *133* (25), 9796–9811. <https://doi.org/10.1021/ja2005303>.
- (43) Cowley, R. E.; Holland, P. L. Ligand Effects on Hydrogen Atom Transfer from Hydrocarbons to Three-Coordinate Iron Imides. *Inorg. Chem.* **2012**, *51* (15), 8352–8361. <https://doi.org/10.1021/ic300870y>.
- (44) See, R. F.; Kruse, R. A.; Strub, W. M. Metal-Ligand Bond Distances in First-Row Transition Metal Coordination Compounds: Coordination Number, Oxidation State, and Specific Ligand Effects. *Inorg. Chem.* **1998**, *37*, 5369–5375. <https://doi.org/10.1021/ic971462p>.
- (45) Hu, M. L.; Miao, Q.; Fang, L. P.; Jin, Z. M. Crystal Structure of Tris(Acetylacetonato)Iron(III), C₁₅H₂₁O₆Fe, at 20 K. *Zeitschrift fur Krist. - New Cryst. Struct.* **2001**, *216* (1–4), 631–632. <https://doi.org/10.1524/ncrs.2001.216.14.631>.
- (46) Wertheim, G. K.; Kingston, W. R.; Herber, R. H. Mössbauer Effect in Iron (III) Acetylacetonate and Chemical Consequences of K Capture in Cobalt (III) Acetylacetonate. *J. Chem. Phys.* **1962**, *37* (4), 687–690. <https://doi.org/10.1063/1.1733147>.
- (47) Korendovych, I. V.; Staples, R. J.; Reiff, W. M.; Rybak-Akimova, E. V. A New High-Spin Iron(III) Complex with a Pentadentate Macrocyclic Amidopyridine Ligand: A Change from Slow Single-Ion Paramagnetic Relaxation to Long-Range Antiferromagnetic Order in a Hydrogen-Bonded Network. *Inorg. Chem.* **2004**, *43* (13), 3930–3941. <https://doi.org/10.1021/ic0351601>.
- (48) Epstein, L. M. Mössbauer Spectra of Some Iron Complexes. *J. Chem. Phys.* **1962**, *36* (10), 2731–2737. <https://doi.org/10.1063/1.1732360>.

- (49) Kovács, K.; Kamnev, A. A.; Shchelochkov, A. G.; Kuzmann, E.; Medzihradzky-Schweiger, H.; Mink, J.; Vértes, A. Mössbauer Spectroscopic Evidence for Iron(III) Complexation and Reduction in Acidic Aqueous Solutions of Indole-3-Butyric Acid. *J. Radioanal. Nucl. Chem.* **2004**, *262* (1), 151–156. <https://doi.org/10.1023/B:JRNC.0000040867.54095.7a>.
- (50) Gütlich, P.; Bill, E.; Trautwein, A. X. *Mössbauer Spectroscopy and Transition Metal Chemistry*; Springer Berlin Heidelberg: Berlin, Heidelberg, 2011. <https://doi.org/10.1007/978-3-540-88428-6>.
- (51) Cotton, S. A. Iron(III) Chloride and Its Coordination Chemistry. *J. Coord. Chem.* **2018**, *71* (21), 3415–3443. <https://doi.org/10.1080/00958972.2018.1519188>.
- (52) Bergstrom, F. W.; Fernelius, W. C. The Chemistry of the Alkali Amides. *Chem. Rev.* **1933**, *12* (1), 43–179. <https://doi.org/10.1021/cr60041a002>.
- (53) *Impurities: Guideline for Residual Solvents Q3C(R8)*; Step 4; International Council for Harmonisation of Technical Requirements for Pharmaceuticals for Human Use, 2021.
- (54) Lithium amides are pyrophoric when exposed to air.
- (55) Burger, B. J.; Bercaw, J. E. Vacuum Line Techniques for Handling Air-Sensitive Organometallic Compounds. In *Experimental Organometallic Chemistry*; American Chemical Society, 1987; pp 79–115. <https://doi.org/10.1021/bk-1987-0357.ch004>.
- (56) Pangborn, A. B.; Giardello, M. A.; Grubbs, R. H.; Rosen, R. K.; Timmers, F. J. Safe and Convenient Procedure for Solvent Purification. *Organometallics* **1996**, *15* (5), 1518–1520. <https://doi.org/10.1021/om9503712>.
- (57) Evans, D. F. The Determination of the Paramagnetic Susceptibility of Substances in Solution by Nuclear Magnetic Resonance. *J. Chem. Soc.* **1959**, 2003–2005. <https://doi.org/10.1039/jr9590002003>.
- (58) Ackermann, L.; Kapdi, A. R.; Schulzke, C. Air-Stable Secondary Phosphine Oxide or Chloride (Pre)Ligands for Cross-Couplings of Unactivated Alkyl Chlorides. *Org. Lett.* **2010**, *12* (10), 2298–2301. <https://doi.org/10.1021/ol100658y>.

Chapter 4.

Progress Towards Suzuki-Miyaura Cross-Coupling Reactions of Alkyl Sulfonate Esters and Unactivated Aryl Boronic Esters Catalyzed by Iron-Based Complexes

4.1 Introduction

While the development of iron-catalyzed cross-coupling methodologies has historically lagged behind its palladium-catalyzed analogues, we have recently developed efficient methods for the iron-catalyzed Suzuki-Miyaura cross-coupling reaction of C(sp³)-halide electrophiles^{1,2} inaccessible by palladium catalysis (see Chapters 2-3). Despite these developments, the analogous palladium-catalyzed reactions remain far more advanced in terms of general applicability and practical utility. One useful class of substrates uniquely accessible to palladium-catalyzed cross-coupling reactions are sulfonate ester electrophiles, which themselves compose a subclass of compounds known as pseudohalides—polyatomic analogues of halides which are commonly used as reagents in organic synthesis because they exhibit similar reactivity to halides.³ Sulfonate esters are usually derived from alcohols through facile reaction with a corresponding sulfonyl chloride and a base (Figure 4.1).⁴⁻⁶ As a result, the large libraries of alcohols available to the pharmaceutical industry⁷ can be easily converted into a diverse collection of reactive electrophiles for incorporation into targeted synthetic intermediates via cross-coupling reactions. Moreover, using sulfonate esters avoids toxicity concerns associated with halogenated compounds,^{8,9} and the aliphatic alcohol precursors are resistant to decomposition via elimination reactions, which can preclude long-term storage of some alkyl halides.

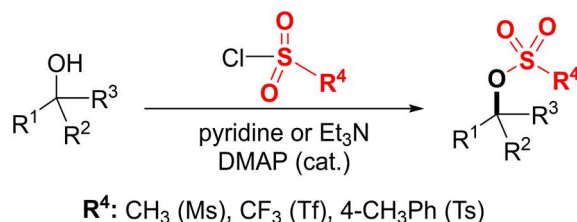
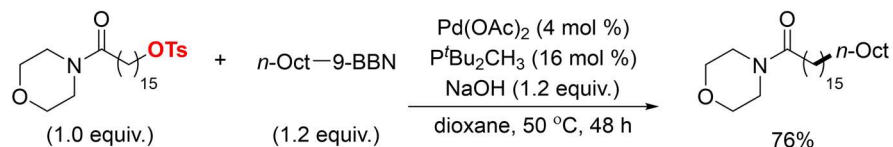


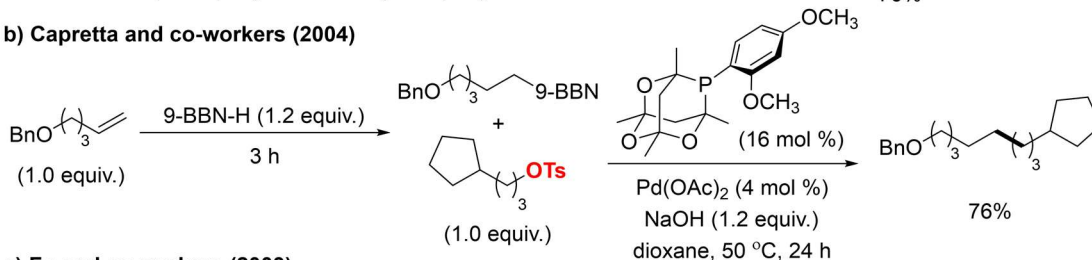
Figure 4.1. Representative synthesis of sulfonate esters from alcohols.

Successful cross-coupling reactions of alkyl sulfonate esters are much less commonly reported in the literature. Examples of palladium-catalyzed cross-coupling reactions of alkyl tosylates are limited to primary electrophiles, and they also require the use of (9-BBN)-boranes (Scheme 4.2a-4.2b),^{22,23} or feature nucleophiles containing other metals (Scheme 4.2c).²⁴ More general examples of cross-coupling reactions of alkyl tosylates have been observed when using first-row transition metal-based catalysts such as iron (Figure 4.2d)^{25,26} and nickel (Figure 4.2e),^{27,28} but these examples are limited to Kumada-type (i.e. requiring Grignard transmetalating reagents) or Negishi-type (i.e. requiring arylzinc transmetalating reagents) reactions of alkyl nucleophiles.

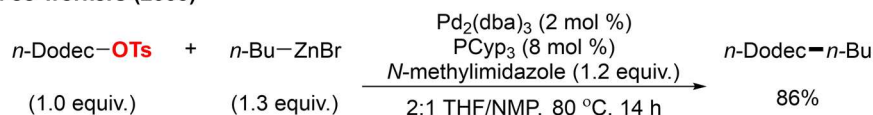
a) Fu and co-workers (2002)



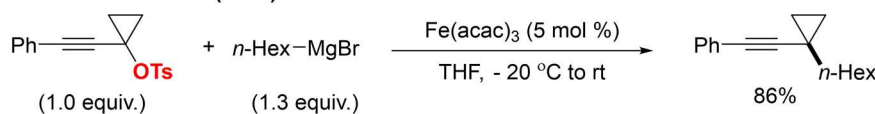
b) Capretta and co-workers (2004)



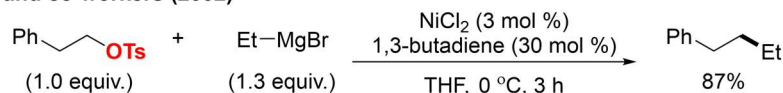
c) Fu and co-workers (2003)



d) Fürstner and co-workers (2016)



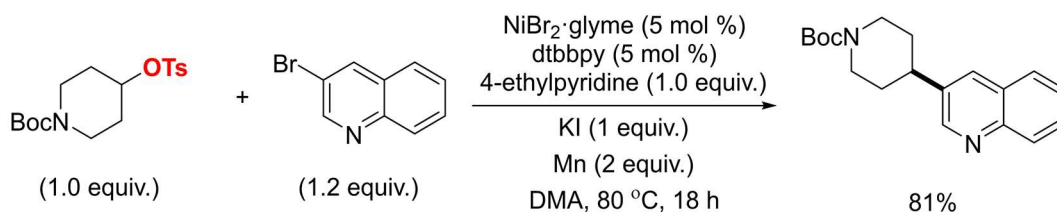
e) Kambe and co-workers (2002)



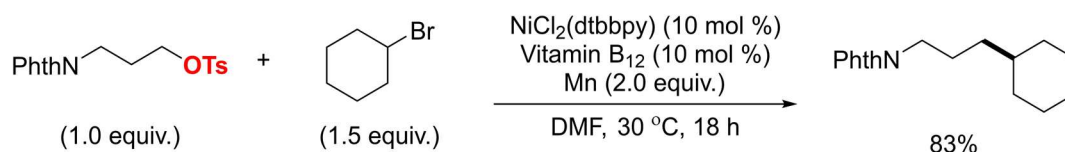
Scheme 4.2. a-c) Examples of palladium-catalyzed cross-coupling reactions of alkyl tosylates, d-e) examples of first-row transition metal-catalyzed cross-coupling reactions of alkyl tosylates.

A recently burgeoning research direction that has proven to be an amenable method for the incorporation of alkyl sulfonate esters is that of reductive cross-electrophile cross-coupling reactions. In contrast to traditional cross-coupling reactions between a preformed organometallic nucleophile and an electrophilic partner, two electrophiles are joined in the presence of a transition metal catalyst and excess reductant, which is needed to regenerate the catalyst. Nickel-catalyzed systems have proven particularly effective for these transformations (Scheme 4.3).²⁹⁻³¹ Molander and co-workers developed a method for the nickel-catalyzed reductive cross-electrophile coupling of heterocycloalkyl tosylates with heteroaryl bromides, improving the functional group tolerance of previously reported methods (Scheme 4.3a).²⁹ In 2019, Komeyama and co-workers demonstrated that a nickel catalyst in combination with cobalt-centered Vitamin B₁₂ could catalyze the reductive cross-electrophile coupling of alkyl tosylates with alkyl halides (Scheme 4.3b).³⁰ Most recently, Jarvo and co-workers demonstrated the intramolecular reductive cross-electrophile coupling of 1,3-dimesylates to form cyclopropanes (Scheme 4.3c).³¹ However, mechanistic studies implicate the formation of the corresponding halides as reaction intermediates, which in turn react with the nickel catalyst to provide the alkyl radicals responsible for carbon-carbon bond formation. Despite these advances, all of these examples of cross-electrophile cross-coupling require the addition of superstoichiometric metal reductants and substrates with significantly divergent rates of oxidative addition in order to avoid dimerization.^{32,33}

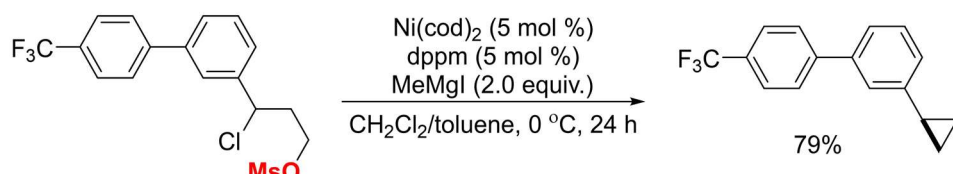
a) Molander and co-workers (2015)



b) Komeyama and co-workers (2019)



c) Jarvo and co-workers (2020)



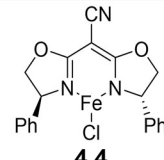
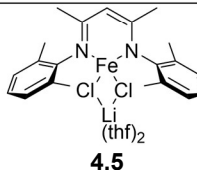
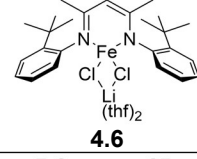
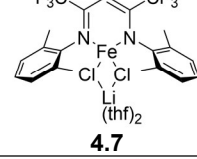
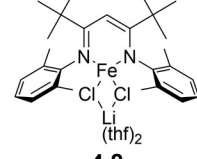
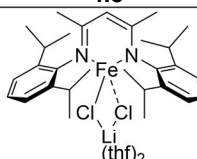
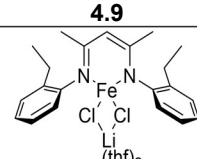
Scheme 4.3. Examples of nickel-catalyzed reductive cross-electrophile cross-coupling reactions involving alkyl sulfonate esters.

In this chapter, we report our progress towards developing a Suzuki-Miyaura cross-coupling reaction between alkyl tosylates and aryl boronic esters catalyzed by an iron-based complex. Such a reaction would take advantage of using the comparatively more stable and inexpensive alkyl tosylates in place of the historically more commonly employed alkyl triflates, leverage the use of the easier-to-handle aryl boronic esters in place of aryl boranes, and avoid the toxicity and scarcity concerns associated with noble metal catalysts such as palladium. In the process of these investigations, mechanistic studies suggest a distinct operative mechanism which can potentially be harnessed to access otherwise incompatible substrates with a single catalyst system.

4.2 Initial discovery and catalyst optimization

During the course of evaluating the substrate scope of the initial Suzuki-Miyaura cross-coupling reaction catalyzed by an iron-based complex supported by a cyanophenylbis(oxazoline) ligand, it was observed that cycloheptyl tosylate (**4.1**) was active for catalytic cross-coupling with phenyl boronic acid pinacol ester (**4.2**, PhB(pin)) to produce the phenylcycloheptane product (**4.3**) in 12% yield (Table 4.1, entry 1). Due to the success and generality of β -diketiminate ligated iron complexes for cross-coupling reactions discussed in Chapter 2, a selection of β -diketiminate iron complexes was evaluated for the cross-coupling reaction of **4.1** and **4.2** at ambient and elevated temperature (50 °C). In all cases, elevated temperatures produced higher yields of **4.3** (Table 4.1, entries 3, 5, 7, 9, 13) than if the reaction were carried out at ambient temperature with the same catalyst (*cf.* Table 4.1, entries 2, 4, 6, 8, 12). Temperatures higher than 50 °C led to similar yields of cross-coupled product. Of the iron complexes tested, complex **4.6** containing 2-*tert*-butylphenylimines on the β -diketiminate ligand generated the cross-coupled product in the highest yield at 50 °C (Table 4.1, entry 5). Using iron complex **4.9** containing 2-isopropylphenylimines on the β -diketiminate ligand, which has previously demonstrated catalytic activity for cycloheptyl bromide when using potassium ethoxide in place of lithium amide at 80 °C,³⁴ did not produce appreciable cross-coupled product at either temperature tested (Table 4.1, entries 10-11). Control reactions in which the iron precatalyst and the amide base were not included produced no cross-coupled product (Table 4.1, entries 14-15). The mass balance of all reactions as analyzed by ¹H NMR was cycloheptyl tosylate. Cycloheptene resulting from elimination of the leaving group, which had been previously observed in reactions of cycloheptyl halides, was not observed.

Table 4.1. Screening of iron-based catalysts for the cross-coupling of cycloheptyl tosylate and phenyl boronic acid pinacol ester.

entry	4.1 (1.0 equiv.) Fe catalyst	4.2 (2.0 equiv.) temperature (°C)	4.3 yield (%)
1 ^a		50 °C	12%
2		25 °C	6%
3		50 °C	19%
4		25 °C	15%
5		50 °C	26%
6		25 °C	20%
7		50 °C	21%
8		25 °C	14%
9		50 °C	19%
10 ^b		25 °C	0%
11 ^b		80 °C	<1%
12		25 °C	4%
13		50 °C	19%
14	No Fe catalyst	25 °C	0%
15 ^c	4.6	25 °C	0%

^a reaction run for 48 h. ^b KOEt (1.2 equiv.) used in place of LiNMeEt. ^c no LiNMeEt used in reaction.

4.3 Inconsistencies in the working mechanistic hypothesis when explaining the reactivity of alkyl sulfonate ester electrophiles

Our previous experience with the Suzuki-Miyaura cross-coupling reaction catalyzed by β -diketiminato iron complexes led to the development of a working mechanistic hypothesis in which an iron amide intermediate is implicated in multiple roles³⁵ (Figure 4.2). In our proposed mechanistic hypothesis, iron precatalyst **I** is activated by salt metathesis with the lithium amide. The resulting iron amide species **II** is bifunctional; it activates the electrophile by halogen abstraction to yield intermediate **III**, and it activates the nucleophile by transmetalation to yield intermediate **IV**. The carbon-centered radical formed by halogen abstraction recombines with **III**, followed by reductive elimination from **V** to deliver the cross-coupled product. Subsequent comproportionation of the resulting low-coordinate solvent-stabilized iron(I) species **VI** with iron(III) species **III** resulting from electrophile activation regenerates iron precatalyst **I** and iron amide **II**, closing the catalytic cycle.

However, key differences arise when the same mechanistic hypothesis is applied towards the reaction of alkyl sulfonate ester electrophiles (Figure 4.2, steps with dashed lines). Firstly, following one turnover of the active catalyst, the regenerated iron-based precatalyst is a putative iron tosylate species **I** which forms lithium tosylate instead of lithium halide following salt metathesis (Figure 4.2, red box). We believe that precipitation of lithium halide acts as a driving force for the precatalyst to enter into the catalytic cycle as iron amide **II**, and the differing solubility properties of the lithium tosylate analogue could alter the equilibrium of the salt metathesis reaction, inhibiting the formation of the amide intermediate. Moreover, an inhibitory effect on product yield could result from the

byproduct remaining in solution. Secondly, our mechanistic hypothesis also implicates **II** in the halide abstraction step, a single-electron process (Figure 4.2, blue box). However, sulfonate ester electrophiles such as alkyl tosylates typically react by two-electron mechanisms, such as those observed in nucleophilic substitution reactions.^{6,36,37} Therefore, it is likely that tosylate electrophiles require a different mechanism of activation from the one originally proposed for the Suzuki-Miyaura cross-coupling reaction of alkyl halides catalyzed by β -diketiminato iron complexes. These two issues informed the course of our investigations in seeking to optimize the yields and generality of this reaction.

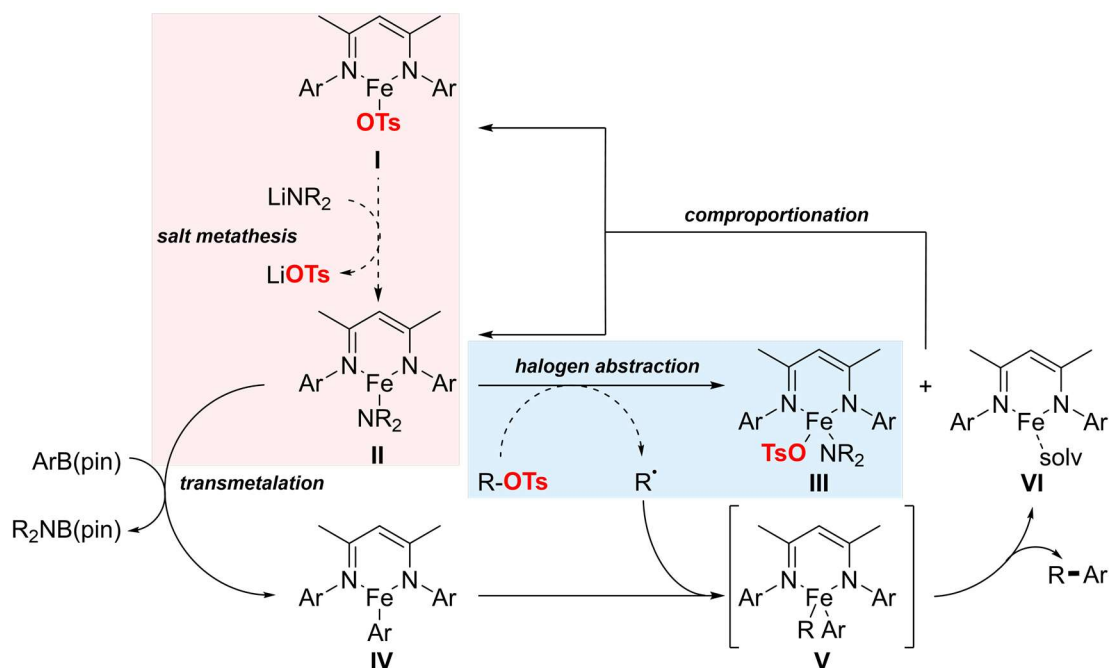


Figure 4.2. Working mechanistic hypothesis for the Suzuki-Miyaura cross-coupling reaction of alkyl halides and unactivated boronic esters catalyzed by β -diketiminato iron(II) complexes applied to alkyl tosylate electrophiles. Changes resulting from replacement of the electrophile with an alkyl tosylate are highlighted.

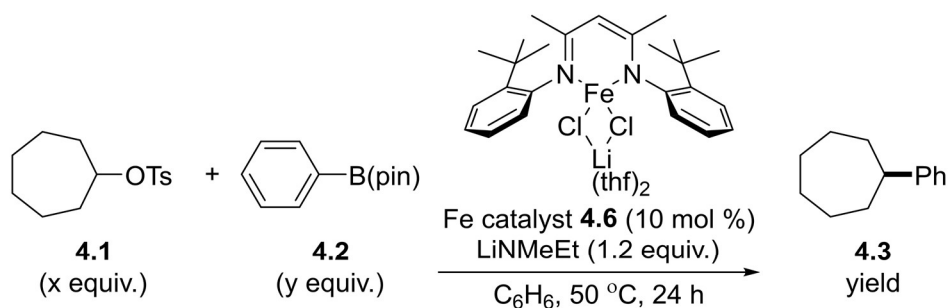
4.4 Optimization of reaction conditions

4.4.1 Screening of substrate equivalents

We then turned our attention to optimizing the ratio of substrates. In the original reaction conditions, an excess of boronic ester was used in order to promote

transmetalation.^{1,2} We had originally hypothesized that the rate of transmetalation needed to be competitive with the rapid rate of halogen abstraction to form a carbon-centered radical for the catalytic cross-coupling to take place (see Chapter 2). The rate of carbon-centered radical formation is dependent on the strength of the bond between carbon and the leaving group;^{38,39} in these reactions, the breaking bond is a C—O sulfonate bond instead of a carbon-halogen bond. Consequently, the new leaving group introduced by using alkyl tosylates may not require an excess of boronic ester in order for the rate of transmetalation to be competitive with that of radical formation. Instead, transmetalation may need to be slowed down (or radical formation accelerated) in order for the rates to be competitive.

Table 4.2. Screening of substrate equivalents for the cross-coupling of cycloheptyl tosylate and phenyl boronic acid pinacol ester catalyzed by an iron-based complex.



entry	equivalents 4.1 (x)	equivalents 4.2 (y)	yield (%)
1	1.0	1.0	14%
2	2.0	1.0	42%
3	3.0	1.0	26%

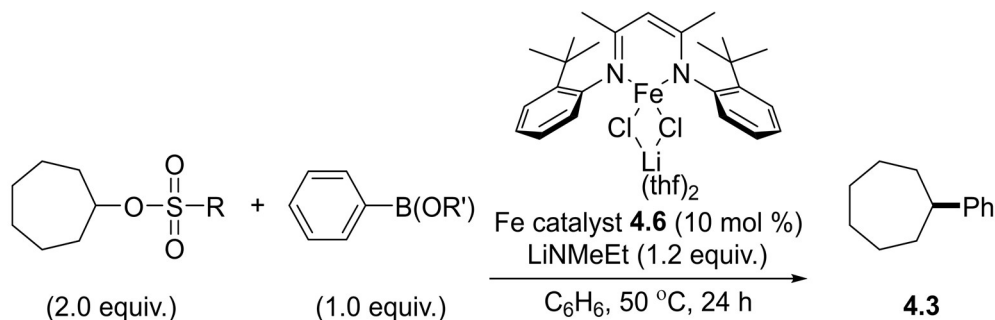
The catalytic cross-coupling reaction was screened for different ratios of **4.1** to **4.2** (Table 4.2). Using catalyst precursor **4.6**, a 1:1 ratio of tosylate to boronic ester produced the cross-coupled product in reduced yields (Table 4.2, entry 1) compared to when a 1:2 ratio of tosylate to boronic ester was used (*cf.* Table 4.1, entry 5). However, when the ratio

of tosylate to boronic ester was reversed such that the **4.1** was in excess (2 equivalents to 1 equivalent of **4.2**), the yield of the reaction increased to 42% (Table 4.2, entry 2). Further increasing the ratio of tosylate to boronic ester was detrimental to reaction yield (Table 4.2, entry 3). The improved yields in the presence of excess tosylate suggests that when using alkyl sulfonate ester electrophiles, the rate of the difficult electrophile activation needs to be promoted in order for successful cross-coupling to occur.

4.4.2 Screening of sulfonate ester identity and boronic ester identity

We next evaluated the effect of the identities of the sulfonate esters and boronic esters used in the cross-coupling reaction (Table 4.3). Employing an aryl sulfonate ester with an electron-donating methoxy substituent at the *para* position resulted in reduced yields in the cross-coupling reaction with PhB(pin) (Table 4.3, entry 2, *cf.* entry 1). On the other hand, an electron-deficient nitro substituent at the *para* position of the sulfonate ester (i.e. nosylate) shut down formation of the cross-coupled product completely (Table 4.3, entry 3). Lastly, a bromo substituent at the *para* position of the sulfonate ester (i.e. brosylate) also resulted in reduced yield (Table 4.3, entry 4). No cross-coupled product was observed when cycloheptyl mesylate was used as the alkyl electrophile (Table 4.3, entry 5). Using a different phenyl boronic ester in the neopentyl glycol ester resulted in lower yields overall when compared to the same reaction with PhB(pin) (Table 4.3, entry 6), but the boronic acid neopentyl ester performed better when the equivalencies of the substrates was reversed (*cf.* Table 4.3, entry 7). Lithium butylmethyl amide provided a further boost in yield of cross-coupled product when the boronic acid neopentyl ester was used (Table 4.3, entry 8). From this evaluation, we decided to move forward with using the tosylates for further optimization of the cross-coupling reaction.

Table 4.3. Screening of sulfonate esters and boronic esters for the cross-coupling of cycloheptyl sulfonate ester and phenyl boronic ester catalyzed by an iron-based complex.



entry	R (sulfonate ester)	B(OR') (boronic ester)	yield (%)
1	4-CH ₃ Ph	B(pin)	42%
2	4-OMePh	B(pin)	19%
3	4-NO ₂ Ph	B(pin)	0%
4	4-BrPh	B(pin)	14%
5	CH ₃	B(pin)	0%
6	4-CH ₃ Ph	B(neo)	5%
7 ^a	4-CH ₃ Ph	B(neo)	16%
8 ^b	4-CH ₃ Ph	B(neo)	19%

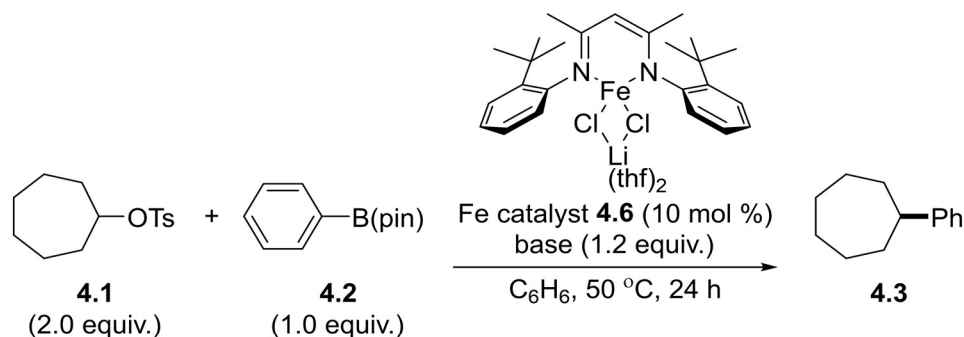
^a 1.0 equiv. cycloheptyl tosylate to 2.0 equiv. PhB(neo), ^b LiNMeBu (1.2 equiv.) used.

4.4.3 Screening of lithium amide bases

We hypothesized that altering the relative solubility of the base in relation to the lithium tosylate byproduct from catalyst activation would shift the equilibrium of the salt metathesis toward the formation of the iron amide. To this end, a screen of lithium amide bases with different *N*-alkyl substituents was conducted (Table 4.4). Lithium amide bases containing longer alkyl chains possess higher solubility in benzene and produced **4.3** in the highest yields (Table 4.4, entries 4-5); however, the yields remained moderate. Critically, it was determined that lithium amide that had been passed through a 250-micron sieve into a uniformly fine powder was necessary for optimal and reproducible yields. This had been previously observed for LiNMeEt in cross-coupling reactions of alkyl halides.¹ When the

LiNMe(ⁿBu) base was introduced without sieving, yields of the cross-coupled product were significantly reduced.

Table 4.4. Screening of lithium amides for the cross-coupling of cycloheptyl tosylate and phenyl boronic acid pinacol ester catalyzed by an iron-based complex.



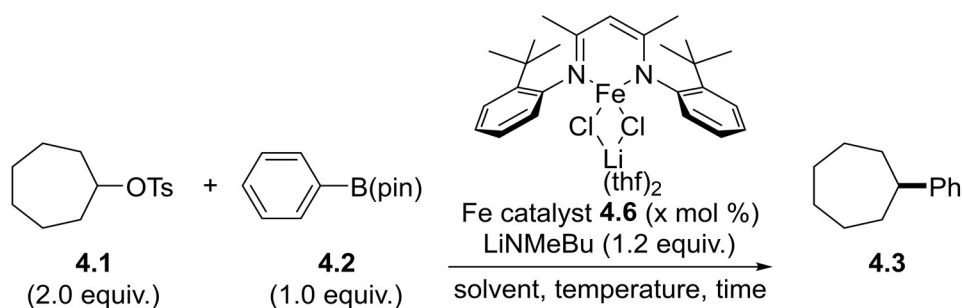
entry	lithium amide	yield (%)
1	LiNMe ₂	32%
2	LiNMeEt	42%
3	LiNEt ₂	27%
4	LiNMe(ⁿ Bu)	47%
5	LiNMe(ⁿ Oct)	47%
6 ^a	LiN(ⁱ Pr) ₂	2%

4.4.4 Screening of reaction conditions

A variety of reaction conditions including solvent, temperature, time, and catalyst loading were assessed next (Table 4.5). The reaction did not proceed in toluene or 2-methyltetrahydrofuran (Table 4.5, entries 2-3), but produced comparable yields in anisole (Table 4.5, entry 4). It was determined that the reaction requires heat to reach optimal yields, but yields plateau and slightly decreased above 50 °C (Table 4.5, entries 5-7). The reaction demonstrated a modest increase in yield when the reaction time was doubled, but we did not feel that this improvement was substantial enough to justify the significantly longer reaction time in future optimization studies (Table 4.5, entry 8). A lower amount of catalyst loading produced comparable yields during the longer reaction time, but the

majority of the cross-coupled product is observed within the first six hours (Table 4.5, entries 9-10). Increased catalyst loading, however, was detrimental for the reaction over the course of 24 hours (Table 4.5, entry 11). It is possible that increased catalyst loading leads to a higher buildup of lithium tosylate, which we believe has an inhibitory effect on the cross-coupling reaction (*vide supra*).

Table 4.5. Screening of reaction conditions including solvent, temperature, time, and catalyst loading for the cross-coupling of cycloheptyl tosylate and phenyl boronic acid pinacol ester catalyzed by an iron-based complex.



entry	cat. loading (x)	solvent	temperature (°C)	time (h)	yield (%)
1	10	benzene	50	24	47%
2	10	toluene	50	24	15%
3	10	2-MeTHF	50	24	0%
4	10	anisole	50	24	43%
5	10	benzene	25	24	17%
6	10	benzene	65	24	44%
7	10	benzene	80	24	40%
8	10	benzene	50	48	51%
9	5	benzene	50	48	41%
10	5	benzene	50	6	28%
11	20	benzene	50	24	34%

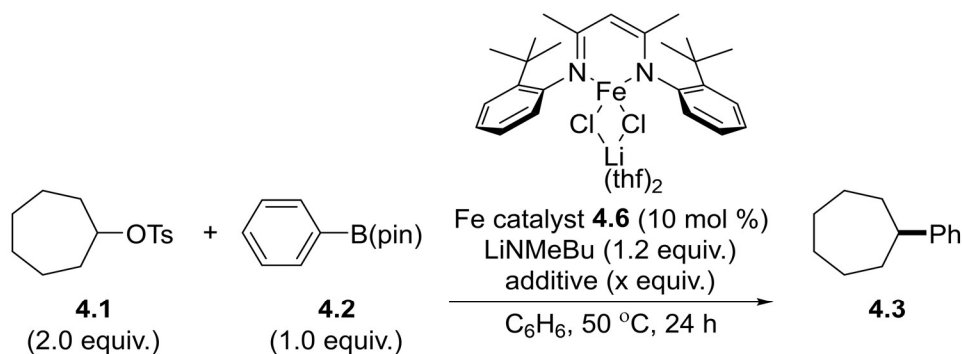
4.4.5 Screening of additive effects

We hypothesized that we could potentially improve the yields of cross-coupling reactions involving alkyl tosylates by addressing some of the mechanistic issues that may arise when the tosylate replaces the halide. One way to do this is by initiating *in situ* anion exchange with the addition of a halide source such as tetrabutylammonium halide, leading

to the formation of a cycloheptyl halide that would subsequently be active for cross-coupling. The addition of tetrabutylammonium chloride did not improve the yields of **4.3** in either stoichiometric or substoichiometric amounts (Table 4.6, entries 2-3, *cf.* entry 1). However, tetrabutylammonium bromide as an additive resulted in a modest increase in yield that was independent of the amount added (Table 4.6, entries 4-5). With both tetrabutylammonium halide salts, a significant byproduct of the reaction was the corresponding unreacted cycloheptyl halide (Table 4.6, entries 2 and 4). It is possible that *in situ* anion exchange occurs to deliver this product, but at a rate that is slower than a catalyst deactivation pathway.

Alternatively, we considered the impact of crown ether additives, hypothesizing that their ability to sequester alkali cations⁴⁰ could impact the equilibrium of salt metathesis by either solubilizing the lithium amide or decreasing the solubility of the lithium tosylate byproducts. Varying equivalencies of 18-crown-6 did not significantly improve yields, although 18-crown-6 is not the appropriately sized crown ether for the lithium cation^{41,42} (Table 4.6, entries 6-8). However, the addition of 1 equivalent of 12-crown-4, which demonstrates the ability to sequester lithium cations,^{41,42} also did not result in improved yields (Table 4.6, entry 9). In fact, lower yields were generally observed.

Table 4.6. Screening of the effect of additives for the cross-coupling of cycloheptyl tosylate and phenyl boronic acid pinacol ester catalyzed by an iron-based complex.



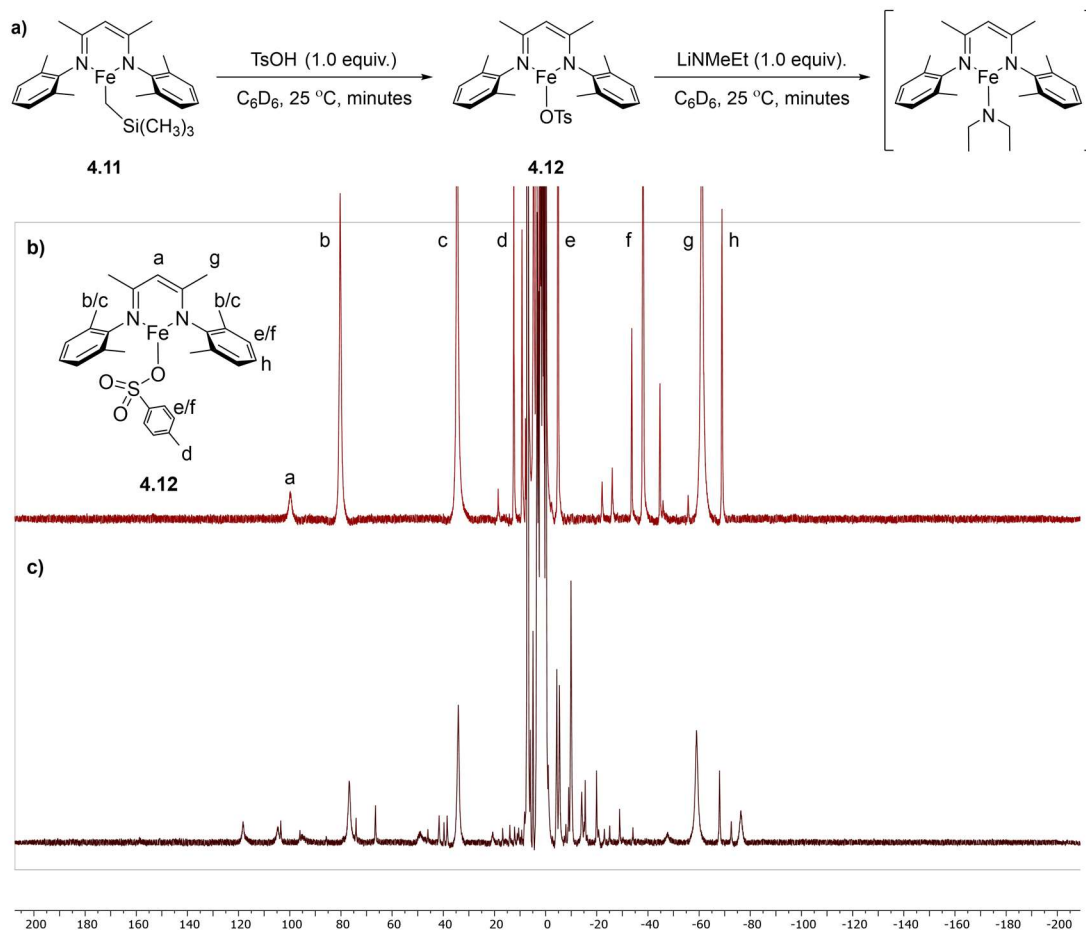
entry	additive	equivalents of additive (x)	yield (%)
1	none	n/a	42%
2 ^a	(<i>n</i> -Bu) ₄ NCl	1.0	23%
3	(<i>n</i> -Bu) ₄ NCl	0.5	44%
4 ^b	(<i>n</i> -Bu) ₄ NBr	1.0	51%
5	(<i>n</i> -Bu) ₄ NBr	0.5	52%
6	18-crown-6	1.5	31%
7	18-crown-6	1.0	49%
8	18-crown-6	0.5	30%
9	12-crown-4	1.0	38%

^a 56% of the cycloheptyl chloride was recovered. ^b 13% of the cycloheptyl bromide was recovered.

4.5 Examining the equilibrium of the salt metathesis step and the inhibitory effect of lithium tosylate

According to our mechanistic hypothesis (Figure 4.2), a putative iron tosylate species **I** forms following one turnover of the active iron catalyst. Earlier studies focused on perturbing the equilibrium of the salt metathesis between the iron tosylate **I** and the lithium amide base, which could be unfavorable for the formation of the catalytically active iron amide species **II**. To assess the capability of the iron tosylate species to act as a suitable precatalyst, we sought to synthesize **4.12** via protonolysis of iron alkyl compound **4.11** (Scheme 4.4a). ¹H NMR spectroscopy of the reaction mixture following the addition of lithium diethylamide to the iron tosylate species was inconclusive and suggested that the

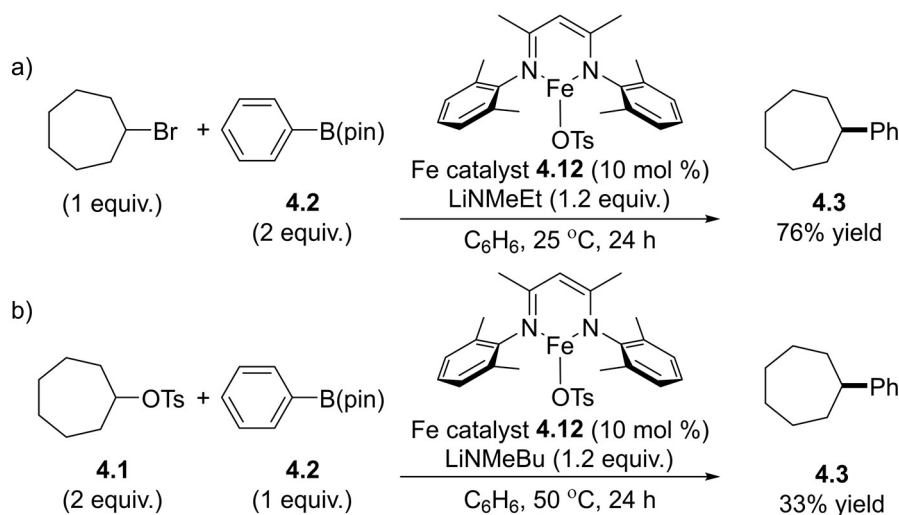
salt metathesis reaction from this compound to the iron amide species did not proceed cleanly (Scheme 4.4b-c).



Scheme 4.4. a) Synthesis of iron tosylate complex supported by β -diketiminato ligand. b) ^1H NMR spectrum in C_6D_6 of **4.12**, c) ^1H NMR spectrum in C_6D_6 of reaction between **4.12** and LiNMeEt

However, using **4.12** as the catalyst precursor in place of the iron halide analogue in the cross-coupling reaction of bromocycloheptane under standard conditions produced the desired product in slightly reduced yield (Scheme 4.5a, *cf.* ref. 2). The iron tosylate **4.12** was similarly effective for the cross-coupling reaction of cycloheptyl tosylate **4.1** under otherwise standard conditions, also producing the desired product in slightly reduced

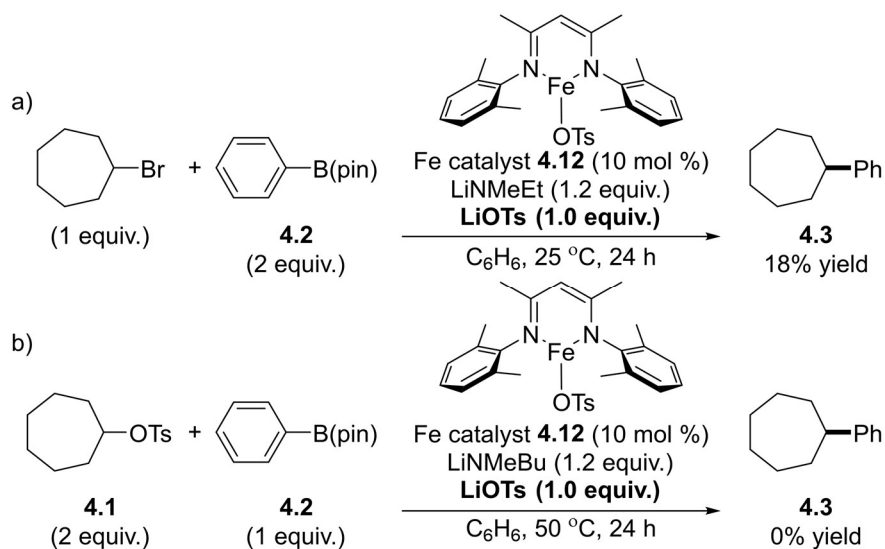
yield (Scheme 4.5b). These results suggest that the iron tosylate species **4.12** generated following one turnover of the catalyst remains catalytically competent, which suggests that the salt metathesis reaction is not prohibitively slow.



Scheme 4.5. a) Cross-coupling reaction of cycloheptyl bromide and phenyl boronic acid pinacol ester catalyzed by iron tosylate complex **4.12**, b) Cross-coupling reaction of cycloheptyl tosylate and phenyl boronic acid pinacol ester catalyzed by iron tosylate complex **4.12**.

While earlier efforts were directed at addressing the role of the lithium tosylate byproduct as a driving force in the equilibrium of the salt metathesis reaction, we had not considered its ability to otherwise serve as an inhibitor. To evaluate its possible inhibitory role, 1 equivalent of lithium tosylate (LiOTs) was added to the cross-coupling reaction of bromocycloheptane and **4.2** catalyzed by iron tosylate complex **4.12**. These conditions had a significantly detrimental impact on product yield, delivering the cross-coupled product **4.3** in only 18% yield (Scheme 4.6a), compared to 76% in its absence (*vide supra*, Scheme 4.5a). Lithium tosylate has a similar effect on the cross-coupling reaction of bromocycloheptane and **4.2** catalyzed by iron complex **4.6**, producing the desired product in 33% yield (compared to 95% without). Likewise, the addition of lithium tosylate to the

cross-coupling reaction of cycloheptyl tosylate **4.1** and **4.2** catalyzed by iron tosylate complex **4.12** completely shut down the reaction (Scheme 4.6b). These results suggest that the cross-coupling reaction is inhibited by lithium tosylate as it is formed in the catalytic cycle.

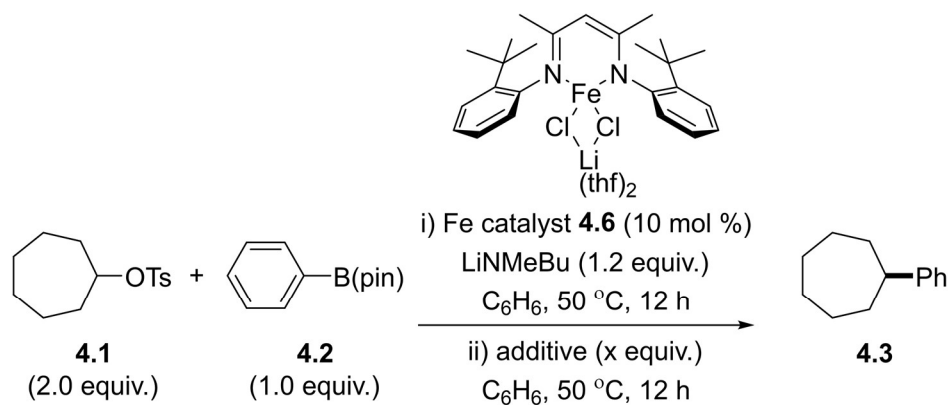


Scheme 4.6. a) Inhibition of the cross-coupling reaction of bromocycloheptane and phenyl boronic acid pinacol ester catalyzed by iron tosylate complex **4.12** with the addition of 1 equiv. lithium tosylate, b) Inhibition of the cross-coupling reaction of cycloheptyl tosylate and phenyl boronic acid pinacol ester catalyzed by iron tosylate complex **4.12** with the addition of 1 equiv. lithium tosylate.

Because our results suggested that the reaction was stalling as a result of inhibitory byproduct formation, we sought to establish conditions that would enable the reaction to re-enter the productive catalytic cycle. We examined the impact of adding equivalents of catalyst or base to “kickstart” the reaction partway through. While adding an extra equivalent of iron halide complex **4.6** after 24 hours of the reaction did not improve the yield (Table 4.7, entry 1), the addition of 1 equivalent of lithium butylmethyl amide resulted in a significant increase in product yield, leading to our current optimized results (Table 4.7, entries 2-3). Using 2 equivalents of lithium butylmethyl amide at the beginning

of the reaction resulted in 48% yield of the desired product, suggesting that the benefit of the excess base is limited to its introduction to the reaction mixture partway through catalysis.

Table 4.7. Screening of the effect of adding reagents halfway through the cross-coupling of cycloheptyl tosylate and phenyl boronic acid pinacol ester catalyzed by an iron-based complex.

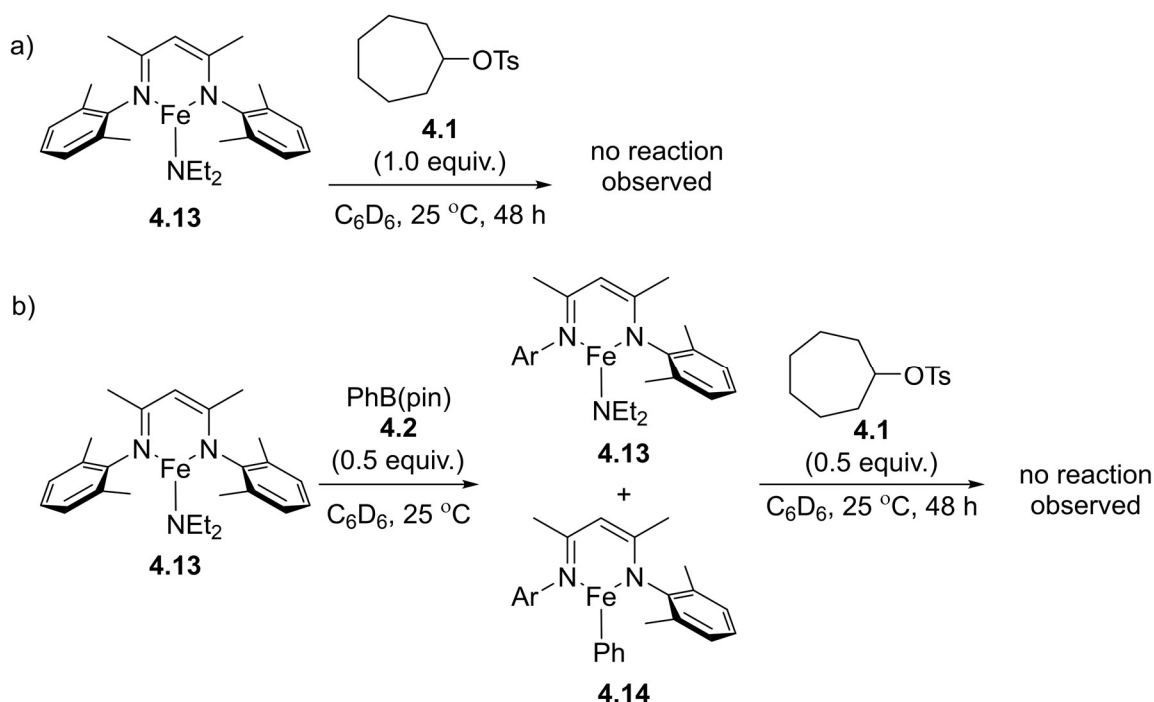


entry	additive	equivalents of additive (x)	yield (%)
1	4.6	0.1	35%
2	LiNMeBu	1.0	68%
3	LiNMeBu (2 nd trial)	1.0	56%

4.6 Examining the possibility of a catalytic cycle featuring two-electron processes

In addition to transmetalation, our mechanistic hypothesis also implicates the iron amide species **II** in the single-electron halide abstraction (Figure 4.2). To assess the capability of the iron amide species to activate cycloheptyl tosylate, iron amide **4.13** was synthesized and reacted with 1 equivalent of **4.1** in an NMR tube (Scheme 4.7a). After 48 hours, no change was observed in the ¹H NMR spectrum of the reaction mixture. An analogous stoichiometric reaction with bromocycloheptane had previously led to a complex mixture of products.³⁴ Similarly, reaction of iron amide **4.13** with 0.5 equivalent of **4.2** to generate a 1:1 mixture of **4.13** and iron phenyl **4.14** *in situ* did not produce the

cross-coupled product following addition of **4.1** (Scheme 4.7b). Previously, an analogous stoichiometric reaction with bromocycloheptane was fast and cleanly produced the desired cross-coupled product. These results suggest that a different mechanism is operative for electrophile activation when alkyl tosylates are used.



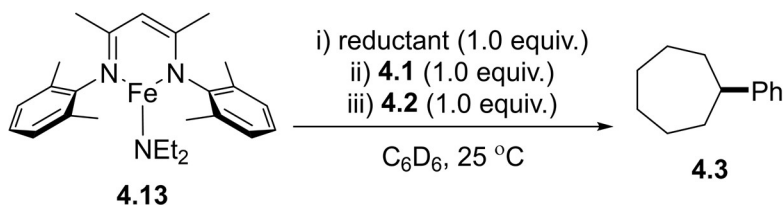
Scheme 4.7. a) Stoichiometric reaction to probe reactivity of cycloheptyl tosylate **4.1** with discretely synthesized iron amide intermediate **4.13**, b) Stoichiometric reaction to probe reactivity of cycloheptyl tosylate **4.1** with *in situ* generated iron intermediates **4.13** and **4.14**.

Alkyl sulfonate esters are known to be excellent substrates for two-electron nucleophilic substitution reactions,^{6,36,37} making it unlikely that activation occurs through the single-electron pathway we have proposed for the iron amide. Conversely, it is unlikely that iron(II)-based intermediates such as the iron amide can engage in two-electron oxidative addition reactions, because such a process would result in the intermediacy of uncommonly observed high-valent non-heme iron(IV) species.^{43–45} The successful formation of cross-coupled product in the catalytic reaction despite the incongruity in

reactivity between **4.1** and **4.13** led us to consider the possibility that a complex with lower valency than the iron(II) precursors investigated in the stoichiometric reactions could be responsible for activation of the electrophile. The significant excess of a reductant such as lithium amide⁴⁶ in relation to the catalyst (1.2 equiv. to 0.1 equiv.) could reduce a population of the iron-based intermediates to a lower oxidation state, which could then participate in a two-electron oxidative addition to activate the alkyl tosylate.

To explore this possibility, stoichiometric reactions of **4.13** were performed with external reductants in order to generate a putative iron(I) compound that could be assessed for reactivity with **4.1** (Table 4.8). While the addition of cobaltocene led to no changes in the ¹H NMR spectrum of **4.13** nor any observed subsequent reaction with **4.1** (Table 4.8, entry 1), addition of potassium graphite to a solution of **4.13** in C₆D₆ led to the formation of a complex mixture of products observed in the ¹H NMR spectrum (Table 4.8, entry 2). Subsequent addition of **4.1** followed by **4.2** resulted in the formation of **4.3** as detected by gas chromatography. Studies using other reductants remain ongoing.

Table 4.8. Stoichiometric reactions of *in situ* reduced iron amide species **4.13** to test for reactivity with cycloheptyl tosylate **4.1** and formation of **4.3**.



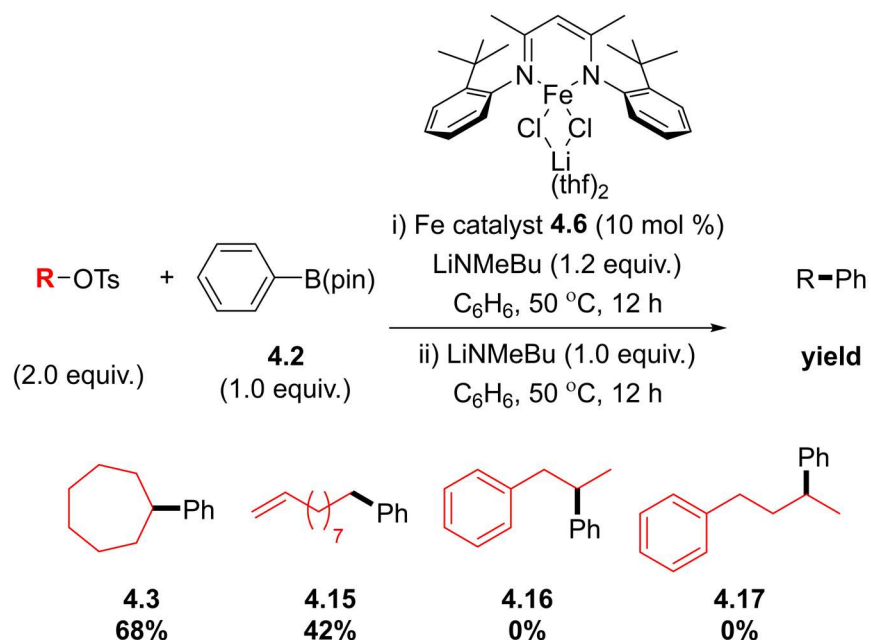
entry	reductant	E° (V, vs. Fc)	reaction after i) observed? ^a	4.3 observed after iii)? ^b
1	CoCp ₂	-1.33	no	no
2	KC ₈	-2.04	yes	yes

^a reaction mixture analyzed by paramagnetic ¹H NMR spectroscopy to assess evidence of reaction between **4.13** and **4.1**. ^b reaction mixture analyzed by gas chromatography to determine presence of **4.3**.

4.7 Evaluation of substrate scope

Other tosylate substrates were screened to evaluate the generality of the cross-coupling reaction (Table 4.9). Primary alkyl tosylate **4.15** could be incorporated. We had targeted a racemic benzylic alkyl tosylate for evaluation because observed inversion of stereochemistry would further support the hypothesis that the cross-coupling reaction proceeds through a two-electron mechanism akin to a bimolecular nucleophilic substitution. However, benzylic tosylates are highly unstable and difficult to synthesize.⁴⁷ The racemic homobenzylic alkyl tosylate **4.16** and racemic alkyl tosylate **4.17** delivered no observed cross-coupled product. At the time of submission of this dissertation, an examination of the substrate scope of aryl boronic esters tolerated by this method had not been conducted and is an opportunity for future study.

Table 4.9. Substrate scope of alkyl tosylates for the Suzuki-Miyaura cross-coupling reaction with **4.2** catalyzed by iron-based complex **4.6**.



4.8 Conclusion and outlook

We report the discovery and optimization of a Suzuki-Miyaura cross-coupling reaction between alkyl tosylates and aryl boronic esters catalyzed by an iron-based complex. The practical implications of being able to use alkyl pseudohalide electrophiles include taking advantage of the wide availability of aliphatic alcohol precursors for incorporation into cross-coupling reactions and avoidance of toxic and unstable alkyl halides. The use of pseudohalide electrophiles are rare for cross-coupling reactions employing first-row transition metal catalysts such as nickel and the use of sp^3 -hybridized substrates are a known limitation for palladium-catalyzed cross-coupling reactions. As a result, a cross-coupling reaction involving an alkyl pseudohalide substrate provides complementary reactivity to that of established methods. The successful cross-coupling reaction of alkyl tosylates catalyzed by iron-based complexes is inconsistent with our understanding of how such electrophiles and transition metal catalysts behave, giving rise to the possibility that a different reaction mechanism may be operative. The ability of iron-based complexes to access different mechanistic manifolds has long been an obstruction to a thorough mechanistic understanding of reactions involving iron. However, the studies presented here demonstrate the potential for harnessing such divergent reactivity to employ a diverse range of otherwise inaccessible substrates through the use of a single transition metal complex. Future directions include extending this method towards incorporating other pseudohalide electrophiles, including but not limited to redox-active esters, phosphonates, and xanthates, and a closer examination of how other ancillary ligand frameworks may impact the efficacy of the cross-coupling reaction.

4.9 Experimental section

General Considerations. Unless stated otherwise, all reactions were carried out in oven-dried glassware in a nitrogen-filled glovebox or using standard Schlenk line techniques.⁴⁸ Solvents including tetrahydrofuran, pentane, and benzene were used after passage through two activated alumina columns under a blanket of argon and then degassed by brief exposure to vacuum.⁴⁹ Deuterated solvents were dried over a sodium/benzophenone pot and distilled prior to their use. Boronic esters were used after passage through alumina under a nitrogen atmosphere. Methylbutylamine and methylethylamine were purchased from TCI America; diethylamine was purchased from Sigma-Aldrich. Amines that were liquids at room temperature were dried over calcium hydride for at least 24 hours and then distilled under vacuum. Lithium amides were passed through a 250-micron sieve to ensure homogenous particle size prior to use. Iron (II) chloride was purchased from Sigma-Aldrich and used without further purification. Alkyl halides were dried over calcium hydride for at least 24 hours and then distilled under vacuum. Nuclear magnetic resonance (NMR) spectra were recorded at ambient temperature on Varian vNMRs operating at 400 MHz, 500 MHz, or 600 MHz for ¹H NMR, at 160 MHz for ¹¹B NMR, and at 125 MHz for {¹H}¹³C NMR. Spectra were referenced using shifts corresponding to solvent residual protic impurities. Boron trifluoride diethyl etherate (BF₃·Et₂O) was used as an external standard for ¹¹B NMR (0.0 ppm). The line listing for NMR spectra of diamagnetic compounds are reported as follows: chemical shift (multiplicity, coupling constant, integration); paramagnetic compounds are reported as follows: chemical shift (peak width at half height, number of protons). All paramagnetic spectra were collected at 25 °C. Solvent suppressed spectra were collected for

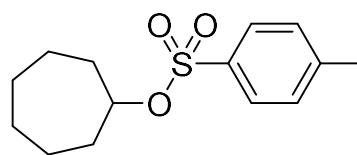
paramagnetic complexes in THF using the PRESAT macro on the vNMR software. Infrared spectra were recorded on a Bruker Alpha attenuated total reflectance infrared spectrometer. High resolution mass spectra were obtained at the Boston College Mass Spectrometry Facility on a JEOL AccuTOF DART instrument.

General procedure for synthesis of β -diketimate iron chloride complexes. To an oven-dried round-bottom flask equipped with stir bar was added β -diketimate ligand (9.8 mmol, 1.0 equiv.) and pentane (40 mL, 0.244 M). This mixture was cooled to $-78\text{ }^{\circ}\text{C}$ and degassed by placing the solution under vacuum for at least 5 minutes. A solution of butyl lithium in hexanes (4.21 mL, 2.3 M, 9.75 mmol) was added dropwise while stirring. In most cases, a white precipitate formed rapidly. The reaction mixture was warmed to room temperature while stirring before the solvent was removed under vacuum. The sealed reaction vessel was transferred into a nitrogen glovebox, where the solid was collected on a frit and washed with cold pentane (5 mL at $-40\text{ }^{\circ}\text{C}$). The solid was dried and weighed to determine stoichiometry for the next step. The collected lithiated ligand (9.8 mmol) was then dissolved in THF (10 mL) in a 20 mL scintillation vial. This solution was added dropwise to a slurry of iron dichloride (9.8 mmol) in THF (10 mL) prepared in a separate scintillation vial equipped with stir bar. This mixture was allowed to stir overnight. The resulting solution was cooled and passed through celite which was washed with additional THF ($\sim 20\text{ mL}$), then concentrated under vacuum. The resulting semi-solid was then washed with pentane, dried, and collected.

General procedure for the iron-catalyzed cross-coupling reaction of aryl boronic esters and alkyl sulfonate esters. In a nitrogen-filled glovebox, iron complex (0.05 mmol, 10 mol %) and lithium ethylmethyl amide (0.60 mmol, 1.2 equiv.) were added

to a 7 mL scintillation vial containing a magnetic stir bar. A 1 mL benzene solution of boronic acid pinacol ester (0.5 mmol, 1.0 equiv.) and alkyl sulfonate ester (1.0 mmol, 2.0 equiv.) was added to the stirring vial followed immediately by benzene (5 mL) and sealing of the reaction vessel. The sealed reaction vessel was removed from the glovebox and heated to 50 °C. The reaction was allowed to stir vigorously and quickly became homogenous. After 24 hours of stirring, the reaction was quenched with a saturated aqueous solution of ammonium chloride (10 mL). The aqueous phase was washed with dichloromethane (3 x 40 mL) and the combined organic phases were dried over sodium sulfate and filtered through celite. Trimethoxybenzene (42 mg, 0.25 mmol) was added as an internal standard before evaporating the solvent *in vacuo*. A spectroscopic yield was determined by ¹H NMR spectroscopy before the crude product was purified by silica column chromatography.

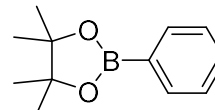
Synthesis of cycloheptyl tosylate (4.1). To oven dried round bottom flask containing stir bar was added cycloheptanol (1.14 g, 9.96 mmol, 1.2



mL) and pyridine (4.87 g, 61.59 mmol, 4.98 mL). The reaction mixture was cooled to 0°C with an ice bath. To the stirring solution of alcohol in pyridine was slowly added 4-methylbenzenesulfonyl chloride (2.85 g, 14.94 mmol). The reaction mixture was allowed to stir overnight, warming to ambient temperature. The reaction mixture was acidified with 15% aqueous HCl (pH ~ 2), extracted with EtOAc (30 mL x 2), and the combined organics washed with DI water (1x) and brine (1x). The combined organic layers were dried over magnesium sulfate and filtered; the filtrate concentrated in vacuo and purified via flash autocolumn chromatography (15% EtOAc in hexanes). ¹H NMR (400 MHz, CDCl₃) δ 7.79

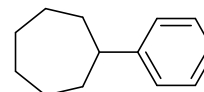
(d, $J = 7.9$ Hz, 2H), 7.32 (d, $J = 7.9$ Hz, 2H), 4.67 (tt, $J = 7.9, 4.7$ Hz, 1H), 2.44 (s, 3H), 1.99 – 1.46 (m, 12H). NMR spectrum is in agreement with literature precedence.⁵⁰

Synthesis of 4,4,5,5-tetramethyl-2-phenyl-1,3,2-dioxaborolane



(4.2). To round bottom flask containing stir bar was added phenyl boronic acid (10 g, 82 mmol, 1.0 equiv.), pinacol (10.2 g, 86 mmol, 1.05 equiv.), and sodium sulfate (11.65 g, 82 mmol). To the flask was added pentane (100 mL) and diethyl ether (50 mL). The reaction mixture was allowed to stir overnight before the crude reaction mixture was passed through a plug of silica, eluting with dichloromethane. The solvent was removed *in vacuo* and the resultant crude white solid (15.5 g, 93%) was passed through a plug of alumina in the glovebox prior to use. ¹H NMR (500 MHz, CDCl₃) δ 1.35 (s, 6H), 7.35-7.39 (m, 2H), 7.43-7.48 (m, 1H), 7.79-7.83 (m, 2H); ¹¹B NMR (500 MHz, CDCl₃) δ 31. NMR spectra are in accordance with literature precedence.⁵¹

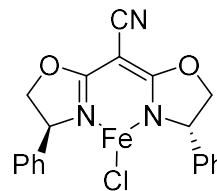
Synthesis of phenylcycloheptane (4.3). Phenylcycloheptane was



synthesized from cycloheptyl tosylate (2.0 equiv.) and phenyl boronic acid pinacol ester according to the general procedures for the iron-catalyzed cross-coupling reaction of aryl boronic esters and alkyl sulfonate esters and purified by silica gel flash column chromatography, eluting with 100% hexanes to afford the product as a colorless oil. $R_f = 0.60$ (100% hexanes). ¹H NMR (500 MHz, CDCl₃): δ 7.23 – 7.33 (m, 2H), 7.08 – 7.23 (m, 2H), 2.66 (tt, $J = 10.7, 3.7$ Hz, 1H), 1.92 (ddt, $J = 13.5, 6.6, 3.3$ Hz, 2H), 1.80 (ddd, $J = 13.4, 6.6, 3.4$ Hz, 2H), 1.46 – 1.78 (m, 8H) ppm. NMR spectrum is in agreement with literature precedence.¹

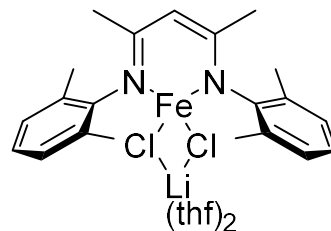
Synthesis of (2,2-bis((S)-4-phenyl-4,5-dihydrooxazol-2-yl)acetonitrile) iron chloride (4.4).

In the glovebox, to a 7 mL scintillation vial equipped with stir bar was added 2,2-bis((S)-4-phenyl-4,5-dihydrooxazol-2-yl)acetonitrile (0.81 g, 2.5 mmol). This was dissolved in THF (3 mL) and sodium hydride (0.065 g, 2.7 mmol) was added using THF (2 mL) to transfer it. This mixture was stirred for 12 hours before being filtered through celite. The celite and vial were rinsed with THF (5 mL). To a 20 mL scintillation vial equipped with a stir bar was added iron dichloride (0.31 g, 2.5 mmol) and THF (5 mL). After stirring for one hour, the Na{2,2-bis((S)-4-phenyl-4,5-dihydrooxazol-2-yl)acetonitrile} solution was added. The solution went from pale yellow-brown to a white suspension almost immediately. After stirring for 12 hours the solvent was removed *in vacuo* and the solid washed with THF and redried. This yielded an off-white solid (0.95 g, 81%). ¹H NMR (500 MHz, THF) δ -30 (*w*_{1/2} = 307 Hz, 4H), -4.2 (*w*_{1/2} = 59 Hz, 2H), -3.8 (*w*_{1/2} = 33 Hz, 4H), -1.1 (*w*_{1/2} = 21 Hz, 2H), 10.8 (*w*_{1/2} = 76 Hz, 2H), 56.8 (*w*_{1/2} = 512 Hz, 1H) ppm. IR: 2203, 1606, 1533, 1440, 1067, 694 cm⁻¹. NMR spectrum is in agreement with literature precedence.¹



Synthesis of 2,4-bis[(2,6-dimethylphenyl)imino]pentane

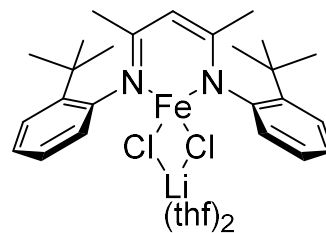
iron chloride complex (4.5). Synthesized according to general procedure using 2,4-bis[(2,6-dimethylphenyl)imino]pentane as the ligand. ¹H NMR (400



MHz, THF) δ -68.7 (*w*_{1/2} = 180 Hz, 6H), -52.0 (*w*_{1/2} = 100 Hz, 2H), -39.7 (*w*_{1/2} = 264 Hz, 1H), 6.2 (*w*_{1/2} = 254 Hz, 12H), 16.1 (*w*_{1/2} = 82 Hz, 4H) ppm. IR: 2916, 1519, 1373, 1038, 760 cm⁻¹. NMR spectrum is in agreement with literature precedence.²

Synthesis of 2,4-bis[(2-*tert*-butylphenyl)imino]pentane iron

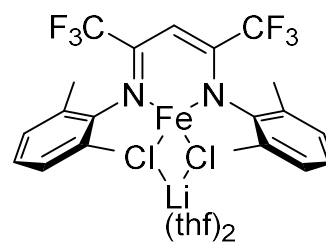
chloride complex (4.6). Synthesized according to general procedure using 2,4-bis[(2-*tert*-butylphenyl)imino]pentane as the ligand. ¹H NMR (of the major rotameric species) (400



MHz, THF) δ -62.3 ($w_{1/2}$ = 137 Hz, 6H), -48.1 ($w_{1/2}$ = 69 Hz, 2H), -46.5 ($w_{1/2}$ = 206 Hz, 1H), -5.1 ($w_{1/2}$ = 210 Hz, 18H), 14.3 ($w_{1/2}$ = 60 Hz, 2H) 16.7 (three overlapping peaks, 4H) ppm. IR: 2914, 1377, 1187, 1037, 754 cm^{-1} . NMR spectrum is in agreement with literature precedence.²

Synthesis of 1,1,1,5,5,5-hexafluoro-2,4-bis[(2,6-dimethylphenyl)imino]pentane iron chloride complex (4.7).

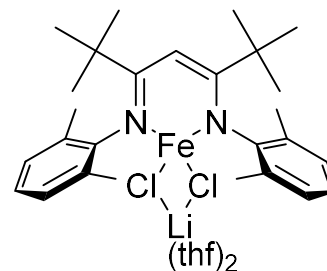
Synthesized according to general procedure using 1,1,1,5,5,5-hexafluoro-2,4-bis[(2,6-dimethylphenyl)imino]pentane as the



ligand. ¹H NMR (400 MHz, THF) δ -53.9 ($w_{1/2}$ = 89 Hz, 1H), 15.5 ($w_{1/2}$ = 356 Hz, 12H), 18.7 ($w_{1/2}$ = 760 Hz, 4H) ppm. IR: 1564, 1173, 1136, 769 cm^{-1} . NMR spectrum is in agreement with literature precedence.²

Synthesis of 2,2,6,6-tetramethyl-3,5-bis[(2,6-dimethylphenyl)imino]heptane iron chloride complex (4.8).

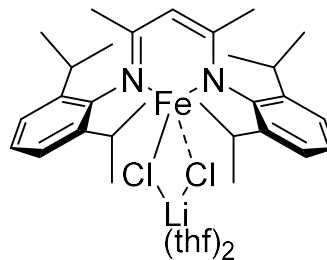
Synthesized according to general procedure using 2,2,6,6-tetramethyl-3,5-bis[(2,6-dimethylphenyl)imino]heptane as the



ligand. ¹H NMR (400 MHz, THF) δ -75.0 ($w_{1/2}$ = 105 Hz, 2H), -51.4 ($w_{1/2}$ = 348 Hz, 1H), 12.8 ($w_{1/2}$ = 152 Hz, 36H), 21.7 ($w_{1/2}$ = 383 Hz, 12H), 22.9 ($w_{1/2}$ = 82 Hz, 4H) ppm. IR: 3301, 1665, 1539, 1320, 752, 691 cm^{-1} . NMR spectrum is in agreement with literature precedence.²

Synthesis of 2,4-bis[(2,6-diisopropylphenyl)imino]pentane

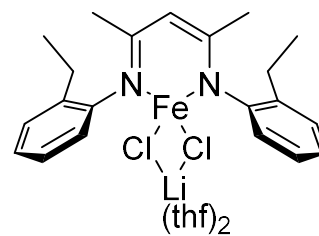
iron chloride complex (4.9). Synthesized according to general procedure using 2,4-bis[(2,6-diisopropylphenyl)imino]pentane as the ligand. ¹H NMR (400



MHz, THF) δ 15.28 ($w_{1/2}$ = 40 Hz, 4H), 2.23 ($w_{1/2}$ = 51 Hz, 12H), -16.55 ($w_{1/2}$ = 115 Hz, 12H), -42.97 ($w_{1/2}$ = 56 Hz, 2H), -63.88 ($w_{1/2}$ = 116 Hz, 6H). NMR spectrum is in agreement with literature precedence.⁵²

Synthesis of 2,4-bis[(2-ethylphenyl)imino]pentane iron

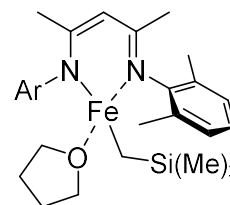
chloride complex (4.10). Synthesized according to general procedure using 2,4-bis[(2-ethylphenyl)imino]pentane as the ligand. ¹H NMR (400 MHz, THF) δ -67.2 ($w_{1/2}$ = 162 Hz, 6H),



-52.1 ($w_{1/2}$ = 187 Hz, 2H), -14.2 ($w_{1/2}$ = 103 Hz, 3H), -11.3 ($w_{1/2}$ = 132 Hz, 3H), 15.9 ($w_{1/2}$ = 289 Hz, 4H) ppm. IR: 2963, 1518, 1373, 1021, 740 cm^{-1} . NMR spectrum is in agreement with literature precedence.²

Synthesis of 2,4-bis[(2,6-dimethylphenyl)imino]pentane iron

CH₂TMS tetrahydrofuran adduct (4.11). In a nitrogen-filled glovebox, to a 7 mL scintillation vial equipped with magnetic stir bar

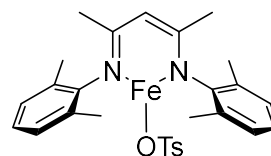


was added 4.5 (800 mg, 1.37 mmol) and pentane (2 mL). This mixture was allowed to cool to -40 °C in the freezer. A solution of LiCH₂TMS (129 mg, 1.0 equiv.) in pentane (1 mL) was added to the stirring reaction mixture. The reaction vessel was sealed and a dark yellow precipitate forms immediately. The reaction was allowed to stir for 1 hour, at which point the precipitate was filtered off through celite and the filtrate concentrated *in vacuo*. The residue was dissolved in pentane and transferred to a vial to recrystallize in the freezer

overnight. The mother liquor was decanted to afford the product as a yellow solid (434 mg, 61% yield). ^1H NMR (400 MHz, C_6D_6) δ 81.30 ($w_{1/2}$ = 294 Hz, 6H), 34.65 ($w_{1/2}$ = 303 Hz, 9H), 3.31 ($w_{1/2}$ = 37 Hz, 4H), 1.58 ($w_{1/2}$ = 12 Hz, 4H), -4.97 ($w_{1/2}$ = 42 Hz, 4H), -61.48 ($w_{1/2}$ = 406 Hz, 12H), -69.12 ($w_{1/2}$ = 68 Hz, 2H). NMR spectrum is in agreement with literature precedence.²

Synthesis of 2,4-bis[(2,6-dimethylphenyl)imino]pentane iron

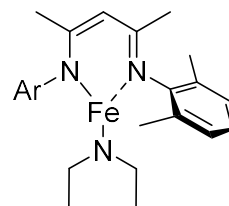
tosylate (4.12). In a nitrogen-filled glovebox, **4.11** (16.5 mg, 0.032 mmol) was weighed into a scintillation vial and dissolved in



deuterated benzene (300 μL). *para*-toluenesulfonic acid (5.46 mg, 0.032 mmol, 1.0 equiv.) was weighed out in a separate scintillation vial and dissolved in deuterated benzene (300 μL). The solutions were combined and the reaction mixture turned bright yellow immediately with formation of a white precipitate. The reaction mixture was decanted and transferred into a J. Young tube, which was sealed and shaken. The product could not be isolated and was carried forward for stoichiometric reactions without further purification. ^1H NMR (500 MHz, C_6D_6) δ 100.05 ($w_{1/2}$ = 704 Hz, 1H), 80.4 ($w_{1/2}$ = 394 Hz, 6H), 34.61 ($w_{1/2}$ = 348 Hz, 6H), 12.5 ($w_{1/2}$ = 97 Hz, 3H), -4.8 ($w_{1/2}$ = 116 Hz, 4H), -37.91 ($w_{1/2}$ = 244 Hz, 4H), -61.05 ($w_{1/2}$ = 509 Hz, 6H), -68.95 ($w_{1/2}$ = 151 Hz, 2H).

Synthesis of 2,4-bis[(2,6-dimethylphenyl)imino]pentane iron *N,N*-

diethylamide (4.13). In the glovebox, to a 20 mL scintillation vial equipped with magnetic stir bar was added **4.11** (200 mg, 390 μmol)

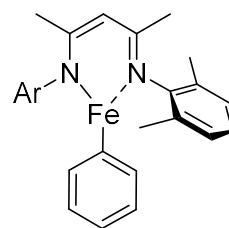


and pentane (5 mL). To this mixture was added diethylamine (40 μL , 1.0 equiv). The resulting mixture was allowed to stir overnight, turning from yellow to red-orange. The reaction vessel was transferred to the freezer to recrystallize overnight. The pentane was

decanted and the resultant red-orange solid washed with fresh cold pentane, and residual pentane removed *in vacuo* to afford the product as a red-orange solid (150 mg, 90% yield). ^1H NMR (400 MHz, C_6D_6) δ 121.30 ($w_{1/2}$ = 780 Hz, 1H), 50.20 ($w_{1/2}$ = 961 Hz, 6H), 37.77 ($w_{1/2}$ = 355 Hz, 6H), -14.89 ($w_{1/2}$ = 97 Hz, 4H), -73.44 ($w_{1/2}$ = 110 Hz, 2H), -78.58 ($w_{1/2}$ = 530 Hz, 12H). IR: 1506, 1378, 1173, 1096, 765 cm^{-1} . NMR spectrum is in agreement with literature precedence.²

Synthesis of 2,4-bis[(2,6-dimethylphenyl)imino]pentane iron

phenyl (4.14). In the glovebox, to a 20 mL scintillation vial was weighed **4.13** (10 mg, 23 μmol , 1.0 equiv.). In the same vial was weighed **4.2** (2.5 mg, 11.5 μmol , 0.5 equiv.). The solids were dissolved



in deuterated benzene (600 μmol) and a rapid color change from orange to dark brown was observed. The reaction mixture was carried forward and used in reactivity studies as a 1:1 mixture of **4.13** and **4.14** without further purification. NMR spectrum displayed signals consistent with both species, and is in agreement with literature precedence.²

Synthesis of 9-decen-1-ylbenzene (4.16). 9-decen-1-ylbenzene was



synthesized from 9-decen-1-yltosylate (2.0 equiv.) and phenyl boronic acid pinacol ester according to the general procedures for the iron-catalyzed cross-coupling reaction of aryl boronic esters and alkyl sulfonate esters and purified by silica gel flash column chromatography, eluting with 100% hexanes to afford the product as a colorless oil. ^1H NMR (400 MHz, CDCl_3) δ), 7.33-7.11 (m, 5H), 5.61 (m, 1H), 4.88-4.73 (m, 2H), 2.59 (t, J = 7.6 Hz, 2H), 1.95 (q, J = 7.4 Hz, 2H), 1.56-1.41 (m, 4H), 1.31-1.17 (m, 8H). NMR spectrum is in agreement with literature precedence.⁵³

4.10 References

- (1) Crockett, M. P.; Tyrol, C. C.; Wong, A. S.; Li, B.; Byers, J. A. Iron-Catalyzed Suzuki–Miyaura Cross-Coupling Reactions between Alkyl Halides and Unactivated Arylboronic Esters. *Org. Lett.* **2018**, *20* (17), 5233–5237. <https://doi.org/10.1021/acs.orglett.8b02184>.
- (2) Crockett, M. P.; Wong, A. S.; Li, B.; Byers, J. A. Rational Design of an Iron-Based Catalyst for Suzuki–Miyaura Cross-Couplings Involving Heteroaromatic Boronic Esters and Tertiary Alkyl Electrophiles. *Angew. Chemie Int. Ed.* **2020**, *59* (13), 5392–5397. <https://doi.org/10.1002/anie.201914315>.
- (3) Smith, M. B.; March, J. *March's Advanced Organic Chemistry: Reactions, Mechanisms, and Structure*, 6th ed.; John Wiley & Sons, Inc.: Hoboken, New Jersey, 2007.
- (4) Kabalka, G. W.; Varma, M.; Varma, R. S.; Srivastava, P. C.; Knapp, F. F. The Tosylation of Alcohols. *J. Org. Chem.* **1986**, *51* (12), 2386–2388. <https://doi.org/10.1021/jo00362a044>.
- (5) Wuts, P. G. M.; Greene, T. W. *Greene's Protective Groups in Organic Synthesis*; John Wiley & Sons, Inc.: Hoboken, NJ, USA, 2006. <https://doi.org/10.1002/0470053488>.
- (6) Tipson, R. S. On Esters of P-Toluenesulfonic Acid. *J. Org. Chem.* **1944**, *09* (3), 235–241. <https://doi.org/10.1021/jo01185a005>.
- (7) Arpe, H.-J. *Industrial Organic Chemistry*, 5th ed.; WILEY-VCH Verlag GmbH & Co. KGaA: Weinheim, 2010.
- (8) Pohl, L. R.; Mico, B. A. Electrophilic Halogens as Potentially Toxic Metabolites of Halogenated Compounds. *Trends Pharmacol. Sci.* **1984**, *5*, 61–64. [https://doi.org/10.1016/0165-6147\(84\)90368-7](https://doi.org/10.1016/0165-6147(84)90368-7).
- (9) Vickers, A. E.; Sloop, T. C.; Lucier, G. W. Mechanism of Action of Toxic Halogenated Aromatics. *Environ. Health Perspect.* **1985**, *59*, 121–128. <https://doi.org/10.1289/ehp.59-1568090>.

- (10) Oh-e, T.; Miyaura, N.; Suzuki, A. Palladium-Catalyzed Cross-Coupling Reaction of Organoboron Compounds with Organic Triflates. *J. Org. Chem.* **1993**, *58* (8), 2201–2208. <https://doi.org/10.1021/jo00060a041>.
- (11) Molander, G. A.; Ito, T. Cross-Coupling Reactions of Potassium Aryltrifluoroborates with Aryl and 1-Alkenyl Trifluoromethanesulfonates. *Org. Lett.* **2001**, *3* (3), 393–396. <https://doi.org/10.1021/ol006896u>.
- (12) Roy, A. H.; Hartwig, J. F. Oxidative Addition of Aryl Tosylates to Palladium(0) and Coupling of Unactivated Aryl Tosylates at Room Temperature. *J. Am. Chem. Soc.* **2003**, *125* (29), 8704–8705. <https://doi.org/10.1021/ja035835z>.
- (13) Nguyen, H. N.; Huang, X.; Buchwald, S. L. The First General Palladium Catalyst for the Suzuki-Miyaura and Carbonyl Enolate Coupling of Aryl Arenesulfonates. *J. Am. Chem. Soc.* **2003**, *125* (39), 11818–11819. <https://doi.org/10.1021/ja036947t>.
- (14) Zhang, L.; Meng, T.; Wu, J. Palladium-Catalyzed Suzuki–Miyaura Cross-Couplings of Aryl Tosylates with Potassium Aryltrifluoroborates. *J. Org. Chem.* **2007**, *72* (24), 9346–9349. <https://doi.org/10.1021/jo7019064>.
- (15) So, C. M.; Lau, C. P.; Chan, A. S. C.; Kwong, F. Y. Suzuki–Miyaura Coupling of Aryl Tosylates Catalyzed by an Array of Indolyl Phosphine–Palladium Catalysts. *J. Org. Chem.* **2008**, *73* (19), 7731–7734. <https://doi.org/10.1021/jo8014819>.
- (16) Bhayana, B.; Fors, B. P.; Buchwald, S. L. A Versatile Catalyst System for Suzuki–Miyaura Cross-Coupling Reactions of C(Sp²)-Tosylates and Mesylates. *Org. Lett.* **2009**, *11* (17), 3954–3957. <https://doi.org/10.1021/ol9015892>.
- (17) So, C. M.; Lau, C. P.; Kwong, F. Y. A General Palladium-Catalyzed Suzuki–Miyaura Coupling of Aryl Mesylates. *Angew. Chemie Int. Ed.* **2008**, *47* (42), 8059–8063. <https://doi.org/10.1002/anie.200803193>.
- (18) Percec, V.; Bae, J. Y.; Hill, D. H. Aryl Mesylates in Metal Catalyzed Homocoupling and Cross-Coupling Reactions. 2. Suzuki-Type Nickel-Catalyzed Cross-Coupling of Aryl Arenesulfonates and Aryl Mesylates with Arylboronic Acids. *J. Org. Chem.* **1995**, *60* (4),

1060–1065. <https://doi.org/10.1021/jo00109a044>.

(19) Kobayashi, Y.; Mizojiri, R. Nickel-Catalyzed Coupling Reaction of Lithium Organoborates and Aryl Mesylates Possessing an Electron Withdrawing Group. *Tetrahedron Lett.* **1996**, *37* (47), 8531–8534. [https://doi.org/10.1016/0040-4039\(96\)01984-3](https://doi.org/10.1016/0040-4039(96)01984-3).

(20) Zim, D.; Lando, V. R.; Dupont, J.; Monteiro, A. L. NiCl₂(PCy₃)₂: A Simple and Efficient Catalyst Precursor for the Suzuki Cross-Coupling of Aryl Tosylates and Arylboronic Acids. *Org. Lett.* **2001**, *3* (19), 3049–3051. <https://doi.org/10.1021/ol016526l>.

(21) Kuroda, J. I.; Inamoto, K.; Hiroya, K.; Doi, T. N-Heterocyclic Carbene Derived Nickel-Pincer Complexes: Efficient and Applicable Catalysts for Suzuki-Miyaura Coupling Reactions of Aryl/Alkenyl Tosylates and Mesylates. *European J. Org. Chem.* **2009**, No. 14, 2251–2261. <https://doi.org/10.1002/ejoc.200900067>.

(22) Netherton, M. R.; Fu, G. C. Suzuki Cross-Couplings of Alkyl Tosylates That Possess β Hydrogen Atoms: Synthetic and Mechanistic Studies. *Angew. Chemie Int. Ed.* **2002**, *41* (20), 3910–3912. [https://doi.org/10.1002/1521-3773\(20021018\)41:20<3910::AID-ANIE3910>3.0.CO;2-W](https://doi.org/10.1002/1521-3773(20021018)41:20<3910::AID-ANIE3910>3.0.CO;2-W).

(23) Brenstrum, T.; Gerristma, D. A.; Adjabeng, G. M.; Frampton, C. S.; Britten, J.; Robertson, A. J.; McNulty, J.; Capretta, A. Phosphaadamantanes as Ligands for Palladium Catalyzed Cross-Coupling Chemistry: Library Synthesis, Characterization, and Screening in the Suzuki Coupling of Alkyl Halides and Tosylates Containing Beta-Hydrogens with Boronic Acids and Alkylboranes. *J. Org. Chem.* **2004**, *69* (22), 7635–7639. <https://doi.org/10.1021/jo048875+>.

(24) Zhou, J.; Fu, G. C. Palladium-Catalyzed Negishi Cross-Coupling Reactions of Unactivated Alkyl Iodides, Bromides, Chlorides, and Tosylates. *J. Am. Chem. Soc.* **2003**, *125* (41), 12527–12530. <https://doi.org/10.1021/ja0363258>.

(25) Fürstner, A.; Leitner, A.; Méndez, M.; Krause, H. Iron-Catalyzed Cross-Coupling Reactions. *J. Am. Chem. Soc.* **2002**, *124* (46), 13856–13863. <https://doi.org/10.1021/ja027190t>.

- (26) Tindall, D. J.; Krause, H.; Fürstner, A. Iron-Catalyzed Cross-Coupling of 1-Alkynylcyclopropyl Tosylates and Related Substrates. *Adv. Synth. Catal.* **2016**, *358* (15), 2398–2403. <https://doi.org/10.1002/adsc.201600357>.
- (27) Terao, J.; Watanabe, H.; Ikumi, A.; Kuniyasu, H.; Kambe, N. Nickel-Catalyzed Cross-Coupling Reaction of Grignard Reagents with Alkyl Halides and Tosylates: Remarkable Effect of 1,3-Butadienes. *J. Am. Chem. Soc.* **2002**, *124* (16), 4222–4223. <https://doi.org/10.1021/ja025828v>.
- (28) Do, H. Q.; Chandrashekar, E. R. R.; Fu, G. C. Nickel/Bis(Oxazoline)-Catalyzed Asymmetric Negishi Arylations of Racemic Secondary Benzylic Electrophiles to Generate Enantioenriched 1,1-Diarylalkanes. *J. Am. Chem. Soc.* **2013**, *135* (44), 16288–16291. <https://doi.org/10.1021/ja408561b>.
- (29) Molander, G. A.; Traister, K. M.; O'Neill, B. T. Engaging Nonaromatic, Heterocyclic Tosylates in Reductive Cross-Coupling with Aryl and Heteroaryl Bromides. *J. Org. Chem.* **2015**, *80* (5), 2907–2911. <https://doi.org/10.1021/acs.joc.5b00135>.
- (30) Komeyama, K.; Michiyuki, T.; Osaka, I. Nickel/Cobalt-Catalyzed C(Sp³)-C(Sp³) Cross-Coupling of Alkyl Halides with Alkyl Tosylates. *ACS Catal.* **2019**, *9* (10), 9285–9291. <https://doi.org/10.1021/acscatal.9b03352>.
- (31) Sanford, A. B.; Thane, T. A.; McGinnis, T. M.; Chen, P.-P.; Hong, X.; Jarvo, E. R. Nickel-Catalyzed Alkyl–Alkyl Cross-Electrophile Coupling Reaction of 1,3-Dimesylates for the Synthesis of Alkylcyclopropanes. *J. Am. Chem. Soc.* **2020**, *142* (11), 5017–5023. <https://doi.org/10.1021/jacs.0c01330>.
- (32) Knappe, C. E. I.; Grupe, S.; Gärtner, D.; Corpet, M.; Gosmini, C.; Jacobi von Wangelin, A. Reductive Cross-Coupling Reactions between Two Electrophiles. *Chem. - A Eur. J.* **2014**, *20* (23), 6828–6842. <https://doi.org/10.1002/chem.201402302>.
- (33) Olivares, A. M.; Weix, D. J. Multimetallic Ni- and Pd-Catalyzed Cross-Electrophile Coupling to Form Highly Substituted 1,3-Dienes. *J. Am. Chem. Soc.* **2018**, *140* (7), 2446–2449. <https://doi.org/10.1021/jacs.7b13601>.

- (34) Crockett, M. P. The Development of Iron Catalysts for Suzuki-Miyaura Cross-Coupling and the Reactivity Discovered Along the Way, PhD thesis, Boston College, 2020.
- (35) Tyrol, C. C.; Yone, N. S.; Gallin, C. F.; Byers, J. A. Iron-Catalysed Enantioconvergent Suzuki–Miyaura Cross-Coupling to Afford Enantioenriched 1,1-Diarylalkanes. *Chem. Commun.* **2020**, *56* (93), 14661–14664. <https://doi.org/10.1039/D0CC05003B>.
- (36) Crossland, R. K.; Wells, W. E.; Shiner, V. J. Sulfonate Leaving Groups, Structure and Reactivity. 2,2,2-Trifluoroethanesulfonate. *J. Am. Chem. Soc.* **1971**, *93* (17), 4217–4219. <https://doi.org/10.1021/ja00746a021>.
- (37) Streitwieser, Jr, A.; Wilkins, C.; Kiehlmann, E. Kinetics and Isotope Effects in Solvolyses of Ethyl Trifluoromethanesulfonate. *J. Am. Chem. Soc.* **1968**, *90* (6), 1598–1601. <https://doi.org/10.1021/ja01008a601>.
- (38) Curran, D. P.; Bosch, E.; Kaplan, J.; Newcomb, M. Rate Constants for Halogen Atom Transfer from Representative α -Halocarbonyl Compounds to Primary Alkyl Radicals. *J. Org. Chem.* **1989**, *54* (8), 1826–1831. <https://doi.org/10.1021/jo00269a016>.
- (39) Beckwith, A. L. J.; Poole, J. S. Factors Affecting the Rates of Addition of Free Radicals to Alkenes - Determination of Absolute Rate Coefficients Using the Persistent Aminoxyl Method. *J. Am. Chem. Soc.* **2002**, *124* (32), 9489–9497. <https://doi.org/10.1021/ja025730g>.
- (40) Pedersen, C. J. Cyclic Polyethers and Their Complexes with Metal Salts. *J. Am. Chem. Soc.* **1967**, *89* (26), 7017–7036. <https://doi.org/10.1021/ja01002a035>.
- (41) Liou, C.-C.; Brodbelt, J. S. Determination of Orders of Relative Alkali Metal Ion Affinities of Crown Ethers and Acyclic Analogs by the Kinetic Method. *J. Am. Soc. Mass Spectrom.* **1992**, *3* (5), 543–548. [https://doi.org/10.1016/1044-0305\(92\)85031-E](https://doi.org/10.1016/1044-0305(92)85031-E).
- (42) Frensdorff, H. K. Stability Constants of Cyclic Polyether Complexes with Univalent Cations. *J. Am. Chem. Soc.* **1971**, *93* (3), 600–606. <https://doi.org/10.1021/ja00732a007>.
- (43) Rohde, J. U.; In, J. H.; Lim, M. H.; Brennessel, W. W.; Bukowski, M. R.; Stubna,

A.; Münck, E.; Nam, W.; Que, L. Crystallographic and Spectroscopic Characterization of a Nonheme Fe(IV)=O Complex. *Science* **2003**, *299* (5609), 1037–1039. <https://doi.org/10.1126/science.299.5609.1037>.

(44) Jensen, M. P.; Costas, M.; Ho, R. Y. N.; Kaizer, J.; Mairata i Payeras, A.; Münck, E.; Que, L.; Rohde, J.-U.; Stubna, A. High-Valent Nonheme Iron. Two Distinct Iron(IV) Species Derived from a Common Iron(II) Precursor. *J. Am. Chem. Soc.* **2005**, *127* (30), 10512–10525. <https://doi.org/10.1021/ja0438765>.

(45) Wang, D.; Farquhar, E. R.; Stubna, A.; Münck, E.; Que, L. A Diiron(IV) Complex That Cleaves Strong C–H and O–H Bonds. *Nat. Chem.* **2009**, *1* (2), 145–150. <https://doi.org/10.1038/nchem.162>.

(46) Bergstrom, F. W.; Fernelius, W. C. The Chemistry of the Alkali Amides. *Chem. Rev.* **1933**, *12* (1), 43–179. <https://doi.org/10.1021/cr60041a002>.

(47) Lee, C.-H.; Yoh, S.-D.; Cheong, D.-Y.; Kim, S.-H.; Park, J.-H. Products Analysis in the Reaction of Substituted 1-Phenylethyl Alcohols with p-Toluenesulfonyl Chloride. *Bull. Korean Chem. Soc.* **2000**, *21* (10), 1049–1051.

(48) Burger, B. J.; Bercaw, J. E. Vacuum Line Techniques for Handling Air-Sensitive Organometallic Compounds. In *Experimental Organometallic Chemistry*; American Chemical Society, 1987; pp 79–115. <https://doi.org/10.1021/bk-1987-0357.ch004>.

(49) Pangborn, A. B.; Giardello, M. A.; Grubbs, R. H.; Rosen, R. K.; Timmers, F. J. Safe and Convenient Procedure for Solvent Purification. *Organometallics* **1996**, *15* (5), 1518–1520. <https://doi.org/10.1021/om9503712>.

(50) Liu, Y.; Xu, Y.; Jung, S.; Chae, J. A Facile and Green Protocol for Nucleophilic Substitution Reactions of Sulfonate Esters by Recyclable Ionic Liquids [Bmim][X]. *Synlett* **2012**, *23* (18), 2692–2698. <https://doi.org/10.1055/s-0032-1317473>.

(51) Potter, B.; Edelstein, E. K.; Morken, J. P. Modular, Catalytic Enantioselective Construction of Quaternary Carbon Stereocenters by Sequential Cross-Coupling Reactions. *Org. Lett.* **2016**, *18* (13), 3286–3289.

<https://doi.org/10.1021/acs.orglett.6b01580>.

(52) Smith, J. M.; Lachicotte, R. J.; Holland, P. L. Tuning Metal Coordination Number by Ancillary Ligand Steric Effects: Synthesis of a Three-Coordinate Iron(II) Complex. *Chem. Commun.* **2001**, No. 17, 1542–1543. <https://doi.org/10.1039/b103635c>.

(53) Toutounchian, N.; Ahmadpour, A.; Heravi, M. M.; Bamoharram, F. F.; Ayati, A.; Deymeh, F. Investigation of Linear Alkylbenzene Synthesis Using Nanotitania-Supported Dawson Heteropolyacid as Catalyst by Statistical Design Approaches. *Res. Chem. Intermed.* **2016**, *42* (4), 3283–3301. <https://doi.org/10.1007/s11164-015-2210-3>.

Appendix A.

Nuclear magnetic resonance spectral data

A.1 Nuclear magnetic resonance spectral data from Chapter 2

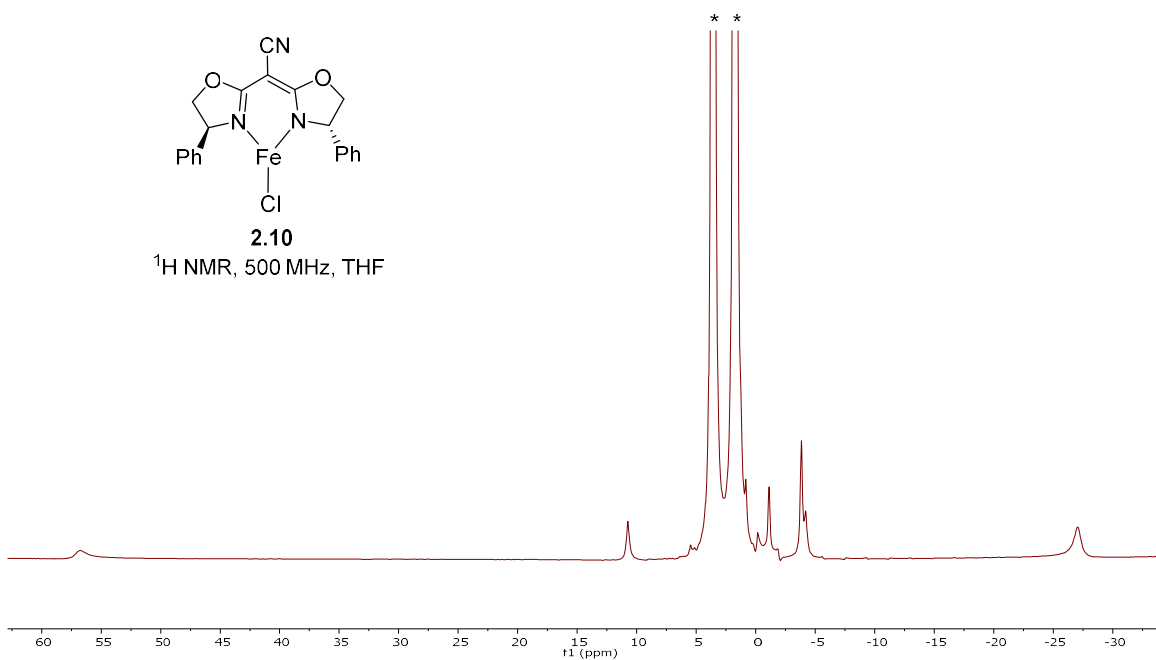


Figure A.1.1. $^1\text{H NMR}$ spectrum of compound **2.10** using solvent suppression for THF peaks.

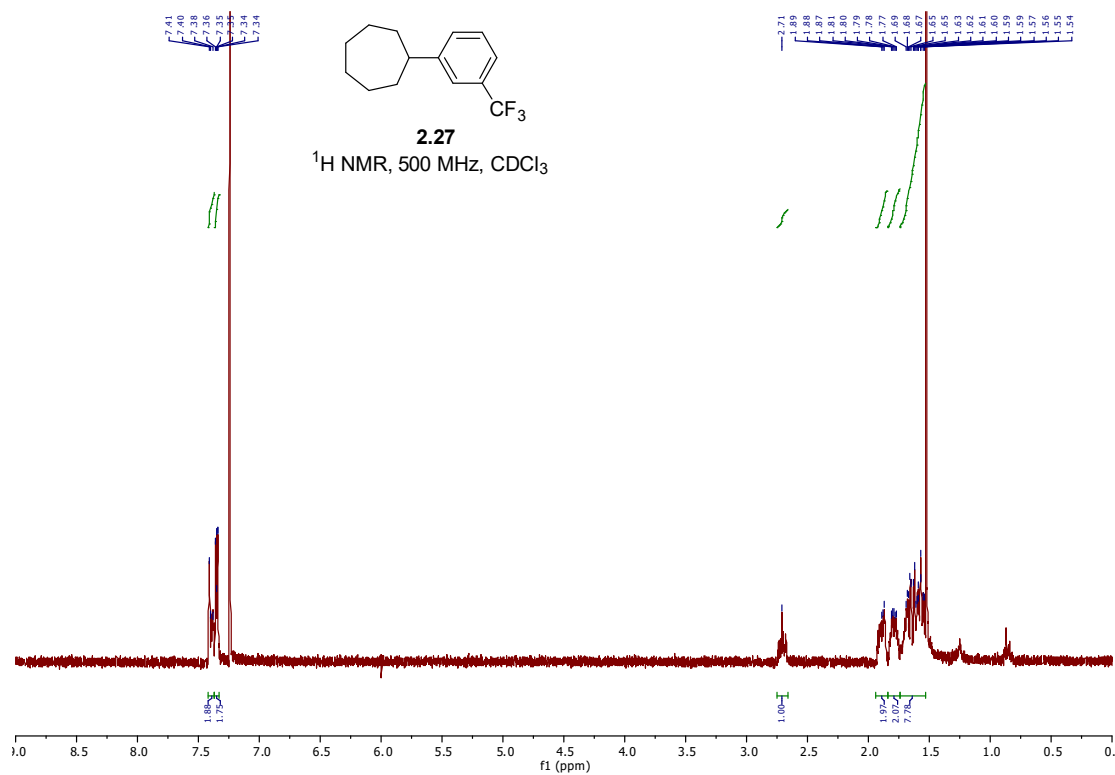


Figure A.1.2. $^1\text{H NMR}$ spectrum of compound **2.27**.

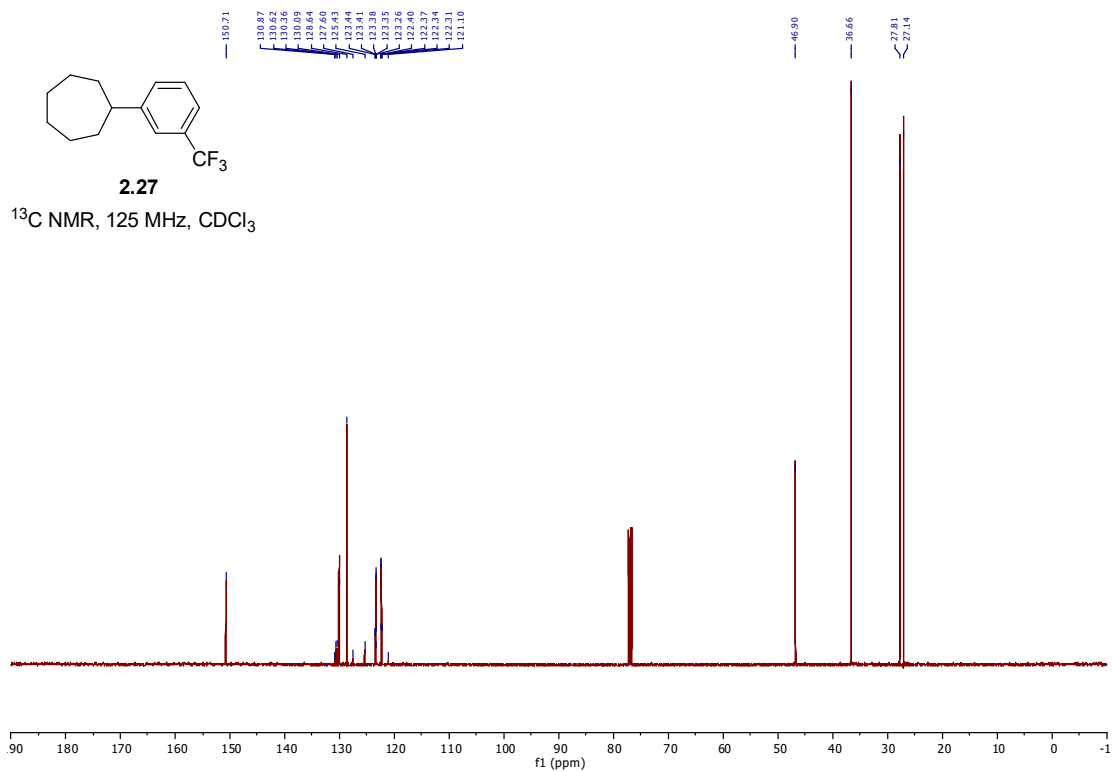


Figure A.1.3. ^{13}C NMR spectrum of compound **2.27**.

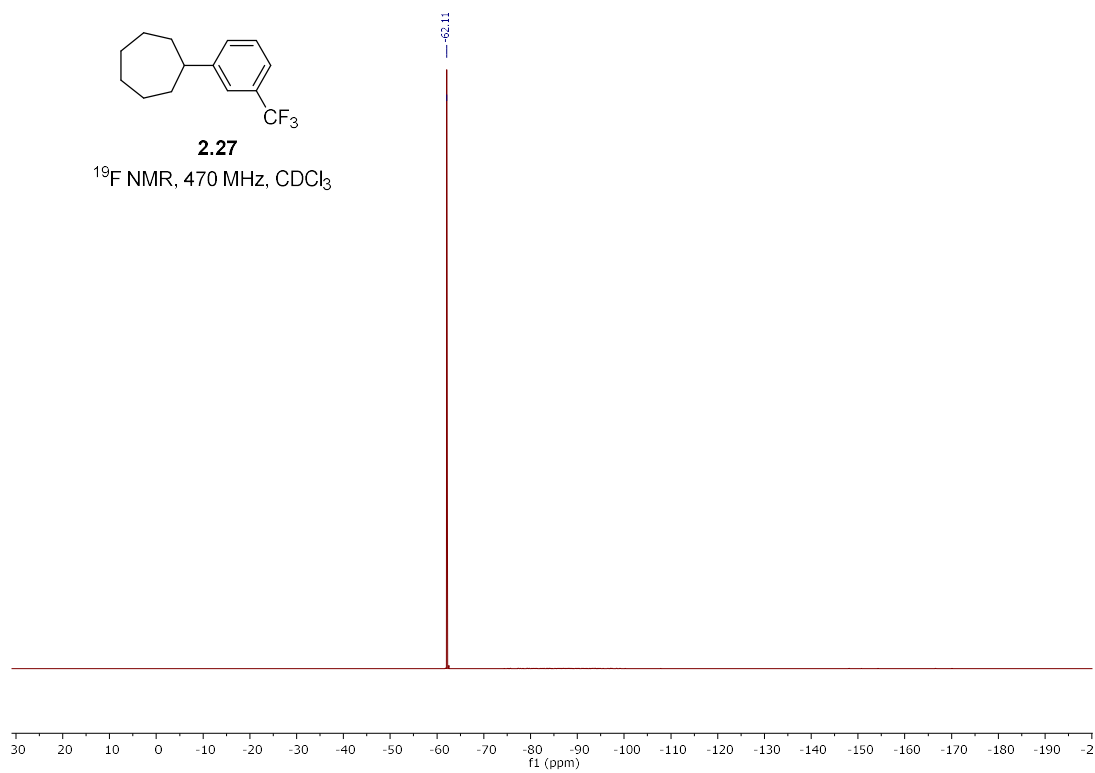


Figure A.1.4. ^{19}F NMR spectrum of compound **2.27**.

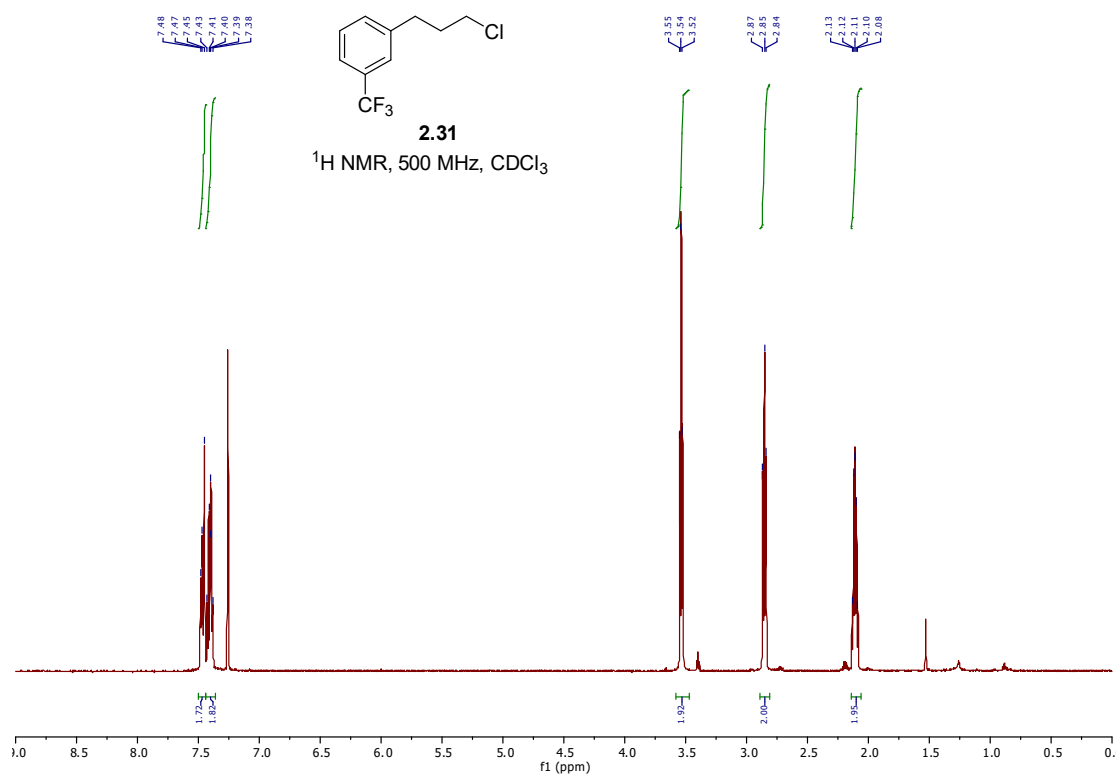


Figure A.1.5. ¹H NMR spectrum of compound 2.31.

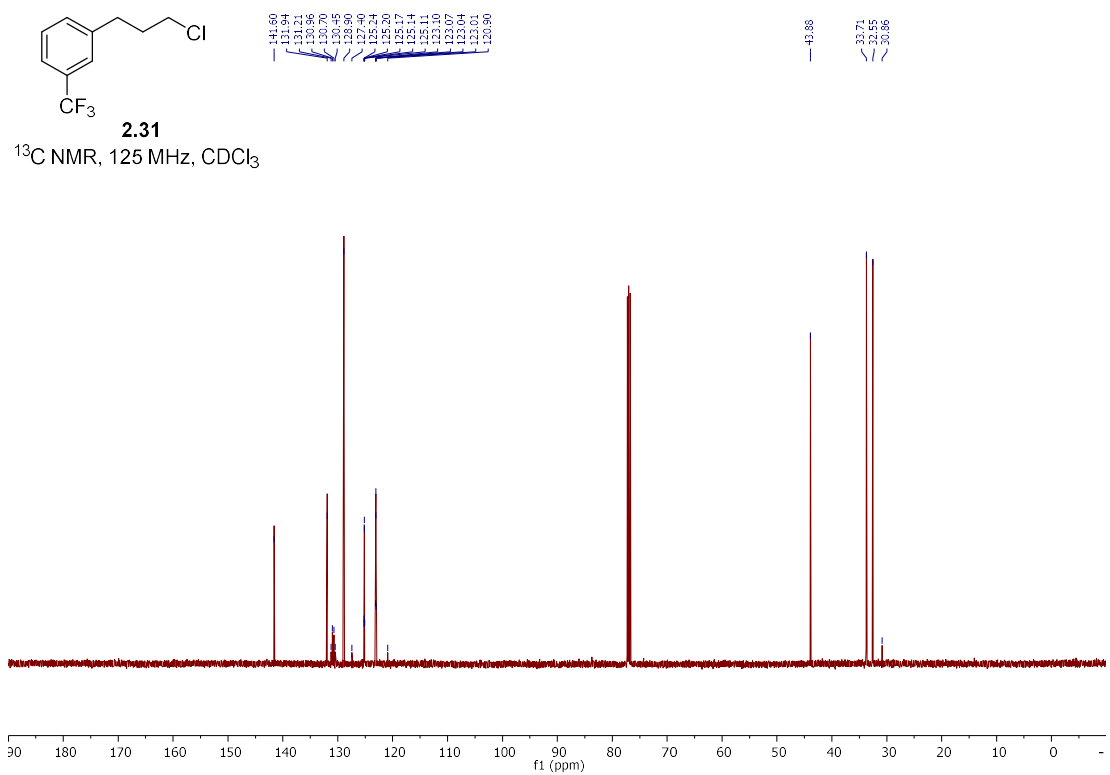


Figure A.1.6. ¹³C NMR spectrum of compound 2.31.

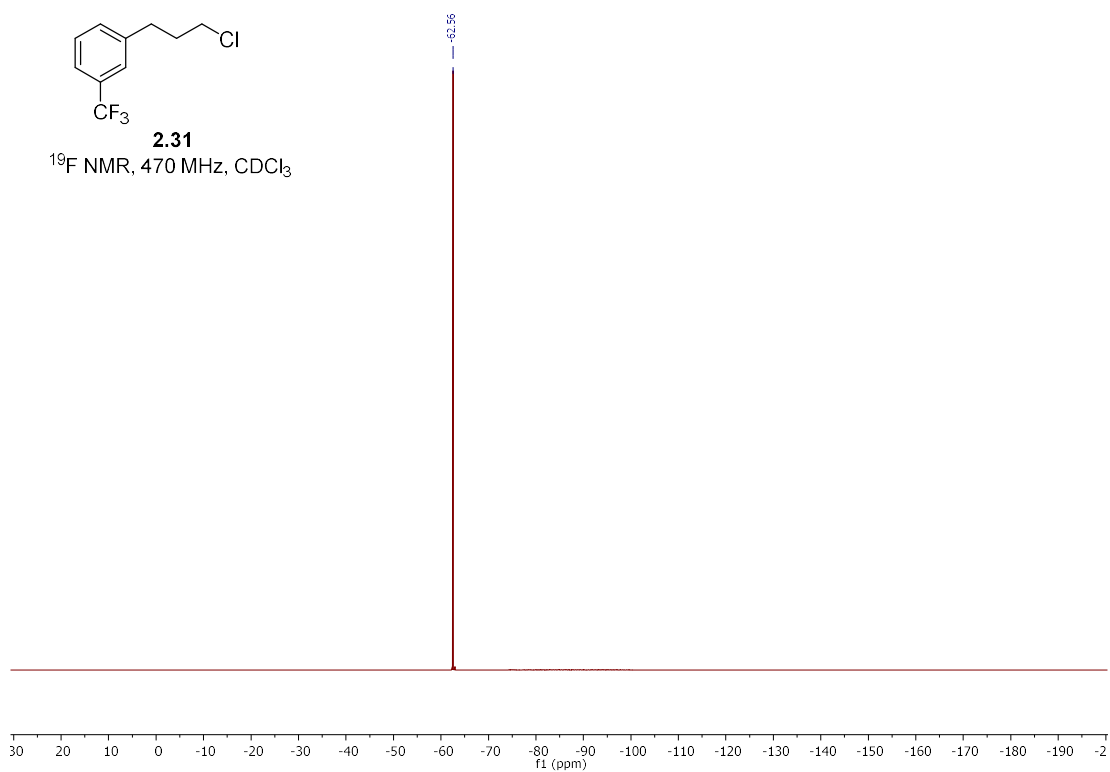


Figure A.1.7. ^{19}F NMR spectrum of compound **2.31**.

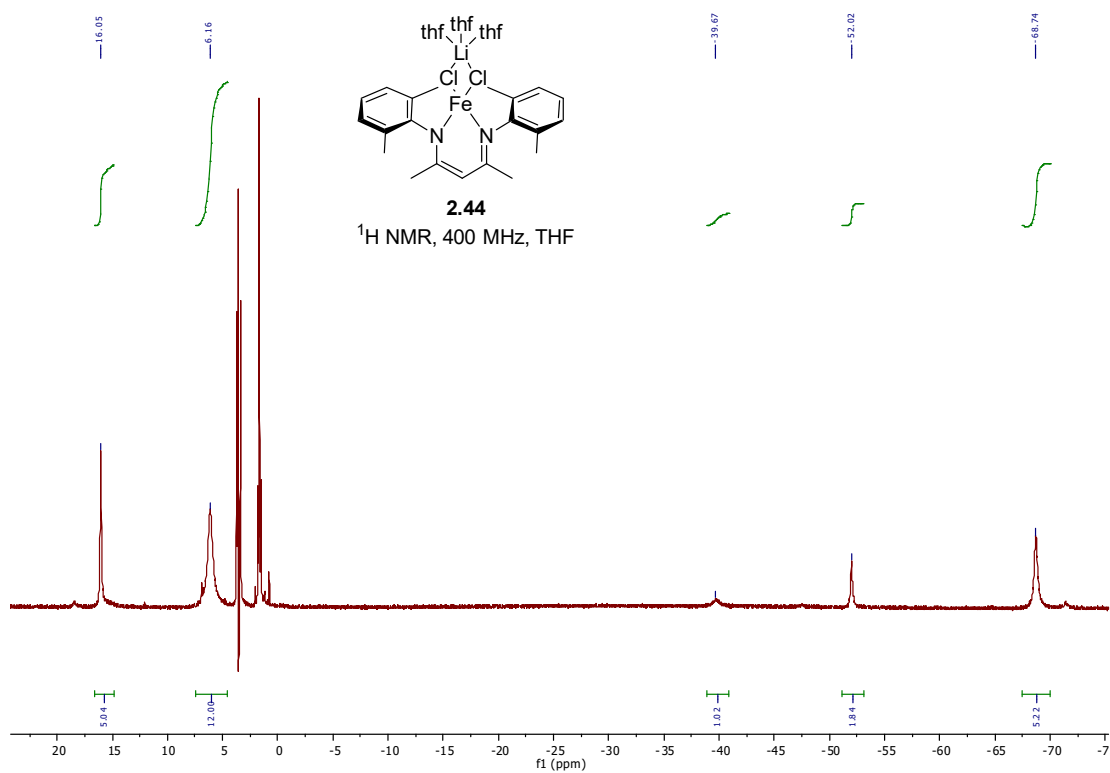


Figure A.1.8. ^1H NMR spectrum of compound **2.44** using solvent suppression for THF peaks.

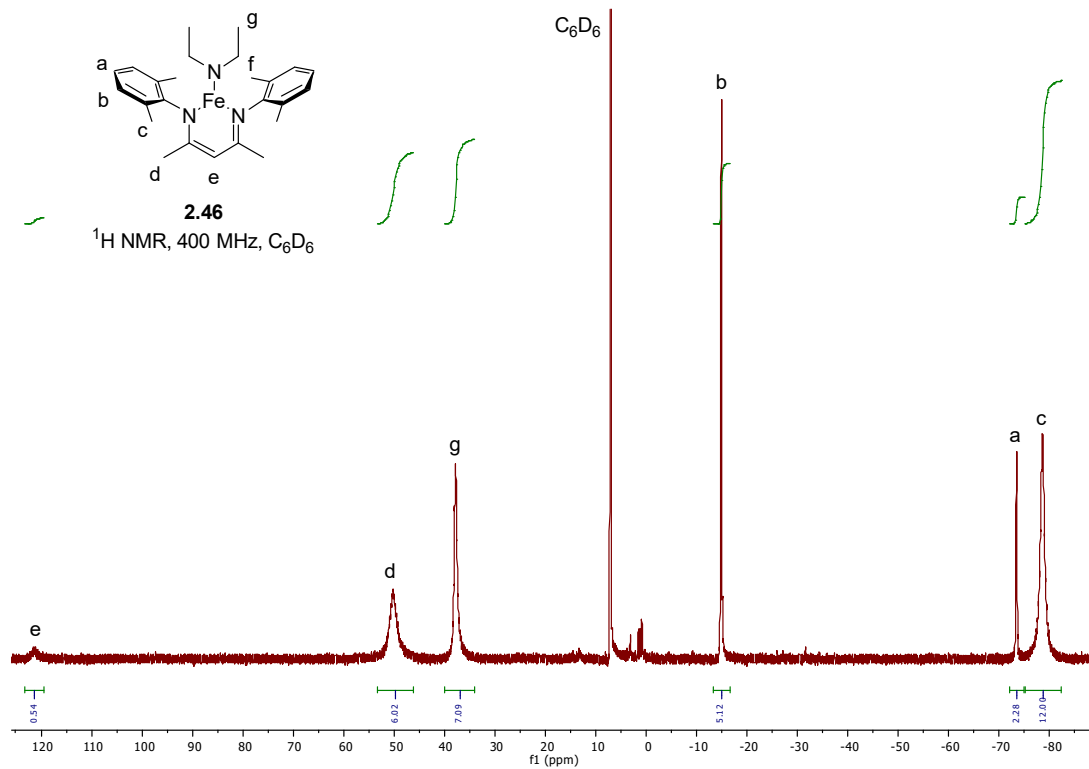


Figure A.1.9. ^1H NMR spectrum of compound **2.46**.

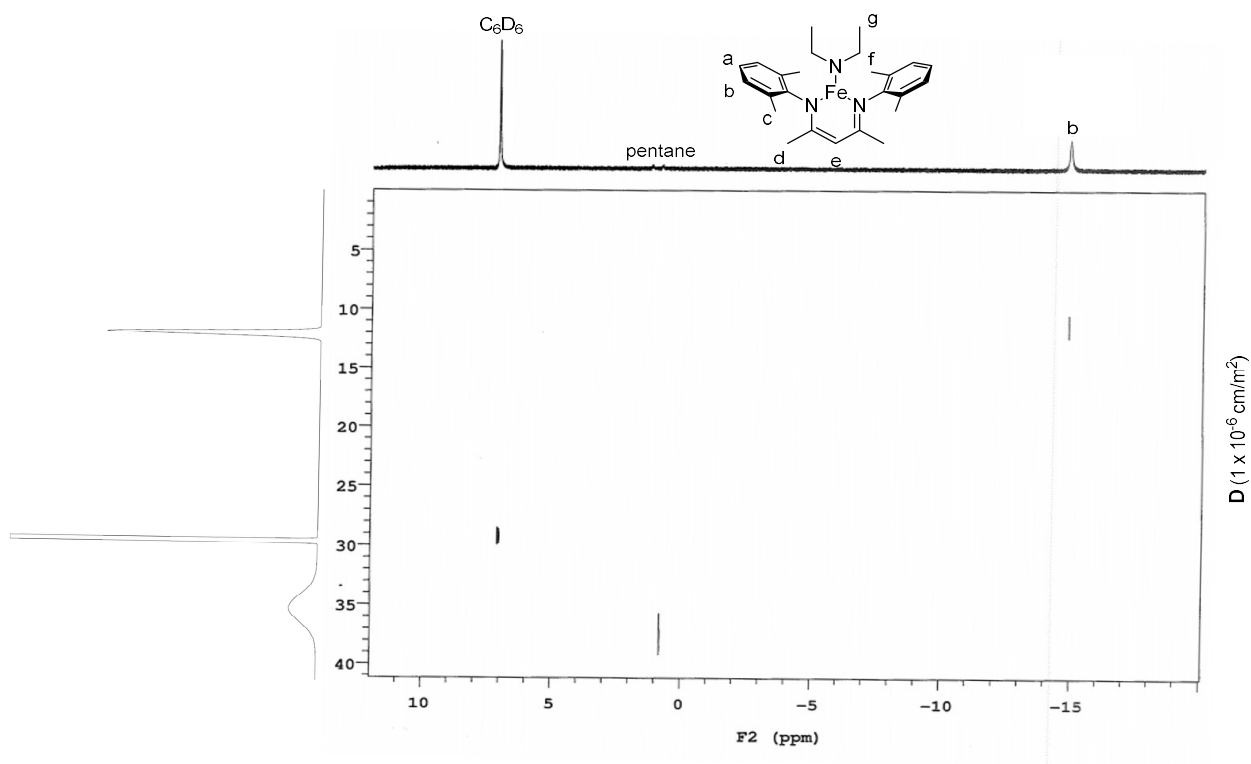


Figure A.1.10. DOSY NMR spectrum of compound **2.46**.

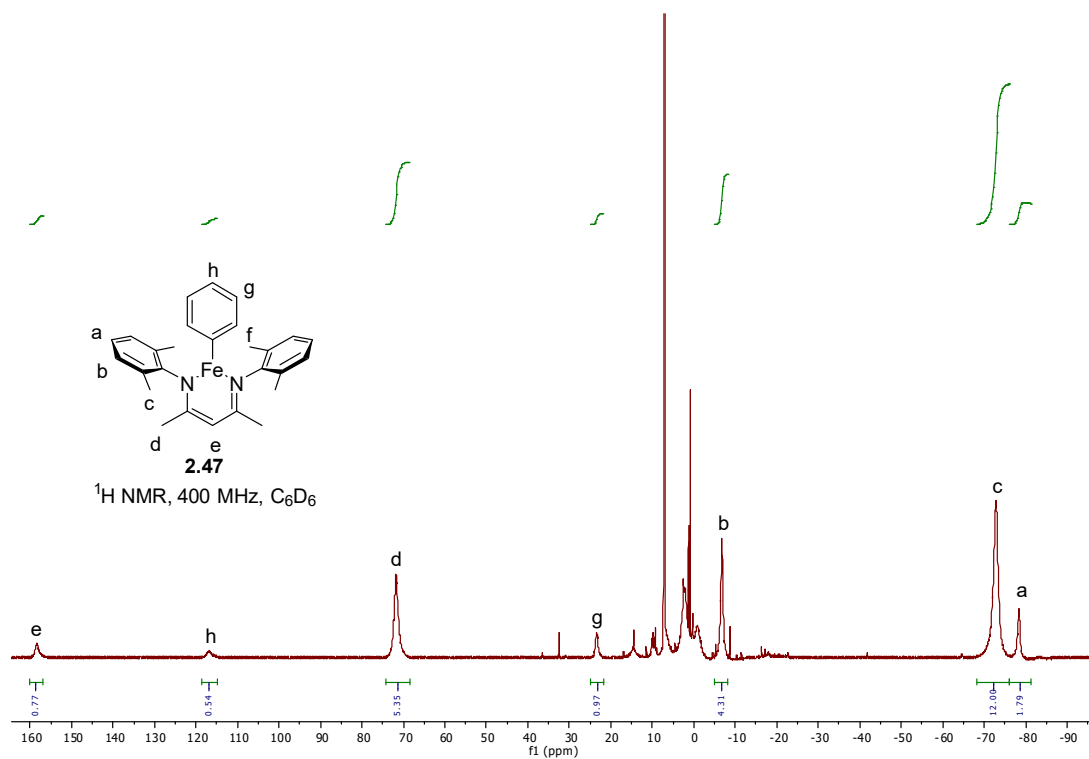


Figure A.1.11. ^1H NMR spectrum of compound **2.47**.

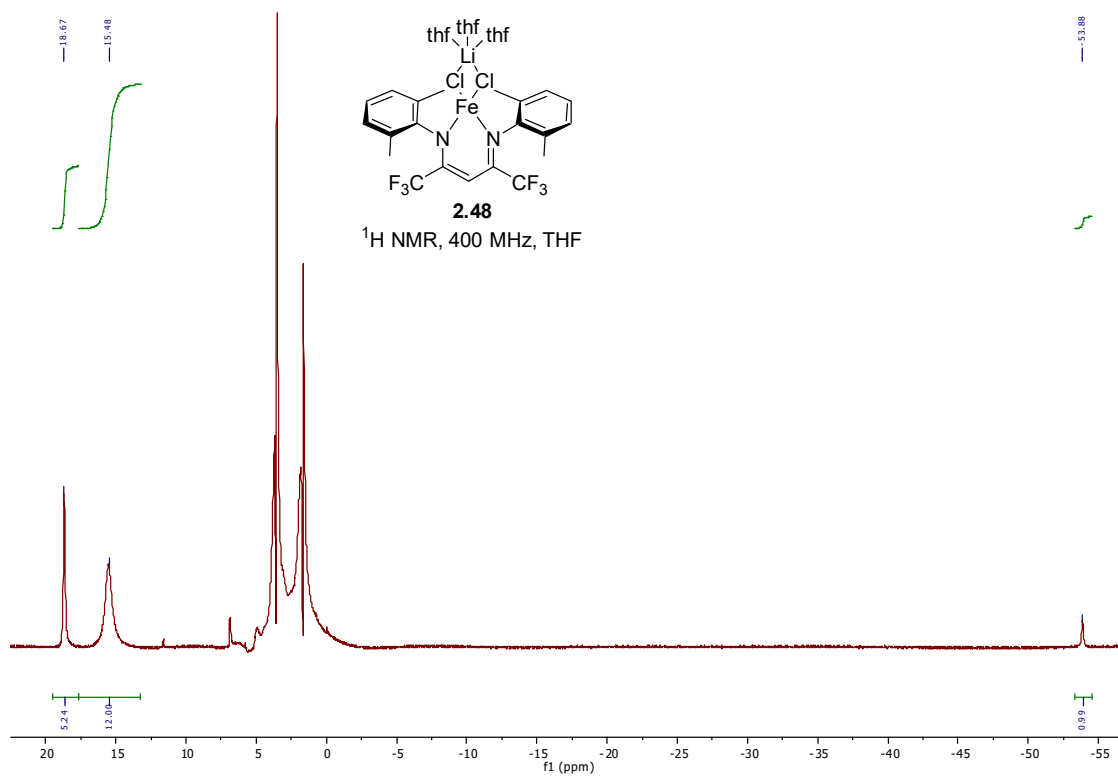


Figure A.1.12. ^1H NMR spectrum of compound **2.48** using solvent suppression for THF peaks.

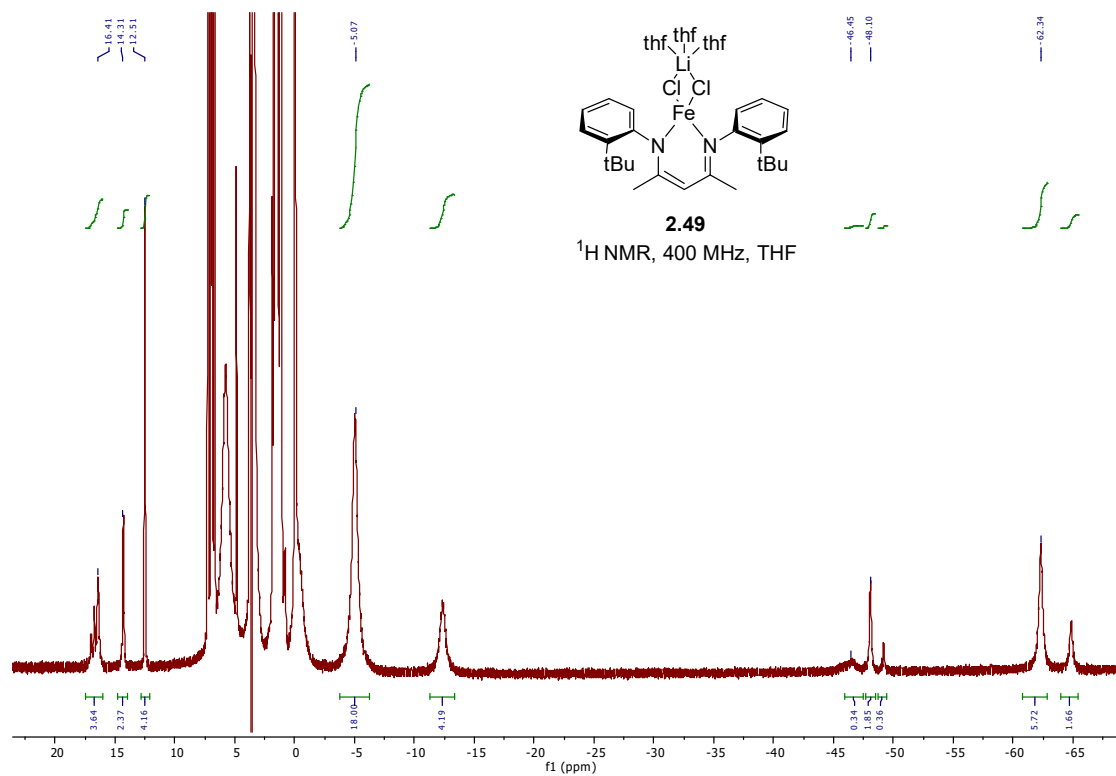


Figure A.1.13. ¹H NMR spectrum of compound **2.49** using solvent suppression for THF peaks.

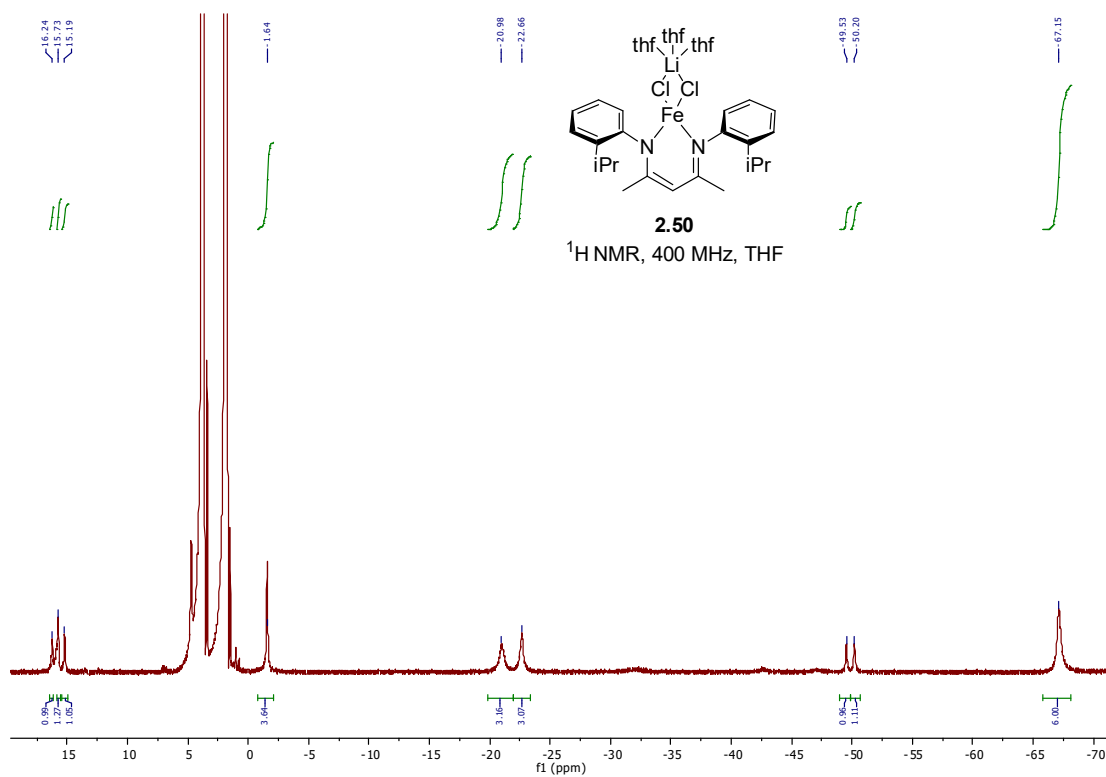


Figure A.1.14. ¹H NMR spectrum of compound **2.50** using solvent suppression for THF peaks.

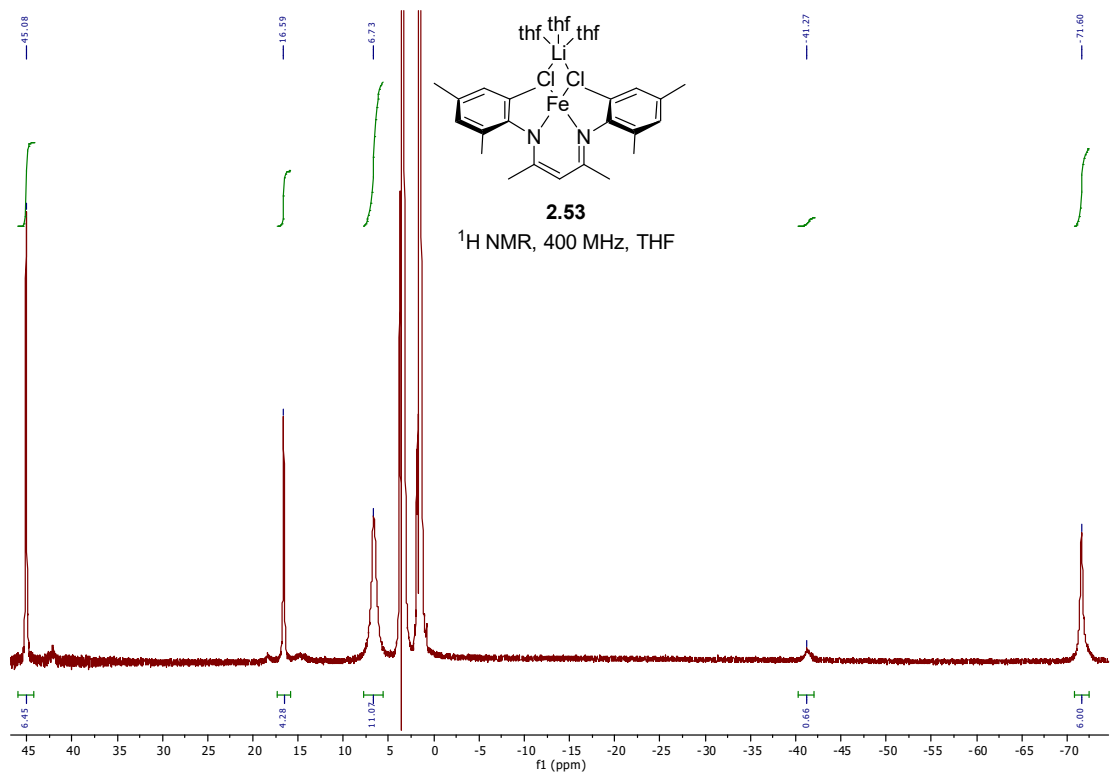


Figure A.1.17. ¹H NMR spectrum of compound **2.53** using solvent suppression for THF peaks.

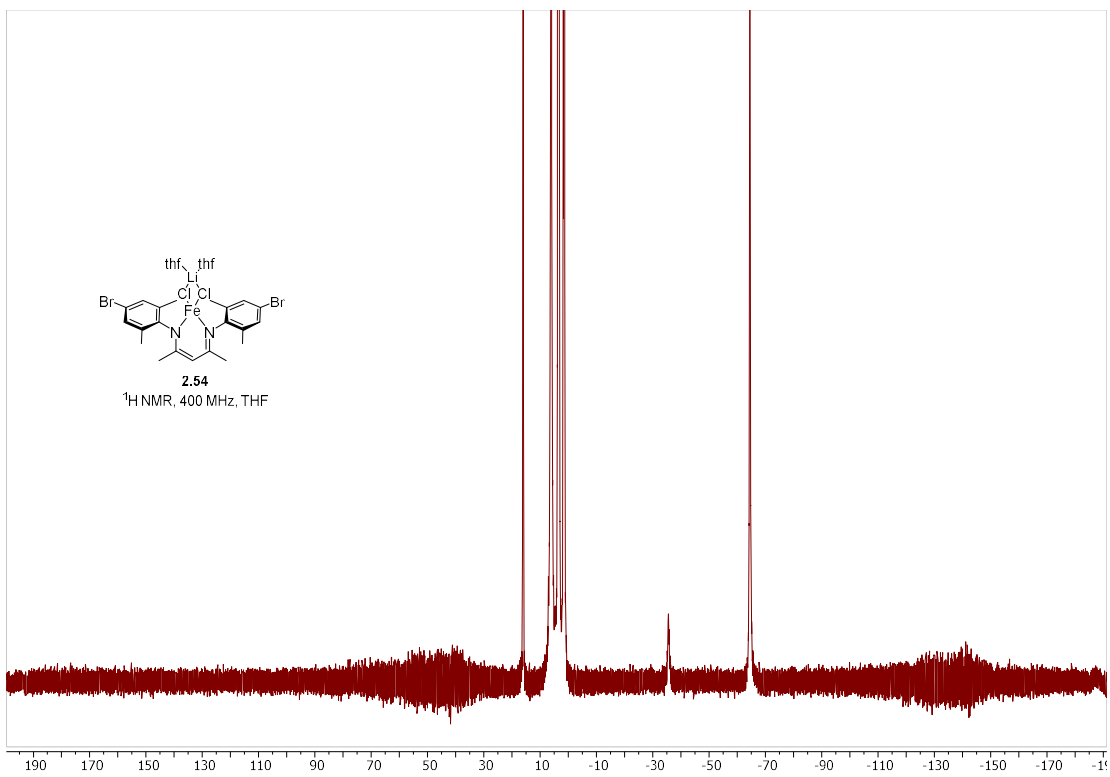


Figure A.1.18. ¹H NMR spectrum of compound **2.54** using solvent suppression for THF peaks.

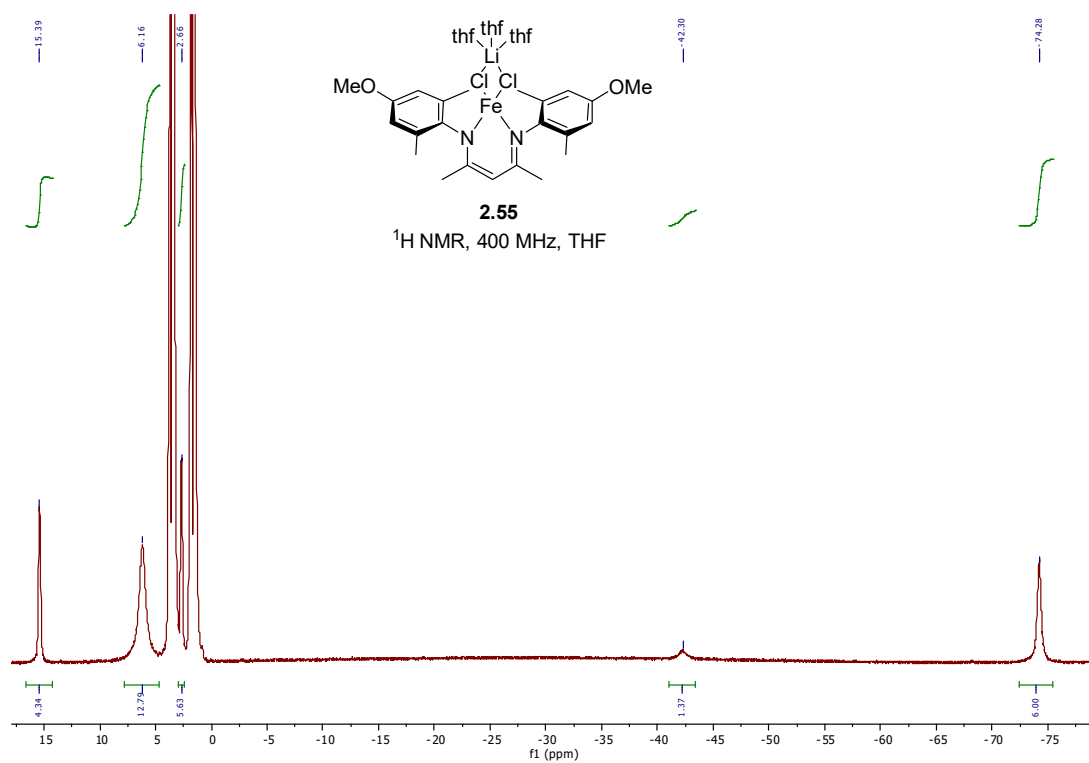


Figure A.1.19. $^1\text{H NMR}$ spectrum of compound **2.55** using solvent suppression for THF peaks.

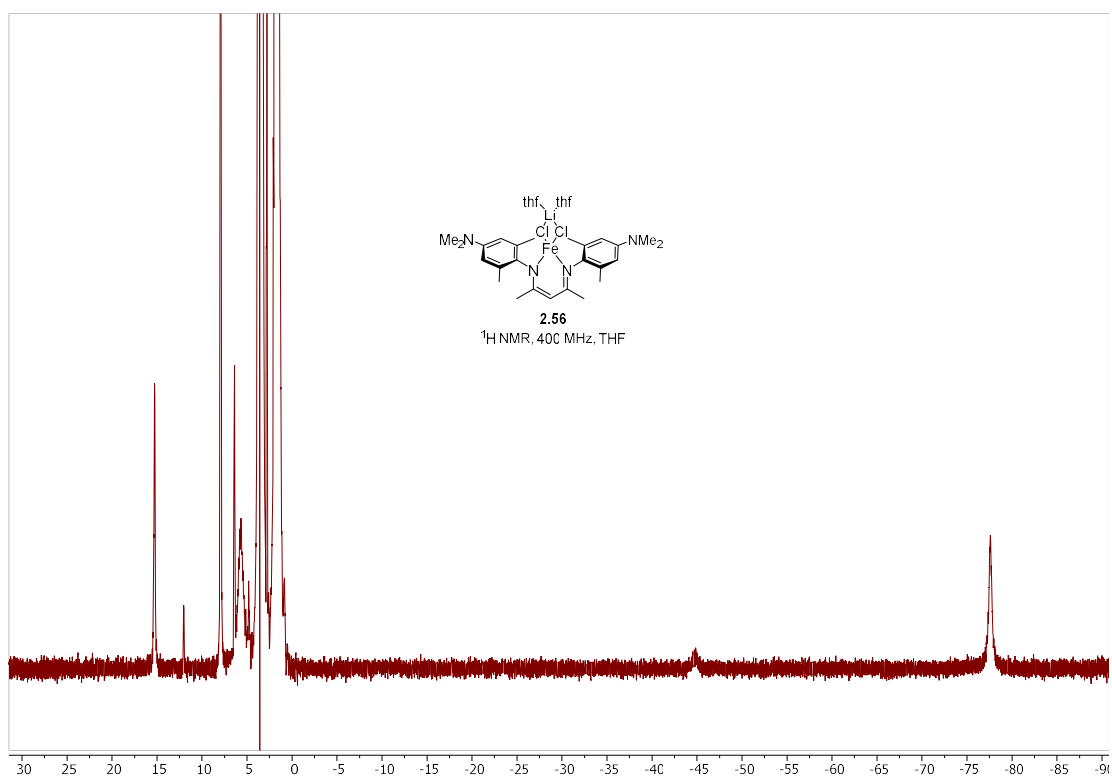


Figure A.1.20. $^1\text{H NMR}$ spectrum of compound **2.56** using solvent suppression for THF peaks.

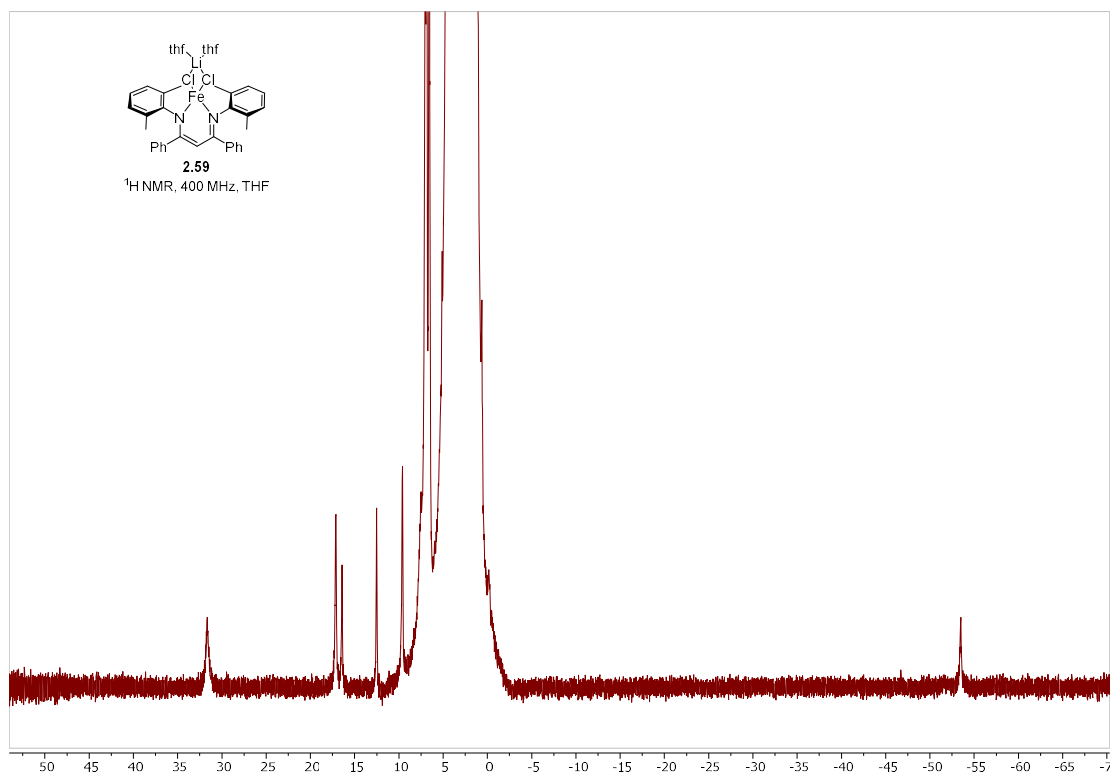


Figure A.1.21. ¹H NMR spectrum of compound **2.59** using solvent suppression for THF peaks.

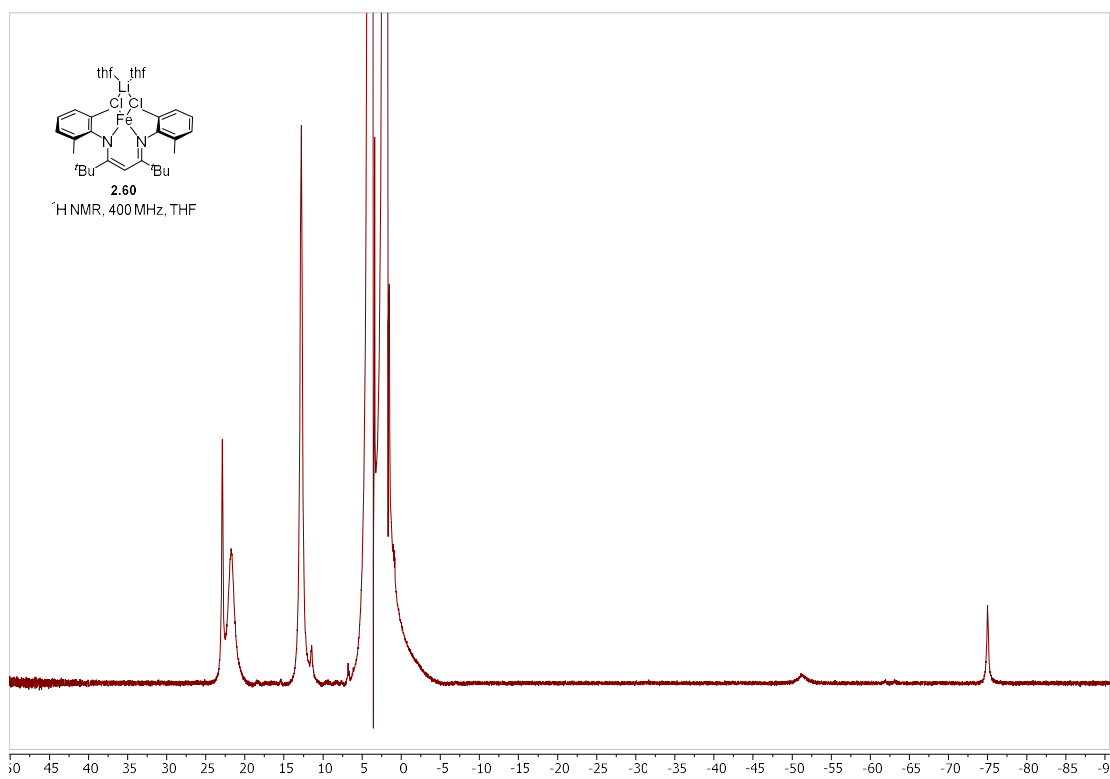


Figure A.1.22. ¹H NMR spectrum of compound **2.60** using solvent suppression for THF peaks.

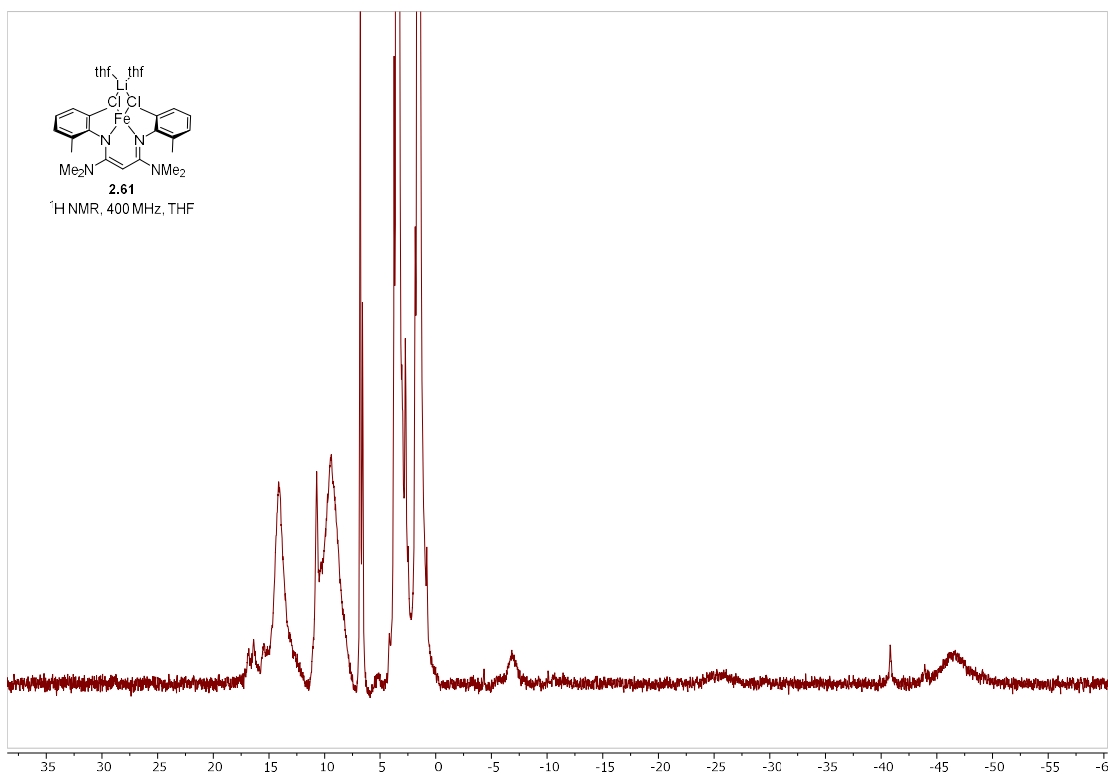


Figure A.1.23. ¹H NMR spectrum of compound **2.61** using solvent suppression for THF peaks.

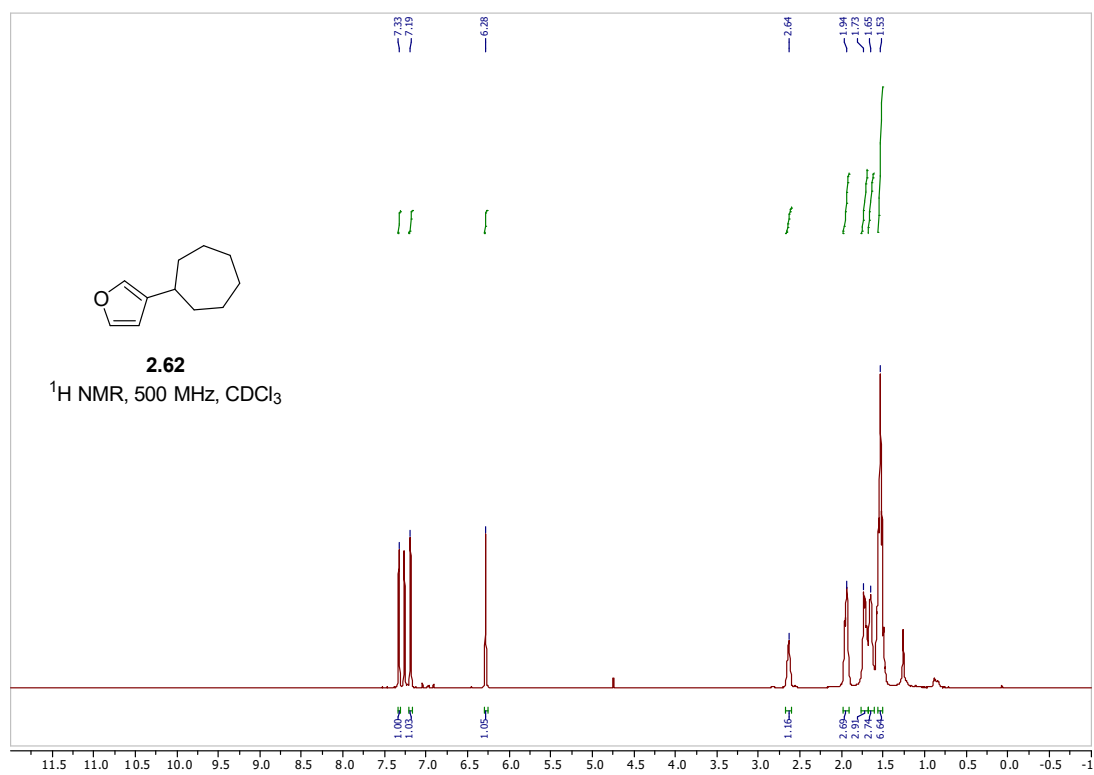


Figure A.1.24. ¹H NMR spectrum of compound **2.62**.

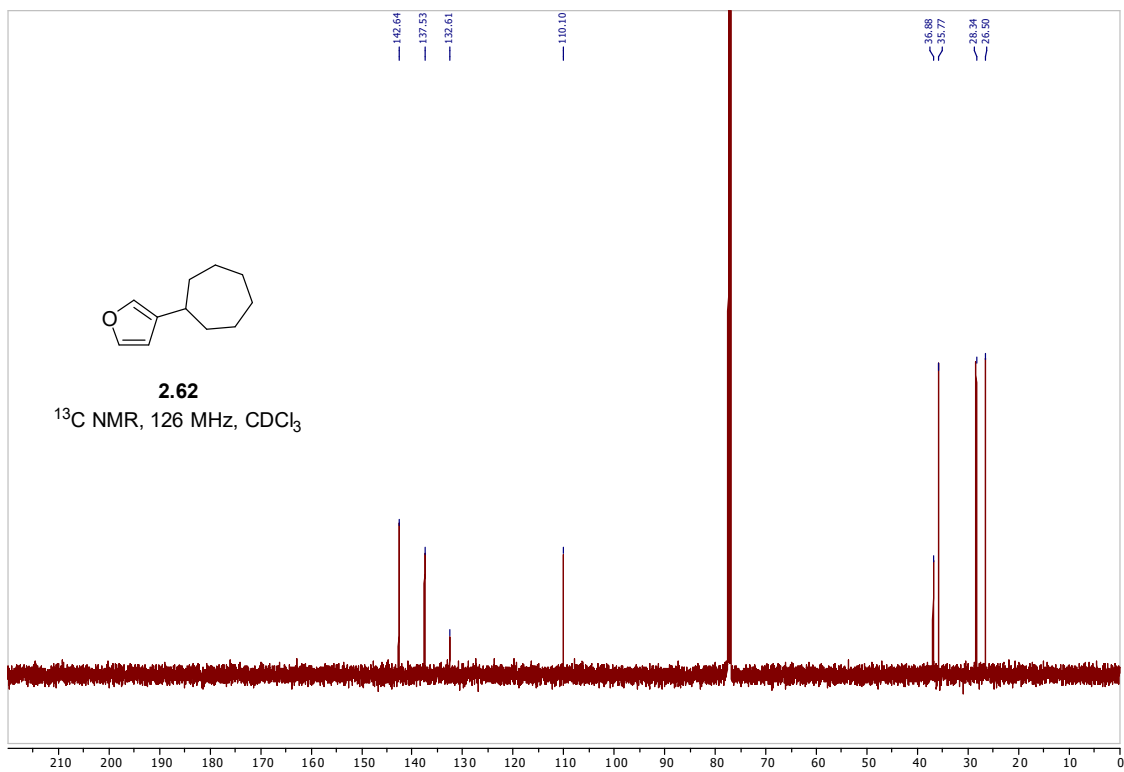


Figure A.1.25. ^{13}C NMR spectrum of compound **2.62**.

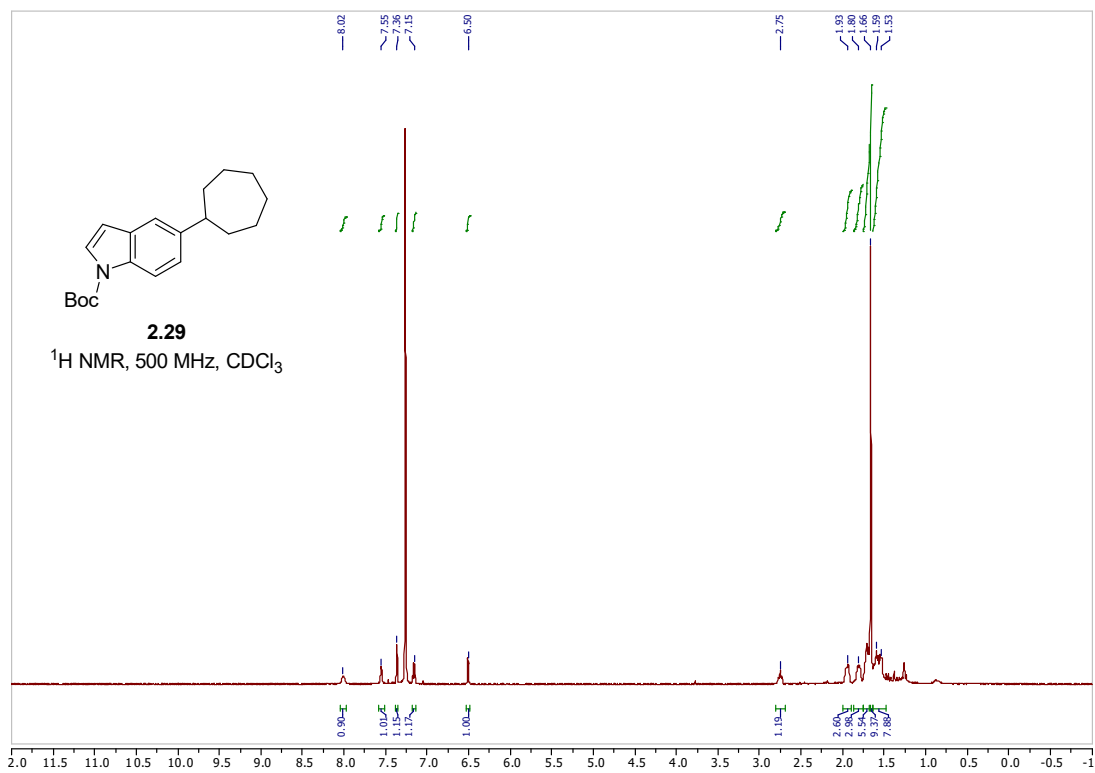


Figure A.1.26. ^1H NMR spectrum of compound **2.29**.

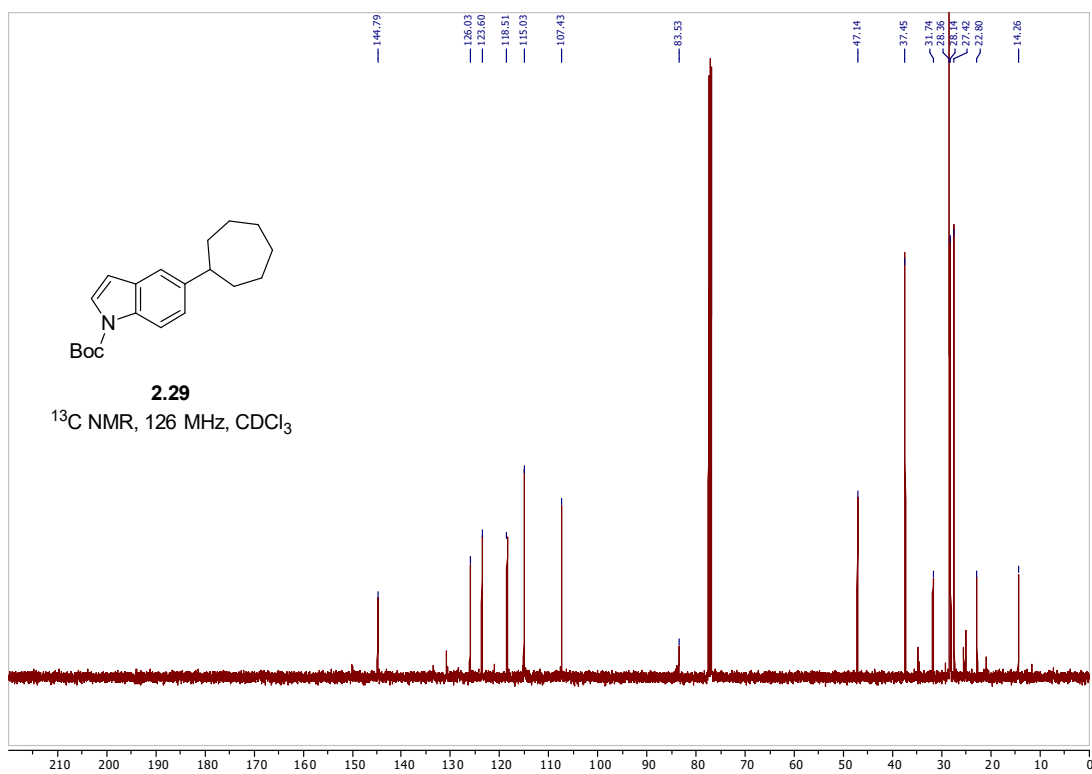


Figure A.1.27. ^{13}C NMR spectrum of compound 2.29.

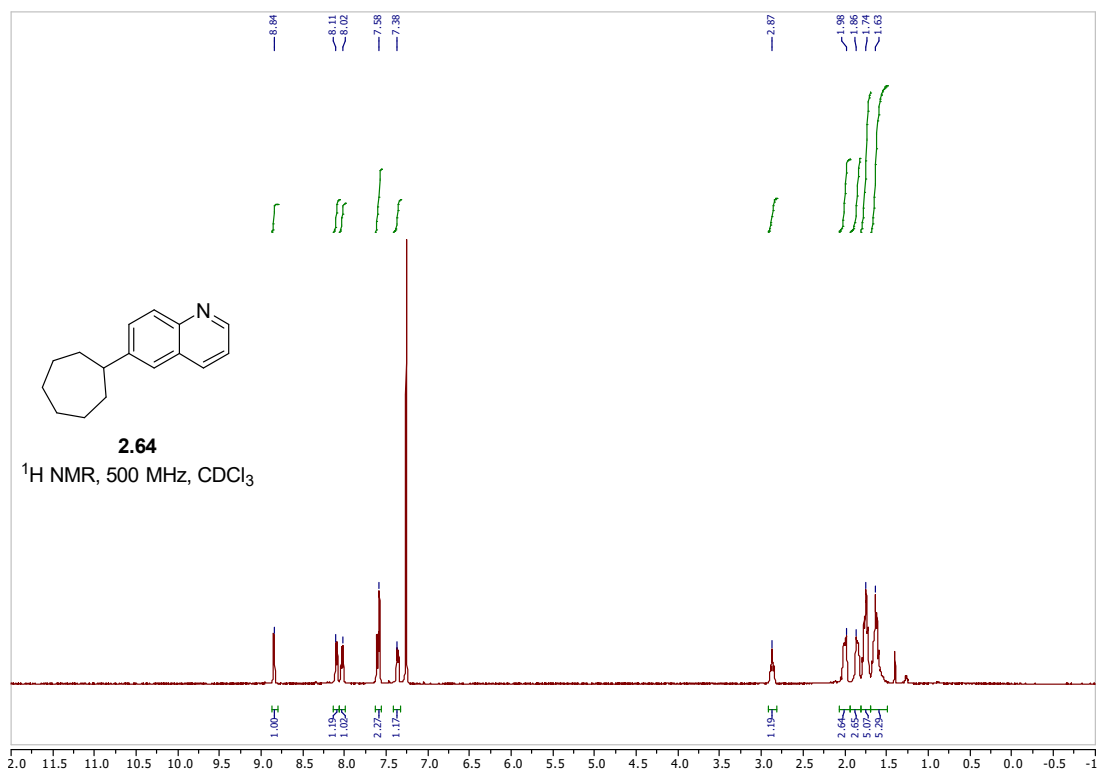


Figure A.1.28. ^1H NMR spectrum of compound 2.64.

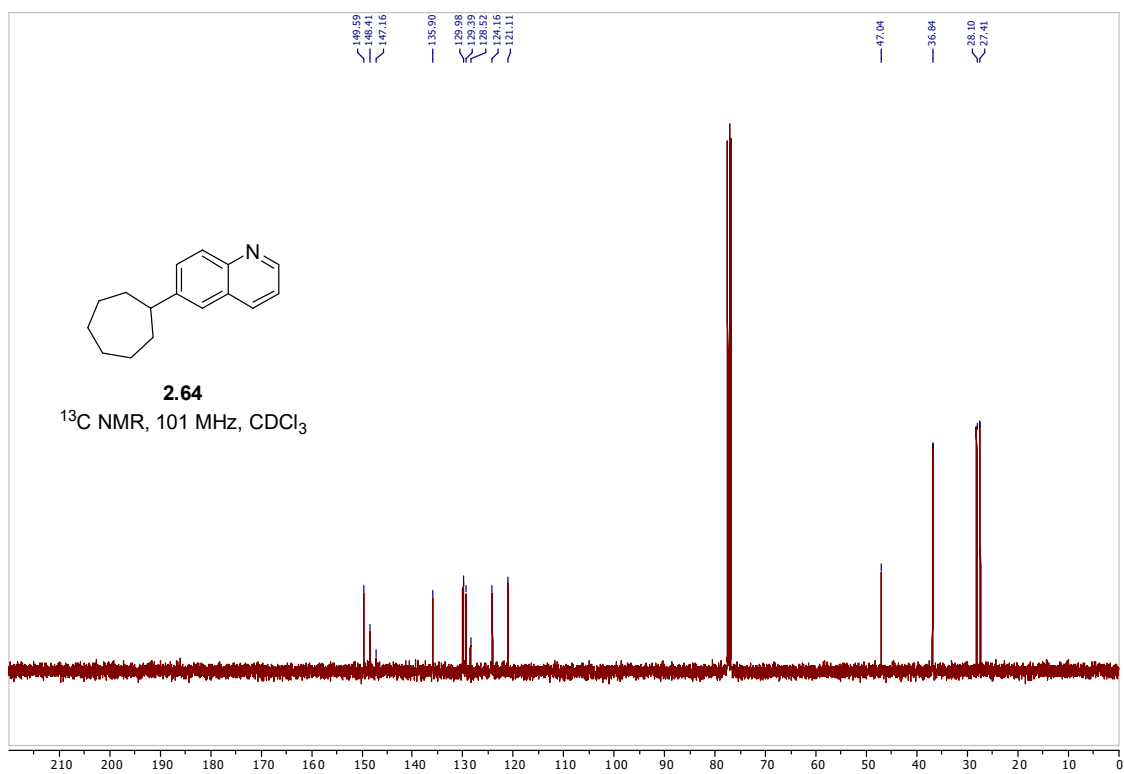


Figure A.1.29. ^{13}C NMR spectrum of compound 2.64.

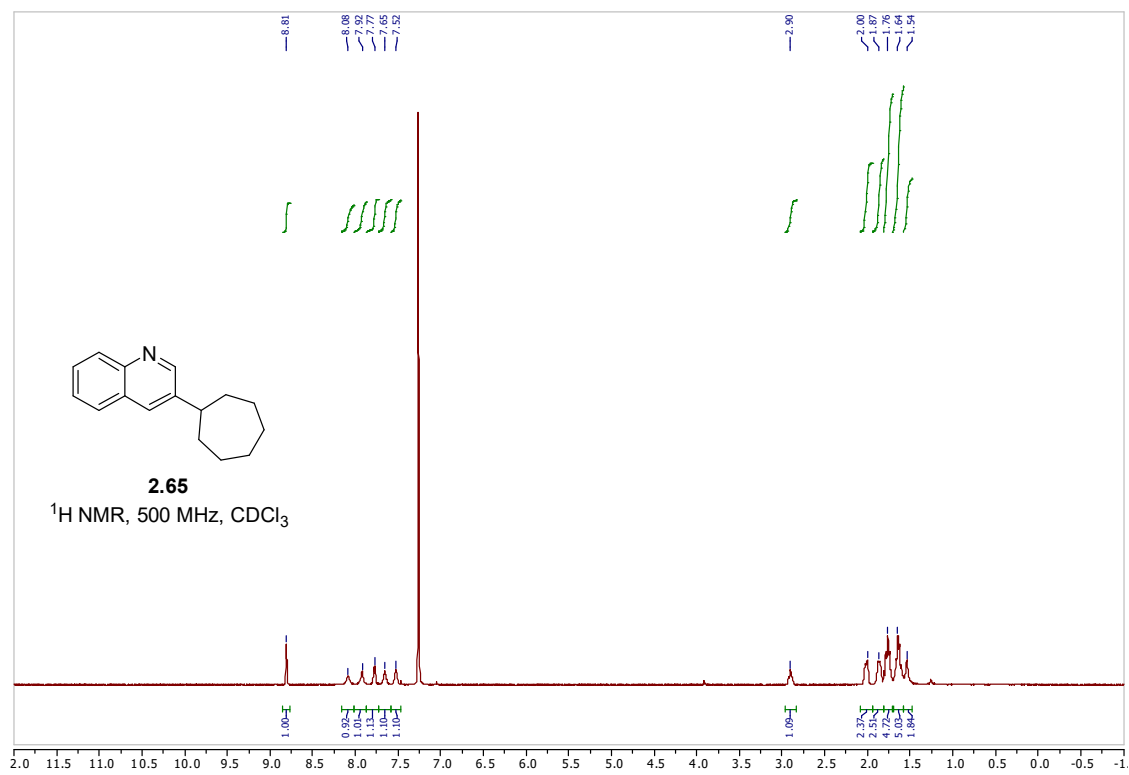


Figure A.1.30. ^1H NMR spectrum of compound 2.65.

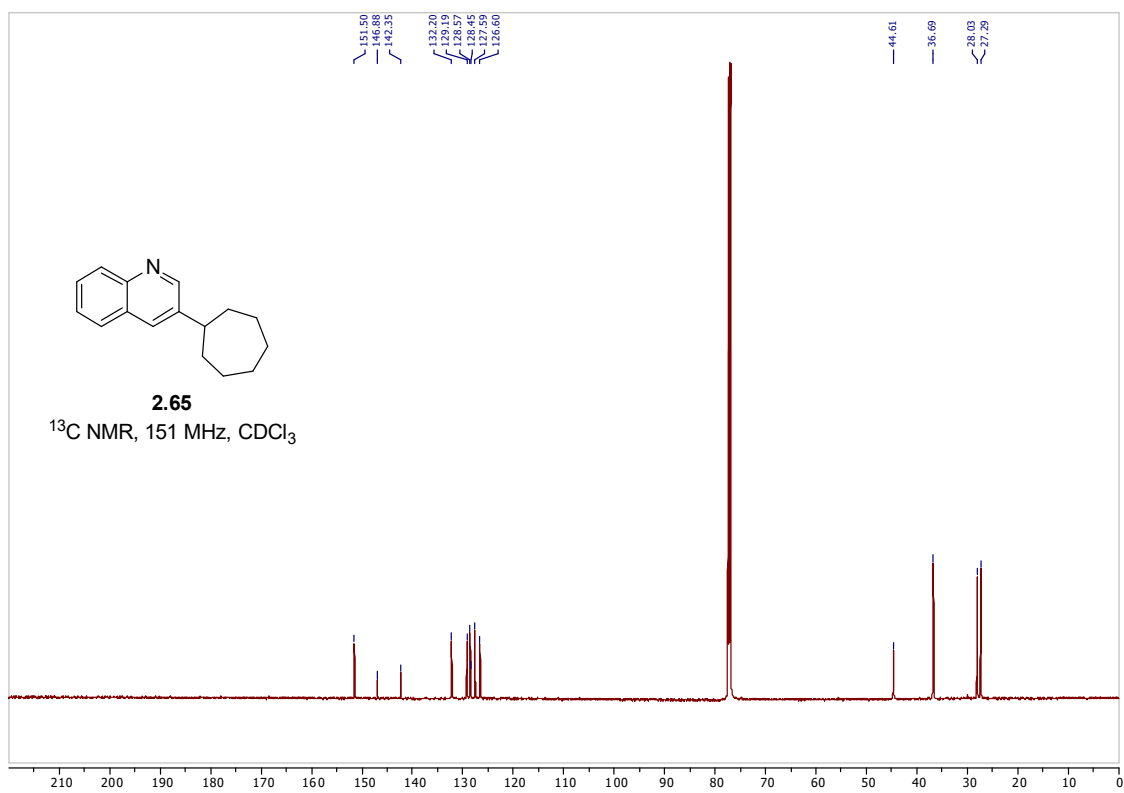


Figure A.1.31. ^{13}C NMR spectrum of compound **2.65**.

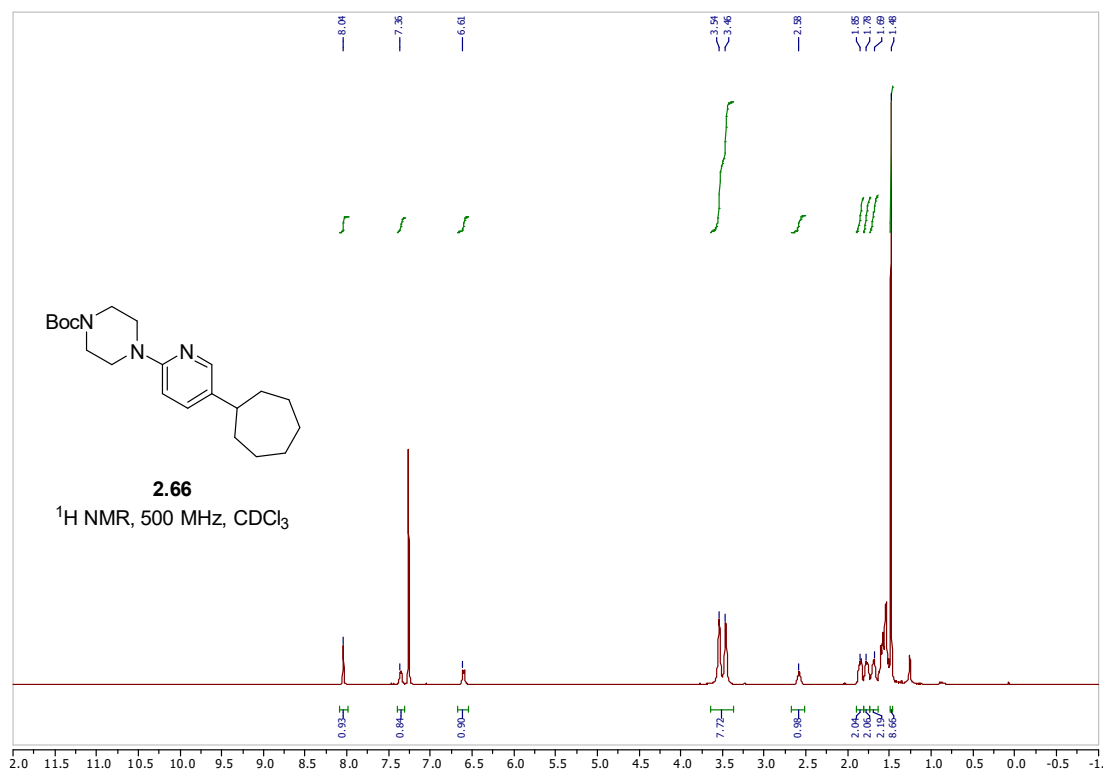


Figure A.1.32. ^1H NMR spectrum of compound **2.66**.

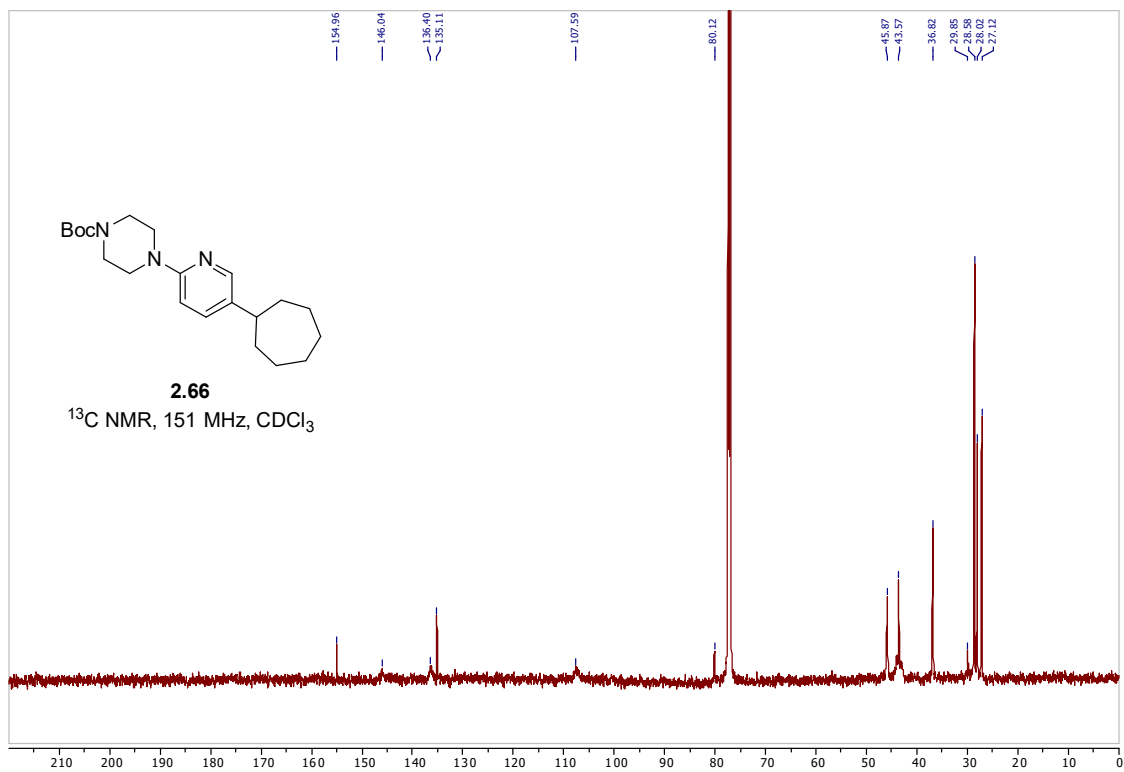


Figure A.1.33. ^{13}C NMR spectrum of compound **2.66**.

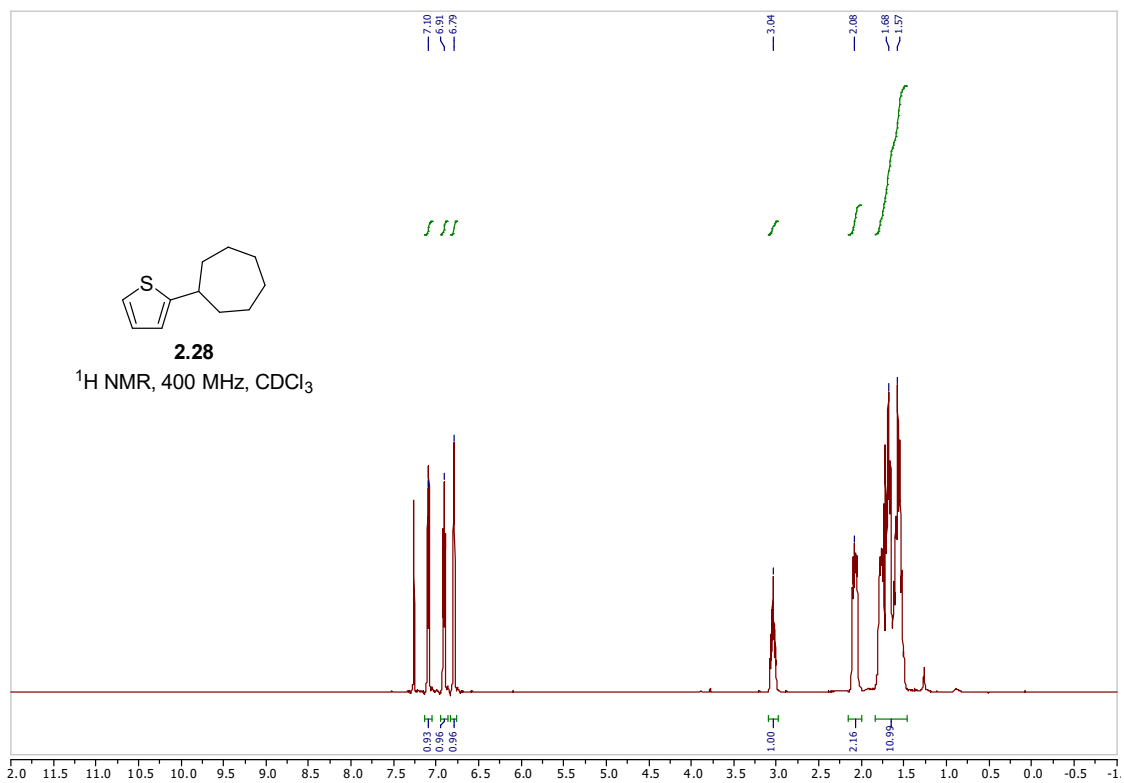


Figure A.1.34. ^1H NMR spectrum of compound **2.28**.

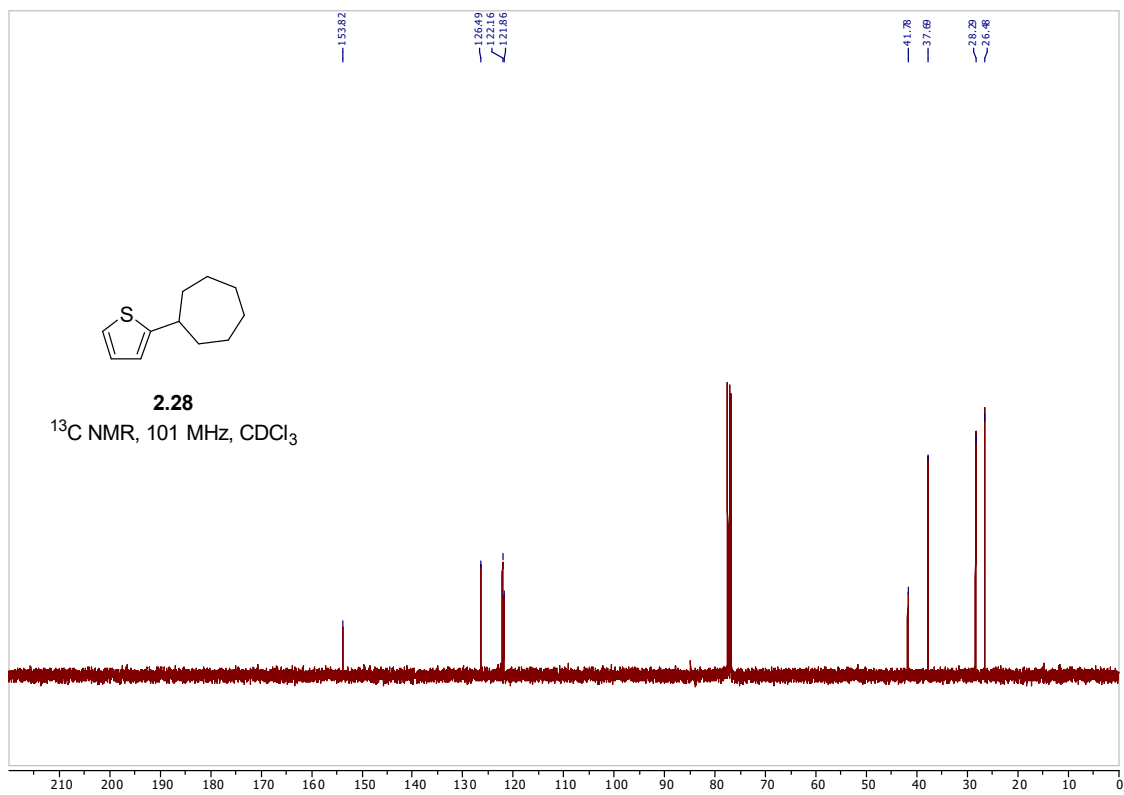


Figure A.1.35. ^{13}C NMR spectrum of compound 2.28.

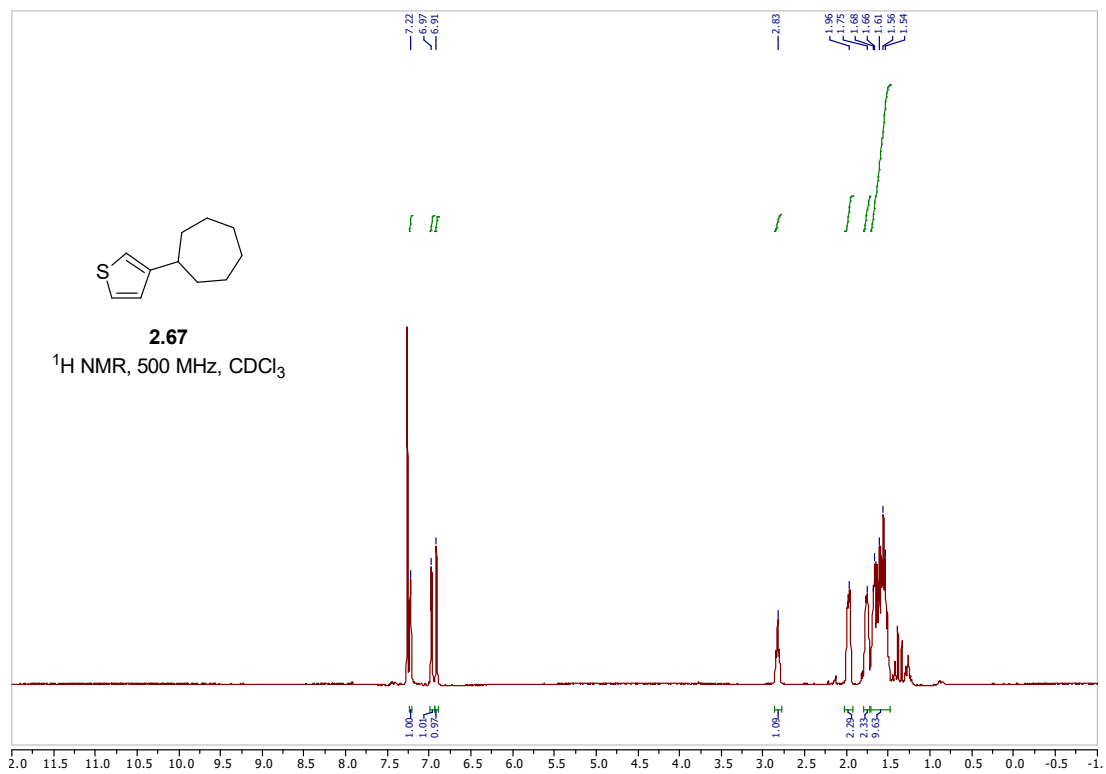


Figure A.1.36. ^1H NMR spectrum of compound 2.67.

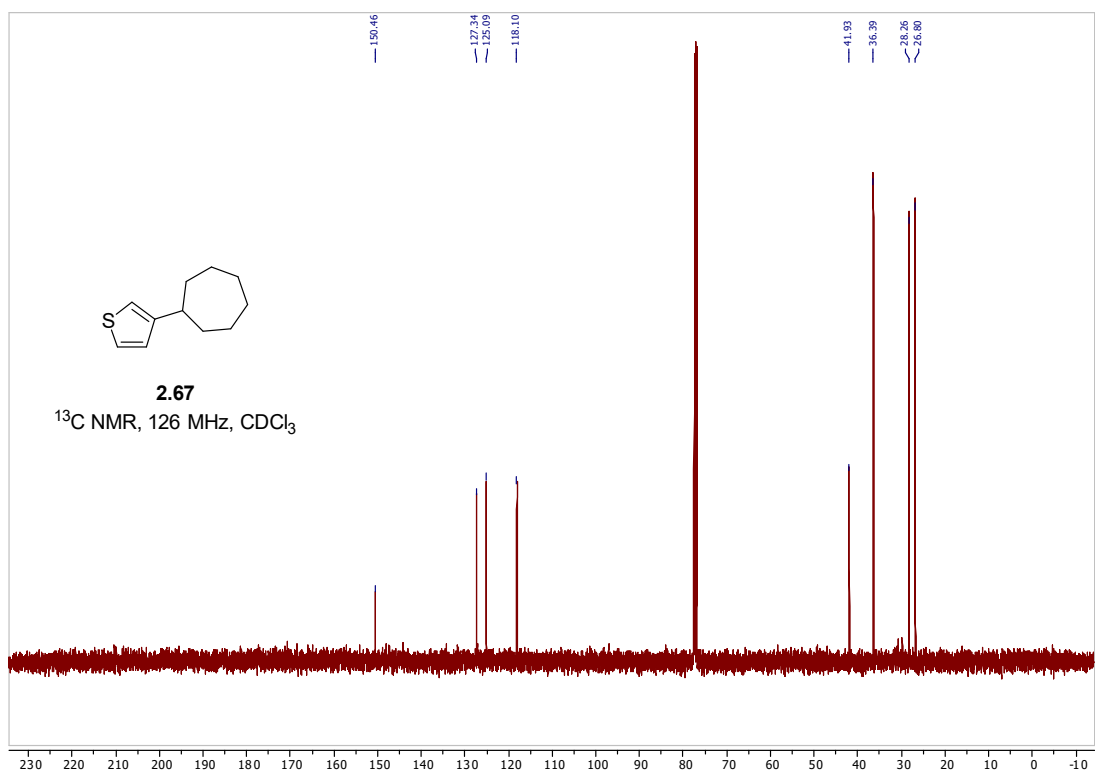


Figure A.1.37. ^{13}C NMR spectrum of compound **2.67**.

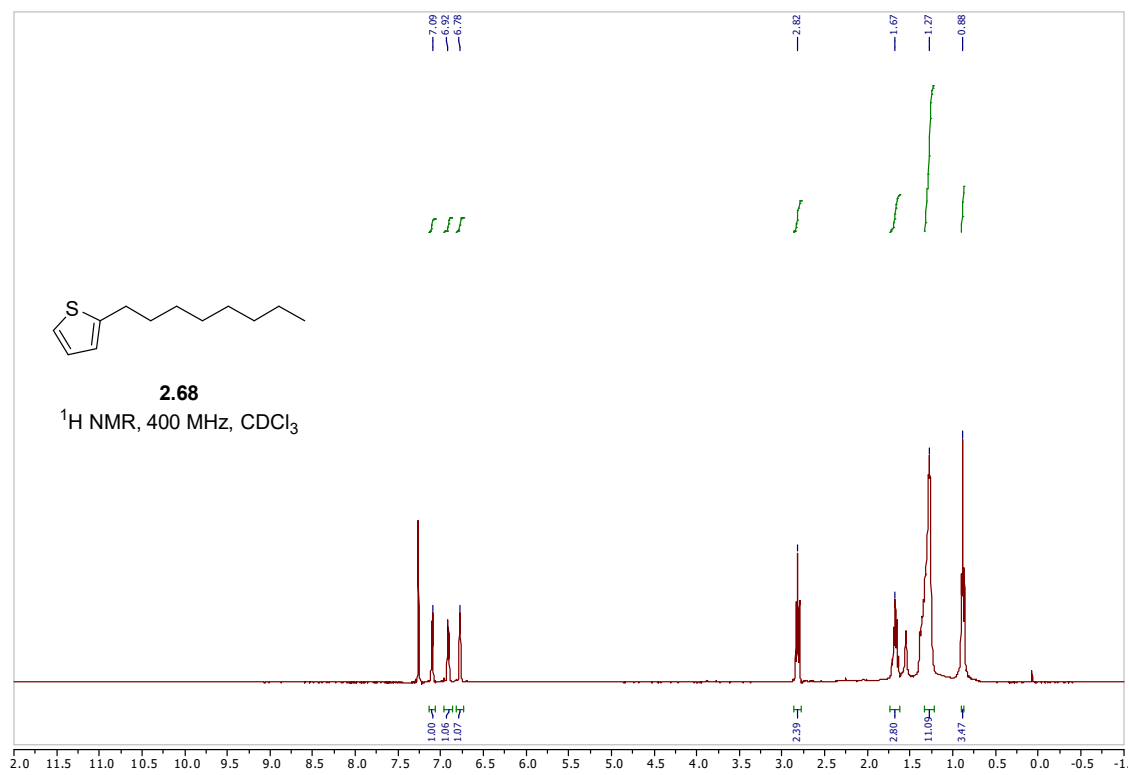


Figure A.1.38. ^1H NMR spectrum of compound **2.68**.

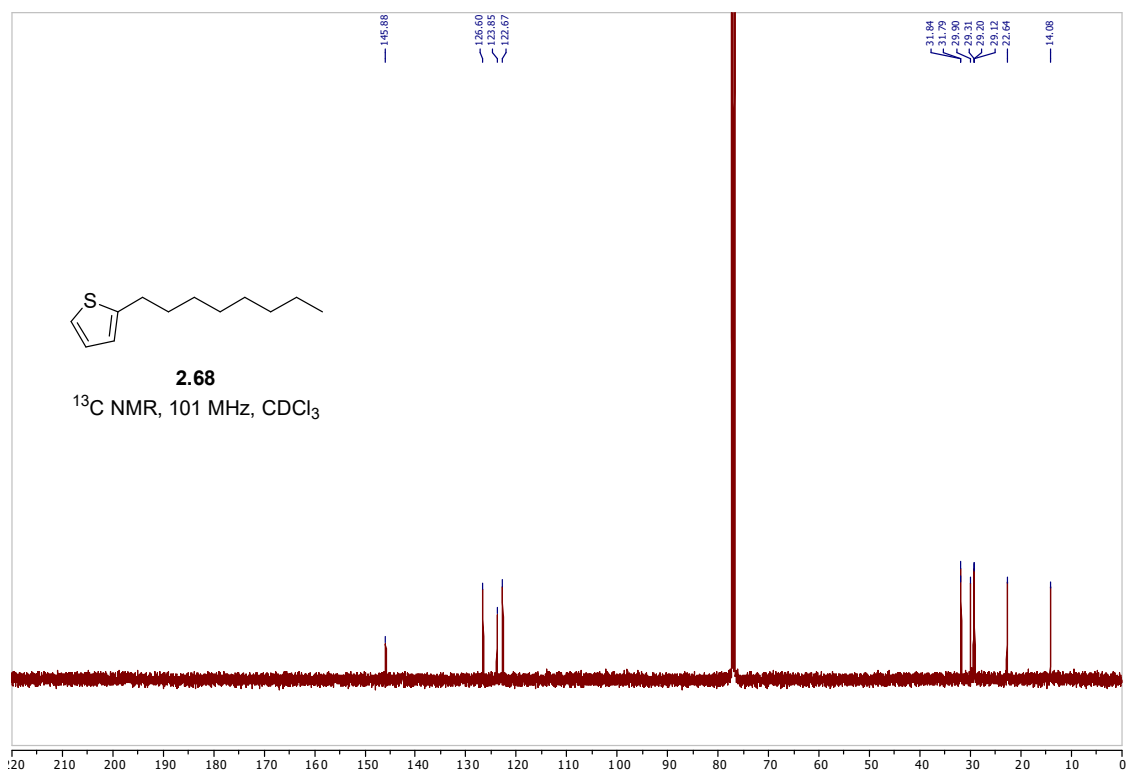


Figure A.1.39. ^{13}C NMR spectrum of compound 2.68.

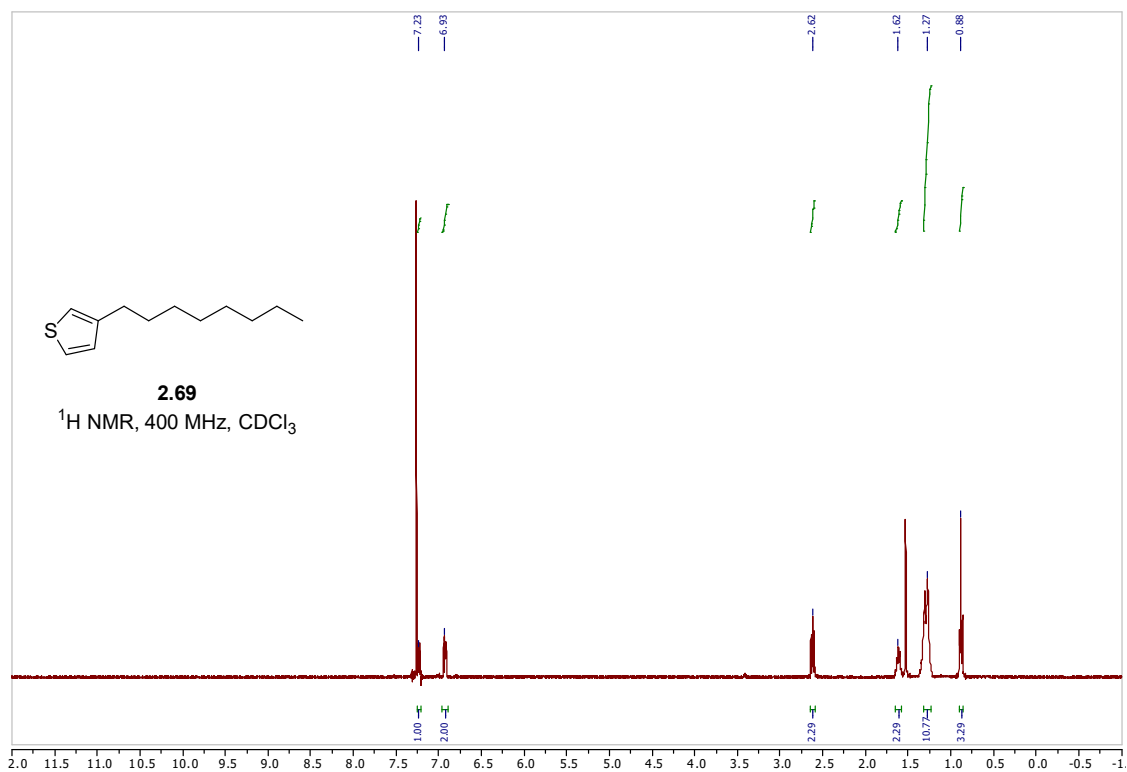


Figure A.1.40. ^1H NMR spectrum of compound 2.69.

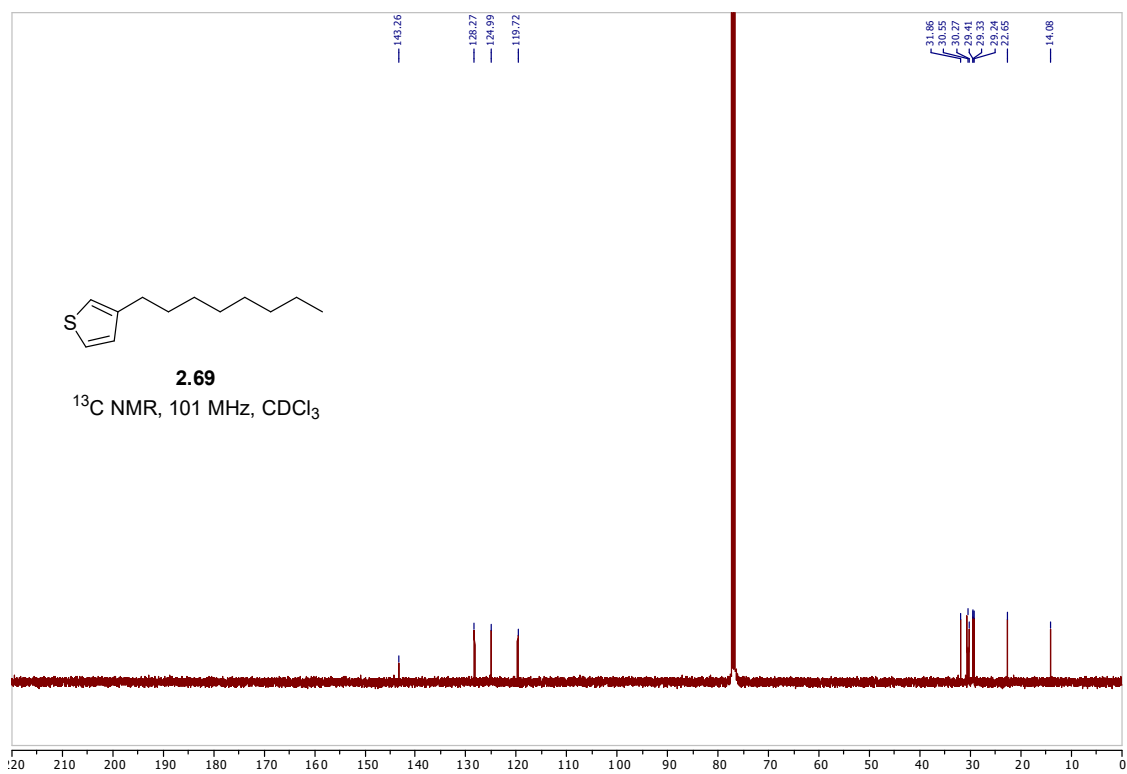


Figure A.1.41. ^{13}C NMR spectrum of compound 2.69.

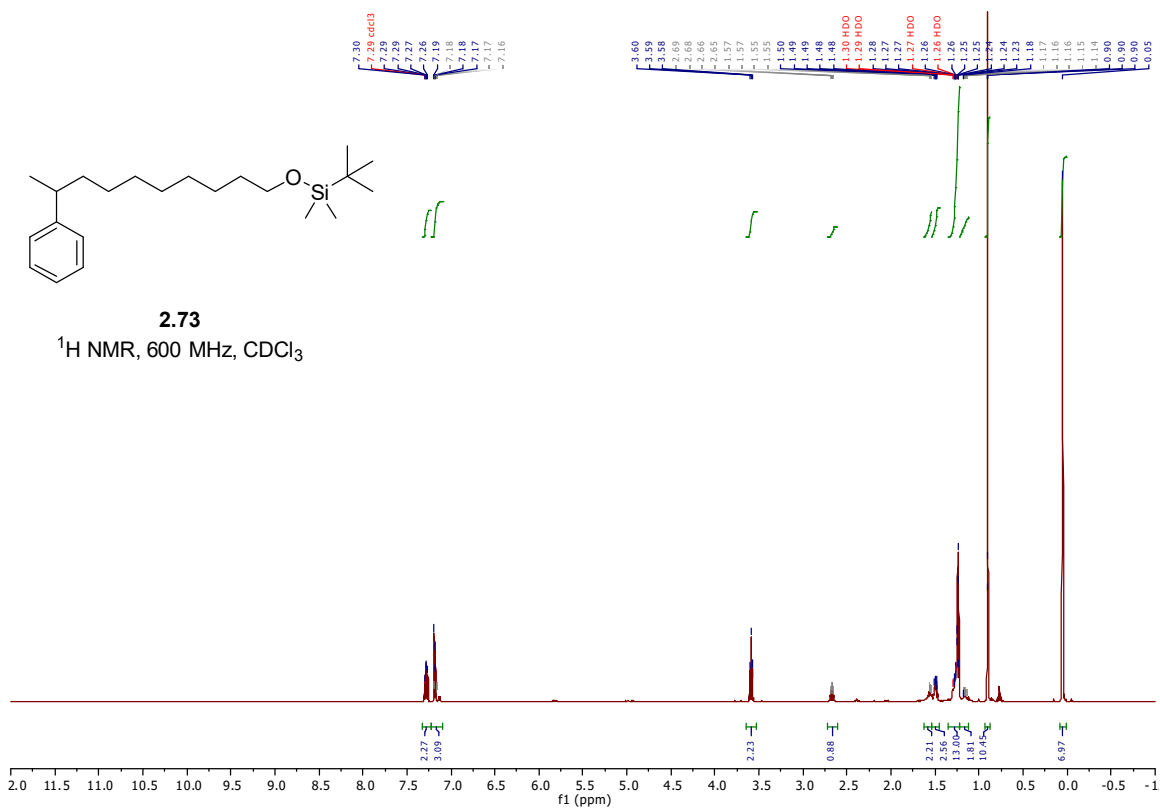


Figure A.1.42. ^1H NMR spectrum of compound 2.73.

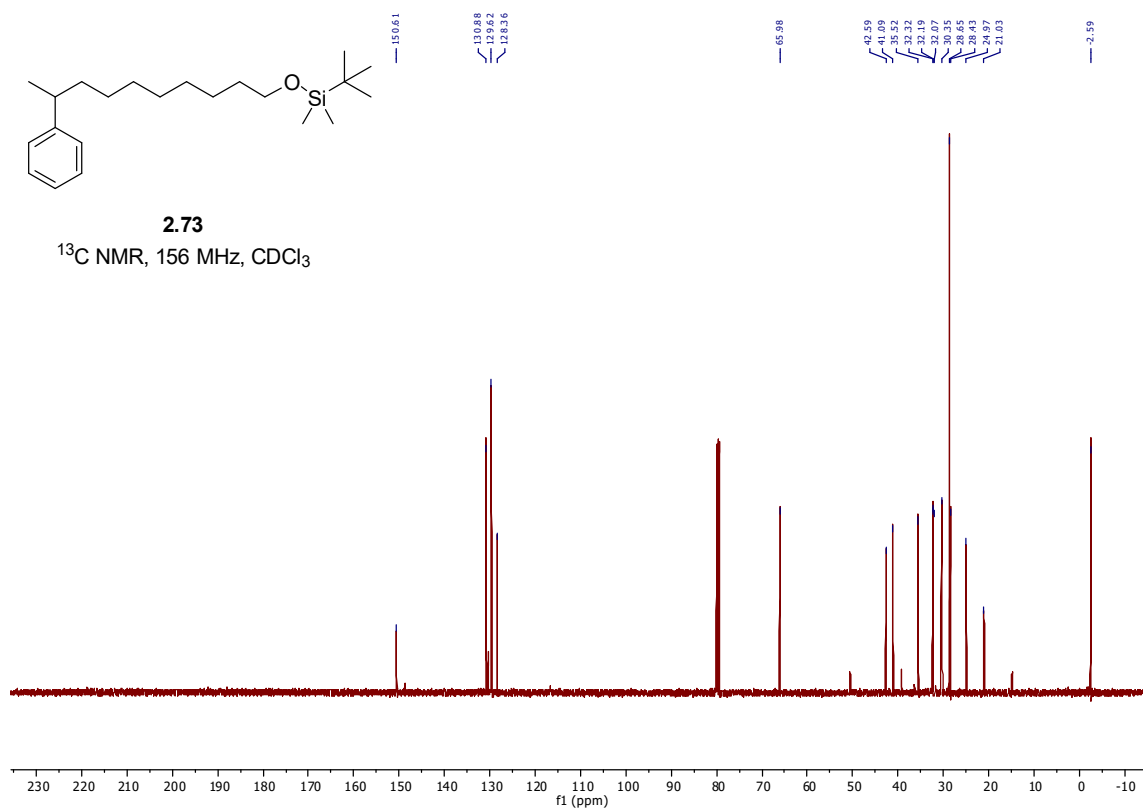


Figure A.1.43. ¹³C NMR spectrum of compound **2.73**.

A.2 Nuclear magnetic resonance spectral data from Chapter 3

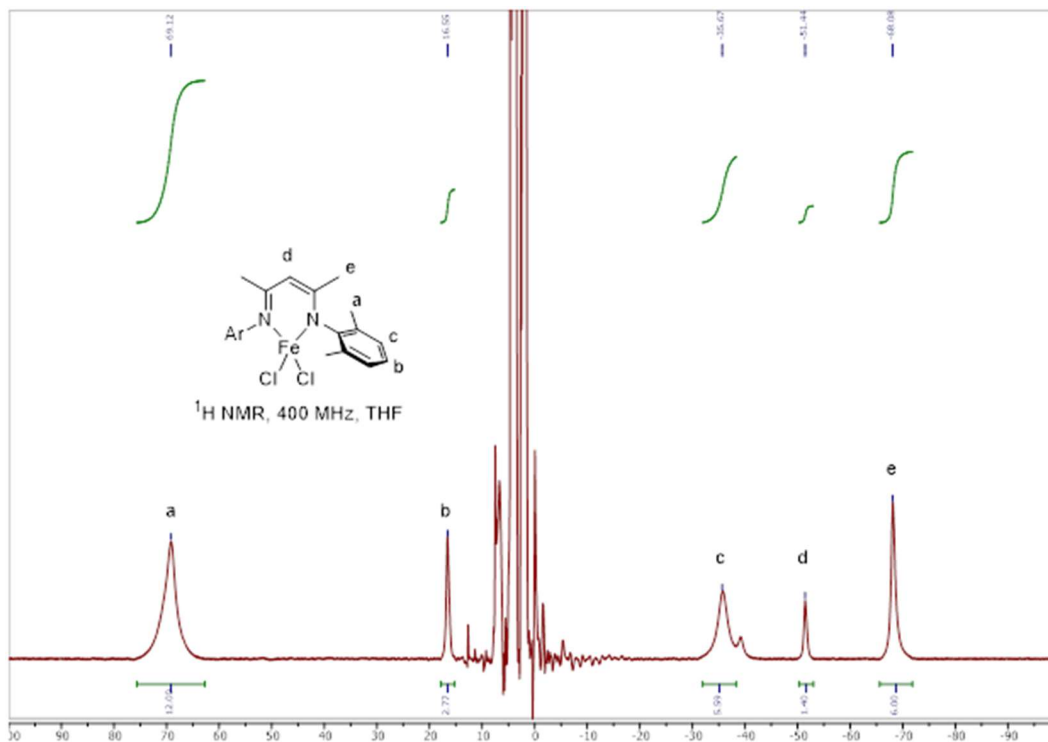


Figure A.2.1. $^1\text{H NMR}$ spectrum of compound 3.2 using solvent suppression for THF peaks.

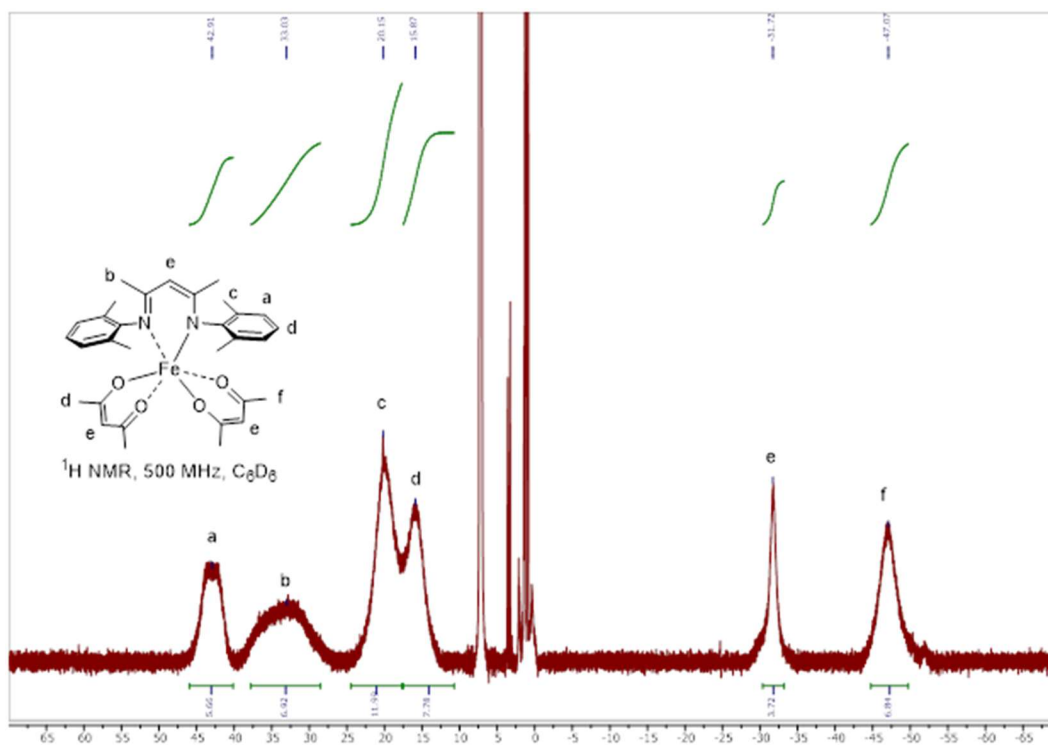


Figure A.2.2. $^1\text{H NMR}$ spectrum of compound 3.3.

A.3 Nuclear magnetic resonance spectral data from Chapter 4

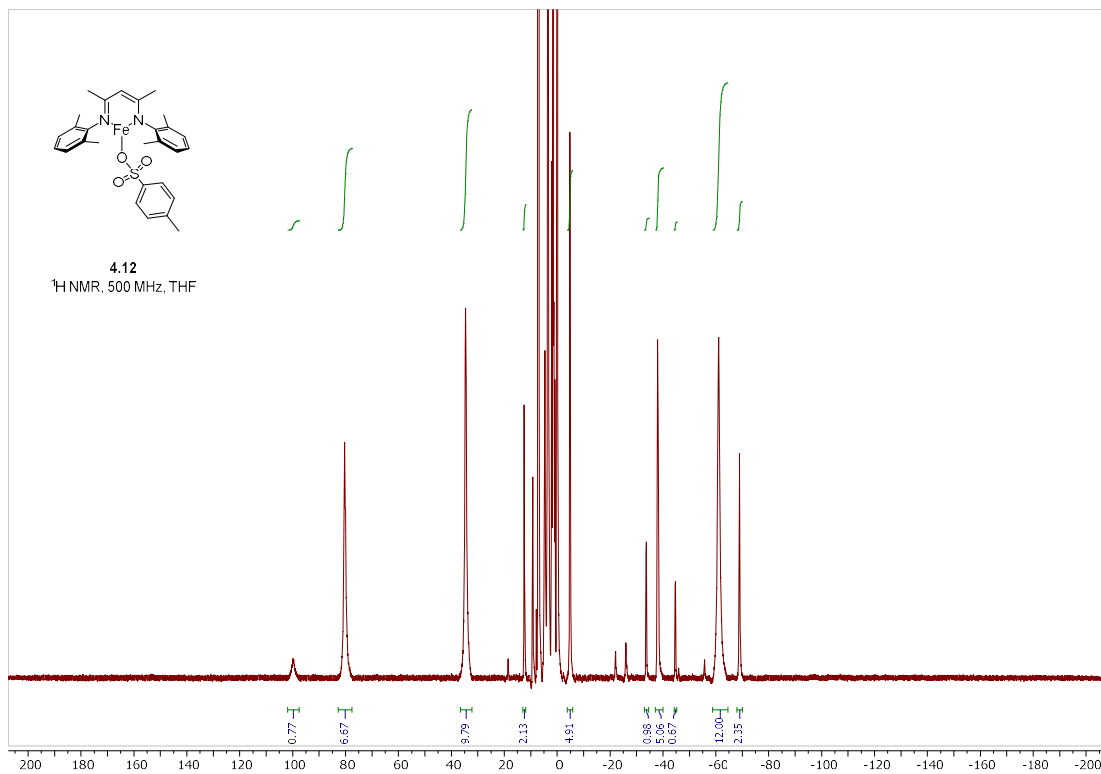


Figure A.3.1. ¹H NMR spectrum of compound 4.12.

Appendix B.

X-ray crystallographic data

B.1 X-ray crystallographic data from Chapter 2

B.1.1. X-ray crystallographic data for compound 2.46

Figure B.1.1.1. ORTEP diagram of compound 2.46

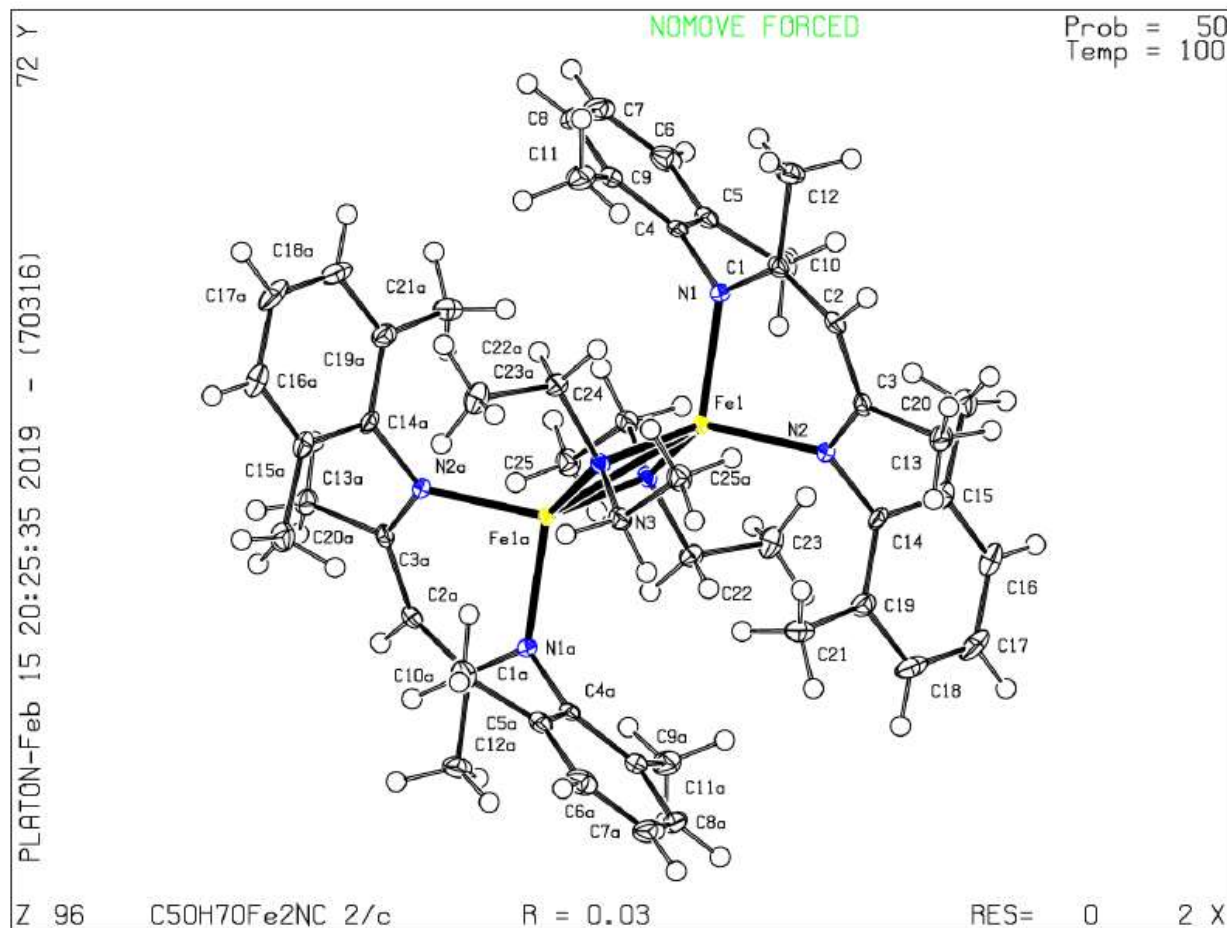


Table B.1.1.1. Crystal data and structure refinement for dimeric 2,4-bis[(2,6-dimethylphenyl)imino]pentane iron *N,N*-diethylamide complex (2.46)

Identification code	C50H70Fe2N6	
Empirical formula	C50 H70 Fe2 N6	
Formula weight	866.82	
Temperature	100(2) K	
Wavelength	1.54178 Å	
Crystal system	Monoclinic	
Space group	6/c	
Unit cell dimensions	a = 15.8079(5) Å	$\alpha = 90^\circ$.
	b = 14.3502(4) Å	$\beta = 109.8450(10)^\circ$.
	c = 21.0653(6) Å	$\gamma = 90^\circ$.
Volume	4494.8(2) Å ³	

Z	4
Density (calculated)	1.281 Mg/m ³
Absorption coefficient	5.480 mm ⁻¹
F(000)	1856
Crystal size	0.480 x 0.260 x 0.100 mm ³
Theta range for data collection	4.282 to 66.599°.
Index ranges	-18<=h<=18, -17<=k<=17, -24<=l<=25
Reflections collected	19773
Independent reflections	3960 [R(int) = 0.0363]
Completeness to theta = 66.599°	99.7 %
Absorption correction	Semi-empirical from equivalents
Max. and min. transmission	0.7528 and 0.4837
Refinement method	Full-matrix least-squares on F ²
Data / restraints / parameters	3960 / 0 / 273
Goodness-of-fit on F ²	1.067
Final R indices [I>2sigma(I)]	R1 = 0.0288, wR2 = 0.0794
R indices (all data)	R1 = 0.0292, wR2 = 0.0798
Extinction coefficient	n/a
Largest diff. peak and hole	0.322 and -0.371 e.Å ⁻³

Table B.1.1.2. Atomic coordinates ($\times 10^4$) and equivalent isotropic displacement parameters ($\text{\AA}^2 \times 10^3$) for dimeric 2,4-bis[(2,6-dimethylphenyl)imino]pentane iron *N,N*-diethylamide complex (**2.46**). $U(\text{eq})$ is defined as one third of the trace of the orthogonalized U^{ij} tensor.

	x	y	z	U(eq)
Fe(1)	7654(1)	3272(1)	5451(1)	9(1)
N(1)	7882(1)	3290(1)	6488(1)	11(1)
N(2)	8003(1)	4654(1)	5448(1)	10(1)
N(3)	6507(1)	2774(1)	4737(1)	10(1)
C(1)	8488(1)	3876(1)	6878(1)	11(1)
C(2)	8929(1)	4563(1)	6626(1)	12(1)
C(3)	8660(1)	4979(1)	5989(1)	11(1)
C(4)	7358(1)	2743(1)	6793(1)	12(1)
C(5)	6474(1)	3048(1)	6692(1)	15(1)
C(6)	5927(1)	2532(1)	6957(1)	21(1)
C(7)	6247(1)	1734(1)	7331(1)	24(1)
C(8)	7119(1)	1456(1)	7447(1)	21(1)
C(9)	7694(1)	1948(1)	7189(1)	16(1)
C(10)	6135(1)	3955(1)	6338(1)	19(1)
C(11)	8655(1)	1614(1)	7385(1)	23(1)
C(12)	8737(1)	3870(1)	7638(1)	19(1)
C(13)	9142(1)	5869(1)	5932(1)	16(1)
C(14)	7604(1)	5317(1)	4916(1)	12(1)
C(15)	7019(1)	6002(1)	5009(1)	15(1)
C(16)	6589(1)	6606(1)	4480(1)	21(1)
C(17)	6732(1)	6544(1)	3870(1)	24(1)
C(18)	7325(1)	5889(1)	3788(1)	22(1)
C(19)	7780(1)	5277(1)	4308(1)	16(1)
C(20)	6841(1)	6098(1)	5664(1)	20(1)
C(21)	8468(1)	4618(1)	4218(1)	21(1)
C(22)	6196(1)	3365(1)	4128(1)	14(1)
C(23)	5625(1)	4207(1)	4166(1)	20(1)
C(24)	5736(1)	2488(1)	4939(1)	14(1)
C(25)	5022(1)	1909(1)	4414(1)	17(1)

Table B.1.1.3. Bond lengths [Å] and angles [°] for dimeric 2,4-bis[(2,6-dimethylphenyl)imino]pentane iron *N,N*-diethylamide complex (**2.46**)

Fe(1)-N(3)	2.0503(12)
Fe(1)-N(2)	2.0601(12)
Fe(1)-N(1)	2.0909(13)
Fe(1)-N(3)#1	2.1275(12)
Fe(1)-Fe(1)#1	2.8494(4)
N(1)-C(1)	1.328(2)
N(1)-C(4)	1.4412(19)
N(2)-C(3)	1.338(2)
N(2)-C(14)	1.4407(19)
N(3)-C(22)	1.4770(19)
N(3)-C(24)	1.4793(19)
C(1)-C(2)	1.410(2)
C(1)-C(12)	1.513(2)
C(2)-C(3)	1.397(2)
C(2)-H(2)	0.935(19)
C(3)-C(13)	1.512(2)
C(4)-C(9)	1.407(2)
C(4)-C(5)	1.409(2)
C(5)-C(6)	1.393(2)
C(5)-C(10)	1.505(2)
C(6)-C(7)	1.384(3)
C(6)-H(6)	0.9500
C(7)-C(8)	1.375(3)
C(7)-H(7)	0.9500
C(8)-C(9)	1.399(2)
C(8)-H(8)	0.9500
C(9)-C(11)	1.510(2)
C(10)-H(10A)	0.9800
C(10)-H(10B)	0.9800
C(10)-H(10C)	0.9800
C(11)-H(11A)	0.9800
C(11)-H(11B)	0.9800
C(11)-H(11C)	0.9800
C(12)-H(12A)	0.9800
C(12)-H(12B)	0.9800
C(12)-H(12C)	0.9800
C(13)-H(13A)	0.9800
C(13)-H(13B)	0.9800
C(13)-H(13C)	0.9800
C(14)-C(19)	1.402(2)
C(14)-C(15)	1.408(2)
C(15)-C(16)	1.393(2)
C(15)-C(20)	1.505(2)

C(16)-C(17)	1.381(3)
C(16)-H(16)	0.9500
C(17)-C(18)	1.378(3)
C(17)-H(17)	0.9500
C(18)-C(19)	1.398(2)
C(18)-H(18)	0.9500
C(19)-C(21)	1.501(2)
C(20)-H(20A)	0.9800
C(20)-H(20B)	0.9800
C(20)-H(20C)	0.9800
C(21)-H(21A)	0.9800
C(21)-H(21B)	0.9800
C(21)-H(21C)	0.9800
C(22)-C(23)	1.527(2)
C(22)-H(22A)	0.9900
C(22)-H(22B)	0.9900
C(23)-H(23A)	0.9800
C(23)-H(23B)	0.9800
C(23)-H(23C)	0.9800
C(24)-C(25)	1.530(2)
C(24)-H(24A)	0.9900
C(24)-H(24B)	0.9900
C(25)-H(25A)	0.9800
C(25)-H(25B)	0.9800
C(25)-H(25C)	0.9800
N(3)-Fe(1)-N(2)	120.34(5)
N(3)-Fe(1)-N(1)	124.49(5)
N(2)-Fe(1)-N(1)	92.24(5)
N(3)-Fe(1)-N(3)#1	94.01(4)
N(2)-Fe(1)-N(3)#1	119.61(5)
N(1)-Fe(1)-N(3)#1	107.82(5)
N(3)-Fe(1)-Fe(1)#1	48.14(3)
N(2)-Fe(1)-Fe(1)#1	137.08(4)
N(1)-Fe(1)-Fe(1)#1	129.49(3)
N(3)#1-Fe(1)-Fe(1)#1	45.87(3)
C(1)-N(1)-C(4)	118.15(12)
C(1)-N(1)-Fe(1)	119.13(10)
C(4)-N(1)-Fe(1)	122.54(9)
C(3)-N(2)-C(14)	116.18(12)
C(3)-N(2)-Fe(1)	117.67(10)
C(14)-N(2)-Fe(1)	126.15(9)
C(22)-N(3)-C(24)	110.21(11)
C(22)-N(3)-Fe(1)	112.78(9)
C(24)-N(3)-Fe(1)	119.73(9)
C(22)-N(3)-Fe(1)#1	106.76(9)

C(24)-N(3)-Fe(1)#1	119.03(9)
Fe(1)-N(3)-Fe(1)#1	85.99(4)
N(1)-C(1)-C(2)	123.69(13)
N(1)-C(1)-C(12)	121.66(13)
C(2)-C(1)-C(12)	114.62(13)
C(3)-C(2)-C(1)	129.18(14)
C(3)-C(2)-H(2)	114.7(11)
C(1)-C(2)-H(2)	114.8(11)
N(2)-C(3)-C(2)	124.37(13)
N(2)-C(3)-C(13)	119.50(13)
C(2)-C(3)-C(13)	116.11(13)
C(9)-C(4)-C(5)	119.82(14)
C(9)-C(4)-N(1)	123.19(14)
C(5)-C(4)-N(1)	116.98(13)
C(6)-C(5)-C(4)	119.54(15)
C(6)-C(5)-C(10)	119.54(15)
C(4)-C(5)-C(10)	120.80(14)
C(7)-C(6)-C(5)	120.80(16)
C(7)-C(6)-H(6)	119.6
C(5)-C(6)-H(6)	119.6
C(8)-C(7)-C(6)	119.44(16)
C(8)-C(7)-H(7)	120.3
C(6)-C(7)-H(7)	120.3
C(7)-C(8)-C(9)	121.96(16)
C(7)-C(8)-H(8)	119.0
C(9)-C(8)-H(8)	119.0
C(8)-C(9)-C(4)	118.37(15)
C(8)-C(9)-C(11)	117.31(15)
C(4)-C(9)-C(11)	124.25(15)
C(5)-C(10)-H(10A)	109.5
C(5)-C(10)-H(10B)	109.5
H(10A)-C(10)-H(10B)	109.5
C(5)-C(10)-H(10C)	109.5
H(10A)-C(10)-H(10C)	109.5
H(10B)-C(10)-H(10C)	109.5
C(9)-C(11)-H(11A)	109.5
C(9)-C(11)-H(11B)	109.5
H(11A)-C(11)-H(11B)	109.5
C(9)-C(11)-H(11C)	109.5
H(11A)-C(11)-H(11C)	109.5
H(11B)-C(11)-H(11C)	109.5
C(1)-C(12)-H(12A)	109.5
C(1)-C(12)-H(12B)	109.5
H(12A)-C(12)-H(12B)	109.5
C(1)-C(12)-H(12C)	109.5
H(12A)-C(12)-H(12C)	109.5

H(12B)-C(12)-H(12C)	109.5
C(3)-C(13)-H(13A)	109.5
C(3)-C(13)-H(13B)	109.5
H(13A)-C(13)-H(13B)	109.5
C(3)-C(13)-H(13C)	109.5
H(13A)-C(13)-H(13C)	109.5
H(13B)-C(13)-H(13C)	109.5
C(19)-C(14)-C(15)	119.87(14)
C(19)-C(14)-N(2)	120.90(13)
C(15)-C(14)-N(2)	119.22(13)
C(16)-C(15)-C(14)	119.25(15)
C(16)-C(15)-C(20)	118.99(15)
C(14)-C(15)-C(20)	121.76(14)
C(17)-C(16)-C(15)	121.01(16)
C(17)-C(16)-H(16)	119.5
C(15)-C(16)-H(16)	119.5
C(18)-C(17)-C(16)	119.55(16)
C(18)-C(17)-H(17)	120.2
C(16)-C(17)-H(17)	120.2
C(17)-C(18)-C(19)	121.37(16)
C(17)-C(18)-H(18)	119.3
C(19)-C(18)-H(18)	119.3
C(18)-C(19)-C(14)	118.84(15)
C(18)-C(19)-C(21)	119.93(14)
C(14)-C(19)-C(21)	121.19(14)
C(15)-C(20)-H(20A)	109.5
C(15)-C(20)-H(20B)	109.5
H(20A)-C(20)-H(20B)	109.5
C(15)-C(20)-H(20C)	109.5
H(20A)-C(20)-H(20C)	109.5
H(20B)-C(20)-H(20C)	109.5
C(19)-C(21)-H(21A)	109.5
C(19)-C(21)-H(21B)	109.5
H(21A)-C(21)-H(21B)	109.5
C(19)-C(21)-H(21C)	109.5
H(21A)-C(21)-H(21C)	109.5
H(21B)-C(21)-H(21C)	109.5
N(3)-C(22)-C(23)	115.92(13)
N(3)-C(22)-H(22A)	108.3
C(23)-C(22)-H(22A)	108.3
N(3)-C(22)-H(22B)	108.3
C(23)-C(22)-H(22B)	108.3
H(22A)-C(22)-H(22B)	107.4
C(22)-C(23)-H(23A)	109.5
C(22)-C(23)-H(23B)	109.5
H(23A)-C(23)-H(23B)	109.5

C(22)-C(23)-H(23C)	109.5
H(23A)-C(23)-H(23C)	109.5
H(23B)-C(23)-H(23C)	109.5
N(3)-C(24)-C(25)	114.79(12)
N(3)-C(24)-H(24A)	108.6
C(25)-C(24)-H(24A)	108.6
N(3)-C(24)-H(24B)	108.6
C(25)-C(24)-H(24B)	108.6
H(24A)-C(24)-H(24B)	107.5
C(24)-C(25)-H(25A)	109.5
C(24)-C(25)-H(25B)	109.5
H(25A)-C(25)-H(25B)	109.5
C(24)-C(25)-H(25C)	109.5
H(25A)-C(25)-H(25C)	109.5
H(25B)-C(25)-H(25C)	109.5

Symmetry transformations used to generate equivalent atoms:

#1 $-x+3/2, -y+1/2, -z+1$

Table B.1.1.4. Anisotropic displacement parameters ($\text{\AA}^2 \times 10^3$) for dimeric 2,4-bis[(2,6-dimethylphenyl)imino]pentane iron *N,N*-diethylamide complex (**2.46**). The anisotropic displacement factor exponent takes the form: $-2\pi^2 [h^2 a^{*2} U^{11} + \dots + 2 h k a^* b^* U^{12}]$

	U11	U22	U33	U23	U13	U12
Fe(1)	13(1)	6(1)	7(1)	-1(1)	2(1)	-1(1)
N(1)	15(1)	9(1)	8(1)	1(1)	3(1)	0(1)
N(2)	14(1)	8(1)	10(1)	1(1)	4(1)	0(1)
N(3)	10(1)	10(1)	9(1)	-1(1)	2(1)	0(1)
C(1)	13(1)	11(1)	10(1)	-1(1)	3(1)	4(1)
C(2)	12(1)	12(1)	10(1)	-4(1)	2(1)	-1(1)
C(3)	12(1)	9(1)	14(1)	-2(1)	6(1)	0(1)
C(4)	19(1)	12(1)	6(1)	-3(1)	4(1)	-4(1)
C(5)	20(1)	15(1)	10(1)	-4(1)	4(1)	-4(1)
C(6)	20(1)	27(1)	16(1)	-6(1)	7(1)	-9(1)
C(7)	32(1)	26(1)	15(1)	-3(1)	10(1)	-16(1)
C(8)	37(1)	15(1)	10(1)	2(1)	6(1)	-7(1)
C(9)	26(1)	13(1)	9(1)	-2(1)	4(1)	-2(1)
C(10)	18(1)	17(1)	21(1)	-2(1)	7(1)	2(1)
C(11)	32(1)	22(1)	14(1)	6(1)	7(1)	9(1)
C(12)	24(1)	22(1)	11(1)	-3(1)	6(1)	-7(1)
C(13)	19(1)	13(1)	16(1)	-1(1)	5(1)	-5(1)
C(14)	14(1)	8(1)	12(1)	3(1)	3(1)	-3(1)
C(15)	17(1)	10(1)	19(1)	1(1)	6(1)	-3(1)
C(16)	20(1)	12(1)	28(1)	6(1)	7(1)	2(1)
C(17)	26(1)	19(1)	23(1)	13(1)	3(1)	0(1)
C(18)	26(1)	25(1)	15(1)	7(1)	7(1)	-4(1)
C(19)	18(1)	14(1)	14(1)	2(1)	5(1)	-4(1)
C(20)	25(1)	15(1)	24(1)	1(1)	12(1)	4(1)
C(21)	27(1)	22(1)	14(1)	2(1)	10(1)	3(1)
C(22)	15(1)	14(1)	12(1)	2(1)	3(1)	2(1)
C(23)	18(1)	15(1)	25(1)	4(1)	5(1)	3(1)
C(24)	16(1)	14(1)	14(1)	-2(1)	7(1)	-1(1)
C(25)	16(1)	16(1)	19(1)	-2(1)	7(1)	-3(1)

B.1.2. X-ray crystallographic data for compound 2.47

Figure B.1.2.1. ORTEP diagram of compound 2.47

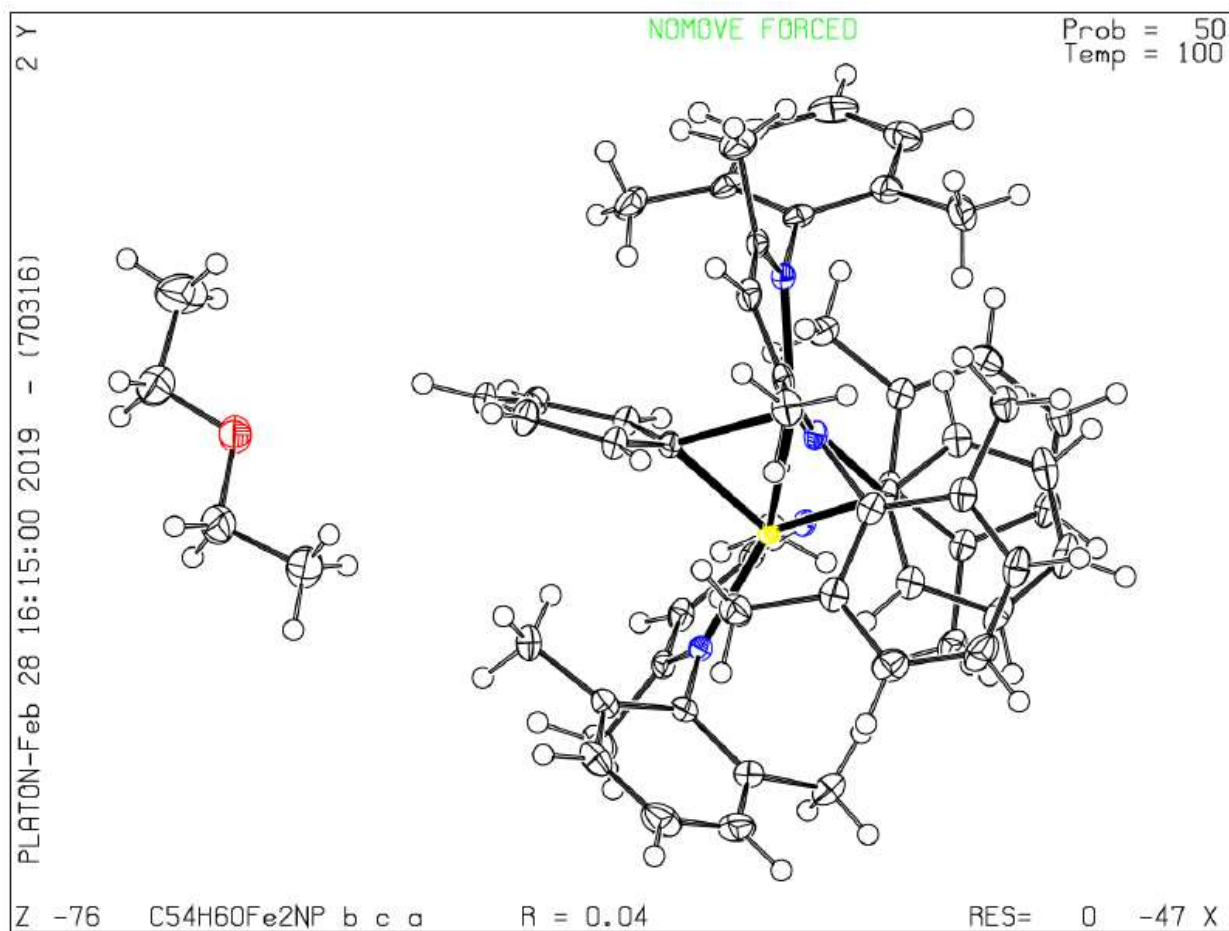


Table B.1.2.1. Crystal data and structure refinement for dimeric 2,4-bis[(2,6-dimethylphenyl)imino]pentane iron phenyl complex (2.47).

Identification code	C54H60Fe2N4(C4H10O)	
Empirical formula	C58 H70 Fe2 N4 O	
Formula weight	950.88	
Temperature	100(2) K	
Wavelength	1.54178 Å	
Crystal system	Orthorhombic	
Space group	Pbca	
Unit cell dimensions	a = 13.5021(4) Å	$\alpha = 90^\circ$.
	b = 22.3216(6) Å	$\beta = 90^\circ$.
	c = 33.1135(10) Å	$\gamma = 90^\circ$.
Volume	9980.0(5) Å ³	
Z	8	
Density (calculated)	1.266 Mg/m ³	

Absorption coefficient	4.990 mm ⁻¹
F(000)	4048
Crystal size	0.480 x 0.400 x 0.280 mm ³
Theta range for data collection	2.669 to 69.544°.
Index ranges	-15<=h<=16, -27<=k<=23, -23<=l<=38
Reflections collected	37898
Independent reflections	9062 [R(int) = 0.0398]
Completeness to theta = 67.679°	98.8 %
Absorption correction	Semi-empirical from equivalents
Max. and min. transmission	0.7532 and 0.4281
Refinement method	Full-matrix least-squares on F ²
Data / restraints / parameters	9062 / 0 / 598
Goodness-of-fit on F ²	1.026
Final R indices [I>2sigma(I)]	R1 = 0.0379, wR2 = 0.0886
R indices (all data)	R1 = 0.0453, wR2 = 0.0931
Extinction coefficient	n/a
Largest diff. peak and hole	0.459 and -0.583 e.Å ⁻³

Table B.1.2.2. Atomic coordinates ($\times 10^4$) and equivalent isotropic displacement parameters ($\text{\AA}^2 \times 10^3$) for dimeric 2,4-bis[(2,6-dimethylphenyl)imino]pentane iron phenyl complex (**2.47**). $U(\text{eq})$ is defined as one third of the trace of the orthogonalized U_{ij} tensor.

	x	y	z	U(eq)
Fe(1)	3350(1)	3847(1)	4006(1)	12(1)
Fe(2)	1949(1)	3201(1)	3642(1)	12(1)
N(1)	3207(1)	4361(1)	4510(1)	15(1)
N(2)	4770(1)	4115(1)	3917(1)	16(1)
N(3)	2088(1)	2413(1)	3347(1)	14(1)
N(4)	508(1)	3287(1)	3470(1)	15(1)
C(1)	3728(2)	4866(1)	4553(1)	17(1)
C(2)	4542(2)	5015(1)	4308(1)	18(1)
C(3)	5084(2)	4647(1)	4047(1)	17(1)
C(4)	2586(2)	4184(1)	4843(1)	17(1)
C(5)	1572(2)	4323(1)	4840(1)	19(1)
C(6)	978(2)	4114(1)	5154(1)	26(1)
C(7)	1372(2)	3777(1)	5464(1)	30(1)
C(8)	2377(2)	3647(1)	5465(1)	27(1)
C(9)	2994(2)	3843(1)	5156(1)	20(1)
C(10)	1129(2)	4684(1)	4504(1)	26(1)
C(11)	4069(2)	3669(1)	5155(1)	23(1)
C(12)	3484(2)	5300(1)	4888(1)	22(1)
C(13)	6097(2)	4874(1)	3920(1)	26(1)
C(14)	5429(1)	3746(1)	3681(1)	17(1)
C(15)	5541(2)	3837(1)	3265(1)	21(1)
C(16)	6127(2)	3438(1)	3049(1)	28(1)
C(17)	6610(2)	2969(1)	3237(1)	33(1)
C(18)	6532(2)	2900(1)	3650(1)	29(1)
C(19)	5952(2)	3289(1)	3879(1)	21(1)
C(20)	5091(2)	4363(1)	3049(1)	28(1)
C(21)	5933(2)	3234(1)	4331(1)	28(1)
C(22)	2685(2)	3046(1)	4193(1)	16(1)
C(23)	3459(2)	2635(1)	4272(1)	18(1)
C(24)	3392(2)	2210(1)	4574(1)	26(1)
C(25)	2525(2)	2155(1)	4794(1)	32(1)
C(26)	1739(2)	2536(1)	4724(1)	26(1)
C(27)	1828(2)	2988(1)	4435(1)	18(1)
C(28)	1571(2)	2300(1)	3011(1)	16(1)
C(29)	748(2)	2641(1)	2893(1)	19(1)
C(30)	200(2)	3053(1)	3123(1)	17(1)
C(31)	2699(2)	1941(1)	3504(1)	14(1)

C(32)	3720(2)	1932(1)	3422(1)	17(1)
C(33)	4302(2)	1491(1)	3602(1)	21(1)
C(34)	3895(2)	1070(1)	3857(1)	23(1)
C(35)	2883(2)	1079(1)	3932(1)	20(1)
C(36)	2275(2)	1509(1)	3756(1)	16(1)
C(37)	4178(2)	2392(1)	3149(1)	24(1)
C(38)	1178(2)	1501(1)	3841(1)	23(1)
C(39)	1839(2)	1767(1)	2752(1)	23(1)
C(40)	-819(2)	3203(1)	2958(1)	30(1)
C(41)	-162(1)	3659(1)	3699(1)	18(1)
C(42)	-666(2)	3405(1)	4027(1)	23(1)
C(43)	-1243(2)	3777(1)	4270(1)	32(1)
C(44)	-1347(2)	4379(1)	4187(1)	32(1)
C(45)	-887(2)	4616(1)	3852(1)	26(1)
C(46)	-296(2)	4264(1)	3599(1)	21(1)
C(47)	-634(2)	2741(1)	4106(1)	32(1)
C(48)	131(2)	4542(1)	3226(1)	27(1)
C(49)	2628(1)	4008(1)	3429(1)	15(1)
C(50)	2729(2)	3833(1)	3022(1)	16(1)
C(51)	2683(2)	4239(1)	2704(1)	18(1)
C(52)	2607(2)	4848(1)	2780(1)	21(1)
C(53)	2546(2)	5043(1)	3176(1)	21(1)
C(54)	2521(2)	4633(1)	3492(1)	18(1)
C(1S)	2875(2)	6122(2)	1608(1)	53(1)
C(2S)	1838(2)	6299(1)	1709(1)	36(1)
C(3S)	542(2)	6088(1)	2162(1)	41(1)
C(4S)	333(2)	5799(1)	2562(1)	36(1)
O(1S)	1543(1)	5980(1)	2058(1)	31(1)

Table B.1.2.3. Bond lengths [Å] and angles [°] for dimeric 2,4-bis[(2,6-dimethylphenyl)imino]pentane iron phenyl complex (**2.47**).

Fe(1)-N(2)	2.0301(17)
Fe(1)-N(1)	2.0356(17)
Fe(1)-C(22)	2.096(2)
Fe(1)-C(49)	2.175(2)
Fe(1)-Fe(2)	2.6664(4)
Fe(2)-N(3)	2.0207(16)
Fe(2)-N(4)	2.0368(17)
Fe(2)-C(22)	2.106(2)
Fe(2)-C(49)	2.142(2)
N(1)-C(1)	1.335(3)
N(1)-C(4)	1.440(3)
N(2)-C(3)	1.332(3)
N(2)-C(14)	1.442(3)
N(3)-C(28)	1.335(3)
N(3)-C(31)	1.436(2)
N(4)-C(30)	1.328(3)
N(4)-C(41)	1.445(3)
C(1)-C(2)	1.405(3)
C(1)-C(12)	1.511(3)
C(2)-C(3)	1.400(3)
C(2)-H(2)	0.9500
C(3)-C(13)	1.518(3)
C(4)-C(9)	1.399(3)
C(4)-C(5)	1.404(3)
C(5)-C(6)	1.394(3)
C(5)-C(10)	1.499(3)
C(6)-C(7)	1.380(3)
C(6)-H(6)	0.9500
C(7)-C(8)	1.388(3)
C(7)-H(7)	0.9500
C(8)-C(9)	1.389(3)
C(8)-H(8)	0.9500
C(9)-C(11)	1.503(3)
C(10)-H(10A)	0.9800
C(10)-H(10B)	0.9800
C(10)-H(10C)	0.9800
C(11)-H(11A)	0.9800
C(11)-H(11B)	0.9800
C(11)-H(11C)	0.9800
C(12)-H(12A)	0.9800
C(12)-H(12B)	0.9800
C(12)-H(12C)	0.9800
C(13)-H(13A)	0.9800

C(13)-H(13B)	0.9800
C(13)-H(13C)	0.9800
C(14)-C(15)	1.400(3)
C(14)-C(19)	1.404(3)
C(15)-C(16)	1.391(3)
C(15)-C(20)	1.504(3)
C(16)-C(17)	1.381(4)
C(16)-H(16)	0.9500
C(17)-C(18)	1.382(4)
C(17)-H(17)	0.9500
C(18)-C(19)	1.394(3)
C(18)-H(18)	0.9500
C(19)-C(21)	1.500(3)
C(20)-H(20A)	0.9800
C(20)-H(20B)	0.9800
C(20)-H(20C)	0.9800
C(21)-H(21A)	0.9800
C(21)-H(21B)	0.9800
C(21)-H(21C)	0.9800
C(22)-C(27)	1.413(3)
C(22)-C(23)	1.414(3)
C(23)-C(24)	1.381(3)
C(23)-H(23)	0.9500
C(24)-C(25)	1.385(4)
C(24)-H(24)	0.9500
C(25)-C(26)	1.380(4)
C(25)-H(25)	0.9500
C(26)-C(27)	1.395(3)
C(26)-H(26)	0.9500
C(27)-H(27)	0.9500
C(28)-C(29)	1.402(3)
C(28)-C(39)	1.511(3)
C(29)-C(30)	1.407(3)
C(29)-H(29)	0.9500
C(30)-C(40)	1.517(3)
C(31)-C(36)	1.398(3)
C(31)-C(32)	1.406(3)
C(32)-C(33)	1.394(3)
C(32)-C(37)	1.500(3)
C(33)-C(34)	1.379(3)
C(33)-H(33)	0.9500
C(34)-C(35)	1.389(3)
C(34)-H(34)	0.9500
C(35)-C(36)	1.390(3)
C(35)-H(35)	0.9500
C(36)-C(38)	1.509(3)

C(37)-H(37A)	0.9800
C(37)-H(37B)	0.9800
C(37)-H(37C)	0.9800
C(38)-H(38A)	0.9800
C(38)-H(38B)	0.9800
C(38)-H(38C)	0.9800
C(39)-H(39A)	0.9800
C(39)-H(39B)	0.9800
C(39)-H(39C)	0.9800
C(40)-H(40A)	0.9800
C(40)-H(40B)	0.9800
C(40)-H(40C)	0.9800
C(41)-C(42)	1.401(3)
C(41)-C(46)	1.402(3)
C(42)-C(43)	1.394(3)
C(42)-C(47)	1.507(3)
C(43)-C(44)	1.380(4)
C(43)-H(43)	0.9500
C(44)-C(45)	1.377(4)
C(44)-H(44)	0.9500
C(45)-C(46)	1.397(3)
C(45)-H(45)	0.9500
C(46)-C(48)	1.498(3)
C(47)-H(47A)	0.9800
C(47)-H(47B)	0.9800
C(47)-H(47C)	0.9800
C(48)-H(48A)	0.9800
C(48)-H(48B)	0.9800
C(48)-H(48C)	0.9800
C(49)-C(50)	1.410(3)
C(49)-C(54)	1.418(3)
C(50)-C(51)	1.389(3)
C(50)-H(50)	0.9500
C(51)-C(52)	1.386(3)
C(51)-H(51)	0.9500
C(52)-C(53)	1.386(3)
C(52)-H(52)	0.9500
C(53)-C(54)	1.391(3)
C(53)-H(53)	0.9500
C(54)-H(54)	0.9500
C(1S)-C(2S)	1.493(4)
C(1S)-H(1SA)	0.9800
C(1S)-H(1SB)	0.9800
C(1S)-H(1SC)	0.9800
C(2S)-O(1S)	1.415(3)
C(2S)-H(2SA)	0.9900

C(2S)-H(2SB)	0.9900
C(3S)-O(1S)	1.414(3)
C(3S)-C(4S)	1.500(4)
C(3S)-H(3SA)	0.9900
C(3S)-H(3SB)	0.9900
C(4S)-H(4SA)	0.9800
C(4S)-H(4SB)	0.9800
C(4S)-H(4SC)	0.9800

N(2)-Fe(1)-N(1)	92.41(7)
N(2)-Fe(1)-C(22)	134.32(7)
N(1)-Fe(1)-C(22)	101.38(7)
N(2)-Fe(1)-C(49)	104.38(7)
N(1)-Fe(1)-C(49)	125.82(7)
C(22)-Fe(1)-C(49)	102.08(8)
N(2)-Fe(1)-Fe(2)	139.87(5)
N(1)-Fe(1)-Fe(2)	127.45(5)
C(22)-Fe(1)-Fe(2)	50.79(6)
C(49)-Fe(1)-Fe(2)	51.30(5)
N(3)-Fe(2)-N(4)	91.98(7)
N(3)-Fe(2)-C(22)	103.48(7)
N(4)-Fe(2)-C(22)	135.21(8)
N(3)-Fe(2)-C(49)	122.15(7)
N(4)-Fe(2)-C(49)	103.68(7)
C(22)-Fe(2)-C(49)	102.84(8)
N(3)-Fe(2)-Fe(1)	128.58(5)
N(4)-Fe(2)-Fe(1)	138.88(5)
C(22)-Fe(2)-Fe(1)	50.44(5)
C(49)-Fe(2)-Fe(1)	52.42(6)
C(1)-N(1)-C(4)	117.24(17)
C(1)-N(1)-Fe(1)	120.78(14)
C(4)-N(1)-Fe(1)	121.91(12)
C(3)-N(2)-C(14)	119.17(17)
C(3)-N(2)-Fe(1)	121.09(14)
C(14)-N(2)-Fe(1)	119.53(13)
C(28)-N(3)-C(31)	117.60(16)
C(28)-N(3)-Fe(2)	121.26(13)
C(31)-N(3)-Fe(2)	121.02(13)
C(30)-N(4)-C(41)	118.98(17)
C(30)-N(4)-Fe(2)	120.33(14)
C(41)-N(4)-Fe(2)	120.32(13)
N(1)-C(1)-C(2)	123.45(19)
N(1)-C(1)-C(12)	120.22(19)
C(2)-C(1)-C(12)	116.27(18)
C(3)-C(2)-C(1)	128.80(19)
C(3)-C(2)-H(2)	115.6

C(1)-C(2)-H(2)	115.6
N(2)-C(3)-C(2)	123.77(19)
N(2)-C(3)-C(13)	119.67(19)
C(2)-C(3)-C(13)	116.53(18)
C(9)-C(4)-C(5)	120.6(2)
C(9)-C(4)-N(1)	119.11(18)
C(5)-C(4)-N(1)	120.18(19)
C(6)-C(5)-C(4)	118.8(2)
C(6)-C(5)-C(10)	120.3(2)
C(4)-C(5)-C(10)	120.84(19)
C(7)-C(6)-C(5)	121.1(2)
C(7)-C(6)-H(6)	119.5
C(5)-C(6)-H(6)	119.5
C(6)-C(7)-C(8)	119.5(2)
C(6)-C(7)-H(7)	120.3
C(8)-C(7)-H(7)	120.3
C(7)-C(8)-C(9)	121.3(2)
C(7)-C(8)-H(8)	119.3
C(9)-C(8)-H(8)	119.3
C(8)-C(9)-C(4)	118.7(2)
C(8)-C(9)-C(11)	120.0(2)
C(4)-C(9)-C(11)	121.3(2)
C(5)-C(10)-H(10A)	109.5
C(5)-C(10)-H(10B)	109.5
H(10A)-C(10)-H(10B)	109.5
C(5)-C(10)-H(10C)	109.5
H(10A)-C(10)-H(10C)	109.5
H(10B)-C(10)-H(10C)	109.5
C(9)-C(11)-H(11A)	109.5
C(9)-C(11)-H(11B)	109.5
H(11A)-C(11)-H(11B)	109.5
C(9)-C(11)-H(11C)	109.5
H(11A)-C(11)-H(11C)	109.5
H(11B)-C(11)-H(11C)	109.5
C(1)-C(12)-H(12A)	109.5
C(1)-C(12)-H(12B)	109.5
H(12A)-C(12)-H(12B)	109.5
C(1)-C(12)-H(12C)	109.5
H(12A)-C(12)-H(12C)	109.5
H(12B)-C(12)-H(12C)	109.5
C(3)-C(13)-H(13A)	109.5
C(3)-C(13)-H(13B)	109.5
H(13A)-C(13)-H(13B)	109.5
C(3)-C(13)-H(13C)	109.5
H(13A)-C(13)-H(13C)	109.5
H(13B)-C(13)-H(13C)	109.5

C(15)-C(14)-C(19)	120.7(2)
C(15)-C(14)-N(2)	121.20(19)
C(19)-C(14)-N(2)	118.14(19)
C(16)-C(15)-C(14)	118.4(2)
C(16)-C(15)-C(20)	119.0(2)
C(14)-C(15)-C(20)	122.5(2)
C(17)-C(16)-C(15)	121.4(2)
C(17)-C(16)-H(16)	119.3
C(15)-C(16)-H(16)	119.3
C(16)-C(17)-C(18)	119.8(2)
C(16)-C(17)-H(17)	120.1
C(18)-C(17)-H(17)	120.1
C(17)-C(18)-C(19)	120.7(2)
C(17)-C(18)-H(18)	119.6
C(19)-C(18)-H(18)	119.6
C(18)-C(19)-C(14)	118.8(2)
C(18)-C(19)-C(21)	120.0(2)
C(14)-C(19)-C(21)	121.1(2)
C(15)-C(20)-H(20A)	109.5
C(15)-C(20)-H(20B)	109.5
H(20A)-C(20)-H(20B)	109.5
C(15)-C(20)-H(20C)	109.5
H(20A)-C(20)-H(20C)	109.5
H(20B)-C(20)-H(20C)	109.5
C(19)-C(21)-H(21A)	109.5
C(19)-C(21)-H(21B)	109.5
H(21A)-C(21)-H(21B)	109.5
C(19)-C(21)-H(21C)	109.5
H(21A)-C(21)-H(21C)	109.5
H(21B)-C(21)-H(21C)	109.5
C(27)-C(22)-C(23)	116.23(19)
C(27)-C(22)-Fe(1)	126.64(15)
C(23)-C(22)-Fe(1)	106.93(14)
C(27)-C(22)-Fe(2)	96.78(14)
C(23)-C(22)-Fe(2)	127.96(15)
Fe(1)-C(22)-Fe(2)	78.77(7)
C(24)-C(23)-C(22)	122.0(2)
C(24)-C(23)-H(23)	119.0
C(22)-C(23)-H(23)	119.0
C(23)-C(24)-C(25)	119.9(2)
C(23)-C(24)-H(24)	120.1
C(25)-C(24)-H(24)	120.1
C(26)-C(25)-C(24)	120.4(2)
C(26)-C(25)-H(25)	119.8
C(24)-C(25)-H(25)	119.8
C(25)-C(26)-C(27)	119.7(2)

C(25)-C(26)-H(26)	120.2
C(27)-C(26)-H(26)	120.2
C(26)-C(27)-C(22)	121.7(2)
C(26)-C(27)-H(27)	119.2
C(22)-C(27)-H(27)	119.2
N(3)-C(28)-C(29)	123.02(19)
N(3)-C(28)-C(39)	119.73(18)
C(29)-C(28)-C(39)	117.19(19)
C(28)-C(29)-C(30)	128.3(2)
C(28)-C(29)-H(29)	115.9
C(30)-C(29)-H(29)	115.9
N(4)-C(30)-C(29)	124.15(19)
N(4)-C(30)-C(40)	120.61(19)
C(29)-C(30)-C(40)	115.19(19)
C(36)-C(31)-C(32)	120.50(18)
C(36)-C(31)-N(3)	119.20(18)
C(32)-C(31)-N(3)	120.23(18)
C(33)-C(32)-C(31)	118.65(19)
C(33)-C(32)-C(37)	120.56(19)
C(31)-C(32)-C(37)	120.78(19)
C(34)-C(33)-C(32)	121.3(2)
C(34)-C(33)-H(33)	119.3
C(32)-C(33)-H(33)	119.3
C(33)-C(34)-C(35)	119.4(2)
C(33)-C(34)-H(34)	120.3
C(35)-C(34)-H(34)	120.3
C(34)-C(35)-C(36)	121.1(2)
C(34)-C(35)-H(35)	119.5
C(36)-C(35)-H(35)	119.5
C(35)-C(36)-C(31)	119.01(19)
C(35)-C(36)-C(38)	119.59(19)
C(31)-C(36)-C(38)	121.40(18)
C(32)-C(37)-H(37A)	109.5
C(32)-C(37)-H(37B)	109.5
H(37A)-C(37)-H(37B)	109.5
C(32)-C(37)-H(37C)	109.5
H(37A)-C(37)-H(37C)	109.5
H(37B)-C(37)-H(37C)	109.5
C(36)-C(38)-H(38A)	109.5
C(36)-C(38)-H(38B)	109.5
H(38A)-C(38)-H(38B)	109.5
C(36)-C(38)-H(38C)	109.5
H(38A)-C(38)-H(38C)	109.5
H(38B)-C(38)-H(38C)	109.5
C(28)-C(39)-H(39A)	109.5
C(28)-C(39)-H(39B)	109.5

H(39A)-C(39)-H(39B)	109.5
C(28)-C(39)-H(39C)	109.5
H(39A)-C(39)-H(39C)	109.5
H(39B)-C(39)-H(39C)	109.5
C(30)-C(40)-H(40A)	109.5
C(30)-C(40)-H(40B)	109.5
H(40A)-C(40)-H(40B)	109.5
C(30)-C(40)-H(40C)	109.5
H(40A)-C(40)-H(40C)	109.5
H(40B)-C(40)-H(40C)	109.5
C(42)-C(41)-C(46)	120.6(2)
C(42)-C(41)-N(4)	118.70(19)
C(46)-C(41)-N(4)	120.70(19)
C(43)-C(42)-C(41)	118.6(2)
C(43)-C(42)-C(47)	120.1(2)
C(41)-C(42)-C(47)	121.2(2)
C(44)-C(43)-C(42)	121.4(2)
C(44)-C(43)-H(43)	119.3
C(42)-C(43)-H(43)	119.3
C(45)-C(44)-C(43)	119.3(2)
C(45)-C(44)-H(44)	120.3
C(43)-C(44)-H(44)	120.3
C(44)-C(45)-C(46)	121.6(2)
C(44)-C(45)-H(45)	119.2
C(46)-C(45)-H(45)	119.2
C(45)-C(46)-C(41)	118.3(2)
C(45)-C(46)-C(48)	118.7(2)
C(41)-C(46)-C(48)	122.9(2)
C(42)-C(47)-H(47A)	109.5
C(42)-C(47)-H(47B)	109.5
H(47A)-C(47)-H(47B)	109.5
C(42)-C(47)-H(47C)	109.5
H(47A)-C(47)-H(47C)	109.5
H(47B)-C(47)-H(47C)	109.5
C(46)-C(48)-H(48A)	109.5
C(46)-C(48)-H(48B)	109.5
H(48A)-C(48)-H(48B)	109.5
C(46)-C(48)-H(48C)	109.5
H(48A)-C(48)-H(48C)	109.5
H(48B)-C(48)-H(48C)	109.5
C(50)-C(49)-C(54)	115.11(18)
C(50)-C(49)-Fe(2)	97.09(13)
C(54)-C(49)-Fe(2)	137.37(16)
C(50)-C(49)-Fe(1)	138.60(15)
C(54)-C(49)-Fe(1)	94.48(14)
Fe(2)-C(49)-Fe(1)	76.28(7)

C(51)-C(50)-C(49)	122.53(19)
C(51)-C(50)-H(50)	118.7
C(49)-C(50)-H(50)	118.7
C(52)-C(51)-C(50)	120.5(2)
C(52)-C(51)-H(51)	119.8
C(50)-C(51)-H(51)	119.8
C(51)-C(52)-C(53)	118.9(2)
C(51)-C(52)-H(52)	120.5
C(53)-C(52)-H(52)	120.5
C(52)-C(53)-C(54)	120.45(19)
C(52)-C(53)-H(53)	119.8
C(54)-C(53)-H(53)	119.8
C(53)-C(54)-C(49)	122.3(2)
C(53)-C(54)-H(54)	118.9
C(49)-C(54)-H(54)	118.9
C(2S)-C(1S)-H(1SA)	109.5
C(2S)-C(1S)-H(1SB)	109.5
H(1SA)-C(1S)-H(1SB)	109.5
C(2S)-C(1S)-H(1SC)	109.5
H(1SA)-C(1S)-H(1SC)	109.5
H(1SB)-C(1S)-H(1SC)	109.5
O(1S)-C(2S)-C(1S)	108.3(2)
O(1S)-C(2S)-H(2SA)	110.0
C(1S)-C(2S)-H(2SA)	110.0
O(1S)-C(2S)-H(2SB)	110.0
C(1S)-C(2S)-H(2SB)	110.0
H(2SA)-C(2S)-H(2SB)	108.4
O(1S)-C(3S)-C(4S)	108.7(2)
O(1S)-C(3S)-H(3SA)	109.9
C(4S)-C(3S)-H(3SA)	109.9
O(1S)-C(3S)-H(3SB)	109.9
C(4S)-C(3S)-H(3SB)	109.9
H(3SA)-C(3S)-H(3SB)	108.3
C(3S)-C(4S)-H(4SA)	109.5
C(3S)-C(4S)-H(4SB)	109.5
H(4SA)-C(4S)-H(4SB)	109.5
C(3S)-C(4S)-H(4SC)	109.5
H(4SA)-C(4S)-H(4SC)	109.5
H(4SB)-C(4S)-H(4SC)	109.5
C(3S)-O(1S)-C(2S)	112.45(19)

Symmetry transformations used to generate equivalent atoms:

Table B.1.2.4. Anisotropic displacement parameters ($\text{\AA}^2 \times 10^3$) for dimeric 2,4-bis[(2,6-dimethylphenyl)imino]pentane iron phenyl complex (**2.47**). The anisotropic displacement factor exponent takes the form: $-2\pi^2 [h^2 a^{*2} U^{11} + \dots + 2 h k a^* b^* U^{12}]$

	U11	U22	U33	U23	U13	U12
Fe(1)	15(1)	9(1)	12(1)	-1(1)	-1(1)	-3(1)
Fe(2)	14(1)	8(1)	14(1)	0(1)	-1(1)	-1(1)
N(1)	20(1)	12(1)	14(1)	0(1)	-1(1)	-1(1)
N(2)	15(1)	16(1)	15(1)	2(1)	-1(1)	-1(1)
N(3)	17(1)	10(1)	14(1)	1(1)	1(1)	0(1)
N(4)	14(1)	13(1)	19(1)	3(1)	-1(1)	-1(1)
C(1)	22(1)	9(1)	18(1)	0(1)	-8(1)	2(1)
C(2)	24(1)	10(1)	21(1)	1(1)	-6(1)	-3(1)
C(3)	18(1)	16(1)	17(1)	5(1)	-6(1)	-4(1)
C(4)	25(1)	12(1)	13(1)	-4(1)	1(1)	-1(1)
C(5)	27(1)	14(1)	18(1)	-4(1)	1(1)	2(1)
C(6)	28(1)	27(1)	24(1)	-4(1)	8(1)	2(1)
C(7)	38(1)	32(1)	22(1)	3(1)	11(1)	0(1)
C(8)	40(1)	24(1)	16(1)	3(1)	1(1)	2(1)
C(9)	27(1)	12(1)	19(1)	-2(1)	-2(1)	0(1)
C(10)	23(1)	28(1)	27(1)	2(1)	1(1)	4(1)
C(11)	28(1)	18(1)	22(1)	1(1)	-5(1)	0(1)
C(12)	29(1)	15(1)	21(1)	-5(1)	-5(1)	0(1)
C(13)	26(1)	26(1)	28(1)	-1(1)	-1(1)	-11(1)
C(14)	15(1)	19(1)	18(1)	-2(1)	1(1)	-6(1)
C(15)	19(1)	26(1)	18(1)	0(1)	2(1)	-11(1)
C(16)	26(1)	35(1)	24(1)	-8(1)	10(1)	-15(1)
C(17)	21(1)	35(1)	43(2)	-15(1)	13(1)	-5(1)
C(18)	20(1)	27(1)	40(2)	-2(1)	2(1)	2(1)
C(19)	17(1)	23(1)	24(1)	-1(1)	-1(1)	-3(1)
C(20)	29(1)	37(1)	17(1)	6(1)	1(1)	-10(1)
C(21)	28(1)	31(1)	26(1)	6(1)	-8(1)	4(1)
C(22)	25(1)	10(1)	14(1)	0(1)	-2(1)	-4(1)
C(23)	25(1)	12(1)	16(1)	-5(1)	-5(1)	-2(1)
C(24)	38(1)	17(1)	23(1)	0(1)	-12(1)	5(1)
C(25)	49(2)	24(1)	22(1)	11(1)	-5(1)	-6(1)
C(26)	36(1)	24(1)	18(1)	5(1)	2(1)	-10(1)
C(27)	25(1)	14(1)	15(1)	-4(1)	-2(1)	-2(1)
C(28)	22(1)	11(1)	16(1)	0(1)	0(1)	-6(1)
C(29)	26(1)	18(1)	13(1)	1(1)	-6(1)	-5(1)
C(30)	18(1)	15(1)	19(1)	5(1)	-4(1)	-4(1)
C(31)	21(1)	7(1)	13(1)	-3(1)	-2(1)	0(1)
C(32)	23(1)	14(1)	15(1)	-3(1)	0(1)	-1(1)

C(33)	20(1)	19(1)	25(1)	-6(1)	1(1)	5(1)
C(34)	31(1)	12(1)	25(1)	0(1)	-4(1)	8(1)
C(35)	32(1)	9(1)	19(1)	0(1)	0(1)	-2(1)
C(36)	23(1)	10(1)	16(1)	-3(1)	-1(1)	-2(1)
C(37)	22(1)	24(1)	27(1)	4(1)	4(1)	-2(1)
C(38)	25(1)	17(1)	28(1)	5(1)	2(1)	-4(1)
C(39)	30(1)	22(1)	17(1)	-7(1)	-4(1)	-2(1)
C(40)	24(1)	29(1)	38(2)	1(1)	-12(1)	1(1)
C(41)	13(1)	19(1)	20(1)	2(1)	-2(1)	0(1)
C(42)	17(1)	28(1)	25(1)	6(1)	0(1)	-1(1)
C(43)	20(1)	47(2)	28(1)	5(1)	7(1)	2(1)
C(44)	23(1)	41(2)	31(2)	-6(1)	2(1)	11(1)
C(45)	23(1)	25(1)	31(1)	0(1)	-4(1)	8(1)
C(46)	17(1)	22(1)	25(1)	4(1)	-3(1)	2(1)
C(47)	26(1)	31(1)	37(2)	13(1)	5(1)	-5(1)
C(48)	28(1)	22(1)	30(1)	10(1)	-2(1)	4(1)
C(49)	15(1)	14(1)	17(1)	2(1)	-1(1)	0(1)
C(50)	19(1)	13(1)	14(1)	-2(1)	0(1)	0(1)
C(51)	21(1)	20(1)	13(1)	0(1)	1(1)	-1(1)
C(52)	25(1)	19(1)	20(1)	9(1)	1(1)	1(1)
C(53)	31(1)	10(1)	23(1)	0(1)	1(1)	0(1)
C(54)	25(1)	15(1)	15(1)	1(1)	0(1)	0(1)
C(1S)	37(2)	92(3)	29(2)	-3(2)	6(1)	0(2)
C(2S)	39(1)	36(1)	32(2)	3(1)	1(1)	-4(1)
C(3S)	36(1)	40(2)	47(2)	15(1)	10(1)	13(1)
C(4S)	42(1)	34(1)	33(2)	3(1)	8(1)	9(1)
O(1S)	32(1)	33(1)	27(1)	5(1)	3(1)	7(1)

B.2 X-ray crystallographic data from Chapter 3

B.2.1. X-ray crystallographic data for compound 3.2

Figure B.2.1.1. ORTEP diagram of compound 3.2

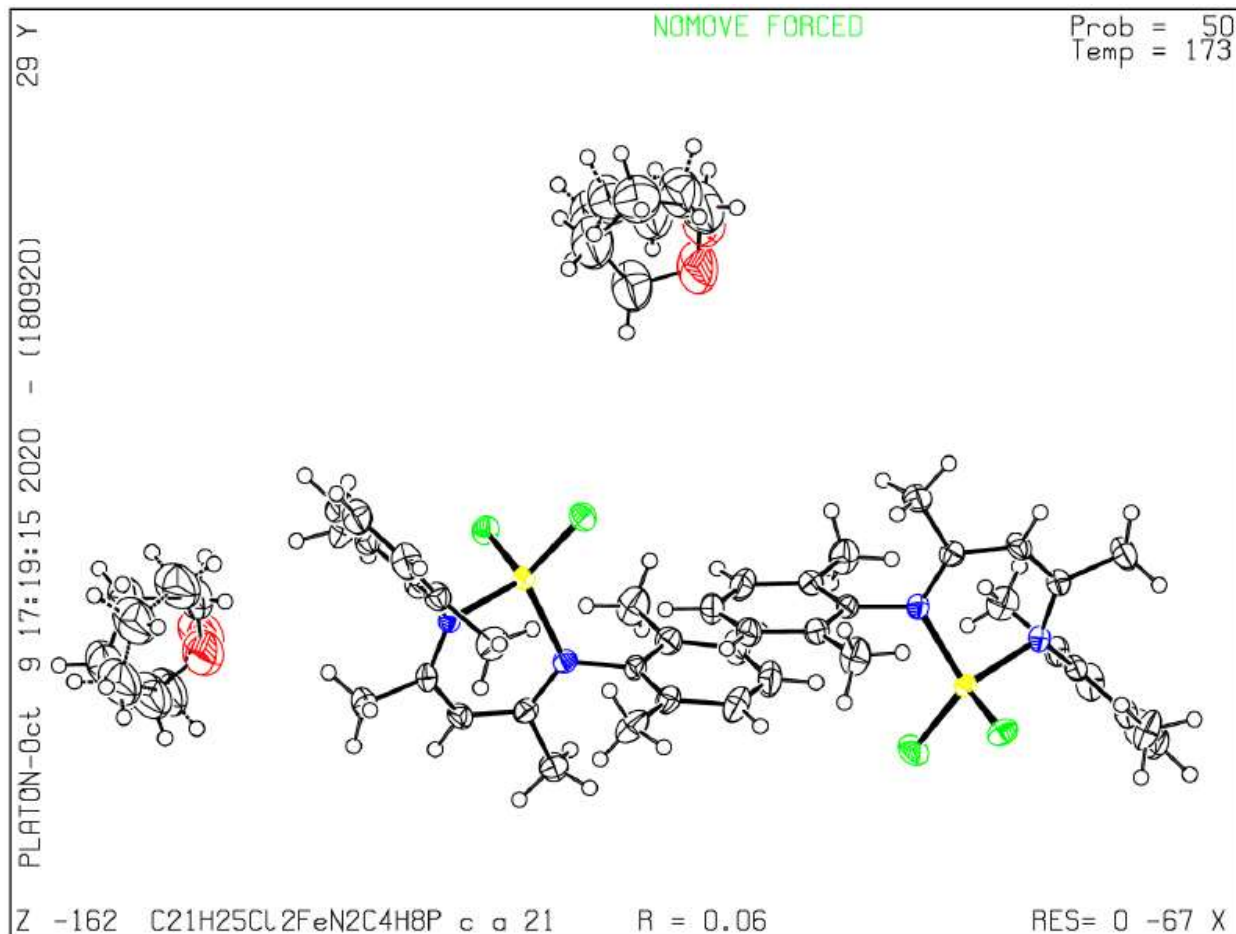


Table B.2.1.1. Crystal data and structure refinement for 2,4-bis[(2,6-dimethylphenyl)imino]pentane iron(III) dichloride complex (3.2).

Identification code	C ₂₁ H ₂₅ Cl ₂ FeN ₂ (C ₄ H ₈ O)	
Empirical formula	C ₂₅ H ₃₃ Cl ₂ Fe N ₂ O	
Formula weight	504.28	
Temperature	173(2) K	
Wavelength	1.54178 Å	
Crystal system	Orthorhombic	
Space group	Pca2 ₁	
Unit cell dimensions	a = 27.8561(11) Å	a = 90°.
	b = 8.6070(4) Å	b = 90°.

	$c = 21.1090(9) \text{ \AA}$	$g = 90^\circ$.
Volume	$5061.0(4) \text{ \AA}^3$	
Z	8	
Density (calculated)	1.324 Mg/m^3	
Absorption coefficient	6.860 mm^{-1}	
F(000)	2120	
Crystal size	$0.260 \times 0.120 \times 0.080 \text{ mm}^3$	
Theta range for data collection	$3.173 \text{ to } 66.654^\circ$.	
Index ranges	$-33 \leq h \leq 32, -10 \leq k \leq 10, -25 \leq l \leq 25$	
Reflections collected	126278	
Independent reflections	8895 [R(int) = 0.0612]	
Completeness to $\theta = 66.654^\circ$	99.6 %	
Absorption correction	Semi-empirical from equivalents	
Max. and min. transmission	0.7528 and 0.5132	
Refinement method	Full-matrix least-squares on F^2	
Data / restraints / parameters	8895 / 551 / 645	
Goodness-of-fit on F^2	1.021	
Final R indices [$I > 2\sigma(I)$]	$R1 = 0.0606, wR2 = 0.1444$	
R indices (all data)	$R1 = 0.0642, wR2 = 0.1470$	
Extinction coefficient	n/a	
Largest diff. peak and hole	$0.625 \text{ and } -0.334 \text{ e.\AA}^{-3}$	

Table B.2.1.2. Atomic coordinates ($\times 10^4$) and equivalent isotropic displacement parameters ($\text{\AA}^2 \times 10^3$) for 2,4-bis[(2,6-dimethylphenyl)imino]pentane iron(III) dichloride complex (**3.2**). $U(\text{eq})$ is defined as one third of the trace of the orthogonalized U^{ij} tensor.

	x	y	z	$U(\text{eq})$
Fe(1)	3835(1)	3683(1)	4155(1)	22(1)
Fe(2)	1450(1)	10965(1)	5778(1)	23(1)
Cl(1)	3851(1)	1134(2)	4068(1)	32(1)
Cl(2)	3824(1)	4607(3)	5118(1)	36(1)
Cl(3)	1449(1)	13510(2)	5876(1)	34(1)
Cl(4)	1401(1)	10059(3)	4812(1)	42(1)
N(1)	4364(2)	4528(8)	3644(3)	24(1)
N(2)	3327(2)	4464(8)	3599(3)	24(1)
N(3)	1990(2)	10175(8)	6275(3)	24(1)
N(4)	954(2)	10168(8)	6346(3)	25(1)
C(1)	4315(3)	4642(9)	3021(4)	27(2)
C(2)	3871(3)	4444(10)	2713(4)	29(2)
C(3)	3409(3)	4462(10)	2978(4)	27(2)
C(4)	4818(3)	4884(10)	3944(4)	26(2)
C(5)	5157(3)	3707(10)	4031(4)	33(2)
C(6)	5583(3)	4083(12)	4337(5)	41(2)
C(7)	5671(3)	5558(14)	4549(5)	45(3)
C(8)	5330(3)	6706(12)	4466(5)	41(2)
C(9)	4895(3)	6382(10)	4162(5)	32(2)
C(10)	5088(3)	2077(12)	3782(6)	46(3)
C(11)	4524(3)	7638(11)	4089(5)	41(2)
C(12)	4746(3)	5064(12)	2629(4)	38(2)
C(13)	2986(3)	4562(13)	2529(4)	39(2)
C(14)	2864(3)	4928(10)	3843(4)	26(2)
C(15)	2778(3)	6514(10)	3905(4)	30(2)
C(16)	2335(3)	6981(12)	4159(5)	44(2)
C(17)	2001(3)	5909(13)	4337(5)	45(2)
C(18)	2089(3)	4335(13)	4268(5)	42(2)

C(19)	2524(3)	3810(10)	4025(4)	33(2)
C(20)	3148(3)	7694(11)	3726(5)	43(2)
C(21)	2613(4)	2090(11)	3959(6)	49(3)
C(22)	1951(3)	10141(10)	6903(4)	27(2)
C(23)	1510(3)	10272(10)	7218(4)	29(2)
C(24)	1042(3)	10157(10)	6969(4)	27(2)
C(25)	2439(3)	9772(10)	5976(4)	25(2)
C(26)	2775(3)	10937(10)	5831(5)	31(2)
C(27)	3194(3)	10488(12)	5528(4)	36(2)
C(28)	3283(3)	8950(12)	5375(4)	40(2)
C(29)	2951(3)	7839(12)	5522(5)	39(2)
C(30)	2522(3)	8216(9)	5826(4)	29(2)
C(31)	2694(3)	12613(11)	6000(6)	46(3)
C(32)	2159(4)	6982(11)	5980(5)	43(2)
C(33)	2393(3)	9881(12)	7300(4)	37(2)
C(34)	634(3)	9913(13)	7426(4)	41(2)
C(35)	487(3)	9770(10)	6105(4)	26(2)
C(36)	407(3)	8209(10)	5940(4)	31(2)
C(37)	-35(3)	7820(12)	5676(5)	41(2)
C(38)	-382(3)	8946(14)	5572(5)	46(3)
C(39)	-296(3)	10453(12)	5741(5)	41(2)
C(40)	132(3)	10904(11)	6016(4)	32(2)
C(41)	790(4)	7000(11)	6032(5)	42(2)
C(42)	210(4)	12576(11)	6206(6)	48(3)
O(1S)	5855(8)	3430(50)	2329(17)	100(7)
C(1S)	6129(13)	3740(70)	1786(13)	97(8)
C(2S)	6632(11)	3950(60)	1990(14)	100(9)
C(3S)	6658(8)	3450(70)	2621(13)	96(9)
C(4S)	6158(10)	3520(50)	2864(12)	88(8)
O(1T)	5900(20)	3150(110)	2470(30)	105(11)
C(1T)	6020(20)	3770(140)	1880(30)	97(11)
C(2T)	6520(20)	4350(120)	1930(30)	96(12)
C(3T)	6650(20)	4270(120)	2570(30)	99(12)
C(4T)	6290(30)	3250(110)	2880(30)	106(12)
O(2S)	3472(4)	1640(20)	7455(7)	104(5)
C(5S)	3819(5)	1300(30)	7002(8)	91(6)

C(6S)	4294(5)	1310(30)	7305(8)	105(6)
C(7S)	4215(7)	1680(30)	7946(9)	103(6)
C(8S)	3692(7)	1590(30)	8060(8)	99(6)
O(2T)	3530(20)	1150(130)	7850(50)	103(12)
C(5T)	3700(30)	-190(120)	7530(60)	105(12)
C(6T)	4210(30)	180(170)	7370(60)	105(6)
C(7T)	4360(30)	1340(190)	7790(70)	100(12)
C(8T)	3940(40)	1790(160)	8170(50)	101(13)

Table B.2.1.3. Bond lengths [\AA] and angles [$^\circ$] for 2,4-bis[(2,6-dimethylphenyl)imino]pentane iron(III) dichloride complex (**3.2**).

Fe(1)-N(2)	1.957(6)
Fe(1)-N(1)	1.967(7)
Fe(1)-Cl(2)	2.183(2)
Fe(1)-Cl(1)	2.202(2)
Fe(2)-N(4)	1.953(7)
Fe(2)-N(3)	1.955(7)
Fe(2)-Cl(4)	2.189(3)
Fe(2)-Cl(3)	2.201(2)
N(1)-C(1)	1.325(11)
N(1)-C(4)	1.446(10)
N(2)-C(3)	1.330(11)
N(2)-C(14)	1.445(10)
N(3)-C(22)	1.331(11)
N(3)-C(25)	1.444(10)
N(4)-C(24)	1.337(11)
N(4)-C(35)	1.440(10)
C(1)-C(2)	1.408(11)
C(1)-C(12)	1.503(11)
C(2)-C(3)	1.402(12)
C(2)-H(2A)	0.9500
C(3)-C(13)	1.517(11)
C(4)-C(9)	1.386(12)
C(4)-C(5)	1.397(12)
C(5)-C(6)	1.389(13)
C(5)-C(10)	1.510(13)
C(6)-C(7)	1.369(15)
C(6)-H(6A)	0.9500
C(7)-C(8)	1.381(15)
C(7)-H(7A)	0.9500
C(8)-C(9)	1.401(12)
C(8)-H(8A)	0.9500
C(9)-C(11)	1.502(12)
C(10)-H(10A)	0.9800

C(10)-H(10B)	0.9800
C(10)-H(10C)	0.9800
C(11)-H(11A)	0.9800
C(11)-H(11B)	0.9800
C(11)-H(11C)	0.9800
C(12)-H(12A)	0.9800
C(12)-H(12B)	0.9800
C(12)-H(12C)	0.9800
C(13)-H(13A)	0.9800
C(13)-H(13B)	0.9800
C(13)-H(13C)	0.9800
C(14)-C(15)	1.392(12)
C(14)-C(19)	1.404(12)
C(15)-C(16)	1.406(12)
C(15)-C(20)	1.495(13)
C(16)-C(17)	1.363(15)
C(16)-H(16A)	0.9500
C(17)-C(18)	1.385(15)
C(17)-H(17A)	0.9500
C(18)-C(19)	1.390(13)
C(18)-H(18A)	0.9500
C(19)-C(21)	1.508(13)
C(20)-H(20A)	0.9800
C(20)-H(20B)	0.9800
C(20)-H(20C)	0.9800
C(21)-H(21A)	0.9800
C(21)-H(21B)	0.9800
C(21)-H(21C)	0.9800
C(22)-C(23)	1.401(12)
C(22)-C(33)	1.507(11)
C(23)-C(24)	1.409(12)
C(23)-H(23A)	0.9500
C(24)-C(34)	1.505(12)
C(25)-C(30)	1.396(11)
C(25)-C(26)	1.405(11)
C(26)-C(27)	1.387(12)

C(26)-C(31)	1.502(13)
C(27)-C(28)	1.384(14)
C(27)-H(27A)	0.9500
C(28)-C(29)	1.367(14)
C(28)-H(28A)	0.9500
C(29)-C(30)	1.392(12)
C(29)-H(29A)	0.9500
C(30)-C(32)	1.503(12)
C(31)-H(31A)	0.9800
C(31)-H(31B)	0.9800
C(31)-H(31C)	0.9800
C(32)-H(32A)	0.9800
C(32)-H(32B)	0.9800
C(32)-H(32C)	0.9800
C(33)-H(33A)	0.9800
C(33)-H(33B)	0.9800
C(33)-H(33C)	0.9800
C(34)-H(34A)	0.9800
C(34)-H(34B)	0.9800
C(34)-H(34C)	0.9800
C(35)-C(40)	1.402(12)
C(35)-C(36)	1.405(12)
C(36)-C(37)	1.393(12)
C(36)-C(41)	1.503(13)
C(37)-C(38)	1.385(15)
C(37)-H(37A)	0.9500
C(38)-C(39)	1.367(15)
C(38)-H(38A)	0.9500
C(39)-C(40)	1.383(13)
C(39)-H(39A)	0.9500
C(40)-C(42)	1.509(13)
C(41)-H(41A)	0.9800
C(41)-H(41B)	0.9800
C(41)-H(41C)	0.9800
C(42)-H(42A)	0.9800
C(42)-H(42B)	0.9800

C(42)-H(42C)	0.9800
O(1S)-C(1S)	1.403(19)
O(1S)-C(4S)	1.414(19)
C(1S)-C(2S)	1.48(2)
C(1S)-H(1S1)	0.9900
C(1S)-H(1S2)	0.9900
C(2S)-C(3S)	1.40(2)
C(2S)-H(2S1)	0.9900
C(2S)-H(2S2)	0.9900
C(3S)-C(4S)	1.48(2)
C(3S)-H(3S1)	0.9900
C(3S)-H(3S2)	0.9900
C(4S)-H(4S1)	0.9900
C(4S)-H(4S2)	0.9900
O(2S)-C(5S)	1.390(16)
O(2S)-C(8S)	1.417(18)
C(5S)-C(6S)	1.471(17)
C(5S)-H(5S1)	0.9900
C(5S)-H(5S2)	0.9900
C(6S)-C(7S)	1.41(2)
C(6S)-H(6S1)	0.9900
C(6S)-H(6S2)	0.9900
C(7S)-C(8S)	1.478(19)
C(7S)-H(7S1)	0.9900
C(7S)-H(7S2)	0.9900
C(8S)-H(8S1)	0.9900
C(8S)-H(8S2)	0.9900
N(2)-Fe(1)-N(1)	94.9(3)
N(2)-Fe(1)-Cl(2)	115.0(2)
N(1)-Fe(1)-Cl(2)	112.7(2)
N(2)-Fe(1)-Cl(1)	107.9(2)
N(1)-Fe(1)-Cl(1)	107.9(2)
Cl(2)-Fe(1)-Cl(1)	116.19(10)
N(4)-Fe(2)-N(3)	95.3(3)
N(4)-Fe(2)-Cl(4)	113.8(2)

N(3)-Fe(2)-Cl(4)	115.1(2)
N(4)-Fe(2)-Cl(3)	106.9(2)
N(3)-Fe(2)-Cl(3)	107.3(2)
Cl(4)-Fe(2)-Cl(3)	116.21(10)
C(1)-N(1)-C(4)	120.6(7)
C(1)-N(1)-Fe(1)	119.6(5)
C(4)-N(1)-Fe(1)	119.5(5)
C(3)-N(2)-C(14)	120.4(7)
C(3)-N(2)-Fe(1)	117.8(5)
C(14)-N(2)-Fe(1)	121.7(5)
C(22)-N(3)-C(25)	120.1(7)
C(22)-N(3)-Fe(2)	118.6(5)
C(25)-N(3)-Fe(2)	121.0(5)
C(24)-N(4)-C(35)	120.7(7)
C(24)-N(4)-Fe(2)	118.5(5)
C(35)-N(4)-Fe(2)	120.4(5)
N(1)-C(1)-C(2)	122.6(7)
N(1)-C(1)-C(12)	118.8(7)
C(2)-C(1)-C(12)	118.5(8)
C(3)-C(2)-C(1)	128.4(8)
C(3)-C(2)-H(2A)	115.8
C(1)-C(2)-H(2A)	115.8
N(2)-C(3)-C(2)	123.4(7)
N(2)-C(3)-C(13)	118.8(7)
C(2)-C(3)-C(13)	117.7(7)
C(9)-C(4)-C(5)	121.8(8)
C(9)-C(4)-N(1)	118.5(7)
C(5)-C(4)-N(1)	119.6(7)
C(6)-C(5)-C(4)	118.0(8)
C(6)-C(5)-C(10)	119.1(8)
C(4)-C(5)-C(10)	122.8(8)
C(7)-C(6)-C(5)	121.5(9)
C(7)-C(6)-H(6A)	119.3
C(5)-C(6)-H(6A)	119.3
C(6)-C(7)-C(8)	119.9(9)
C(6)-C(7)-H(7A)	120.1

C(8)-C(7)-H(7A)	120.1
C(7)-C(8)-C(9)	120.7(9)
C(7)-C(8)-H(8A)	119.6
C(9)-C(8)-H(8A)	119.6
C(4)-C(9)-C(8)	118.1(8)
C(4)-C(9)-C(11)	121.9(8)
C(8)-C(9)-C(11)	119.9(8)
C(5)-C(10)-H(10A)	109.5
C(5)-C(10)-H(10B)	109.5
H(10A)-C(10)-H(10B)	109.5
C(5)-C(10)-H(10C)	109.5
H(10A)-C(10)-H(10C)	109.5
H(10B)-C(10)-H(10C)	109.5
C(9)-C(11)-H(11A)	109.5
C(9)-C(11)-H(11B)	109.5
H(11A)-C(11)-H(11B)	109.5
C(9)-C(11)-H(11C)	109.5
H(11A)-C(11)-H(11C)	109.5
H(11B)-C(11)-H(11C)	109.5
C(1)-C(12)-H(12A)	109.5
C(1)-C(12)-H(12B)	109.5
H(12A)-C(12)-H(12B)	109.5
C(1)-C(12)-H(12C)	109.5
H(12A)-C(12)-H(12C)	109.5
H(12B)-C(12)-H(12C)	109.5
C(3)-C(13)-H(13A)	109.5
C(3)-C(13)-H(13B)	109.5
H(13A)-C(13)-H(13B)	109.5
C(3)-C(13)-H(13C)	109.5
H(13A)-C(13)-H(13C)	109.5
H(13B)-C(13)-H(13C)	109.5
C(15)-C(14)-C(19)	122.0(8)
C(15)-C(14)-N(2)	117.2(7)
C(19)-C(14)-N(2)	120.8(8)
C(14)-C(15)-C(16)	117.9(8)
C(14)-C(15)-C(20)	121.6(8)

C(16)-C(15)-C(20)	120.5(8)
C(17)-C(16)-C(15)	120.8(9)
C(17)-C(16)-H(16A)	119.6
C(15)-C(16)-H(16A)	119.6
C(16)-C(17)-C(18)	120.8(9)
C(16)-C(17)-H(17A)	119.6
C(18)-C(17)-H(17A)	119.6
C(17)-C(18)-C(19)	120.8(9)
C(17)-C(18)-H(18A)	119.6
C(19)-C(18)-H(18A)	119.6
C(18)-C(19)-C(14)	117.8(9)
C(18)-C(19)-C(21)	119.8(8)
C(14)-C(19)-C(21)	122.4(8)
C(15)-C(20)-H(20A)	109.5
C(15)-C(20)-H(20B)	109.5
H(20A)-C(20)-H(20B)	109.5
C(15)-C(20)-H(20C)	109.5
H(20A)-C(20)-H(20C)	109.5
H(20B)-C(20)-H(20C)	109.5
C(19)-C(21)-H(21A)	109.5
C(19)-C(21)-H(21B)	109.5
H(21A)-C(21)-H(21B)	109.5
C(19)-C(21)-H(21C)	109.5
H(21A)-C(21)-H(21C)	109.5
H(21B)-C(21)-H(21C)	109.5
N(3)-C(22)-C(23)	122.9(7)
N(3)-C(22)-C(33)	119.3(7)
C(23)-C(22)-C(33)	117.8(7)
C(22)-C(23)-C(24)	129.0(8)
C(22)-C(23)-H(23A)	115.5
C(24)-C(23)-H(23A)	115.5
N(4)-C(24)-C(23)	122.3(7)
N(4)-C(24)-C(34)	119.6(7)
C(23)-C(24)-C(34)	118.0(8)
C(30)-C(25)-C(26)	121.7(7)
C(30)-C(25)-N(3)	118.3(7)

C(26)-C(25)-N(3)	120.0(7)
C(27)-C(26)-C(25)	117.5(8)
C(27)-C(26)-C(31)	120.2(8)
C(25)-C(26)-C(31)	122.3(8)
C(28)-C(27)-C(26)	121.7(9)
C(28)-C(27)-H(27A)	119.2
C(26)-C(27)-H(27A)	119.2
C(29)-C(28)-C(27)	119.6(8)
C(29)-C(28)-H(28A)	120.2
C(27)-C(28)-H(28A)	120.2
C(28)-C(29)-C(30)	121.5(9)
C(28)-C(29)-H(29A)	119.3
C(30)-C(29)-H(29A)	119.3
C(29)-C(30)-C(25)	118.1(8)
C(29)-C(30)-C(32)	120.8(8)
C(25)-C(30)-C(32)	121.1(7)
C(26)-C(31)-H(31A)	109.5
C(26)-C(31)-H(31B)	109.5
H(31A)-C(31)-H(31B)	109.5
C(26)-C(31)-H(31C)	109.5
H(31A)-C(31)-H(31C)	109.5
H(31B)-C(31)-H(31C)	109.5
C(30)-C(32)-H(32A)	109.5
C(30)-C(32)-H(32B)	109.5
H(32A)-C(32)-H(32B)	109.5
C(30)-C(32)-H(32C)	109.5
H(32A)-C(32)-H(32C)	109.5
H(32B)-C(32)-H(32C)	109.5
C(22)-C(33)-H(33A)	109.5
C(22)-C(33)-H(33B)	109.5
H(33A)-C(33)-H(33B)	109.5
C(22)-C(33)-H(33C)	109.5
H(33A)-C(33)-H(33C)	109.5
H(33B)-C(33)-H(33C)	109.5
C(24)-C(34)-H(34A)	109.5
C(24)-C(34)-H(34B)	109.5

H(34A)-C(34)-H(34B)	109.5
C(24)-C(34)-H(34C)	109.5
H(34A)-C(34)-H(34C)	109.5
H(34B)-C(34)-H(34C)	109.5
C(40)-C(35)-C(36)	121.4(8)
C(40)-C(35)-N(4)	121.3(7)
C(36)-C(35)-N(4)	117.3(7)
C(37)-C(36)-C(35)	117.9(8)
C(37)-C(36)-C(41)	120.9(8)
C(35)-C(36)-C(41)	121.2(8)
C(38)-C(37)-C(36)	120.8(9)
C(38)-C(37)-H(37A)	119.6
C(36)-C(37)-H(37A)	119.6
C(39)-C(38)-C(37)	120.0(9)
C(39)-C(38)-H(38A)	120.0
C(37)-C(38)-H(38A)	120.0
C(38)-C(39)-C(40)	121.8(9)
C(38)-C(39)-H(39A)	119.1
C(40)-C(39)-H(39A)	119.1
C(39)-C(40)-C(35)	118.0(8)
C(39)-C(40)-C(42)	120.2(8)
C(35)-C(40)-C(42)	121.8(8)
C(36)-C(41)-H(41A)	109.5
C(36)-C(41)-H(41B)	109.5
H(41A)-C(41)-H(41B)	109.5
C(36)-C(41)-H(41C)	109.5
H(41A)-C(41)-H(41C)	109.5
H(41B)-C(41)-H(41C)	109.5
C(40)-C(42)-H(42A)	109.5
C(40)-C(42)-H(42B)	109.5
H(42A)-C(42)-H(42B)	109.5
C(40)-C(42)-H(42C)	109.5
H(42A)-C(42)-H(42C)	109.5
H(42B)-C(42)-H(42C)	109.5
C(1S)-O(1S)-C(4S)	108.5(15)
O(1S)-C(1S)-C(2S)	107.5(15)

O(1S)-C(1S)-H(1S1)	110.2
C(2S)-C(1S)-H(1S1)	110.2
O(1S)-C(1S)-H(1S2)	110.2
C(2S)-C(1S)-H(1S2)	110.2
H(1S1)-C(1S)-H(1S2)	108.5
C(3S)-C(2S)-C(1S)	106.8(17)
C(3S)-C(2S)-H(2S1)	110.4
C(1S)-C(2S)-H(2S1)	110.4
C(3S)-C(2S)-H(2S2)	110.4
C(1S)-C(2S)-H(2S2)	110.4
H(2S1)-C(2S)-H(2S2)	108.6
C(2S)-C(3S)-C(4S)	105.5(17)
C(2S)-C(3S)-H(3S1)	110.6
C(4S)-C(3S)-H(3S1)	110.6
C(2S)-C(3S)-H(3S2)	110.6
C(4S)-C(3S)-H(3S2)	110.6
H(3S1)-C(3S)-H(3S2)	108.8
O(1S)-C(4S)-C(3S)	106.4(17)
O(1S)-C(4S)-H(4S1)	110.4
C(3S)-C(4S)-H(4S1)	110.4
O(1S)-C(4S)-H(4S2)	110.4
C(3S)-C(4S)-H(4S2)	110.4
H(4S1)-C(4S)-H(4S2)	108.6
C(5S)-O(2S)-C(8S)	108.1(12)
O(2S)-C(5S)-C(6S)	109.1(12)
O(2S)-C(5S)-H(5S1)	109.9
C(6S)-C(5S)-H(5S1)	109.9
O(2S)-C(5S)-H(5S2)	109.9
C(6S)-C(5S)-H(5S2)	109.9
H(5S1)-C(5S)-H(5S2)	108.3
C(7S)-C(6S)-C(5S)	106.1(13)
C(7S)-C(6S)-H(6S1)	110.5
C(5S)-C(6S)-H(6S1)	110.5
C(7S)-C(6S)-H(6S2)	110.5
C(5S)-C(6S)-H(6S2)	110.5
H(6S1)-C(6S)-H(6S2)	108.7

C(6S)-C(7S)-C(8S)	107.4(13)
C(6S)-C(7S)-H(7S1)	110.2
C(8S)-C(7S)-H(7S1)	110.2
C(6S)-C(7S)-H(7S2)	110.2
C(8S)-C(7S)-H(7S2)	110.2
H(7S1)-C(7S)-H(7S2)	108.5
O(2S)-C(8S)-C(7S)	106.2(13)
O(2S)-C(8S)-H(8S1)	110.5
C(7S)-C(8S)-H(8S1)	110.5
O(2S)-C(8S)-H(8S2)	110.5
C(7S)-C(8S)-H(8S2)	110.5
H(8S1)-C(8S)-H(8S2)	108.7

Symmetry transformations used to generate equivalent atoms:

Table B.2.1.4. Anisotropic displacement parameters ($\text{\AA}^2 \times 10^3$) for 2,4-bis[(2,6-dimethylphenyl)imino]pentane iron(III) dichloride complex (**3.2**). The anisotropic displacement factor exponent takes the form: $-2p^2 [h^2 a^* U_{11} + \dots + 2 h k a^* b^* U_{12}]$

	U ₁₁	U ₂₂	U ₃₃	U ₂₃	U ₁₃	U ₁₂
Fe(1)	21(1)	25(1)	22(1)	0(1)	0(1)	2(1)
Fe(2)	20(1)	27(1)	22(1)	0(1)	0(1)	0(1)
Cl(1)	32(1)	24(1)	41(1)	1(1)	4(1)	1(1)
Cl(2)	40(1)	42(1)	26(1)	-6(1)	1(1)	6(1)
Cl(3)	33(1)	26(1)	42(1)	4(1)	-6(1)	1(1)
Cl(4)	45(1)	54(1)	25(1)	-7(1)	0(1)	0(1)
N(1)	19(3)	26(4)	26(4)	-1(3)	0(3)	0(3)
N(2)	21(3)	25(3)	25(3)	0(3)	-3(3)	-1(3)
N(3)	20(3)	26(3)	25(3)	-2(3)	1(3)	0(3)
N(4)	21(3)	25(3)	27(4)	-3(3)	1(3)	0(3)
C(1)	25(4)	26(4)	29(4)	-5(3)	5(3)	2(3)
C(2)	30(4)	37(5)	21(4)	-3(3)	0(3)	0(4)
C(3)	27(4)	27(4)	27(4)	-3(3)	-4(3)	4(3)
C(4)	20(4)	33(4)	24(4)	-1(3)	0(3)	-6(3)
C(5)	24(4)	36(5)	38(5)	2(4)	4(4)	-3(4)
C(6)	22(4)	56(6)	46(6)	0(5)	-3(4)	8(4)
C(7)	25(5)	71(7)	39(6)	-8(5)	-5(4)	-8(5)
C(8)	34(5)	50(6)	40(5)	-14(5)	-1(4)	-11(4)
C(9)	29(4)	38(5)	30(4)	-3(4)	1(4)	-3(4)
C(10)	29(5)	38(5)	72(7)	-2(5)	2(5)	6(4)
C(11)	44(5)	32(5)	48(6)	-6(4)	-4(5)	-2(4)
C(12)	32(5)	48(6)	35(5)	-2(4)	7(4)	-5(4)
C(13)	30(5)	56(6)	30(5)	-1(4)	-5(4)	1(5)
C(14)	18(4)	37(5)	23(4)	-1(3)	-2(3)	3(3)
C(15)	23(4)	33(5)	34(5)	-3(4)	-4(3)	2(3)
C(16)	32(5)	50(5)	51(6)	-16(5)	-8(5)	13(4)
C(17)	26(5)	64(7)	46(6)	-11(5)	4(4)	7(5)
C(18)	24(4)	57(6)	46(6)	0(5)	5(4)	-6(4)

C(19)	26(4)	40(5)	33(5)	0(4)	-2(4)	-3(4)
C(20)	34(5)	29(5)	66(7)	4(5)	-10(5)	3(4)
C(21)	35(5)	39(6)	75(8)	5(5)	4(5)	-10(4)
C(22)	25(4)	28(4)	28(4)	-1(3)	-2(3)	-1(3)
C(23)	31(4)	38(5)	19(4)	-5(3)	1(3)	-2(4)
C(24)	26(4)	28(4)	26(4)	-2(3)	2(3)	0(3)
C(25)	17(4)	34(4)	23(4)	1(3)	-1(3)	0(3)
C(26)	25(4)	34(4)	33(5)	5(4)	2(4)	-1(3)
C(27)	21(4)	52(6)	34(5)	5(4)	2(3)	-2(4)
C(28)	29(5)	56(6)	35(5)	-2(4)	5(4)	9(4)
C(29)	33(5)	39(5)	46(5)	-6(4)	0(4)	12(4)
C(30)	27(4)	31(4)	29(4)	5(4)	4(4)	2(3)
C(31)	34(5)	33(5)	69(7)	-1(5)	8(5)	-9(4)
C(32)	44(5)	27(5)	56(6)	-3(4)	7(5)	1(4)
C(33)	30(5)	55(6)	25(4)	-1(4)	-7(4)	-1(4)
C(34)	31(5)	65(7)	29(5)	-5(5)	6(4)	-6(5)
C(35)	21(4)	35(4)	21(4)	-3(3)	1(3)	-3(3)
C(36)	23(4)	35(5)	35(5)	-5(4)	2(3)	-3(3)
C(37)	33(5)	44(5)	45(6)	-17(4)	1(4)	-11(4)
C(38)	25(5)	71(7)	43(6)	-14(5)	-4(4)	-4(5)
C(39)	25(4)	55(6)	42(5)	-3(5)	-3(4)	8(4)
C(40)	26(4)	39(5)	30(5)	-6(4)	5(3)	-1(4)
C(41)	44(5)	29(5)	52(6)	-3(4)	0(4)	-4(4)
C(42)	31(5)	37(5)	76(8)	-9(5)	1(5)	10(4)
O(1S)	59(9)	161(19)	81(14)	14(13)	1(8)	3(11)
C(1S)	70(15)	160(20)	60(11)	-4(14)	0(10)	-13(17)
C(2S)	59(12)	170(20)	69(12)	7(14)	12(10)	1(15)
C(3S)	50(10)	170(20)	72(11)	8(16)	6(9)	10(14)
C(4S)	49(12)	150(20)	64(10)	13(13)	10(9)	7(14)
O(1T)	66(16)	160(30)	80(20)	15(19)	6(14)	-27(19)
C(1T)	51(18)	160(30)	76(18)	10(20)	10(14)	-20(20)
C(2T)	56(19)	160(30)	77(16)	14(19)	7(15)	-20(20)
C(3T)	57(17)	160(30)	77(17)	10(20)	2(14)	-20(20)
C(4T)	60(20)	170(30)	85(18)	30(20)	5(15)	-20(20)
O(2S)	48(6)	168(13)	97(9)	-5(9)	3(5)	-9(8)
C(5S)	56(8)	144(16)	74(9)	-27(10)	-9(6)	-6(10)

C(6S)	55(7)	184(17)	77(9)	-23(12)	-11(7)	-2(10)
C(7S)	80(10)	155(17)	74(10)	-11(11)	-19(9)	6(12)
C(8S)	85(11)	132(15)	81(9)	-22(11)	4(9)	-20(12)
O(2T)	67(17)	160(20)	80(20)	-10(20)	-3(18)	-3(19)
C(5T)	62(16)	160(20)	90(20)	-20(20)	-5(19)	0(18)
C(6T)	55(7)	184(17)	77(9)	-23(12)	-11(7)	-2(10)
C(7T)	69(19)	160(30)	70(20)	-10(20)	0(20)	-2(19)
C(8T)	70(20)	160(30)	80(20)	-10(20)	-1(19)	0(20)

Table B.2.1.5. Hydrogen coordinates ($\times 10^4$) and isotropic displacement parameters ($\text{\AA}^2 \times 10^3$) for 2,4-bis[(2,6-dimethylphenyl)imino]pentane iron(III) dichloride complex (**3.2**).

	x	y	z	U(eq)
H(2A)	3886	4277	2269	35
H(6A)	5818	3298	4400	49
H(7A)	5967	5793	4752	54
H(8A)	5392	7727	4617	49
H(10A)	4772	1994	3580	70
H(10B)	5339	1843	3471	70
H(10C)	5108	1337	4134	70
H(11A)	4646	8606	4272	62
H(11B)	4456	7795	3638	62
H(11C)	4229	7330	4309	62
H(12A)	4655	5104	2180	57
H(12B)	4867	6083	2761	57
H(12C)	4998	4281	2688	57
H(13A)	3102	4548	2090	58
H(13B)	2772	3675	2599	58
H(13C)	2810	5530	2606	58
H(16A)	2267	8056	4208	53
H(17A)	1704	6246	4511	54
H(18A)	1850	3605	4389	51
H(20A)	3022	8739	3804	65
H(20B)	3438	7534	3982	65
H(20C)	3228	7582	3277	65
H(21A)	2933	1919	3781	74
H(21B)	2591	1596	4376	74
H(21C)	2371	1638	3676	74
H(23A)	1529	10466	7660	35
H(27A)	3426	11254	5423	43

H(28A)	3574	8669	5170	48
H(29A)	3013	6786	5415	47
H(31A)	2382	12723	6210	68
H(31B)	2948	12964	6286	68
H(31C)	2698	13244	5613	68
H(32A)	1882	7458	6191	64
H(32B)	2053	6477	5588	64
H(32C)	2304	6208	6261	64
H(33A)	2306	9886	7750	55
H(33B)	2536	8875	7191	55
H(33C)	2626	10711	7217	55
H(34A)	757	9936	7861	62
H(34B)	396	10740	7371	62
H(34C)	483	8903	7344	62
H(37A)	-100	6771	5566	49
H(38A)	-679	8670	5382	55
H(39A)	-538	11212	5668	49
H(41A)	1074	7483	6222	63
H(41B)	670	6181	6313	63
H(41C)	876	6549	5621	63
H(42A)	530	12691	6393	72
H(42B)	183	13243	5832	72
H(42C)	-33	12880	6518	72
H(1S1)	6012	4698	1575	116
H(1S2)	6104	2869	1482	116
H(2S1)	6850	3322	1720	120
H(2S2)	6727	5052	1957	120
H(3S1)	6871	4135	2871	115
H(3S2)	6783	2372	2645	115
H(4S1)	6095	2638	3155	106
H(4S2)	6104	4501	3097	106
H(1T1)	5804	4633	1763	117
H(1T2)	6002	2961	1548	117
H(2T1)	6738	3698	1671	116
H(2T2)	6540	5434	1775	116
H(3T1)	6643	5322	2764	119

H(3T2)	6976	3837	2618	119
H(4T1)	6430	2208	2954	127
H(4T2)	6194	3693	3294	127
H(5S1)	3808	2085	6659	110
H(5S2)	3755	269	6815	110
H(6S1)	4449	283	7266	126
H(6S2)	4504	2100	7104	126
H(7S1)	4333	2743	8039	124
H(7S2)	4387	940	8223	124
H(8S1)	3610	606	8279	119
H(8S2)	3583	2470	8324	119
H(5T1)	3512	-389	7147	126
H(5T2)	3686	-1110	7812	126
H(6T1)	4411	-763	7412	126
H(6T2)	4229	551	6926	126
H(7T1)	4489	2243	7555	120
H(7T2)	4618	934	8072	120
H(8T1)	3960	1376	8602	121
H(8T2)	3909	2936	8189	121

Table B.2.1.6. Torsion angles [°] for 2,4-bis[(2,6-dimethylphenyl)imino]pentane iron(III) dichloride complex (**3.2**).

C(4)-N(1)-C(1)-C(2)	-174.2(8)
Fe(1)-N(1)-C(1)-C(2)	11.6(11)
C(4)-N(1)-C(1)-C(12)	3.2(12)
Fe(1)-N(1)-C(1)-C(12)	-171.0(6)
N(1)-C(1)-C(2)-C(3)	15.9(14)
C(12)-C(1)-C(2)-C(3)	-161.5(9)
C(14)-N(2)-C(3)-C(2)	162.1(8)
Fe(1)-N(2)-C(3)-C(2)	-22.2(11)
C(14)-N(2)-C(3)-C(13)	-14.8(12)
Fe(1)-N(2)-C(3)-C(13)	160.9(6)
C(1)-C(2)-C(3)-N(2)	-9.6(15)
C(1)-C(2)-C(3)-C(13)	167.2(9)
C(1)-N(1)-C(4)-C(9)	92.5(10)
Fe(1)-N(1)-C(4)-C(9)	-93.2(8)
C(1)-N(1)-C(4)-C(5)	-90.1(10)
Fe(1)-N(1)-C(4)-C(5)	84.1(8)
C(9)-C(4)-C(5)-C(6)	-1.0(13)
N(1)-C(4)-C(5)-C(6)	-178.2(8)
C(9)-C(4)-C(5)-C(10)	-178.2(9)
N(1)-C(4)-C(5)-C(10)	4.5(13)
C(4)-C(5)-C(6)-C(7)	0.0(14)
C(10)-C(5)-C(6)-C(7)	177.3(10)
C(5)-C(6)-C(7)-C(8)	0.8(16)
C(6)-C(7)-C(8)-C(9)	-0.6(16)
C(5)-C(4)-C(9)-C(8)	1.2(13)
N(1)-C(4)-C(9)-C(8)	178.5(8)
C(5)-C(4)-C(9)-C(11)	-177.9(9)
N(1)-C(4)-C(9)-C(11)	-0.6(13)
C(7)-C(8)-C(9)-C(4)	-0.4(14)
C(7)-C(8)-C(9)-C(11)	178.7(9)
C(3)-N(2)-C(14)-C(15)	-82.0(10)
Fe(1)-N(2)-C(14)-C(15)	102.5(8)
C(3)-N(2)-C(14)-C(19)	99.8(10)

Fe(1)-N(2)-C(14)-C(19)	-75.7(9)
C(19)-C(14)-C(15)-C(16)	0.0(13)
N(2)-C(14)-C(15)-C(16)	-178.2(8)
C(19)-C(14)-C(15)-C(20)	178.3(8)
N(2)-C(14)-C(15)-C(20)	0.1(13)
C(14)-C(15)-C(16)-C(17)	-0.1(14)
C(20)-C(15)-C(16)-C(17)	-178.4(10)
C(15)-C(16)-C(17)-C(18)	-0.4(16)
C(16)-C(17)-C(18)-C(19)	1.0(16)
C(17)-C(18)-C(19)-C(14)	-1.0(15)
C(17)-C(18)-C(19)-C(21)	179.6(10)
C(15)-C(14)-C(19)-C(18)	0.5(13)
N(2)-C(14)-C(19)-C(18)	178.7(8)
C(15)-C(14)-C(19)-C(21)	179.9(9)
N(2)-C(14)-C(19)-C(21)	-1.9(13)
C(25)-N(3)-C(22)-C(23)	-169.5(8)
Fe(2)-N(3)-C(22)-C(23)	16.2(11)
C(25)-N(3)-C(22)-C(33)	7.8(12)
Fe(2)-N(3)-C(22)-C(33)	-166.5(6)
N(3)-C(22)-C(23)-C(24)	13.5(15)
C(33)-C(22)-C(23)-C(24)	-163.8(9)
C(35)-N(4)-C(24)-C(23)	168.7(8)
Fe(2)-N(4)-C(24)-C(23)	-18.3(11)
C(35)-N(4)-C(24)-C(34)	-7.3(12)
Fe(2)-N(4)-C(24)-C(34)	165.7(7)
C(22)-C(23)-C(24)-N(4)	-12.3(15)
C(22)-C(23)-C(24)-C(34)	163.8(9)
C(22)-N(3)-C(25)-C(30)	88.6(10)
Fe(2)-N(3)-C(25)-C(30)	-97.2(8)
C(22)-N(3)-C(25)-C(26)	-92.8(10)
Fe(2)-N(3)-C(25)-C(26)	81.4(9)
C(30)-C(25)-C(26)-C(27)	0.4(13)
N(3)-C(25)-C(26)-C(27)	-178.2(8)
C(30)-C(25)-C(26)-C(31)	-179.0(9)
N(3)-C(25)-C(26)-C(31)	2.4(13)
C(25)-C(26)-C(27)-C(28)	-0.4(14)

C(31)-C(26)-C(27)-C(28)	179.0(9)
C(26)-C(27)-C(28)-C(29)	0.3(15)
C(27)-C(28)-C(29)-C(30)	-0.2(15)
C(28)-C(29)-C(30)-C(25)	0.2(14)
C(28)-C(29)-C(30)-C(32)	179.6(9)
C(26)-C(25)-C(30)-C(29)	-0.3(13)
N(3)-C(25)-C(30)-C(29)	178.3(8)
C(26)-C(25)-C(30)-C(32)	-179.7(8)
N(3)-C(25)-C(30)-C(32)	-1.0(12)
C(24)-N(4)-C(35)-C(40)	89.9(10)
Fe(2)-N(4)-C(35)-C(40)	-83.0(8)
C(24)-N(4)-C(35)-C(36)	-92.3(9)
Fe(2)-N(4)-C(35)-C(36)	94.8(8)
C(40)-C(35)-C(36)-C(37)	0.9(13)
N(4)-C(35)-C(36)-C(37)	-176.8(8)
C(40)-C(35)-C(36)-C(41)	179.6(8)
N(4)-C(35)-C(36)-C(41)	1.8(12)
C(35)-C(36)-C(37)-C(38)	0.9(14)
C(41)-C(36)-C(37)-C(38)	-177.8(9)
C(36)-C(37)-C(38)-C(39)	-1.5(16)
C(37)-C(38)-C(39)-C(40)	0.2(16)
C(38)-C(39)-C(40)-C(35)	1.6(15)
C(38)-C(39)-C(40)-C(42)	-179.0(10)
C(36)-C(35)-C(40)-C(39)	-2.1(13)
N(4)-C(35)-C(40)-C(39)	175.5(8)
C(36)-C(35)-C(40)-C(42)	178.5(9)
N(4)-C(35)-C(40)-C(42)	-3.9(13)
C(4S)-O(1S)-C(1S)-C(2S)	3(5)
O(1S)-C(1S)-C(2S)-C(3S)	12(5)
C(1S)-C(2S)-C(3S)-C(4S)	-21(5)
C(1S)-O(1S)-C(4S)-C(3S)	-16(5)
C(2S)-C(3S)-C(4S)-O(1S)	23(5)
C(8S)-O(2S)-C(5S)-C(6S)	-11(3)
O(2S)-C(5S)-C(6S)-C(7S)	0(3)
C(5S)-C(6S)-C(7S)-C(8S)	11(3)
C(5S)-O(2S)-C(8S)-C(7S)	17(3)

C(6S)-C(7S)-C(8S)-O(2S)

-18(3)

Symmetry transformations used to generate equivalent atoms:

B.2.2. X-ray crystallographic data for compound 3.3

Figure B.2.2.1. ORTEP diagram of compound 3.3

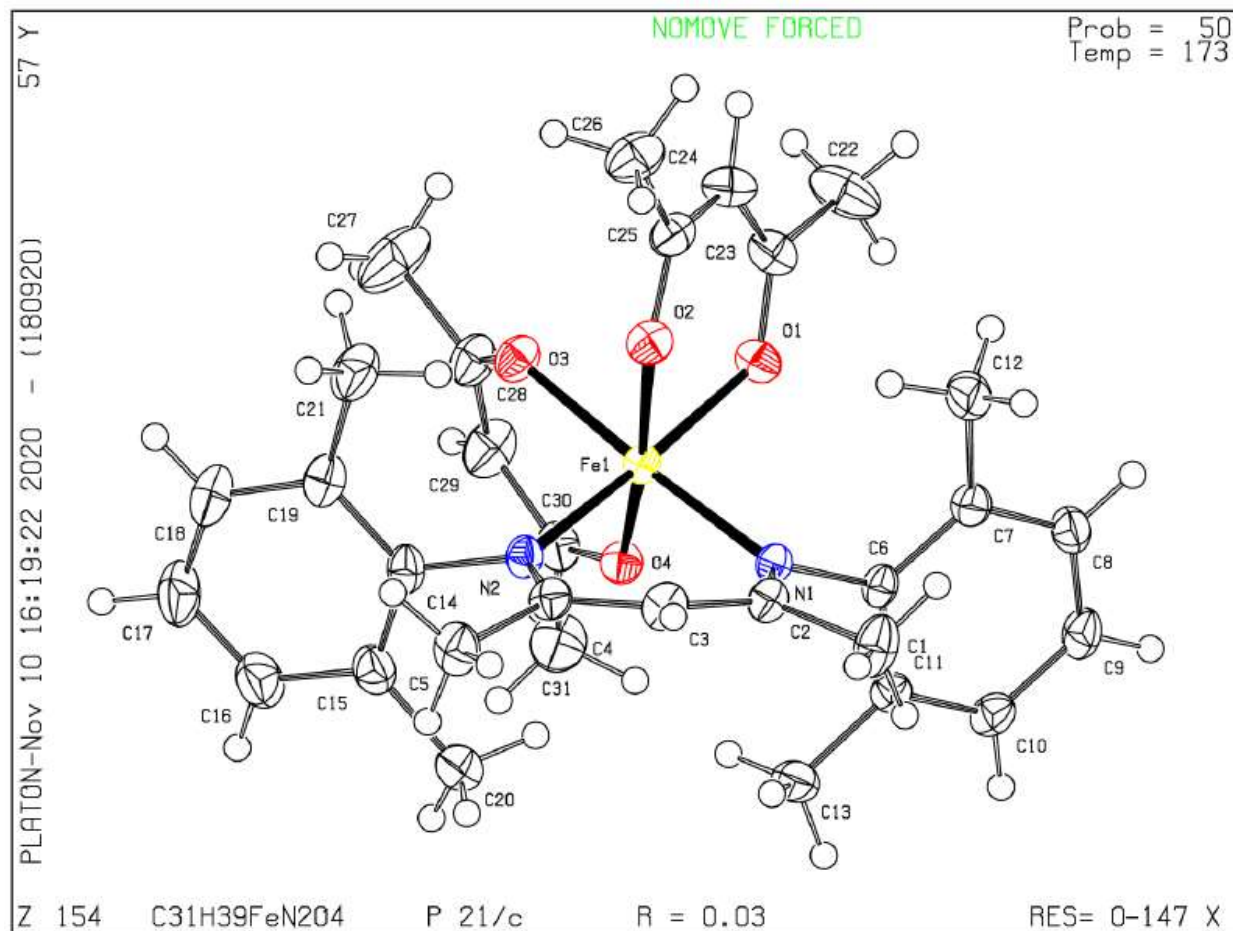


Table B.2.2.1. Crystal data and structure refinement for 2,4-bis[(2,6-dimethylphenyl)imino]pentane iron(III) bis(acetylacetonate) complex (3.3).

Identification code	C31H39FeN2O4	
Empirical formula	C31 H39 Fe N2 O4	
Formula weight	559.49	
Temperature	173(2) K	
Wavelength	1.54178 Å	
Crystal system	Monoclinic	
Space group	P2 ₁ /c	
Unit cell dimensions	a = 8.5730(7) Å	a = 90°.
	b = 15.7016(13) Å	b = 92.127(3)°.
	c = 22.1488(17) Å	g = 90°.
Volume	2979.4(4) Å ³	

Z	4
Density (calculated)	1.247 Mg/m ³
Absorption coefficient	4.346 mm ⁻¹
F(000)	1188
Crystal size	0.480 x 0.220 x 0.100 mm ³
Theta range for data collection	3.451 to 66.673°.
Index ranges	-10<=h<=10, -18<=k<=18, -26<=l<=25
Reflections collected	61955
Independent reflections	5172 [R(int) = 0.0377]
Completeness to theta = 66.673°	97.9 %
Absorption correction	Semi-empirical from equivalents
Max. and min. transmission	0.7528 and 0.4395
Refinement method	Full-matrix least-squares on F ²
Data / restraints / parameters	5172 / 0 / 353
Goodness-of-fit on F ²	1.085
Final R indices [I>2sigma(I)]	R1 = 0.0300, wR2 = 0.0775
R indices (all data)	R1 = 0.0331, wR2 = 0.0787
Extinction coefficient	n/a
Largest diff. peak and hole	0.283 and -0.279 e.Å ⁻³

Table B.2.2.2. Atomic coordinates ($\times 10^4$) and equivalent isotropic displacement parameters ($\text{\AA}^2 \times 10^3$) for 2,4-bis[(2,6-dimethylphenyl)imino]pentane iron(III) bis(acetylacetonate) complex (**3.3**). $U(\text{eq})$ is defined as one third of the trace of the orthogonalized U_{ij} tensor.

	x	y	z	$U(\text{eq})$
Fe(1)	3432(1)	2625(1)	5975(1)	19(1)
O(1)	1352(1)	3191(1)	5748(1)	26(1)
O(2)	4405(1)	3749(1)	5747(1)	26(1)
O(3)	3192(1)	3174(1)	6802(1)	27(1)
O(4)	2295(1)	1624(1)	6319(1)	24(1)
N(1)	3608(1)	2125(1)	5118(1)	20(1)
N(2)	5626(2)	2160(1)	6187(1)	22(1)
C(1)	5023(2)	1946(1)	4177(1)	37(1)
C(2)	4972(2)	2102(1)	4851(1)	23(1)
C(3)	6418(2)	2170(1)	5159(1)	26(1)
C(4)	6727(2)	2099(1)	5782(1)	24(1)
C(5)	8388(2)	1893(1)	5976(1)	32(1)
C(6)	2249(2)	1866(1)	4765(1)	21(1)
C(7)	1363(2)	2455(1)	4429(1)	24(1)
C(8)	35(2)	2169(1)	4109(1)	28(1)
C(9)	-386(2)	1320(1)	4108(1)	29(1)
C(10)	533(2)	738(1)	4428(1)	27(1)
C(11)	1849(2)	998(1)	4761(1)	22(1)
C(12)	1843(2)	3371(1)	4368(1)	35(1)
C(13)	2846(2)	360(1)	5100(1)	31(1)
C(14)	6051(2)	1957(1)	6806(1)	25(1)
C(15)	5916(2)	1114(1)	7002(1)	30(1)
C(16)	6306(2)	924(1)	7603(1)	40(1)
C(17)	6834(3)	1550(1)	7996(1)	46(1)
C(18)	6978(2)	2375(1)	7794(1)	41(1)
C(19)	6585(2)	2600(1)	7201(1)	30(1)
C(20)	5418(2)	416(1)	6572(1)	37(1)

C(21)	6793(2)	3506(1)	7000(1)	40(1)
C(22)	-653(2)	4219(1)	5699(1)	48(1)
C(23)	1052(2)	3980(1)	5752(1)	30(1)
C(24)	2177(2)	4626(1)	5786(1)	33(1)
C(25)	3777(2)	4482(1)	5770(1)	27(1)
C(26)	4893(2)	5224(1)	5776(1)	39(1)
C(27)	2318(3)	3554(2)	7756(1)	61(1)
C(28)	2399(2)	2933(1)	7241(1)	32(1)
C(29)	1655(2)	2148(1)	7278(1)	38(1)
C(30)	1694(2)	1527(1)	6833(1)	28(1)
C(31)	1011(3)	663(1)	6956(1)	43(1)

Table B.2.2.3. Bond lengths [Å] and angles [°] for 2,4-bis[(2,6-dimethylphenyl)imino]pentane iron(III) bis(acetylacetonate) complex (**3.3**).

Fe(1)-O(4)	2.0142(11)
Fe(1)-O(2)	2.0238(11)
Fe(1)-O(1)	2.0384(11)
Fe(1)-O(3)	2.0409(11)
Fe(1)-N(2)	2.0559(13)
Fe(1)-N(1)	2.0653(12)
O(1)-C(23)	1.266(2)
O(2)-C(25)	1.272(2)
O(3)-C(28)	1.265(2)
O(4)-C(30)	1.276(2)
N(1)-C(2)	1.330(2)
N(1)-C(6)	1.4374(19)
N(2)-C(4)	1.330(2)
N(2)-C(14)	1.441(2)
C(1)-C(2)	1.514(2)
C(1)-H(1A)	0.9800
C(1)-H(1B)	0.9800
C(1)-H(1C)	0.9800
C(2)-C(3)	1.397(2)
C(3)-C(4)	1.400(2)
C(3)-H(3)	0.9500
C(4)-C(5)	1.508(2)
C(5)-H(5A)	0.9800
C(5)-H(5B)	0.9800
C(5)-H(5C)	0.9800
C(6)-C(7)	1.395(2)
C(6)-C(11)	1.405(2)
C(7)-C(8)	1.393(2)
C(7)-C(12)	1.503(2)
C(8)-C(9)	1.380(3)
C(8)-H(8)	0.9500
C(9)-C(10)	1.385(2)
C(9)-H(9)	0.9500

C(10)-C(11)	1.387(2)
C(10)-H(10)	0.9500
C(11)-C(13)	1.501(2)
C(12)-H(12A)	0.9800
C(12)-H(12B)	0.9800
C(12)-H(12C)	0.9800
C(13)-H(13A)	0.9800
C(13)-H(13B)	0.9800
C(13)-H(13C)	0.9800
C(14)-C(15)	1.398(2)
C(14)-C(19)	1.402(2)
C(15)-C(16)	1.392(2)
C(15)-C(20)	1.503(2)
C(16)-C(17)	1.378(3)
C(16)-H(16)	0.9500
C(17)-C(18)	1.377(3)
C(17)-H(17)	0.9500
C(18)-C(19)	1.390(3)
C(18)-H(18)	0.9500
C(19)-C(21)	1.502(3)
C(20)-H(20A)	0.9800
C(20)-H(20B)	0.9800
C(20)-H(20C)	0.9800
C(21)-H(21A)	0.9800
C(21)-H(21B)	0.9800
C(21)-H(21C)	0.9800
C(22)-C(23)	1.509(2)
C(22)-H(22A)	0.9800
C(22)-H(22B)	0.9800
C(22)-H(22C)	0.9800
C(23)-C(24)	1.400(3)
C(24)-C(25)	1.392(3)
C(24)-H(24)	0.9500
C(25)-C(26)	1.507(2)
C(26)-H(26A)	0.9800
C(26)-H(26B)	0.9800

C(26)-H(26C)	0.9800
C(27)-C(28)	1.505(3)
C(27)-H(27A)	0.9800
C(27)-H(27B)	0.9800
C(27)-H(27C)	0.9800
C(28)-C(29)	1.393(3)
C(29)-C(30)	1.388(3)
C(29)-H(29)	0.9500
C(30)-C(31)	1.507(2)
C(31)-H(31A)	0.9800
C(31)-H(31B)	0.9800
C(31)-H(31C)	0.9800
O(4)-Fe(1)-O(2)	169.96(4)
O(4)-Fe(1)-O(1)	90.12(4)
O(2)-Fe(1)-O(1)	85.62(4)
O(4)-Fe(1)-O(3)	85.63(4)
O(2)-Fe(1)-O(3)	84.97(4)
O(1)-Fe(1)-O(3)	85.50(5)
O(4)-Fe(1)-N(2)	95.03(5)
O(2)-Fe(1)-N(2)	89.12(5)
O(1)-Fe(1)-N(2)	174.73(5)
O(3)-Fe(1)-N(2)	93.80(5)
O(4)-Fe(1)-N(1)	95.93(5)
O(2)-Fe(1)-N(1)	93.30(5)
O(1)-Fe(1)-N(1)	91.84(5)
O(3)-Fe(1)-N(1)	176.93(5)
N(2)-Fe(1)-N(1)	88.71(5)
C(23)-O(1)-Fe(1)	126.92(11)
C(25)-O(2)-Fe(1)	126.87(10)
C(28)-O(3)-Fe(1)	129.73(11)
C(30)-O(4)-Fe(1)	130.34(10)
C(2)-N(1)-C(6)	117.31(12)
C(2)-N(1)-Fe(1)	120.99(10)
C(6)-N(1)-Fe(1)	121.43(9)
C(4)-N(2)-C(14)	117.72(13)

C(4)-N(2)-Fe(1)	122.50(10)
C(14)-N(2)-Fe(1)	119.57(10)
C(2)-C(1)-H(1A)	109.5
C(2)-C(1)-H(1B)	109.5
H(1A)-C(1)-H(1B)	109.5
C(2)-C(1)-H(1C)	109.5
H(1A)-C(1)-H(1C)	109.5
H(1B)-C(1)-H(1C)	109.5
N(1)-C(2)-C(3)	124.02(14)
N(1)-C(2)-C(1)	120.08(14)
C(3)-C(2)-C(1)	115.82(14)
C(2)-C(3)-C(4)	127.38(14)
C(2)-C(3)-H(3)	116.3
C(4)-C(3)-H(3)	116.3
N(2)-C(4)-C(3)	123.14(14)
N(2)-C(4)-C(5)	120.62(14)
C(3)-C(4)-C(5)	116.14(14)
C(4)-C(5)-H(5A)	109.5
C(4)-C(5)-H(5B)	109.5
H(5A)-C(5)-H(5B)	109.5
C(4)-C(5)-H(5C)	109.5
H(5A)-C(5)-H(5C)	109.5
H(5B)-C(5)-H(5C)	109.5
C(7)-C(6)-C(11)	120.78(14)
C(7)-C(6)-N(1)	121.13(14)
C(11)-C(6)-N(1)	118.09(13)
C(8)-C(7)-C(6)	118.41(15)
C(8)-C(7)-C(12)	119.00(15)
C(6)-C(7)-C(12)	122.49(15)
C(9)-C(8)-C(7)	121.41(15)
C(9)-C(8)-H(8)	119.3
C(7)-C(8)-H(8)	119.3
C(8)-C(9)-C(10)	119.55(15)
C(8)-C(9)-H(9)	120.2
C(10)-C(9)-H(9)	120.2
C(9)-C(10)-C(11)	120.90(15)

C(9)-C(10)-H(10)	119.6
C(11)-C(10)-H(10)	119.6
C(10)-C(11)-C(6)	118.89(14)
C(10)-C(11)-C(13)	120.41(14)
C(6)-C(11)-C(13)	120.70(14)
C(7)-C(12)-H(12A)	109.5
C(7)-C(12)-H(12B)	109.5
H(12A)-C(12)-H(12B)	109.5
C(7)-C(12)-H(12C)	109.5
H(12A)-C(12)-H(12C)	109.5
H(12B)-C(12)-H(12C)	109.5
C(11)-C(13)-H(13A)	109.5
C(11)-C(13)-H(13B)	109.5
H(13A)-C(13)-H(13B)	109.5
C(11)-C(13)-H(13C)	109.5
H(13A)-C(13)-H(13C)	109.5
H(13B)-C(13)-H(13C)	109.5
C(15)-C(14)-C(19)	121.11(15)
C(15)-C(14)-N(2)	119.01(14)
C(19)-C(14)-N(2)	119.88(15)
C(16)-C(15)-C(14)	118.72(16)
C(16)-C(15)-C(20)	120.07(16)
C(14)-C(15)-C(20)	121.17(15)
C(17)-C(16)-C(15)	120.74(18)
C(17)-C(16)-H(16)	119.6
C(15)-C(16)-H(16)	119.6
C(18)-C(17)-C(16)	119.87(17)
C(18)-C(17)-H(17)	120.1
C(16)-C(17)-H(17)	120.1
C(17)-C(18)-C(19)	121.65(18)
C(17)-C(18)-H(18)	119.2
C(19)-C(18)-H(18)	119.2
C(18)-C(19)-C(14)	117.90(17)
C(18)-C(19)-C(21)	119.58(16)
C(14)-C(19)-C(21)	122.48(15)
C(15)-C(20)-H(20A)	109.5

C(15)-C(20)-H(20B)	109.5
H(20A)-C(20)-H(20B)	109.5
C(15)-C(20)-H(20C)	109.5
H(20A)-C(20)-H(20C)	109.5
H(20B)-C(20)-H(20C)	109.5
C(19)-C(21)-H(21A)	109.5
C(19)-C(21)-H(21B)	109.5
H(21A)-C(21)-H(21B)	109.5
C(19)-C(21)-H(21C)	109.5
H(21A)-C(21)-H(21C)	109.5
H(21B)-C(21)-H(21C)	109.5
C(23)-C(22)-H(22A)	109.5
C(23)-C(22)-H(22B)	109.5
H(22A)-C(22)-H(22B)	109.5
C(23)-C(22)-H(22C)	109.5
H(22A)-C(22)-H(22C)	109.5
H(22B)-C(22)-H(22C)	109.5
O(1)-C(23)-C(24)	124.76(16)
O(1)-C(23)-C(22)	116.06(16)
C(24)-C(23)-C(22)	119.17(16)
C(25)-C(24)-C(23)	123.97(16)
C(25)-C(24)-H(24)	118.0
C(23)-C(24)-H(24)	118.0
O(2)-C(25)-C(24)	124.49(15)
O(2)-C(25)-C(26)	115.51(15)
C(24)-C(25)-C(26)	120.00(16)
C(25)-C(26)-H(26A)	109.5
C(25)-C(26)-H(26B)	109.5
H(26A)-C(26)-H(26B)	109.5
C(25)-C(26)-H(26C)	109.5
H(26A)-C(26)-H(26C)	109.5
H(26B)-C(26)-H(26C)	109.5
C(28)-C(27)-H(27A)	109.5
C(28)-C(27)-H(27B)	109.5
H(27A)-C(27)-H(27B)	109.5
C(28)-C(27)-H(27C)	109.5

H(27A)-C(27)-H(27C)	109.5
H(27B)-C(27)-H(27C)	109.5
O(3)-C(28)-C(29)	124.73(15)
O(3)-C(28)-C(27)	115.56(16)
C(29)-C(28)-C(27)	119.70(16)
C(30)-C(29)-C(28)	123.84(16)
C(30)-C(29)-H(29)	118.1
C(28)-C(29)-H(29)	118.1
O(4)-C(30)-C(29)	124.88(15)
O(4)-C(30)-C(31)	116.23(15)
C(29)-C(30)-C(31)	118.87(15)
C(30)-C(31)-H(31A)	109.5
C(30)-C(31)-H(31B)	109.5
H(31A)-C(31)-H(31B)	109.5
C(30)-C(31)-H(31C)	109.5
H(31A)-C(31)-H(31C)	109.5
H(31B)-C(31)-H(31C)	109.5

Symmetry transformations used to generate equivalent atoms:

Table B.2.2.4. Anisotropic displacement parameters ($\text{\AA}^2 \times 10^3$) for 2,4-bis[(2,6-dimethylphenyl)imino]pentane iron(III) bis(acetylacetonate) complex (**3.3**). The anisotropic

displacement factor exponent takes the form: $-2p^2 [h^2 a^{*2} U^{11} + \dots + 2 h k a^* b^* U^{12}]$

	U ¹¹	U ²²	U ³³	U ²³	U ¹³	U ¹²
Fe(1)	17(1)	21(1)	19(1)	0(1)	2(1)	-1(1)
O(1)	22(1)	24(1)	32(1)	3(1)	1(1)	0(1)
O(2)	25(1)	25(1)	28(1)	0(1)	4(1)	-5(1)
O(3)	31(1)	28(1)	23(1)	-2(1)	5(1)	-5(1)
O(4)	24(1)	24(1)	25(1)	1(1)	1(1)	-2(1)
N(1)	19(1)	22(1)	20(1)	-1(1)	0(1)	-2(1)
N(2)	19(1)	26(1)	21(1)	-1(1)	-2(1)	0(1)
C(1)	29(1)	58(1)	23(1)	-5(1)	5(1)	-4(1)
C(2)	24(1)	26(1)	21(1)	-1(1)	3(1)	-4(1)
C(3)	19(1)	32(1)	27(1)	-2(1)	6(1)	-4(1)
C(4)	18(1)	24(1)	29(1)	-2(1)	0(1)	-3(1)
C(5)	20(1)	42(1)	36(1)	-2(1)	-2(1)	0(1)
C(6)	18(1)	27(1)	17(1)	-2(1)	1(1)	-1(1)
C(7)	26(1)	26(1)	22(1)	0(1)	1(1)	0(1)
C(8)	25(1)	33(1)	25(1)	1(1)	-3(1)	4(1)
C(9)	21(1)	38(1)	28(1)	-5(1)	-5(1)	-3(1)
C(10)	25(1)	25(1)	30(1)	-5(1)	0(1)	-4(1)
C(11)	20(1)	24(1)	24(1)	-3(1)	2(1)	1(1)
C(12)	45(1)	27(1)	33(1)	6(1)	-7(1)	-4(1)
C(13)	27(1)	24(1)	40(1)	-1(1)	-4(1)	2(1)
C(14)	19(1)	34(1)	22(1)	0(1)	-2(1)	0(1)
C(15)	26(1)	35(1)	30(1)	2(1)	-3(1)	4(1)
C(16)	45(1)	40(1)	33(1)	9(1)	-3(1)	2(1)
C(17)	56(1)	58(1)	23(1)	6(1)	-7(1)	-2(1)
C(18)	44(1)	52(1)	25(1)	-6(1)	-6(1)	-7(1)
C(19)	27(1)	39(1)	25(1)	-3(1)	-1(1)	-4(1)
C(20)	43(1)	28(1)	39(1)	2(1)	-9(1)	3(1)

C(21)	45(1)	40(1)	34(1)	-4(1)	-5(1)	-15(1)
C(22)	31(1)	38(1)	74(2)	15(1)	10(1)	9(1)
C(23)	29(1)	29(1)	31(1)	6(1)	5(1)	4(1)
C(24)	37(1)	22(1)	40(1)	0(1)	5(1)	2(1)
C(25)	36(1)	24(1)	22(1)	0(1)	4(1)	-6(1)
C(26)	44(1)	31(1)	43(1)	-4(1)	7(1)	-12(1)
C(27)	93(2)	57(1)	35(1)	-17(1)	27(1)	-27(1)
C(28)	36(1)	37(1)	22(1)	-3(1)	4(1)	-4(1)
C(29)	46(1)	43(1)	25(1)	0(1)	12(1)	-13(1)
C(30)	25(1)	31(1)	27(1)	5(1)	-1(1)	-5(1)
C(31)	53(1)	36(1)	40(1)	8(1)	2(1)	-16(1)

Table B.2.2.5. Hydrogen coordinates ($\times 10^4$) and isotropic displacement parameters ($\text{\AA}^2 \times 10^3$) for 2,4-bis[(2,6-dimethylphenyl)imino]pentane iron(III) bis(acetylacetonate) complex (**3.3**).

	x	y	z	U(eq)
H(1A)	4592	1382	4082	55
H(1B)	6107	1974	4053	55
H(1C)	4404	2382	3961	55
H(3)	7292	2277	4918	31
H(5A)	8736	2282	6300	49
H(5B)	9063	1959	5631	49
H(5C)	8447	1305	6123	49
H(8)	-595	2566	3887	33
H(9)	-1300	1138	3890	35
H(10)	257	152	4419	32
H(12A)	2195	3473	3958	53
H(12B)	2695	3497	4661	53
H(12C)	950	3741	4444	53
H(13A)	2729	436	5535	46
H(13B)	3941	443	5003	46
H(13C)	2518	-217	4983	46
H(16)	6206	356	7744	47
H(17)	7099	1413	8404	55
H(18)	7354	2801	8067	49
H(20A)	6299	254	6327	56
H(20B)	4554	618	6308	56
H(20C)	5076	-79	6802	56
H(21A)	6176	3883	7250	60
H(21B)	6440	3562	6576	60
H(21C)	7898	3662	7043	60
H(22A)	-1274	3713	5594	71
H(22B)	-809	4652	5384	71

H(22C)	-982	4448	6086	71
H(24)	1827	5197	5823	39
H(26A)	5254	5343	6193	59
H(26B)	4360	5728	5607	59
H(26C)	5790	5085	5533	59
H(27A)	3375	3678	7916	91
H(27B)	1702	3307	8077	91
H(27C)	1824	4083	7612	91
H(29)	1088	2029	7629	45
H(31A)	581	419	6578	65
H(31B)	178	721	7245	65
H(31C)	1828	288	7126	65

Table B.2.2.6. Torsion angles [°] for 2,4-bis[(2,6-dimethylphenyl)imino]pentane iron(III) bis(acetylacetonate) complex (**3.3**).

C(6)-N(1)-C(2)-C(3)	-166.96(15)
Fe(1)-N(1)-C(2)-C(3)	18.9(2)
C(6)-N(1)-C(2)-C(1)	9.6(2)
Fe(1)-N(1)-C(2)-C(1)	-164.51(13)
N(1)-C(2)-C(3)-C(4)	14.0(3)
C(1)-C(2)-C(3)-C(4)	-162.66(17)
C(14)-N(2)-C(4)-C(3)	171.33(15)
Fe(1)-N(2)-C(4)-C(3)	-13.9(2)
C(14)-N(2)-C(4)-C(5)	-4.8(2)
Fe(1)-N(2)-C(4)-C(5)	169.89(12)
C(2)-C(3)-C(4)-N(2)	-17.0(3)
C(2)-C(3)-C(4)-C(5)	159.31(17)
C(2)-N(1)-C(6)-C(7)	-90.94(18)
Fe(1)-N(1)-C(6)-C(7)	83.13(16)
C(2)-N(1)-C(6)-C(11)	88.00(17)
Fe(1)-N(1)-C(6)-C(11)	-97.93(14)
C(11)-C(6)-C(7)-C(8)	2.8(2)
N(1)-C(6)-C(7)-C(8)	-178.28(14)
C(11)-C(6)-C(7)-C(12)	-173.39(15)
N(1)-C(6)-C(7)-C(12)	5.5(2)
C(6)-C(7)-C(8)-C(9)	-1.8(2)
C(12)-C(7)-C(8)-C(9)	174.56(16)
C(7)-C(8)-C(9)-C(10)	-0.4(3)
C(8)-C(9)-C(10)-C(11)	1.6(2)
C(9)-C(10)-C(11)-C(6)	-0.5(2)
C(9)-C(10)-C(11)-C(13)	-179.33(15)
C(7)-C(6)-C(11)-C(10)	-1.7(2)
N(1)-C(6)-C(11)-C(10)	179.37(13)
C(7)-C(6)-C(11)-C(13)	177.09(14)
N(1)-C(6)-C(11)-C(13)	-1.8(2)
C(4)-N(2)-C(14)-C(15)	-88.95(18)
Fe(1)-N(2)-C(14)-C(15)	96.16(16)
C(4)-N(2)-C(14)-C(19)	91.32(19)

Fe(1)-N(2)-C(14)-C(19)	-83.57(16)
C(19)-C(14)-C(15)-C(16)	0.7(3)
N(2)-C(14)-C(15)-C(16)	-179.02(15)
C(19)-C(14)-C(15)-C(20)	-176.98(16)
N(2)-C(14)-C(15)-C(20)	3.3(2)
C(14)-C(15)-C(16)-C(17)	-0.8(3)
C(20)-C(15)-C(16)-C(17)	176.91(19)
C(15)-C(16)-C(17)-C(18)	0.1(3)
C(16)-C(17)-C(18)-C(19)	0.7(3)
C(17)-C(18)-C(19)-C(14)	-0.8(3)
C(17)-C(18)-C(19)-C(21)	-178.8(2)
C(15)-C(14)-C(19)-C(18)	0.1(3)
N(2)-C(14)-C(19)-C(18)	179.80(16)
C(15)-C(14)-C(19)-C(21)	178.02(17)
N(2)-C(14)-C(19)-C(21)	-2.3(3)
Fe(1)-O(1)-C(23)-C(24)	14.7(2)
Fe(1)-O(1)-C(23)-C(22)	-166.83(13)
O(1)-C(23)-C(24)-C(25)	5.6(3)
C(22)-C(23)-C(24)-C(25)	-172.77(17)
Fe(1)-O(2)-C(25)-C(24)	-19.8(2)
Fe(1)-O(2)-C(25)-C(26)	160.52(11)
C(23)-C(24)-C(25)-O(2)	-3.0(3)
C(23)-C(24)-C(25)-C(26)	176.66(16)
Fe(1)-O(3)-C(28)-C(29)	9.4(3)
Fe(1)-O(3)-C(28)-C(27)	-172.13(16)
O(3)-C(28)-C(29)-C(30)	0.0(3)
C(27)-C(28)-C(29)-C(30)	-178.5(2)
Fe(1)-O(4)-C(30)-C(29)	2.6(2)
Fe(1)-O(4)-C(30)-C(31)	-176.27(12)
C(28)-C(29)-C(30)-O(4)	-6.2(3)
C(28)-C(29)-C(30)-C(31)	172.67(19)

Symmetry transformations used to generate equivalent atoms:

Appendix C.

Assorted spectral data

C.1 Mössbauer and electron paramagnetic resonance spectral data from Chapter 3

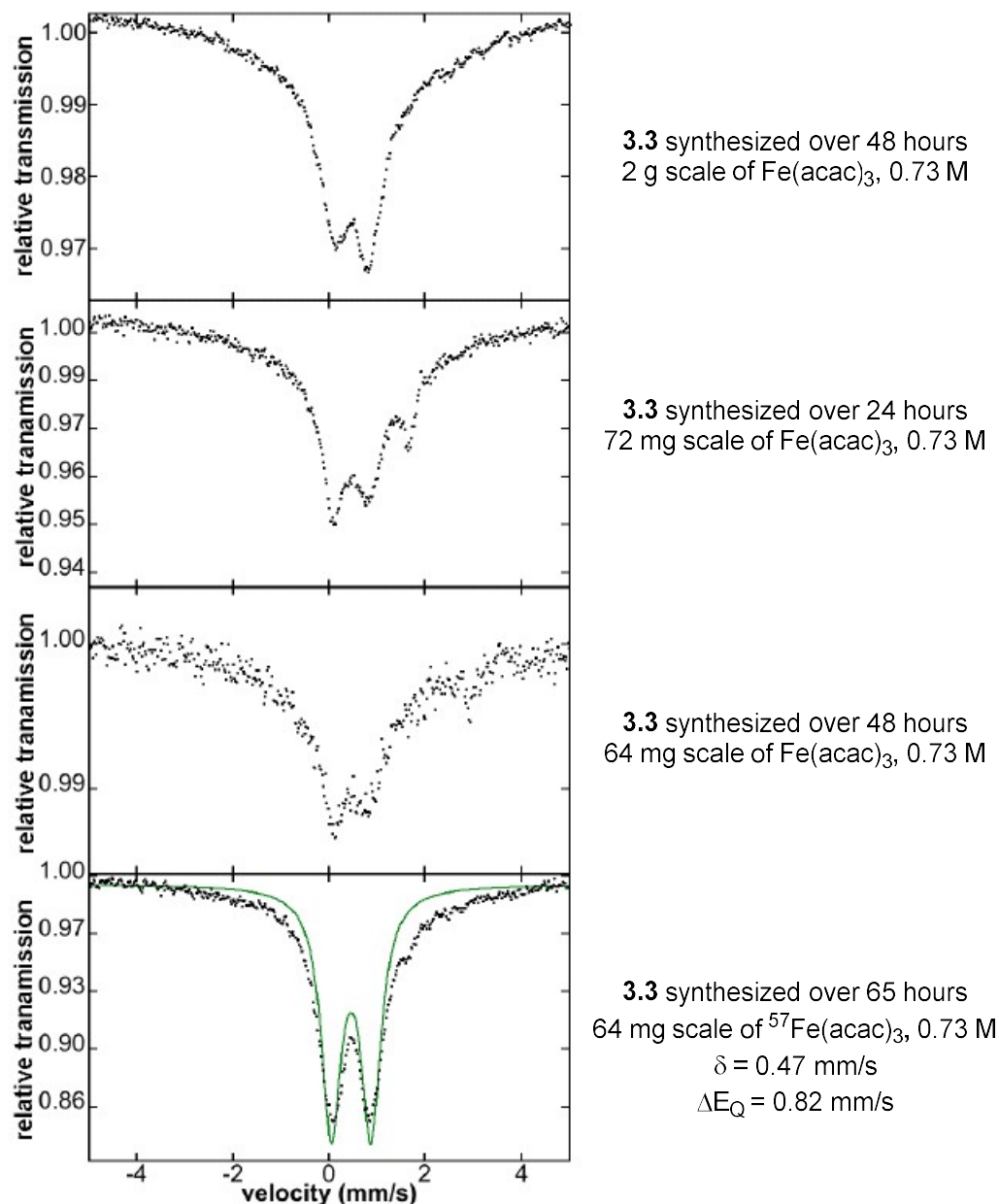


Figure C.1.1. Mössbauer spectra of **3.3** synthesized at various concentrations. The fourth spectrum is a sample of ^{57}Fe -enriched **3.3**, which displays reduced signal broadening (though signal broadening is common for Fe(III) complexes)

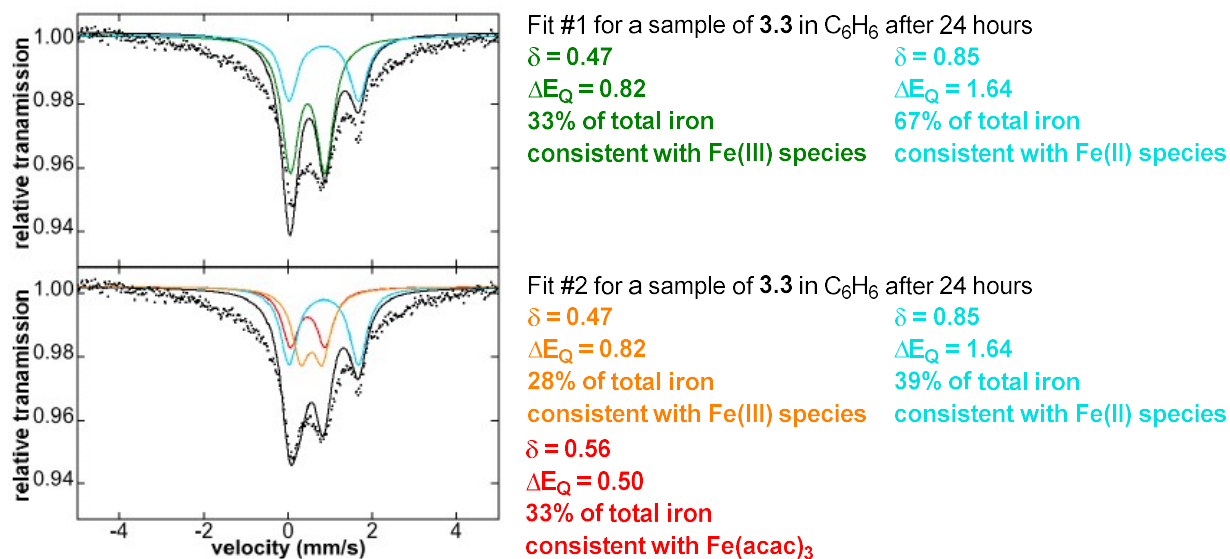


Figure C.1.2. Two possible fits for the Mössbauer spectra of a sample of **3.3** dissolved in C_6H_6 after 24 hours. The compound is converted into a mixture of iron species in solution. At this time, the iron speciation of the compound in solution is unclear.

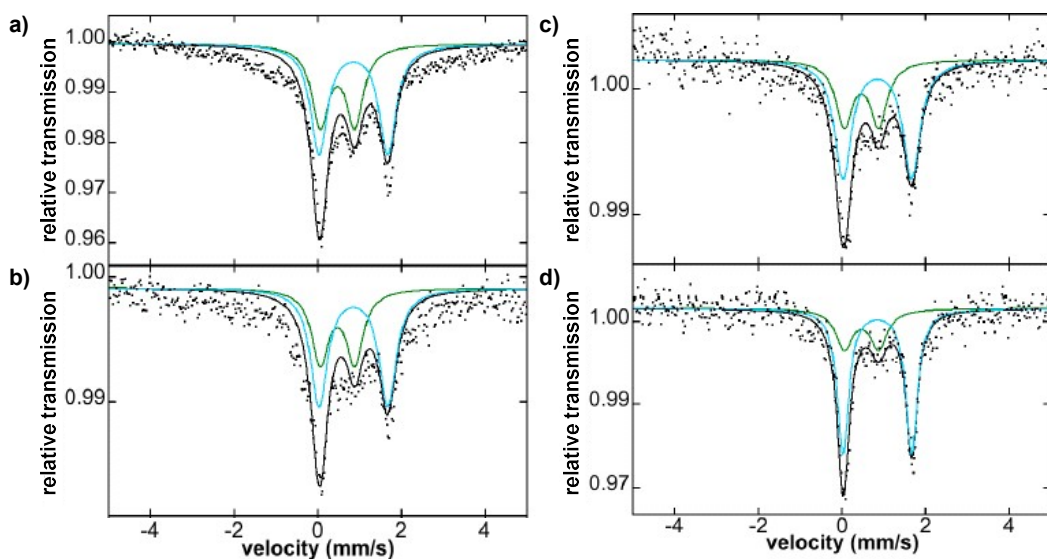


Figure C.1.3. a) 80 K ^{57}Fe Mössbauer spectra of **3.3** in C_6H_6 , b) 80 K ^{57}Fe Mössbauer spectra of **3.3** 5 minutes following the addition of 1 equivalent LiNMeEt in C_6H_6 , c) 80 K ^{57}Fe Mössbauer spectra of **3.3** 5 minutes following the addition of 1 equivalent PhB(pin) in C_6H_6 , d) 80 K ^{57}Fe Mössbauer spectra of **3.3** 5 minutes following the addition of 1 equivalent LiNMeEt and 1 equivalent PhB(pin) in C_6H_6 . All spectra feature two iron species in varying ratios, with the following parameters: green component, $\delta = 0.47$ mm/s, $|\Delta E_Q| = 0.82$ mm/s; blue component, $\delta = 0.85$ mm/s, $|\Delta E_Q| = 1.64$ mm/s.

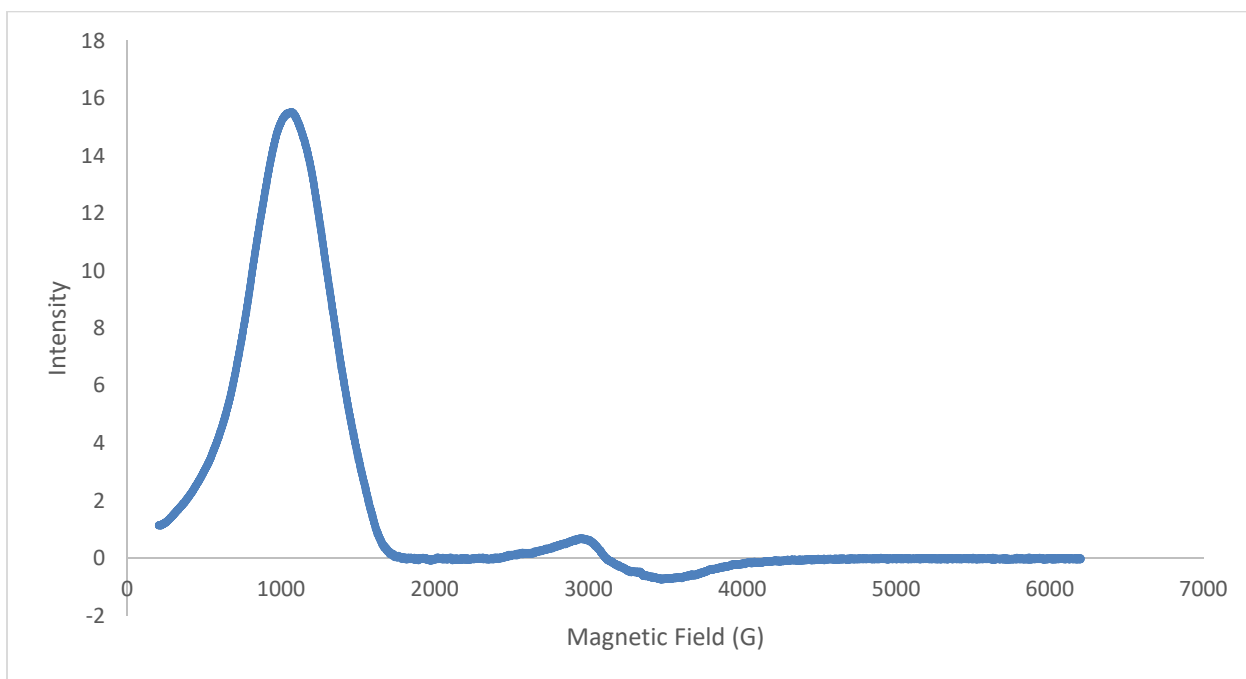


Figure C.1.4. Electron paramagnetic spectrum of **3.3** in C_6H_6 at 10 K.

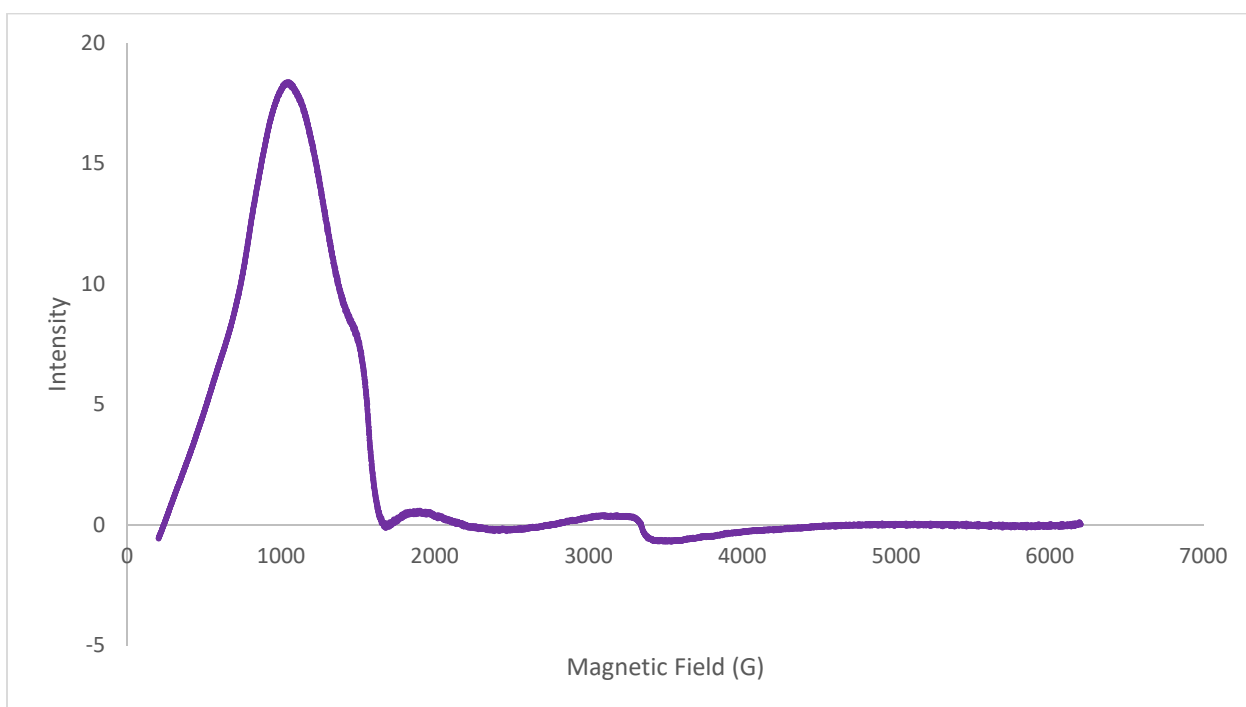


Figure C.1.5. Electron paramagnetic spectrum of **3.3** following the addition of 1 equivalent of LiNMeEt in C_6H_6 at 10 K.

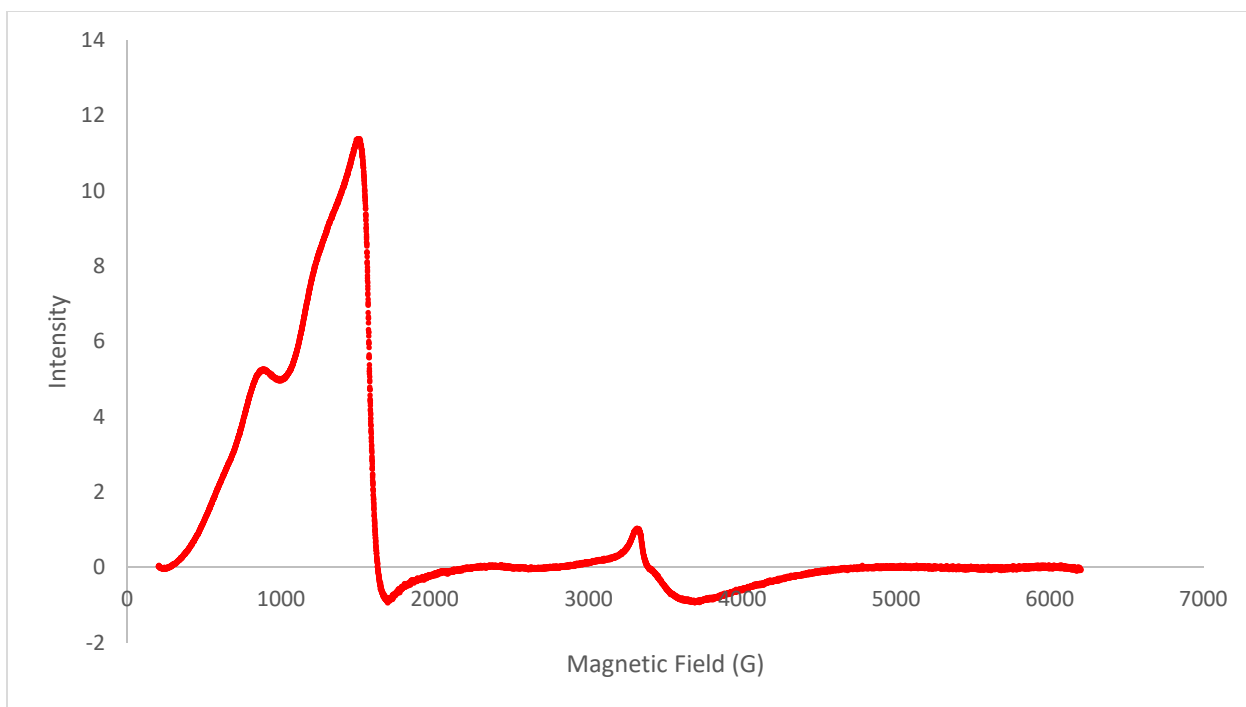


Figure C.1.6. Electron paramagnetic spectrum of **3.3** following the addition of 2 equivalents of LiNMeEt in C₆H₆ at 10 K.